Habilitation à Diriger des Recherches

Vincent Boudon

Laboratoire de Physique de l'Université de Bourgogne
UMR CNRS 5027

Habilitation à Diriger des Recherches

présentée par

Vincent BOUDON

Soutenue le 9 avril 2004, devant la commission d'examen composée de :

J.-M. Flaud	Directeur de Recherches CNRS (Université Paris-Sud)	*Rapporteur*
M. Herman	Professeur (Université Libre de Bruxelles)	*Rapporteur*
M. Joyeux	Chargé de Recherches CNRS (Université Joseph Fourier, Grenoble)	*Examinateur*
R. Poli	Professeur (Université de Bourgogne, Dijon)	*Examinateur*
M. Quack	Professeur (Ecole Polytechnique Fédérale de Zürich)	*Rapporteur*
P. Senet	Professeur (Université de Bourgogne, Dijon)	*Examinateur*
V. Tyuterev	Professeur (Université de Reims Champagne-Ardenne)	*Examinateur*

Remerciements

J'adresse mes plus vifs remerciements à Hubert BERGER et Jean-Paul CHAMPION, respectivement ancien et actuel directeur de Laboratoire de Physique de l'Université de Bourgogne, ainsi qu'à tous ses membres pour l'accueil qu'ils m'ont réservé depuis ma nomination en tant que Chargé de Recherches CNRS.

J'éprouve une reconnaissance toute particulière envers Martin QUACK et tous les membres de son groupe pour leur accueil chaleureux lors de mon stage post-doctoral à l'Ecole Polytechnique Fédérale de Zürich.

Très grands remerciements également à Maud ROTGER pour sa gentillesse, son soutien constant et pour les thématiques qu'elle a développées ces dernières années et dont il est en partie fait état dans ce rapport. La partie consacrée à la spectroscopie rovibronique n'aurait pas pu être ce qu'elle est sans le très brillant travail de thèse de Michaël REY. Ce travail doit également beaucoup à Michel LOETE pour son soutien et ses conseils, tant sur le plan scientifique que sur celui des différentes démarches que j'ai eues à accomplir. Merci aussi à Gérard PIERRE pour ses conseils et pour les différents travaux auxquels il m'a permis de participer (en particulier concernant SF_6), à Christian WENGER pour son aide précieuse en informatique, à Françoise MICHELOT pour tout ce qui concerne le traitement algébrique, à Hans-Rudolf JAUSLIN et à tous les membres de l'équipe "Spectroscopie et Dynamique Moléculaire – Phénomènes Non-Linéaires et Champs Intenses" pour les discussions enrichissantes que j'ai pu avoir avec eux au cours de ces dernières années. Une pensée amicale aussi pour Jacques MORET-BAILLY, mon ancien directeur de thèse.

Sur le plan théorique merci à Boris ZHILINSKII et Dimitrii SADOVSKII (Dunkerque) pour m'avoir initié à l'approche topologique, ainsi qu'à Boris SARTAKOV (Moscou).

Ces remerciements ne sauraient être complets sans mentionner les différents collègues expérimentateurs avec qui j'ai eu le plaisir de travailler et sans lesquels beaucoup des travaux présentés ici n'auraient jamais vu le jour : Michael HIPPLER, Hans HOLLENSTEIN, Ulrich SCHMITT, Yabai HE (Zürich), Hans BÜRGER, Helge WILLNER, El Bachir MKADMI (Wuppertal), Michel HERMAN (Bruxelles), Dioniso BERMEJO (Madrid), Nelly LACOME, Pierre ASSELIN (Paris), Daniel AVIGNANT (Clermont-Ferrand) et Henry SELIG (Jérusalem). Pardon à tous leurs collaborateurs que je n'aurais pas cités.

Je remercie enfin les membres du jury et en particulier Martin QUACK, Jean-Marie FLAUD et Michel HERMAN pour avoir accepté de rapporter ce travail.

Table des matières

Première partie

Introduction

Ce rapport d'habilitation présente une synthèse des activités de recherche que j'ai menées ces huit dernières années. Il couvre l'année d'Attaché Temporaire d'Enseignement et de Recherche (ATER) que j'ai effectuée au Laboratoire de Physique de l'Université de Bourgogne (LPUB) après ma thèse de doctorat, mon année de stage post-doctoral effectuée à l'Ecole Polytechnique Fédérale (ETH) de Zürich (Suisse) ainsi que la période consécutive à ma nomination en tant que Chargé de Recherche (CR) CNRS au LPUB en 1997.

Le deuxième partie de ce document est réservée à un développement synthétique de mon *curriculum vitæ*. J'y résume mon parcours scientifique, en soulignant à la fois la variété des thèmes abordés et la cohérence d'ensemble de ma démarche. Je présente les responsabilités que j'assume au LPUB ainsi que les collaborations locales, nationales et internationales que j'ai développées. Enfin, je décris mon rôle concernant les activités et l'animation scientifiques de l'équipe et du Laboratoire au sein desquels je travaille.

Les troisième et quatrième parties de ce rapport sont dédiées aux sujets de recherche et à la présentation des résultats. J'ai distingué d'une part les recherches concernant la spectroscopie rovibrationnelle dans un état électronique singulet (Partie III) et d'autre part celles concernant la spectroscopie rovibronique dans un état électronique dégénéré (Partie IV). Cette seconde thématique est au coeur du projet de recherche présenté lors de ma candidature au CNRS. Les résultats sont présentés sous la forme de quatorze articles reproduits dans le présent rapport. J'ai choisi ceux-ci comme les plus significatifs parmi mes trente-neuf publications acceptées ou soumises au moment de la rédaction de cette habilitation. Un extrait d'acte de colloque constituant une introduction générale au problème de la spectroscopie rovibronique dans les toupies sphériques est également inclus. Afin de présenter les différents thèmes et de les situer dans le contexte général, j'ai pris le parti de rédiger des textes introductifs. J'ai également ajouté quelques compléments concernant des projets en cours. J'espère que cela facilitera la lecture de ce rapport. L'ensemble de mes travaux sont basés sur les méthodes de théorie des groupes et de formalisme tensoriel développées et employées au sein du groupe de spectroscopie moléculaire du LPUB. Je n'ai pas rappelé ici le détail de ces méthodes, ce qui prendrait trop de place. Mais la plupart des articles inclus comportent une première partie de rappel des points essentiels de ce formalisme.

Enfin, la dernière partie récapitule l'ensemble de ma production scientifique. J'y distingue les articles dans des revues à comité de lecture (P), les contributions à des ouvrages collectifs (B), les actes de colloques (A), les conférences invitées (I), les posters présentées lors de colloques (C), les communications orales présentées lors de colloques (O) et enfin les séminaires (S).

Deuxième partie

Curriculum Vitæ

I – Etat civil

Nom, Prénom : Boudon, Vincent.
Né le : 25 février 1969 à Ermont (95).
Nationalité : Français.
Situation familiale : Célibataire.
Adresse : 43E rue de Mulhouse, F-21000 DIJON, France.

II – Fonction et coordonnées professionnelles

Fonction : Chargé de Recherches CNRS 1ère classe (CR1).
Section CNRS : 04.

Unité d'affectation : UMR 5027,
Laboratoire de Physique de l'Université de Bourgogne (LPUB),
(Directeur : Pr. Jean-Paul Champion).

Adresse : LPUB, 9 Av. A. Savary, B.P. 47 870, F-21078 DIJON Cedex, France.
Téléphone : +33 (0)3 80 39 59 17.
Fax : +33 (0)3 80 39 59 71.
E-mail : `Vincent.Boudon@u-bourgogne.fr`
Page Web : `http://www.u-bourgogne.fr/LPUB/Boudon/Vincent.html`

III – Formations et emplois occupés

1. Septembre 1991 – juin 1992 : DEA de Physique

Diplôme d'Etudes Approfondies (DEA) "Matière et Rayonnement" au Laboratoire de Physique de l'Université de Bourgogne.

2. Septembre 1992 – août 1995 : Thèse

Allocataire-Moniteur au Laboratoire de Physique de l'Université de Bourgogne.

3. Septembre 1995 – juillet 1996 : ATER

Attaché Temporaire d'Enseignement et de Recherche (ATER) au Laboratoire de Physique de l'Université de Bourgogne.

4. Août 1996 – septembre 1997 : Stage postdoctoral

Groupe du Pr. Martin Quack,
Laboratorium für Physikalische Chemie,
Ecole Polytechnique Fédérale (ETH) de Zürich (Suisse).

Août 1996 – Septembre 1997.

Sujet : Spectroscopie en jet moléculaire supersonique d'hexafluorures métalliques (WF_6, ReF_6) et de molécules chirales (CDFClBr).

Stage financé par le *Fonds National Suisse*.

5. Depuis septembre 1997 : CR CNRS

Chargé de Recherches CNRS au Laboratoire de Physique de l'Université de Bourgogne.

IV – Titres et diplômes universitaires

DEA de Physique "Matière et Rayonnement :
Juin 1992, au Laboratoire de Physique de l'Université de Bourgogne (Dijon).
Mention très bien.
Responsable de stage : Pr. J. Moret-Bailly.
Sujet: Les Hexafluorures à Nombre Impair d'Electrons.

Thèse de doctorat :
Soutenue le 26 mai 1995 au Laboratoire de Physique de l'Université de Bourgogne (Dijon).
Mention très honorable avec les félicitations du jury.
Directeurs de thèse : Pr. J. Moret-Bailly et Pr. F. Michelot.
Sujet: Spectroscopie des Hexafluorures à Nombre Impair d'Electrons.

V – Parcours scientifique

1. Thématiques abordées

Les trois paragraphes suivants résument brièvement les travaux scientifiques effectués après ma thèse (1995–2003).

• LPUB (1995 – 1996)

Durant mon année d'ATER au LPUB, j'ai poursuivi et complété mon travail de thèse sur la spectroscopie des hexafluorures colorés. Des expériences d'absorption à basse résolution ont été réalisées à Dijon (collaboration avec Maud Rotger) et ont permis l'enregistrement des spectres proche infrarouge – visible – ultraviolet de plusieurs molécules (WF_6, ReF_6, OsF_6, IrF_6, PtF_6).

Des spectres Raman spontané des ces mêmes molécules ont été enregistrés dans les laboratoires des sociétés Jobin-Yvon (Longjumeau, collaboration avec An Tuan Nguyen) et Dilor (Lille, collaboration avec Bernard Roussel).

Deux collaborations ont été mises en place avec le Pr. Daniel Avignant (Université Blaise Pascal, Clermont-Ferrand) et le Pr. Henry Selig (Université de Jérusalem, Israël) pour la synthèse d'échantillons des ces espèces.

De plus, une expérience de spectroscopie d'absorption saturée dans le visible (région des 630 nm) a été mise en place et testée avec succès sur la molécule d'iode, I_2 (collaboration avec Maud Rotger). Un court séjour dans le groupe du Pr. Welf Kreiner (Université d'Ulm, Allemagne), spécialiste de cette technique, a été effectué dans ce cadre (*cf.* paragraphe 5, ci-dessous). Des essais d'absorption saturée sur IrF_6 (bande ν_3, état électronique excité e) se sont révélés infructueux : ce type de molécules très lourdes nécessite l'utilisation de techniques de simplification des spectres.

• ETH Zürich (1996 – 1997)

Mon stage postdoctoral au sein du groupe du Pr. Martin Quack m'a permis de m'initier aux techniques de spectroscopie d'absorption infrarouge à haute résolution et en jet supersonique. Cette dernière technique est indispensable à la simplification (par le refroidissement des molécules) des spectres des espèces lourdes comme les hexafluorures métalliques. Deux types d'expériences ont été réalisées :

- Une expérience "*transformée de Fourier (FTIR) + jet supersonique*" utilisant un spectromètre Bomem DA.002. Collaboration avec Hans Hollenstein et Ulrich Schmitt.
- Une expérience "*diode laser + jet fente supersonique*". Collaboration avec Yabai He et Maud Rotger.

Dans les deux cas, des pompes adaptées aux molécules fluorées corrosives ont été utilisées. Les spectres froids ($T_{\text{rot}} \leq 50$ K) des molécules suivantes ont été enregistrés :

- WF_6 (bande ν_3). Le spectre de cette espèce à sous-couche complète a pu être analysé jusqu'à $J = 48$ (nombre quantique rotationnel), complétant ainsi les travaux précédents (de M. Takami, au Japon, en particulier).
- ReF_6 (région de la bande ν_3). Les tous premiers spectres froids et résolus (pour ce qui concerne l'expérience de spectroscopie par diode laser) de cette molécule à sous-couche électronique incomplète ont été enregistrés. L'état électronique de base de ReF_6 est quatre fois dégénéré. Nous reviendrons abondamment sur cette molécule dans la partie IV de ce rapport, puisque l'exploitation des ces spectres a constitué (et constitue encore) un des éléments majeurs de mes travaux de recherche effectués par la suite.
- $CDCl_3$. En abondance naturelle, le spectre de cette molécule est complexe, du fait des deux isotopes du chlore.
- CDBrClF. Il s'agit d'une molécule chirale.

Les deux dernières molécules concernent des projets spécifiques du groupe du Pr. Martin Quack. Nous ne les détaillerons pas ici.

• LPUB (depuis 1997)

Depuis ma nomination au Laboratoire de Physique de l'Université de Bourgogne (LPUB) en tant que Chargé de Recherches CNRS, mon activité scientifique vise à diversifier les thèmes abordés en physique moléculaire au LPUB et à rechercher de nouveaux champs d'applications. Ces travaux s'appuient sur la longue expérience du Laboratoire concernant la spectroscopie des molécules à haut degré de symétrie et les techniques associées (hamiltoniens et moments de transition effectifs, formalisme tensoriel, théorie des groupes, ...), en cherchant à les étendre à de nouveaux types de problèmes. Ils s'orientent autour de deux axes principaux :

- *Premièrement*, l'analyse de spectres de vibration-rotation de molécules de différentes symétries dans un état électronique non-dégénéré.
- *Deuxièmement*, la spectroscopie des molécules dans un état électronique dégénéré, travail amorcé lors de ma thèse puis lors de mon stage postdoctoral (1996-97) au sein du groupe du Pr. Martin Quack à l'ETH Zürich et qui a constitué mon projet de recherche lors de ma candidature au CNRS.

La description détaillée des travaux de cette période 1997–2003 constituera bien entendu l'essentiel de ce rapport (*cf.* parties III et IV).

♢ **Spectroscopie moléculaire à haute résolution et analyse de spectres** Mes travaux dans le domaine de la vibration-rotation des molécules "classiques" (à sous-couche électronique complète) concernent un certain nombre de molécules pour lesquelles il s'agit soit d'étudier des systèmes de niveaux (isolés ou en groupes appelés polyades) complexes, soit d'élaborer de nouveaux outils théoriques, voire d'aborder ces deux aspects simultanément. Dans tous les cas, un autre souci important a été de rendre les résultats accessibles à la communauté sous forme de programmes et de banques de données spectroscopiques. Succinctement, les différents travaux entrepris concernent les sujets suivants :

- *La spectroscopie de l'hexafluorure de soufre (SF_6)* a connu récemment un important regain d'intérêt depuis que cette espèce s'est révélée être un gaz à effet de serre important dont la concentration dans l'atmosphère terrestre augmente rapidement (7 % par an). Seule la bande fondamentale ν_3 (vers 10.5 μm) étant bien connue jusqu'à présent, ce qui est insuffisant pour pouvoir effectuer des diagnostics atmosphériques précis, j'ai tout d'abord été amené à mettre au point un jeu de programmes adaptés au calcul de spectres des molécules octaédriques (HTDS). A l'aide de celui-ci, et dans le cadre des plusieurs collaborations avec des expérimentateurs (spectroscopie infrarouges et Raman), diverses bandes (fondamentales, combinaisons, bandes chaudes) ont pu être analysées, améliorant significativement la connaissance de cette molécule.
- *Spectroscopie des polyades élevées du méthane.* Les besoins récents en matière de spectroscopie du méthane chaud (combustions dans les moteurs fusées, atmosphères de naines brunes, ...) nécessitent l'étude de niveaux vibrationnellement très excités. Dans la suite des travaux précédemment réalisés au LPUB sur les quatre premières polyades de CH_4, une première analyse de la très complexe cinquième polyade (icosade, 20 niveaux vibrationnels en interaction) a été entreprise (spectres du groupe du Pr. Martin Quack, ETH Zürich), avec des premiers résultats significatifs pour la région 13.2 – 13.4 μm (bande $\nu_2 + 2\nu_3$).
- *Spectroscopie de diverses molécules à haute symétrie.* Dans le cadre de plusieurs collaborations avec des équipes expérimentales (dont, en particulier, le Pr. Hans Bürger à l'Université de Wuppertal, Allemagne) et en vue de diverses applications, des spectres de plusieurs molécules toupies sphériques "exotiques" et mal connues ont été analysés : P_4, GeF_4, GeD_4, SeF_6 et $Mo(CO)_6$. Ces études ont également été l'occasion d'aborder l'approche semi-classique et classique de la structure des niveaux rovibrationnels (collaboration avec le Pr. Boris Zhilinskií et Dimitrií Sadovskií de l'Université du Littoral à Dunkerque).

– *Contribution au développement de modèles tensoriels pour des molécules non-sphériques.* En collaboration avec Maud Rotger et le Pr. Michel Loëte au LPUB, j'ai également participé au développement de modèles tensoriels permettant d'étendre l'approche "dijonnaise" aux molécules quasi-sphériques (SF_5Cl, SO_2F_2) ainsi qu'à l'éthylène (C_2H_4). Dans ce dernier cas, le but est l'étude de l'adsorption de cette molécule dans les zéolithes, avec inclusion de l'effet Stark et du confinement dans le modèle (collaboration avec des collègues chimistes du LRRS [1] à Dijon). De plus, une approche *ab initio* a été entreprise sur la molécule SF_5Cl.

– *Banques de données spectroscopiques.* L'ensemble de ces résultats est accessible sous la forme des banques de données STDS, HTDS, C_{4v}TDS, C_{2v}TDS, D_{2h}TDS et du programme GROUP dédié au formalisme tensoriel (*cf.* `http://www.u-bourgogne.fr/LPUB/shTDS.html`).

♢ **Spectroscopie moléculaire dans un état électronique dégénéré** Les espèces moléculaires (molécules, ions, radicaux libres) à sous-couche électronique incomplète interviennent dans de nombreux domaines : réactions chimiques, milieux en combustion, milieu interstellaire, atmosphères planétaires et cométaires, ... *etc.* Ces systèmes possèdent des états électroniques dégénérés impliquant des couplages complexes (Jahn-Teller, ...) entre tous les degrés de liberté moléculaires : électroniques, vibrationnels et rotationnels (couplages dits rovibroniques).

Nous avons choisi pour aborder ce type de problème d'étudier les systèmes modèles que sont les hexafluorures et les hexacarbonyles de métaux de transition qui sont des molécules stables ayant une structure électronique analogue à celle d'ions ou de radicaux libres, avec en particulier un état électronique de base généralement dégénéré.

Ce travail de longue haleine, qui a été entrepris lors de ma thèse, a été poursuivi lors de mon stage postdoctoral à l'ETH Zürich d'un point de vue expérimental, puis au LPUB du point de vue théorie et analyse depuis ma nomination, en particulier dans le cadre de la thèse de Michaël Rey que j'ai co-encadrée avec le Pr. Michel Loëte. Il s'est agi, d'une part, de mettre au point un formalisme adéquat et, d'autre part, de tenter d'analyser les toutes premières données expérimentales disponibles pour ce type de molécules :

– *Développement d'un formalisme adapté.* Après une reformulation tensorielle des couplages vibroniques sur la base des méthodes utilisées au LPUB en vibration-rotation, une nouveau modèle pour le développement des opérateurs hamiltonien et moments de transition effectifs a été mis au point (thèse de M. Rey) afin de pouvoir modéliser les spectres à haute résolution de toute bande vibrationnelle dans des états électroniques doublets, triplets ou quadruplets. Une construction adaptée des opérateurs électroniques a été introduite. Ce modèle évite en particulier les problèmes de matrices infinies apparaissant dans le traitement usuel de l'effet Jahn-Teller. De nouveaux outils ont été mis en place, en particulier concernant la symétrisation des états de moment angulaire demi-entier. L'approche algébrique des couplages vibroniques (collaboration avec F. Michelot) ainsi que l'approche semi-classique de la structure des niveaux vibroniques ont également été abordées. L'idée est ici d'aboutir à un ensemble d'outils le plus complet possible pour une approche globale de la spectroscopie rovibronique dans un état électronique dégénéré, à l'exemple de ce qui existe pour la rotation-vibration.

– *Application aux molécules $V(CO)_6$ et ReF_6.* Ce modèle a été appliqué (thèse de Michaël Rey) à deux jeux de données obtenus récemment : des spectres d'absorption en jet moléculaire supersonique de $V(CO)_6$ (collaboration avec Pierre Asselin et collègues, LADIR, Paris) et de ReF_6 (obtenus lors de mon stage postdoctoral à l'ETH Zürich, groupe du Pr. Martin Quack). Le profil de la bande fondamentale la plus intense de chacune de ces molécules (état électronique de base respectivement trois et quatre fois dégénéré) sont parfaitement reproduits. Une première étude qualitative des spectres à haute résolution de ReF_6 permet déjà d'en reproduire les structures typiques.

Cette thématique très complexe nécessitera encore de nombreux développements. L'extension de

1. Laboratoire de Recherche sur la Réactivité des Solides.

ce type d'étude (modèles + analyse) au radicaux CH_3O et CH_3S, très importants en chimie atmosphérique, est maintenant envisagée à court terme.

2. Diffusion des résultats

- 39 publications dans des revues à comité de lecture.
- 2 contributions à des ouvrages collectifs.
- 2 actes de colloques ("proceedings" à comité de lecture).
- 5 conférences invitées.
- 62 contributions (orales ou posters) à des conférences.
- 4 séminaires dans des laboratoires étrangers, 1 séminaire en entreprise.

La liste complète des travaux est fournie en annexe (partie VI).

3. Collaborations scientifiques locales

- Dr. Maud Rotger (LPUB).
- Pr. Michel Loëte (LPUB).
- Pr. Gérard Pierre (LPUB).
- Pr. Jean-Paul Champion (LPUB).
- Dr. Tony Gabard (LPUB).
- Dr. Jean-Marc Simon (LRRS).

4. Collaborations scientifiques nationales et internationales

- Groupe du Pr. Martin Quack, ETH Zürich (Suisse).
- Groupe du Pr. Hans Bürger, Université de Wuppertal (Allemagne).
- Groupe du Pr. Michel Herman, Université Libre de Bruxelles (Belgique).
- Pr. Boris Zhilinskií, Dr. Dimitrií Sadovskií, Université du Littoral, Dunkerque.
- Pr. Daniel Avignant, Université Blaise Pascal (Clermont-Ferrand).
- Pr. Henry Selig, Université de Jérusalem (Israël).
- Pr. Nelly Lacome et collègues, LADIR, Université Pierre et Marie Curie (Paris).
- Pr. Dionisio Bermejo, Université de Madrid (Espagne).
- Pr. Boris Sartakov, General Physics Institute RAS, Moscou (Russie).

5. Séjours de courte durée à l'étranger

- **Du 04/12 au 08/12 1995**, séjour à l'Abteilung Chemische Physik – Gruppe Laseranwendungenden, groupe du Pr. Welf Kreiner, Universität Ulm (Allemagne). Spectroscopie d'absorption saturée.
- **Du 27/04 au 03/05 1998**, séjour au Laboratorium für Physikalische Chemie, groupe du Pr. Martin Quack, ETH Zürich (Suisse). Spectroscopie par transformée de Fourier dans un jet supersonique de ReF_6.
- **Du 01/03 au 12/03 1999**, séjour au Laboratorium für Physikalische Chemie, groupe du Pr. Martin Quack, ETH Zrich (Suisse). Spectroscopie par transformée de Fourier dans un jet supersonique de ReF_6.

6. Reconnaissance scientifique

En 2001 et 2002, referee pour deux articles de revues internationales (*Chirality* et *Journal of Molecular Spectroscopy*).

VI – Encadrement

1. Encadrements de stagiaires

- De septembre 1998 à juin 1999, **co-encadrement** (avec le Pr. M. Loëte du LPUB) **d'un stagiaire de DEA**, Michaël Rey, sur l'"*Approche tensorielle des couplages rovibroniques dans les molécules octaédriques*".
- De septembre 1999 à octobre 2002, **co-direction** (sous la direction du Pr. Michel Loëte) **d'un thésard**, Michaël Rey, sur la "*Théorie des spectres rovibroniques des molécules octaédriques : Hamiltonien et moments de transition*". Thèse soutenue le 24 octobre 2002.
- De septembre 2003 à juin 2004, **co-encadrement** (avec le Pr. M. Loëte du LPUB) **d'un stagiaire de DEA**, Abdollatyf El Hilali, sur le "*Développement d'un modèle rovibronique pour la spectroscopie des radicaux méthoxy (CH_3O) et thiométhyle (CH_3S)*".

2. Participations à des jurys

- **Rapporteur** de la thèse de Christophe Van-Hecke sur le sujet "*Analyse qualitative des spectres de rotation-vibration: influence du potentiel intramoléculaire*". Thèse soutenue le 14 février 2001 à Dunkerque et dirigée par le Pr. Boris Zhilinskií.
- **Membre** (en tant que co-directeur) du jury de la thèse de Michaël Rey sur le sujet "*Théorie des spectres rovibroniques des molécules octaédriques : Hamiltonien et moments de transition*". Thèse soutenue le 24 octobre 2002 et co-dirigée avec le Pr. Michel Loëte.

VII – Animation scientifique

1. Participation à l'organisation de colloques

- Participation à l'organisation du *16th Colloquium on High-Resolution Molecular spectroscopy* (HRMS Dijon, 6–10 Septembre 1999) : Organisation générale, gestion du site Web, participation à la réalisation du livre de résumés.
- Participation à l'*Atelier sur la Spectroscopie de Molécules Piégées dans les Solides* organisée à Dijon le 26 mai 2003 par Maud Rotger dans le cadre du réseau SpecMo du CNRS.
- Participation à l'organisation du *18th Colloquium on High-Resolution Molecular spectroscopy* (HRMS Dijon, 8–12 Septembre 2003) : Organisation générale, gestion du site Web,

  `http://www.u-bourgogne.fr/LPUB/HRMS`

  participation à la réalisation du livre de résumés.
- Depuis Septembre 2003, membre du comité scientifique des colloques HRMS (Dijon 2003, Salmanque 2005, ...).
- Préparation de l'organisation d'une école d'été intitulée *Molecules Trapped in Solids* prévue en septembre 2004 à Dijon.

2. Animation d'un groupe de travail

Animation avec le Pr. Hans R. Jauslin d'un groupe de travail intitulé "Résonances et Bifurcations" au sein du LPUB, avec pour but principal de permettre aux personnes du laboratoire travaillant en physique moléculaire et en physique non-linéaire déchanger des idées. Les thèmes abordés concernent les problmes de résonances en spectroscopie moléculaire et dans les processus multiphotoniques, les calculs *ab initio*, ... *etc.* Dans ce cadre, diverses personnalités extrieures ont été invitées : Pr. Boris Zhilinskií (Dunkerque), Pr. Walter Thiel (Max Planck Institut, Mülheim, Allemagne), ...

3. Financements obtenus

- **1998 :** Financement par la Région Bourgogne de l'achat d'une diode laser et de deux détecteurs adaptés à l'étude de la région des 12 μm, afin de compléter l'équipement de spectroscopie par diodes laser du laboratoire (collaboration avec M. Rotger).

- **2003 :** Financement par le Programme National de Chimie Atmosphérique (PNCA) du projet "*Spectre du méthane (positions et intensités) dans les régions 1,6 – 2 μm et 1.3 – 1.5 μm*".
- **2003 :** Paiement par le CEA Saclay de calculs de spectres de la bande $3\nu_3$ de $^{235}UF_6$ et $^{238}UF_6$.

VIII – Enseignement et diffusion de l'information scientifique et technique

1. Enseignements dispensés

- En 1992–1996, en tant qu'allocataire-moniteur puis ATER, enseignements à l'Université de Bourgogne, en 1er cycle (DEUG A) : Travaux Dirigés (TD) et Travaux Pratiques (TP) d'électromagnétisme et d'optique.
- En 2002–2003, 12,5 heures de cours au sein du DEA "Matière et Rayonnement" de l'Université de Bourgogne. Cours de "*Physique Moléculaire*" (en remplacement du Pr. Michel Loëte).
- En 2003–2004, 8 heures de cours au sein de ce même DEA sur "*Les Etats et Transitions Electroniques des Molécules*" (nouveau cours).

2. Multimédia et diffusion de l'information scientifique

- Fin 2001 – début 2002, création d'un site consacré à l'enseignement de l'optique matricielle (niveau DEUG) contenant des applets Java illustrant la construction des images à travers des lentilles minces ou des miroirs dans l'approximation de Gauss :

  `http://eunomie.u-bourgogne.fr/Optique`

  Ce travail a été rémunéré par l'Université de Bourgogne.

- En janvier 2003, participation à la mise en place et à l'animation du stand du LPUB au Salon des Métiers "*Forcing 2003*" de Dijon. A cette occasion, une présentation multimédia (diaporama PowerPoint, animations, films vidéo) des activités de recherche au sein du Laboratoire a été mise au point.
- En janvier 2004, participation à la mise en place et à l'animation du stand du LPUB au Salon des Métiers "*Forcing 2004*" de Dijon.

IX – Responsabilités administratives et collectives

1. Responsabilités administratives

- Membre titulaire de la Commission de Spécialistes de Physique (28–29–30èmes sections) de l'Université de Bourgogne.
- Membre suppléant de la Commission de Spécialistes de Physique (29–30èmes sections) de l'Université de Reims Champagne - Ardenne.
- Membre élu du Conseil de Laboratoire du LPUB.
- Depuis début 2002, gestion des finances de l'équipe Spectroscopie et Dynamique Moléculaire – Phénomènes Non-Linéaires et Champs Intenses dont le coordonnateur est le Pr. Hans R. Jauslin.

2. Responsabilités informatiques

- Je suis membre de la Commission Informatique du LPUB.
- Responsable (Webmaster) du site Web du *18th Colloquium on High-Rsesolution Molecular spectroscopy* (Dijon, 8–12 Septembre 2003) :

  `http://www.u-bourgogne.fr/LPUB/HRMS`
- Responsable (Webmaster) du site Web du *Laboratoire de Physique de l'Université de Bourgogne* :

  `http://www.u-bourgogne.fr/LPUB/`

ainsi que de celui de l'équipe *Spectroscopie et Dynamique Moléculaire – Phénomènes Non-Linéaires et Champs Intenses* :

`http://www.u-bourgogne.fr/LPUB/tSM.html`

– Responsable de l'informatique au sein de l'équipe *Spectroscopie et Dynamique Moléculaire*. Dans ce cadre, mise en place un serveur Macintosh sous MacOS X Server, qui est utilisé, entre autres, comme serveur Intranet pour le Laboratoire.

Troisième partie

Spectroscopie Moléculaire à Haute Résolution et Analyse de Spectres

TROISIÈME PARTIE

Chapitre

1

Spectroscopie de l'Hexafluorure de Soufre

Publications P9, P12, P18, P20, P28, P33, P34, P37, P39
Articles de revue B1,B2

1.1 Introduction

La molécule SF_6 suscite depuis quelques années un regain d'intérêt important. En effet, ce composé apparaît désormais comme un polluant atmosphérique non-négligeable et le protocole de Kyoto l'a classé parmi les gaz à effet de serre dont les émissions doivent être réduites et la concentration suivie de près. L'hexafluorure de soufre est rejeté dans l'atmosphère par diverses industries (électriques, en particulier). Comme le montre la Figure 1.1, si la concentration actuelle de SF_6 dans l'atmosphère terrestre est relativement faible, celle-ci augmente à un rythme assez inquiétant. Tout le problème est que, d'une part, la durée de vie des cette molécule très inerte est extrêmement longue dans l'atmosphère ($\sim$ 3200 ans) et que, d'autre part, sa capacité d'effet de serre est énorme, 23900 fois celle de CO_2 [1].

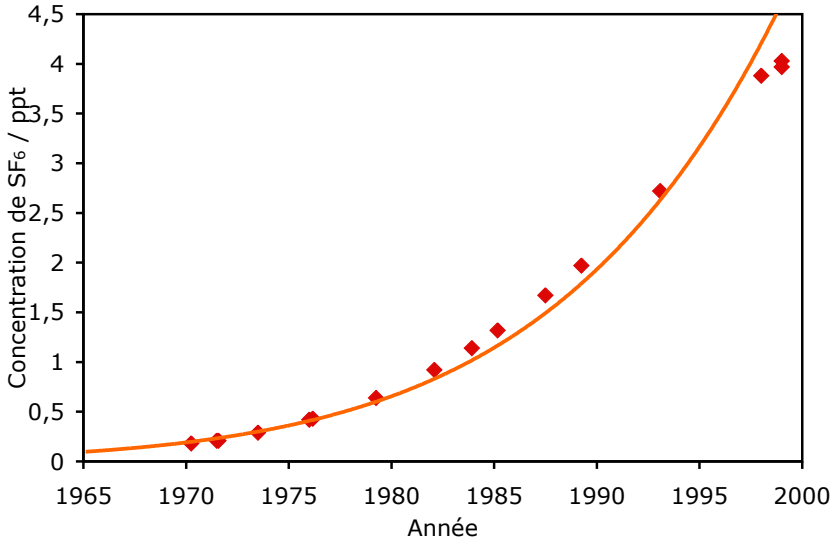

FIG. 1.1 – *Augmentation de la concentration de SF_6 dans l'atmosphère terrestre. Source : W. T. Sturges, School of Environmental Sciences, University of East Anglia (Norwich, Royaume Uni) et* `http://cdiac.esd.ornl.gov/trends/otheratg/sturges/sturges.html`. *Mesures effectuées à Dôme Concordia, Est Antarctique.*

1. Cette valeur est ce qu'on appelle le *Global Warming Potential (GWP)* ; cela signifie qu'une seule molécule de SF_6, en termes d'effet de serre, est équivalente à 23900 molécules de CO_2.

La détection et la mesure de concentration de SF_6 dans l'atmosphère nécessitent une modélisation précise des spectres d'absorption de cette molécule. Or, jusqu'à ces dernières années, sa spectroscopie à haute résolution était paradoxalement assez mal connue. En effet, si la bande d'élongation ν_3 (~ 948 cm^{-1}) a été analysée avec un très grande précision par différents auteurs [B1], l'ensemble des autres niveaux vibrationnels ont été très peu étudiés.

1.2 Particularités de SF_6

TAB. 1.1 – *Les modes normaux de vibration de SF_6 (nombres d'onde en cm^{-1}) pour les différents isotopomères (abondance naturelle donnée entre parentheses).*

Mode normal	ν_1	ν_2	ν_3	ν_4	ν_5	ν_6
Symétrie dans O_h	A_{1g}	E_g	F_{1u}	F_{1u}	F_{2g}	F_{2u}
Dégénérescence	1	2	3	3	3	3
Activité	Raman	Raman	Infrarouge	Infrarouge	Raman	Inactif
Type	Elongation			Pliage		
$^{32}SF_6$ (95.02 %)	774.545	643.375	948.103	614.982	523.5	346.9
$^{33}SF_6$ (0.75 %)	–	–	939.131	613.6	–	–
$^{34}SF_6$ (4.21 %)	774.602	–	930.678	612.209	–	–
$^{36}SF_6$ (0.02 %)	–	–	915.1	–	–	–

La Table 1.1 rappelle les caractéristiques des six modes normaux de vibration de SF_6. Nous pouvons faire les quelques remarques suivantes :

- Pour ce type de molécule centrosymétrique, les bandes de parité g ne sont observables qu'en spectroscopie Raman (pas en absorption). D'une manière générale, les niveaux vibrationnels de parité g et u n'interagissent pas entre eux [2].
- La région d'intense absorption est celle de ν_3. Mais SF_6 possédant des vibrations de pliage de relativement bas nombre d'onde, celles-ci sont à l'origine de nombreuses bandes chaudes. L'étude de la région d'intense absorption, ν_3, essentielle pour les problèmes d'effet de serre ne requiert donc pas seulement l'analyse de la fondamentale, mais aussi des nombreuses bandes chaudes présentes dans les spectres. Pour mémoire, notons qu'à température ambiante, seulement 32 % des molécules SF_6 sont dans l'état vibrationnel de base (voire Figure 1.2). Cette région spectrale étant particulièrment dense, l'analyse des bandes chaudes est difficile.
- La fondamentale ν_6, qui est la plus basse en énergie, est inactive tant en absorption infrarouge qu'en diffusion Raman. Or, le niveau $v_6 = 1$ est le principal "générateur" de bandes chaudes.

Afin de résoudre le problème des bandes chaudes dans la région ν_3, il apparaît par conséquent nécessaire d'étudier l'ensemble des niveaux vibrationnels les plus bas (niveaux fondamentaux, harmoniques et de combinaison). Les cas de $v_6 = 1$ est le plus problématique, le seul moyen (indirect) de l'atteindre étant d'utiliser des niveaux de combinaison impliquant le mode ν_6.

Rappelons enfin que les bandes harmoniques ou de combinaison de ce type de molécule toupie sphérique possèdent un nombre variable de sous-niveaux de différentes symétries.

1.3 Analyses de bandes rovibrationnelles

Les travaux que j'ai effectués ces dernières années concernant SF_6 m'ont permis d'analyser plusieurs bandes vibrationnelles de cette molécule [B1], en collaboration avec différentes équipes expérimentales

2. Sauf à invoquer la violation de parité, phénomène de toute façon négligeable ici.

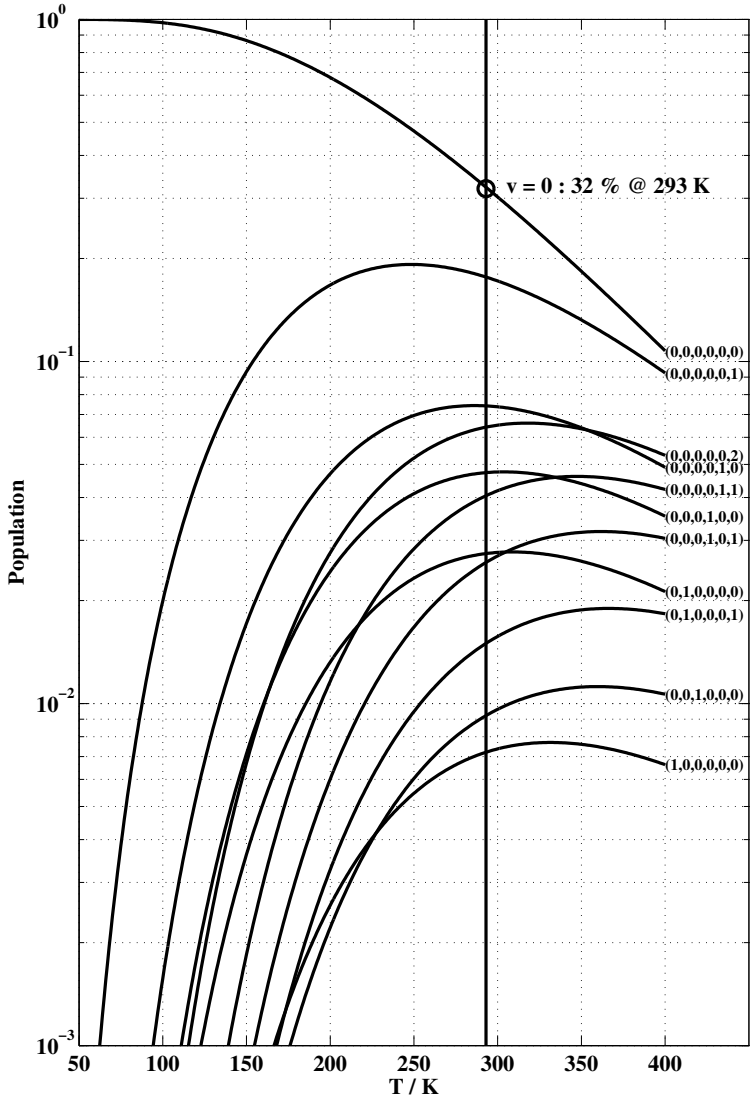

FIG. 1.2 – *Population des premiers niveaux vibrationnels de SF_6 (notés $[v_1v_2v_3v_4v_5v_6]$) en fonction de la température.*

à Madrid, Bruxelles, Paris et Wuppertal. Si quelques analyses ont permis d'améliorer et de compléter les travaux antérieurs d'autres auteurs, il s'est aussi agi, pour plusieurs bandes, de la toute première analyse à haute résolution.

En particulier, le problème du mode ν_6 a été abordé grâce à la première analyse détaillée d'une bande de combinaison, $\nu_2 + \nu_6$ [P9]. Ce travail a été complété par la suite par une analyse simultanée de ce même spectre infrarouge et du spectre Raman de la bande ν_2 [P18].

Deux bandes Raman ont été étudiées pour la première fois à haute résolution : ν_2 [P18], déjà citée, et ν_5 [P28]. Récemment, le spectre infrarouge de la bande de combinaison $\nu_2 + \nu_4$ [P37] a lui aussi fait l'objet d'une analyse complète et ce jusqu'à des valeurs élevées du nombre quantique rotationnel ($J = 112$).

L'ensemble de ces travaux ont permis d'améliorer la connaissance spectroscopique de SF_6. Mais d'autres niveaux vibrationnels doivent encore être étudiés avant de pouvoir aborder complètement le problème des bandes chaudes dans la région ν_3. Les niveaux de SF_6 ne présentant pas de structure en polyades vibrationnelles claire (voir Figure 1.3), il sera nécessaire d'envisager un ajustement global de l'ensemble des niveaux les plus bas.

L'essentiel des travaux portent sur l'isotopomère principal $^{32}SF_6$ (95.02 % en abondance naturelle). Mais, à chaque fois que cela a été possible, les isotopomères mineurs ont également été étudiés.

Ces analyses ont été réalisées à l'aide d'un formalisme tensoriel adapté aux molécules octaédriques

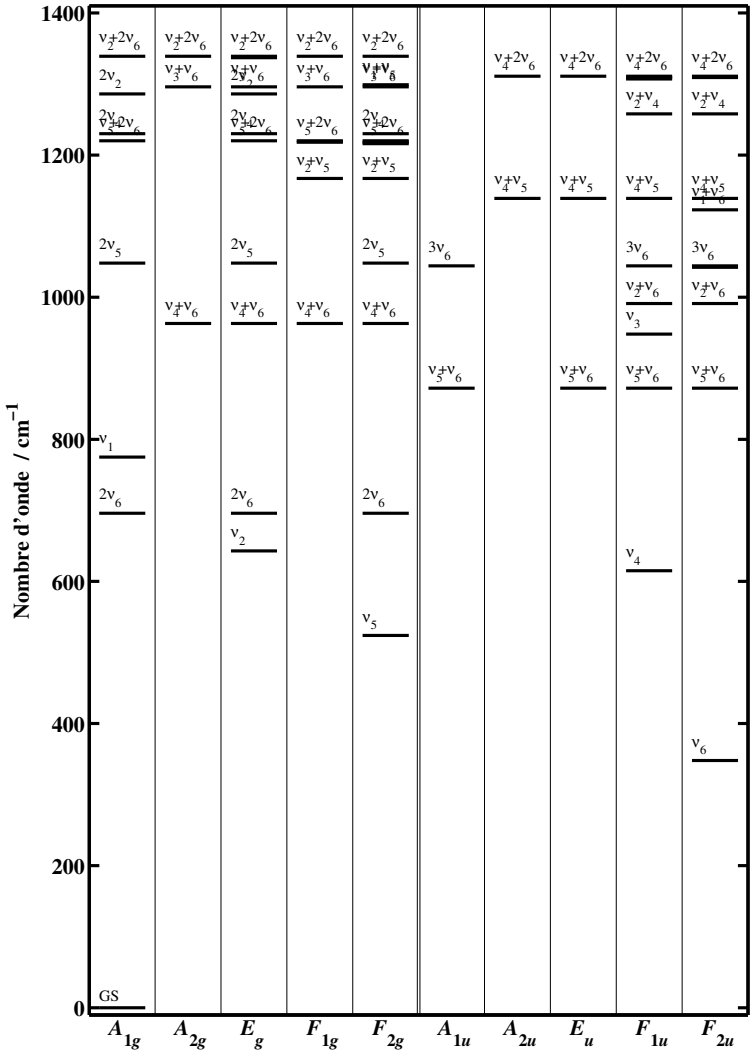

FIG. 1.3 – *Les premiers niveaux vibrationnels de SF_6 classés par symétrie.*

de type XY_6 [P12] (voir Chapitre 3) implanté dans la suite de programmes HTDS [P16] (voir Chapitre 5).

1.4 Articles-clés

Sont reproduits ici deux articles illustrant les avancées récentes que j'ai pu effectuer sur la spectroscopie rovibrationnelle de SF_6, en collaboration avec des collègues expérimentateurs européens.

- [**P20 :** *J. Mol. Spectrosc.*, **205**, 304–311 (2001)] présente l'étude du spectre d'absorption infrarouge de la région de la bande fondamentale ν_4. Ce travail comprend la toute première analyse d'une bande chaude de SF_6, à savoir $\nu_4 + \nu_6 - \nu_6$, qui a bénéficié des résultats obtenus précédemment sur ν_6 (voir ci-dessus). Le région ν_4 est spectralement moins dense que la région ν_3. Dans ce même article, la bande ν_3 de l'isotopomère $^{34}SF_6$ est également prise en compte.
- [**P39 :** soumis au *J. Mol. Spectrosc.* (2003)] concernant l'étude du spectre Raman de la région ν_1 et du spectre double résonance Raman-Raman de la bande $2\nu_1 - \nu_1$ pour $^{32}SF_6$ et $^{34}SF_6$. Plusieurs bandes chaudes ont pu être analysées. Ce travail, en conjugaison avec l'ensemble des autres analyses que j'ai effectuées a permis la première détermination spectroscopique de la longueur de liaison de SF_6. Celle-ci est en parfait accord avec les plus récents calculs *ab initio*.

Journal of Molecular Spectroscopy **205,** 304–311 (2001)
doi:10.1006/jmsp.2000.8267, available online at http://www.idealibrary.com on IDEAL®

High-Resolution Spectroscopy and Analysis of the ν_4 Bending Region of SF_6 near 615 cm^{-1}

V. Boudon,* G. Pierre,* and H. Bürger†

*Laboratoire de Physique de l'Université de Bourgogne, UMR CNRS no. 5027, 9, Avenue Alain Savary BP 47870, F-21078 Dijon Cedex, France; and †Anorganische Chemie, Universität-Gesamthochschule, D-42097 Wuppertal, Germany

E-mail: boudon@jupiter.u-bourgogne.fr

Received September 12, 2000

The high-resolution Fourier transform spectrum of the ν_4 bending region of SF_6 near 615 cm^{-1} has been recorded at 213 K. We were able to perform a simultaneous analysis of the ν_4 and $\nu_4 + \nu_6 - \nu_6$ bands of the main isotopomer, namely $^{32}SF_6$. This is the first detailed analysis of a hot band for this molecule. The ν_4 band of $^{34}SF_6$ was also analyzed and the Q branch of the ν_4 band of $^{33}SF_6$ was identified. In both cases we used the HTDS software developed in Dijon.

Key Words: molecular spectroscopy; spherical top; SF_6; hot band.

1. INTRODUCTION

Sulfur hexafluoride appears to be a species of growing importance in the field of atmospheric physics and chemistry since it is now recognized as a pollutant that can contribute to the greenhouse effect (*1, 2*). SF_6 concentration in Earth's atmosphere is presently small but increases at a rate of around 7% per year due to industrial emissions (*3, 4*). This small concentration is also used to understand gas transport and circulation phenomena in the middle atmosphere (*5, 6*).

However, except for the well-known ν_3 stretching fundamental (*7*), the spectroscopy of SF_6 is still widely unexplored. We have contributed recently to the study of this molecule by analyzing high-resolution spectra of the ν_2 and $\nu_2 + \nu_6$ bands (*8, 9*).

We present here a study of the ν_4 bending region near 615 cm^{-1} which completes and extends the work of Kim *et al.* (*10*) performed with intermediate resolution (0.04 cm^{-1}) Fourier transform infrared (FTIR) spectroscopy and Doppler-limited high-resolution (0.0001 cm^{-1}) measurements using a 200- to 400-m optical path diode–laser spectrometer. The present FTIR spectrum of this region has been recorded in Wuppertal at a resolution (1/maximum optical path difference) of 0.0028 cm^{-1} and a temperature of 213 K.

Using the tensorial formalism (*11*) and the HTDS software (*12*) developed in Dijon for XY_6 octahedral molecules, we were able to perform a simultaneous analysis of the ν_4 bending fundamental of the $^{32}SF_6$ species together with the $\nu_4 + \nu_6 - \nu_6$ hot band. This is the first analysis of a hot band ever performed for this molecule. We were also able to analyze the ν_4 band of the $^{34}SF_6$ isotopomer (4.21% in natural abundance).

In Section 2 we give some experimental details; then in Section 3 we briefly recall the basic features of the theory used, and finally we explain the details of the analyses in Section 4 and discuss some of the results in Section 5.

2. EXPERIMENTAL

The infrared spectrum of SF_6 was recorded at −60°C using a stainless steel cell of 220 mm length outfitted with CsBr windows. A pressure of 2.8 mb (at room temperature) was adjusted. A Bruker 120 HR interferometer equipped with a Globar source, a KBr beam splitter, and a liquid-He-cooled Si:B detector was used. Radiation > 800 cm^{-1} was eliminated using a cooled 12.5-mm-long pass filter. The resolution (1/maximum optical path difference) was adjusted to 2.8×10^{-3} cm^{-1}, and in total 743 scans were collected. Calibration was done by comparison with lines of residual H_2O in the interferometer in the 500–550 cm^{-1} range as quoted in Ref. (*13*). Wavenumber precision of sharp, unblended lines is better than 2×10^{-4} cm^{-1}.

An overview spectrum of the ν_4 region is shown at the bottom of Fig. 1.

3. THEORETICAL MODEL

The theoretical model used in this paper is based on the tensorial formalism and the vibrational extrapolation methods developed in Dijon. These methods have already been explained for example in Refs. (*14*) and (*11*) and they are implemented in the HTDS software (*12*) used to perform the present analyses. Thus, we just briefly recall here the basic principles.

Let us consider an XY_6 molecule for which the vibrational levels are grouped in a series of polyads designed by P_k ($k = 0, \ldots, n$), P_0 being the ground state (GS). The Hamiltonian operator can be put in the following form (after performing some contact transformations)

0022-2852/01 $35.00

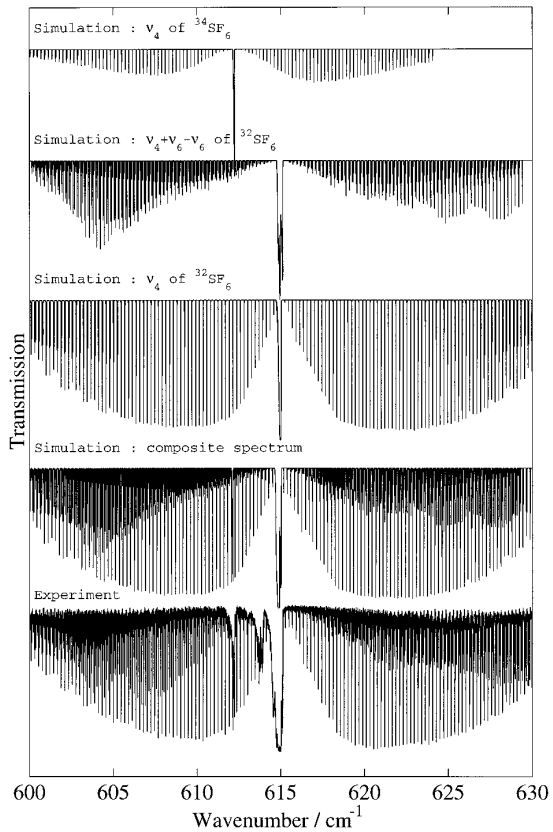

FIG. 1. Experimental and simulated spectra for $^{32}SF_6$ and $^{34}SF_6$ in the ν_4 region.

$$\mathcal{H} = \mathcal{H}_{\{P_0 \equiv GS\}} + \mathcal{H}_{\{P_1\}} + \cdots + \mathcal{H}_{\{P_n\}}, \quad [1]$$

where $\mathcal{H}_{\{P_k\}}$ contains only rovibrational operators which have no matrix elements within the $P_{k'<k}$ basis sets. The different terms are written in the form

$$\mathcal{H}_{\{P_k\}} = \sum_{\text{all indexes}} t^{\Omega(K,n\Gamma)\Gamma_v\Gamma_{v'}}_{\{s\}\{s'\}} T^{\Omega(K,n\Gamma)\Gamma_v\Gamma_{v'}}_{\{s\}\{s'\}}. \quad [2]$$

In this equation the $t^{\Omega(K,n\Gamma)\Gamma_v\Gamma_{v'}}_{\{s\}\{s'\}}$ are the parameters and the $T^{\Omega(K,n\Gamma)\Gamma_v\Gamma_{v'}}_{\{s\}\{s'\}}$ are the rovibrational operators defined as follows

$$T^{\Omega(K,n\Gamma)\Gamma_v\Gamma_{v'}}_{\{s\}\{s'\}} = \beta[R^{\Omega(K,n\Gamma)} \otimes {}^{\epsilon}V^{\Gamma_v\Gamma_{v'}(\Gamma)}_{\{s\}\{s'\}}]^{(A_{1g})}, \quad [3]$$

where β is a numerical factor equal to $\sqrt{[\Gamma_v]}\,(-\sqrt{3}/4)^{\Omega/2}$ if $(K, n\Gamma) = (0_g, 0A_{1g})$, and equal to 1 otherwise.

The rovibrational operators $T^{\Omega(K,n\Gamma)\Gamma_v\Gamma_{v'}}_{\{s\}\{s'\}}$ are obtained by coupling of a rotational operator $R^{\Omega(K,n\Gamma)}$ of degree Ω and a vibrational operator ${}^{\epsilon}V^{\Gamma_v\Gamma_{v'}(\Gamma)}_{\{s\}\{s'\}}$ of degree Ω_v. The order of each individual term is defined as $\Omega + \Omega_v - 2$.

The effective Hamiltonian for polyad P_n is obtained by projecting $\mathcal{H}$ in the P_n Hilbert subspace, i.e.,

$$H^{\langle P_n\rangle} = P^{\langle P_n\rangle}\mathcal{H}P^{\langle P_n\rangle}, \quad = H^{\langle P_n\rangle}_{\{GS\}} + \cdots + H^{\langle P_n\rangle}_{\{P_k\}} + \cdots + H^{\langle P_n\rangle}_{\{P_n\}}. \quad [4]$$

In order to analyze the ν_4 and $\nu_4 + \nu_6 - \nu_6$ bands, we use the following effective Hamiltonians:

- The ground state effective Hamiltonian,

$$\tilde{H}^{\langle GS\rangle} = \tilde{H}^{\langle GS\rangle}_{\{GS\}}, \quad [5]$$

- The ν_4 effective Hamiltonian,

$$\tilde{H}^{\langle \nu_4\rangle} = \tilde{H}^{\langle \nu_4\rangle}_{\{GS\}} + \tilde{H}^{\langle \nu_4\rangle}_{\{\nu_4\}}, \quad [6]$$

- The $\nu_4 + \nu_6$ effective Hamiltonian,

$$\tilde{H}^{\langle \nu_4+\nu_6\rangle} = \tilde{H}^{\langle \nu_4+\nu_6\rangle}_{\{GS\}} + \tilde{H}^{\langle \nu_4+\nu_6\rangle}_{\{\nu_6\}} + \tilde{H}^{\langle \nu_4+\nu_6\rangle}_{\{\nu_4\}} + \tilde{H}^{\langle \nu_4+\nu_6\rangle}_{\{\nu_4+\nu_6\}}. \quad [7]$$

In order to calculate transition intensities, we developed the dipole-moment operator through the zeroth order using the same methods (*11*).

We use a coupled vibrational basis taking into account the six vibrational modes of XY_6 molecules (of respective symmetry A_{1g}, E_g, F_{1u}, F_{1u}, F_{2g}, and F_{2u}). The Hamiltonian and dipole-moment matrix elements are calculated in the coupled rovibrational basis

$$|[\Psi_r^{(J,nC)} \otimes \Psi_v^{(C_v)}]^{(\Gamma)}\rangle, \quad [8]$$

as described in Ref. (*11*). In Eq. [8], the $\Psi_v^{(C_v)}$'s and $\Psi_r^{(J,nC)}$'s are harmonic oscillator and rotational wavefunctions, respectively.

4. ANALYSIS

The infrared spectrum of the ν_4 band of $^{32}SF_6$ has a very simple structure with well-separated J clusters, which make it relatively straightforward to analyze. The band apparently shows no perturbation from other vibrational levels. This was already noticed by Kim *et al.* (*10*) who were able to perform an analysis of the room-temperature spectrum up to very high J values (>150). They used a very simple Bobin and Fox (*15*) model. These authors also analyzed the ν_4 band of $^{34}SF_6$ using the same techniques. They observed several hot bands but did not analyze them in detail.

As shown in Figs. 2–5, the hot band structure is greatly simplified when observed at low temperature. The $\nu_4 + \nu_6 - \nu_6$ band originating from the very low ν_6 (346.9 cm^{-1}) inactive fundamental level clearly dominates, although some other hot bands (very likely $\nu_4 + 2\nu_6 - 2\nu_6$ and $\nu_4 + \nu_5 - \nu_5$) are visible, especially in the Q-branch region (Fig. 2). As it can be

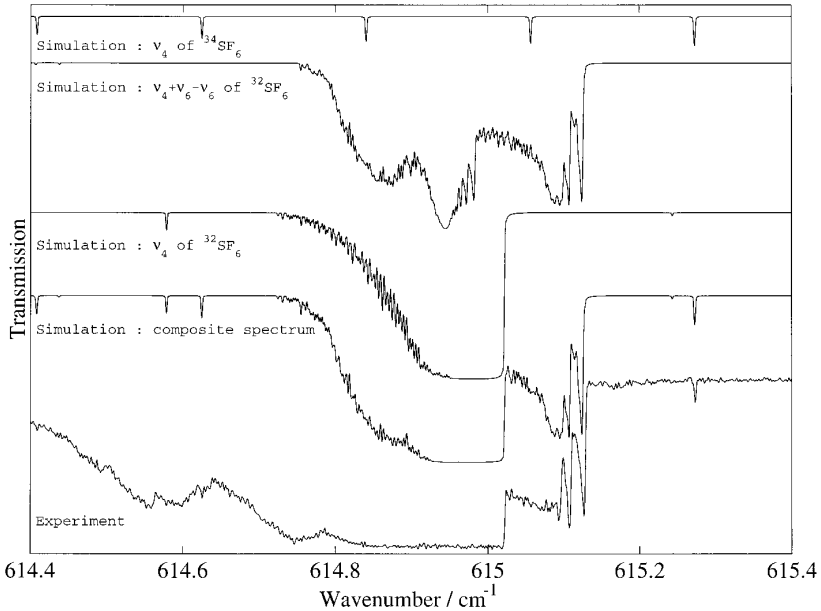

FIG. 2. Experimental and simulated spectra in the $^{32}SF_6$ Q-branch region.

seen in Figs. 3–5, most of the P and R lines of $\nu_4 + \nu_6 - \nu_6$ appear between the ν_4 J clusters, which makes it possible to perform detailed assignments and analysis.

We first made a new analysis of ν_4 of $^{32}SF_6$ as an isolated band in order to get parameter values for the Dijon tensorial formalism (*14, 11*) described in the previous section. We started from the parameters of Kim *et al.* (*10*). The correspondence between the Bobin and Fox parameters (*15*) and the "usual" parameters (*16*) is given in Ref. (*17*) and that with our formalism is given in Ref. (*14*) and in Table 1. For the reasons

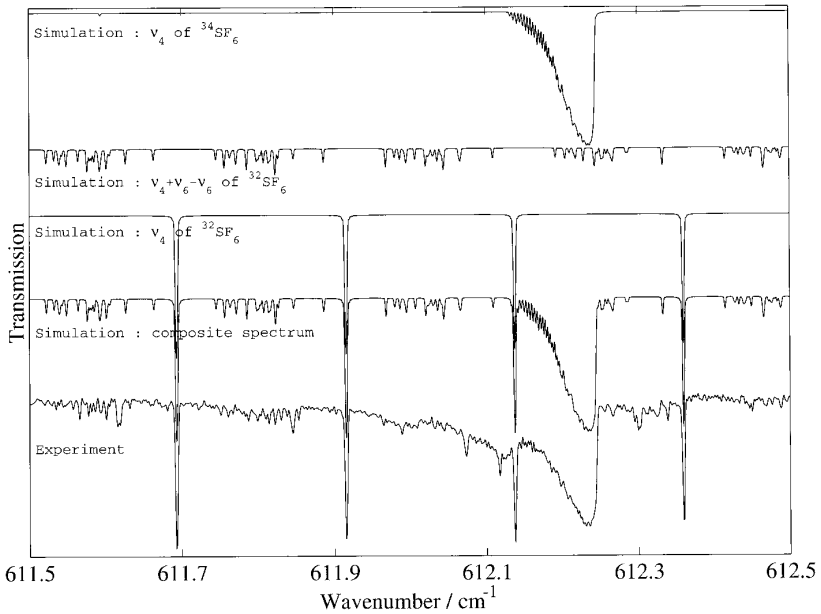

FIG. 3. Experimental and simulated spectra in the $^{34}SF_6$ Q-branch region.

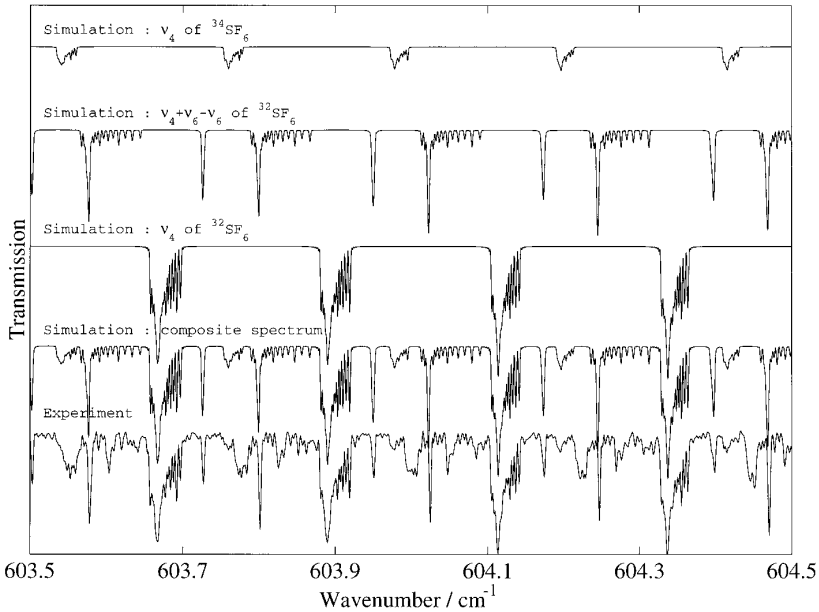

FIG. 4. Experimental and simulated spectra in the *P*-branch region.

mentioned above, the assignments were easy to realize. $\tilde{H}^{\langle\nu_4\rangle}_{\{GS\}}$ and $\tilde{H}^{\langle\nu_4\rangle}_{\{\nu_4\}}$ were developed to the sixth and fourth order, respectively. The ground state parameters were fixed to the values of Ref. (*7*). As is usual for heavy molecules, the *Q* branch is not sufficiently resolved to allow assignments of *Q* lines. In this case, the parameters $t^{2(2,0E_g)F_{1u}F_{1u}}_{\{4\}\{4\}}$ and $t^{2(2,0F_{2g})F_{1u}F_{1u}}_{\{4\}\{4\}}$ cannot be determined simultaneously (*18*). Thus, we decided to adjust $t^{2(2,0E_g)F_{1u}F_{1u}}_{\{4\}\{4\}}$ manually until the *Q*-branch profile was correct and then we fixed it to the value obtained in this way,

$$t^{2(2,0E_g)F_{1u}F_{1u}}_{\{4\}\{4\}} = 1.02654 \times 10^{-5}\ \text{cm}^{-1} \qquad [9]$$

in all further fits.

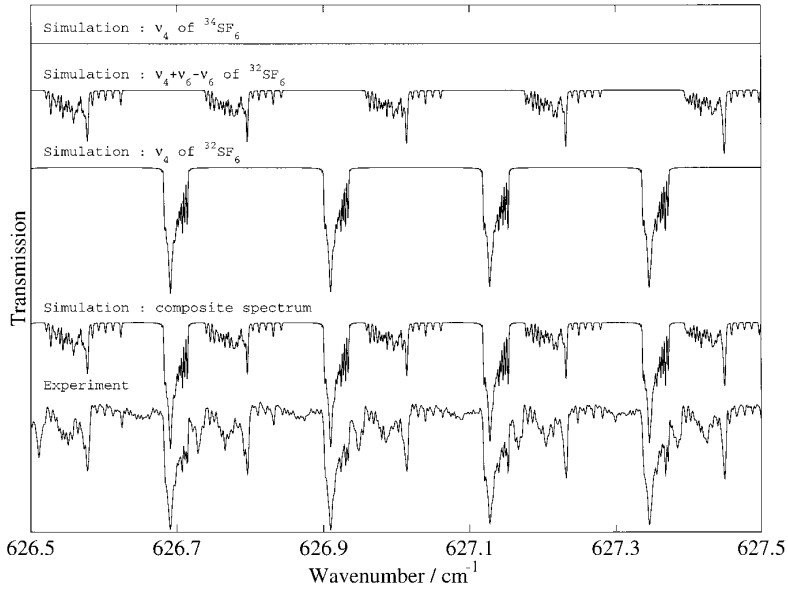

FIG. 5. Experimental and simulated spectra in the *R*-branch region.

TABLE 1
Parameters for the ν_4 and $\nu_4 + \nu_6$ Bands of $^{32}SF_6$

Vibrational level	Order in $\widetilde{H}$	Parameter $t^{\Omega(K,n\Gamma)\Gamma_v\Gamma'_v}_{\{s\}\{s'\}}$ $\Omega(K,n\Gamma)$	$\{s\}$ Γ_v	$\{s'\}$ Γ'_v	Value/cm^{-1}	"Usual" notation [16,14] and comments	Constrain
Ground state	0	$2(0,0A_{1g})$	$000000A_{1g}$	$000000A_{1g}$	$9.1078389192 \times 10^{-2}$	B_0	Fixed
	2	$4(0,0A_{1g})$	$000000A_{1g}$	$000000A_{1g}$	$-6.3369998149 \times 10^{-9}$	$-D_0$	Fixed
		$4(4,0A_{1g})$	$000000A_{1g}$	$000000A_{1g}$	$1.8196943510 \times 10^{-10}$	$-(\sqrt{15}/4\sqrt{2})D_{0t}$	Fixed
	4	$6(0,0A_{1g})$	$000000A_{1g}$	$000000A_{1g}$	$-1.5890094350 \times 10^{-13}$	H_0	Fixed
		$6(4,0A_{1g})$	$000000A_{1g}$	$000000A_{1g}$	$1.0083389785 \times 10^{-14}$	$3\sqrt{5}/16\sqrt{2})H_{4t}$	Fixed
		$6(6,0A_{1g})$	$000000A_{1g}$	$000000A_{1g}$	$-1.0615255469 \times 10^{-16}$	$-(\sqrt{231}/64\sqrt{2})H_{4t}$	Fixed
	6	$8(0,0A_{1g})$	$000000A_{1g}$	$000000A_{1g}$	$5.9060087823 \times 10^{-19}$	L_0	Fixed
		$8(4,0A_{1g})$	$000000A_{1g}$	$000000A_{1g}$	$6.5795734511 \times 10^{-20}$	$-(3\sqrt{15}/64\sqrt{2})L_{4t}$	Fixed
		$8(6,0A_{1g})$	$000000A_{1g}$	$000000A_{1g}$	$-8.9391941374 \times 10^{-21}$	$(3\sqrt{77}/256\sqrt{2})L_{6t}$	Fixed
		$8(8,0A_{1g})$	$000000A_{1g}$	$000000A_{1g}$	$-9.6703402824 \times 10^{-22}$	$(1/32\sqrt{33})L_{8t}$	Fixed
$v_6 = 1$	0	$0(0,0A_{1g})$	$000001F_{2u}$	$000001F_{2u}$	346.9	ν_6	Fixed
	1	$1(1,0F_{1g})$	$000001F_{2u}$	$000001F_{2u}$	−0.3103(23)	$3\sqrt{2}B\zeta_6$ (ν_6 Coriolis)	
	2	$2(0,0A_{1g})$	$000001F_{2u}$	$000001F_{2u}$	$-2.2062929503 \times 10^{-5}$	$B_3 - B_0$	Fixed
		$2(2,0E_g)$	$000001F_{2u}$	$000001F_{2u}$	$-2.6343685366 \times 10^{-5}$	$-(1/2)\alpha^6_{220} - 6\alpha^6_{224}$	Fixed
		$2(2,0F_{2g})$	$000001F_{2u}$	$000001F_{2u}$	$5.2830499700 \times 10^{-5}$	$-(3/4)\alpha^6_{220} + 6\alpha^6_{224}$	Fixed
	3	$3(1,0F_{1g})$	$000001F_{2u}$	$000001F_{2u}$	$1.9129608827 \times 10^{-7}$	$-(3\sqrt{3}/4\sqrt{2}F^6_{110}$	Fixed
		$3(3,0F_{1g})$	$000001F_{2u}$	$000001F_{2u}$	$-3.7106303207 \times 10^{-7}$	$(3/\sqrt{5}/2)F^6_{134}$	Fixed
$v_4 = 1$	0	$0(0,0A_{1g})$	$000100F_{1u}$	$000100F_{1u}$	614.98196(15)	ν_4	
	1	$1(1,0F_{1g})$	$000100F_{1u}$	$000100F_{1u}$	$-8.36914(43) \times 10^{-2}$	$3\sqrt{2}B\zeta_4$ (ν_4 Coriolis)	
	2	$2(0,0A_{1g})$	$000100F_{1u}$	$000100F_{1u}$	$-1.9670(71) \times 10^{-5}$	$B_4 - B_0$	
		$2(2,0E_g)$	$000100F_{1u}$	$000100F_{1u}$	$1.0265400000 \times 10^{-5}$	$-(1/2)\alpha^4_{220} - 6\alpha^4_{224}$	Fixed
		$2(2,0F_{2g})$	$000100F_{1u}$	$000100F_{1u}$	$-1.6681(62) \times 10^{-5}$	$-(3/4)\alpha^4_{220} + 6\alpha^4_{224}$	
	3	$3(1,0F_{1g})$	$000100F_{1u}$	$000100F_{1u}$	$-3.345(28) \times 10^{-8}$	$-(3\sqrt{3}/4\sqrt{2}F^4_{110}$	
		$3(3,0F_{1g})$	$000100F_{1u}$	$000100F_{1u}$	$1.712(16) \times 10^{-7}$	$(3/\sqrt{5}/2)F^4_{134}$	
	4	$4(0,0A_{1g})$	$000100F_{1u}$	$000100F_{1u}$	$-1.93(70) \times 10^{-10}$	$-(D_4 - D_0)$	
		$4(2,0E_g)$	$000100F_{1u}$	$000100F_{1u}$	0.0		Fixed
		$4(2,0F_{2g})$	$000100F_{1u}$	$000100F_{1u}$	0.0		Fixed
		$4(4,0A_{1g})$	$000100F_{1u}$	$000100F_{1u}$	0.0		Fixed
		$4(4,0E_g)$	$000100F_{1u}$	$000100F_{1u}$	0.0		Fixed
		$4(4,0F_{2g})$	$000100F_{1u}$	$000100F_{1u}$	0.0		Fixed
$v_4 = v_6 = 1$	2	$0(0,0A_{1g})$	$000101A_{2g}$	$000101A_{2g}$	0.2224(25)	A_{2g} sublevel	
	4	$2(0,0A_{1g})$	$000101A_{2g}$	$000101A_{2g}$	$1.6(1.0) \times 10^{-6}$		
		$2(2,0E_g)$	$000101A_{2g}$	$000101E_g$	$2.002(66) \times 10^{-5}$		
		$2(2,0F_{2g})$	$000101A_{2g}$	$000101F_{1g}$	0.0		Fixed
	3	$1(1,0F_{1g})$	$000101A_{2g}$	$000101F_{2g}$	0.0	A_{2g}–F_{2g} Coriolis	Fixed
	2	$0(0,0A_{1g})$	$000101E_g$	$000101E_g$	−0.1823(14)	E_g sublevel	
	4	$2(0,0A_{1g})$	$000101E_g$	$000101E_g$	0.0		Fixed
		$2(2,0E_g)$	$000101E_g$	$000101E_g$	$-4.98(96) \times 10^{-6}$		
	3	$1(1,0F_{1g})$	$000101E_g$	$000101F_{1g}$	$-3.585(91) \times 10^{-4}$	E_g–F_{1g} Coriolis	
	4	$2(2,0F_{2g})$	$000101E_g$	$000101F_{1g}$	0.0		Fixed
	3	$1(1,0F_{1g})$	$000101E_g$	$000101F_{2g}$	$2.71(14) \times 10^{-4}$	E_g–F_{2g} Coriolis	
	4	$2(2,0F_{2g})$	$000101E_g$	$000101F_{2g}$	0.0		Fixed
	2	$0(0,0A_{1g})$	$000101F_{1g}$	$000101F_{1g}$	0.0689(12)	F_{1g} sublevel	
	3	$1(1,0F_{1g})$	$000101F_{1g}$	$000101F_{1g}$	$-3.03(22) \times 10^{-4}$	F_{1g} Coriolis	
	4	$2(0,0A_{1g})$	$000101F_{1g}$	$000101F_{1g}$	$-4.49(45) \times 10^{-6}$		
		$2(2,0E_g)$	$000101F_{1g}$	$000101F_{1g}$	$5.2(1.0) \times 10^{-6}$		
		$2(2,0F_{2g})$	$000101F_{1g}$	$000101F_{1g}$	$5.86(90) \times 10^{-6}$		
	3	$1(1,0F_{1g})$	$000101F_{1g}$	$000101F_{2g}$	$1.400(18) \times 10^{-3}$	F_{1g}–F_{2g} Coriolis	
	4	$2(2,0E_g)$	$000101F_{1g}$	$000101F_{2g}$	$-4.05(38) \times 10^{-6}$		
		$2(2,0F_{2g})$	$000101F_{1g}$	$000101F_{2g}$	0.0		Fixed
	2	$0(0,0A_{1g})$	$000101F_{2g}$	$000101F_{2g}$	−0.1577(11)	F_{2g} sublevel	
	3	$1(1,0F_{1g})$	$000101F_{2g}$	$000101F_{2g}$	$3.234(25) \times 10^{-3}$	F_{2g} Coriolis	
	4	$2(0,0A_{1g})$	$000101F_{2g}$	$000101F_{2g}$	$5.23(34) \times 10^{-6}$		
		$2(2,0E_g)$	$000101F_{2g}$	$000101F_{2g}$	$-1.43(11) \times 10^{-5}$		
		$2(2,0F_{2g})$	$000101F_{2g}$	$000101F_{2g}$	0.0		Fixed

Then, we started a simultaneous analysis of ν_4 and $\nu_4 + \nu_6 - \nu_6$ of $^{32}SF_6$. $\tilde{H}^{\langle\nu_4+\nu_6\rangle}_{\{GS\}}$, $\tilde{H}^{\langle\nu_4+\nu_6\rangle}_{\{\nu_6\}}$, $\tilde{H}^{\langle\nu_4+\nu_6\rangle}_{\{\nu_4\}}$, and $\tilde{H}^{\langle\nu_4+\nu_6\rangle}_{\{\nu_4+\nu_6\}}$ were developed to the sixth, third, fourth, and fourth order, respectively. The $\nu_4(F_{1u}) + \nu_6(F_{2u})$ vibrational level has four sublevels since

$$F_{1u} \otimes F_{2u} = A_{2g} \oplus E_g \oplus F_{1g} \oplus F_{2g}. \quad [10]$$

As a first step, we thus made several tries to find the correct relative positions of these sublevels. The order E_g, F_{1g}, F_{2g},

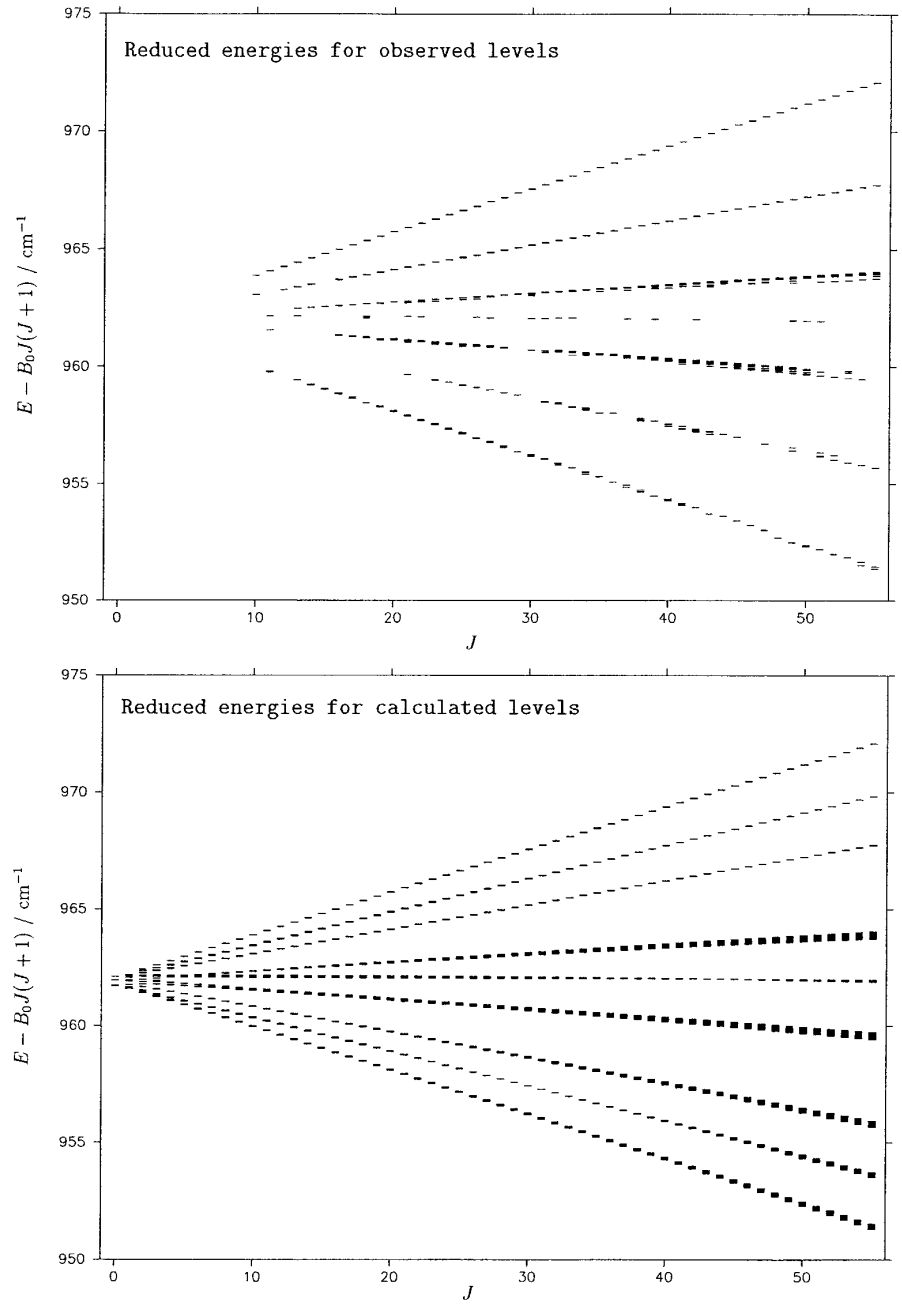

FIG. 6. Observed a calculated reduced energies for the $\nu_4 + \nu_6$ level of $^{32}SF_6$.

A_{2g} with increasing wavenumbers was found to be the correct one, since only this order leads to an acceptable Q-branch profile (see Fig. 2). We were then able to perform many assignments and to get a satisfying fit of 26 parameters with a global standard deviation of 0.959×10^{-3} cm^{-1}. The ground state parameters were again fixed to the values of Ref. (*7*) and those of ν_6 to the values of Ref. (*9*), except for $t^{1(1,3)F_{1g})F_{2u}F_{2u}}_{\{6\}\{6\}}$, which was fitted. The parameters obtained in this analysis are listed in Table 1 and the fit statistics are given in Table 2. The four sublevels of $\nu_4 + \nu_6$ with symmetry A_{2g}, E_g, F_{1g}, and F_{2g} are found to lie at 962.104, 961.700, 961.950, and 961.724 cm^{-1}, respectively. Figure 6

TABLE 2
Fit Statistics

Molecule	Band	Number of data	J_{max}	RMS†
$^{32}SF_6$	ν_4	1891	95	0.36
$^{32}SF_6$	$\nu_4+\nu_6-\nu_6$	943	65	1.58
$^{34}SF_6$	ν_4	103	55	0.41

† Root Mean Square / 10^{-3} cm^{-1}

shows the observed and calculated reduced energy levels for the $\nu_4 + \nu_6$ level.

An isolated band study was also performed for the ν_4 band of the $^{34}SF_6$ isotopomer again starting from the parameters of Kim *et al.* The results are given in Tables 2 and 3. $\tilde{H}^{\langle\nu_4\rangle}_{\{GS\}}$ and $\tilde{H}^{\langle\nu_4\rangle}_{\{\nu_4\}}$ were developed to the sixth and fourth order, respectively. The ground state parameters were fixed to the values of $^{32}SF_6$ (*7*). The value of $t^{2(2,0E_g)F_{1u}F_{1u}}_{\{4\}\{4\}}$ was fixed to that of $^{32}SF_6$ obtained as explained above.

5. DISCUSSION

Figures 1 to 5 show synthetic spectra calculated with the parameters obtained in the present fits. We can see that several lines are still not reproduced. These belong to other hot bands, still to be analyzed.

SF_6 in natural abundance contains four isotopomers in the following proportions: $^{32}SF_6$ (95.02%), $^{33}SF_6$ (0.75%), $^{34}SF_6$ (4.21%), and $^{36}SF_6$ (0.02%). The present data enable us to find the position of the ν_4 Q branch of $^{33}SF_6$ as explained now. The ν_4 band center m_4 can be calculated through (*15*)

$$m_4 = t^{0(0,0A_{1g})F_{1u}F_{1u}}_{\{3\}\{3\}} - \frac{\sqrt{2}}{3}\, t^{1(1,0F_{1g})F_{1u}F_{1u}}_{\{3\}\{3\}} + \frac{2}{5}\,(t^{2(2,0Eg)F_{1u}F_{1u}}_{\{3\}\{3\}} + t^{2(2,0F_{2g})F_{1u}F_{1u}}_{\{3\}\{3\}}) + \cdots, \quad [11]$$

which leads to

$$m_4(^{32}SF_6) \simeq 615.0214\ \text{cm}^{-1}, \quad [12]$$

$$m_4(^{34}SF_6) \simeq 612.2443\ \text{cm}^{-1}. \quad [13]$$

This gives the following isotope shifts for the ν_4 band of SF_6

$$\frac{\Delta\nu_4(32-34)}{2} \simeq 1.3886\ \text{cm}^{-1}, \quad [14]$$

which is very close to the value (1.385 cm^{-1}) given by McDowell in Ref. (*19, 20*). We can now calculate the position of the ν_4 band center of $^{33}SF_6$:

$$m_4(^{33}SF_6) \simeq 613.6328\ \text{cm}^{-1}. \quad [15]$$

This enables us to identify the weak Q-branch peak of this rare isotopomer among the remaining unidentified Q branches as shown in Fig. 7.

TABLE 3
Parameters for the ν_4 Band of $^{34}SF_6$

Vibrational level	Order in $\tilde{H}$	Parameter $t^{\Omega(K,n\Gamma)\Gamma_v\Gamma'_v}_{\{s\}\{s'\}}$ $\Omega(K,n\Gamma)$	$\{s\}$ Γ_v	$\{s'\}$ Γ'_v	Value/cm^{-1}	"Usual" notation and comments	Constraint
Ground state	0	$2(0,0A_{1g})$	$000000A_{1g}$	$000000A_{1g}$	$9.1078389192\times10^{-2}$	B_0	Fixed
	2	$4(0,0A_{1g})$	$000000A_{1g}$	$000000A_{1g}$	$-6.3369998149\times10^{-9}$	$-D_0$	Fixed
		$4(4,0A_{1g})$	$000000A_{1g}$	$000000A_{1g}$	$1.8196943510\times10^{-10}$	$-(\sqrt{15}/4\sqrt{2})D_{0t}$	Fixed
	4	$6(0,0A_{1g})$	$000000A_{1g}$	$000000A_{1g}$	$-1.5890094350\times10^{-13}$	H_0	Fixed
		$6(4,0A_{1g})$	$000000A_{1g}$	$000000A_{1g}$	$1.0083389785\times10^{-14}$	$3\sqrt{5}/16\sqrt{2})H_{4t}$	Fixed
		$6(6,0A_{1g})$	$000000A_{1g}$	$000000A_{1g}$	$-1.0615255469\times10^{-16}$	$-(\sqrt{231}/64\sqrt{2})H_{4t}$	Fixed
	6	$8(0,0A_{1g})$	$000000A_{1g}$	$000000A_{1g}$	$5.9060087823\times10^{-19}$	L_0	Fixed
		$8(4,0A_{1g})$	$000000A_{1g}$	$000000A_{1g}$	$6.5795734511\times10^{-20}$	$-(3\sqrt{15}/64\sqrt{2})L_{4t}$	Fixed
		$8(6,0A_{1g})$	$000000A_{1g}$	$000000A_{1g}$	$-8.9391941374\times10^{-21}$	$(3\sqrt{77}/256\sqrt{2})L_{6t}$	Fixed
		$8(8,0A_{1g})$	$000000A_{1g}$	$000000A_{1g}$	$-9.6703402824\times10^{-22}$	$(1/32\sqrt{33})L_{8t}$	Fixed
$v_4=1$	0	$0(0,0A_{1g})$	$000100F_{1u}$	$000100F_{1u}$	612.20980(24)	ν_4	
	1	$1(1,0F_{1g})$	$000100F_{1u}$	$000100F_{1u}$	$-7.3202(18)\times10^{-2}$	$3\sqrt{2}B\zeta_4$ (ν_4 Coriolis)	
	2	$2(0,0A_{1g})$	$000100F_{1u}$	$000100F_{1u}$	$-2.112(66)\times10^{-5}$	B_4-B_0	
		$2(2,0E_g)$	$000100F_{1u}$	$000100F_{1u}$	$1.0265400000\times10^{-5}$	$-(1/2)\alpha^4_{220}-6\alpha^4_{224}$	Fixed
		$2(2,0F_{2g})$	$000100F_{1u}$	$000100F_{1u}$	$-1.682(60)\times10^{-5}$	$-(3/4)\alpha^4_{220}+6\alpha^4_{224}$	
	3	$3(1,0F_{1g})$	$000100F_{1u}$	$000100F_{1u}$	$-5.41(67)\times10^{-8}$	$-(3\sqrt{3}/4\sqrt{2}F^4_{110}$	
		$3(3,0F_{1g})$	$000100F_{1u}$	$000100F_{1u}$	$2.52(38)\times10^{-8}$	$(3/\sqrt{5}/2)F^4_{134}$	
	4	$4(0,0A_{1g})$	$000100F_{1u}$	$000100F_{1u}$	$-9.3(3.7)\times10^{-10}$	$-(D_4-D_0)$	
		$4(2,0E_g)$	$000100F_{1u}$	$000100F_{1u}$	0.0		Fixed
		$4(2,0F_{2g})$	$000100F_{1u}$	$000100F_{1u}$	0.0		Fixed
		$4(4,0A_{1g})$	$000100F_{1u}$	$000100F_{1u}$	0.0		Fixed
		$4(4,0E_g)$	$000100F_{1u}$	$000100F_{1u}$	0.0		Fixed
		$4(4,0F_{2g})$	$000100F_{1u}$	$000100F_{1u}$	0.0		Fixed

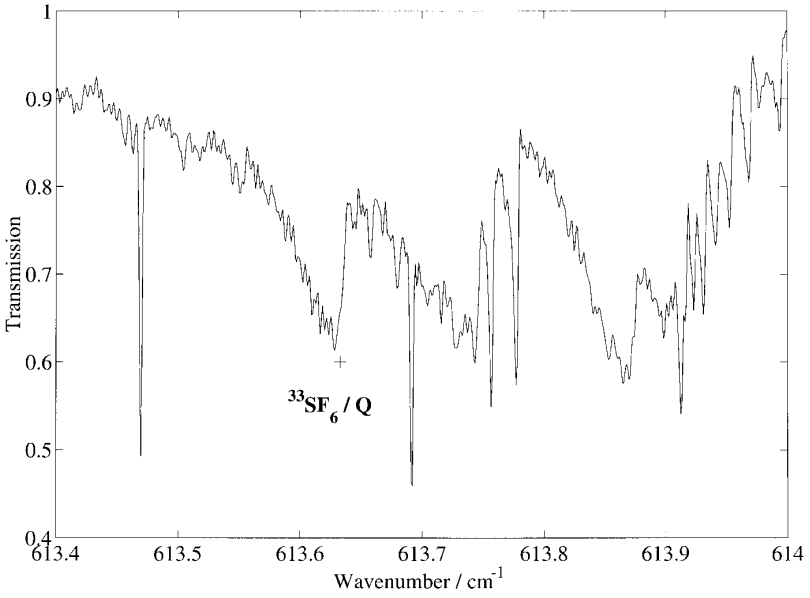

FIG. 7. The ν_4 Q branch of $^{33}SF_6$ (calculated position indicated by the cross).

6. CONCLUSION

This very first analysis of a hot band of the SF_6 molecule was made possible thanks to the use of a set of programs called HTDS (highly spherical top data system) (*12*), in reference to the set of programs called STDS (spherical top data system written for XY_4 molecules (*21*)). This set of programs can be accessed through ftp (user anonymous) at jupiter.u-bourgogne.fr or on the web at the URL http://www.u-bourgogne.fr/LPUB/shTDS.html.

The analysis of the other hot bands visible in the present spectrum would require some new data: in particular, for the analysis of $\nu_4 + \nu_5 - \nu_5$, it would be useful to get a high-resolution Raman spectrum of ν_5 (near 525 cm^{-1}).

Work is presently in progress to analyze hot bands in the ν_3 stretching region of SF_6 near 910 cm^{-1} which are of primary importance for the modeling of the atmospheric absorption of this species.

ACKNOWLEDGMENTS

Région Bourgogne is gratefully acknowledged for supporting the Laboratoire de Physique de l'Université de Bourgogne. H.B. thanks the Deutsche Forschungsgemeinschaft for financial support.

REFERENCES

1. M. Khalil, *Annu. Rev. Energy Environ.* **24,** 645–661 (1999).
2. C. Dervos and P. Vassiliou, *Air Waste Manage. Assoc.* **50,** 137–141 (2000).
3. L. Geller, J. Elkins, J. Lobert, A. Clarke, D. Hurst, J. Butler, and R. Myers, *Geophys. Res. Lett.* **24,** 675–678 (1997).
4. C. Volk, J. Elkins, D. Fahey, G. Dutton, J. Gilligan, M. Loewenstein, J. Podolske, K. Chan, and M. Gunson, *J. Geophys. Res.* **102,** 25543–25564 (1997).
5. E. Manzini and J. Feichter, *J. Geophys. Res.* **104,** 31097–31108 (1999).
6. E. Kjellström, J. Feitcher, and G. Hoffman, *Tellus* **52B,** 1–18 (2000).
7. O. Acef, C. Bordé, A. Clairon, G. Pierre, and B. Sartakov, *J. Mol. Spectrosc.* **199,** 188–204 (2000).
8. V. Boudon, M. Hepp, M. Herman, I. Pak, and G. Pierre, *J. Mol. Spectrosc.* **192,** 359–367 (1998).
9. D. Bermejo, R. Martínez, E. Loubignac, V. Boudon, and G. Pierre, *J. Mol. Spectrosc.* **201,** 164–171 (2000).
10. K. Kim, W. Person, D. Seitz, and B. Krohn, *J. Mol. Spectrosc.* **76,** 322–340 (1979).
11. N. Cheblal, M. Loëte, and V. Boudon, *J. Mol. Spectrosc.* **197,** 222–231 (1999).
12. C. Wenger, V. Boudon, J.-P. Champion, and G. Pierre, *J. Quant. Spectrosc. Radiat. Transfer* **66,** 1–16 (2000).
13. G. Guelachvili and K. N. Rao, "Handbook of Infrared Standard," Academic Press, San Diego, 1986.
14. J.-P. Champion, M. Loëte, and G. Pierre, *in* "Spectroscopy of the Earth's Atmosphere and Interstellar Medium" (K. N. Rao and A. Weber, Eds.), Academic Press, San Diego, 1992, pp. 339–422.
15. B. Bobin and K. Fox, *J. Phys. (Paris)* **34,** 571–582 (1973).
16. A. Robiette, D. Gray, and F. Birss, *Mol. Phys.* **32,** 1591–1607 (1976).
17. J. P. Aldridge, E. G. Brock, H. Filip, H. Flicker, K. Fox, H. W. Galbraith, R. F. Holland, K. C. Kim, B. J. Krohn, D. W. Magnuson, W. B. Maier II, R. S. McDowell, C. W. Patterson, W. B. Person, D. F. Smith, and G. K. Werner, *J. Chem. Phys.* **83,** 34–48 (1985).
18. V. Boudon, E. Mkadmi, H. Bürger, and G. Pierre, *Chem. Phys. Lett.* **305,** 21–27 (1999).
19. R. McDowell, B. Krohn, H. Flicker, and M. C. Vasquez, *Spectrochim. Acta A* **42,** 371–385 (1986).
20. R. McDowell, *Spectrochim. Acta A* **42,** 1053–1057 (1986).
21. C. Wenger and J.-P. Champion, *J. Quant. Spectrosc. Radiat. Transfer* **59,** 471–480 (1998).

High-Resolution Raman spectroscopy of the ν_1 region and Raman-Raman double resonance spectroscopy of the $2\nu_1 - \nu_1$ band of $^{32}SF_6$ and $^{34}SF_6$. Determination of the equilibrium bond length of sulfur hexafluoride.

V. Boudon

Laboratoire de Physique de l'Université de Bourgogne, CNRS UMR 5027, 9, Avenue Alain Savary, BP 47870, F-21078 Dijon Cedex, France
E-Mail: Vincent.Boudon@u-bourgogne.fr

J. L. Doménech and D. Bermejo

Instituto de Estructura de la Materia, CSIC Serrano 123, 28006 Madrid, Spain
E-Mail: dbermejo@iem.cfmac.csic.es

H. Willner

Fachbereich 9 – Anorganische Chemie, Bergische Universität Wuppertal, D-42097 Wuppertal, Germany
E-Mail: willner@uni-wuppertal.de

Abstract

The ν_1 region of $^{32}SF_6$ and $^{34}SF_6$ has been studied by stimulated Raman spectroscopy. For both isotopomers, a detailed analysis has been performed. Several hot bands ($\nu_1 + \nu_6 - \nu_6$, $\nu_1 + 2\nu_6 - 2\nu_6$, $\nu_1 + \nu_5 - \nu_5$) have been taken into account to calculate synthetic spectra that satisfactorily reproduce the experimental data. These results, together with the previous studies of the other fundamental bands have allowed us to determine the equilibrium bond length of sulfur hexafluoride as $r_e = 1.5560(1)$ Å, in very good agreement with recent *ab initio* calculations. The $2\nu_1 - \nu_1$ band has also been studied for both isotopomers by Raman-Raman double resonance spectroscopy and the resulting spectra have been analyzed. In this case, a striking difference is observed between the two isotopomers, since the $2\nu_1 - \nu_1$ band of $^{34}SF_6$ appears to have a very narrow structure that could not be rotationally resolved under the present experimental conditions. All analyses have been performed thanks to the HTDS program suite (http://www.u-bourgogne.fr/LPUB/hTDS.html) dedicated to octahedral XY_6 molecules.

Key words: Sulfur hexafluoride, Stimulated Raman Spectroscopy, High Resolution, Double Resonance, Hot Bands

1 Introduction

Sulfur hexafluoride is a species of growing importance in the field of atmospheric physics and chemistry [1] as a pollutant that can contribute to the greenhouse effect [2,3]. SF_6 concentration in the Earth's atmosphere is increasing at a rate of about 7 % per year due to industrial emissions and this very inert molecule has an extremely long lifetime in the atmosphere (*ca.* 3200 years) [4,5]. SF_6 is included as one of the species to control in the Kyoto protocol [6–8].

However, as we have shown in a recent review article [9] and in previous papers [10–14], the spectroscopy of this molecule, which is essential for quantitative measurements in the atmosphere, is still insufficiently known. In particular, the region of the ν_3 fundamental near 948 cm^{-1} is of primary importance since its very strong absorption is responsible for the huge greenhouse capabilities of SF_6. Although the $v_3 = 1$ level itself is very well determined [15], the hot bands in this region which largely contribute to the absorption (the ground state population is only 30 % at 300 K [9]) are very poorly known. The study of these hot bands requires the investigation of many vibrational bands, including fundamentals, combinations and harmonics. Moreover, SF_6 being a centrosymmetric species, many of its vibrational levels (those with g parity) are infrared inactive and can only be studied using Raman techniques. Another important problem concerning SF_6 spectroscopy is the ν_6 vibrational mode which is inactive both in infrared absorption and in Raman scattering. Since this is the vibrational mode that has the lowest energy (347 cm^{-1} region), it largely contributes to hot bands. The only mean to obtain informations about ν_6 is to study combination levels implying this vibration.

The present paper is a new contribution to this topic concerning the stimulated Raman spectrum of the totally symmetric ν_1 stretching band and its associated hot bands ($\nu_1+\nu_6-\nu_6$, $\nu_1+2\nu_6-2\nu_6$, $\nu_1+\nu_5-\nu_5$), as well as the Raman-Raman double resonance spectrum of $2\nu_1 - \nu_1$. It completes our recent studies of the SF_6 Raman-active fundamentals which were published in References [11] (ν_2) and [13] (ν_5). This work has been realized for the two main isotopomers of SF_6, namely $^{32}SF_6$ (95.02 % natural abundance) and $^{34}SF_6$ (4.21 % natural abundance). For $^{34}SF_6$, we have used an isotopically pure sample. The ν_1 region of SF_6 has already been studied at high resolution by Esherick and Owyoung [16] ($^{32}SF_6$) and by Volkov *et al.* [17] ($^{34}SF_6$). Our contribution improves these previous studies by integrating higher J values and more hot bands. Moreover,

it has allowed us to obtain effective Hamiltonian parameters in the "Dijon" tensorial formalism and thus to complete the HDTS database [18] that we have built for octahedral XY_6 molecules. Combining all recent high resolution analyses (infrared and Raman) of the fundamental bands of SF_6, we are able to give a precise estimate of the equilibrium bond length $r_e = r_{S-F}$ of this molecule.

Double resonance spectroscopy of $2\nu_1-\nu_1$ has never been attempted before. We observe an impressive difference for this spectrum between $^{32}SF_6$ and $^{34}SF_6$, since the $2\nu_1 - \nu_1$ band of $^{34}SF_6$ appears to have a very narrow ("collapsed") rotational structure which was impossible to resolve under our experimental conditions.

2 Experiment

2.1 Synthesis of the $^{34}SF_6$ sample

70 mg of isotopic enriched sulphur powder (2 mmol ^{34}S, 94.3%, Oak Ridge, Tennessee) is placed in a 50 ml glass bulb equipped with a glass valve with PTFE piston (Young, London). After evacuation and cooling to −196 °C, 7 mmol of fluorine from a stainless steel vacuum line are slowly introduced into the glass vessel. Most of the sulphur burns under this condition and the residue reacts at room temperature. At −196 °C the excess of fluorine is pumped off and then 3 ml of NaOH solution (2 mol.l^{-1}) is slowly introduced through the valve into the cold and evacuated glass bulb. In order to hydrolyze and to absorb all by-products such as SiF_4, CO_2, SOF_2, *etc*, the content of the bulb is shaken at room temperature for 20 minutes. Finally the gaseous products are separated by trap-to-trop condensation in vacuum in a series of traps held at −30, −90, −196 °C. The trap at −196 °C contains 1.8 mmol $^{34}SF_6$ of high purity, checked by IR spectroscopy. The product is stored in flame-sealed glass ampoules under liquid nitrogen in a long-term Dewar vessel. The ampoules are opened and resealed by use of an ampoule key [19].

2.2 Stimulated Raman spectroscopy of the ν_1 region

The inverse Raman spectrometer at the IEM in Madrid was used for recording the spectra. It is based on the design by Esherick and Owyoung and its implementation at the IEM has been described often (eg. [20,21]) so only the most relevant details pertaining to this experiment will be given. The probe beam is a cw single mode Ar^+ laser operated at 529 nm with $\sim$ 650 mW, actively

frequency stabilized and locked to an hyperfine transition of $^{130}Te_2$. Its frequency is known with an absolute accuracy of $\sim 1:10^8$ [22] and its linewidth (due to the residual frequency jitter) is less than 500 kHz. The pump beam is generated by pulsed amplification in a three stages amplifier of a single mode cw ring dye laser, in order to obtain pulses with Fourier limited linewidth. The pulsed dye amplifier is pumped by an injection-seeded, cavity-extended and frequency-doubled Nd:YAG laser, that supplies near gaussian (spatially and temporally, 12 ns FWHM) pulses. The dyes used were Rhodamine 110 in the ring dye laser and Fluorescein in the amplifier, obtaining ~ 5 mJ per pulse with the same temporal and spatial characteristics of the Nd:YAG laser. The instrument apparatus function is the convolution of the lineshapes of both lasers and is therefore limited by the Fourier transform of the time profile of the pump pulses, *i.e.* $\sim 3 \times 10^{-3}$ cm^{-1}. When the wavenumber difference of both lasers matches that of a Raman transition, a transient decrease of the power of the probe beam is observed. This transient signal, that follows the temporal profile of the pump laser, is boxcar averaged over 10 shots of the pump laser as it is scanned. The plot of the averaged transient signal intensity versus the pump-probe wavenumber difference renders the Raman spectrum. The scan of the ring dye laser is linearized and calibrated after the recording of the spectra using the simultaneously recorded transmission fringes of a high finesse Fabry Perot interferometer of 150 MHz free spectral range, and the visible absorption spectrum of $^{127}I_2$. The absolute accuracy of the wavenumber scale is 1×10^{-3} cm^{-1} limited by the I_2 standard, although the internal precision is better ($\sim 1 \times 10^{-4}$ cm^{-1}). The sample was placed in an 80 cm long glass cell with fused silica windows mounted at Brewster angle, and a triple pass configuration was adopted. Except for the windows mounts, the cell body has a double jacket. The outermost cavity is pumped out for thermal insulation, while cold Nitrogen, boiled from liquid Nitrogen tank with a regulated immersed heater, can flow through the intermediate jacket, and the the sample is placed in the innermost tube where the temperature is monitored by a type K thermocouple. Since the Raman signal is generated mostly in the focal region of the lasers and this is rather short (~ 6 mm), good temperature uniformity and little contribution to the signal from warmer molecules near the windows are obtained. Spectra were recorded at 297 K (room temperature) and also at 197 K in order to deplete the lower levels of hot bands and facilitate initial assignments. Pressures were 600 Pa for the room temperature spectra and 250 Pa for the cold ones. Two recordings where averaged in all studied bands in order to increase the signal-to-noise ratio.

2.3 Raman-Raman double resonance spectroscopy of the $2\nu_1 - \nu_1$ band

The $2\nu_1 - \nu_1$ band is barely observable at room temperature, since its lower level is at 774.5 cm^{-1} and only ~ 0.7 % of the molecules are expected in this

state at room temperature. Besides it is overlapped by the tails of ν_1 and the associated hot bands from ν_5 and ν_6. In order to have a significantly larger fraction of molecules in the ν_1 state, a Raman-Raman double resonance technique has been employed. Using two pulsed lasers whose frequency difference is tuned to the frequency of the ν_1 band, a significant increase of the population of the $v_1 = 1$ level can be achieved via an stimulated Raman process. After a delay of about 15 ns the pump-probe pair described in Section 2.2 interacts with the sample yielding the spectrum of the transition $2\nu_1 - \nu_1$. This technique has also been described elsewhere [23,24] and, again, only the most relevant details will be given. The 1.06 μm radiation from the Nd:YAG laser remaining after the frequency doubling mentioned in Section 2.2, passes through a BBO crystal, and its frequency doubled output pumps a tunable pulsed dye laser, using in this case Rhodamine 575. The still remaining 1.06 μm radiation is sent to a KDP crystal whose frequency doubled output constitutes the other pulsed beam of the pumping process. Typical energies per pulse reaching the sample are 25 mJ in the pulsed dye laser and 30 mJ in the doubled Nd:YAG laser. The wavenumber difference of these two lasers is tuned to the maximum of the ν_1 band, and, since the bandwidth of this process is ~ 0.2 cm^{-1} (basically the linewidth of the pulsed dye laser) mainly the rovibrational levels within this bandwidth are populated, hence the need of a delay before the spectroscopy pair of lasers interacts with the sample, in aid of rotational population redistribution. The sample pressure in these experiments was 600 Pa and the temperature was 170 K. Low temperature is preferred in this case because it increases the population of the vibrational ground level (it is only 30 % at room temperature) and it also narrows the distribution of populated rotational levels in this state, therefore increasing the efficiency of the pumping process.

3 Theoretical model

The theoretical model used in this paper is based on the tensorial formalism and the vibrational extrapolation methods developed in Dijon. These methods have already been explained for example in Ref. [25,26]. If we consider an XY_6 molecule for which the vibrational levels are grouped in a series of polyads designed by P_k ($k = 0, \ldots, n$), P_0 being the Ground State (GS), the Hamiltonian operators can be put in the following form (after performing some contact transformations):

$$\mathcal{H} = \mathcal{H}_{\{P_0 \equiv GS\}} + \mathcal{H}_{\{P_1\}} + \ldots + \mathcal{H}_{\{P_n\}}, \qquad (1)$$

where the $\mathcal{H}_{\{P_k\}}$ contain rovibrational operators which have no matrix elements within the $P_{k'<k}$ basis sets. The different terms are written in the form

$$\mathcal{H}_{\{P_k\}} = \sum_{\text{all indexes}} t^{\Omega(K,n\Gamma)\Gamma_v\Gamma_{v'}}_{\{s\}\{s'\}} T^{\Omega(K,n\Gamma)\Gamma_v\Gamma_{v'}}_{\{s\}\{s'\}}. \tag{2}$$

In this equation the $t^{\Omega(K,n\Gamma)\Gamma_v\Gamma_{v'}}_{\{s\}\{s'\}}$ term is the parameter and $T^{\Omega(K,n\Gamma)\Gamma_v\Gamma_{v'}}_{\{s\}\{s'\}}$ the rovibrational operator defined as

$$T^{\Omega(K,n\Gamma)\Gamma_v\Gamma_{v'}}_{\{s\}\{s'\}} = \beta \left[{}^{\epsilon}V^{\Gamma_v\Gamma_{v'}(\Gamma)}_{\{s\}\{s'\}} \otimes R^{\Omega(K,n\Gamma)} \right]^{(A_{1g})}, \tag{3}$$

where β is a numerical factor equal to $\sqrt{3}\left(-\sqrt{3}/4\right)^{\Omega/2}$ if $(K, n\Gamma) = (0, 0A_1)$, and equal to 1 otherwise. As shown by Equation (3), the rovibrational operators $T^{\Omega(K,n\Gamma)\Gamma_v\Gamma_{v'}}_{\{s\}\{s'\}}$ are obtained by coupling of a rotational operator $R^{\Omega(K,n\Gamma)}$ of degree Ω (in the angular momentum components J_x, J_y or J_z) and a vibrational operator ${}^{\epsilon}V^{\Gamma_v\Gamma_{v'}(\Gamma)}_{\{s\}\{s'\}}$ of degree Ω_v (in creation or annihilation operators). The order of each individual term is $\Omega + \Omega_v - 2$.

The effective Hamiltonian for polyad P_n is obtained by projecting $\mathcal{H}$ in the P_n Hilbert subspace, i.e.,

$$H^{\langle P_n\rangle} = P^{\langle P_n\rangle}\mathcal{H}P^{\langle P_n\rangle} = H^{\langle P_n\rangle}_{\{GS\}} + \ldots + H^{\langle P_n\rangle}_{\{P_k\}} + \ldots + H^{\langle P_n\rangle}_{\{P_n\}}. \tag{4}$$

This corresponds to the so-called "vibrational extrapolation": the effective Hamiltonian for a given polyad contains all the parameters for the lower polyads. This allows to study a molecule by climbing up the polyad ladder, one polyad after the other. Each time a new polyad is studied, the terms that are added to the effective Hamiltonien consists, in principle, in small contributions.

For the analysis of ν_1 and its hot bands, we need the following effective Hamiltonians:

- The ν_1 effective Hamiltonian,

$$H^{\langle\nu_1\rangle} = H^{\langle\nu_1\rangle}_{\{\text{GS}\}} + H^{\langle\nu_1\rangle}_{\{\nu_1\}}. \tag{5}$$

- The $2\nu_1$ effective Hamiltonian,

$$H^{\langle 2\nu_1\rangle} = H^{\langle 2\nu_1\rangle}_{\{\text{GS}\}} + H^{\langle 2\nu_1\rangle}_{\{\nu_1\}} + H^{\langle 2\nu_1\rangle}_{\{2\nu_1\}}. \tag{6}$$

- The $\nu_1 + \nu_6$ effective Hamiltonian,

$$H^{\langle\nu_1+\nu_6\rangle} = H^{\langle\nu_1+\nu_6\rangle}_{\{\text{GS}\}} + H^{\langle\nu_1+\nu_6\rangle}_{\{\nu_6\}} + H^{\langle\nu_1+\nu_6\rangle}_{\{\nu_1\}} + H^{\langle\nu_1+\nu_6\rangle}_{\{\nu_1+\nu_6\}}. \tag{7}$$

- The $\nu_1 + 2\nu_6$ effective Hamiltonian,

$$H^{\langle\nu_1+2\nu_6\rangle} = H^{\langle\nu_1+2\nu_6\rangle}_{\{\mathrm{GS}\}} + H^{\langle\nu_1+2\nu_6\rangle}_{\{\nu_6\}} + H^{\langle\nu_1+2\nu_6\rangle}_{\{2\nu_6\}} + H^{\langle\nu_1+2\nu_6\rangle}_{\{\nu_1\}} + H^{\langle\nu_1+2\nu_6\rangle}_{\{\nu_1+\nu_6\}} + H^{\langle\nu_1+2\nu_6\rangle}_{\{\nu_1+2\nu_6\}}. \quad (8)$$

- The $\nu_1 + \nu_5$ effective Hamiltonian,

$$H^{\langle\nu_1+\nu_5\rangle} = H^{\langle\nu_1+\nu_5\rangle}_{\{\mathrm{GS}\}} + H^{\langle\nu_1+\nu_5\rangle}_{\{\nu_5\}} + H^{\langle\nu_1+\nu_5\rangle}_{\{\nu_1\}} + H^{\langle\nu_1+\nu_5\rangle}_{\{\nu_1+\nu_5\}}. \quad (9)$$

In order to calculate Raman intensities, the effective polarizability operator is expressed using similar methods [26]. Since experimental Raman intensities cannot be precisely determined, this operator is expanded up to order zero only. All the bands involved in the present study correspond to an increase of one quantum on the ν_1 mode and thus, in each case, the zeroth order polarizability always correspond to the same single operator symbolically denoted $P^{0(0,0A_{1g})A_{1g}A_{1g}}_{\{\mathrm{GS}\}\{\nu_1\}}$. Since we will only consider here relative intensities, the corresponding parameter is simply fixed to 1.

4 Analysis

The contributions of the ground state (GS), ν_6, $2\nu_6$, ν_5, ν_1, $\nu_1 + \nu_6$, $\nu_1 + 2\nu_6$, $\nu_1+\nu_5$ and $2\nu_1$ to the various effective Hamiltonians have been expanded up to order 6, 3, 2, 3, 4, 3 ,4 ,4 and 6, respectively. The GS and ν_6 parameters have been fixed to the values obtained in Ref. [11] and those of ν_5 have been fixed to the values from Ref. [13]. For the GS, $v_6 = 1$ and $v_5 = 1$ levels, we took the same parameters for $^{32}SF_6$ and $^{34}SF_6$. While this is fully justified for the GS whose isotopic dependency can be considered as negligible, for the $v_6 = 1$ and $v_5 = 1$ levels there is, of course, an isotopic shift. However, this one is presently not known precisely since no study of $^{34}SF_6$ has been yet performed for these levels. Nevertheless, since we only study here difference bands like $\nu_1 + \nu_6 - \nu_6$ and $\nu_1 + \nu_5 - \nu_5$, the fact that we ignore the isotopic shift on ν_6 and ν_5 does not change the results.

All the analyses were performed thanks to the HTDS software [18]. We detail below the results for the various bands that we were able to analyze. The effective Hamiltonian parameters are summarized in Tables 1 (ν_1 and $2\nu_1-\nu_1$) and 2 (hot bands). The ground state parameters have not been repeated in Table 2. In these two Tables, we have indicated in the last column the correspondence between our tensorial notation for parameters and the usual "Robiette" notation [27,25]. We can notice that, due to the vibrational extrapolation scheme used in our model (see Section 3), most of the parameters that are specific to a given combination or harmonic level are in fact corrections to the parameters of the levels below. This is why, in the last column, many parameters are denoted by the letter Δ. For instance, for the ν_1 band, this is the difference

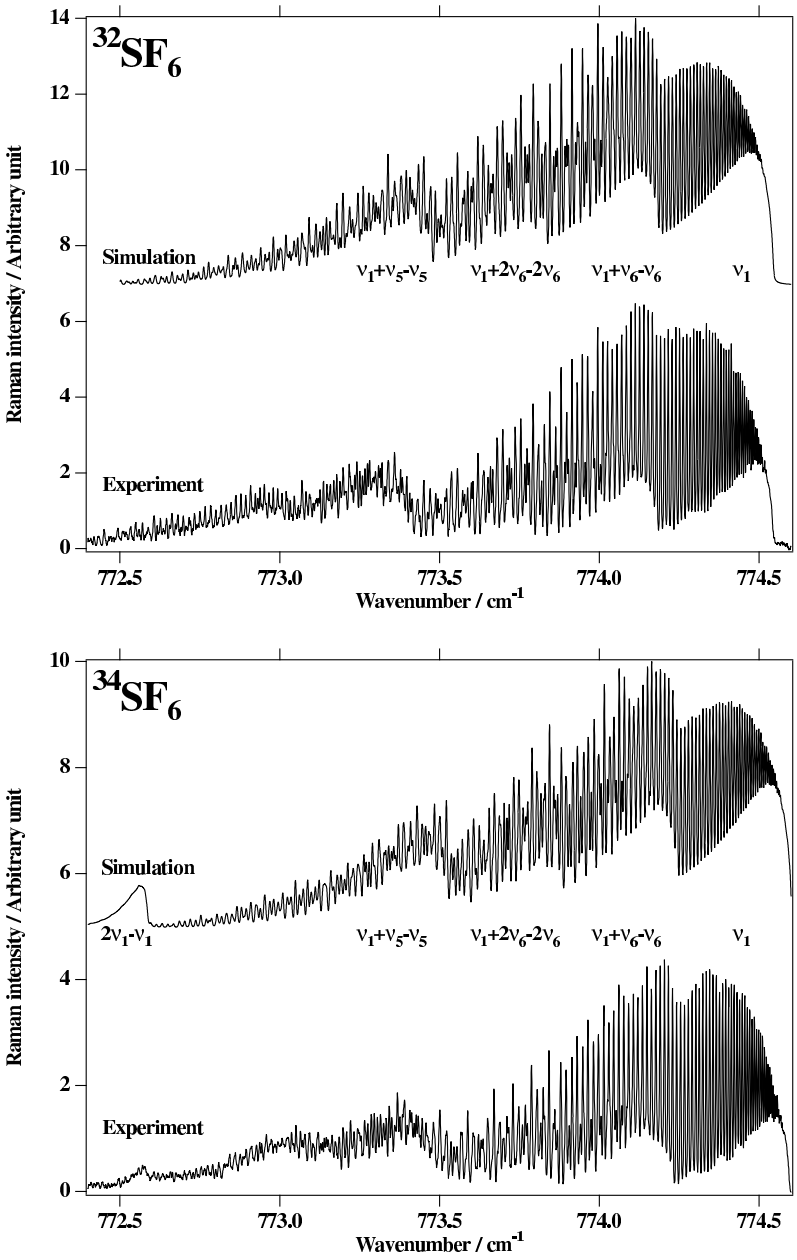

Fig. 1. Overview of the Raman spectra of the ν_1 region of $^{32}SF_6$ and $^{34}SF_6$ at room temperature compared to the simulations.

$\Delta B_1 = B_1 - B_0$ which is fitted rather than the B_1 rotational constant itself. In the same way, ΔD_{1t} means $D_{1_t} - D_{0t}$, ΔB_{11} means $B_{11} - B_1$ (where B_{11} stands for the $v_1 = 2$ rotational constant), *etc.* For combination levels like $v_1 = v_6 = 1$, we have $\Delta B_{16} = B_{16} + B_0 - B_1 - B_6$, *etc.*

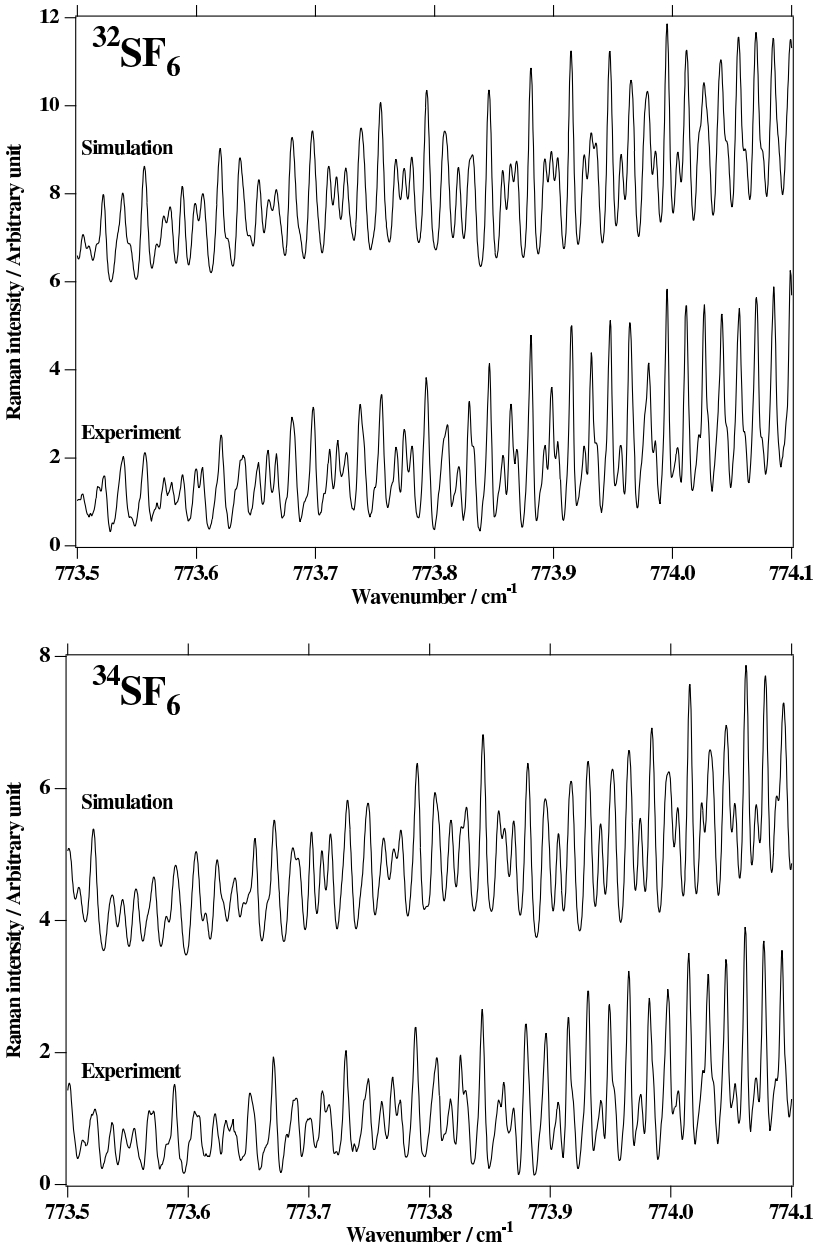

Fig. 2. Part of the $\nu_1 + \nu_6 - \nu_6$ region of $^{32}SF_6$ and $^{34}SF_6$ at room temperature compared to the simulations.

4.1 The ν_1 fundamental

For the ν_1 fundamental itself, we started the study by using the parameters from Refs [16,17]. We were thus able to assign significantly more lines (up to higher J values) than in these previous studies and our fits lead to quite more precise parameter values. Our results are summarized in Table 1. We have combined data from our cold and room temperature spectra. It was possible to fit fourth order parameters. Their contribution appears to be more important for $^{34}SF_6$ than for $^{32}SF_6$.

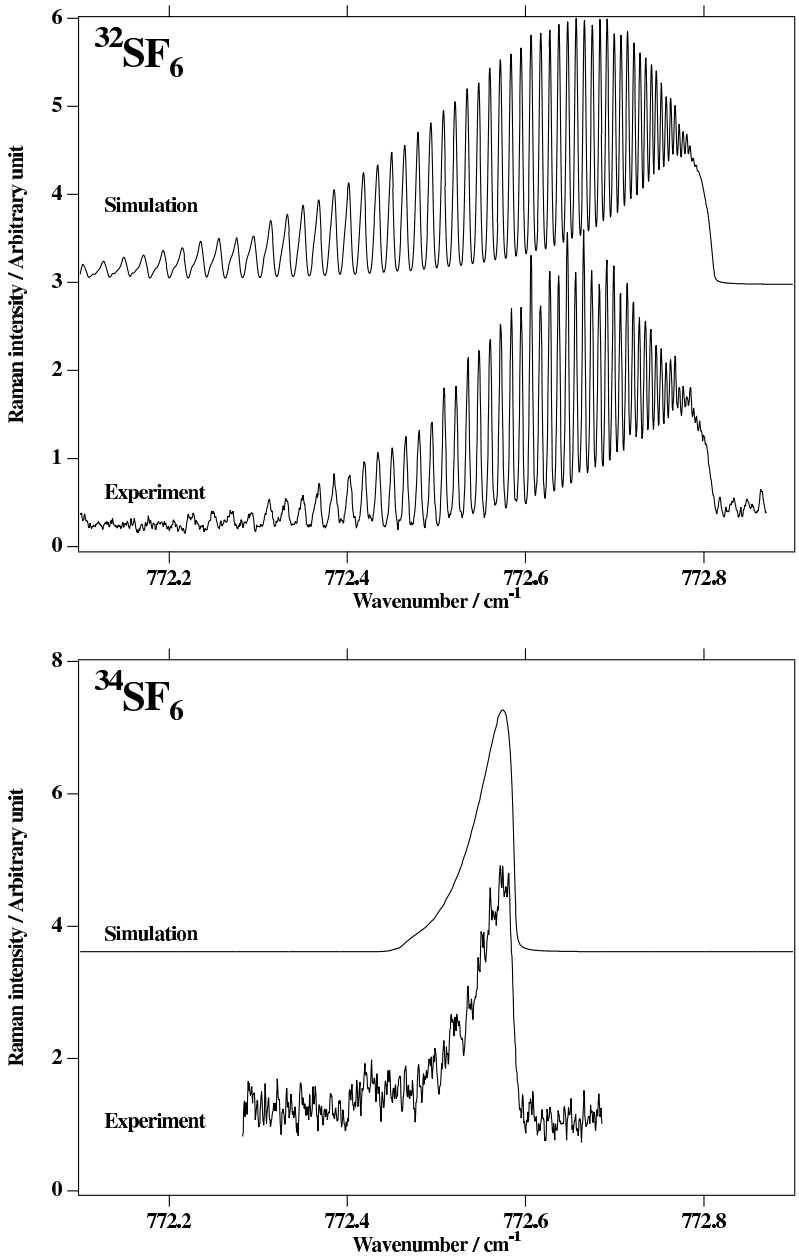

Fig. 3. The $2\nu_1 - \nu_1$ double resonance spectrum of $^{32}SF_6$ and $^{34}SF_6$ at 170 K compared to the simulations.

4.2 Hot bands in the ν_1 region

As it has been shown in Ref. [29] and as it can be seen in Figure 1 many hot bands appear at room temperature in the ν_1 region. Again by combining our cold and room temperature spectra we were able to obtain a good fit of the "main" hot band, namely $\nu_1 + \nu_6 - \nu_6$. For $^{32}SF_6$ this improves the study of Ref. [16]. Contrary to this previous work, we did not fit the correction to the rotational constant ΔB_{16} (which would be a 4th order contribution) but rather the correction to the Coriolis parameter $\Delta(B\zeta)_{16} = (B\zeta)_{16} - (B\zeta)_6$

Table 1
Effective hamiltonian parameters and fit statistics for ν_1 and $2\nu_1 - \nu_1$.

Parameter $t^{\Omega(K,n\Gamma)\Gamma_v\Gamma'_v}_{\{s\}\{s'\}}$			$^{32}SF_6$	$^{34}SF_6$	"Usual" notation
$\Omega(K,n\Gamma)$	$\{s\}\Gamma_v$	$\{s'\}\Gamma'_v$	Value / cm^{-1} †	Value / cm^{-1} †	(Refs. [27,25,28])
Ground state					
$2(0,0A_{1g})$	$000000A_{1g}$	$000000A_{1g}$	$9.1078389192 \times 10^{-2}$		B_0
$4(0,0A_{1g})$	$000000A_{1g}$	$000000A_{1g}$	$-6.3369998149 \times 10^{-9}$		$-D_0$
$4(4,0A_{1g})$	$000000A_{1g}$	$000000A_{1g}$	$1.8196943510 \times 10^{-10}$		$-(\sqrt{15}/4\sqrt{2})D_{0t}$
$6(0,0A_{1g})$	$000000A_{1g}$	$000000A_{1g}$	$-1.5890094350 \times 10^{-13}$		H_0
$6(4,0A_{1g})$	$000000A_{1g}$	$000000A_{1g}$	$1.0083389785 \times 10^{-14}$		$(3\sqrt{5}/16\sqrt{2})H^0_{4t}$
$6(6,0A_{1g})$	$000000A_{1g}$	$000000A_{1g}$	$-1.0615255469 \times 10^{-16}$		$-(\sqrt{231}/64\sqrt{2})H^0_{6t}$
$8(0,0A_{1g})$	$000000A_{1g}$	$000000A_{1g}$	$5.9060087823 \times 10^{-19}$		L_0
$8(4,0A_{1g})$	$000000A_{1g}$	$000000A_{1g}$	$6.5795734511 \times 10^{-20}$		$-(3\sqrt{15}/64\sqrt{2})L^0_{4t}$
$8(6,0A_{1g})$	$000000A_{1g}$	$000000A_{1g}$	$-8.9391941374 \times 10^{-21}$		$(3\sqrt{77}/256\sqrt{2})L^0_{6t}$
$8(8,0A_{1g})$	$000000A_{1g}$	$000000A_{1g}$	$-9.6703402824 \times 10^{-22}$		$(1/32\sqrt{33})L^0_{8t}$
$v_1 = 1$ level.					
$0(0,0A_{1g})$	$100000A_{1g}$	$100000A_{1g}$	774.544759(56)	774.60264(17)	ν_1
$2(0,0A_{1g})$	$100000A_{1g}$	$100000A_{1g}$	$-1.10574(24) \times 10^{-4}$	$-1.0437(10) \times 10^{-4}$	ΔB_1
$4(0,0A_{1g})$	$100000A_{1g}$	$100000A_{1g}$	$9.8(1.9) \times 10^{-12}$	$-2.58(11) \times 10^{-10}$	$-\Delta D_1$
$4(4,0A_{1g})$	$100000A_{1g}$	$100000A_{1g}$	0.0	$2.50(68) \times 10^{-12}$	$-(\sqrt{15}/4\sqrt{2})\Delta D_{1t}$
σ/ cm^{-1}			0.247	0.601	
J_{max} / Number of data			120 / 91	98 / 82	
$v_1 = 2$ level					
$0(0,0A_{1g})$	$200000A_{1g}$	$200000A_{1g}$	$-1.73476(26)$	-2.015	$2X_{11}$
$2(0,0A_{1g})$	$200000A_{1g}$	$200000A_{1g}$	$-1.243(35) \times 10^{-5}$	8.5×10^{-5}	ΔB_{11}
$4(0,0A_{1g})$	$200000A_{1g}$	$200000A_{1g}$	$-4.870(96) \times 10^{-9}$	0.0	$-\Delta D_{11}$
$4(4,0A_{1g})$	$200000A_{1g}$	$200000A_{1g}$	0.0	0.0	$-(\sqrt{15}/4\sqrt{2})\Delta D_{11t}$
σ/ cm^{-1}			0.611	—	
J_{max} / Number of data			98 / 48	—	

† Standard deviation is indicated in the unit of the last two digits for fitted parameters, the others being fixed.

σ is the root mean square of $\nu_{obs} - \nu_{calc}$.

(which is a 3rd order contribution). This seems more reasonable due to the relative contributions of these terms. The $\nu_1 + \nu_6 - \nu_6$ hot band of $^{34}SF_6$ has been analyzed here for the first time since it was not fitted in Ref. [17]. Figure 2 shows the $\nu_1+\nu_6-\nu_6$ region for both isotopomers, compared to the simulation.

It was also possible to perform a fit of $\nu_1+\nu_5-\nu_5$ of $^{32}SF_6$ using the ν_5 parameters from Ref. [13]. Since the ν_5 band of $^{34}SF_6$ has not yet been analyzed, we did not intend to fit the $\nu_1+\nu_5-\nu_5$ hot band for this isotopomer. We just used the same ν_5 and $\nu_1+\nu_5$ parameters to simulate spectra for both isotopomers.

Figure 1 shows the overview of the ν_1 region compared to our simulations. For these, we also included the $\nu_1+2\nu_6-2\nu_6$ hot band by simply fixing the $\nu_1+2\nu_6$ specific parameters to zero and by moving by hand the $2\nu_6$ anharmonicity

parameters to a value which puts this hot band at the correct position. These anharmonicity constants were taken identical for both isotopomers.

For $^{34}SF_6$, the small band near 772.6 cm^{-1} has been identified to be $2\nu_1-\nu_1$ and was included in the simulation using the results from the next paragraph. Some other hot band appear around 773 cm^{-1}. According to Ref. [29], this includes contributions from several complicated bands like $\nu_1 + (\nu_6 + \nu_4) - (\nu_6 + \nu_4)$. No attempt to analyze these additional hot bands has been performed here.

Table 2 summarizes all these hot band results. Our anharmonicity constants X_{16} and X_{15} are in good agreement with those of Ref. [29].

4.3 Equilibrium bond length of sulfur hexafluoride

The present fit of ΔB_1, combined with B_0 [15] and the ΔB values for all the other fundamentals of $^{32}SF_6$, namely ν_2 [11], ν_3 [15], ν_4 [12], ν_5 [13] and ν_6 [10,11], allows us to calculate the r_e equilibrium bond length of sulfur hexafluoride. To do this, we use the formula [30]

$$B_e = B_0 - \frac{1}{2}\sum_{i=1}^{6} \Delta B_i d_i = \frac{h}{32\pi^2 c m_F r_e^2}, \tag{10}$$

where $\Delta B_i = B_i - B_0$ and d_i is the degeneracy of oscillator i ($d_1 = 1$, $d_2 = 2$, $d_3 = d_4 = d_5 = d_6 = 3$). Given the high accuracy of all ΔB values and neglecting the electronic effects we can thus estimate

$$r_e = 1.5560(1) \text{ Å}. \tag{11}$$

This value is very close to the most recent *ab initio* results [31] and to the force field calculation of Krohn and Overend [32] that both give $r_e = 1.5561$ Å. Up to our knowledge, Equation (11) represents the first direct experimental determination of r_e of SF_6.

4.4 The $2\nu_1 - \nu_1$ band

As Figure 3 shows, the $2\nu_1 - \nu_1$ spectrum of $^{32}SF_6$ is quite simple. Its analysis was straightforward, using vibrational extrapolation from ν_1. The results are shown in Table 1. We find an anharmonicity constant $X_{11} \simeq -0.867$ cm^{-1}, in good agreement with the value -0.896 cm^{-1} reported in Ref. [28] in which much lower precision data were used.

The $^{34}SF_6$ case is much more intriguing since in this case the rotational structure is completely collapsed into a narrow unresolved band. In fact,

Table 2
Effective hamiltonian parameters and fit statistics for $\nu_1+\nu_6-\nu_6$ and $\nu_1+\nu_5-\nu_5$.

Parameter $t^{\Omega(K,n\Gamma)\Gamma_v\Gamma'_v}_{\{s\}\{s'\}}$			$^{32}SF_6$	$^{34}SF_6$	"Usual" notation
$\Omega(K,n\Gamma)$	$\{s\}\Gamma_v$	$\{s'\}\Gamma'_v$	Value / cm^{-1} †	Value / cm^{-1} †	(Refs. [27,25,28])
			$v_6=1$ level		
$0(0,0A_{1g})$	$000001F_{2u}$	$000001F_{2u}$	346.9		ν_6
$1(1,0F_{1g})$	$000001F_{2u}$	$000001F_{2u}$	−0.31032909393		$3\sqrt{2}(B\zeta)_6$
$2(0,0A_{1g})$	$000001F_{2u}$	$000001F_{2u}$	$-0.22062929503\times10^{-4}$		ΔB_6
$2(2,0E_g)$	$000001F_{2u}$	$000001F_{2u}$	$-0.26343685366\times10^{-4}$		$-\alpha^6_{220}/2-6\alpha^6_{224}$
$2(2,0F_{2g})$	$000001F_{2u}$	$000001F_{2u}$	$0.52830499700\times10^{-4}$		$-3\alpha^6_{220}/4+6\alpha^6_{224}$
$3(1,0F_{1g})$	$000001F_{2u}$	$000001F_{2u}$	$0.19129608827\times10^{-6}$		$-(3\sqrt{3}/4\sqrt{2})F^6_{110}$
$3(3,0F_{1g})$	$000001F_{2u}$	$000001F_{2u}$	$-0.37106303207\times10^{-6}$		$(3\sqrt{5}/2)F^6_{134}$
			$v_6=2$ level		
$0(0,0A_{1g})$	$000002A_{1g}$	$000002A_{1g}$	−0.13		(A_{1g} sublevel)
$0(0,0A_{1g})$	$000002E_g$	$000002E_g$	−0.13		(E_g sublevel)
$0(0,0A_{1g})$	$000002F_{2g}$	$000002F_{2g}$	−0.13		(F_{2g} sublevel)
			$v_5=1$ level		
$0(0,0A_{1g})$	$000010F_{2g}$	$000010F_{2g}$	524.03074724		ν_5
$1(1,0F_{1g})$	$000010F_{2g}$	$000010F_{2g}$	−0.19000327358		$3\sqrt{2}(B\zeta)_5$
$2(0,0A_{1g})$	$000010F_{2g}$	$000010F_{2g}$	$-0.16017985186\times10^{-3}$		ΔB_5
$2(2,0E_g)$	$000010F_{2g}$	$000010F_{2g}$	$0.22320710649\times10^{-3}$		$-\alpha^5_{220}/2-6\alpha^5_{224}$
$2(2,0F_{2g})$	$000010F_{2g}$	$000010F_{2g}$	$-0.24308388824\times10^{-4}$		$-3\alpha^5_{220}/4+6\alpha^5_{224}$
$3(1,0F_{1g})$	$000010F_{2g}$	$000010F_{2g}$	$-0.52728567909\times10^{-7}$		$-(3\sqrt{3}/4\sqrt{2})F^5_{110}$
$3(3,0F_{1g})$	$000010F_{2g}$	$000010F_{2g}$	$0.33933691037\times10^{-7}$		$(3\sqrt{5}/2)F^5_{134}$
			$v_1=v_6=1$ level		
$0(0,0A_{1g})$	$100001F_{2u}$	$100001F_{2u}$	$-3.5924(14)\times10^{-1}$	$-3.60199(89)\times10^{-1}$	X_{16}
$1(1,0F_{1g})$	$100001F_{2u}$	$100001F_{2u}$	$2.01(54)\times10^{-5}$	$1.82(51)\times10^{-5}$	$3\sqrt{2}\Delta(B\zeta)_{16}$
σ/ cm^{-1}			0.704	0.518	
J_{max} / Number of data			88 / 39	78 / 37	
			$v_1=1$, $v_6=2$ level		
$0(0,0A_{1g})$	$100002A_{1g}$	$100002A_{1g}$	0.0		(A_{1g} sublevel)
$0(0,0A_{1g})$	$100002E_g$	$100002E_g$	0.0		(E_g sublevel)
$0(0,0A_{1g})$	$100002F_{2g}$	$100002F_{2g}$	0.0		(F_{2g} sublevel)
			$v_1=v_5=1$ level		
$0(0,0A_{1g})$	$100010F_{2g}$	$100010F_{2g}$	−1.08140(67)	−1.08140	X_{15}
$1(1,0F_{1g})$	$100010F_{2g}$	$100010F_{2g}$	$-2.788(18)\times10^{-3}$	-2.788×10^{-5}	$3\sqrt{2}\Delta(B\zeta)_{15}$
$2(2,0A_{1g})$	$100010F_{2g}$	$100010F_{2g}$	$2.077(16)\times10^{-5}$	2.077×10^{-5}	ΔB_{15}
$2(2,0E_g)$	$100010F_{2g}$	$100010F_{2g}$	0.0	0.0	—
$2(2,0F_{2g})$	$100010F_{2g}$	$100010F_{2g}$	0.0	0.0	—
σ/ cm^{-1}			1.643	—	
J_{max} / Number of data			88 / 45	—	

† Standard deviation is indicated in the unit of the last two digits for fitted parameters, the others being fixed.

σ is the root mean square of $\nu_{obs}-\nu_{calc}$. See Table 1 for ground state parameters.

as can be seen in Figure 1, this band can be observed in the room temperature spectrum of the $^{34}SF_6$ isotopomer as opposed to the case of the $^{32}SF_6$ isotopomer. By moving parameters by hand, we found that an anharmonicity constant $X_{11} \simeq 1.0075$ cm^{-1} and a rotational constant correction $\Delta B_{11} = B_{11} - B_1 \simeq 8.5 \times 10^{-5}$ cm^{-1} gives a satisfactory reproduction of the band profile, as shown in Figure 3. We have presently no explanation for this big difference between the two isotopomers. Further investigation of the neighbor bands would be necessary to identify a possible perturber. However, at the present time, vibrational levels in the vicinity of $v_1 = 2$ (1550 cm^{-1} region) are not known.

5 Conclusion

We have been able to perform a detailed analysis of the ν_1 region and of the $2\nu_1 - \nu_1$ band of $^{32}SF_6$ and $^{34}SF_6$. We have found that the $v_2 = 1$ vibrational level of $^{34}SF_6$ has an extremely narrow rotational structure, compared to that of $^{32}SF_6$. The equilibrium bond length of SF_6 has be estimated.

These results will be now used for the analysis of infrared spectra of combination bands implying quanta of ν_1, like $\nu_1+\nu_3$ or $\nu_1+\nu_4$, for instance. A further step would be to attempt a global fit of all the lowest SF_6 vibrational levels. We also intend to complete the work on the $^{34}SF_6$ isotopomer by studying its ν_2 and ν_5 Raman-active fundamentals.

The HTDS software [18] used to perform the present analyses can be freely downloaded though the World Wide Web at the URL:

`http://www.u-bourgogne.fr/LPUB/shTDS.html`

It has been updated to include the parameter files resulting from the present study.

Acknowledgments

Région Bourgogne is gratefully acknowledged for supporting the Laboratoire de Physique de l'Université de Bourgogne. JLD and DB acknowledge the financial support of the Ministry of Science and Technology under the project REN2002-01618.

References

[1] T. Reddmann, R. Ruhnke, W. Kouker, J. Geophys. Res. 106 (D13) (2001) 14525–14537.

[2] M. Khalil, Annu. Rev. Energy Environ 24 (1999) 645–661.

[3] C. Dervos, P. Vassiliou, Air & Waste Manage. Assoc. 50 (2000) 137–141.

[4] L. Geller, J. Elkins, J. Lobert, A. Clarke, D. Hurst, J. Butler, R. Myers, Geophys. Res. Lett. 24 (6) (1997) 675–678.

[5] C. Volk, J. Elkins, D. Fahey, G. Dutton, J. Gilligan, M. Loewenstein, J. Podolske, K. Chan, M. Gunson, J. Geophys. Res. 102 (D21) (1997) 25543–25564.

[6] J. Reilly, M. Mayer, J. Harnisch, Environmental Modeling and Assessment 7 (2002) 217–229.

[7] J. Harnisch, N. Höhne, Environ. Sci. & Pollut. Res. 9 (5) (2002) 315–320.

[8] J. Harnisch, D. de Jager, J. Gale, O. Stobbe, Environ. Sci. & Pollut. Res. 9 (6) (2002) 369–374.

[9] V. Boudon, G. Pierre, Rovibrational spectroscopy of sulphur hexafluoride : A review, in: S. G. Pandalai (Ed.), Recent research developments in molecular spectroscopy, Vol. 1, Transworld Research Network, Trivandrum, India, 2002, pp. 25–55.

[10] V. Boudon, M. Hepp, M. Herman, I. Pak, G. Pierre, J. Mol. Spectrosc. 192 (1998) 359–367.

[11] D. Bermejo, R. Martínez, E. Loubignac, V. Boudon, G. Pierre, J. Mol. Spectrosc. 201 (2000) 164–171.

[12] V. Boudon, G. Pierre, H. Bürger, J. Mol. Spectrosc. 205 (2001) 304–311.

[13] V. Boudon, D. Bermejo, J. Mol. Spectrosc. 213 (2002) 139–144.

[14] V. Boudon, N. Lacome, J. Mol. Spectrosc. 222 (2003) *in press.*

[15] O. Acef, C. Bordé, A. Clairon, G. Pierre, B. Sartakov, J. Mol. Spectrosc. 199 (2000) 188–204.

[16] P. Esherick, A. Owyoung, J. Mol. Spectrosc. 92 (1982) 162–169.

[17] S. Y. Volkov, D. N. Kozlov, M. R. Malikov, V. V. Smirnov, Sov. J. Quantum Electron. 14 (9) (1985) 1240–1242.

[18] C. Wenger, V. Boudon, J.-P. Champion, G. Pierre, J. Quant. Spectrosc. Radiat. Transfer 66 (1) (2000) 1–16.

[19] W. Gombler, H. Willner, J. Phys. E: Sci. Instrum. 20 (1987) 1286–1288.

[20] A. Owyoung, C. W. Patterson, R. S. McDowell, Chem. Phys. Lett. 59 (1978) 156–162.

[21] J. Santos, J. L. D. P. Cancio, J. Rodríguez, D. Bermejo, Laser Chem. 12 (1992) 53–63.

[22] P. Cancio, D. Bermejo, J. Opt. Soc. Am. B 14 (1997) 1305–1311.

[23] D. Bermejo, P. Cancio, G. D. Lonardo, L. Fusina, J. Chem. Phys. 108 (1998) 7224–7228.

[24] D. Bermejo, R. Z. Martínez, G. D. Lonardo, L. Fusina, J. Chem. Phys. 111 (1999) 519–524.

[25] J.-P. Champion, M. Loëte, G. Pierre, Spherical top spectra, in: K. N. Rao, A. Weber (Eds.), Spectroscopy of the Earth's atmosphere and interstellar medium, Academic Press, San Diego, 1992, pp. 339–422.

[26] N. Cheblal, M. Loëte, V. Boudon, J. Mol. Spectrosc. 197 (1999) 222–231.

[27] A. Robiette, D. Gray, F. Birss, Mol. Phys. 32 (6) (1976) 1591–1607.

[28] R. McDowell, B. Krohn, Spectrochim. Acta. 42A (2/3) (1986) 371–385.

[29] A. Aboumajd, H. Berger, R. Saint-Loup, J. Mol. Spectrosc. 78 (1979) 486–492.

[30] D. L. Gray, A. G. Robiette, Mol. Phys. 37 (6) (1979) 1901–1920.

[31] I. V. Kochikov, Y. I. Tarasov, V. P. Spiridonov, G. M. Kuramshina, A. S. Saakjan, A. G. Yagola, J. Mol. Struct. 550–551 (2000) 429–438.

[32] B. J. Krohn, J. Overend, J. Phys. Chem. 88 (1984) 564–574.

Troisième partie

Chapitre

2

Spectroscopie des Polyades Elevées du Méthane

Publication P33
Article de revue B2
Proceeding A1

2.1 Introduction

La molécule de méthane est un sujet d'étude majeur pour l'équipe de spectroscopie moléculaire du Laboratoire depuis de très nombreuses années. Il fut même à l'origine du développement du modèle tensoriel pour les toupies sphériques. Récemment, un regain d'intérêt important est apparu pour la spectroscopie des états excités de CH_4, d'une part dans le domaine de l'astrophysique (atmosphères des naines brunes et des exoplanètes) [A1] et, d'autre part, dans le domaine des combustions (moteurs-fusées à méthane). Bien entendu, cette molécule est aussi un gaz à effet de serre et constitue un des polluants majeurs de l'atmosphère terrestre [P33,B2].

Personnellement, je ne me suis impliqué dans cette thématique que récemment, et ce sur les deux points suivants :

- D'une part, j'ai intégré à la base de donnée STDS (voir Chapitre III.5) les résultats récents concernant l'octade (troisième polyade) et la tétradécade (quatrième polyade) issus de la thèse d'Olivier Robert.
- D'autre part, j'ai pu réaliser un analyse préliminaire de la région de la bande $\nu_2+2\nu_3$ appartenant à l'icosade (cinquième polyade), en collaboration avec Michael Hippler et le Pr. Martin Quack (ETH Zürich, Suisse).

Dans ce chapitre, je commence par effectuer quelques rappels généraux sur la spectroscopie de CH_4, puis je présente les résultats obtenus récemment dans la région de l'icosade. Je reproduis également un article général sur les outils développés au Laboratoire pour la spectrsocopie des gaz à effet de serre.

2.2 La spectroscopie du méthane

La caractéristique essentielle des spectres du méthane est le regroupement des niveaux en *polyades*, les fréquences fondamentales des modes normaux satisfaisant la relation approximative

$$\nu_1 \simeq \nu_3 \simeq 2\nu_2 \simeq 2\nu_4. \tag{III.2.1}$$

Rappelons que $\nu_1(A_1)$ et $\nu_3(F_2)$ sont les modes d'élongation et que $\nu_2(E)$ et $\nu_4(F_2)$ sont les modes de pliage. Nous pouvons définir les polyades du méthane de la manière suivante : un niveau vibrationnel (v_1,v_2,v_3,v_4) appartient à la polyade P_n si

$$n = 2(v_1 + v_3) + v_2 + v_4. \tag{III.2.2}$$

La figure 2.1 représente schématiquement les six premières polyades vibrationnelles de CH_4.

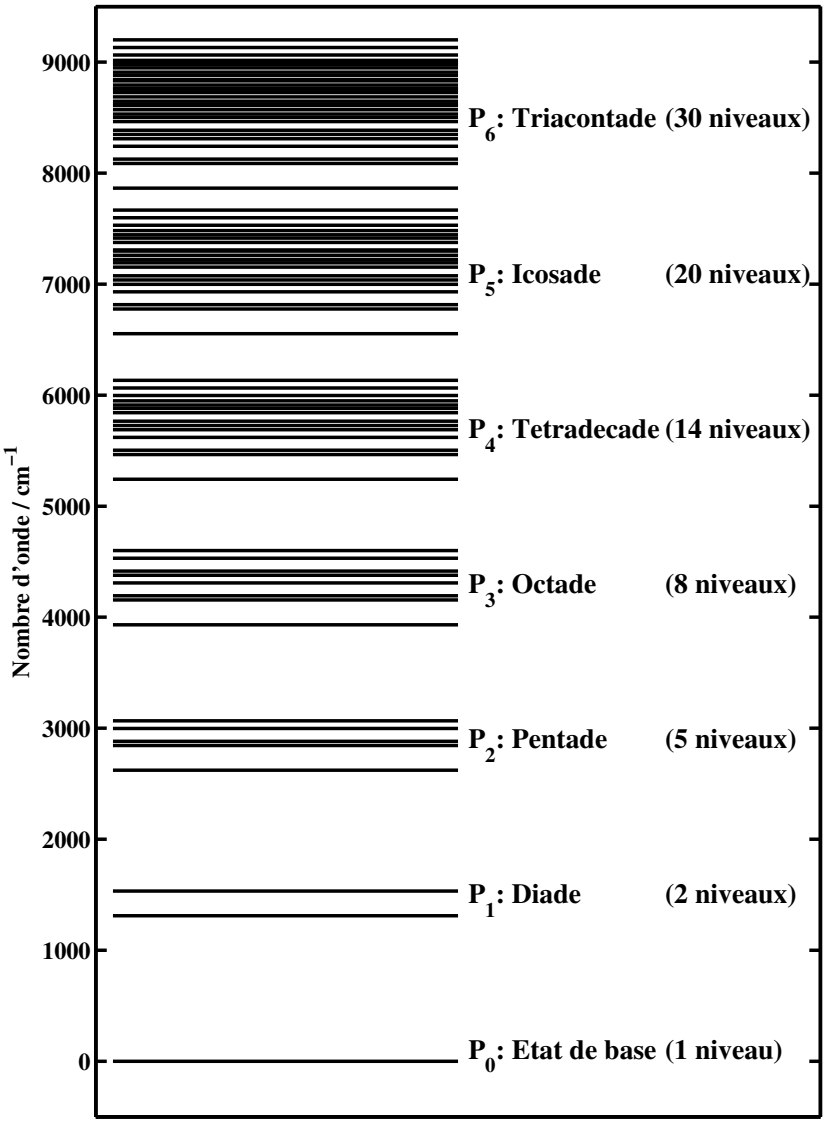

FIG. 2.1 – *Les polyades vibrationnelles de CH_4.*

Cette structure particulière justifie pleinement l'utilisation de la technique dite d'*extrapolation vibrationnelle* [1]. Brièvement, celle-ci consiste à écrire l'hamiltonien tensoriel comme une somme de contributions pour chaque polyade,

$$\mathcal{H} = \mathcal{H}_{\{P_0 \equiv \mathrm{GS}\}} + \mathcal{H}_{\{P_1\}} + \ldots + \mathcal{H}_{\{P_k\}} + \ldots + \mathcal{H}_{\{P_{n-1}\}} + \mathcal{H}_{\{P_n\}} + \ldots \qquad \text{(III.2.3)}$$

L'hamiltonien effectif pour une polyade P_n donnée est alors obtenu par projection dans le sous-espace de Hilbert correspondant,

$$H^{<P_n>} = P^{<P_n>}\mathcal{H}P^{<P_n>} = H^{<P_n>}_{\{\mathrm{GS}\}} + H^{<P_n>}_{\{P_1\}} + \ldots + H^{<P_n>}_{\{P_k\}} + \ldots + H^{<P_n>}_{\{P_{n-1}\}} + H^{<P_n>}_{\{P_n\}}. \qquad \text{(III.2.4)}$$

Ainsi, l'hamiltonien effectif de chaque polyade contient les opérateurs, et donc les paramères, associés à toutes les polyades inférieures. Les "nouveaux" paramètres associés à la polyade étudiée sont, en principe, des "petites corrections". Par exemple, si nous prenons l'exemple élémentaire d'une bande fondamentale, son hamiltonien effectif contiendra la constante rotationnelle B_0, issue de l'analyse de l'état de base, et la "correction" $\Delta B = B_1 - B_0$, plutôt que la constante B_1 de l'état $v = 1$.

En pratique, cette approche permet l'analyse des polyades les unes après les autres et s'est avérée jusqu'à présent très productive.

1. Celle-ci est en réalité utilisée pour l'ensemble des analyses présentées dans ce rapport ; mais il est clair qu'elle est pleinement adaptée au cas du méthane, molécule pour laquelle elle a été développée à l'origine.

A l'heure actuelle, on peut considérer que les analyses de l'état de base, de la diade, de la pentade et de l'octade [2] sont achevées, tant du point de vue des fréquences que des intensités. L'analyse de la tétradécade n'est encore que partielle [3].

2.3 Avancées récentes : l'icosade de CH_4

Récemment, j'ai pu entreprendre une première étude concernant l'icosade du méthane, grâce à des spectres FTIR et CRDS enregistrés par Michael Hippler à l'ETH Zürich (Suisse). Il s'agit bien évidemment d'une polyade extrêmement complexe, avec 20 niveaux vibrationnels correspondant à 134 sous-niveaux en interaction. L'analyse complète de cette polyade représente un travail considérable qui prendra de nombreuses années. Je me suis pour l'instant intéressé à la région de la bande la plus intense, $\nu_2 + 2\nu_3$.

TAB. 2.1 – *Nombre de paramètres spécifiques pour l'hamiltonien effectif de l'icosade*

Polyade	P_0	P_1	P_2	P_3	P_4	P_5
	Etat de base	Diade	Pentade	Octade	Tétradécade	Icosade
Ordre du devel.	6	6	4	4	4	7
Nb. param. H	10	62	134	253	248	6469

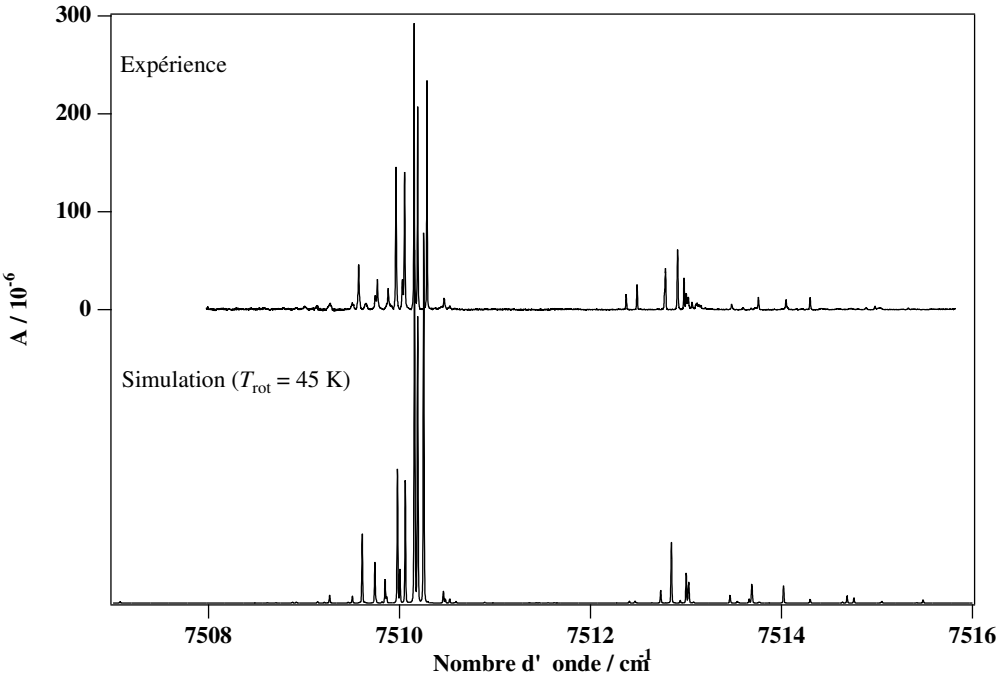

FIG. 2.2 – *Détail de la branche Q de $\nu_2 + 2\nu_3$ (spectre CRD de Michael Hippler, ETH Zürich, Suisse), comparé à l'expérience.*

La Table 2.1 donne le nombre de paramètres pour les différentes contributions à l'hamiltonien de l'icosade. Cette table appelle quelques commentaires. Afin d'avoir suffisamment de paramètres ajustables pour la bande $\nu_2 + 2\nu_3$, il m'a été nécessaire de développer la contribution de l'icosade jusqu'à l'ordre 7, d'où un très grand nombre de paramètres (mais dont seulement un tout petit nombre sont ajustés dans la suite). Ceci peut sembler disproportionné au regard des contributions de l'octade et de la tétradécade. Mais il faut préciser que les paramètres de la tétradécade utilisés proviennent du meilleur ajustement global réalisé par Olivier Robert, cette analyse étant encore très incomplète. Une

2. J.-C. Hilico, O. Robert, M. Loëte, S. Toumi, A. S. Pine and L. R. Brown, *J. Mol. Spectrosc.*, **208**, 1–13 (2001).
3. O. Robert, J.-C. Hilico, M. Loëte, J.-P. Champion and L. R. Brown, *J. Mol. Spectrosc.*, **2009**, 14–23 (2001).

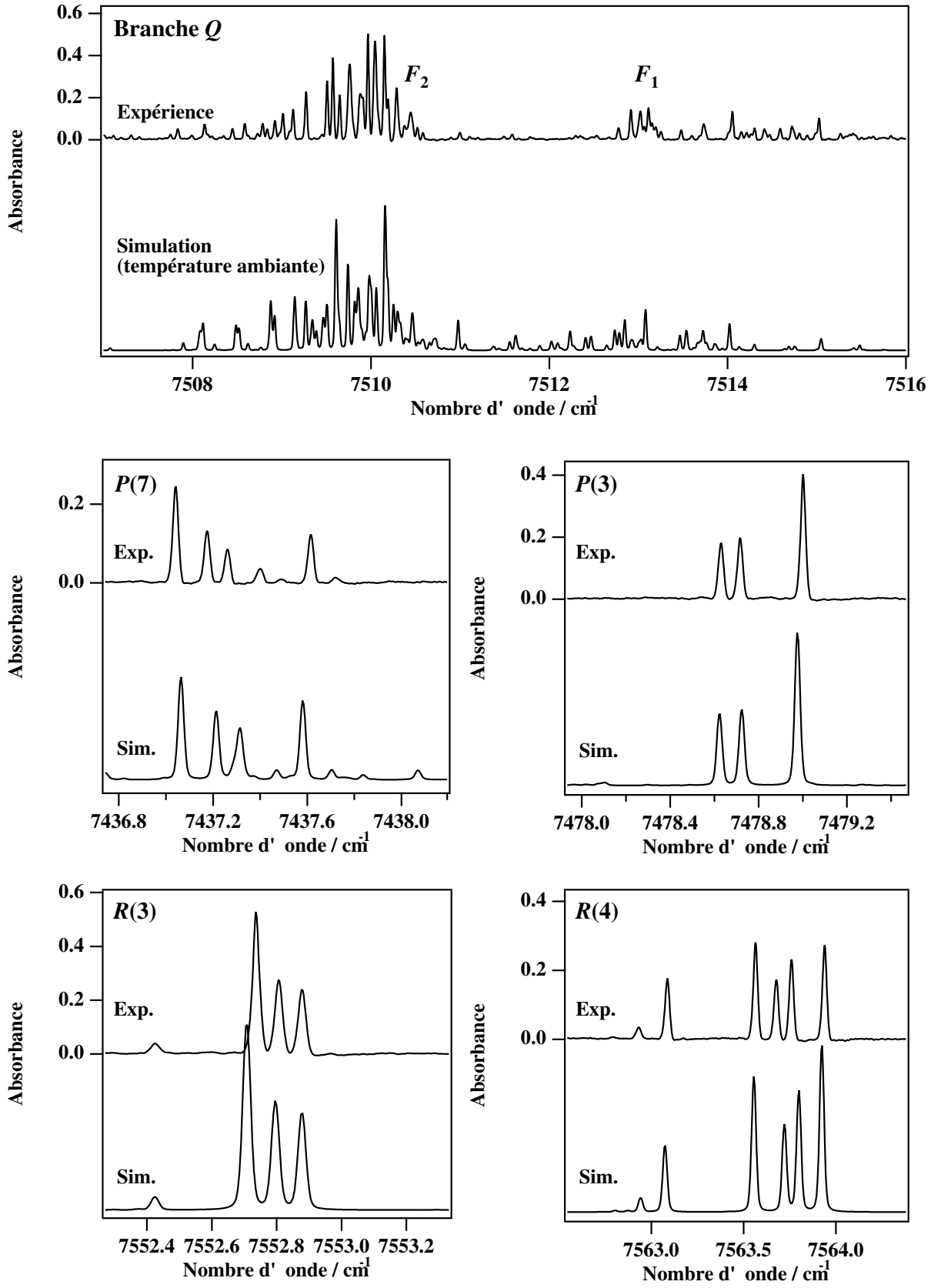

FIG. 2.3 – *Portions de la bande $\nu_2 + 2\nu_3$ (spectre FT de Michael Hippler, ETH Zürich, Suisse), comparées à l'expérience.*

analyse "finale" de la tétradécade nécessiterait probablement un développement à l'ordre 6. Même pour l'octade, il est permis de se demander si un développement à l'ordre 5 ne permettrait pas d'améliorer encore les résultats existants (*cf.* note 2 page 53).

J'ai abordé l'analyse de la région $\nu_2+2\nu_3$ en utilisant, d'une part, l'étude préliminaire de M. Hippler et M. Quack[4] et, d'autre part, les résultats d'un calcul *ab initio* récent[5] concernant les positions des six sous-niveaux vibrationnels de cette bande. J'ai décalé les valeurs de cette dernière référence de $+11$ cm^{-1} afin de faire correspondre le sous-niveau "actif" F_2 avec la principale branche Q observée dans cette région. J'ai alors pu attribuer un certain nombre de raies et effectuer un ajustement dans les conditions suivantes :

- 25 paramètres ajustés pour $\nu_2 + 2\nu_3$ (7 pour le sous-niveau F_1, 7 pour le sous-niveau F_2, 7 pour l'interaction $F_1 - F_2$, et 4 pour un des sous-niveaux E).
- Les paramètres purement vibrationnels pour les sous-niveaux A_1, A_2 et pour le second sous-niveau E sont restés fixés aux valeurs *ab initio*[5].
- Tous les autres paramètres de $\nu_2 + 2\nu_3$ ont été fixés à 0.
- La position d'un des sous-niveaux F_2 de $3\nu_2 + \nu_3$ a été ajustée.
- Le moment dipolaire a été développé à l'ordre 3, ce qui donne 44 paramètres d'intensité. 26 d'entre eux ont été fixés manuellement à des valeurs donnant un profil raisonnable pour l'ensemble de l'icosade, les autres restant fixés à 0.

J'ai ainsi pu effectuer 164 attributions et obtenir un RMS de 71.15×10^{-3} cm^{-1}. Les Figures 2.2 et 2.3 illustrent le résultat. La Table 2.2 donne les positions ajustées des sous-niveaux de $\nu_2 + 2\nu_3$, comparées au calcul *ab initio*[5].

TAB. 2.2 – *Positions des sous-niveaux de* $\nu_2 + 2\nu_3$.

Sous-niveau (symmétrie)	Ajusté / cm^{-1}	Calculé / cm^{-1} †	Ajusté−Calculé / cm^{-1}
A_1	7557.26	7546.94	+10.32
A_2	7546.62	7533.95	+12.67
E	7459.55	7440.53	+19.02
E	7554.61	7540.01	+14.60
F_1	7512.77	7501.09	+11.68
F_2	7510.29	7498.83	+11.46

† Calcul *ab initio*, voir note 5 au bas de cette page.

Il est clair que ceci n'est qu'un travail très préliminaire. Michaël Rey, actuellement en stage post-doctoral au sein du groupe du Pr. Martin Quack (ETH Zürich, Suisse) tente actuellement de poursuivre cette analyse. Il a pu très récemment améliorer significativement les résultats décrits ci-dessus.

2.4 Perspectives

Les applications concernant le méthane chaud (atmosphères stellaires, combustions) nécessiteront de "grimper" encore plus haut dans l'échelle des polyades. Des spectres de ces polyades supérieures existent d'ores et déjà, comme l'illustre la Figure 2.4 avec la polyade P_6 (triacontade).

Il apparaît cependant évident que, pour des polyades aussi élevées et complexes, la méthode utilisée jusqu'à présent atteint ses limites, le nombre de paramètres nécessaires explosant littéralement.

Pour aller plus loin, d'autres méthodes devront être mises en place. Nous pouvons penser principalement à trois axes de recherche :

- Une meilleure utilisation des calculs *ab initio* afin de déterminer les paramètres réellement pertinents.
- Une approche d'extrapolation statistique des niveaux élevés, thème déjà abordé au Laboratoire par Jean-Paul Champion.

4. M. Hippler and M. Quack, *J. Chem. Phys.*, **116**(14), 6045–6055) (2002).
5. X.-G. Wang and T. Carrington Jr., *J. Chem. Phys.*, **119**(1), 101–117 (2003).

– L'utilisation d'une approche classique du type de celle que nous avons utilisée pour la molécule P_4 [P26], en collaboration avec Dimitrii Sadovskii à Dunkerque (thèse de Christophe Van-Hecke dont j'ai été rapporteur). Grossièrement, la méthode consiste à partir d'un modèle classique simple à peu de paramètres et d'en déduire, par transformations de contact, les valeurs des paramètres de l'hamiltonien effectif.

Une demande de bourse post-doctorale sur cette thématique a été présentée cette année à la Région Bourgogne.

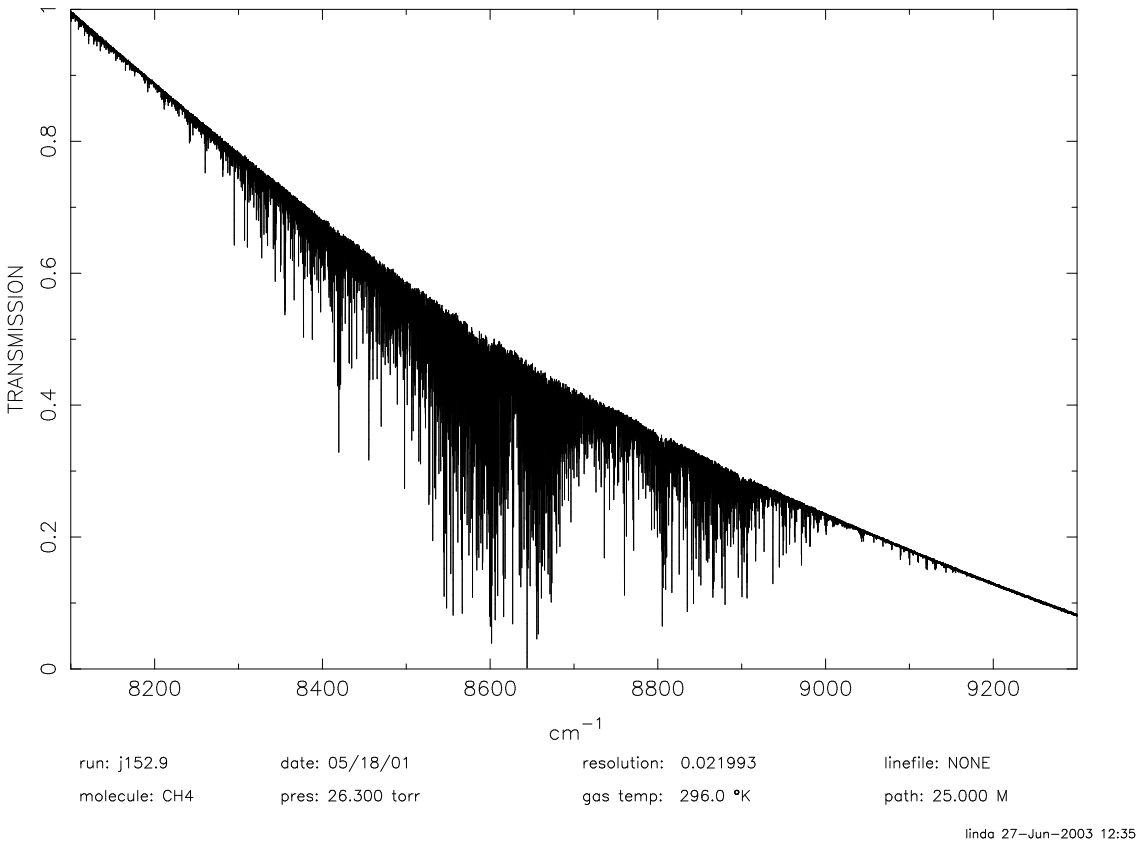

FIG. 2.4 – *La triacontade de CH_4. Source : L. R. Brown, JPL (Pasadena, USA).*

2.5 Article-clé

Est reproduit ici un article très général sur la spectroscopie de certains gaz à effet de serre, dont le méthane.

– [**P33 :** *Env. Chem. Lett.*, **1**, 86–91 (2003)] présente les outils développés au laboratoire pour la spectroscopie de CH_4, SF_6 et CF_4.

Environ Chem Lett (2003) 1:86–91
DOI 10.1007/s10311-002-0009-0

ORIGINAL PAPER

V. Boudon · J.-P. Champion · T. Gabard · G. Pierre · M. Loëte · C. Wenger

Spectroscopic tools for remote sensing of greenhouse gases CH_4, CF_4 and SF_6

Accepted: 13 September 2002 / Published online: 7 February 2003

Abstract Highly symmetrical molecules such as CH_4, CF_4 or SF_6 are known to be atmospheric pollutants and greenhouse gases. High-resolution spectroscopy in the infrared is particularly suitable for the monitoring of gas concentration and radiative transfers in the earth's atmosphere. This technique requires extensive theoretical studies for the modeling of the spectra of such molecules (positions, intensities and shapes of absorption lines). Here, we have developed powerful tools for the analysis and the simulation of absorption spectra of highly symmetrical molecules. These tools have been implemented in the spherical top data system (STDS) and highly-spherical top data system (HTDS) software available at http://www.u-bourgogne.fr/LPUB/shTDS.html. They include a compilation of modeled data obtained during the last 20 years. An overview of our latest results in this domain will be presented.

Keywords Greenhouse gases · Molecular spectroscopy · Simulation · CH_4 · SF_6 · CF_4 · Climate change

Introduction

Among the various gaseous pollutants that are present in the earth's atmosphere, the greenhouse gases require careful monitoring for the global warming survey. These species are very strong absorbers in the infrared region and some of them are chemically "inert" in the sense that they hardly react with other molecules and thus have a long or even extremely long lifetime in the atmosphere. These compounds have various natural or non-natural sources. The most abundant greenhouse gas is carbon dioxide (CO_2). Nonetheless, several other gases, even if present in much lower quantities, must be taken into account since their absorption is much stronger than that of CO_2. Table 1 shows selected data about important greenhouse gases, and especially their so-called "global warming potential" (GWP). This value compares the ability of a given molecule to trap heat in the atmosphere compared to CO_2 (that has thus a GWP equal to 1). More precisely, the GWP of a greenhouse gas is the ratio of global warming (both direct and indirect), also known as radiative forcing, between one unit mass of a greenhouse gas and one unit mass of carbon dioxide over a period of time.

The quantitative remote sensing of molecular species in the atmosphere is usually done by means of infrared absorption spectroscopy, either from the ground or from balloons (Pieroni et al. 2001) or satellites. It is thus necessary to develop precise models able to reproduce molecular absorption spectra in both frequency and intensity. CH_4, CF_4 and SF_6 are highly symmetrical molecules. Such compounds, also called "spherical-top" molecules have complex vibration – rotation spectra, which require specific theoretical treatment. During the last 40 years, our group has developed models for handling such complex spherical-top spectra (Moret-Bailly 1959, Champion et al. 1992). Spectrum calculations and fitting programs implementing these methods, as well as results from analyses, are available using the STDS (Wenger and Champion 1998) and HTDS (Wenger et al. 2000) software.

The aim of the present paper is to give an overview of what can be done with the STDS and HTDS tools in the field of greenhouse gas spectroscopy. Thus, after recalling a very few basic properties of XY_4 and XY_6 molecules and their spectroscopy, we will review the cases of methane, sulfur hexafluoride and carbon tetrafluoride.

V. Boudon can also be reached at http://www.u-bourgogne.fr/LPUB/tSM.html.

V. Boudon (✉) · J.-P. Champion · T. Gabard · G. Pierre · M. Loëte · C. Wenger
Laboratoire de Physique de l'Université de Bourgogne,
CNRS UMR 5027, 9 Av. A. Savary,
21078 Dijon Cedex, France
e-mail: Vincent.Boudon@u-bourgogne.fr

Table 1 Selected data about important greenhouse gases. Concentration is given in parts per trillion (10^{12}) in volume (pptv)

Gas	Global warming potential	Lifetime (years)	Concentration (pptv)	Annual increase (%)
CO_2[a, b]	1	~250	0.360×10^9	0.4
CH_4[a, b]	21	~12	1.720×10^6	1.6
CF_4[a, b]	6,500	~50,000	75.0	1.0
SF_6[a, c]	23,900	~3,200	3.8	8.0
SF_5CF_3[d]	22,200	~3,500	0.12	–

[a] http://www.epa.gov [b] Khalil 1999 [c] Geller et al. 1997 [d] Sturges et al. 2000

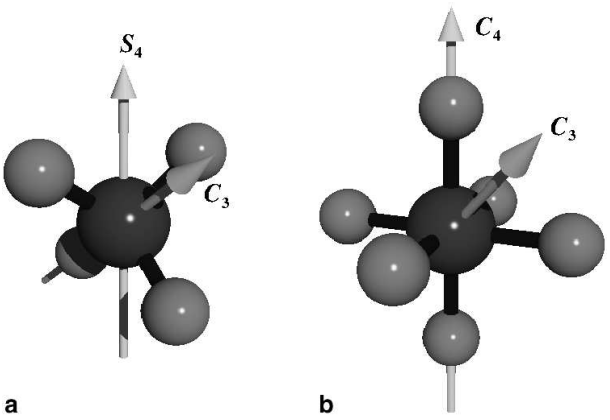

Fig. 1 a A tetrahedral molecule like CH_4. **b** An octahedral molecule like SF_6. Examples of symmetry axes are given (C_3 and C_4 are rotations of $2\pi/3$ and $2\pi/4$, respectively, and S_4 is a rotation of $2\pi/4$ combined with an inversion of all coordinates). The spectra strongly depend on these symmetry properties

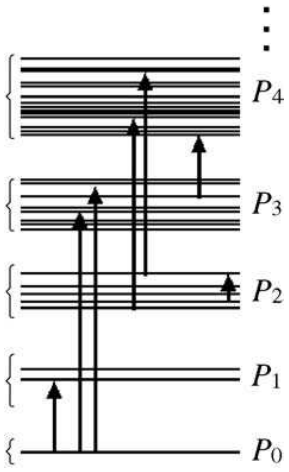

Fig. 2 Vibrational polyads for a molecule and examples of possible absorption transitions. Such a structure results in well-defined absorption windows, as shown in Fig. 3a in the case of methane

Theoretical considerations

Readers interested in the detailed theory of spherical-top spectra can refer to several of our previous papers (Champion et al. 1992; Cheblal et al. 1999). In this section, we will focus on the specific aspects of the methods developed and used in our group.

In order to determine gas concentrations in the atmosphere, it is necessary to compare in situ or remote spectroscopic measurements with synthetic spectra. This requires the calculation of transition frequencies and intensities. Both depend strongly on the symmetry of the molecule. Here, we consider so-called "spherical-top" molecules (molecules whose ellipsoid of inertia is a sphere), i.e., either tetrahedral molecules of type XY_4 or octahedral molecules of type XY_6. Their symmetry point group is thus either T_d or O_h, respectively. Examples of such molecules with their main symmetry elements are shown in Fig. 1.

Tetrahedral XY_4 molecules possess four fundamental frequencies of vibration, usually labeled by ν_1, ν_2, ν_3 and ν_4. Vibrations ν_1 and ν_3 correspond to stretching motions, while ν_2 and ν_4 correspond to bending motions. It is possible to observe the ν_3 and ν_4 fundamental frequencies in infrared absorption and all four fundamental frequencies using the Raman scattering technique. This can be explained by symmetry considerations that we will not develop here.

In the same way, octahedral XY_6 molecules have six fundamental frequencies of vibration, usually labeled by ν_1, ν_2, ν_3, ν_4, ν_5 and ν_6. Vibrations ν_1, ν_2 and ν_3 are stretching modes, while ν_4, ν_5 and ν_6 are bending modes. Only the ν_3 and ν_4 fundamental frequencies can be observed by infrared absorption, while only ν_1, ν_2 and ν_5 can be observed using Raman scattering. The ν_6 mode is optically inactive. This last point has some consequences that we will discuss later for SF_6.

Each vibrational band has a very complex rotational structure. The specificities of our approach for the analysis and the calculation of rotation-vibration spectra of these species can be summarized as follows:

- The fundamental, harmonic and combination bands of vibration are usually grouped in packets called *polyads*. Figure 2shows a schematic example of a vibrational polyad scheme of a molecule. The existence of such polyads results in well-defined absorption regions or "windows" in the spectra. Our method consists of a step-by-step study of the different polyads: P_0(the ground state), P_1, P_2, ...

All these techniques are implemented in the programs included in the STDS (Wenger and Champion 1998) and

HTDS (Wenger et al. 2000) packages. Moreover, specific methods have also been developed for the modeling of line shifts and line broadenings that are induced by collisions between molecules. This is essential for the remote sensing of gas mixtures like the earth's atmosphere. This point will be discussed later when dealing with the case of methane.

Methane (CH_4)

Methane is a relatively abundant constituent of planetary atmospheres. It is also one of the major greenhouse gases on earth (Table 1) with many natural, industrial or agricultural sources. As a result, remote sensing applications require good knowledge of its spectroscopic parameters: position, intensity, air-broadened line width, lower-state transition energy, self-broadened line width, temperature dependence of the air-broadened width and the air-broadened pressure shift. In recent years, laboratory studies have resulted in significant revisions of these molecular line parameters in the public databases (Rothman et al. 1992; Rothman et al. 1998; Goldman et al. 2000).

The main difficulties in modeling the vibration – rotation spectrum of methane arise from the existence of essential degeneracies (induced by symmetry properties), accidental resonances (between stretching and bending vibrational motions) and broad rotational fine structure (large inertia constant).

The accuracy of the modeling of the methane infrared (IR) spectrum is enough to satisfy the needs of atmospheric applications: a few 10^{-3} cm^{-1} for line positions and a few percent for line intensities, including $^{12}CH_4$, $^{13}CH_4$ and CH_3D.

The low-resolution overview infrared spectrum of methane plotted in Fig. 3a reflects its polyad structure. Numerous experimental and theoretical studies have been devoted to its analysis over decades. At present, the lower polyads (P_0: ground state – P_1: *dyad* – P_2: *pentad* – P_3: *octad) covering the region from 0 to 4,850 cm*$^{-1}$ *can be considered as well known.*

Appropriate effective frequency and intensity models have been developed and applied to analyses of the ground state (Champion et al. 1989a; Roche and Champion 1991), in the range below 10 μm, the dyad (Brown et al. 1989; Champion et al. 1989b; Roche and Champion 1991; Ouardi et al. 1996) from 5 to 10 μm (see Fig. 4), and the pentad (Hilico et al. 1994; Féjard et al. 2000) from 3 to 5 μm. The analysis of the next polyad (octad) observed from 2 to 3 μm has recently been performed (Hilico et al. 2001). The upper polyad (tetradecad, P_4) is only partially analyzed (Robert et al. 2001).

The line parameters of the dyad system (ν_2 and ν_4 interacting bands) are modeled with an accuracy of 0.00006 cm^{-1} for positions and 3% for intensities respectively. For the pentad system (ν_1, ν_3, $2\nu_2$, $\nu_2+\nu_4$, $2\nu_4$) around 3 μm, the accuracy achieved is 0.002 cm^{-1} for

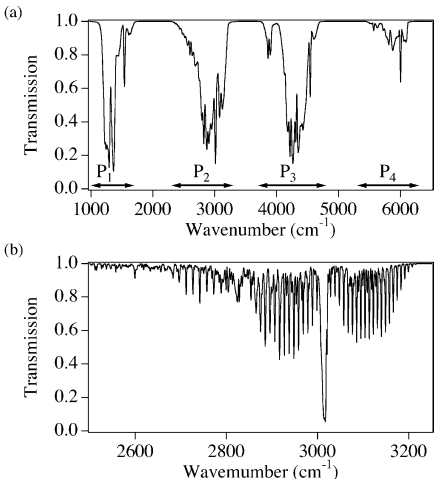

Fig. 3 Simulation of the infrared absorption spectrum of methane at different resolutions. **a** is an overview of the first polyads in the

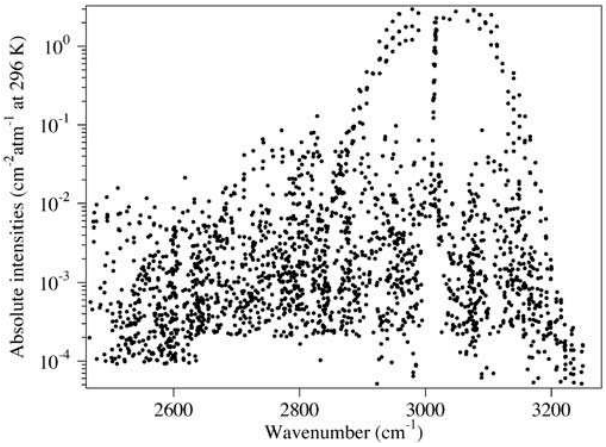

Fig. 4 Distribution of measured line intensities in the region of the ν_3 band of methane. Each *dot* represents a transition. The intensity scale is logarithmic, showing that strong as well as very weak transitions are considered in the analysis

positions and 3% for intensities (see Fig. 4). Selected transitions from the ν_3 band of CH_4 are proposed as secondary standards with absolute accuracy of 0.002 cm^{-1} for positions and 2% for intensities. Figure 3b shows an overview of the strongest ν_3 band. Of course, all the lines shown on this last figure have their own complex substructure that can be observed at higher resolution.

In addition to $^{12}CH_4$, the next two main isotopomers ($^{13}CH_4$ and CH_3D) contribute also significantly to the absorption spectrum. They have motivated several works. In particular, a global analysis of nine interacting bands of CH_3D in the 3 μm region has been published recently (Nikitin et al. 2002). Further details, updates and refer-

ences are available at http://www.u-bourgogne.fr/LPUB/methane/metspec.htm

Let us now say a few words about the problem of line shapes which we illustrate with the case of methane. As already explained, the remote sensing and detection of such molecular species as spherical tops in the atmosphere is usually done through the measurements of spectra in the infrared region. In most of the thermodynamic conditions encountered in this medium, a given spectrum cannot be modeled as a simple sum of profiles over all the individual lines. While the line widths do depend on the individual quantum numbers of the lines, the collisional transfers of populations in the lower and upper states of the transitions induce a phenomenon known as "line-mixing", or collisional coupling of lines (Pieroni et al. 1999, 2000, 2001; Grigoriev et al. 2001). As a consequence, the spectrum of a given vibrational band must be calculated as a whole, to give satisfactory agreement with the measurements.

Sulfur hexafluoride, SF_6

Some new interest in sulfur hexafluoride studies has appeared recently, since this compound has proved to be a species of growing importance in the field of atmospheric physics and chemistry (Reddmann et al. 2001). In fact, it is now recognized as a pollutant that can contribute to the greenhouse effect (Khalil 1999; Dervos and Vassiliou 2000). This molecule is a by-product of electrical industries. Because of its chemical stability and diffusion properties, it is also the "air" in "Nike Air" shoes. At present, the concentration of SF_6 in the earth's atmosphere is small, but increases at a rate of about 7% per year due to industrial emissions (Geller et al. 1997; Volk et al. 1997). Moreover, its lifetime in the atmosphere is very long, reaching 3,200 years (Geller et al. 1997; Volk et al. 1997) or maybe even more (Reddmann et al. 2001) as shown in Table 1. This molecule is also observed at low altitude, near large urban areas (Ho and Schlosser 2000). The small, but regularly increasing SF_6 concentration is also used to understand gas transport and circulation phenomena in the middle atmosphere (Eklund 1999; Hall et al. 1999; Khalil 1999; Manzini and Feichter 1999; Ray et al. 1999; Kjellström et al. 2000) or to monitor the distribution of other pollutants such as chlorofluorocarbons (CFCs) (Hurst et al. 1997; Wamsley et al. 1998; Romashkin et al. 1999). For all these reasons, correct quantitative measurements and monitoring of SF_6 in the earth's atmosphere is necessary.

However, as we have shown in Boudon and Pierre (2002) and in earlier papers (Boudon et al. 1998, 2001; Bermejo et al. 2000), that the spectroscopy of this molecule is still not very well known. The present knowledge about SF_6 spectroscopy is very limited compared to methane for instance. In particular, the region of the ν_3 fundamental frequency near 948 cm^{-1} is of great importance since its very strong absorption is responsible for the huge greenhouse capabilities of SF_6.

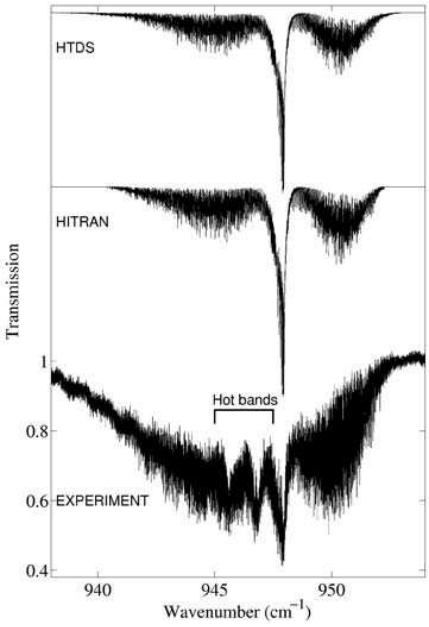

Fig. 5 Comparison between STDS and HITRAN simulations of the ν_3 stretching fundamental of SF_6 with an experimental spectrum from N. Lacome

Nevertheless, if the ν_3=1 level itself is very well known (Acef et al. 2000), the hot bands in this region, which largely contribute to the absorption (remember that the ground state population is only 30% at 300 K), are very poorly known. The knowledge of these hot bands requires the study of many other vibrational states, especially those with low energy.

Up to now, only one hot band of SF_6 has been analyzed in detail: $\nu_4+\nu_6-\nu_6$ in the ν_4 bending region (Boudon et al. 2001). Several vibrational levels have been analyzed with the aim of understanding the much denser ν_3 region. However, this work is in progress and still requires a lot of effort, from both the experimental and theoretical sides. One important technical difficulty arising when dealing with octahedral molecules like SF_6 is related to the ν_6 bending mode. This vibration, which is the lowest in energy and thus very important for hot band generation, is inactive in both infrared absorption and Raman scattering (see Theoretical considerations). Thus, some of our recent works (Boudon et al. 1998, 2001), although they do not concern the ν_3 region directly, intended to collect indirect information on this mode through the analysis of combination levels associated with this vibration. The final aim of this is the analysis of $\nu_3+\nu_6-\nu_6$.

Figure 5 shows a comparison between data from the existing databases and an actual experimental spectrum of the ν_3 region. While in this case the HTDS simulation and the HITRAN data (Rothman et al. 1992; Rothman et al. 1998) give quite similar results, the lack of hot band data is very clear when compared to the real spectrum. We are presently working on the analysis of the most important

90

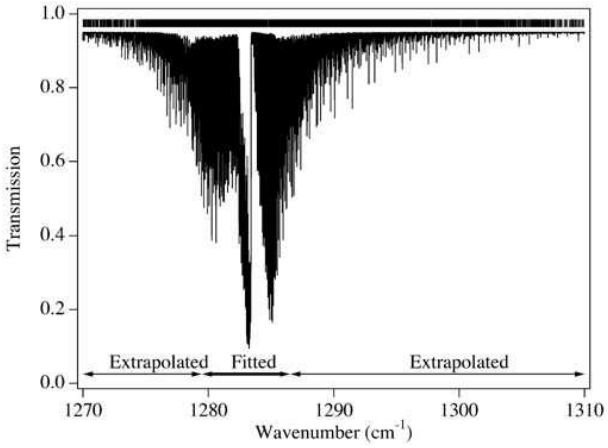

Fig. 6 Absorption spectrum of the ν_3 band of CF_4 at 296 K calculated using STDS. The parameters provided in STDS in this case were obtained through a fit up to J=40. Higher J values are extrapolated

hot bands in the region, namely $\nu_3+\nu_6-\nu_6$ and $\nu_3+\nu_5-\nu_5$. The last one should benefit from our recent study of the Raman spectrum of ν_5 (Boudon and Bermejo 2002).

As for methane, the problem of line broadening of SF_6 transitions in an SF_6/N_2 mixture has been treated recently in the case of the ν_3 band (Gamache et al. 2001).

Tetrafluoromethane (CF_4)

The spherical top data system (STDS) and highly-spherical top data system (HTDS) databases contain parameters for several other spherical-top molecules. The most interesting as far as atmospheric absorption is concerned is CF_4. As for SF_6, this is an important greenhouse gas with an extremely long lifetime in the atmosphere as shown in Table 1 and in several references (Harnisch et al. 1996; Khalil 1999). Furthermore, CF_4 is one of the most important polyfluorocarbons (PFCs) measured in the earth's atmosphere. It is one of the by-products of aluminum manufacturing. Its concentration is increasing at ~1% per year. However, the CF_4 spectroscopy is even less known than that of SF_6. Figure 6 shows an example of STDS calculation for the very strongly absorbing ν_3 stretching fundamental (Gabard et al. 1995) and also illustrates how the spectrum calculations can be extrapolated to higher J values than those that were measured experimentally.

Conclusion

We have presented the spherical top data system (STDS) and highly-spherical top data system (HTDS) spectroscopic tools for the simulation of spherical-top spectra. Compared to other classical databases such as HITRAN (high-resolution transmission molecular absorption database; Rothman et al. 1992, 1998; Goldman et al. 2000), these packages offer the advantage that they not only provide computed lists of measured transition frequencies and intensities, but rather programs and parameter files that allow the user to calculate spectra for specific physical conditions. This allows extrapolation to higher temperatures, pressures, or excited levels, within some reasonable limits, of course.

We have discussed the examples of CH_4, SF_6 and CF_4. It is clear that, even for the widely studied methane molecule, a lot of work still has to be done for the complete and precise modeling of the absorption spectra. Our group will thus continue its efforts in this direction. At the same time, similar tools will be developed for other types of molecules, which are also of atmospheric interest.

Acknowledgments Région Bourgogne is gratefully acknowledged for supporting the Laboratoire de Physique de l'Université de Bourgogne. The authors thank Pr. N. Lacome (LADIR/Université Pierre et Marie Curie, Paris, France) for providing the SF_6 experimental spectrum of Fig. 5, and Pr. H.R. Jauslin (LPUB/Université de Bourgogne) for carefully reading and correcting the manuscript.

References

Acef O, Bordé CJ, Clairon A, Pierre G, Sartakov B (2000) New accurate fit of an extended set of saturation data for the ν3 band of SF6: comparison of Hamiltonians in the spherical and cubic tensor formalisms. J Mol Spectrosc 199:188–204

Bermejo D, Martínez RZ, Loubignac E, Pierre G (2000) Simultaneous analysis of the ν2 Raman and ν2+ν6 infrared spectra of the SF6 molecule. J Mol Spectrosc 201:164–171

Boudon V, Bermejo D (2002) First high resolution Raman spectrum and analysis of the ν5 bending fundamental of SF6. J Mol Spectrosc 213:139–144

Boudon V, Pierre G (2002) Rovibrational spectroscopy of sulphur hexafluoride: a review. In: Recent research developments in molecular spectroscopy, vol. 1. Transworld Research Network, Trivandrum, India, pp 339–422

Boudon V, Hepp M, Herman M, Pak I, Pierre G (1998) High-resolution jet-cooled spectroscopy of SF6: the ν2+ν6 combination band of 32SF6 and the ν3 band of the rare isotopomers. J Mol Spectrosc 192:359–367

Boudon V, Bürger H, MKadmi EB (2001) High resolution spectroscopy and analysis of the ν4 bending region of SF6 near 615 cm–1. J Mol Spectrosc 205:304–311

Brown LR, Loëte M, Hilico JC (1989) Line strengths of the ν2 and ν4 bands of 12CH4 and 13CH4. J Mol Spectrosc 133:273–311

Champion JP, Hilico JC, Brown LR (1989a) The vibrational ground state of 12CH4 and 13CH4. J Mol Spectrso. 133:244–255

Champion JP, Hilico JC, Wenger C, Brown LR (1989b) Analysis of the ν2/ν4 dyad of 12CH4 and 13CH4. J Mol Spectrosc 133:256–272

Champion JP, Loëte M, Pierre G (1992) Spherical top spectra. In: Rao KN, Weber A (eds) Spectroscopy of the earth's atmosphere and interstellar medium, Academic Press, New York, pp339–422

Cheblal N, Loëte M, Boudon V (1999) Development of the dipole moment and polarizability operators of octahedral molecules. J Mol Spectrosc 197:222–231

Dervos CT, Vassiliou P (2000) Sulphur hexafluoride (SF6): Global environmental effects and toxic byproduct formation. Air Waste Manage Assoc 50:137–141

Eklund B (1999) Comparison of line- and point-source releases of tracer gases. Atmos Environ 33:1065–1071

Féjard L, Champion JP, Jouvard JM, Brown LR, Pine AS (2000) The intensities of methane in the 3–5 μm region revisited. J Mol Spectrosc 201:83–94

Gabard T, Nikitin A, Champion JP, Pierre G, Pine AS (1995) 2ν3 band of 12CF4 and its simultaneous analysis with ν3. J Mol Spectrosc 170:431–448

Gamache RR, Lacome N, Pierre G, Gabard T (2001) Nitrogen broadening of SF6 transitions in the ν3 band. J Mol Struct 599:279–292

Geller LS, Elkins JW, Lobert JM, Clarke AD, Hurst DF, Butler JH, Myers RC (1997) Tropospheric SF6: Observed latitudinal distribution and trends, derived emissions and interhemispheric exchange time. Geophys Res Lett 24:675–678

Goldman A, Gamache RR, Perrin A, Flaud JM, Rinsland CP, Rothman LS (2000) HITRAN partition functions and weighted transition-moments squared. J Quant Spectrosc Radiat Transfer 66:455–86

Grigoriev IM, Filippov NN, Tonkov NN, Gabard T, Le Doucen R (2001) Estimation of line parameters under line mixing effects: the ν3 band of CH4 in helium. J Quant Spectrosc Radiat Transfer 69:189–204

Hall TM, Waugh DW, Borering KA, Plumb RA (1999) Evaluation of transport in stratospheric models. J Geophys Res 104:18815–18839

Harnisch J, Brochers R, Fabian P, Gäggeler HW, Schrotterer U (1996) Effect of natural tetrafluoromethane. Nature 384:32

Hilico JC, Champion JP, Toumi S, Tyuterev VG, Tashkun SA (1994) New analysis of the pentad system of methane and prediction of the (pentad-pentad) spectrum. J Mol Spectrosc 168:455–476

Hilico JC, Robert O, Loëte M, Toumi S, Pine AS, Brown LR (2001) Analysis of the interacting octad system of 12CH4. J Mol Spectrosc 208:1–13

Ho DT, Schlosser P (2000) Atmospheric SF6 near a large urban area. Geophys Res Lett 27:1679–1682

Hurst DF, Balkwin PS, Myers RC, Elkins JW (1997) Behavior of trace gas mixing ratios on a very tall tower in North Carolina. J Geophys Res 102:8825–8835

Khalil MA (1999) Non-CO2 greenhouse gases in the atmosphere. Annu Rev Energy Environ 24:645–661

Kjellström E, Feitcher J, Hoffman G (2000) Transport of SF6 and 14CO2 in the atmospheric general circulation model ECHAM4. Tellus 52B:1–18

Manzini E, Feichter J (1999) Simulation of the SF6 tracer with the middle atmosphere MAECHAM4 model: Aspects of the large-scale transport. J Geophys Res 104:31097–31108

Moret-Bailly J (1959) Introduction au calcul de l'énergie de vibration-rotation des molécules à symétrie sphérique. Cah Phys 112:476–494

Nikitin A, Brown LR, Féjard L, Champion JP, Tyuterev VG (2002) Analysis of the CH3D nonad from 2000 to 3300 cm–1. J Mol Spectrosc 216:225–251

Ouardi O, Hilico JC, Loëte M, Brown LR (1996) The hot bands of methane between 5 and 10 μm. J. Mol. Spectrosc. 180:311–322

Pieroni D, Van-Thanh N, Brodbeck C, Claveau C, Valentin A, Hartmann JM, Gabard T, Champion JP, Bermejo D, Domenech JL (1999) Experimental and theoretical study of line mixing in methane spectra. I. The N2 broadened ν3 band at room temperature. J Chem Phys 110:7717–7732

Pieroni D, Van-Than N, Brodbeck C, Hartman JM, Gabard T, Champion JP, Bermejo D, Domenech JL, Claveau C, Valentin A (2000) Experimental and theoretical study of line mixing in methane spectra. IV. Influence of the temperature and of the band. J Chem Phys 113:5776–5783

Pieroni D, Hartmann JM, Camy-Peyret C, Jeseck P, Payan S (2001) Influence of line mixing on absorption by CH4 in atmospheric balloon-borne spectra near 3.3 μm. J Quant Spectrosc Radiat Transfer 68:117–133

Ray EA, Moore FL, Elkins JW, Dutton GS, Fahey DW, Vömel H, Oltmans SJ, Rosenlof KH (1999) Transport into the northern hemisphere lowermost stratosphere revealed by in situ tracer measurements. J Geophys Res 104:26565–26580

Reddmann T, Ruhnke R, Kouker W (2001) Three dimensional model simulations of SF6 with mesospheric chemistry. J Geophys Res 106:14525–14537

Robert O, Hilico JC, Loëte M, Champion JP, Brown LR (2001) First assignment and line strengths of the 4ν4 band of 12CH4 near 1.9 μm. J Mol Spectrosc 209:14–23

Roche C, Champion JP (1991) Analysis of dyad—dyad transitions of 12CH4 and 13CH4. Can J Phys 69:40–51

Romashkin PA, Hurst DF, Elkins JW, Dutton GS, Wamsley PR (1999) Effect of the tropospheric trend on the stratospheric tracer—tracer correlations: Methyl chloroform. J Geophys Res 104:26643–26652

Rothman LS, Gamache RR, Tiping RH, Rinsland CP, Smith MAH, Benner DC, Malathy Devi V, Flaud JM, Camy-Peyret C, Perrin A, Goldman A, Massie ST, Brown LR, Toth RA (1992) The HITRAN molecular database: editions of 1991 and 1992. J Quant Spectrosc Radiat Transfer 48:469–507

Rothman LS, Rinsland CP, Goldman A, Massie ST, Edwards DP, Flaud JM, Perrin A, Camy-Peyret C, Dana V, Mandin JY, Schroeder J, McCann A, Gamache RR, Wattsin RB, Yoshino K, Chance KV, Juck KW, Brown LR, Nemtchechin V, Varanasi P (1998) The HITRAN molecular spectroscopic database and HAWKS (HITRAN atmospheric workstation): 1996 edition. J Quant Spectrosc Radiat Transfer 60:665–710

Sturges WT, Wallington TJ, Hurley MD, Shine KP, Shira K, Engel A, Oram DE, Penkett SA, Mulvaney R, Brenninkmeijer CAM (2000) A potent greenhouse gas identified in the atmosphere: SF5CF3. Science 289:611–613

Volk CM, Elkins JW, Fahey DW, Dutton GS, Gilligan JM, Loewenstein M, Podolske JR, Chan KR, Gunson MR (1997) Evaluation of sources gas lifetimes from stratospheric observations. J Geophys Res 102:25543–25564

Wamsley PR, Elkins JW, Fahey, DW, Dutton GS, Volk CM, Myers RC, Montzka SA, Butler JH, Clarke AD, Fraser PJ, Steele LP, Lucarelli MP, Atlas EL, Schauffler SM, Blake DR, Rowland FS, Sturges WT, Lee JM, Penkett SA, Engel A, Stimpfle RM, Chan KR, Weisenstein DK, Ko MKW, Salawitch RJ (1998) Distribution of halon-1211 in the upper troposphere and the 1994 total bromine budget. J Geophys Res 103:1513–1526

Wenger C, Champion JP (1998) Spherical Top Data System (STDS) software for the simulation of spherical top spectra. J Quant Spectrosc Radiat Transfer 59:471–480

Wenger C, Boudon V, Champion JP, Pierre G (2000) Highly-Spherical Top Data System (HTDS) software for the spectrum simulation of octahedral XY6 molecules. J Quant Spectrosc Radiat Transfer 66:1–16

TROISIÈME PARTIE

Chapitre

3

Spectroscopie de Diverses Molécules à Haute Symétrie

Publications P10, P15, P17, P21, P22, P26, P29, P31, P34

3.1 Introduction

Outre CH_4 et SF_6 abordées dans les chapitres précédents, la famille des molécules toupies sphériques comprend de nombreuses autres espèces dont beaucoup présentent des intérêts variés, tant sur le plan fondamental que sur celui des applications réelles ou potentielles. Les outils théoriques ou informatiques mis en place pour l'étude du méthane ou de l'hexafluorure de soufre m'ont également permis de réaliser un certain nombre d'analyses sur certaines de ces molécules "exotiques", en collaboration avec plusieurs équipes expérimentales.

3.2 Les molécules étudiées

Je présente ici succinctement les différentes molécules toupies sphériques que j'ai été amené à étudier ces dernières années.

P_4 (phosphore blanc). Cette molécule constitue la plus simple possible des toupies sphériques, puisqu'elle consiste en quatre atomes identiques disposés en un tétraèdre régulier. Elle ne possède que trois modes normaux de vibration : $\nu_1(A_1)$, $\nu_2(E)$ et $\nu_3(F_2)$. Seul $\nu_3(F_2)$ est actif en absorption infrarouge [P10]. La structure géométrique très simple et le petit nombre de modes vibrationnels de P_4 ont permis une étude de sa structure rovibrationnelle par l'approche classique, menant à quelques prédictions intéressantes [P26], qui restent toutefois à confirmer expérimentalement.

GeD_4 et GeF_4 (germane et tétrafluorure de germanium). Les molécules à base de germanium sont difficiles à étudier du fait des cinq isotopes de cet élément présents en abondance naturelle. En collaboration avec le groupe du Pr. Hans Bürger àWuppertal (Allemagne), nous avons pu étudier les spectres d'échantillons isotopiques de $^{70}GeD_4$ [P31] et $^{70}GeF_4$ [P21].

SeF_6 (hexafluorure de sélénium). Certains isotopomères de cette molécule très similaire à SF_6 ont des applications médicales. J'ai participé à l'analyse de la bande de pliage ν_4 de $^{80}SeF_6$ [P22].

WF_6 (hexafluorure de tungstène). J'ai été amené à enregistrer des spectres d'absorption infrarouge en jet supersonique (transformée de Fourier et diode laser) de cette molécule lourde lors de mon stage post-doctroal au sein du groupe du Pr. Martin Quack à l'ETH Zürich [P29]. Ce travail était un préliminaire à l'étude de la molécule "open-shell" ReF_6 dont nous reparlerons au Chapitre IV.3.

$Mo(CO)_6$ (hexacarbonyle de molybdène). Les carbonyles de métaux de transition présentent une absorption extrêmement intense dans la région de l'élongation C–O, vers 2000 cm^{-1}. En collaboration avec Pierre Asselin et ses collègues (Université Pierre et Marie Curie, Paris), nous avons étudié le spectre d'absorption en jet supersonique de la bande ν_6. Ce travail était un préliminaire à l'étude de la molécule "open-shell" $V(CO)_6$ dont nous reparlerons au Chapitre IV.2

3.3 Articles-clés

Sont reproduits ici quatre articles illustrant quelques résultats originaux.

- [**P10 :** *Chem. Phys. Lett.*, **305**, 21–27 (1999)] présente l'étude du spectre d'absorption infrarouge de la bande d'élongation ν_3 de la molécule P_4.
- [**P31 :** *J. Mol. Spectrosc.*, **216**, 408–418 (2002)] concerne l'analyse de l'ensemble des bandes fondamentales de la molécule $^{70}GeD_4$. Ce travail a permis la première détermination expérimentale précise de la longueur de liaison du germane.
- [**P12 :** *J. Mol. Spectrosc.*, **197**, 222–231 (1999)] présente le formalisme tensoriel adapté aux molécules octaédriques de type XY_6. Le cas de l'effet Stark pour ces molécules est également abordé dans cet article.
- [**P17 :** *J. Mol. Spectrosc.*, **201**, 95–108 (2000)] concerne l'étude semi-classique de la structure rovibrationnelle de la bande ν_6 d'élongation C–O de $Mo(CO)_6$, réalisée en collaboration avec des collègues de l'Université du Littoral à Dunkerque. La structure des niveaux d'énergie rotationnelle est très particulière du fait d'une constante de Coriolis anormalement petite dans le niveau vibrationnel $v_6 = 1$. L'analyse semi-classique permet de comprendre certains aspects étonnants de cette structure.

ELSEVIER

14 May 1999

Chemical Physics Letters 305 (1999) 21–27

CHEMICAL PHYSICS LETTERS

High-resolution Fourier transform infrared spectroscopy and analysis of the ν_3 fundamental band of P_4

V. Boudon [a,*], E.B. Mkadmi [b], H. Bürger [b], G. Pierre [a]

[a] *Laboratoire de Physique de l'Université de Bourgogne–CNRS, B.P. 47 870, F-21078 Dijon, France*
[b] *Anorganische Chemie, Universität-Gesamthochschule, D-42097 Wuppertal, Germany*

Received 25 January 1999; in final form 1 March 1999

In Memoriam Marco Haeser

Abstract

We present the first high-resolution infrared absorption study of the ν_3 fundamental of white phosphorus, P_4. This spectrum has been analyzed using the STDS (Spherical Top Data System) software. The band center lies at 466.286 cm^{-1}. With the approximation $(B\zeta)_3 = -B_0/2$, we found that the ground-state bond length is $r_0 = 219.58$ pm. This value is consistent with that of ab initio studies reported previously but significantly different from a value obtained from a Raman study.

1. Introduction

In spite of its fundamental importance as a well-known metastable modification of a ubiquitous, common element of technical importance the structure and spectroscopic parameters of the free P_4 molecule are not known at high accuracy. Experimental studies related to the structure of P_4 are (i) an old gas phase electron diffraction study yielding $r_g \approx r_0$(P–P) = 2.21(2) Å [1] and (ii) a low-temperature X-ray diffraction study of crystalline white phosphorus giving a P–P bond length of 2.209 ± 0.005 Å [2]. Since P_4 has no permanent dipole moment and is therefore not amenable to microwave spectroscopy, (iii) the vibration–rotation Raman spectrum of the ν_2 band studied by Brassington et al. [3] provided the hitherto unique experimental information on the ground-state (GS) rotational constant $B_0 = 0.11015 \pm 0.00005$ cm^{-1}, from which $r_0 = 2.2228 \pm 0.0005$ Å was calculated.

This apparently very accurate P–P bond length has been seriously called into question by two recent high-level ab initio calculations [4,5]. These definitely rule out P–P bond lengths greater than 2.20 Å, and their best estimates, after applying empirical corrections, are $r_e = 2.194$ Å [4] and $r_e = 2.186 \pm 0.001$ Å[5]. With the help of the ab initio anharmonic force field a 'true' r_0 value, 2.191 ± 0.001 Å, was predicted [5], which is more than 0.03 Å shorter than that deduced from the Raman experiment [3].

Less disputable but nevertheless numerically not consistent is the location of the three vibrational fundamentals of P_4. In the most recent Raman study

* Corresponding author. Fax: +33 3 80 39 59 17; e-mail: boudon@jupiter.u-bourgogne.fr

0009-2614/99/$ - see front matter
PII: S0009-2614(99)00348-6

of P_4 at 540 K [6] the following band centers have been determined:

$\nu_1(A_1)$	600.51 ± 0.01 cm^{-1}
$\nu_2(E)$	360.813 ± 0.014 cm^{-1}
$\nu_3(F_2)$	466.925 ± 0.009 cm^{-1}

The wavenumbers of ν_1 and ν_3 represent the centers of the Q branches. The ν_1 to ν_3 wavenumbers differ by 5–6 cm^{-1} from those obtained at 580 K that were reported by Bosworth et al. [7]. The only infrared (IR)-active fundamental ν_3 has been studied at low resolution in the gas phase at 503 K, and the band center was located at 464.5 cm^{-1}[8].

The authors of Ref. [5] do not endorse these figures and they believe that hardly any discrepancy exceeding a few cm^{-1} is possible with regard to their 'best' values, which are 625, 374 and 472 cm^{-1}, respectively, for ν_1, ν_2 and ν_3. Part of this apparent discrepancy is ascribed to the fact that at the elevated temperatures of the relevant measurements a shift to small wavenumber is expected due both to vibrational and rotational population of highly excited states [5].

In order to measure a state-resolved rovibrational band of P_4 in the IR, to determine the ground- and excited-state rotational constants B_0 and B_3, to settle the disagreement concerning the structure of P_4, and to determine the band center of ν_3, we have performed a high-resolution IR study of this band at the lowest temperature feasible, 413 K. We have resolved the Q branch and the tetrahedral fine structure of the J clusters in the P and R branches and unambiguously determined several spectroscopic parameters up to third order that enable a satisfactory reproduction of the experimental spectrum by a simulation. Here we report our results.

2. Experiment

Measurements were performed using a Bruker 120HR interferometer employing an external stainless steel cell of 140 cm length and 8 cm inner diameter equipped with KBr windows. The parallel external beam of the interferometer was used in conjunction with an external detector chamber similar to the arrangement described in Ref. [9]. During the experiment the cell was heated to 140°C. The interferometer was equipped with a globar source, a 3.5 μm Mylar beam splitter and a liquid helium-cooled B:Si detector. A 12.5 μm low-pass filter was used, and the 370–800 cm^{-1} region studied. The

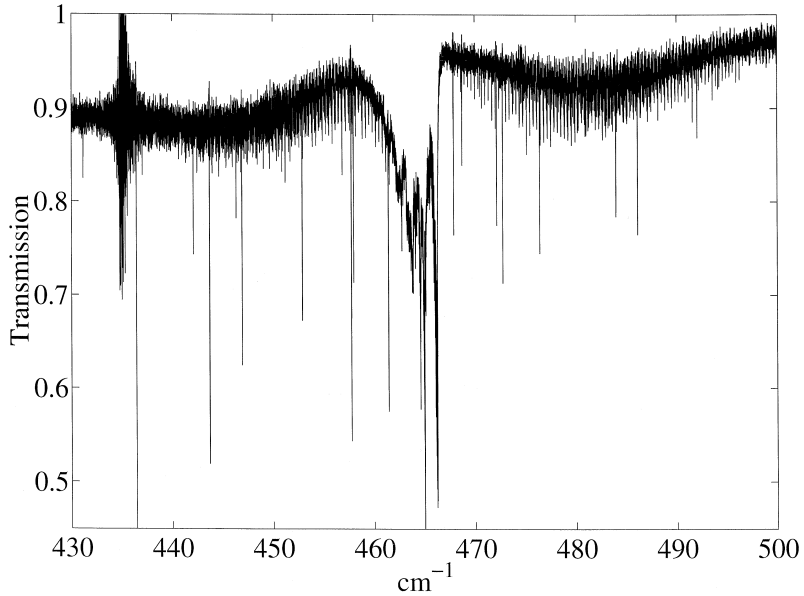

Fig. 1. Global view of the ν_3 band of P_4.

Table 1
Effective parameters for the ν_3 band of P_4. The standard deviation is given in parentheses, in the units of the last two digits

Level	Order	Parameter	$t^{\Omega(K,n\Gamma)\Gamma_v\Gamma'_v}_{\{s\}\{s'\}}$		Value/cm^{-1}	Notation of Robiette et al.	Constraint
		$\Omega(K,n\Gamma)$	$\{s\}\Gamma_v$	$\{s'\}\Gamma' - v$			
GS	0	2(0,0A$_1$)	000A$_1$	000A$_1$	0.1128757(25)	B_0	
	2	4(0,0A$_1$)	000A$_1$	000A$_1$	-2.0347×10^{-8}	$-D_0$	Fixed
		4(4,0A$_1$)	000A$_1$	000A$_1$	-4.5675×10^{-10}	$-(\sqrt{15}/4\sqrt{2})D_{0t}$	Fixed
$\nu_3=1$	0	0(0,0A$_1$)	001F$_2$	001F$_2$	466.17262(20)	ν_3	
	1	1(1,0F$_1$)	001F$_2$	001F$_2$	Fixed to $3\sqrt{2}\,B_0\zeta_3$ with $\zeta_3=-1/2$		
	2	2(0,0A$_1$)	001F$_2$	001F$_2$	$2.387(15)\times10^{-5}$	B_3-B_0	
		2(2,0E)	001F$_2$	001F$_2$	$-4.893(36)\times10^{-5}$	$-(1/2)\alpha_{220}-6\alpha_{224}$	
		2(2,0F$_2$)	001F$_2$	001F$_2$	2.080×10^{-4}	$-(3/4)\alpha_{220}+6\alpha_{224}$	Fixed
	3	3(1,0F$_1$)	001F$_2$	001F$_2$	$-5.385(35)\times10^{-7}$	$-(3\sqrt{3}/4\sqrt{2})F_{110}$	
		3(3,0F$_1$)	001F$_2$	001F$_2$	$-3.342(26)\times10^{-7}$	$(3\sqrt{5}/2)F_{134}$	
		656 lines fitted	$J_{max}=63$	$\sigma=2.54\times10^{-3}$ cm^{-1}			

resolution (1/maximum optical path difference) was adjusted to 6×10^{-3} cm^{-1}, and trapezoidal apodization applied. A total of 22 scans were collected, and a signal-to-noise ratio of the power spectrum of ca. 50 was achieved. Calibration was done with H_2O lines taken from Ref. [10] in the 500–550 cm^{-1} region. Wavenumber accuracy is 1×10^{-3} cm^{-1}.

P_4 was evaporated from a heated glass container in a flow of Ar passing beforehand through a capillary of 100 cm length and 0.6 mm diameter to avoid back diffusion. This container the temperature of which was adjusted to ca. 120°C was connected to the absorption cell. The absorption cell was continuously pumped, removed P_4 being condensed in a

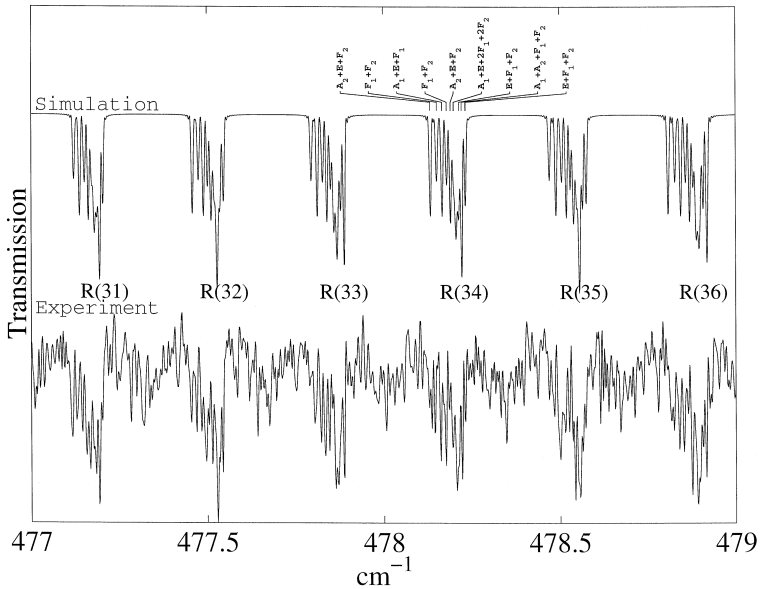

Fig. 2. Detailed portion in the *R*-branch of the ν_3 band of P_4 compared to the simulation. The *J* values are indicated. Symmetry assignments are shown for the *R*(34) cluster.

liquid nitrogen trap to which a pressure gauge was connected. A capillary in the vacuum line served to adjust the pumping efficiency such that a total gas pressure of ca. 3000 Pa was maintained in the absorption cell.

3. Theory

X_4 molecules like phosphorus possess three normal modes of vibration, say ν_1, ν_2 and ν_3, of respective symmetry A_1, E and F_2 in the T_d point group [11,6]. $\nu_3(F_2)$ is the only IR-active fundamental (the two others are Raman active).

The theoretical model described below to develop the Hamiltonian operator is based on the tensorial formalism and vibrational extrapolation methods used in Dijon. These methods have already been explained for example in Ref. [12]. We recall here the basic principles and their application to the case of an X_4 tetrahedral molecule.

If we consider an X_4 molecule for which the vibrational levels are grouped in a series of polyads designed by P_k ($k=0,\ldots,n$), P_0 being the ground state (GS), the Hamiltonian operator can be put in the following form (after performing some contact transformations):

$$\mathscr{H} = \mathscr{H}_{\{P_0 \equiv \mathrm{GS}\}} + \mathscr{H}_{\{P_1\}} + \cdots + \mathscr{H}_{\{P_k\}} + \cdots + \mathscr{H}_{\{P_{n-1}\}} + \mathscr{H}_{\{P_n\}}. \quad (1)$$

Terms like $\mathscr{H}_{\{P_k\}}$ contain rovibrational operators which have no matrix elements within the $P_{k'>k}$ basis sets. The effective Hamiltonian for polyad P_n is obtained by projecting $\mathscr{H}$ in the P_n Hilbert subspace, i.e.

$$H^{\langle P_n\rangle} = P^{\langle P_n\rangle}\mathscr{H}P^{\langle P_n\rangle} = H^{\langle P_n\rangle}_{\{\mathrm{GS}\}} + H^{\langle P_n\rangle}_{\{P_1\}} + \cdots + H^{\langle P_n\rangle}_{\{P_k\}} + \cdots + H^{\langle P_n\rangle}_{\{P_{n-1}\}} + H^{\langle P_n\rangle}_{\{P_n\}}. \quad (2)$$

The different terms are written in the form

$$\mathscr{H}_{\{P_k\}} = \sum_{\text{all indexes}} t^{\Omega(K,n\Gamma)\Gamma_v\Gamma'_v}_{\{s\}\{s'\}} \times \left[{}^{\varepsilon}V^{\Omega_v(\Gamma_v\Gamma'_v)\Gamma}_{\{s\}\{s'\}} \otimes R^{\Omega(K,n\Gamma)}\right]^{(A_1)}. \quad (3)$$

In this equation, the $t^{\Omega(K,n\Gamma)\Gamma_v\Gamma'_v}_{\{s\}\{s'\}}$ are the parameters to be determined. ${}^{\varepsilon}V^{\Omega_v(\Gamma_v\Gamma'_v)\Gamma}_{\{s\}\{s'\}}$ and $R^{\Omega(K,n\Gamma)}$ are vibrational and rotational operators of respective degree Ω_v and Ω. Their construction is described in Ref. [12]. Again, the vibrational operators only have

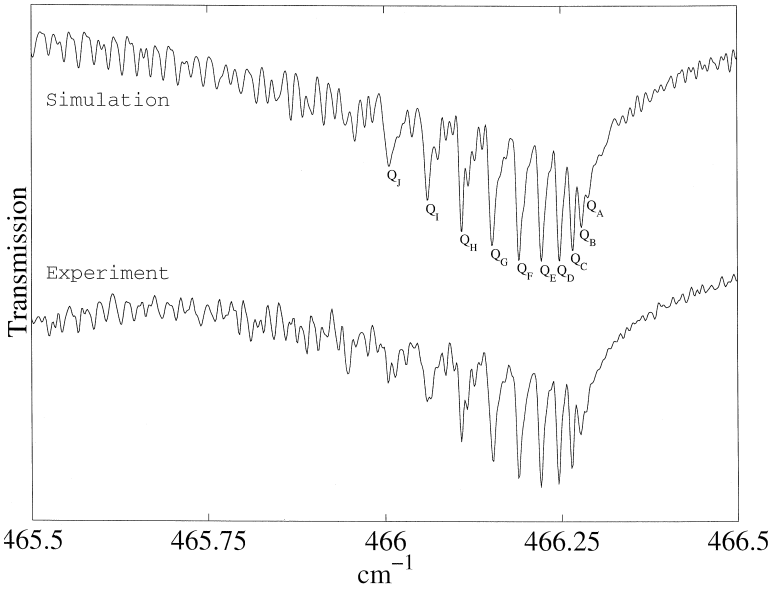

Fig. 3. Detailed portion in the Q-branch of the ν_3 band of P_4 compared to the simulation. The sub-bandhead labels according to Fig. 2 of Ref. [15] are indicated.

matrix elements within the $P_{k' \leqslant k}$ basis sets. The order of each individual term is $\Omega + \Omega_v - 2$.

Such a Hamiltonian development scheme enables the treatment of any polyad system. In this work however, since we only consider an isolated fundamental band, we will use only the two following effective Hamiltonians:

- The GS effective Hamiltonian,

$$H^{\langle \mathrm{GS} \rangle} = H^{\langle \mathrm{GS} \rangle}_{\{\mathrm{GS}\}} . \tag{4}$$

- The ν_3 stretching fundamental effective Hamiltonian,

$$H^{\langle \nu_3 \rangle} = H^{\langle \nu_3 \rangle}_{\{\mathrm{GS}\}} + H^{\langle \nu_3 \rangle}_{\{\nu_3\}} . \tag{5}$$

A dipole moment operator is developed in the same way, but, in the case we study in this Letter, it reduces to a single trivial operator. As we do not consider absolute intensities, the corresponding parameter is set to one.

We use a vibrational basis in the coupled form

$$\left| \Psi_v^{(C_v)} \right\rangle = \left| \left[\Psi_{v_1}^{(A_1)} \otimes \Psi_{v_2}^{(l_2,C_2)} \otimes \Psi_{v_3}^{(l_3,n_3C_3)} \right]^{(C_v)} \right\rangle , \tag{6}$$

the Ψs being harmonic oscillator wavefunctions. The Hamiltonian and dipole moment matrix elements are calculated in the coupled rovibrational basis

$$\left| \left[\Psi_v^{(C_v)} \otimes \Psi_r^{(J,nC)} \right]^{(\Gamma)} \right\rangle , \tag{7}$$

$\Psi_r^{(J,nC)}$ being a rotational wavefunction.

4. Analysis of the ν_3 spectrum

All the calculations and fits were realized using the STDS (Spherical Top Data System) program chain developed in Dijon (see Ref. [13]). As this software is designed for the study of tetrahedral XY_4 molecules with four normal modes of vibration ($\nu_1(A_1)$, $\nu_2(E)$, $\nu_3(F_2)$ and $\nu_4(F_2)$) we simply used it by considering the $\nu_3(F_2)$ fundamental of P_4 as a $\nu_3(F_2)$ fundamental of an XY_4 molecule. In order to get a correct vibrational partition function, the ν_4 frequency was set to an arbitrarily high value.

Here, $\mathscr{H}_{\{\mathrm{GS}\}}$ is developed to second order and $\mathscr{H}_{\{\nu_3\}}$ is developed to third order. The assignments of the ν_3 band of P_4 were realized as follows. We first made preliminary simulations using ab initio GS parameters from Ref. [5] and with the band center placed at the maximum of the most prominent Q branch feature of Fig. 1. As X_4 molecules only have one F_2 vibration, the zeta sum rule [14] reduces to $\zeta_3 = -1/2$. We thus approximated $t^{1(1,0F_1)F_2F_2}_{\{3\}\{3\}} = 3\sqrt{2}(B\zeta)_3$ by $-3B_0/\sqrt{2}$. Several trials were made for different values of $t^{2(2,0E)F_2F_2}_{\{3\}\{3\}}$, $t^{2(2,0F_2)F_2F_2}_{\{3\}\{3\}}$ being set to zero. This procedure enabled us to assign many lines in the P and R branches. Since the Q branch consists of several hundreds of unresolved transitions in a very small frequency range, this was too dense to allow any assignment in this region.

Then, it was possible to perform a parameter fit using a least-squares fit method. The fit was realized using the following constraints:

- $t^{1(1,0F_1)F_2F_2}_{\{3\}\{3\}}$ was fixed to $-3B_0/\sqrt{2}$ and B_0 was fitted. In view of the smallness of the difference

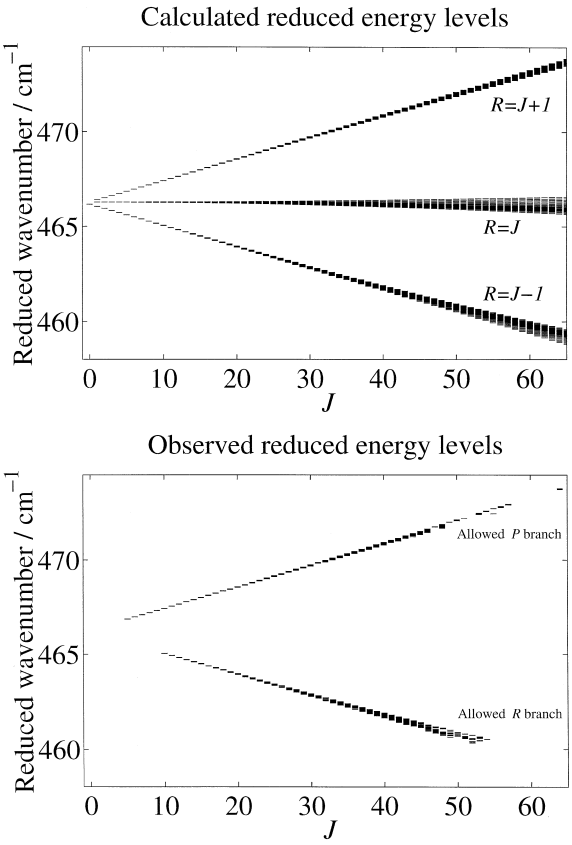

Fig. 4. Reduced energies for the ν_3 band of P_4. The top diagram shows only the levels corresponding to lines that could be observed and assigned. The values of the R quantum number are indicated ($R = J - l$ where l is the vibrational quantum number).

$(B_3 - B_0)$, 2.39×10^{-5} cm^{-1}, it does not matter for the conclusions whether B_0 or B_3 is used.

- the other GS parameters where fixed to their ab initio values,
- $t_{\{3\}\{3\}}^{2(2,0F_2)F_2F_2}$ was fixed to zero in a first step since it is not possible to fit it simultaneously with $t_{\{3\}\{3\}}^{2(2,0E)F_2F_2}$ if no Q branch assignments are available.

Since the Q branch shows a characteristic sub-band-head structure (Fig. 3) [15], it was possible to adjust manually the value of $t_{\{3\}\{3\}}^{2(2,0F_2)F_2F_2}$ as follows: this parameter was set to different values and each time the other parameters were fitted again with the same constraints as above. This was repeated until the Q branch simulation was correct. Table 1 shows the result of the final fit. Six hundred and fifty six P and R transitions were assigned and the root-mean-square deviation is 2.54×10^{-3} cm^{-1}. The maximum J values that could be assigned in the P and R branches were 54 and 63, respectively.

As can be seen in Fig. 2 and Fig. 3, the simulation is very satisfactory. Fig. 4 shows the reduced energy levels obtained by subtracting the scalar terms, i.e.

$$E_{\mathrm{red}} = E - \sum_{\Omega} t_{\{0\}\{0\}}^{\Omega(0,0A_1)A_1A_1} \left(J(J+1)\right)^{\Omega/2}$$
$$= E - B_0 J(J+1) + D_0 J^2(J+1)^2. \qquad (8)$$

The top of the figure displays only levels corresponding to the transitions that could be assigned.

5. Discussion

The band center m can be calculated through [16]:

$$m = t_{\{3\}\{3\}}^{0(0,0A_1)F_2F_2} - \frac{\sqrt{2}}{3} t_{\{3\}\{3\}}^{1(1,0F_1)F_2F_2} + \tfrac{2}{5}\left(t_{\{3\}\{3\}}^{2(2,0E)F_2F_2} + t_{\{3\}\{3\}}^{2(2,0F2)F_2F_2}\right) + \cdots, \qquad (9)$$

and we find

$$m = 466.286\,\mathrm{cm}^{-1}. \qquad (10)$$

The strict selection rules that apply to spherical top rovibrational spectra make it impossible to determine B_0 from GS combination differences (this is the same as for the axial rotational constant in symmetric top molecules). Thus, as mentioned above, we were forced to make the assumption that $(B\zeta)_3 \simeq B_0\zeta_3$ which is only approximative. Although this assumption is based on two approximations, namely $B_0 \simeq B_3$, which is correct within 0.02% (see Table 1), and the neglect of any v-dependance of ζ_3, this appears to be justified.

If we calculate the GS bond length using our B_0 value, we get

$$r_0 = \sqrt{\frac{h}{8\pi^2 c m_P B_0}} = 219.58\,\mathrm{pm}, \qquad (11)$$

($m_P = 5.143397 \times 10^{-26}$ kg) which is close to the 219.1 pm ab initio value [5]. Moreover, if we make two new fits by varying ζ_3 by $\pm 1\%$ (which would be a pessimistic error; in CH_4, for instance, the zeta sum rule is verified with a much better precision [17]), we obtain $r_0 = 219.22$ and 219.95 pm, respectively. These results seem to definitely rule out the high r_0 value derived from the Raman study of Ref. [3].

The hot bands that appear in the experimental spectrum could not be analyzed here because of their complexity. They should be dominated by $\nu_3 + \nu_2 - \nu_2$ since ν_2(E) is the lowest fundamental band at 360.813 cm^{-1} [6,3]. The understanding of this hot band would probably require first the analysis of the $\nu_2 + \nu_3$ combination band.

6. Conclusions

We have been able to locate the ν_3 fundamental band of P_4 unambiguously in the gas phase, and resolved the rotational structure. We conclude that, with the assumption that $(B\zeta)_3 \simeq -B_0/2$, we can support the ab initio structural parameters for P_4 [4,5] rather than those from Raman spectroscopy [3]. The difference between our ν_3 value and the ab initio calculation [5] is 6 cm^{-1} which is an acceptable discrepancy. This corresponds to 'a few cm^{-1}' as mentioned in Ref. [5].

Acknowledgements

The 'Région Bourgogne' is gratefully acknowledged for its support to the 'Laboratoire de Physique de l'Université de Bourgogne'. EBM gratefully acknowledges support by the Max-Planck-Gesellschaft zur Förderung der Wissenschaften.

References

[1] L.B. Maxwell, S.B. Hendricks, V. Mosley, J. Chem. Phys. 3 (1935) 699.
[2] A. Simon, H. Borrmann, H. Craubner, Phosphorus Sulfur 30 (1987) 507.
[3] N. Brassington, H. Edwards, D. Long, J. Raman. Spectrosc. 11 (1981) 346.
[4] M. Häser, O. Treutler, J. Chem. Phys. 102 (1995) 3703.
[5] B. Persson, R. Taylor, T. Lee, J. Chem. Phys. 107 (1997) 5051.
[6] H. Edwards, J. Mol. Struct. 295 (1993) 95.
[7] Y.M. Bosworth, R.J.H. Clark, D.M. Rippon, J. Mol. Spectrosc. 46 (1970) 240.
[8] H. Gutowsky, C. Hoffman, J. Am. Chem. Soc. 72 (1950) 5751.
[9] M. Birk, M. Winnewisser, E.A. Cohen, J. Mol. Spectrosc. 136 (1985) 402.
[10] Guelachvili, K.N. Rao, Handbook of Infrared Standards, Academic Press, San Diego, CA, 1986.
[11] R. McDowell, Spectrochim. Acta 27A (1971) 773.
[12] J.-P. Champion, M. Loëte, G. Pierre, in: K.N. Rao, A. Weber (Eds.), Spectroscopy of the Earth's Atmosphere and Interstellar Medium, Academic Press, San Diego, CA, 1992, pp. 339–422.
[13] C. Wenger, J.-P. Champion, J. Quantum Spectrosc. Radiat. Transfer 59 (1998) 471.
[14] D. Lepard, Can. J. Phys. 44 (1966) 461.
[15] E. Brock, B. Krohn, R. McDowell, C. Patterson, D. Smith, J. Mol. Spectrosc. 76 (1979) 301.
[16] B. Bobin, K. Fox, J. Phys. (Paris) 34 (1973) 571.
[17] D.L. Gray, A.G. Robiette, Mol. Phys. 37 (1979) 1901.

Journal of Molecular Spectroscopy **216,** 408–418 (2002)
doi:10.1006/jmsp.2002.8662

Study of the Fundamental Bands of $^{70}GeD_4$ by High-Resolution Raman and Infrared Spectroscopy: First Experimental Determination of the Equilibrium Bond Length of Germane

G. Pierre,* V. Boudon,* E. B. MKadmi,† H. Bürger,† D. Bermejo,‡ and R. Martínez‡

*Laboratoire de Physique de l'Université de Bourgogne, CNRS UMR 5027, 9 Av. A. Savary, BP 47 870, F-21078, Dijon Cedex, France; †Anorganische Chemie, FB9 Universität GH, D-42097 Wuppertal, Germany; and ‡Instituto de Estructura de la Materia CSIC, Serrano 119-123, 28006 Madrid, Spain

E-mail: Gerard.Pierre@u-bourgogne.fr, Vincent.Boudon@u-bourgogne.fr, buerger1@uni-wuppertal.de, dbermejo@fresno.csis.es

Received April 8, 2002; in revised form July 16, 2002

The four fundamental bands of $^{70}GeD_4$ have been analyzed using the STDS software developed in Dijon (http://www.u-bourgogne.fr/LPUB/sTDS.html). Both infrared and Raman spectra were used to observe all fundamental bands. Infrared spectra of monoisotopic $^{70}GeD_4$ were recorded in the regions 600 and 1500 cm^{-1} using the Bruker 120HR interferometer at Wuppertal. The resolution (1/maximum optical path difference) was between 2.3 and 3.3×10^{-3} cm^{-1} for the ν_3 and ν_4 infrared-active fundamental bands as well as for the interacting ν_2 band. A high-resolution stimulated Raman spectrum of the ν_1 band has been recorded in Madrid. The instrumental resolution of the Raman spectrum was 3.3×10^{-3} cm^{-1}. We have performed a global fit of the ground state, ν_2/ν_4 bending dyad, and ν_1/ν_3 stretching dyad. We have used 1146, 139, and 676 assigned lines for ν_2/ν_4, ν_1, and ν_3, respectively. The standard deviation is 2.2×10^{-3} cm^{-1} for the bending dyad, 1.6×10^{-3} cm^{-1} for the ν_3 infrared lines, and 1.7×10^{-3} cm^{-1} for the ν_1 Raman lines. These results enabled us to perform the first experimental determination of the equilibrium bond length of germane as $r_e = 1.5173(1)$ Å.

Key Words: high resolution infrared spectroscopy; Raman; germane isotopomers.

1. INTRODUCTION

In the series of MD_4 molecular species (M = C, Si, Ge, or Sn) high-resolution studies are missing only for GeD_4, while low-resolution Raman and infrared spectra have been reported (*1*). One reason for this deficiency is certainly the isotopic effect of Ge, which has five isotopes with quite comparable natural abundance. This, of course, complicates the spectra considerably. However, the spectroscopic knowledge of GeD_4 is interesting in itself since it would add valuable information on the structure of germane. It is thus challenging to overcome the difficulties due to isotopes in order to obtain detailed spectra and to analyze them. Moreover, since only the complete set of rovibrational parameters can provide the information required to determine the equilibrium structure, the study should be as global as possible. Another interesting question concerning this molecule would be to see how overtones of GeD_4 fit between SiD_4 (which shows no local mode behavior) and SnD_4 (local mode behavior at $\upsilon_{stretch} = 3$ (*2*)).

We have circumvented the isotopic problem by synthesizing monoisotopic $^{70}GeD_4$ and present here the first high-resolution study of this molecule. We have realized a global fit of the four fundamentals, using Fourier transform infrared spectra of the bending dyad ν_2/ν_4 and of the stretching fundamental ν_3 (both recorded in Wuppertal), as well as a Raman spectrum of the ν_1 totally symmetric stretching (recorded in Madrid). Due to the strong interaction between ν_2 and ν_4, forbidden lines appear in the bending dyad infrared spectrum, which also allowed us to fit some of the ground state parameters. The analysis has been realized thanks to the STDS software (*3*) developed in Dijon for tetrahedral spherical tops.

After presenting the Raman and infrared experiments, we briefly recall the basic principles of the tensorial formalism that we use for such molecules. We then detail the results of the global analysis of our $^{70}GeD_4$ data and give a preliminary estimate of the r_e equilibrium bond length for germane.

2. EXPERIMENTAL DETAILS

2.1. Material

$^{70}GeD_4$ was made from $^{70}GeO_2$ (97.1% ^{70}Ge) by dropwise addition of a solution of GeO_2 and $NaBD_4$ in KOD/D_2O to a solution (30%) of D_3PO_4 in D_2O (*4*). The gaseous products were separated in a standard vacuum line and $^{70}GeD_4$ was obtained by fractional condensation.

2.2. Raman Experiment

The spectrum has been recorded with the high-resolution Raman spectrometer of the Instituto de Estructura de la Materia

Supplementary data for this article may be found on the journal home page.

0022-2852/02 $35.00

in Madrid, described elsewere (*5, 6*). It follows the quasi-continuous wave (*q*-CW) scheme first proposed by Esherick and Owyoung (*7*). The probe beam is a frequency-fixed CW Ar^+ laser and the pump beam is produced by pulse-amplifying the CW output of a ring dye laser in a three-stage dye amplifier pumped by an injection-seeded Nd:YAG laser. The frequency of the pump laser is scanned and when the frequency difference between pump and probe lasers matches a Raman-active transition of the medium, a transient power transfer from the upper frequency laser (Ar^+ CW in our experiment) to the lower frequency one (pulsed dye) is observed. This transient signal is proportional to the Raman scattering cross section of the transition.

In this experiment, the Ar^+ laser was operated single-mode at 514 nm, 800 mW, locked in a double loop scheme. In the first loop, it was locked to a transmission fringe of a 300 MHz FSR confocal Fabry–Perot étalon. In the second loop, the étalon was locked to the a_3 hyperfine component of the $P(13)$ 43–0 $B^3\Pi^+_{0u} \leftarrow X^1\Sigma^+_g$ absorption of the $^{127}I_2$ molecule by a polarization spectroscopy setup (*8*). The resulting bandwidth, mainly determined by the residual jitter, was about 500 kHz, FWHM. For the pump laser, the ring dye laser was operated with rhodamine 110 and the dye amplifier with rhodamine 6G. The spectral bandwidth of this laser is limited by the Fourier transform of its nearly Gaussian temporal profile (12 ns FWHM) to about 3×10^{-3} cm^{-1}. As the apparatus function of the spectrometer depends on the convolution of the spectral profile of both the probe and pump lasers, the second one limits the spectral resolution to the above-mentioned value. Lenses of focal length 0.5 m have been used to focus and recollimate the laser beams in and out of the sample. This relatively high focal length has been chosen in order to decrease as much as possible the AC Stark effect associated with the pump laser field (*6, 9*). Several spectra were recorded at pump laser energies ranging between 1.3 and 8.0 mJ per pulse to estimate the wavenumber shifts due to this effect. For the $J = 7$ to 9 multiplets used for the test, broadening was very apparent as the laser energy increased, but the shift was nearly zero as expected for a Q-branch (*9*). We determined a shift of -5×10^{-5} cm^{-1}/mJ with an uncertainty of 100%. A peak energy of about 1.3 mJ was finally used, as we estimated that for the resolution and accuracy of our experiment no significant shift and broadening were present under these conditions. In this way, isolated lines near the band origin fit reasonably well to a Gaussian of 0.004 cm^{-1} FWHM. The convolution of the Doppler width (0.0021 cm^{-1}) and an apparatus function of 0.003 cm^{-1} assumed to be Gaussian yields a total width of 0.0037 cm^{-1}. As the apparatus function is not exactly Gaussian, we believe the observed linewidth is consistent with the assumption of no significant AC Stark broadening.

The pressure of the sample was also limited to 100 Pa in order to avoid pressure broadening and shifts. A triple pass configuration was used in order to increase the signal-to-noise ratio of the spectrum.

2.3. Infrared Experiment

Altogether four spectra have been recorded with a Bruker 120 HR interferometer. For the bending fundamentals ν_2 and ν_4 two spectra were measured in the 430 to 750 cm^{-1} range using a Globar source, a KBr beam splitter, and a liquid-He-cooled Si:B detector. A resolution (1/maximum optical path difference) of 3.3×10^{-3} cm^{-1} was achieved. A cell of length 28 cm was used, and pressures of 50 and 300 Pa were chosen. The number of scans was 110 and 1061. Calibration was performed in the region 500–525 cm^{-1} using H_2O lines (*10*).

For the study of the stretching region, two spectra were recorded in the range 1230–2350 cm^{-1} employing a Globar source, a KBr beam splitter, and an MCT 800 detector. A resolution of 3.3×10^{-3} cm^{-1} was achieved, and a 28-cm-long cell was used. The pressures were 43 and 750 Pa, respectively, and 478 and 226 scans were collected. Calibration was done with H_2O lines in the region 1600–1700 cm^{-1} [10].[1]

Figure 1 shows an overview of the FTIR spectrum of the bending and stretching dyad regions.

3. THEORY

The theoretical model used in this contribution is based on the tensorial formalism and the vibrational extrapolation methods developed in Dijon. These methods have already been explained, for example, in Refs. (*11, 12*) and they are implemented in the STDS software (*3*) used to perform the present analyses. Thus, we just briefly recall here the basic principles.

Let us consider an XY_4 molecule for which the vibrational levels are grouped in a series of polyads designated by P_k ($k = 0, \ldots, n$), P_0 being the ground state (GS). The Hamiltonian operator can be put in the form (after some contact transformations)

$$\mathcal{H} = \mathcal{H}_{\{P_0 \equiv GS\}} + \mathcal{H}_{\{P_1\}} + \cdots + \mathcal{H}_{\{P_n\}}, \qquad [1]$$

where $\mathcal{H}_{\{P_k\}}$ contains only rovibrational operators which have no matrix elements within the $P_{k' \lt k}$ basis sets. The different terms are written in the form

$$\mathcal{H}_{\{P_k\}} = \sum_{\text{all indexes}} t^{\Omega(K,n\Gamma)\Gamma_v\Gamma_{v'}}_{\{s\}\{s'\}} T^{\Omega(K,n\Gamma)\Gamma_v\Gamma_{v'}}_{\{s\}\{s'\}}. \qquad [2]$$

In this equation the $t^{\Omega(K,n\Gamma)\Gamma_v\Gamma_{v'}}_{\{s\}\{s'\}}$ are the parameters and the $T^{\Omega(K,n\Gamma)\Gamma_v\Gamma_{v'}}_{\{s\}\{s'\}}$ are the rovibrational operators defined as

$$T^{\Omega(K,n\Gamma)\Gamma_v\Gamma_{v'}}_{\{s\}\{s'\}} = \beta\left[R^{\Omega(K,n\Gamma)} \otimes {}^{\epsilon} V^{\Gamma_v\Gamma_{v'}(\Gamma)}_{\{s\}\{s'\}}\right]^{(A_1)}, \qquad [3]$$

[1] According to recent calibration standards (*24*) the band centers of ν_1 and ν_3 are too large by 0.350×10^{-3} cm^{-1}. Otherwise the lower and higher pressure spectra in their respective regions match each other within better than 0.2×10^{-3} cm^{-1}.

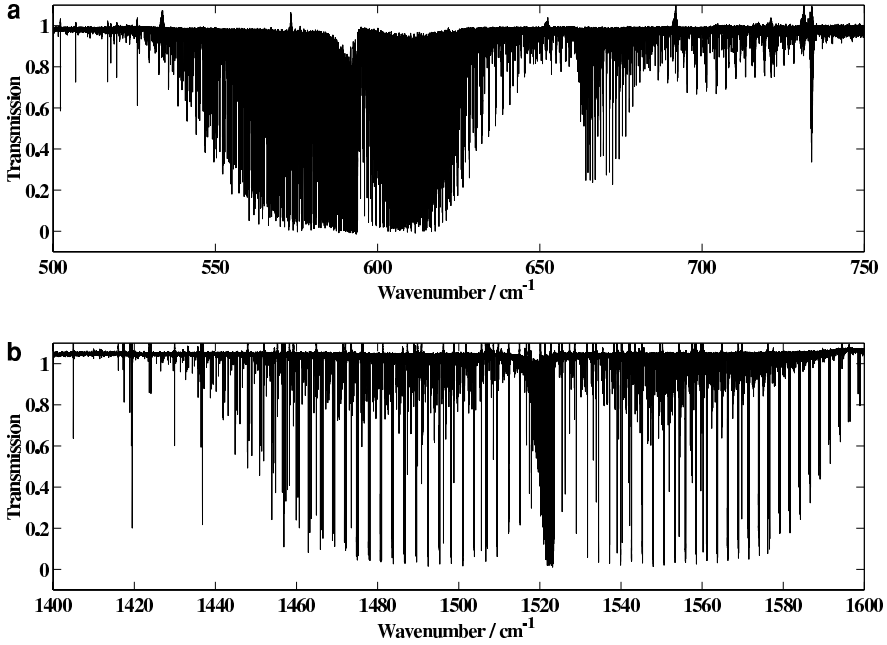

FIG. 1. Overview of the FTIR spectrum of the bending dyad (a) and of the stretching dyad (b) regions. In (a), the forbidden Q lines of ν_2 appear clearly near 670 cm^{-1}.

where β is a numerical factor equal to $\sqrt{[\Gamma_v]}(-\sqrt{3}/4)^{\Omega/2}$ if $(K, n\Gamma) = (0, 0A_1)$, and equal to 1 otherwise. The rovibrational operators $T^{\Omega(K,n\Gamma)\Gamma_v\Gamma_{v'}}_{\{s\}\{s'\}}$ are obtained by coupling of a rotational operator $R^{\Omega(K,n\Gamma)}$ of degree Ω (in the rotational angular momentum components J_x, J_y, and J_z) and symmetry Γ and a vibrational operator ${}^{\epsilon}V^{\Gamma_v\Gamma_{v'}(\Gamma)}_{\{s\}\{s'\}}$.

As detailed in Ref. (*11*), these vibrational operators are themselves obtained from the coupling of elementary creation (a^+) and annihilation (a) operators with a total degree Ω_v. Γ_v and $\Gamma_{v'}$ are the respective symmetries of the creation and anihilation parts and $\varepsilon = \pm 1$ is the symmetry against time reversal. Of course, $\Gamma_v \otimes \Gamma_{v'} \supset \Gamma$, so the rovibrational operator is totally symmetric (A_{1g} species). The order of each individual term is defined as $\Omega + \Omega_v - 2$. The effective Hamiltonian for polyad P_n is obtained by projecting $\mathcal{H}$ in the P_n Hilbert subspace, i.e.,

$$\begin{aligned} H^{\langle P_n\rangle} &= P^{\langle P_n\rangle}\mathcal{H}P^{\langle P_n\rangle}, \\ &= H^{\langle P_n\rangle}_{\{GS\}} + \cdots + H^{\langle P_n\rangle}_{\{P_k\}} + \cdots + H^{\langle P_n\rangle}_{\{P_n\}}. \end{aligned} \quad [4]$$

In order to analyze the fundamental bands of GeD_4, we use the following effective Hamiltonians:

- The ground state effective Hamiltonian,

$$\tilde{H}^{\langle GS\rangle} = \tilde{H}^{\langle GS\rangle}_{\{GS\}}. \quad [5]$$

- The ν_2/ν_4 bending dyad effective Hamiltonian,

$$\tilde{H}^{\langle \nu_2/\nu_4\rangle} = \tilde{H}^{\langle \nu_2/\nu_4\rangle}_{\{GS\}} + \tilde{H}^{\langle \nu_2\rangle}_{\{\nu_2/\nu_4\}} + \tilde{H}^{\langle \nu_4\rangle}_{\{\nu_2/\nu_4\}} + \tilde{H}^{\langle \nu_2/\nu_4\rangle}_{\{\nu_2/\nu_4\}}. \quad [6]$$

- The ν_1/ν_3 stretching dyad effective Hamiltonian,

$$\tilde{H}^{\langle \nu_1/\nu_3\rangle} = \tilde{H}^{\langle \nu_1/\nu_3\rangle}_{\{GS\}} + \tilde{H}^{\langle \nu_1\rangle}_{\{\nu_1/\nu_3\}} + \tilde{H}^{\langle \nu_3\rangle}_{\{\nu_1/\nu_3\}} + \tilde{H}^{\langle \nu_1/\nu_3\rangle}_{\{\nu_1/\nu_3\}}. \quad [7]$$

In order to calculate transition intensities, we developed the dipole moment (for infrared absorption) and polarizability (for Raman scattering) operators through the zeroth order using the same methods (*11*).

We use a coupled vibrational basis taking into account the four vibrational modes of XY_4 molecules (with respective symmetry A_1, E, F_2, and F_2). The Hamiltonian, dipole moment, and polarizability matrix elements are calculated in the coupled rovibrational basis

$$\left|\left[\Psi_r^{(J,nC)} \otimes \Psi_v^{(C_v)}\right]^{(\Gamma)}\right\rangle, \quad [8]$$

as described in Ref. (*11*). In Eq. [8], the $\Psi_v^{(C_v)}$'s and $\Psi_r^{(J,nC)}$'s are harmonic oscillator and rotational wavefunctions, respectively.

TABLE 1
Values of the Ground State Parameters

Order	H_{mn}	Parameter	Value/cm^{-1}[a]
0	02	$t^{2(0,A_1)}_{\{0\}\{0\}}$	1.3530633(54)
2	04	$t^{4(0,A_1)}_{\{0\}\{0\}}$	$-6.994(10)\times10^{-6}$
2	04	$t^{4(4,A_1)}_{\{0\}\{0\}}$	$-2.308(18)\times10^{-7}$
4	06	$t^{6(0,A_1)}_{\{0\}\{0\}}$	$1.426(14)\times10^{-9}$
4	06	$t^{6(4,A_1)}_{\{0\}\{0\}}$	$-9.91(18)\times10^{-11}$
4	06	$t^{6(6,A_1)}_{\{0\}\{0\}}$	$-5.4(1.2)\times10^{-12}$
6	08	$t^{8(0,A_1)}_{\{0\}\{0\}}$	$-9.59(13)\times10^{-13}$
6	08	$t^{8(4,A_1)}_{\{0\}\{0\}}$	$2.47(72)\times10^{-15}$
6	08	$t^{8(6,A_1)}_{\{0\}\{0\}}$	$-4.08(66)\times10^{-15}$
6	08	$t^{8(8,A_1)}_{\{0\}\{0\}}$	$-6.09(21)\times10^{-15}$

[a] The standard deviation (1σ) is given in parentheses.

4. ANALYSIS

In order to analyze the ν_2, ν_3, and ν_4 infrared bands together with the Raman spectrum of ν_1, we used the effective Hamiltonians described before. The parameters of these Hamiltonians are obtained by simultaneous fitting of the different spectra. After a preliminary assignment and study of each dyad (the bending dyad ν_2/ν_4 and the stretching dyad ν_1/ν_3) separately, we fitted the whole set of lines simultaneously. The two dyads and ground state parameters are determined using all possible assignments of experimental lines. In this way, 139 Raman lines of ν_1 for J values between 0 and 23 and 240, 676, and 906 lines of ν_2, ν_3 and ν_4, respectively, for J values up to 29 are used.

We developed the Hamiltonian up to sixth order for the ground state and the bending state ν_2/ν_4 and up to the fifth order for the stretching state ν_1/ν_3. However, one of the fourth order parameters of ν_1 and the fourth and fifth order parameters of the

TABLE 2
Values of the Bending Dyad Parameters

Order	H_{mn}	$t^{\Omega(K,n,\Gamma)}_{\{i\}\{j\}}$	Value/cm^{-1}[a] $t_{\{2\}\{2\}}$	$t_{\{2\}\{4\}}$	$t_{\{4\}\{4\}}$
0	20	$t^{0(0,\ A_1)}$	660.82647(23)		594.92632(13)
0	21	$t^{1(1,\ F_1)}$		−1.74169(11)	3.045292(33)
2	22	$t^{2(0,\ A_1)}$	$8.1948(25)\times10^{-3}$		$-4.8422(11)\times10^{-3}$
2	22	$t^{2(2,\ E)}$	$3.3848(25)\times10^{-3}$		$7.3359(17)\times10^{-3}$
2	22	$t^{2(2,\ F_2)}$		$-3.8606(55)\times10^{-3}$	$-1.02166(23)\times10^{-2}$
3	23	$t^{3(1,\ F_1)}$		$1.483(12)\times10^{-5}$	$1.71933(66)\times10^{-4}$
3	23	$t^{3(3,\ A_2)}$	$-1.0343(12)\times10^{-4}$		
3	23	$t^{3(3,\ F_1)}$		$6.311(16)\times10^{-5}$	$1.38993(82)\times10^{-4}$
3	23	$t^{3(3,\ F_2)}$		$2.120(37)\times10^{-5}$	
4	24	$t^{4(0,\ A_1)}$	$2.654(69)\times10^{-7}$		$-8.714(27)\times10^{-7}$
4	24	$t^{4(2,\ E)}$	$-7.985(39)\times10^{-7}$		$3.814(24)\times10^{-7}$
4	24	$t^{4(2,\ F_2)}$		$-3.123(44)\times10^{-7}$	$8.374(39)\times10^{-7}$
4	24	$t^{4(4,\ A_1)}$	$-4.765(17)\times10^{-7}$		$4.197(13)\times10^{-7}$
4	24	$t^{4(4,\ E)}$	$9.898(65)\times10^{-7}$		0.0[b]
4	24	$t^{4(4,\ F_1)}$		$-4.26(12)\times10^{-7}$	
4	24	$t^{4(4,\ F_2)}$		$6.806(33)\times10^{-7}$	$1.785(55)\times10^{-7}$
5	25	$t^{5(1,\ F_1)}$		0.0[b]	$7.095(50)\times10^{-9}$
5	25	$t^{5(3,\ A_2)}$	$-1.59(18)\times10^{-9}$		
5	25	$t^{5(3,\ F_1)}$		0.0[b]	$1.180(76)\times10^{-9}$
5	25	$t^{5(3,\ F_2)}$		0.0[b]	
5	25	$t^{5(5,\ 0F_1)}$		0.0[b]	0.0[b]
5	25	$t^{5(5,\ 1F_1)}$		0.0[b]	0.0[b]
5	25	$t^{5(5,\ F_2)}$		0.0[b]	
6	26	$t^{6(0,\ A_1)}$	0.0[b]		$5.430(33)\times10^{-10}$
6	26	$t^{6(2,\ E)}$	$-1.284(25)\times10^{-10}$		0.0[b]
6	26	$t^{6(2,\ F_2)}$		0.0[b]	$1.751(23)\times10^{-10}$
6	26	$t^{6(4,\ A_1)}$	0.0[b]		$9.198(79)\times10^{-11}$
6	26	$t^{6(4,\ E)}$	$3.324(73)\times10^{-10}$		0.0[b]
6	26	$t^{6(4,\ F_1)}$		0.0[b]	
6	26	$t^{6(4,\ F_2)}$		0.0[b]	$5.49(37)\times10^{-11}$
6	26	$t^{6(6,\ A_1)}$	$1.58(35)\times10^{-11}$		$-2.135(73)\times10^{-11}$
6	26	$t^{6(6,\ E)}$	$-4.87(43)\times10^{-11}$		$8.14(15)\times10^{-11}$
6	26	$t^{6(6,\ F_1)}$		0.0[b]	
6	26	$t^{6(6,\ 0F_2)}$		0.0[b]	0.0[b]
6	26	$t^{6(6,\ 1F_2)}$		0.0[b]	$-3.52(21)\times10^{-11}$

[a] The standard deviation (1σ) is given in parentheses.
[b] Fixed value.

TABLE 3
Values of the Stretching Dyad Parameters

Order	H_{mn}	$t^{\Omega(K,n,\Gamma)}_{\{i\}\{j\}}$	Value/cm^{-1a} $t_{\{1\}\{1\}}$	$t_{\{1\}\{3\}}$	$t_{\{3\}\{3\}}$
0	20	$t^{0(0,\ A_1)}$	1510.51692(63)		1523.41352(12)
0	21	$t^{1(0,\ F_1)}$			$-1.50737(32) \times 10^{-1}$
2	22	$t^{2(0,\ A_1)}$	$-6.3311(34) \times 10^{-3}$		$-5.30045(90) \times 10^{-3}$
2	22	$t^{2(2,\ E)}$			$1.1174(17) \times 10^{-3}$
2	22	$t^{2(2,\ F_2)}$		$2.756(17) \times 10^{-3}$	$-1.4924(14) \times 10^{-3}$
3	23	$t^{3(1,\ F_1)}$			$-8.501(55) \times 10^{-6}$
3	23	$t^{3(3,\ F_1)}$			$2.046(66) \times 10^{-6}$
3	23	$t^{3(3,\ F_2)}$		$-4.70(61) \times 10^{-6}$	
4	24	$t^{4(0,\ A_1)}$	0.0[b]		0.0[b]
4	24	$t^{4(2,\ E)}$			$1.56(17) \times 10^{-8}$
4	24	$t^{4(2,\ F_2)}$		0.0[b]	0.0[b]
4	24	$t^{4(4,\ A_1)}$	$1.44(16) \times 10^{-8}$		$3.78(57) \times 10^{-9}$
4	24	$t^{4(4,\ E)}$			0.0[b]
4	24	$t^{4(4,\ F_2)}$		0.0[b]	$-9.36(34) \times 10^{-8}$
5	25	$t^{5(1,\ F_1)}$			0.0[b]
5	25	$t^{5(3,\ F_1)}$			$-2.263(57) \times 10^{-9}$
5	25	$t^{5(3,\ F_2)}$		0.0[b]	
5	25	$t^{5(5,0F_1)}$			0.0[b]
5	25	$t^{5(5,1F_1)}$			$2.12(67) \times 10^{-10}$
5	25	$t^{5(5,\ F_2)}$		0.0[b]	

[a] The standard deviation (1σ) is given in parentheses.
[b] Fixed value.

interaction between ν_1 and ν_3 were not determined and were thus fixed to zero. Because the interaction between ν_2 and ν_4 is not as strong as in methane or silane the $t_{\{2\}\{4\}}$ interacting parameters of fifth and sixth order were also fixed to zero. Some other parameters were also fixed to zero according to the ambiguity theory (*13–16*).

Because the accuracy of the Δ^{exp} experimental data is, for the higher J values, better than that of the model (Δ^{th}), we used a weighted least-squares fit procedure. The weight ω_i of each set i of data is equal to one over the square of the estimated accuracy Δ_i,

$$\omega_i = \frac{1}{\Delta_i^2}, \qquad [9]$$

with

$$\Delta_i^2 = \left(\Delta_i^{\text{th}}\right)^2 + \left(\Delta_i^{\text{exp}}\right)^2. \qquad [10]$$

In this study, the effective Hamiltonian of the stretching dyad converges faster than that of the bending dyad. Thus, the following considerations are more convenient for the bending part of the effective Hamiltonian. The accuracy of the Hamiltonian model is considered to have the same order of magnitude as that of the energy contribution of the neglected terms. In the present analysis, the seventh order is the lowest one to be neglected. For the two dyad terms, the neglected energy contribution is estimated to have the order of magnitude

$$\Delta_i^{\text{th}} = P_{\text{neglected}} \times J^7 = 1.0 \times 10^{-13} \times J^7. \qquad [11]$$

This value gives for $J = 29$

$$\Delta_i^{\text{th}} \simeq 2 \times 10^{-3}\ \text{cm}^{-1}. \qquad [12]$$

The experimental wavenumber accuracy of infrared experimental lines is estimated to be $\Delta_i^{\text{exp}} = 3 \times 10^{-4}$ cm^{-1} while the Raman line accuracy is approximately 10^{-3} cm^{-1}.

To determine the values of effective Hamiltonian parameters, we minimize the following dimensionless quantity Q in the least-squares procedure:

$$Q = \sum_i \frac{\left(f_i^{\text{exp}} - f_i^{\text{cal}}\right)^2}{\Delta_i^2}. \qquad [13]$$

Tables 1 to 3 show the values of the fitted effective parameters for the ground state, bending dyad, and stretching dyad, respectively. Table 4 shows detailed statistics concerning this global fit.

5. DISCUSSION

Figures 2 to 4 show comparisons of experimental and calculated spectra in different parts of the bending dyad. In particular,

TABLE 4
Fit Statistics: SD Is the Standard Deviation

	ν_1		ν_2		ν_3		ν_4	
J	Number of data	SD/cm^{-1}	Number of data	SD/cm^{-1}	Number of data	SD/cm^{-1}	Number of data	SD/cm^{-1}
0	1	0.0013						
1	1	0.0015			4	0.0008	3	0.0012
2	2	0.0011			6	0.0008	4	0.0008
3	3	0.0010			9	0.0009	8	0.0007
4	4	0.0009	3	0.0007	11	0.0010	10	0.0009
5	4	0.0007	4	0.0008	14	0.0012	12	0.0010
6	6	0.0006	7	0.0010	16	0.0010	14	0.0009
7	6	0.0007	15	0.0017	19	0.0008	17	0.0009
8	7	0.0012	15	0.0013	21	0.0015	18	0.0008
9	8	0.0016	19	0.0023	24	0.0007	21	0.0009
10	9	0.0051	17	0.0018	27	0.0012	24	0.0007
11	9	0.0007	19	0.0013	26	0.0005	24	0.0009
12	11	0.0012	21	0.0013	24	0.0005	29	0.0014
13	11	0.0007	18	0.0015	29	0.0006	33	0.0010
14	7	0.0007	17	0.0027	29	0.0008	36	0.0016
15	4	0.0008	7	0.0019	30	0.0010	34	0.0010
16	6	0.0008	14	0.0040	30	0.0010	39	0.0014
17	5	0.0004	4	0.0029	32	0.0015	37	0.0011
18	8	0.0008	6	0.0010	36	0.0020	47	0.0013
19	7	0.0006	6	0.0023	35	0.0010	47	0.0011
20	4	0.0005	7	0.0020	39	0.0015	48	0.0012
21	6	0.0011	7	0.0015	38	0.0015	50	0.0016
22	6	0.0014	8	0.0016	43	0.0021	56	0.0017
23	4	0.0041	7	0.0012	42	0.0019	43	0.0010
24			8	0.0017	43	0.0033	50	0.0021
25			7	0.0035	29	0.0039	51	0.0018
26			1	0.0024	20	0.0060	45	0.0027
27			3	0.0019			48	0.0042
28							40	0.0053
29							18	0.0088
Total	139	0.0017	240	0.0020	676	0.0015	906	0.0014

Fig. 4 displays the region of forbidden lines where quite strong ν_2 lines appear thanks to the coupling with ν_4. Figure 5 shows the calculated reduced energy levels, obtained by subtracting the scalar term, i.e.,

$$E_{\text{red}} = E - \sum_{\Omega} t^{\Omega(0,0A_1)A_1A_1}_{\{0\}\{0\}} (J(J+1))^{\Omega/2}$$
$$= E - B_0 J(J+1) + D_0 J^2(J+1)^2 - \cdots. \quad [14]$$

Figure 6 compares experiment and simulation for the Q branch of ν_3 and Fig. 7 illustrates this the Raman spectrum of ν_1. A detail of the Raman spectrum showing some Q multiplets of ν_1 is displayed in Fig. 8. The calculated reduced energies for the stretching dyad are shown in Fig. 9.

The present results allow us to calculate the r_e equilibrium bond length. To do this, we use the formula (*17*)

$$B_e = B_0 + \sum_{i=1}^{4} \alpha_i \frac{d_i}{2}, \quad [15]$$

where

$$\alpha_i = -\Delta B_i = -t^{2(0,A_1)\Gamma_i\Gamma_i}_{\{i\}\{i\}} = B_0 - B_i \quad [16]$$

and d_i is the degeneracy of oscillator i ($d_1 = 1$, $d_2 = 2$, $d_3 = d_4 = 3$). The B_e value obtained in this way leads to $r_e = 1.5173$ Å. Although the uncertainty is not easy to determine, given the high accuracy of our ΔB values (see Tables 2 and 3) and neglecting the electronic effects, we estimate it to be 1×10^{-4} Å,

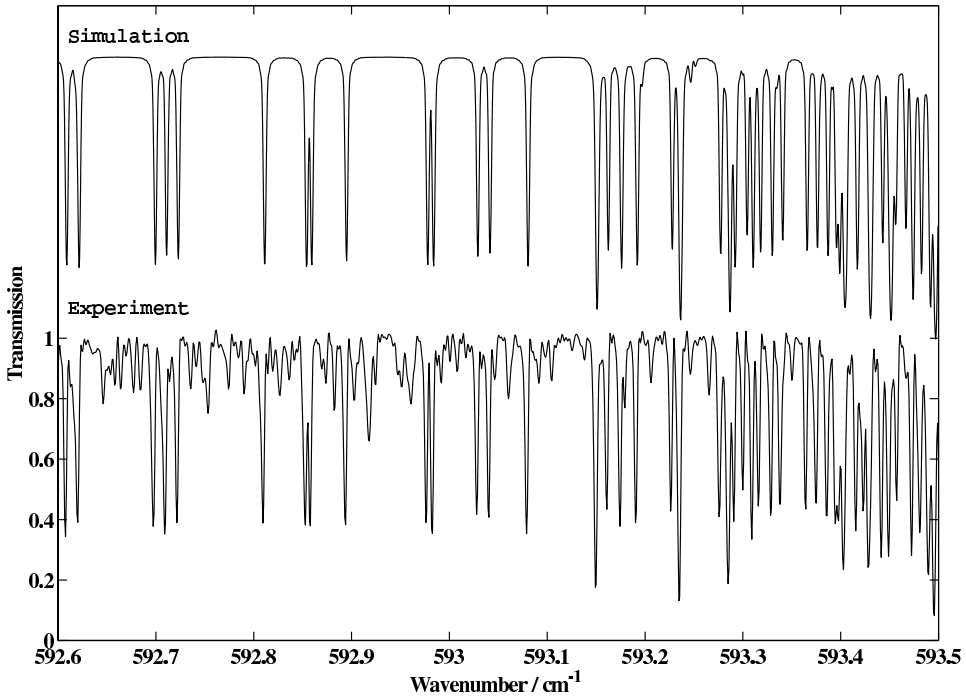

FIG. 2. Part of the FTIR spectrum in the ν_4 Q-branch region, compared to the simulation.

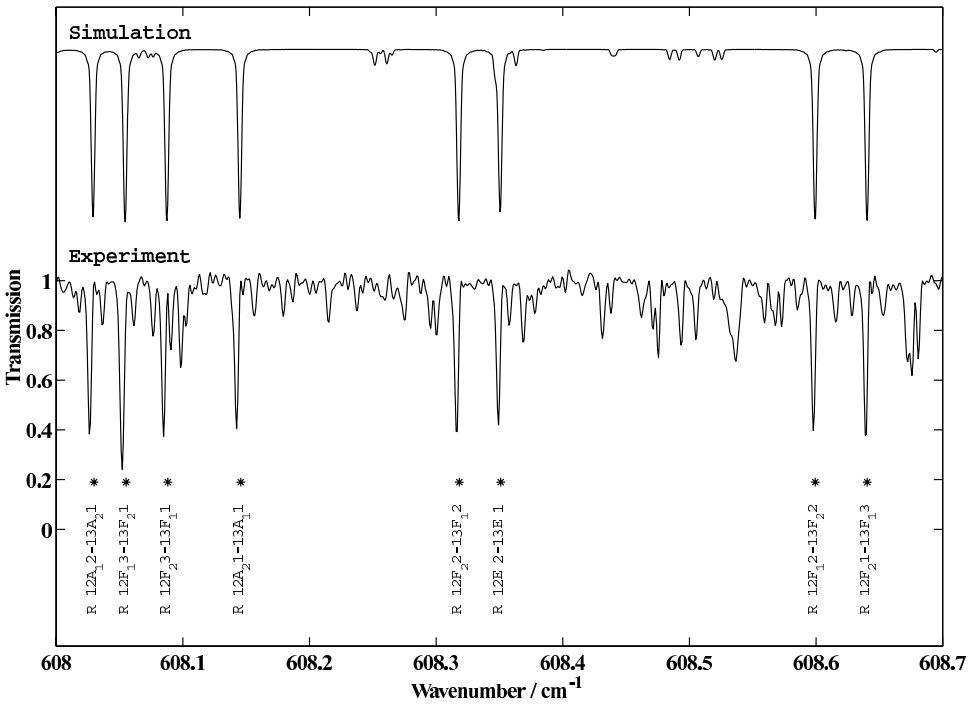

FIG. 3. Part of the FTIR spectrum in the ν_4 R-branch region, compared to the simulation. Some assignments of ν_4 $R(12)$ lines are shown.

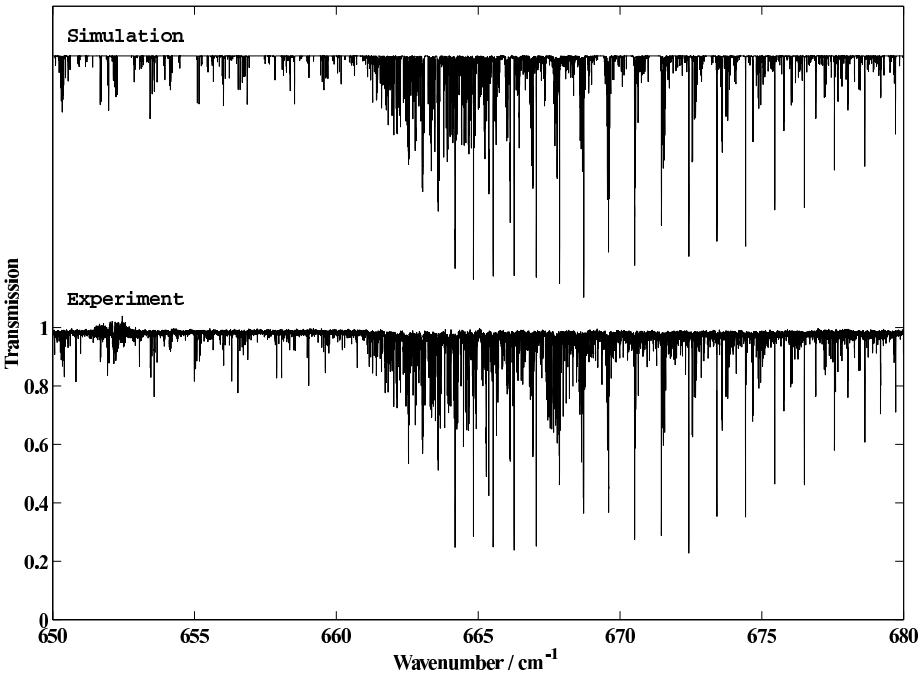

FIG. 4. Part of the FTIR spectrum of the ν_2/ν_4 bending dyad, compared to the simulation. This region shows forbidden lines from the ν_4 *R* branch and from the ν_2 *Q* branch.

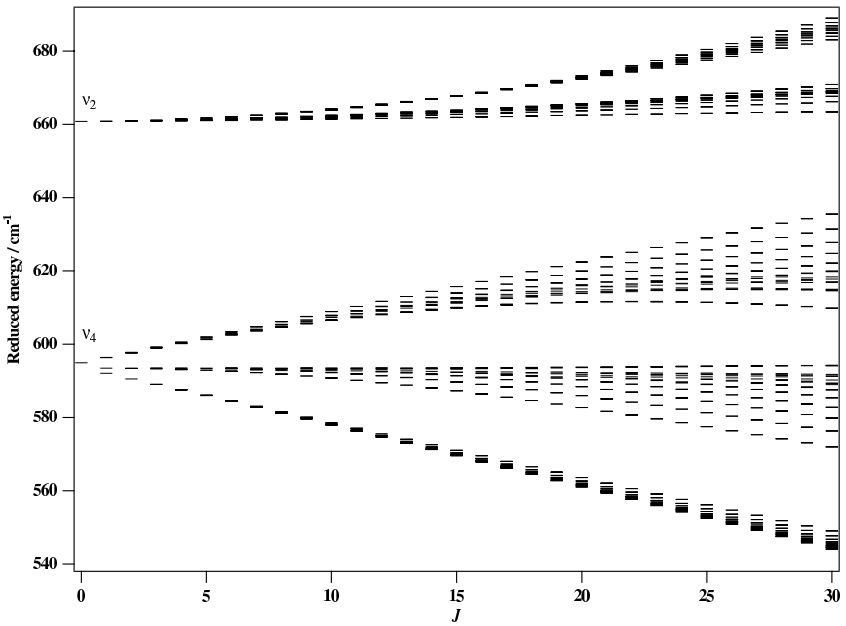

FIG. 5. Calculated reduced energy levels for the ν_2/ν_4 bending dyad.

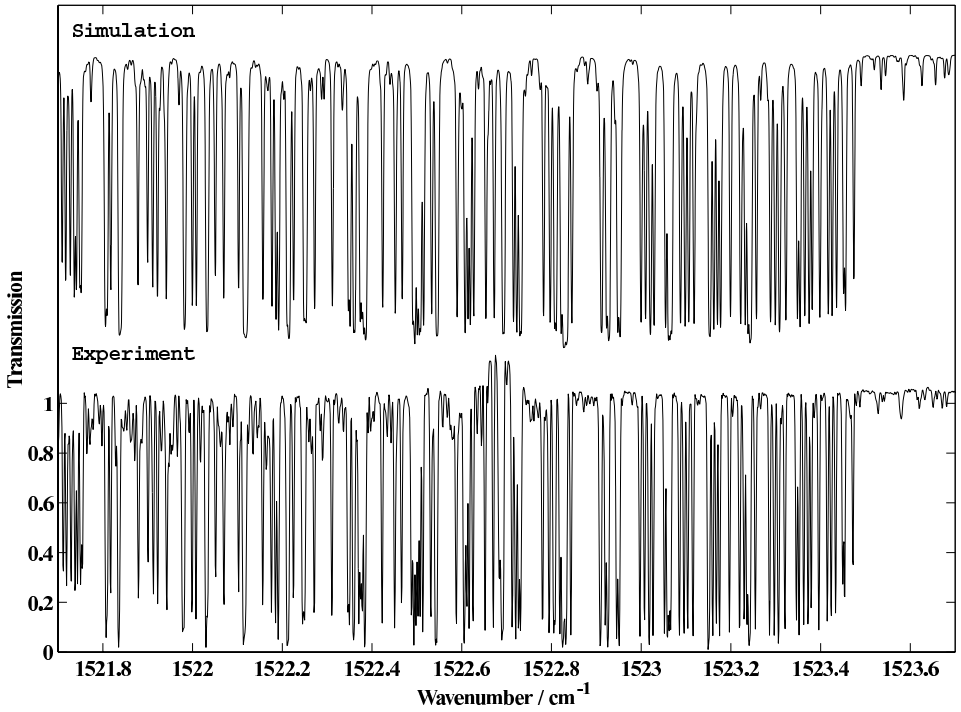

FIG. 6. Part of the FTIR spectrum in the ν_3 Q branch region, compared to the simulation.

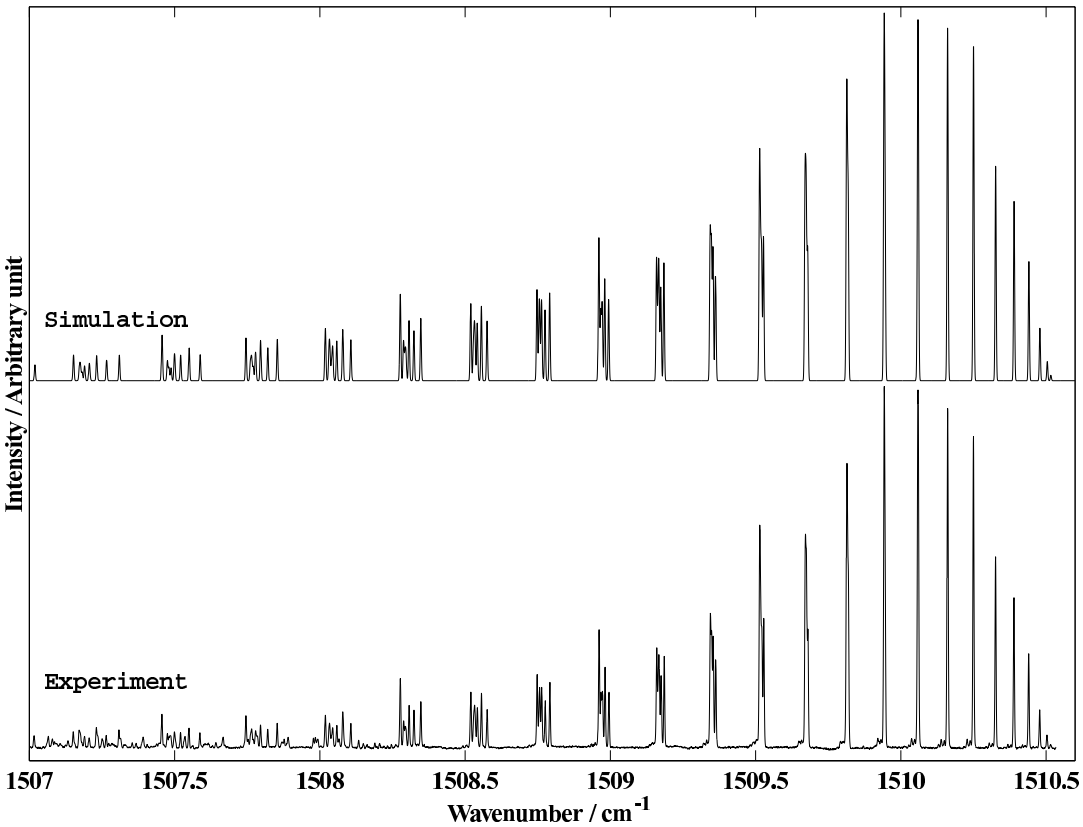

FIG. 7. Raman spectrum of the ν_1 totally symmetric stretching band, compared to the simulation.

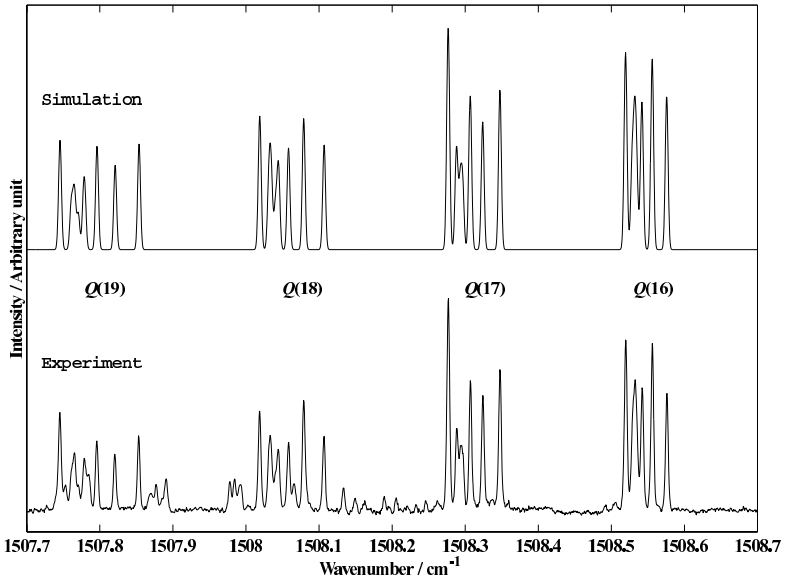

FIG. 8. Portion of the Raman spectrum of the ν_1 band, compared to the simulation.

giving finally

$$r_e = 1.5173(1)\ \text{Å}. \qquad [17]$$

This constitutes the first experimental determination of the equilibrium bond length of germane (r_e being the same for all isotopomers) since it uses the first complete set of fully determined non zero α_i values. The existing parameters for GeH_4 itself (*18*) are not reliable for such a calculation since the full set of four α_i values has never been determined for any of the various GeH_4 isotopomers.

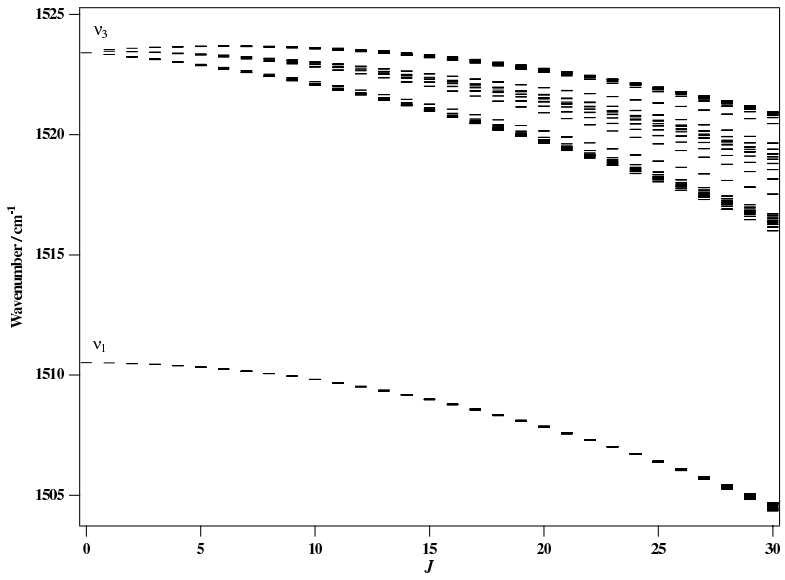

FIG. 9. Calculated reduced energy levels for the ν_1/ν_3 stretching dyad.

6. CONCLUSION

We have performed the first high-resolution spectroscopic study of GeD_4 using monoisotopic $^{70}GeD_4$ by realizing a global fit of the bending and stretching dyads. Complete tables of measured and assigned transitions (infrared and Raman) are available on the journal's home page. The analysis has been performed thanks to the STDS software (3), which can be freely downloaded at the URL `http://www.u-bourgogne.fr/LPUB/sTDS.html`.

These results can now be used in conjunction with those concerning the various isotopomers of GeH_4 (*18–23*) for a better determination of the potential of germane. As already mentionned in the Introduction, it would also be interesting to study the overtones of $^{70}GeD_4$ and their rotational structure in comparison with the other MD_4 species.

ACKNOWLEDGMENTS

D. Bermejo thanks the DGESIC, Ministerio de Educacion y Cultura, for final support of this work in the framework of Project PB97-1196, and also J. L. Doménech, who read the manuscript and made interesting suggestions. The Région Bourgogne is gratefully acknowledged for supporting the Laboratoire de Physique de l'Université de Bourgogne. Support by the Deutsche Forschungsgemeinschaft is gratefully acknowledged.

REFERENCES

1. H. W. Kattenberg, R. Elst, and A. Oskam, *J. Mol. Spectrosc.* **47,** 55–63 (1972).
2. M. Halonen, L. Halonen, H. Bürger, and W. Jerzembeck, *J. Chem. Phys.* **108,** 9285–9290 (1998).
3. C. Wenger and J.-P. Champion, *J. Quant. Spectrosc. Radiat. Transfer* **59,** 471–480 (1998).
4. G. Brauer, "Handbuch der Präparativen Anorganischen Chemie," Vol. 2 Enke, Stuttgart, 1978.
5. D. Bermejo, J. Santos, P. Cancio, J. P. Doménech, C. Domingo, J. M. Orza, J. Ortigoso, and R. Escribano, *J. Raman Spectrosc.* **21,** 197–201 (1990).
6. J. Santos, P. Cancio, J. P. Doménech, J. Rodriguez, and D. Bermejo, *Laser Chem.* **12,** 53–63 (1992).
7. P. Esherick and A. Owyoung, *in* "Advances in Infrared and Raman Spectroscopy," (R. J. H. Clark and R. E. Hester, Eds.), Vol. 9, pp. 130–187. Heyden, London, 1982.
8. M. Raab and A. Weber, *J. Opt. Soc. Am. B* **2,** 1476–1479 (1985).
9. J. Nibler, *in* "Applied Laser Spectroscopy," (W. Demtröder and M. Inguscio, Eds.), pp. 316–318. Plenum, New York, 1990.
10. G. Guelachvili and K. N. Rao, "Handbook of Infrared Standards." Academic Press, Orlando, FL, 1986.
11. J.-P. Champion, M. Loëte, and G. Pierre, *in* "Spectroscopy of the Earth's Atmosphere and Interstellar Medium," (K. N. Rao and A. Weber, Eds.), pp. 339–422. Academic Press, San Diego, 1992.
12. N. Cheblal, M. Loëte, and V. Boudon, *J. Mol. Spectrosc.* **197,** 222–231 (1999).
13. V. I. Perevalov, V. G. Tyuterev, and B. I. Zhilinskiĭ, *Chem. Phys. Lett.* **104,** 455–461 (1984).
14. V. I. Perevalov, V. G. Tyuterev, and B. I. Zhilinskiĭ, *J. Mol. Spectrosc.* **103,** 147–159 (1984).
15. V. I. Perevalov, V. G. Tyuterev, and B. I. Zhilinskiĭ, *J. Mol. Spectrosc.* **111,** 1–19 (1985).
16. V. G. Tyuterev, J.-P. Champion, G. Pierre, and V. I. Perevalov, *J. Mol. Spectrosc.* **120,** 49–78 (1986).
17. D. L. Gray and A. G. Robiette, *Mol. Phys.* **37,** 1901–1920 (1979).
18. P. Lepage, J.-P. Champion, and A. G. Robiette, *J. Mol. Spectrosc.* **89,** 440–448 (1981).
19. I. Ozier and A. Rosenberg, *Can. J. Phys.* **51,** 1882–1895 (1973).
20. P. Lepage, R. Brégier, and R. Saint-Loup, *C. R. Acad Sci. Paris B* **283,** 179–180 (1976).
21. S. J. Daunt, G. W. Halsey, K. Fox, R. J. Lovell, and N. M. Gailar, *J. Chem. Phys.* **68,** 1319–1321 (1978).
22. G. Magerl, W. Schupita, E. Bonek, and W. A. Kreiner, *J. Chem. Phys.* **72,** 395–398 (1980).
23. W. A. Kreiner, R. Opferkuch, A. G. Robiette, and P. H. Turner, *J. Mol. Spectrosc.* **85,** 442–448 (1981).
24. G. Guelachvili *et al.*, *Pure Appl. Chem.* **69,** 193–208 (1996).

Journal of Molecular Spectroscopy **197,** 222–231 (1999)
Article ID jmsp.1999.7902, available online at http://www.idealibrary.com on IDEAL®

Development of the Dipole Moment and Polarizability Operators of Octahedral Molecules

N. Cheblal, M. Loëte, and V. Boudon

Laboratoire de Physique de l'Université de Bourgogne-CNRS, B.P. 47 870, F-21078 Dijon, France

Received December 14, 1998; in revised form May 26, 1999

We present a development of the dipole moment and polarizability operators of octahedral molecules, using a tensorial formalism analogous to the one developed for tetrahedral molecules. These operators are involved in the calculation of the intensities of rovibrational transitions as well as in the calculation of the Stark effect. Expressions for the matrix elements are derived. Two simplified models for the study of the Stark effect in such molecules are also proposed and discussed. © 1999 Academic Press

1. INTRODUCTION

The theory of transition moments operators (dipole moment or polarizability) is essential for the study and prediction of rovibrational transition intensities in polyatomic molecules. The tensorial formalism developed in Dijon for the expansion of the Hamiltonian operator of spherical top molecules has also been applied to the transition moment operators, as summarized in a review article (*1*). In this paper, however, only the case of tetrahedral (point group T_d) molecules was treated. Nevertheless, it appears that octahedral (point group O_h) molecules also form an important family of spherical top species as it can be seen in Table 1. The ν_3 fundamental stretching band of SF_6 is probably the most precisely measured band ever in molecular spectroscopy, as far as the frequencies are concerned (*2–4*). However, apart from this specific case, since these heavy species have been up to now substantially less studied than XY_4 molecules (like CH_4, SiH_4, . . .), there are only a very few data concerning their transition moments (*6*) (see Table 2). For several molecules in Table 1, there exist spectra for which a theoretical model for the interpretation of intensities would be necessary. This does not concern only fundamental bands anymore; for example, the high-resolution spectrum of the $\nu_2 + \nu_6$ combination band of $^{32}SF_6$ has been recently investigated (*5*).

The aim of this paper is to provide a tensorial development of the transition moment operators. This enables the determination of the matrix elements which appear in intensity calculations for rovibrational electric dipole and Raman transitions. As we make extensive use of tensorial formalism, the reader not familiar with this viewpoint should refer to Ref. (*1*) where it has been explained in detail. Section 2 recalls the basic theory of transition moment operators and Section 3 deals more specifically with the case of octahedral molecules. The differences with the tetrahedral case and especially the fundamental role of the parity in the O_h group are explained in detail. The last section of this article is dedicated to the study of the Stark effect in octahedral molecules. We will see that a static Stark effect cannot lead to the determination of the dipole moment (unlike the case of T_d molecules) since it only implies the polarizability. Thus, such a static effect would probably be very small (although there exists no estimation of the polarizability). However, the huge electric fields involved by the use of powerful pulsed lasers in spectroscopy experiments induce lineshifts and deformations due to the dynamic Stark effect, as shown experimentally by Reuss and coworkers (*7–10*). In this case coupling terms involving the dipole moment must be taken into account. Two simplified models which could serve as a starting point for the study of such phenomena will be described.

2. BASIC PRINCIPLES

In this section, we recall briefly the basic principles of the expansion of transition moment operators. This is valuable for any polyatomic molecule and can be found in detail for example in Ref. (*11*).

2.1. Transformed Operators

Successive Van Vleck contact transformations are generally applied to the Hamiltonian and transition moment operators. The aim of these contact transformations is to introduce appropriate basis functions in which the transformed Hamiltonian $\tilde{H}$ has a completely diagonal or block diagonal form with respect to some vibrational subspace. These subspaces of close vibrational levels correspond to the so-called polyads.

If A represents either H (Hamiltonian), μ (dipole moment), or α (polarizability), the transformed operator $\tilde{A}$ is given by

TABLE 1
Octahedral Molecules with a Nondegenerate Electronic Ground State

Type	Generic name	Molecules
XY_6	Hexafluorides	SF_6, CrF_6, SeF_6, MoF_6, TeF_6, WF_6, PtF_6, PoF_6, UF_6, PuF_6
	Hexachlorides	SCl_6, $SeCl_6$, $TeCl_6$, $MoCl_6$, WCl_6, UCl_6
$X(YZ)_6$	Hexacarbonyls	$Cr(CO)_6$, $Mo(CO)_6$, $W(CO)_6$
X_8Y_8	Cubane	C_8H_8

Note. Hexachlorides, hexacarbonyls, and cubane are octahedral only if equivalent atoms are identical (same isotope).

$$\tilde{A} = TAT^{-1} = A + i[S, A] + \frac{1}{2}[S, [S, A]] + \ldots, \quad \text{with } T = e^{iS}. \qquad [1]$$

S is a Hermitian operator and is called the generator of the contact transformation. It has been shown that S is necessarily a sum of rovibrational operators (*1*).

2.2. Dipole Moment

The dipole moment components in the laboratory-fixed frame (LFF) μ_Θ (with $\Theta = X$, Y or Z) can be related to the components μ_θ (with $\theta = x$, y or z) in the molecule-fixed frame (MFF) through

$$\mu_\Theta = \sum_\theta \lambda_{\Theta,\theta}\mu_\theta, \qquad [2]$$

where the $\lambda_{\Theta,\theta}$ are the direction cosines.

In the small amplitude motion approximation one can expand each component μ_θ as a power series in the dimensionless normal coordinates $q_{s,\sigma}$ (where s is the oscillator index and the σ are its components)

TABLE 2
Values (in Debye) of the Zeroth Order Dipole Moment Parameters for the ν_3 and ν_4 Fundamentals of SF_6 and UF_6 (from Ref. 6)

Parameter	SF_6	UF_6	Notation of other authors †
$\left\lvert\mu^{0(0,0A_{1g})A_{1g}F_{1u}}_{\{0\}\{\nu_3\}}\right\rvert$	0.672	0.667	$\sqrt{3}\,\lvert\langle\mu_{0,3}\rangle\rvert = \sqrt{\frac{3}{2}}\,\lvert\mu_3\rvert$
$\left\lvert\mu^{0(0,0A_{1g})A_{1g}F_{1u}}_{\{0\}\{\nu_4\}}\right\rvert$	0.232	0.17	$\sqrt{3}\,\lvert\langle\mu_{0,4}\rangle\rvert = \sqrt{\frac{3}{2}}\,\lvert\mu_4\rvert$

† We have $\mu_i = \left(\frac{\partial\mu_\theta}{\partial q_{i,\theta}}\right)_e$, $i = 3$ or 4.

$$\mu_\theta = \mu^e_\theta + \sum_{s,\sigma}\left(\frac{\partial\mu_\theta}{\partial q_{s,\sigma}}\right)_e q_{s,\sigma} + \frac{1}{2}\sum_{s,\sigma,s',\sigma'}\left(\frac{\partial^2\mu_\theta}{\partial q_{s,\sigma}\partial q_{s',\sigma'}}\right)_e q_{s,\sigma}q_{s',\sigma'} + \ldots, \qquad [3]$$

where μ^e_θ is the permanent dipole moment of the molecule (if it exists). The other terms are induced by molecular vibrations.

One can show that the LFF components of the transformed dipole moment can be written in the symmetrized form (*1*)

$$\tilde{\mu}_\Theta = \frac{1}{2}\sum_\theta (\lambda_{\Theta,\theta}\tilde{\mu}_\theta + \tilde{\mu}_\theta\lambda_{\Theta,\theta}). \qquad [4]$$

Like the contact transformation generator S, $\tilde{\mu}_\theta$, and $\tilde{\mu}_\Theta$ are also sums of rovibrational operators, as implied by Eq. 1.

To establish the expressions of $\tilde{\mu}_\theta$ and $\tilde{\mu}_\Theta$, it is necessary to introduce in a first step the spherical components of the dipole moment operator. The LFF spherical components, denoted $\mu^{(1)}_m$, are related to the MFF ones $\mu^{(1)}_k$ through (*1*)

$$\mu^{(1)}_m = \sum_k \mathcal{D}^{(1)}_{km}\mu^{(1)}_k, \qquad [5]$$

where the $\mathcal{D}^{(1)}_{km}$ are Wigner's harmonic functions (*12*) (k, $m = -1$, 0 or 1). The Cartesian and spherical components in both frames are linked through the relations:

$$\mu_\Theta = \sum_m \langle 1; m|\Theta\rangle\mu^{(1)}_m, \qquad [6]$$

$$\mu_\theta = \sum_k \langle 1; k|\theta\rangle\mu^{(1)}_k, \qquad [7]$$

where the $\langle 1; m|\Theta\rangle$ and $\langle 1; k|\theta\rangle$ are called Stone coefficients (*13*).

2.3. Polarizability

The application of an electric field E to the molecules, induces a dipole moment, defined as

$$\mu_{\Theta_1} = \sum_{\Theta_2} \alpha_{\Theta_1\Theta_2} E_{\Theta_2}, \quad [8]$$

where $\alpha_{\Theta_1\Theta_2}$ is a LFF component of the polarizability tensor. It can be related to the MFF components $\alpha_{\theta_1\theta_2}$ through

$$\alpha_{\Theta_1\Theta_2} = \sum_{\theta_1,\theta_2} \lambda_{\Theta_1,\theta_1}\lambda_{\Theta_2,\theta_2}\alpha_{\theta_1\theta_2}. \quad [9]$$

As for the dipole moment, the small amplitude motion approximation allows to develop the $\alpha_{\theta_1\theta_2}$ as a series of dimensionless normal coordinates like

$$\alpha_{\theta_1\theta_2} = \alpha^e_{\theta_1\theta_2} + \sum_{s,\sigma} \left(\frac{\partial\alpha_{\theta_1\theta_2}}{\partial q_{s,\sigma}}\right)_e q_{s,\sigma} + \frac{1}{2}\sum_{s,\sigma,s',\sigma'} \left(\frac{\partial^2\alpha_{\theta_1\theta_2}}{\partial q_{s,\sigma}\partial q_{s',\sigma'}}\right)_e q_{s,\sigma}q_{s',\sigma'} + \ldots, \quad [10]$$

where $\alpha^e_{\theta_1\theta_2}$ is the permanent polarizability (if it exists). The other terms are induced by molecular vibrations.

Just as for the dipole moment one has to consider the transformed polarizability and in the LFF we have (*14*)

$$\tilde{\alpha}_{\Theta_1\Theta_2} = \frac{1}{2}\sum_{\theta} (\lambda_{\Theta_1,\theta_1}\lambda_{\Theta_2,\theta_2}\tilde{\alpha}_{\theta_1\theta_2} + \tilde{\alpha}_{\theta_1\theta_2}\lambda_{\Theta_1,\theta_1}\lambda_{\Theta_2,\theta_2}). \quad [11]$$

The spherical components in the LFF ($\alpha^{(L)}_m$) and in the MFF ($\alpha^{(L)}_k$) are linked through

$$\alpha^{(L)}_m = \sum_k \mathcal{D}^{(L)}_{km}\alpha^{(L)}_k, \quad [12]$$

where L takes only the values 0 and 2. For the $\mathcal{D}^{(L)}_{km}$ Wigner's harmonics (*12*)

$$\begin{cases} L = 0 \Rightarrow m, k = 0, \\ L = 2 \Rightarrow m, k = 0, \pm 1, \pm 2. \end{cases} \quad [13]$$

Finally, we have

$$\alpha_{\Theta_1\Theta_2} = \sum_{L,m} \langle L; m|\Theta_1\Theta_2\rangle \alpha^{(L)}_m, \quad [14]$$

$$\alpha_{\theta_1\theta_2} = \sum_{L,k} \langle L; k|\theta_1\theta_2\rangle \alpha^{(L)}_k, \quad [15]$$

where the $\langle L; m|\Theta_1\Theta_2\rangle$ and $\langle L; k|\theta_1\theta_2\rangle$ are Stone coefficients (*13*).

TABLE 3
Symmetry of the Hamiltonian (H), Dipole Moment (μ), and Polarizability (α) Operators Expressed in the Molecule-Fixed Frame (MFF) and Laboratory-Fixed Frame (LFF) for Molecules Belonging to the T_d and O_h Symmetry Groups

Operator	T_d		O_h	
	MFF	LFF	MFF	LFF
H	A_1	A_1	A_{1g}	A_{1g}
μ	F_2	A_2	F_{1u}	A_{1u}
α	$A_1 \oplus E \oplus F_2$	A_1	$A_{1g} \oplus E_g \oplus F_{2g}$	A_{1g}

3. TENSORIAL FORMALISM FOR OCTAHEDRAL MOLECULES

In this section, we will focus on the particularities of the tensorial expressions of the transition moments in the O_h group. Table 3 shows the symmetries of the Hamiltonian, the dipole moment, and the polarizability operators in the LFF and MFF for T_d and O_h molecules.

3.1. Expression of the Hamiltonian

The expression of the Hamiltonian developed using the tensorial formalism in the O_h group is very close to the one used for tetrahedral molecules (T_d group) (*1*). Compared to T_d (isomorphous to O), the O_h group has an additional index to characterize its irreducible representations (irreps): the parity (g or u). H should belong to the totally symmetric irrep, which is A_{1g}. So, the initial (untransformed) Hamiltonian is expanded as a series of rovibrational operators $T^{\Omega(K_g,n\Gamma_g)\alpha_1\Gamma_{1\chi}\alpha_2\Gamma_{2\chi}}_{\{n_s\}\{m_s\}}$ as

$$H = \sum_{\text{all indexes}} t^{\Omega(K_g,n\Gamma_g)\alpha_1\Gamma_{1\chi}\alpha_2\Gamma_{2\chi}}_{\{n_s\}\{m_s\}} T^{\Omega(K_g,n\Gamma_g)\alpha_1\Gamma_{1\chi}\alpha_2\Gamma_{2\chi}}_{\{n_s\}\{m_s\}}, \quad (\chi = g \text{ or } u). \quad [16]$$

The $t^{\Omega(K_g,n\Gamma_g)\alpha_1\Gamma_{1\chi}\alpha_2\Gamma_{2\chi}}_{\{n_s\}\{m_s\}}$ are the parameters of the model. The coupled rovibrational operators

$$T^{\Omega(K_g,n\Gamma_g)\alpha_1\Gamma_{1\chi}\alpha_2\Gamma_{2\chi}}_{\{n_s\}\{m_s\}} = (R^{\Omega(K_g,n\Gamma_g)} \otimes {}^{\epsilon}V^{\alpha_1\Gamma_{1\chi}\alpha_2\Gamma_{2\chi}(\Gamma_g)}_{\{n_s\}\{m_s\}})^{(A_{1g})} \quad [17]$$

are constructed exactly in the same way as in T_d (*1*). The parity of the rotational operator $R^{\Omega(K_g,n\Gamma_g)}$ being always taken as g (by convention), that of the vibrational operator $V^{\alpha_1\Gamma_{1\chi}\alpha_2\Gamma_{2\chi}(\Gamma_g)}_{\{n_s\}\{m_s\}}$ is necessarily g too. The expression of the rotational and vibrational operators is detailed in Ref. (*1*). In Eq. [17], ϵ is the symmetry under time reversal and is related to the rotational degree Ω through

$$\epsilon = (-1)^{\Omega}. \quad [18]$$

The transformed Hamiltonian has the same form as the initial one (Eq. 16),

$$\tilde{H} = \sum_{\text{all indexes}} \tilde{t}^{\Omega(K_g,n\Gamma_g)\alpha_1\Gamma_{1\chi}\alpha_2\Gamma_{2\chi}}_{\{n_s\}\{m_s\}} T^{\Omega(K_g,n\Gamma_g)\alpha_1\Gamma_{1\chi}\alpha_2\Gamma_{2\chi}}_{\{n_s\}\{m_s\}}, \quad [19]$$

where the transformed parameter set $\{\tilde{t}^{\Omega(K_g,n\Gamma_g)\alpha_1\Gamma_{1\chi}\alpha_2\Gamma_{2\chi}}_{\{n_s\}\{m_s\}}\}$ depends on both the initial parameter set $\{t^{\Omega(K_g,n\Gamma_g)\alpha_1\Gamma_{1\chi}\alpha_2\Gamma_{2\chi}}_{\{n_s\}\{m_s\}}\}$ and on the set of parameters of the contact transformation operator S.

In the following, we use a coupled rovibrational basis denoted

$$|\Psi^{(C_\tau)}_{M\sigma}\rangle = |[\Psi^{(J_g,nC_{rg})}_M \otimes \Psi^{(C_{v\tau})}_v]^{(C_\tau)}_\sigma\rangle. \quad [20]$$

Here, $\Psi^{(J_g,nC_{rg})}_M$ is a rotational function of symmetry C_{rg} (n is a multiplicity index (*1*)), and $\Psi^{(C_{v\tau})}_v$ is a vibrational function of symmetry $C_{v\tau}$. J is the rotational quantum number, M is the LFF spherical component, C_τ the rovibrational symmetry with component σ, and $\tau = g$ or u is the parity. M is generally omitted for simplicity.

The Hamiltonian eigenfunctions are linear combinations of such functions and we denote them

$$|\Phi^{(JC_\tau\alpha)}_{M\sigma}\rangle, \quad [21]$$

where α numbers the energy levels in increasing order within a (J, C_τ) block.

The general expression of the matrix elements of the Hamiltonian operators is given in the Appendix.

3.2. Expression of the Dipole Moment

Each component of the initial (untransformed) dipole moment in the MFF is expanded as a series of purely vibrational operators (see Eq. 3),

$$\mu^{(F_{1u})}_\theta = \sum_{\text{all indexes}} \mu^{\alpha_1\Gamma_{1\chi}\alpha_2\Gamma_{2\bar{\chi}}(F_{1u})}_{\{n_s\}\{m_s\}} V^{\alpha_1\Gamma_{1\chi}\alpha_2\Gamma_{2\bar{\chi}}(F_{1u})}_{\{n_s\}\{m_s\}\theta}, \quad [22]$$

$$(\chi = g \text{ or } u,\ \bar{\chi} = \chi \otimes u).$$

Here, the overall parity is u and $\epsilon = +1$. The $\mu^{\alpha_1\Gamma_{1\chi}\alpha_2\Gamma_{2\bar{\chi}}(F_{1u})}_{\{n_s\}\{m_s\}}$ are the dipole moment parameters.

As the contact transformation generator is expanded as a series of rovibrational operators (*1*), the transformed dipole moment,

$$\tilde{\mu}^{(F_{1u})}_\theta = \sum_{\{i\}} \tilde{\mu}^{\{i\}} M^{(\{i\},F_{1u})}_\theta, \quad [23]$$

is also formed by a series of rovibrational operators

$$M^{(\{i\},F_{1u})}_\theta = (R^{\Omega(K_g,n_t\Gamma_{rg})} \otimes \epsilon V^{\alpha_1\Gamma_{1\chi}\alpha_2\Gamma_{2\bar{\chi}}(\Gamma_{vu})}_{\{n_s\}\{m_s\}})^{(F_{1u})}_\theta, \quad [24]$$

with

$$\epsilon = (-1)^\Omega. \quad [25]$$

For sake of simplicity, we represent all the indexes in Eq. 24 by the symbol $\{i\}$. The $\tilde{\mu}^{\{i\}}$ are the transformed dipole moment parameters. It can be shown that the LFF components of the transformed dipole moment can be expressed using Eqs. 4 and 6 as

$$\tilde{\mu}^{(A_{1u})}_\Theta = \sqrt{3} \sum_m \langle 1; m|\Theta\rangle \sum_{\{i\}} \tilde{\mu}^{\{i\}} [C^{(1_g,F_{1g})} \otimes M^{(\{i\},F_{1u})}]^{(A_{1u})}. \quad [26]$$

This expression involves the direction cosines tensor, $C^{(1_g,F_{1g})}$, which is the tensor of $\lambda_{\Theta,\theta}$ coefficients of Eq. 2. The square brackets represent the symmetrized tensor product defined as

$$[A^{(\Gamma_1)} \otimes B^{(\Gamma_2)}]^{(\Gamma)} = \frac{1}{2}((A^{(\Gamma_1)} \otimes B^{(\Gamma_2)})^{(\Gamma)} + (-1)^{\Gamma_1+\Gamma_2+\Gamma}(B^{(\Gamma_2)} \otimes A^{(\Gamma_1)})^{(\Gamma)}). \quad [27]$$

We finally recall that the intensity of the dipole transition between the molecular rovibrational states $\tilde{\Phi}_i$ (with energy E_i) and $\tilde{\Phi}_f$ (with energy E_f) is calculated through

$$S_{if} = K_{if} g_i e^{-hcE_i/kT} \sum_{M_i,M_f} |\langle\tilde{\Phi}_i|\tilde{\mu}_Z|\tilde{\Phi}_f\rangle|^2, \quad [28]$$

where K_{if} is a numerical coefficient (depending on the transition frequency and on the temperature) and g_i is the spin statistical weight of state $\tilde{\Phi}_i$. The sum is realized over the spherical components M_i and M_f of the two states in the LFF. The Appendix gives the general expressions for the matrix elements of the transformed dipole moment operators.

3.3. Expression of the Polarizability

The polarizability operator is expanded in the same way. For the MFF components of the initial (untransformed) polarizability, we get

$$\alpha^{(L_g,\Gamma_g)}_\theta = \sum_{\text{all indexes}} \alpha^{\alpha_1\Gamma_{1\chi}\alpha_2\Gamma_{2\chi}(\Gamma_g)}_{\{n_s\}\{m_s\}} V^{\alpha_1\Gamma_{1\chi}\alpha_2\Gamma_{2\chi}(\Gamma_g)}_{\{n_s\}\{m_s\}\theta}, \quad [29]$$

$$(\chi = g \text{ or } u),$$

where θ is a component of the operator $\alpha^{(L_g,\Gamma_g)}$. The overall parity is g and $\epsilon = +1$. The $\alpha^{\alpha_1\Gamma_{1\chi}\alpha_2\Gamma_{2\chi}(\Gamma_g)}_{\{n_s\}\{m_s\}}$ are the polarizability parameters.

Just as for the dipole moment (see above), the transformed polarizability,

$$\tilde{\alpha}_{\theta}^{(L_g,\Gamma_g)} = \sum_{\{i\}} \tilde{\alpha}^{(\{i\},\Gamma_g)} P_{\theta}^{(\{i\},\Gamma_g)}, \qquad [30]$$

is expanded as a series of rovibrational operators,

$$P_{\theta}^{(\{i\},\Gamma_g)} = (R^{\Omega(K_g,n_r\Gamma_{rg})} \otimes {}^{\epsilon}V_{\{n_s\}\{m_s\}}^{\alpha_1\Gamma_{1X}\alpha_2\Gamma_{2\chi}(\Gamma_{vg})})_{\theta}^{(\Gamma_g)}. \qquad [31]$$

The symbol $\{i\}$ represents all the indexes in Eq. 31. The $\tilde{\alpha}^{(\{i\},\Gamma_g)}$ are the transformed parameters and

$$\epsilon = (-1)^{\Omega}. \qquad [32]$$

The LFF components of the transformed polarizability are

$$\begin{aligned}\tilde{\alpha}_{\Theta_1\Theta_2}^{(A_{1g})} = {} & \langle 0;\, 0|\Theta_1\Theta_2\rangle \sum_{\{i\}} \tilde{\alpha}^{(\{i\},A_{1g})}[C^{(0_g,A_{1g})} \otimes P^{(\{i\},A_{1g})}]^{(A_{1g})} \\ & + \sqrt{2} \sum_{m} \langle 2;\, m|\Theta_1\Theta_2\rangle \sum_{\{i\}} \tilde{\alpha}^{(\{i\},E_g)} \\ & \times [C^{(2_g,E_g)} \otimes P^{(\{i\},E_g)}]^{(A_{1g})} \\ & + \sqrt{3} \sum_{m} \langle 2;\, m|\Theta_1\Theta_2\rangle \sum_{\{i\}} \tilde{\alpha}^{(\{i\},F_{2g})} \\ & \times [C^{(2_g,F_{2g})} \otimes P^{(\{i\},F_{2g})}]^{(A_{1g})}\end{aligned} \qquad [33]$$

with Θ_1, $\Theta_2 = X$, Y, or Z. The first term (A_{1g} symmetry) in this expression represents the isotropic part of the polarizability, the two other terms (E_g and F_{2g} symmetry) are the anisotropic part.

The intensity of Raman transitions is expressed as

$$I_{if} = R_{if} g_i e^{-hcE_i/kT} \sum_{\Theta,\Theta'} \sum_{M_i,M_f} |\langle \tilde{\Phi}_i|\tilde{\alpha}_{\Theta\Theta'}|\tilde{\Phi}_f\rangle|^2. \qquad [34]$$

The general expression for the matrix elements of the transformed polarizability operators is given in the Appendix.

3.4. Selection Rules

Let us consider two rovibrational wavefunctions, say $|\Psi_{M\sigma}^{(C_\tau)}\rangle$ and $|\Psi_{M'\sigma'}^{(C'_{\tau'})}\rangle$. The selection rules come directly from the expressions of the matrix elements given in the Appendix and from the properties of the different coupling symbols involved (*1, 12*). These rules are presented in Table 4 for the different operators. The rule concerning J comes from the nonzero condition of the K isoscalar factors (see Appendix); the rule $C' = C$ comes from the fact that all three operators are of symmetry A_1 in the LFF (see Table 1), while the parity selection rule depends on the parity of the operator under consideration.

TABLE 4
Selection Rules for the Hamiltonian ($\tilde{H}$), Dipole Moment ($\tilde{\mu}$), and Polarizability ($\tilde{\alpha}$) Operators

	$\tilde{H}$	$\tilde{\mu}$	$\tilde{\alpha}^{(0)}$	$\tilde{\alpha}^{(2)}$
ΔJ	0	0, ±1	0	0, ±1, ±2
ΔM	0	0, ±1	0	0, ±1, ±2
Symmetry	$C' = C$	$C' = C$	$C' = C$	
Parity	$\tau' = \tau$	$\tau' \neq \tau$	$\tau' = \tau$	
Component	$\sigma' = \sigma$	$\sigma' = \sigma$	$\sigma' = \sigma$	

Note. $\tilde{\alpha}^{(0)}$ and $\tilde{\alpha}^{(2)}$ are the isotropic and anisotropic parts of the polarizability, respectively.

3.5. Discussion

The above selection rules show that the most important difference between the O_h and T_d groups is for the dipole moment which is of F_{1u} (resp. A_{1u}) symmetry in MFF (resp. LFF) in O_h, while it is of F_2 (resp. A_2) symmetry in T_d. Moreover, in O_h, one has to take the parity into account. In particular, dipole-induced transitions (absorption or emission) can only occur between states of opposite parity (only $g \leftrightarrow u$ transitions). As a consequence, pure rotational transitions in a given vibrational state are forbidden. Polarizability-induced (Raman) transitions can only occur between states of the same parity (only $g \leftrightarrow g$ or $u \leftrightarrow u$ transitions). The bands observed in absorption (or emission) spectra of octahedral molecules cannot be observed in Raman spectra and reciprocally. This is completely different from the case of tetrahedral molecules.

4. STARK EFFECT

In this section, we develop an application of the formalism detailed in the preceding sections to the Stark effect. We present here the basic principles and two simplified models to treat the Stark effect. These results could be used as a starting point for the study of octahedral molecules submitted to a time-dependent electric field (like a pulsed laser), i.e., of the dynamic Stark effect.

4.1. Basic Principles

Let us suppose that we have developed a transformed Hamiltonian $\tilde{H}$ (in order to isolate the polyads) for the molecules in the absence of any external electric field, as well as the corresponding transformed transition moments. If a electric field **E** is applied to the molecules, the Hamiltonian becomes

$$\tilde{H}^S = \tilde{H} + {}^{\mu}\tilde{H} + {}^{\alpha}\tilde{H}, \qquad [35]$$

where ${}^{\mu}\tilde{H}$ and ${}^{\alpha}\tilde{H}$ are interaction terms between a molecule and the field, i.e.,

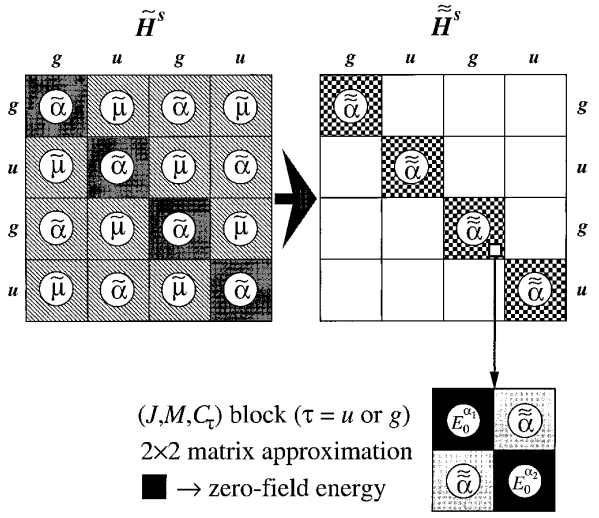

FIG. 1. The 2 × 2 matrix approximation for the Stark effect in the weak field approximation. Rows and columns represent polyads with alternatively g or u parity.

$$^{\mu}\tilde{H} = -\tilde{\boldsymbol{\mu}} \cdot \mathbf{E}, \qquad [36]$$

$$^{\alpha}\tilde{H} = -\tilde{\boldsymbol{\alpha}}\text{:}\mathbf{E}\text{:}\mathbf{E}. \qquad [37]$$

$\tilde{H}$ is block-diagonal (one block per polyad), but $\tilde{\boldsymbol{\mu}}$ and $\tilde{\boldsymbol{\alpha}}$ are not. So the Stark Hamiltonian $\tilde{H}^S$ is not block-diagonal and the polyads defined for zero-field are not isolated anymore. However, if the nondiagonal energy contribution is small enough (weak field case), one can perform a second contact transformation (this one is field-dependent) to isolate the polyads again, that is

$$\tilde{\tilde{H}}^S = \tilde{H} - \tilde{\boldsymbol{\mu}} \cdot \mathbf{E} - \tilde{\boldsymbol{\alpha}}\text{:}\mathbf{E}\text{:}\mathbf{E}. \qquad [38]$$

Doing so, the contribution of the nondiagonal terms is removed to higher orders of the development.

4.2. Application to Octahedral Molecules

Considering the parity selection rules (see Section 3.4), one can see that the dipole moment being of parity u it can only connect polyads of opposite parity, while the polarizability (g parity) connects only blocks with the same parity (see left part of Fig. 1). As a consequence, the dipole moment has no matrix elements within the diagonal blocks (see also the rule implying the absence of pure rotational transitions, in paragraph 3.5). $\tilde{\boldsymbol{\mu}}$ appears only in the nondiagonal blocks. After the contact transformation (right part of Fig. 1), $\tilde{\boldsymbol{\mu}}$ disappears. Thus, from Eq. 38, $\tilde{\tilde{H}}^S$can be written in the form

$$\tilde{\tilde{H}}^S = \tilde{H} - \tilde{\tilde{\boldsymbol{\alpha}}}\text{:}\mathbf{E}\text{:}\mathbf{E}. \qquad [39]$$

This is different from the case of tetrahedral molecules (*1*) for which the diagonal blocks depend on $\tilde{\tilde{\boldsymbol{\mu}}}$ like in Eq. 38. The parameters of $\tilde{\tilde{\boldsymbol{\mu}}}$ for T_d molecules can be determined through the observation of the static Stark effect (*15–19*).

If we consider an isolated polyad, the polarizability selection rules (see Section 3.4) are such that $\Delta J = 0, \pm 1$, or ± 2. Thus, the Stark matrix is an infinite band matrix. As a first step, we can neglect interactions between levels with different J values. As we have also the selection rule $C' = C$ (see Section 3.4), we can restrict our study to a single (J, C_τ) block ($\tau = u$ or g).

Let us take an electrical field polarized in the LFF along the (OZ) axis. In this case, only the $\tilde{\alpha}_{ZZ}$ component of the polarizability is involved and we can write

$$\tilde{\tilde{H}}^S = \tilde{H} - \tilde{\alpha}_{ZZ}^{(A_{1g})} E_Z^2. \qquad [40]$$

We have here the simplified selection rule $\Delta M = 0$ which comes from the nonzero conditions of the Stone coefficients (*13*). So we can finally restrict ourselves to the study of a single (J, M, C_τ) block. Formally, the expression of the doubly transformed polarizability $\tilde{\tilde{\alpha}}$ is the same as that of the transformed polarizability $\tilde{\alpha}$. If we replace the Stone coefficients in Eq. 33 by their values (*13*), we obtain

$$\begin{aligned}\tilde{\tilde{\alpha}}_{ZZ}^{(A_{1g})} = &-\frac{1}{\sqrt{3}}\,\tilde{\alpha}^{([i],A_{1g})}[C^{(0,A_{1g})} \otimes P^{([i],A_{1g})}]^{(A_{1g})} \\ &-\frac{2}{\sqrt{3}}\,\tilde{\alpha}^{([i],E_g)}[C^{(2,E_g)} \otimes P^{([i],E_g)}]^{(A_{1g})} \\ &-\sqrt{2}\,\tilde{\alpha}^{([i],F_{2g})}[C^{(2,F_{2g})} \otimes P^{([i],F_{2g})}]^{(A_{1g})}.\end{aligned} \qquad [41]$$

The matrix elements within a (J, M, C_τ) block are then

$$\begin{aligned}\langle \tilde{\Phi}_{M\sigma}^{(JC_\tau\alpha_1)} | \tilde{\tilde{\alpha}}_{ZZ}^{(A_{1g})} | \tilde{\Phi}_{M\sigma}^{(JC_\tau\alpha_2)} \rangle = &-\sqrt{\frac{2J+1}{3}}\, I(\alpha_1, \alpha_2) \\ &+\sqrt{\frac{2}{3}}\,\frac{2[3M^2 - J(J+1)](2J+1)}{\sqrt{(2J+3)(2J+2)(2J+1)2J(2J-1)}} \\ &\times A(\alpha_1, \alpha_2),\end{aligned} \qquad [42]$$

where the $\tilde{\Phi}$ are the zero-field Hamiltonian eigenfunctions. For sake of clarity, the specific contributions of the isotropic and anisotropic parts (see Eq. 54 in the Appendix) are simply represented by $I(\alpha_1, \alpha_2)$ and $A(\alpha_1, \alpha_2)$, respectively. The J and M dependence comes from the expression of the $3j$ symbol of Eq. 56 (see Appendix). Equation 42 is

the one which is useful in practice for Stark effect calculations. Values for the $I(\alpha_1, \alpha_2)$ and $A(\alpha_1, \alpha_2)$ coefficients can be obtained from the authors upon request. This can be rearranged in the form

$$\langle\tilde{\Phi}^{(JC_\tau\alpha_1)}_{M\sigma}|-\tilde{\alpha}^{(A_{1g})}_{ZZ}E_Z^2|\tilde{\Phi}^{(JC_\tau\alpha_2)}_{M\sigma}\rangle = (\mathcal{I}(\alpha_1, \alpha_2) + \mathcal{A}(\alpha_1, \alpha_2)M^2)E_Z^2. \quad [43]$$

These matrix elements are proportional to E_Z^2, the coefficient comprising a constant plus another part which is quadratic in M.

4.3. 2 × 2 Matrix Approximation

Practically, inside the (J, M, C_τ) blocks, there appear couples of very close energy levels. If the electric field is not too strong, we can restrict ourselves to the study of these two levels; in this case, the Stark effect is simply described by a 2 × 2 matrix (see also lowest part of Fig. 1),

$$\begin{matrix} |\tilde{\Phi}^{(JC_\tau\alpha_1)}_{M\sigma}\rangle & \\ \begin{pmatrix} \tilde{E}_0^{\alpha_1} & \\ (\mathcal{I}(\alpha_1, \alpha_2) + \mathcal{A}(\alpha_1, \alpha_2)M^2)E_Z^2 & \end{pmatrix} & \begin{matrix} \\ |\tilde{\Phi}^{(JC_\tau\alpha_2)}_{M\sigma}\rangle \end{matrix} \\ & \begin{matrix} (\mathcal{I}(\alpha_1, \alpha_2) + \mathcal{A}(\alpha_1, \alpha_2)M^2)E_Z^2 \\ \tilde{E}_0^{\alpha_2} \end{matrix} \end{matrix}. \quad [44]$$

The diagonal terms are the displaced energies,

$$\tilde{E}_0^{\alpha_i} = E_0^{\alpha_i} + (\mathcal{I}(\alpha_i, \alpha_i) + \mathcal{A}(\alpha_i, \alpha_i)M^2)E_Z^2, \quad [45]$$

$E_0^{\alpha_2}$ being the zero-field energy ($i = 1, 2$). The eigenvalues $E^+(M)$ and $E^-(M)$ of this matrix are given by

$$E^{\pm}(M) = \frac{\tilde{E}_0^{\alpha_1} + \tilde{E}_0^{\alpha_2}}{2} \pm \frac{\sqrt{(\tilde{E}_0^{\alpha_1} - \tilde{E}_0^{\alpha_2})^2 + 4(\mathcal{I}(\alpha_1, \alpha_2) + \mathcal{A}(\alpha_1, \alpha_2)M^2)^2E_Z^4}}{2}. \quad [46]$$

Let us consider the two limit cases. The weak field case,

$$(\tilde{E}_0^{\alpha_1} - \tilde{E}_0^{\alpha_2})^2 \gg 4(\mathcal{I}(\alpha_1, \alpha_2) + \mathcal{A}(\alpha_1, \alpha_2)M^2)^2E_Z^4. \quad [47]$$

The eigenvalues can be expanded as

$$E^{\alpha_1}(M) = \tilde{E}_0^{\alpha_1} + \frac{(\mathcal{I}(\alpha_1, \alpha_2) + \mathcal{A}(\alpha_1, \alpha_2)M^2)^2E_Z^4}{(\tilde{E}_0^{\alpha_1} - \tilde{E}_0^{\alpha_2})} + \ldots, \quad [48]$$

$$E^{\alpha_2}(M) = \tilde{E}_0^{\alpha_2} - \frac{(\mathcal{I}(\alpha_1, \alpha_2) + \mathcal{A}(\alpha_1, \alpha_2)M^2)^2E_Z^4}{(\tilde{E}_0^{\alpha_1} - \tilde{E}_0^{\alpha_2})} + \ldots \quad [49]$$

To this order of development, the Stark effect is quartic in E_Z. The isotropic part shifts the levels independently of M, while the anisotropic part induces a splitting which is smaller than the distance between the two zero-field energy levels, as shown on Fig. 2a.

The strong field case,

$$(\tilde{E}_0^{\alpha_1} - \tilde{E}_0^{\alpha_2})^2 \ll 4(\mathcal{I}(\alpha_1, \alpha_2) + \mathcal{A}(\alpha_1, \alpha_2)M^2)^2E_Z^4. \quad [50]$$

Here, the Stark energies are expanded as

$$E^{\pm}(M) = \frac{\tilde{E}_0^{\alpha_1} + \tilde{E}_0^{\alpha_2}}{2} \pm (\mathcal{I}(\alpha_1,\alpha_2) + \mathcal{A}(\alpha_1,\alpha_2)M^2)E_Z^2 + \ldots \quad [51]$$

To this order of development, the Stark effect is quadratic in E_Z. The anisotropic term induces a splitting which is greater than the zero-field energy separation, as shown on Fig. 2b.

4.4. 4 × 4 Matrix Approximation

We have seen in the preceding sections that the 2 × 2 matrix approximation is valuable only if the electric field-induced interactions between the different polyads are relatively weak. If this is not the case, we have to take these interactions explicitly into account.

Let us consider, for example, two interacting polyads of opposite parity (Fig. 3). We now choose two relatively well isolated couples of levels, one in each of the two polyads. These two couples of levels are coupled by the transformed dipole moment $\tilde{\mu}$ (right part of Fig. 3). We thus obtain a 4 × 4 matrix which corresponds to the simultaneous study of a four-level system and of the dipole-induced transitions between them (lowest part of Fig. 3). The off-diagonal 2 × 2 block depends on $\tilde{\mu}$ and represents the transition moments. Its matrix elements are linear in M and in E_Z.

If we consider two interacting polyads of the same parity (g or u), the off-diagonal block depends only on $\tilde{\alpha}$ and represents Raman transition moments.

This scheme is the one that could be used for the study of the dynamical Stark effect.

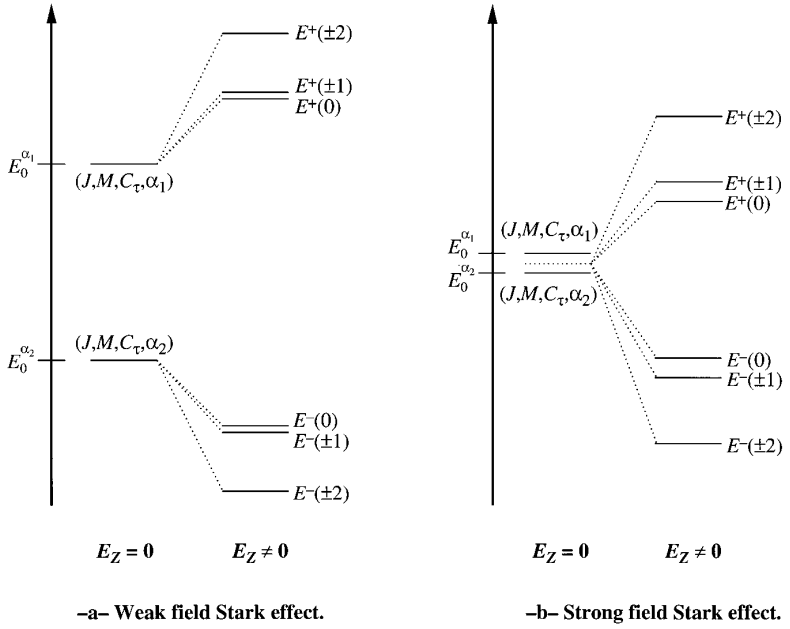

FIG. 2. Energy level scheme for weak (a) and strong (b) static Stark effect.

5. CONCLUSION

In this paper, we have explained the methods to expand the transition moment operators for octahedral molecules using a tensorial formalism. We have shown the main differences between the O_h and T_d cases. The formulas necessary to calculate the matrix elements of these operators have been given as well as the related selection rules. The parity selection rule plays an important role in O_h molecules and is the most important source of differences with T_d molecules. A new version of the STDS software developed in Dijon for the calculation of XY_4 molecular spectra (*20*) has been recently released for the case of XY_6 molecules (*21*); it uses the formulas derived in the present paper for intensity calculations.

Two simplified models for the study of the Stark effect in octahedral molecules have been detailed. This could serve as a starting point for the study of octahedral molecules interacting with electric fields, either static or time-dependent.

Another interesting extension of this work would be the study of electronic transitions in octahedral molecules. Some species like ReF_6, IrF_6, PuF_6, $V(CO)_6$, . . . are open-shell systems with low-lying electronic states. These ones (including the ground electronic state) can be degenerate. We have already started to study the problem of Hamiltonian expansion in the case of (ro)vibronic couplings in such degenerate electronic states (*22–24*). We now intend to extend this study to the expansion of the transition moment operators for rovibronic transitions (either inside a given electronic state, or more generally between two different electronic states). The complete understanding of rovibronic transitions in highly symmetric molecules is still an open question which could be interesting for many other molecular problems (spectroscopy of molecular ions, free radicals, etc.).

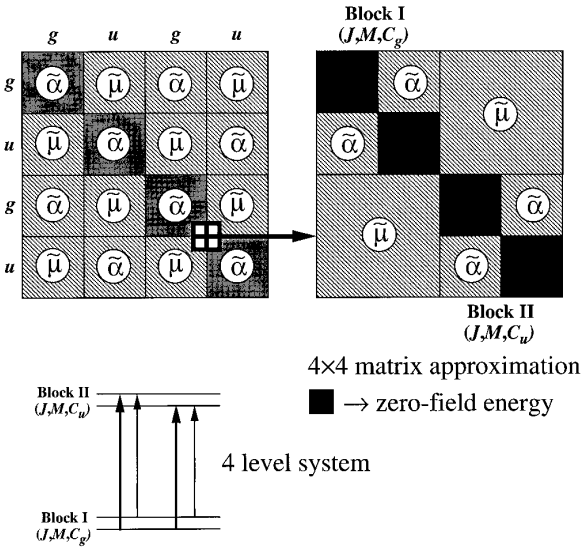

FIG. 3. The 4 × 4 matrix approximation for static Stark effect.

APPENDIX

Matrix Elements of the Hamiltonian Operators

$$\langle[\Psi^{(J_g,n'C'_{rg})}\otimes\Psi_{v'}^{(C'_{v\tau})}]_\sigma^{(C_\tau)}|(R^{\Omega(K_g,n_r\Gamma_g)}\otimes\epsilon V_{\{n_s\}\{m_s\}}^{\alpha_1\Gamma_{1\chi}\alpha_2\Gamma_{2\chi}(\Gamma_g)})^{(A_{1g})}|[\Psi^{(J_g,nC_{rg})}\otimes\Psi_v^{(C_{v\tau})}]_\sigma^{(C_\tau)}\rangle$$
$$=\delta_{J',J}(-1)^{\Gamma+C+C_r+C'_r}\frac{(-1)^J}{\sqrt{[\Gamma]}}K\begin{pmatrix}J_g & K_g & J_g\\ n'C'_{rg} & n_r\Gamma_g & nC_{rg}\end{pmatrix}\begin{Bmatrix}C'_{rg} & C'_{v\tau} & C_\tau\\ C_{v\tau} & C_{rg} & \Gamma_g\end{Bmatrix}\langle J_g\|R^{\Omega(K_g,n\Gamma)}\|J_g\rangle\langle\Psi_{v'}^{(C'_{v\tau})}\|\epsilon V_{\{n_s\}\{m_s\}}^{\alpha_1\Gamma_{1\chi}\alpha_2\Gamma_{2\chi}(\Gamma_g)}\|\Psi_v^{(C_{v\tau})}\rangle. \quad [52]$$

Matrix Elements of the Dipole Moment Operators

$$\langle[\Psi^{(J'_g,n'C'_{rg})}\otimes\Psi_{v'}^{(C'_{v\tau'})}]_\sigma^{(C_{\tau'})}|[C^{(1_g,F_{1g})}\otimes M^{([i],F_{1u})}]^{(A_{1u})}|[\Psi^{(J_g,nC_{rg})}\otimes\Psi_v^{(C_{v\tau})}]_\sigma^{(C_\tau)}\rangle$$
$$=-\frac{(-1)^{C'_v+C'_r}}{2}\langle J'_g\|C^{(1_g)}\|J_g\rangle\langle\Psi_{v'}^{(C'_{v\tau'})}\|\epsilon V_{\{n_s\}\{m_s\}}^{\alpha_1\Gamma_{1\chi}\alpha_2\Gamma_{2\chi}(\Gamma_{vu})}\|\Psi_v^{(C_{v\tau})}\rangle\Bigg\{(-1)^{C+\Gamma_v+\Gamma_r}\langle J'_g\|R^{\Omega(K_g)}\|J'_g\rangle\sum_{C''_r}\Bigg[\begin{Bmatrix}\Gamma_{vu} & C_{rg} & C'_{rg}\\ C_{\tau'} & C'_{v\tau'} & C_{v\tau}\end{Bmatrix}$$
$$\times\begin{Bmatrix}\Gamma_{vu} & C_{rg} & C'_{rg}\\ C''_{rg} & \Gamma_{rg} & F_{1u}\end{Bmatrix}\sum_{n''}K\begin{pmatrix}1_g & J_g & J'_g\\ 0F_{1g} & nC_{rg} & n''C''_{rg}\end{pmatrix}K\begin{pmatrix}K_g & J'_g & J'_g\\ n_r\Gamma_{rg} & n''C''_{rg} & n'C'_{rg}\end{pmatrix}\Bigg]+(-1)^{J+J'}(-1)^{C'}\langle J_g\|R^{\Omega(K_g)}\|J_g\rangle \quad [53]$$
$$\times\sum_{C''_r}\Bigg[\begin{Bmatrix}\Gamma_{vu} & C'_{rg} & C_{rg}\\ C_\tau & C_{v\tau} & C'_{v\tau'}\end{Bmatrix}\begin{Bmatrix}\Gamma_{vu} & C'_{rg} & C_{rg}\\ C''_{rg} & \Gamma_{rg} & F_{1u}\end{Bmatrix}\sum_{n''}K\begin{pmatrix}1_g & J_g & J'_g\\ 0F_{1g} & n''C''_{rg} & n'C'_{rg}\end{pmatrix}K\begin{pmatrix}K_g & J_g & J_g\\ n_r\Gamma_{rg} & nC_{rg} & n''C''_{rg}\end{pmatrix}\Bigg]\Bigg\}.$$

Matrix Elements of the Polarizability Operators

$$\langle[\Psi^{(J'_g,n'C'_{rg})}\otimes\Psi_{v'}^{(C'_{v\tau})}]_\sigma^{(C_\tau)}|[C^{(L_g,\Gamma_g)}\otimes P^{([i],\Gamma_g)}]^{(A_{1g})}|[\Psi^{(J_g,nC_{rg})}\otimes\Psi_v^{(C_{v\tau})}]_\sigma^{(C_\tau)}\rangle$$
$$=\frac{1}{2}(-1)^{C'_v+C'_r+C}\langle J'_g\|C^{(L_g)}\|J_g\rangle\langle\Psi_{v'}^{(C'_{v\tau})}\|\epsilon V_{\{n_s\}\{m_s\}}^{\alpha_1\Gamma_{1\chi}\alpha_2\Gamma_{2\chi}(\Gamma_{vg})}\|\Psi_v^{(C_{v\tau})}\rangle\Bigg\{\begin{matrix}C'_{v\tau} & C'_{rg} & C_\tau\\ C_{rg} & C_{v\tau} & \Gamma_{vg}\end{matrix}\Bigg\}\Bigg\{(-1)^{J+J'}\langle J_g\|R^{\Omega(K_g)}\|J_g\rangle$$
$$\times\sum_{C''_r}\Bigg[\begin{Bmatrix}\Gamma_{vg} & \Gamma_{rg} & \Gamma_g\\ C''_{rg} & C'_{rg} & C_{rg}\end{Bmatrix}\sum_{n''}K\begin{pmatrix}L_g & J_g & J'_g\\ 0\Gamma_g & nC_{rg} & n''C''_{rg}\end{pmatrix}K\begin{pmatrix}K_g & J_g & J_g\\ n_r\Gamma_{rg} & n''C''_{rg} & nC_{rg}\end{pmatrix}\Bigg]+(-1)^{\Gamma_r+\Gamma_v}\langle J_g\|R^{\Omega(K_g)}\|J_g\rangle \quad [54]$$
$$\times\sum_{C''_r}\Bigg[\begin{Bmatrix}\Gamma_{vg} & \Gamma_{rg} & \Gamma_g\\ C''_{rg} & C_{rg} & C'_{rg}\end{Bmatrix}\sum_{n''}K\begin{pmatrix}L_g & J_g & J'_g\\ 0\Gamma_g & n''C''_{rg} & n'C'_{rg}\end{pmatrix}K\begin{pmatrix}K_g & J'_g & J'_g\\ n_r\Gamma_{rg} & n'C'_{rg} & n''C''_{rg}\end{pmatrix}\Bigg]\Bigg\}.$$

Notes

The K's are isoscalar factors for the $O(3)\supset O_h$ group chain and the $\{\ldots\}$ are $6C$ coefficients for the O_h group (*1*).

Only nonvanishing matrix elements are considered in the above formula. Here, we have

$$[J]=2J+1, \quad [55]$$

and $[C]$ is the dimension of the irreducible representation C. In relations [53] and [54], the $C^{(L_g)}$-reduced matrix elements are given by (*1*)

$$\langle\Psi_{M'}^{(J'_g)}\|C_m^{(L_g)}\|\Psi_M^{(J_g)}\rangle=(-1)^{1+J'-M'}\sqrt{[J][J']}\begin{pmatrix}J' & L & J\\ -M' & m & M\end{pmatrix}. \quad [56]$$

REFERENCES

1. J.-P. Champion, M. Loëte, and G. Pierre, *in* "Spectroscopy of the Earth's Atmosphere and Interstellar Medium" (K. N. Rao and A. Weber, Eds.), pp. 339–422, Academic Press, New York, 1992.
2. J. P. Aldridge, H. Filip, H. Flicker, R. F. Holland, R. S. McDowell, N. G. Nereson, and K. Fox, *J. Mol. Spectrosc.* **58,** 165–168 (1975).
3. Ch. J. Bordé, M. Ouhayoun, A. van Lerberghe, C. Salomon, S. Arvillier, C. D. Cantrell, and J. Bordé, *in* "Laser Spectroscopy IV, Proceedings of the 4th International Conference, Rottac-Engern, June 1979," (H. Walter and K. W. Rothe, Ed.), Springer-Verlag, New York, 1979.
4. M. O. Acef, Ch. J. Bordé, G. Pierre, and B. G. Sartakov, in press.
5. V. Boudon, M. Hepp, M. Herman, and G. Pierre, *J. Mol. Spectrosc.* **192,** 359–367 (1998).
6. W. B. Person and B. J. Krohn, *J. Mol. Spectrosc.* **98,** 229–257 (1983).
7. S. Te Lintel Hekkert, A. F. Linskens, B. G. Sartakov, G. Pierre, and J. Reuss, *Chem. Phys.* **173,** 9–16 (1993).
8. S. Te Lintel Hekkert, A. F. Linskens, I. Holleman, B. G. Sartakov, G. Pierre, and J. Reuss, *Chem. Phys.* **176,** 171–184 (1993).

9. S. Te Lintel Hekkert, A. F. Linskens, B. G. Sartakov, G. Pierre, and J. Reuss, *Chem. Phys.* **177,** 181–189 (1993).
10. A. F. Linskens, N. Dam, B. Sartakov, and J. Reuss, *J. Mol. Spectrosc.* **180,** 207–217 (1996).
11. D. Papoušek and M. R. Aliev, *Molecular vibrational-rotational spectra,* Elsevier, Amsterdam-Oxford-New York (1982).
12. A. R. Edmonds, *Angular momentum in quantum mechanics,* Princeton University Press, Princeton (1982).
13. A. J. Stone, *Mol. Phys.* **29,** 1461–1471 (1975).
14. A. Boutahar and M. Loëte, *Can. J. Phys.* **69,** 26–35 (1990).
15. A. Ainetschian, W. A. Kreiner, M.-P. Coquard, and M. Loëte, *J. Mol. Spectrosc.* **161,** 264–268 (1993).
16. V. I. Perevalov, M.-P. Coquard, and M. Loëte, *J. Mol. Spectrosc.* **169,** 484–501 (1995).
17. M.-P. Coquard, M. Loëte, A. Ainetschian, and W. A. Kreiner, *J. Mol. Spectrosc.* **170,** 251–265 (1995).
18. M.-P. Coquard and M. Loëte, *J. Mol. Spectrosc.* **172,** 485–502 (1995).
19. M. Loëte, M.-P. Coquard, Y. Ohshima, and M. Takami, *J. Chem. Phys.* **102**(12), 4819–4822 (1995).
20. Ch. Wenger and J.-P. Champion, *J. Quant. Spectrosc. Radiat. Transfer* **59,** 471–480 (1998).
21. Ch. Wenger, V. Boudon, J.-P. Champion, and G. Pierre, *J. Quant. Spectrosc. Radiat. Transfer,* in press.
22. V. Boudon and F. Michelot, *J. Mol. Spectrosc.* **165,** 554–579 (1994).
23. V. Boudon, F. Michelot, and J. Moret-Bailly, *J. Mol. Spectrosc.* **166,** 449–470 (1994).
24. V. Boudon, M. Rotger, and D. Avignant, *J. Mol. Spectrosc.* **175,** 327–339 (1996).

Journal of Molecular Spectroscopy **201,** 95–108 (2000)
doi:10.1006/jmsp.2000.8070, available online at http://www.idealibrary.com on IDEAL®

Analysis of the "Unusual" Vibrational Components of Triply Degenerate Vibrational Mode ν_6 of $Mo(CO)_6$ Based on the Classical Interpretation of the Effective Rotation–Vibration Hamiltonian

G. Dhont,* D. Sadovskiĭ,* B. Zhilinskiĭ,* and V. Boudon†

*MREID, Université du Littoral, 145 av. M. Schumann, F-59140 Dunkerque, France; and †Laboratoire de Physique de l'Université de Bourgogne, CNRS, B.P. 47870, F-21078 Dijon Cedex, France

E-mail: zhilin@univ-littoral.fr, boudon@jupiter.u-bourgogne.fr

Received September 14, 1999; in revised form January 14, 2000

Rotational structure of the triply degenerate vibrational state $\nu_6(F_{1u})$ of the octahedral molecule $Mo(CO)_6$ is analyzed qualitatively on the basis of classical mechanics. We show that the energy level redistribution between the vibrational components of $\nu_6(F_{1u})$ occurs due to rotational excitation and is related to the formation of singular points of classical rotational energy surfaces. The singularity is stable under small variations of parameters of the effective rovibrational Hamiltonian. Parameters responsible for the persistence of this phenomenon are specified. Comparison with quantum calculations demonstrates the high qualitative and quantitative accuracy of our classical analysis. © 2000 Academic Press

Key Words: rovibrational interactions; spherical top molecules; quantum-classical correspondence.

1. INTRODUCTION

Modern spectroscopic studies produce an increasing amount of information on the rotational structure of different vibrational states of a constantly widening variety of molecules. Typically this information is represented as a list of effective parameters which can be used to reproduce quantum energies, transition frequencies, and intensities with sufficiently high precision. On the other hand, we can use the same effective parameters to describe global qualitative features of the systems of energy levels and corresponding spectral transitions. For example, we can study formation of vibrational bands, energy level clusters, modification of the cluster structure, etc. Such qualitative analysis attracts increasing attention of spectroscopists. It is mainly based on the theory of classical dynamical systems which at the first sight does not seem to be very relevant to "purely" quantum systems such as a simple molecule in a specific quantum vibrational state. At the same time, several classical approaches were used very successfully over the last two decades to interpret quantum effects observed in rotational, vibrational, and electronic structure (see Refs. (*1–19*)). In fact, once the advantages of qualitative classical analysis are appreciated in full, this analysis will become a natural complement of practically every spectroscopic study.

Classical interpretation of molecular spectra was pioneered by Dorney and Watson (*1*), who successfully explained the existence of six- and eightfold degenerate clusters of rotational levels of spherical top molecules in terms of stable classical rotation (precession) around six and eight symmetry axes of the type C_4 and C_3, respectively. This approach was largely advanced in the works by Harter and co-workers (*2, 3, 4, 6*), who introduced the so-called *rotational energy surface* (RES) to describe the structure of quantum rotational multiplet of a nondegenerate isolated vibrational state (*4*). Pavlichenkov and Zhilinskiĭ (*5*) considered and interpreted quantum analogues of classical bifurcations of RESs which occur naturally when rotational excitation (i.e., quantum number J) increases. The RES construction was generalized to a group of quasi-degenerate vibrational levels in (*6, 7*). Crossings of the RESs representing such a group, known also as *diabolic points,* were analyzed in (*8*). General rules governing level redistribution which takes place at such crossings in tetrahedral molecules were formulated in a series of works by Brodersen and Zhilinskiĭ (*14, 15, 16*). Generalizations to other systems, such as vibrational polyads, formulation of the qualitative analysis on the basis of topological and group theoretical arguments, and examples are discussed in (*12, 11, 17*). In this work we present classical qualitative *and* quantitative interpretation of the effective quantum Hamiltonian of the octahedral molecule $Mo(CO)_6$ whose triply degenerate vibrational state ν_6 reconstructed by Asselin *et al.* (*20*) is of a quite unusual rovibrational structure. Reference (*20*) describes the first high-resolution spectroscopic study of this heavy spherical top. The authors where able to fit data from the ν_6 band up to $J = 74$.

2. EFFECTIVE HAMILTONIAN AND QUANTUM-CLASSICAL CORRESPONDENCE

The octahedral molecule $Mo(CO)_6$ possesses 13 normal modes of vibration (*21*). We study the triply degenerate C–O

0022-2852/00 $35.00

stretch fundamental state ν_6 of symmetry F_{1u}. This vibrational state can be considered as isolated because (i) among the six C–O stretch fundamentals ($A_{1g} + E_g + F_{1u}$), it is the only state of the u symmetry type; (ii) for the O_h molecules interactions between u and g states are forbidden; and (iii) C–O stretch fundamentals lie in the 2000 cm^{-1} region, well above all other vibrations, of the molecule (stretches Mo–C, bends C–Mo–C, and Mo–C–O, etc.).

2.1. *Effective Quantum Rotation–Vibration Hamiltonian*

The effective Hamiltonian $\tilde{H}$ for the isolated $v_6 = 1$ vibrational state can be represented as a series of coupled terms $H^{\Omega(K,n\Gamma)}$ constructed from vibrational and rotational tensor operators, $V^{(\Gamma)}$ and $R^{\Omega(K,n\Gamma)}$, respectively,

$$H^{\Omega(K,n\Gamma)} = [V^{(\Gamma)} \otimes R^{\Omega(K,n\Gamma)}]^{(A_{1g})}. \quad [1]$$

Vibrational operators are in turn built as symmetrized tensor products of creation and annihilation operators for mode ν_6, $a_6^{+(F_{1u})}$, and $a_6^{(F_{1u})}$,

$$V^{\Gamma}_{\sigma} = [a_6^{+(F_{1u})} \otimes a_6^{(F_{1u})}]^{(\Gamma)}_{\sigma}, \quad [2]$$

while rotational tensor operators are constructed from elementary angular momentum operators J_x, J_y, and J_z (*22*). Including all possible rovibrational operators up to order three, we obtain the Hamiltonian

$$\begin{aligned}\tilde{H} = {} & k_1 V^{(A_{1g})} + k_2 R^{2(0_g,A_{1g})} + k_3 H^{1(1_g,F_{1g})} \\ & + k_4 H^{2(0_g,A_{1g})} + k_5 H^{2(2_g,E_g)} + k_6 H^{2(2_g,F_{2g})} \\ & + k_7 H^{3(1_g,F_{1g})} + k_8 H^{3(3_g,F_{1g})}.\end{aligned} \quad [3]$$

The first three terms in $\tilde{H}$ describe the degenerated three dimensional harmonic oscillator, the spherical-top rigid rotor, and the Coriolis interaction, respectively. Parameters k_i ($i = 1, \ldots, 8$) are related to those in Ref. (*20*) as shown in Table 1. Parameters k_1, k_2, and k_4 define the scalar contribution to the rotational energy

$$E_s(\mathcal{J}) = \frac{1}{\sqrt{3}} k_1 - \frac{4}{\sqrt{3}} k_2 \mathcal{J}^2 - \frac{4}{3} k_4 \mathcal{J}^2, \quad [4]$$

where

$$\mathcal{J} = \sqrt{J(J+1)} \quad [5]$$

is the amplitude of the angular momentum and J is the rotation quantum number. The term $E_s(\mathcal{J})$ is common to all levels within the rotational multiplet of ν_6. Consequently, parameters k_1, k_2, and k_4 are of no interest to the study of the internal structure of this multiplet. For convenience we will ignore k_2 and plot the so-called "reduced energies" calculated with k_2 set to zero.

TABLE 1
Parameters of the Effective Rovibrational Hamiltonian for the ν_6 Fundamental Band of $Mo(CO)_6$

Parameter			Value (cm^{-1})
This work	Notation of Asselin *et al.* [20]	Notation of Robiette *et al.* [24]	
k_1	$\sqrt{3}t^{0(0,A_{1g})F_{1u}F_{1u}}_{\{6\}\{6\}}$	$\sqrt{3}\nu_6$	3473.60352
k_2	$-\frac{\sqrt{3}}{4}t^{2(0,A_{1g})A_{1g}A_{1g}}_{\{0\}\{0\}}$	$-\frac{\sqrt{3}}{4}B_0$	(Set to 0)
k_3	$-\frac{1}{\sqrt{3}}t^{1(1,F_{1g})F_{1u}F_{1u}}_{\{6\}\{6\}}$	$-\sqrt{6}(B\zeta)_6$	2.10×10^{-4}
k_4	$-\frac{3}{4}t^{2(0,A_{1g})F_{1u}F_{1u}}_{\{6\}\{6\}}$	$-\frac{3}{4}(B_6 - B_0)$	9.6390×10^{-6}
k_5	$\frac{1}{\sqrt{2}}t^{2(2,E_g)F_{1u}F_{1u}}_{\{6\}\{6\}}$	$-\frac{\sqrt{2}}{4}\alpha_{220}$	
		$-3\sqrt{2}\alpha_{224}$	-7.07×10^{-6}
k_6	$\frac{1}{\sqrt{3}}t^{2(2,F_{2g})F_{1u}F_{1u}}_{\{6\}\{6\}}$	$-\frac{\sqrt{3}}{4}\alpha_{220}$	
		$+2\sqrt{3}\alpha_{224}$	7.68×10^{-7}
k_7	$-\frac{1}{\sqrt{3}}t^{3(1,F_{1g})F_{1u}F_{1u}}_{\{6\}\{6\}}$	$\frac{3\sqrt{2}}{8}F_{110}$	8.83×10^{-9}
k_8	$-\frac{1}{\sqrt{3}}t^{3(3,F_{1g})F_{1u}F_{1u}}_{\{6\}\{6\}}$	$-\frac{\sqrt{15}}{2}F_{134}$	-8.03×10^{-9}

Note. Numerical values are taken from Ref. (*20*).

2.2. *Classical Symbol and Rotational Energy Surfaces (RES)*

We follow Refs. (*3, 6, 7, 10*) where the quantum description of the vibrational part of the Hamiltonian is combined with the classical description of the rotational degrees of freedom. Using the vibrational basis functions

$$\{|v_{6x}, v_{6y}, v_{6z}\rangle\} = \{|1, 0, 0\rangle, |0, 1, 0\rangle, |0, 0, 1\rangle\}, \quad [6]$$

and expanding all tensor notation in [3] we get the following matrix of the Hamiltonian $\tilde{H}$,

$$\tilde{H} = \begin{pmatrix} H_{11} & H_{21}^* & H_{31}^* \\ H_{21} & H_{22} & H_{32}^* \\ H_{31} & H_{32} & H_{33} \end{pmatrix}, \quad [7]$$

with

$$H_{11} = \frac{1}{\sqrt{3}} k_1 - \frac{4}{\sqrt{3}} k_2 \mathcal{J}^2 - \frac{4}{3} k_4 \mathcal{J}^2 - \frac{2\sqrt{2}}{3} k_5 (2J_x^2 - J_y^2 - J_z^2),$$

$$H_{22} = \frac{1}{\sqrt{3}} k_1 - \frac{4}{\sqrt{3}} k_2 \mathcal{J}^2 - \frac{4}{3} k_4 \mathcal{J}^2 - \frac{2\sqrt{2}}{3} k_5 (2J_y^2 - J_z^2 - J_x^2),$$

$$H_{33} = \frac{1}{\sqrt{3}} k_1 - \frac{4}{\sqrt{3}} k_2 \mathcal{J}^2 - \frac{4}{3} k_4 \mathcal{J}^2 - \frac{2\sqrt{2}}{3} k_5 (2J_z^2 - J_x^2 - J_y^2),$$

$$H_{21} = -\frac{2}{\sqrt{3}} k_6 (J_x J_y + J_y J_x) + \frac{i}{\sqrt{6}} \left(2k_3 - \frac{8}{\sqrt{3}} k_7 \mathcal{J}^2 + \frac{4\sqrt{2}}{\sqrt{5}} k_8 (2J_z^2 - 3J_x^2 - 3J_y^2 + 1) \right) J_z,$$

$$H_{31} = -\frac{2}{\sqrt{3}} k_6 (J_x J_z + J_z J_x) - \frac{i}{\sqrt{6}} \left(2k_3 - \frac{8}{\sqrt{3}} k_7 \mathcal{J}^2 + \frac{4\sqrt{2}}{\sqrt{5}} k_8 (2J_y^2 - 3J_z^2 - 3J_x^2 + 1) \right) J_y,$$

$$H_{32} = -\frac{2}{\sqrt{3}} k_6 (J_y J_z + J_z J_y) + \frac{i}{\sqrt{6}} \left(2k_3 - \frac{8}{\sqrt{3}} k_7 \mathcal{J}^2 + \frac{4\sqrt{2}}{\sqrt{5}} k_8 (2J_x^2 - 3J_y^2 - 3J_z^2 + 1) \right) J_x, \quad [8]$$

In these formulae rotational operators J_x, J_y, and J_z are converted to classical dynamical variables

$$(J_x, J_y, J_z) = \mathcal{J}(\sin\theta \cos\phi, \sin\theta \sin\phi, \cos\theta), \quad [9]$$

where angles ϕ and θ define the axis of rotation and $\mathcal{J}$ is the constant amplitude of the classical angular momentum. The angles (θ, ϕ) are the coordinates on the classical phase space for the rotational motion, called rotational *phase sphere* (*4, 6, 7, 8*). Diagonalization of matrix [7] for a given value of $\mathcal{J}$ and for each direction (θ, ϕ) gives three eigenvalues $E_i^{\mathcal{J}}(\theta, \phi)$ ($i = -1$, 0, and $+1$) which represent three classical rotational energy surfaces defined as functions on the rotational phase sphere.

TABLE 2
Principal Stationary Rotation Axes of an Octahedral Molecule

axis	$[J_x, J_y, J_z]$	(θ, ϕ)	number
C_4	$[0, 0, 1]$	$(0, 0)$	3
C_3	$[1, 1, 1]/\sqrt{3}$	$(\arctan\sqrt{2}, \pi/4)$	4
C_2	$[1, 1, 0]/\sqrt{2}$	$(\pi/2, \pi/4)$	6

Note. Coordinates for the particular axes used in this work and number of equivalent axes of each symmetry type.

2.3. *Energy of Rotation around Principal Stationary Axes*

We are particularly interested in the values of $E_i^J(\theta, \phi)$ for stationary axes of rotation. Principal stationary axes of any O_h symmetric molecule are its symmetry axes C_4, C_3, and C_2. The O_h group has several equivalent by symmetry axes of each kind and naturally the value of E_i^J for each of the equivalent axes is the same. More precisely, equivalent by symmetry points (θ, ϕ) form an orbit of *equivalent* points on the rotational phase sphere. The principal axes are *always* stationary, and moreover, axes C_4 and C_3 should be stable for any generic Hamiltonian. This means that generically functions E_i^J have a nondegenerate maximum, a minimum, or a saddle at the corresponding points on the phase sphere for any J. These points form *critical orbits* (*23*) with local symmetry C_2, C_3, and C_4. The C_4 and C_3 points can either be a maximum or a minimum, while the C_2 point can also be a saddle. To calculate E_i^J we choose one representative in each critical orbit indicated in Table 2.

Simple analytical expressions can be found for the energies on the critical orbits by diagonalizing the matrix [7]. For C_4 axes we obtain

$$E_0(\mathcal{J}) = E_s(\mathcal{J}) - \frac{4\sqrt{2}}{3} k_5 \mathcal{J}^2,$$

$$E_{\pm1}(\mathcal{J}) = E_s(\mathcal{J}) + \frac{2\sqrt{2}}{3} k_5 \mathcal{J}^2 \pm \sqrt{\frac{2}{3}} k_3 \mathcal{J} \mp \frac{4\sqrt{2}}{3} k_7 \mathcal{J}^3 \pm \frac{4}{\sqrt{15}} k_8 (2\mathcal{J}^3 + \mathcal{J}), \quad [10]$$

where E_s is the scalar contribution [4]. The three eigenvalues for C_3 axes are

$$E_0(\mathcal{J}) = E_s(\mathcal{J}) - \frac{8\sqrt{3}}{9} k_6 \mathcal{J}^2,$$

$$E_{\pm1}(\mathcal{J}) = E_s(\mathcal{J}) + \frac{4\sqrt{3}}{9} k_6 \mathcal{J}^2 \pm \sqrt{\frac{2}{3}} k_3 \mathcal{J} \mp \frac{4\sqrt{2}}{3} k_7 \mathcal{J}^3 \mp \frac{4}{\sqrt{15}} k_8 \left(\frac{4}{3} \mathcal{J}^3 - \mathcal{J} \right). \quad [11]$$

The three eigenvalues for C_2 axes are

$$E_0(\mathcal{J}) = E_s(\mathcal{J}) - \frac{\sqrt{2}}{3} k_5 \mathcal{J}^2 - \frac{2}{\sqrt{3}} k_6 \mathcal{J}^2,$$

$$E_{\pm 1}(\mathcal{J}) = E_s(\mathcal{J}) + \frac{\sqrt{2}}{6} k_5 \mathcal{J}^2 + \frac{1}{\sqrt{3}} k_6 \mathcal{J}^2 \pm \frac{1}{6} \mathcal{J} \sqrt{3a^2 \mathcal{J}^2 + 6b^2}, \quad [12]$$

with

$$a = 2k_6 - \sqrt{6}\, k_5,$$

$$b = 2k_3 - \frac{8}{\sqrt{3}} k_7 \mathcal{J}^2 + \sqrt{\frac{2}{5}} k_8 (4 - 2\mathcal{J}^2). \quad [13]$$

It should be pointed out that the rotational structure of a triply degenerate state of a spherical top molecule has been studied numerically by Harter and co-workers (*3*) using a simpler model. Equations [10], [11], and [12] give an analytical classical description for a more elaborated effective Hamiltonian [3].

2.4. Quantum-Classical Correspondence

Figure 1 gives a general idea of the correspondence between our formulae for the classical stationary rotation energies $E_i(\mathcal{J})$ and the structure of quantum multiplet obtained in (*20*). Contrary to the quantum spectrum which appears quite complicated due to a great number of individual levels, the classical RES "spectrum" is strikingly simple. Yet this simple classical description retains all essential qualitative information on the system of quantum levels in a very concise and efficient way. To understand more how it works notice first that the splitting of the multiplet is well delimited by an absolute maximum and minimum $E_i(\mathcal{J})$ at each given J, then identify three groups of quantum levels which form three diverging "branches" as the value J increases and remark how well the three groups of classical values $E_i^{C_4}(\mathcal{J})$, $E_i^{C_2}(\mathcal{J})$, and $E_i^{C_3}(\mathcal{J})$ represent branches $i = 0$ and ± 1. As first shown in (*1*), each sufficiently stable equilibrium $E_i(\mathcal{J})$ corresponds to a regular sequence of quasi-degenerated groups of quantum levels called *clusters*. The number of levels in each cluster equals the number of equivalent stationary points of RES which in turn equals twice (to account for two directions of classical rotation) the number of equivalent axes. Thus for $J > 15$ we observe a particularly prominent series of sixfold clusters in the upper part of the ν_6 multiplet. These clusters correspond to stable rotation around C_4 axes.

2.4.1. Regular cluster sequences. Cluster sequences can be well reproduced using an oscillator approximation near each stable stationary point of RES. If the frequency of the oscillator

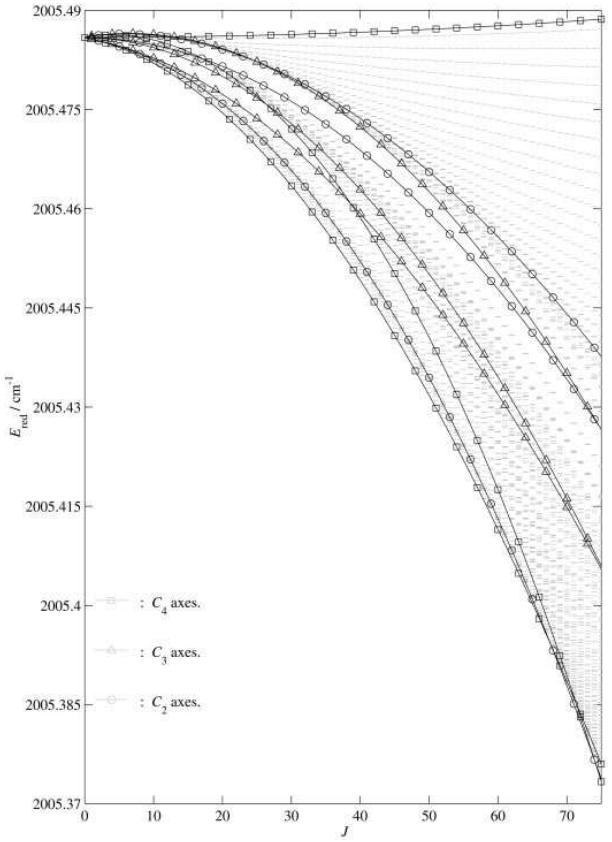

FIG. 1. Quantum (gray horizontal bars) and semiclassical energies $E_i(J)$ with $i = 0, \pm 1$ (solid lines) in the interval $0 \leq J \leq 75$.

is sufficiently large in comparison to the rotational quantum $B\mathcal{J}$ then the corresponding quantum spectrum has a regular sequence of levels with different projection of the angular momentum on the particular stationary axis, $m = J, J - 1, \ldots$. To find the harmonic part (the frequency) of the oscillator potential and to estimate the stability of the stationary point (*10*) of RES, we calculate the value of Hessian:

$$h_i^J(\theta, \phi) = \left(\frac{\partial^2 E_i^J}{\partial \theta^2}\right)\left(\frac{\partial^2 E_i^J}{\partial \phi^2}\right) - \left(\frac{\partial^2 E_i^J}{\partial \theta \partial \phi}\right)^2. \quad [14]$$

Positive and negative values of h_i^J correspond to stable and unstable classical rotation, respectively. A zero Hessian $h_i^J = 0$ for some critical value J_c indicates a bifurcation in the limiting classical problem and a modification of the rotational cluster structure.

2.4.2. Branches of levels. "Typical" rotational multiplets of triply degenerate fundamentals of spherical top molecules consist of three branches (*25*) also called *vibrational components*. The branches are formed due to the Coriolis interaction term which is

typically dominant, at least when the values of J are sufficiently low. When J increases, such branches diverge linearly. At each given J the number of levels $2R + 1$ in each branch is defined by the quantum number $R = J - 1$, J, and $J + 1$ and hence the branches are labeled by $i = -1, 0, 1$. The structure is, of course, a textbook example of angular momentum coupling: the angular momentum $\mathbf{R}$ is a sum of $\mathbf{J}$ and the angular momentum $\mathbf{l} = 1$ of the triply degenerate vibrational mode, the corresponding coupling term $\mathbf{l} \cdot \mathbf{J}$ describes Coriolis interaction.

As has already been noted in (*20*), the first-order Coriolis interaction constant k_3 of the ν_6 state is so small (see Table 1) that at $J \approx 10$ the contribution of the second-order terms with constants k_5 and k_6 surpasses that of the Coriolis term. This results in a very different branch structure which is formed at higher values of J. Classical energies reproduce this transition qualitatively correctly. Many interesting phenomena can be seen and are analyzed in the next sections.

The main phenomenon which corresponds in the classical limit to the change of the branch structure of the quantum spectrum is the formation of the degeneracy points (singularities or diabolic points) of RESs (*7, 8*). Typically two RESs become degenerated at some isolated value J_{crit} and depending on the nature of singularity, the Hessian function $h_i(J)$ has a particular discontinuity. When this happens the RESs are no longer isolated and we should consider the connected surfaces as one multivalued function. Formation of an isolated degeneracy point of RESs is reflected in the quantum energy spectrum as a redistribution of energy levels between branches, or in other words as a reorganization of vibrational components (*8*).

In Section 3 we characterize briefly possible changes of the branch structure of the rotational multiplet $v_6^{F_{1u}} = 1$ of an octahedral molecule on the basis of the theory for tetrahedral molecules developed in (*14, 15, 16*). In Section 4 we return to the analysis of the concrete situation in $Mo(CO)_6$.

3. VIBRATIONAL COMPONENTS OF OCTAHEDRAL MOLECULES

Rotational structure of degenerated vibrational states of spherical top molecules exhibits distinct rotational multiplets for each vibrational component (branch). These multiplets are particularly visible at sufficiently low rotational excitation.

Analysis of possible decompositions of all rotational states into several distinct components begins with the observation that all rotational levels of the vibrational state $\nu_6(F_{1u})$ at a given J form a reducible representation of the O_h group which can be written symbolically as

$$\Gamma_{\text{rv}} = F_{1u} \times \mathcal{D}^{(J_g)}, \qquad [15]$$

where $\mathcal{D}^{(J_g)}$ stands for the decomposition of the irreducible representation (J_g) of the $O(3)$ group with respect to the O_h group. When all these rovibrational levels decompose into three rotational branches, the reducible representation Γ_{rv} should be represented as a sum of three contributions,

$$\Gamma_{\text{rv}} = \sum_{i=1}^{3} \Gamma_i \times \mathcal{D}^{((J+\Delta_i)_g)}, \qquad [16]$$

where Δ_i and Γ_i are independent on J and $\mathcal{D}^{((J+\Delta_i)_g)}$ denotes a reducible representation of the $O(3)$ group with the effective weight $J + \Delta_i$. Naturally $\Delta_1 + \Delta_2 + \Delta_3 = 0$. Each number Δ_i defines an effective rotational quantum number of the corresponding vibrational component (branch) i and therefore the number of rotational states in this component.

The one-dimensional representations of the O_h group Γ_1, Γ_2, and Γ_3 which enter in [16] are effective symmetries of the corresponding vibrational components $i = 1, 2, 3$. The O_h group has four one-dimensional representations and the corresponding four possible types of vibrational components are

$$A_{1g} \times \mathcal{D}^{((J+\Delta)_g)} \equiv \mathcal{D}_{1g}^{(J+\Delta)}, \qquad [17]$$

$$A_{1u} \times \mathcal{D}^{((J+\Delta)_g)} \equiv \mathcal{D}_{1u}^{(J+\Delta)}, \qquad [18]$$

$$A_{2g} \times \mathcal{D}^{((J+\Delta)_g)} \equiv \mathcal{D}_{2g}^{(J+\Delta)}, \qquad [19]$$

$$A_{2u} \times \mathcal{D}^{((J+\Delta)_g)} \equiv \mathcal{D}_{2u}^{(J+\Delta)}. \qquad [20]$$

(Above we introduce full and shortened notation.)

In our case the symmetry of the vibrational state ν_6 is F_{1u} and consequently all Γ_i should be of type u, i.e., either A_{1u} or A_{2u}. The well-known first-order Coriolis splitting of the F_{1u} vibrational state into three components with effective quantum numbers $R = J + 1$, J, and $J - 1$ corresponds to a particular form of the decomposition [16]

$$F_{1u} \times \mathcal{D}^{(J_g)} = \sum_{\delta=0,\pm1} A_{1u} \times \mathcal{D}^{((J+\delta)_g)} \qquad [21]$$

$$= \mathcal{D}_{1u}^{(J+1)} + \mathcal{D}_{1u}^{(J)} + \mathcal{D}_{1u}^{(J-1)} \qquad [22]$$

(represented both in full and short notation).

By means of a formal group-theoretical analysis similar to that in (*14*) we can find all possible decompositions of the rotational multiplet [15] into three vibrational components. Below are some examples of such alternative decompositions:

$$F_{1u} \times \mathcal{D}^{(J_g)} = \mathcal{D}_{1u}^{(J\pm1)} + \mathcal{D}_{2u}^{(J\mp3)} + \mathcal{D}_{2u}^{(J\pm2)}, \qquad [23]$$

$$F_{1u} \times \mathcal{D}^{(J_g)} = \mathcal{D}_{2u}^{(J\pm1)} + \mathcal{D}_{1u}^{(J\mp3)} + \mathcal{D}_{2u}^{(J\pm2)}. \qquad [24]$$

When we describe possible decompositions into individual vibrational components, we should also consider what elementary modifications of the band structure can occur when rota-

tional excitation increases, i.e., when the value of J, the only parameter, is varied.

In the next section we will observe one of the unusual decompositions [23] in the structure of rovibrational energy levels reconstructed from the experimental data for the ν_6 band of $Mo(CO)_6$. At low values of J we will also observe the familiar structure [22] and analyze how this structure is rearranged when J increases.

4. QUALITATIVE ANALYSIS OF THE ROTATIONAL STRUCTURE OF THE $\nu_6 = 1$ STATE OF $Mo(CO)_6$

Qualitative analysis of the rotational structure of a degenerate vibrational state has two steps. First we describe individual vibrational components (branches) and study their eventual modifications occurring when rotational excitation increases. Next we consider the rotational cluster structure of each individual vibrational component and its possible modifications.

As we already noted in Section 2.4.2 above, the first-order Coriolis interaction constant k_3 of the $\nu_6 = 1$ state of $Mo(CO)_6$ is so small that the three Coriolis components originally formed at low J interact strongly and $R = J - 1, J, J + 1$ is no longer a good quantum number when J increases. The structure of the three components changes when $J \approx 8$.

4.1. The $0 \leq J \leq 25$ Region

To understand the situation let us first focus on the low J region shown in Fig. 2. For $J < 8$, we can see the three Coriolis components containing $2J - 1$, $2J + 1$, and $2J + 3$ levels, respectively. The corresponding decomposition [22] can be confirmed by comparing the symmetries of the calculated quantum states to the decomposition $\mathcal{D}^{(R)}$ of the weight-R irreducible representation of the rotation group $O(3)$ into irreducible representations of O_h multiplied by the appropriate factor $\Gamma_i = A_{1u}$ defined in [21]. As an example consider the rotational multiplet for $J = 5$

$$J = 5 \begin{cases} R = J - 1 = 4 \begin{cases} A_1 & 2005.486454 \\ F_1 & 2005.486473 \\ E & 2005.486485 \\ F_2 & 2005.486510 \end{cases} \\ R = J = 5 \begin{cases} F_1 & 2005.485724 \\ E & 2005.485746 \\ F_2 & 2005.485935 \\ F_1 & 2005.485974 \end{cases} \cdot \\ R = J + 1 = 6 \begin{cases} E & 2005.484519 \\ F_2 & 2005.484530 \\ A_2 & 2005.484570 \\ F_2 & 2005.484672 \\ F_1 & 2005.484710 \\ A_1 & 2005.484746 \end{cases} \end{cases}$$

(Parity is always u and has been omitted, wavenumbers are in reciprocal centimeters, degeneracy of levels A, E, and F is 1, 2, and 3.)

When the value of J increases above $J \approx 8$ we can see in Fig. 2 that a number of levels leave the middle branch (formerly $R = J$) and join the upper branch. The three branches persist at the values $J > 8$ but the number of levels in each branch is different. To reproduce this decomposition in terms of an auxiliary quantum number R such that the number of levels in each branch equals $2R + 1$, we should define $R = J + 1$, $J - 3$, and $J + 2$. As an example consider the multiplet for $J = 10$

$$J = 10 \begin{cases} R = J + 2 = 12\ (\times A_{2u}) \begin{cases} A_2 & 2005.485843 \\ F_2 & 2005.485850 \\ E & 2005.485854 \\ F_1 & 2005.486106 \\ F_2 & 2005.486130 \\ E & 2005.486191 \\ F_1 & 2005.486202 \\ A_1 & 2005.486277 \\ F_1 & 2005.486285 \\ F_2 & 2005.486291 \\ A_2 & 2005.486296 \end{cases} \\ R = J - 3 = 7\ (\times A_{2u}) \begin{cases} F_2 & 2005.484712 \\ E & 2005.484761 \\ F_1 & 2005.484798 \\ A_1 & 2005.484876 \\ F_1 & 2005.485019 \\ F_2 & 2005.485048 \end{cases} \cdot \\ R = J + 1 = 11\ (\times A_{1u}) \begin{cases} F_1 & 2005.482186 \\ F_2 & 2005.482192 \\ A_2 & 2005.482409 \\ F_2 & 2005.482444 \\ E & 2005.482468 \\ F_1 & 2005.482583 \\ F_2 & 2005.482778 \\ E & 2005.482822 \\ F_1 & 2005.482847 \end{cases} \end{cases}$$

(The parity index u common to all levels is omitted; wavenumbers are in reciprocal centimeters.) To confirm that the new decomposition is of the type [23], we multiply the standard irreducible representations $\mathcal{D}^{(J+2)}$ (upper component) and $\mathcal{D}^{(J-3)}$ (central component) of the $O(3)$ group by A_{2u} to get the true rovibrational symmetries with respect to the O_h group.

It follows that we should use different good quantum numbers for the values of J below and above $J \approx 8$. The modification of the good quantum numbers proceeds as follows:

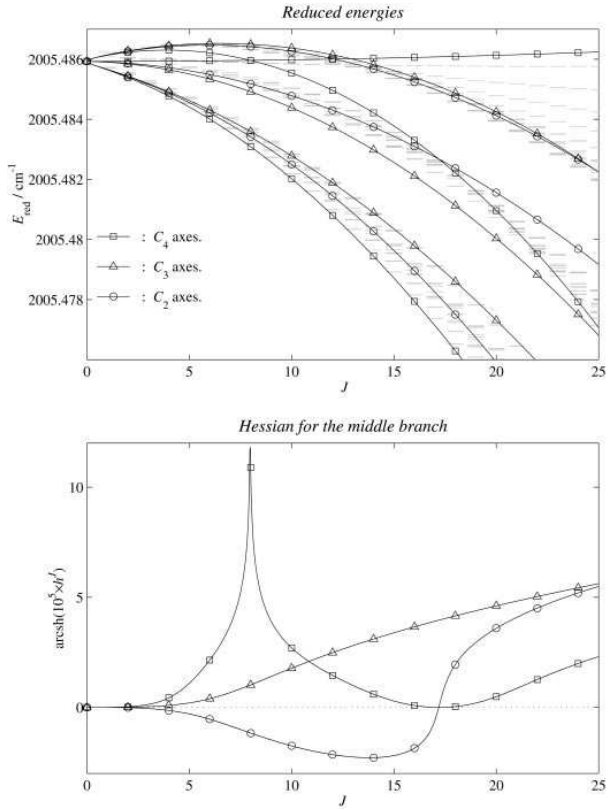

FIG. 2. Above: quantum and classical energies in the interval $0 \le J \le 25$ shown by gray horizontal bars and solid curves, respectively. Below: Hessian values h' for the middle branch $E_0(J)$ at points C_2, C_3, and C_4 shown as $\mathrm{arcsh}(10^5 \times h'(\theta, \phi))$ in order to increase the range of the plot.

$$\mathcal{D}_{1u}^{(J-1)} \rightarrow \mathcal{D}_{2u}^{(J+2)} : 2(J-1)+1 \overset{+6}{\longrightarrow} 2(J+2)+1,$$

$$\mathcal{D}_{1u}^{(J)} \rightarrow \mathcal{D}_{2u}^{(J-3)} : 2J+1 \overset{-6}{\longrightarrow} 2(J-3)+1,$$

$$\mathcal{D}_{1u}^{(J+1)} \rightarrow \mathcal{D}_{1u}^{(J+1)}.$$

Only the two upper components are involved. The upper component gains six levels while the central component loses six levels. This exchange of six levels can be symbolically represented as a "transition" between the symmetry labels of vibrational components

$$\mathcal{D}_{1u}^{(J)} + \mathcal{D}_{1u}^{(J-1)} \overset{J \approx 8}{\longrightarrow} \mathcal{D}_{2u}^{(J-3)} + \mathcal{D}_{2u}^{(J+2)}. \qquad [25]$$

Note that as in the case of the T_d symmetry (*14*), the label $\mathcal{D}_{1u}^{(K)} \equiv A_{1u} \times \mathcal{D}^{(K_g)}$ can be rewritten as $\mathcal{D}^{(K_u)}$. However, the representation $\mathcal{D}_{2u}^{(K)} \equiv A_{2u} \times \mathcal{D}^{(K_g)}$ cannot be replaced by another representations of the $O(3)$ group with the identical decomposition into irreducible representations of O_h. That is why the specific double index notation for vibrational components should be used in [25] and elsewhere.

Modification of the labeling scheme for the two upper components (branches) is a result of rotation–vibrational coupling. When the labeling of the components changes at $J \approx 8$, the two classical rotational energy surfaces representing upper and central components of the ν_6 (solid lines in Fig. 2, top) form a *conical intersection point,* also called a diabolic point, in the direction (θ, ϕ) corresponding to the C_4 axes. At the same time the Hessian value goes to infinity (Fig. 2, bottom). The formation of the conical intersection of the two upper RES is illustrated in Fig. 3. There are six conical points formed simultaneously at six equivalent C_4-symmetric points on the phase sphere (two points for each C_4 axis). Since, as suggested in (*8*), each conical point corresponds to the redistribution of one energy level, there are six levels, i.e., a sixfold cluster, transferred between the two components.

Figure 4 summarizes how the RESs change when the value of J increases from $J = 2$ to $J = 11$. These sufficiently low J values can give the impression that the application of classical analysis may not be adequate for the description of quantum energy level system. At the same time the numerical comparison between classical and exact quantum results for the

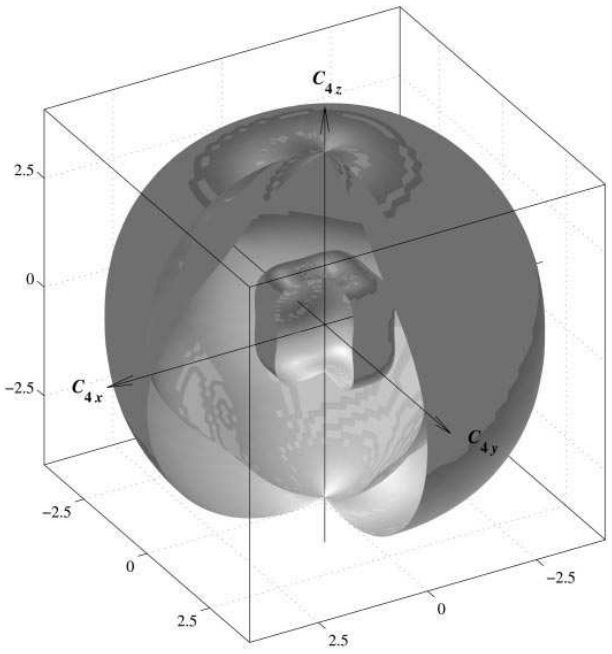

FIG. 3. Rovibrational energy surfaces $E_i^J(\theta, \phi) - E_s$ with $i = 1, 2, 3$, $J = 8$, and $E_s = 2005.482\ \mathrm{cm}^{-1}$. Coordinates are chosen along the three C_4 symmetry axes (arrows) and are labeled in $10^{-3}\ \mathrm{cm}^{-1}$.

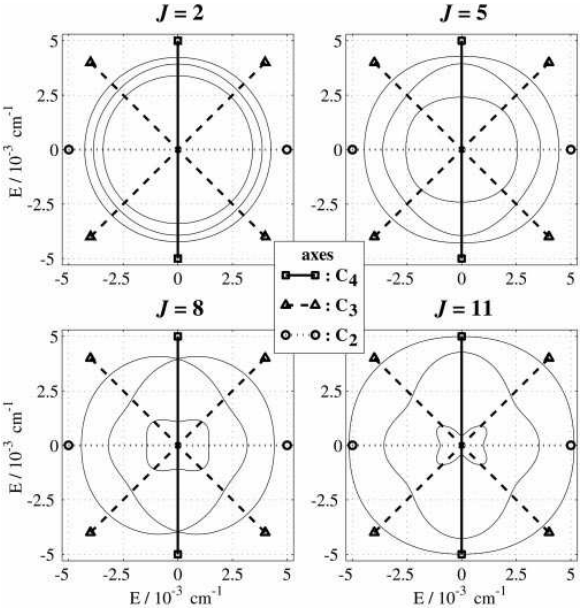

FIG. 4. Cuts of the rotational energy surfaces in the plane $\phi = \pi/4$ for different values of J; we took $E_s = 2005.482$ cm^{-1} (see Fig. 3), except in the case $J = 11$ where we took $E_s = 2005.481$ cm^{-1} for the internal surface.

corresponding Hamiltonian demonstrates the reliability of purely classical analysis. The fact that the rearrangement of branches is a purely topological phenomenon in classical limit ensures its stability under perturbation for quantum Hamiltonian as well. This means that even inclusion of higher order tensorial coupling terms into the Hamiltonian cannot modify the redistribution phenomenon without the appearance of new degeneracy points which in principle can be moved from high J region due to strong perturbation. Such a possibility is not quite realistic because of precise experimental information about rotational structure in the $J = 0$–74 region. Before and after the conical intersection at $J = 8$ we can clearly see three distinct RESs which correspond to three components (branches) of the $\nu_6 = 1$ state. After $J \approx 8$ the decomposition of the rotational multiplet and the labeling scheme remain unchanged up to $J \approx 60$. Our effective rovibrational Hamiltonian is truncated at the third order and is, naturally, less reliable at higher values of J. To the extent this Hamiltonian allows extrapolation we can suggest as to what changes in the structure of the three components may occur. This somewhat formal mathematical analysis is briefly discussed in Section 6.

4.2. *Cluster Structure of the Three Branches*

Once the decomposition of the rotational energy levels into three components (branches) is described, and the redistribution of levels between components occurring near $J = 8$ is understood in terms of connecting RESs, we can further study the cluster structure in each individual component using the corresponding RES. Near maximum and minimum energy of each component we can observe well-pronounced rotational clusters of different kinds which correspond most precisely to the classical rotation around stable stationary axes C_3, C_4, and in some cases C_2. Information on these extremum clusters is presented in Table 3.

The cluster structure in Table 3 corresponds very closely to the classical RES extrema shown by solid lines in Figs. 1 and 2. For example, at the highest and the lowest energy of the lowest component $\mathcal{D}_{1u}^{(J+1)}$ we find eightfold and sixfold degenerate clusters, respectively; they correspond to eight maxima and six minima on the RES in the direction of the C_3 and C_4 symmetry axes.

When $J \simeq 25$, the upper component $\mathcal{D}_{2u}^{(J+2)}$ has 12-fold degenerate clusters at its low energy end and the corresponding RES has a "shallow" global minimum at the 12 points with local symmetry C_2 (Fig. 2). The same component has regular sequences of well-pronounced sixfold clusters starting down from the maximum energy. The corresponding RES maximum is very "deep." In fact the depth of this maximum can be estimated from the large gap between the energy of classical rotation around the C_4 axes and that of rotation around other stationary axes (distance between the corresponding solid lines in Fig. 2). Of course, the quantitative characteristics of the high stability of the rotation around C_4 (and the large depth of the maximum on the RES) is given by the large positive Hessian value at the C_4 point which also gives the frequency of the

TABLE 3
Rotational Clusters with Maximum and Minimum Energy in Each of the Three Components (Branches) of the $\nu_6 = 1$ State of $Mo(CO)_6$ at Different Values of J

component	$J \leq 8$	$J \simeq 12$	$J \simeq 25$	$25 < J \leq 40$
upper	$\mathcal{D}_{1u}^{(J-1)}$ {max $8(C_3)$, min $6(C_4)$}	$\mathcal{D}_{2u}^{(J+2)}$ {max $8(C_3)$, min $6(C_4)$}	$\mathcal{D}_{2u}^{(J+2)}$ {max $6(C_4)$, min $12(C_2)$}	$\mathcal{D}_{2u}^{(J+2)}$ {max $6(C_4)$, min $8(C_3)$}
middle	$\mathcal{D}_{1u}^{(J)}$ {max $6(C_4)$, min $8(C_3)$}	$\mathcal{D}_{2u}^{(J-3)}$ {max $6(C_4)$, min $8(C_3)$}	$\mathcal{D}_{2u}^{(J-3)}$ {max $12(C_2)$, min $6(C_4)$}	$\mathcal{D}_{2u}^{(J-3)}$ {max $12(C_2)$, min $6(C_4)$}
lower	$\mathcal{D}_{1u}^{(J+1)}$ {$8(C_3)$, $6(C_4)$}	$\mathcal{D}_{1u}^{(J+1)}$ {$8(C_3)$, $6(C_4)$}	$\mathcal{D}_{1u}^{(J+1)}$ {$8(C_3)$, $6(C_4)$}	$\mathcal{D}_{1u}^{(J+1)}$ {$8(C_3)$, $6(C_4)$}

Note. In each case we indicate the symmetry label of the component, the degeneracy of the clusters, and the type of the corresponding stable rotation axes.

harmonic oscillator approximation for the regular sequence of the C_4 clusters.

A detailed description of elementary modifications of the cluster structure of each component can be given in terms of bifurcations of corresponding RESs (*5, 26*). The method has been well developed in the earlier study of different rotation–vibration multiplets of spherical top molecules (*7, 10, 11, 15*) and practically all bifurcations we observe in this work have already been described before. Thus two bifurcations of the RES corresponding to the central component happen quickly in what appears an "organized" sequence (*7, 27*) when the value of J changes from $J = 16$ to $J = 19$. The moment of each bifurcation can be determined precisely as the moment when the corresponding value of Hessian h^J becomes zero (Fig. 2, bottom). After these bifurcations, rotation around the C_2 axis becomes stable, the C_2 points on the RES become global maxima which are deep enough for the distinct 12-fold clusters to form at $J \approx 25$.

4.3. The $J > 25$ Region

As we can see in Fig. 1, the situation becomes more complicated at higher values of J. At the values of $25 < J \leq 40$, we observe three distinct components (branches) described by $R = J + 1$, $J - 3$, $J + 2$, respectively. Rotational clusters at maximum and minimum energies of each branch are given in Table 3.

The structure of the upper component $\mathcal{D}_{2u}^{(J+2)}$ remains unchanged up to $J \approx 75$ (see Table 3). After $J = 25$ the C_3 minimum on the corresponding RES becomes lower than the C_2 minimum, and the corresponding eightfold clusters can be seen formed at the lower energy end of this component. A large number of sixfold clusters already mentioned above can be well seen at top energies. The corresponding C_4 maximum becomes very deep.

At first sight the structure of the two lower components is more complicated. Starting with $J \approx 40$ the two multiplets begin to overlap in energy (see Fig. 1). For $J > 40$ the C_4 minimum of the $\mathcal{D}_{2u}^{(J-3)}$ (central) RES becomes lower than the C_3 maximum of the $\mathcal{D}_{1u}^{(J+1)}$ (lowest) RES. This, however, does not lead to any qualitative changes in the structure of the two components because the two RES do *not* connect and remain distinct all the way until (at least) $J \approx 70$. Mixing of the wavefunctions localized near the respective C_4 minima of $\mathcal{D}_{2u}^{(J-3)}$ and C_3 maxima of $\mathcal{D}_{1u}^{(J+1)}$ is only possible due to tunneling and is small. The cluster structure of the two components is indicated in Table 3.

5. QUANTUM-CLASSICAL CORRESPONDENCE AND THE DIRECTION OF REDISTRIBUTION

Comparison of classical energies of stationary points (critical orbits) on the two RESs near the conical intersection (diabolic point) and the corresponding part of the quantum energy level spectrum (Fig. 2, top) clearly shows that the levels which transfer between the two components (branches) follow the classical energy at one of the critical points on the RESs involved in the intersection. On the other hand, the classical analysis of the corresponding RESs does not indicate any preference as to which critical point the quantum level should "follow."

In our particular case the two RESs connect at the six C_4 points when $J \approx 8$ and a sixfold cluster is transferred from the central to the upper component (see Fig. 2). We can easily verify that the only terms of the effective Hamiltonian [3] that are essential to the existence of the conical intersection at the C_4 point are the Coriolis term $H^{1(1_g,F_{1g})}$ and the second-order term $H^{2(2_g,E_g)}$ (in the notation of Section 2.1). While a sufficiently large variation of the two respective constants k_3 and k_5 can eliminate the intersection, contributions from other terms in [3] can only modify the energy of the conical point or the value of J at which the intersection occurs. Consequently, a simple model Hamiltonian

$$k_3 H^{1(1_g,F_{1g})} + k_5 H^{2(2_g,E_g)} \qquad [26]$$

can be used to study all qualitative aspects of the energy level redistribution phenomenon in question. If in this model Hamiltonian we set the values of k_3 and k_5 to those in Table 1, the two energies of classical rotation around the C_4 axis (C_4 points on the two RESs) coincide when

$$\sqrt{J(J+1)} = \frac{1}{\sqrt{12}} \left| \frac{k_3}{k_5} \right| \Rightarrow J_{\text{sing}} \approx 8.09, \qquad [27]$$

which is very close to the real value $J \approx 7.97$ for the complete Hamiltonian [3].

In Fig. 5 we compare the quantum energy level spectrum of the model Hamiltonian [26] to the corresponding energy of classical rotation around the C_4 axis. The real situation is reproduced when the Coriolis constant $k_3 > 0$ and $k_5 < 0$ (Fig. 5, top). It can be clearly seen in this figure that classical C_4 curves are in a sense symmetrical with respect to the value J_{sing} at which they cross. On the other hand, quantum energy level pattern breaks this symmetry. Furthermore, a simple change of the sign of the Coriolis term constant $k_3 \rightarrow -k_3$ in [26] does not modify the classical energies. At the same time, changing signs of k_3 flips the quantum energy pattern (Fig. 5, bottom) so that the energy level transfer occurs in the opposite direction when J increases. Of course, changing the sign also modifies the number of quantum levels in each component and thus affects their internal structure.

We now analyze Fig. 5 in more detail. When $J < 8$ we find the familiar structure formed due to the first-order Coriolis interaction. If $k_3 > 0$ the upper, central, and lower branches are labeled by the quantum number $R = J - 1$, J, and $J + 1$, respectively. This order is reversed when $k_3 < 0$. In the former

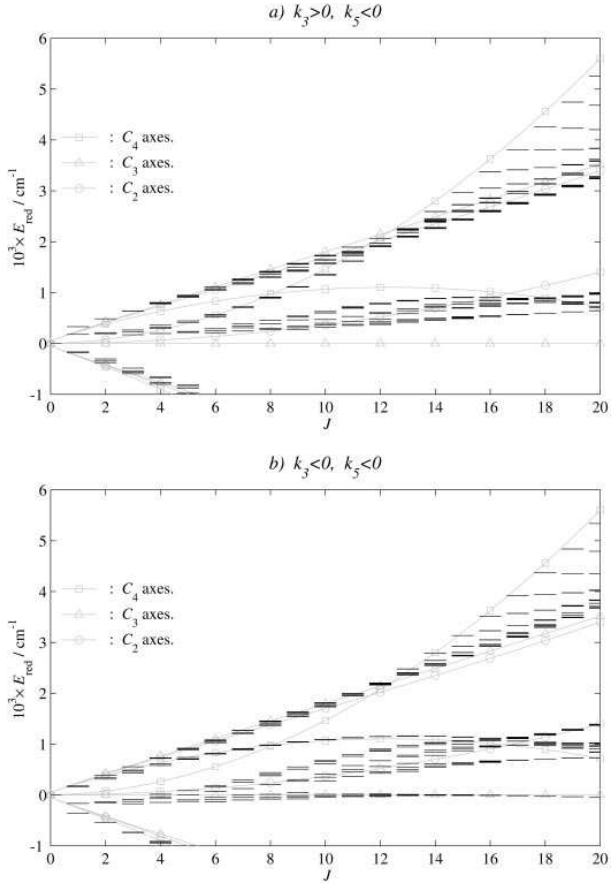

FIG. 5. Quantum (solid horizontal bars) and classical (gray curves) energies for the simple two-parameter model [26] which exhibits different level redistribution for $k_3 > 0$ (top) and $k_3 < 0$ (bottom).

case ($k_3 > 0$, Fig. 5, top), the sixfold cluster moves from the $R = J$ branch to the $R = J - 1$ branch when the value of J increases and passes $J_{sing} = 8$. In other words,

$$\mathcal{D}_{1u}^{(J-1)} \rightarrow \mathcal{D}_{2u}^{(J+2)},$$
$$\mathcal{D}_{1u}^{(J)} \rightarrow \mathcal{D}_{2u}^{(J-3)}, \quad k_3 > 0. \qquad [28]$$

Alternatively ($k_3 < 0$, Fig. 5, bottom), this cluster moves down from the upper branch with $R = J + 1$ to the central branch with $R = J$,

$$\mathcal{D}_{1u}^{(J+1)} \rightarrow \mathcal{D}_{2u}^{(J-2)},$$
$$\mathcal{D}_{1u}^{(J)} \rightarrow \mathcal{D}_{2u}^{(J-3)}, \quad k_3 < 0. \qquad [28]$$

In both cases the sixfold cluster leaves the component with a larger number of levels and joins the "less crowded" component with initially fewer levels. Furthermore, we can show that redistribution in the opposite direction

$$[\mathcal{D}_{1u}^{(J-1)}, \mathcal{D}_{1u}^{(J)}] \overset{?}{\rightarrow} [\mathcal{D}_{\alpha u}^{(J-4)}, \mathcal{D}_{\beta u}^{(J+3)}], \quad k_3 > 0, \qquad [30]$$

$$[\mathcal{D}_{1u}^{(J+1)}, \mathcal{D}_{1u}^{(J)}] \overset{?}{\rightarrow} [\mathcal{D}_{\alpha u}^{(J+4)}, \mathcal{D}_{\beta u}^{(J-3)}], \quad k_3 < 0, \qquad [31]$$

where α and β take the values 1 or 2, is strictly forbidden. Thus in the case of [30] the decomposition of

$$\mathcal{D}_{\alpha u}^{(J-4)} + \mathcal{D}_{\beta u}^{(J+3)}$$

into irreducible representations of O_h should equal the decomposition of

$$\mathcal{D}_{1u}^{(J-1)} + \mathcal{D}_{1u}^{(J)},$$

which is impossible because no pair (α, β) can satisfy this additional restriction.

Further analysis of Fig. 5 shows that changing the sign of the Coriolis parameter k_3 not only alters the direction of the level transfer but also affects other aspects of cluster structure. Comparing top and bottom plots in Fig. 5 we can see that they differ in the position of clusters at the extremes of the branches. Normally we expect to find quantum levels inside the energy interval designated by the global maximum and minimum of the RES. This regular situation can be well seen near the C_4 maximum of the upper RES (Figs. 1, 2, and 5) where the oscillator like sequences of sixfold clusters begin one half of a quantum (one half the energy difference between the first two clusters in the sequence) below the classical limit energy. However, near other extremes of the two components the situation is different. Thus in the case $k_3 < 0$ (Fig. 5, bottom) an eightfold cluster of the central component is located right at the minimum classical energy corresponding to the rotation around the C_3 axis. The same component in the case $k_3 > 0$ (Fig. 5, top) does not have such cluster, and of course the sixfold cluster is moving along the classical C_4 energy curve when transferring between the components.

Finally, alternation of the sign of k_3 can be given a clear physical interpretation. The rotational part of the Coriolis term $H^{1(1_g,F_{1g})}$ is a rotational tensor of odd degree, namely $R_\alpha^{1(1_g,F_{1g})} = 2\hat{J}_\alpha$ with $\alpha = x, y, z$. Consequently, changing the sign of k_3 (and simultaneously of all parameters of the so-called "imaginary" terms $H^{\Omega(K_g,\Gamma)}$ with odd degree Ω of the rotational part) can be interpreted as changing the sign of the commutation relation between the angular momentum operators

$$[J_\alpha, J_\beta] = +\epsilon_{\alpha\beta\gamma}J_\gamma \rightarrow [J_\alpha, J_\beta] = -\epsilon_{\alpha\beta\gamma}J_\gamma,$$

with ϵ the totally antisymmetric tensor and α, β, γ standing for x, y, or z. The "+" relation holds in the laboratory fixed coordinate frame, whereas the "−" relation applies in the molecule-fixed frame. The same classical Hamiltonian matrix symbol can be associated with two quantum operators which differ in the signs of all odd Ω terms.

6. ASYMPTOTIC BEHAVIOR AND POSSIBLE HIGHER ORDER CONNECTION AT LARGE J

As we already mentioned above, our effective Hamiltonian is much less reliable at large values of J. Inclusion of higher order tensorial contributions to the effective Hamiltonian can seriously modify the qualitative structure of rotational bands in the $J > 60$ region where the number of experimental data is insufficient for the detailed reconstruction of the effective Hamiltonian. However it exhibits an interesting and rare behavior near $J = 70$, which we would like to mention. According to this Hamiltonian the two lowest RESs cross each other at the C_4 points when $J \simeq 71.36$. In contrast to the conical intersection at $J \approx 8$, this intersection is parabolic and corresponds to the step in the Hessian value computed at the corresponding C_4 points in the interval $J = 70 \cdots 75$ (Fig. 6).

Another interesting feature of the structure of the three components at high J is the near degeneracy of the C_4 minima of the two lower RES which lie much lower than the C_4 maximum of the upper RES. To explain this structure we can consider the limit of very high rotational excitation (large J) where the amplitude of the $\nu_6 = 1$ vibrations is small compared to the centrifugal distortion of the molecule. In this limit we consider vibrations about a J-dependent equilibrium configuration whose symmetry is generally lower than the O_h symmetry of the $J = 0$ equilibrium. This limit has been studied extensively in (*28, 29*).

Depending on the orientation of the rotation axis the distortion of the $J = 0$ equilibrium is different. Rotation around stationary axes C_4, C_3, and C_2 breaks the O_h symmetry of the equilibrium configuration down to D_{4h}, D_{3d}, and D_{2h}, respectively. Neither of these groups have, of course, triply degenerate irreducible representations, and therefore the triply degenerate vibrational mode $\nu_6(F_{1u})$ of the O_h symmetric molecule will split. Near the D_{4h} and D_{3d} equilibria the ν_6 mode splits into a nondegenerate and a doubly degenerate mode; near the D_{2h} equilibrium the ν_6 mode splits into a sum of three nondegenerate modes. This explains qualitatively why it is natural to expect that in the large J limit the two C_4 energies and the two C_3 energies become nearly degenerate while the three C_2 energies remain separated.

7. PURELY CLASSICAL ANALYSIS OF THE ROVIBRATIONAL HAMILTONIAN

So far our analysis was based on the classical limit of the rotational operators and on quantum three-state description of the vibrational problem. In this way we obtained three rotational energy surfaces (RESs) which represented three vibrational components. We can also introduce a completely classical limit where both rotation and vibration are treated classically. In this section we account briefly for the remarkable fact of the *exact* correspondence of the formulae [10], [11], and [12] obtained by the RES method and the results of the classical study of the relative equilibria (stationary points on the classical phase space defined by the critical orbits of the symmetry group) of the classical rotation–vibration Hamiltonian.

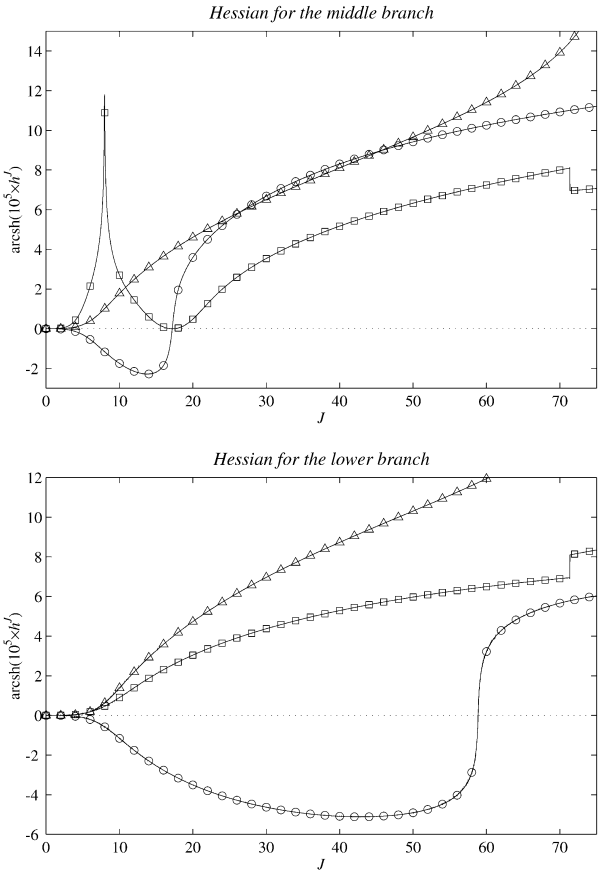

FIG. 6. Hessian values $\text{arcsh}(10^5 \times h'(\theta, \phi))$, at the stationary points of the central component $E_0(\mathcal{J})$ and lower component $E_+(\mathcal{J})$ of $\nu_6 = 1$ for J up to 75.

7.1. Classical Limit of the Vibrational Problem

To construct a purely classical analog of the quantum Hamiltonian [3] we should transform quantum operators of vibrational coordinates and conjugated momenta $(\hat{q}_i, \hat{p}_i)$, $i = 1, 2, 3$ of the triply degenerate oscillator to classical variables. To this end it suffices to replace $(\hat{q}_i, \hat{p}_i)$ for classical variables $(q_i,$

p_i). Equivalently, the classical analogs of the three creation and annihilation operators are the three complex variables together with their conjugates (*30*)

$$(a_k^+, a_k) \rightarrow (z_k^*, z_k) = (q_k + ip_k, q_k - ip_k), \quad k = 1, 2, 3.$$

A less trivial task is to understand the topology of the corresponding classical vibrational phase space. To do this we should realize that our problem contains an approximate integral of motion

$$\mathcal{N} = \frac{1}{2}(z_1 z_1^* + z_2 z_2^* + z_3 z_3^*) \qquad [32]$$

corresponding to the polyad quantum number n (total number of quanta in the ν_6 mode) of the quantum Hamiltonian. This integral is the harmonic oscillator part of the vibrational Hamiltonian or equally the sum of actions of the three one-dimensional oscillators. The assumption that n is preserved introduces an approximate dynamical symmetry. Reduction of this oscillator symmetry (see, for example Appendix B in (*31*)) leads from the initial six-dimensional Euclidean phase-space R_6 to a reduced-phase space of real dimension 4 which is a complex projective space CP_2. This space can be described in terms of homogeneous quadratic polynomials constructed of z and z^*; these polynomials are $su(3)$ analogs of the angular momenta J_x, J_y, J_z which describe the rotational sphere S_2. Analysis of the topological and group-theoretical features related with this model was initiated in (*9*) and continued later in (*12, 13*). Vibrational polyads of different kinds were intensively studied by Kellman (*32*). A numerical semiclassical analysis of the internal structure of vibrational polyads of a triply degenerate mode was suggested in (*33*).

7.2. Critical Orbits on the Classical Phase Space

Our classical analysis is very similar to the RES analysis of the purely rotational problem with classical phase-space S_2. We recall that in this latter familiar problem we look for stationary points of RES which in the presence of symmetry can be found, at least in the simplest possible situation, entirely from the action of the symmetry group on S_2. Thus in the case of cubic symmetry we find *isolated* points on S_2 which are fixed with regard to particular symmetry operations (rotation around particular axes C_4, C_3, and C_2). Operations which leave a particular point invariant form the local symmetry group of the point. This group is called a *stabilizer*. Other operations map the point to other points on S_2. All such points form an *orbit*. Since the points with local symmetry C_4, C_3, and C_2 are isolated, the corresponding orbits are *critical* (*23*). Any RES must have stationary points at the points in the critical orbits. In general, critical orbits correspond to *relative equilibria* of the problem, the set of equilibria of the reduced Hamiltonian which correspond to principal periodic orbits of the original problem (*29*). The values of the rotational Hamiltonian on the critical orbits or the energies of relative equilibria describe the cluster structure of the quantum multiplet.

The total classical phase space of our model rovibrational Hamiltonian for the $\nu_6(F_{1u})$ mode is the product $CP_2 \times S_2$ (for other examples of classical phase spaces of this kind see (*11, 17*)). Due to the action of the symmetry group O_h there are several critical orbits on this space. These critical orbits are necessarily stationary points of any smooth Morse function defined over $CP_2 \times S_2$. Critical orbits are defined entirely by the action of the O_h group on the vibrational and rotational spaces CP_2 and S_2, respectively. More precisely, since the spatial inversion does not modify angular momentum components and quadratic vibrational polynomials, the action of the O_h group reduces to that of the O group. (The image of O_h in the space of rotational and quadratic vibrational variables is O.) The action of the O group on CP_2 has been studied in detail in (*9*), and the action of this group on the rotational space S_2 [on (J_x, J_y, J_z)] is, of course, well known. The seven critical orbits of the O group action on the $CP_2 \times S_2$ space are characterized in Table 4, where for each orbit we specify its stabilizer on the total space, and on the vibrational and rotational subspaces CP_2 and S_2, the number of points in the orbit, and the branch assignment in the limiting case of normal Coriolis splitting. Positions of these critical orbits can be obtained directly from Table 4 of Ref. (*9*) and from the positions of critical orbits of the O group action on S_2. In Table 4 we give these positions in terms of complex vibrational coordinates z_k, $k = 1, 2, 3$ and rotational coordinates J_a, $a = x, y, z$. Since the energy (and everything else) is exactly the same for all points on the same critical orbit, only one point in each orbit is represented.

7.3. Other Stationary Points on $CP_2 \times S_2$

All points in the critical orbits in Table 4 are stationary points of any Morse function (a smooth function with only nondegenerate stationary points) defined on our phase space $CP_2 \times S_2$. However, using simple topology arguments we can show that such function should also have additional stationary points. We can also suggest that an O-symmetric Morse function on $CP_2 \times S_2$ would have two additional noncritical C_2 orbits of stationary points. Using the description of the O group action (*9*), we find that the points in question project on C_2-invariant spheres S_2 in CP_2. It is possible to characterize them further by taking the time reversal symmetry of our rovibrational Hamiltonian into account. Action of time reversal operation T on the classical variables

$$(z_1, z_2, z_3, J_x, J_y, J_z) \rightarrow (z_1^*, z_2^*, z_3^*, -J_x, -J_y, -J_z) \qquad [33]$$

is equivalent to simultaneous complex conjugation on CP_2 and inversion on S_2. Since the Hamiltonian itself is, of course,

TABLE 4
Critical Orbits of the Action of the O Group and Stationary Points of the Hamiltonian Function on the Classical Phase-Space $CP_2 \times S_2$

stabilizer of the orbit total	vib	rot	position on CP_2 (z_1, z_2, z_3)	position on S_2 (J_1, J_2, J_3)	type of orbit	number of points	component assignment
C_4	D_4	C_4	$\mathcal{N}(1,0,0)$	$\mathcal{J}(1,0,0)$	critical	6	central
C_4	C_4	C_4	$\frac{\mathcal{N}}{\sqrt{2}}(0,1,+i)$	$\mathcal{J}(1,0,0)$	critical	6	upper/lower
C_4	C_4	C_4	$\frac{\mathcal{N}}{\sqrt{2}}(0,1,-i)$	$\mathcal{J}(1,0,0)$	critical	6	lower/upper
C_3	D_3	C_3	$\frac{\mathcal{N}}{\sqrt{3}}(1,1,1)$	$\frac{\mathcal{J}}{\sqrt{3}}(1,1,1)$	critical	8	central
C_3	C_3	C_3	$\frac{\mathcal{N}}{2}\left(\frac{2}{\sqrt{3}}, -\frac{1}{\sqrt{3}} - i, -\frac{1}{\sqrt{3}} + i\right)$	$\frac{\mathcal{J}}{\sqrt{3}}(1,1,1)$	critical	8	upper/lower
C_3	C_3	C_3	$\frac{\mathcal{N}}{2}\left(\frac{2}{\sqrt{3}}, -\frac{1}{\sqrt{3}} + i, -\frac{1}{\sqrt{3}} - i\right)$	$\frac{\mathcal{J}}{\sqrt{3}}(1,1,1)$	critical	8	lower/upper
C_2	D_2	C_2	$\frac{\mathcal{N}}{\sqrt{2}}(0,1,1)$	$\frac{\mathcal{J}}{\sqrt{2}}(0,1,1)$	critical	12	central
$C_2 \wedge T_2$	$C_2 \wedge T_2$	$C_2 \wedge T_2$	$\frac{\mathcal{N}}{\sqrt{1+x^2}}\left(ix, \frac{1}{\sqrt{2}}, -\frac{1}{\sqrt{2}}\right)$	$\frac{\mathcal{J}}{\sqrt{2}}(0,1,1)$	non-critical	12	upper/lower
$C_2 \wedge T_2$	$C_2 \wedge T_2$	$C_2 \wedge T_2$	$\frac{\mathcal{N}}{\sqrt{1+y^2}}\left(iy, \frac{1}{\sqrt{2}}, -\frac{1}{\sqrt{2}}\right)$	$\frac{\mathcal{J}}{\sqrt{2}}(0,1,1)$	non-critical	12	lower/upper

Note. Reversing symmetry T_2 is used to restrict noncritical C_2 orbits to the corresponding invariant submanifold S_1 where the two orbits x and y represent the two stationary points of a generic Hamiltonian function.

invariant with respect to T, we can extend its initial symmetry group (*36*) from the spatial group O_h to $O_h \wedge T$ which on $CP_2 \times S_2$ becomes $O \wedge T$.

Analysis of the $O \wedge T$ action on $CP_2 \times S_2$ indicates the presence of a one-dimensional stratum formed by 12-point orbits whose stabilizer is the four-element group

$$C_2 \times T_2 = [Id,\ C_2',\ (C_4^2 \circ T),\ (C_2'' \circ T)].$$

(The C_2 subgroup of this group contains the C_2' element and the second-order-2 subgroup T_2 contains a reversing operation $T_2 = C_2'' \circ T$; the so-called "diagonal" axes C_2' and C_2'' are orthogonal to one of the C_4 axes.) This stratum is a union of 12 isolated S_1 circles. Each circle lies on the corresponding C_2-invariant sphere with stabilizer C_2'. A Morse function has two stationary points on S_1. These points are at the same time stationary on the C_2-invariant sphere in CP_2 and on the complete space $CP_2 \times S_2$ due to the $O \wedge T$ symmetry action. Of course, the exact position of the two stationary points depends on the concrete Hamiltonian function, but restricting this function to one of the invariant circles greatly facilitates the computation.

7.4. *Energy of Relative Equilibria*

Having done all preparatory analysis described above and having transformed our Hamiltonian [3] to its classical analogue $\mathcal{H}(z, J)$ we can appreciate the results. Indeed, we obtain the energies of all relative equilibria corresponding to critical orbits (in particular the energies of all C_4 and C_3 symmetric relative equilibria) after a trivial substitution of classical dynamical variables z and J in the Hamiltonian function $\mathcal{H}$ for the coordinates of the points in Table 4. If the scaling constant corresponding to the value of the oscillator integral $\mathcal{N}$ is set to 1, resulting analytic expressions are *identical* to those in Eqs. [10], [11], and [12] obtained from the analysis of the eigenvalues of the 3×3 matrix Hamiltonian [7] for the $\nu_6 = 1$ state.

To find explicitly the position of the two remaining C_2-symmetric stationary points and the energy of the corresponding relative equilibria, we restrict our classical Hamiltonian $\mathcal{H}$ to the S_1 subspace of CP_2 indicated in Table 4. The coordinates x and y of the two points are defined in terms of the polar coordinate ϕ on the circle S_1. They are obtained as solutions of a simple quadratic equation in ϕ defining the minimum and the maximum of $\mathcal{H}$ on S_1. Of course, positions x and y of the noncritical stationary points depend on the Hamiltonian parameters and the values of $\mathcal{J}$. As before, after replacing variables

z and J for the coordinates of the C_2 symmetric points in Table 4 and using the solutions for x and y (with $\mathcal{N} = 1$) we obtain expressions which can be transformed to form [12].

8. CONCLUSION

We once again demonstrated the advantages and usefulness of the simple classical approach to the analysis of rovibrational energy level system of concrete molecules. Using this approach we gave a complete concise qualitative description of the complicated rotational structure of the $\nu_6 = 1$ state of $Mo(CO)_6$.

We demonstrated how the global features of the rovibrational energy level patterns can be described and interpreted using simple classical mechanical models based on the concept of the rotational energy surface. Description of all stationary points and singularities in our classical model provides a way to understand and characterize all possible energy level structures, including energy intervals with regular sequences of states related to regular dynamical behavior and exceptional states and energy regions related to singularities. We do not, of course, characterize all individual quantum states, a nearly impossible task if our models are meant to be applicable at increasingly high energies where the number and density of states grow rapidly. The obvious advantage of the method is that the complexity of our calculations does not increase with the increase of the rotational excitation.

Our purely classical study (Section 7) based on $CP_2 \times S_2$ and the striking correspondence of its results to the RES calculations deserves by right further serious research which we plan for the near future. In general such classical study should be increasingly accurate in the analysis of the corresponding quantum system in the limit of high rotational *and* vibrational excitations. Nevertheless, our results indicate strongly that the analysis of classical relative equilibria on $CP_2 \times S_2$ can be very useful even in the study of low excited vibrational states which previously were always considered as exclusively quantum systems.

ACKNOWLEDGMENT

Région Bourgogne is gratefully acknowledged for supporting Laboratoire de Physique de l'Université de Bourgogne.

REFERENCES

1. A. J. Dorney and J. K. G. Watson, *J. Mol. Spectrosc.* **42,** 135–148 (1972).
2. W. G. Harter and C. W. Patterson, *J. Chem. Phys.* **66,** 4872–4885 (1977).
3. W. G. Harter, C. W. Patterson, and H. W. Galbraith, *J. Chem. Phys.* **69,** 4896–4907 (1978).
4. W. G. Harter and C. Patterson, *J. Chem. Phys.* **80,** 4241–4261 (1984).
5. I. Pavlichenkov and B. Zhilinskiĭ, *Chem. Phys.* **100,** 339 (1985); *Ann. Phys.* **184,** 1–32 (1988).
6. W. G. Harter, *Comp. Phys. Rep.* **8,** 319–394 (1988).
7. D. Sadovskiĭ and B. Zhilinskiĭ, *Mol. Phys.* **65,** 109–128 (1988).
8. V. Pavlov-Verevkin, D. Sadovskiĭ, and B. Zhilinskiĭ, *Europhys. Lett.* **6,** 573–578 (1988). [An entirely classical interpretation of the redistribution phenomenon and diabolic points is given in (*19*) where this phenomenon is associated with classical *monodromy*.]
9. B. Zhilinskiĭ, *Chem. Phys.* **137,** 1–13 (1989).
10. V. Krivtsun, D. Sadovskiĭ, and B. Zhilinskiĭ, *J. Mol. Spectrosc.* **139,** 126–146 (1990).
11. D. Sadovskiĭ and B. Zhilinskiĭ, *Phys. Rev. A: Gen. Phys.* **47,** 2653–2671 (1993).
12. D. Sadovskiĭ and B. Zhilinskiĭ, *Phys. Rev. A: Gen. Phys.* **48,** 1035–1044 (1993).
13. N. Fulton, J. Tennyson, D. A. Sadovskiĭ, and B. I. Zhilinskiĭ, *J. Chem. Phys.* **99,** 906–918 (1993).
14. B. Zhilinskiĭ and S. Brodersen, *J. Mol. Spectrosc.* **163,** 326–338 (1994).
15. S. Brodersen and B. Zhilinskiĭ, *J. Mol. Spectrosc.* **172,** 303–318 (1995).
16. S. Brodersen and B. Zhilinskiĭ, *J. Mol. Spectrosc.* **169,** 1–17 (1995).
17. B. Zhilinskiĭ, *Spectrochim. Acta A* **52,** 881–900 (1996).
18. L. Michel and B. Zhilinskiĭ, Technical Report No. IHES/P/97/54, Institut des Hautes Etudes Scientifiques Bures-sur-Yvette (France) (unpublished).
19. D. A. Sadovskiĭ and B. Zhilinskiĭ, *Phys. Lett. A* **256,** 235–244 (1999).
20. P. Asselin, P. Soulard, L. Manceron, V. Boudon, and G. Pierre, *J. Mol. Struct.,* in press.
21. L. Jones, R. McDowell, and M. Goldblatt, *Inorg. Chem.* **8,** 2340–2363 (1969).
22. J.-P. Champion, M. Loëte, and G. Pierre, *in* "Spectroscopy of the Earth's Atmosphere and Interstellar Medium," (K. N. Rao and A. Weber, Eds.), Academic Press, San Diego, 1992, pp. 339–422.
23. L. Michel, *Rev. Mod. Phys.* **52,** 617–651 (1980).
24. A. Robiette, D. Gray, and F. Birss, *Mol. Phys.* **32,** 1591–1607 (1976).
25. G. Herzberg, "Molecular Spectra and Structure. II. Infrared and Raman Spectra of Polyatomic Molecules," Van Nostrand, New York, 1966.
26. I. M. Pavlichenkov, *Phys. Rep.* **226,** 173–279 (1993).
27. G. Pierre, D. Sadovskiĭ, and B. Zhilinskiĭ, *Europhys. Lett.* **10,** 409–414 (1989).
28. I. Kozin, R. M. Roberts, and J. Tennyson, *J. Chem. Phys.* **111,** 140–150 (1999).
29. J. Montaldi and R. M. Roberts, *J. Nonlinear Sci.* **9,** 53–88 (1999).
30. V. Bargmann, *Comm. Pure Appl. Math.* **14,** 187–214 (1961).
31. R. Cushman and L. M. Bates, "Global Aspects of Classical Integrable Systems," Birkhauser, Basel, 1997.
32. M. Kellman, *in* "Molecular Dynamics and Spectroscopy by Stimulated Emission Pumping," (H.-L. Day and R. Field, Eds.), World Scientific, Singapore, 1995, pp. 1–60.
33. C. Patterson, *J. Chem. Phys.* **83,** 4618–4632 (1985).
34. D. A. Sadovskiĭ, B. I. Zhilinskiĭ, and L. Michel, *Phys. Rev. A: Gen. Phys.* **53,** 4064–4067 (1996).
35. D. A. Sadovskiĭ and B. I. Zhilinskiĭ, *Phys. Rev. A: Gen. Phys.* **57,** 2867–2884 (1998).
36. [Similar extension of a spatial symmetry group by reversing operations has turned out to be extremely useful in the qualitative analysis of many problems, such as the simple model three-level Hamiltonian with $SU(3)$ dynamical symmetry (*12*) and the Hamiltonian of the hydrogen atom in the presence of external electric and magnetic fields (*18, 34, 35*).]

Troisième partie

Chapitre

4

Modèles Tensoriels pour des Molécules Non-Sphériques

Publications P13, P14, P25, P27, P30, P32, P36, P38

4.1 Introduction

Le formalisme tensoriel développé et utilisé au sein du groupe de Dijon depuis plus de 30 ans est souvent considéré, à tort, comme une machinerie théorique complexe, uniquement destinée à la spectroscopie rovibrationnelle des molécules de type toupies sphériques. Diverses extensions de ce type de formalisme ont été réalisées récemment. Nous reparlerons longuement au cours de la Partie IV de l'extension concernant la spectroscopie rovibronique. Dans le domaine rovibrationnel, Maud Rotger a mis en place au LPUB plusieurs projets concernant l'utilisation du formalisme tensoriel pour des molécules non-sphériques. J'ai participé à ces projets, en particulier en ce qui concerne leur élaboration théorique.

Rappelons brièvement que les deux principaux avantages du formalisme tensoriel "à la dijonnaise" sont i) le développement systématique des opérateurs hamiltonien et moment de transition pour une polyade et un ordre donnés, et ii) la technique d'extrapolation vibrationnelle, décrite au Chapitre III.2.

4.2 Molécules quasi-sphériques

Dans le cas d'une molécule toupie symétrique ou asymétrique dérivant d'une toupie sphérique par substitution d'un ou plusieurs atomes, il peut être intéressant d'utiliser un formalisme dérivant de celui utilisé pour les espèces tétraédriques ou octaédriques. On procède alors à une réorientation dans le sous-groupe de la molécule "déformée". Nous nous sommes ainsi intéressés plus précisément aux deux types de problèmes suivants ;

– Les molécules du type X_2Y_2 de symétrie C_{2v}. On travaille alors dans le chaîne de groupes

$$O(3) \supset T_d \supset C_{2v}. \tag{III.4.1}$$

– Les molécules du type XY_5Z de symétrie C_{4v}. On travaille alors dans le chaîne de groupes

$$O(3) \supset O_h \supset C_{4v}. \tag{III.4.2}$$

Le formalisme correspondant s'obtient en réorientant les tenseurs et les bases de $O(3) \supset T_d$ ou $O(3) \supset O_h$ à l'aide d'une matrice $\widetilde{G}$,

$$\left| j,nC,\widetilde{C}\widetilde{\sigma} \right\rangle = \sum_{\sigma} {}^{(C)}\widetilde{G}^{\sigma}_{\widetilde{C}\widetilde{\sigma}} \left| j,nC\sigma \right\rangle . \tag{III.4.3}$$

cette matrice étant déterminée par une méthode de projection. $\widetilde{C}$ est une représentation irréductible de C_{2v} ou de C_{4v} et $\widetilde{\sigma}$ est l'une de ses composantes.

Les formalisme [P13,P14,P30] et les programmes [P27] nécessaires ont été développés pour ces deux chaînes de groupes et appliqué aux molécules SO_2F_2 [P36] et SF_5Cl [P25,P38].

4.3 Spectroscopie de l'éthylène

J'ai également participé à la mise en place d'un formalisme tensoriel adapté aux molécules de type X_2Y_4 de symétrie D_{2h} comme l'éthylène, C_2H_4 [P32]. Ce travail se fait dans le cadre de la thèse de Wilfried Raballand (co-dirigée par Maud Rotger et Michel Loëte) et dans le cadre d'une collaboration avec Jean-Marc Simon et ses collègues du Laboratoire de Recherches sur la Réactivité des Solides (LRRS) à Dijon. L'idée est à terme de modéliser les spectres de molécules d'éthylène adsorbées dans une zéolithe de type ZSM-5. Dans ce but, l'effet Stark (de part les champs électriques très intenses régnant à l'intérieur de la zéolithe) et les termes de confinement stérique sont en cours d'intégration dans le modèle.

4.4 Article-clé

Est reproduit ici un article illustrant l'utilisation du formalisme tensoriel dans le cas d'une molécule de type toupie quasi-sphérique.

– [**P38 :** *J. Mol. Spectrosc.*, **222**, 172–179 (2003)] présente une comparaison entre l'analyse de l'état vibrationnel de base de SO_2F_2 utilisant le formalisme usuel des toupies asymétriques et celle utilisant le formalisme tensoriel adapté aux molécules quasi-tétraédriques. Cette molécule étant extrêmement proche de la symétrie tétraédrique, l'approche "toupie sphérique déformée" semble prometteuse ici. Nous envisageons dans un proche avenir l'analyse des premières polyades de SO_2F_2 à l'aide de ce formalisme, l'approche toupie asymétrique standard semblant poser de nombreux problèmes.

Available online at www.sciencedirect.com
SCIENCE DIRECT®
Journal of Molecular Spectroscopy 222 (2003) 172–179
Journal of MOLECULAR SPECTROSCOPY
www.elsevier.com/locate/jms

The ground state rotational spectrum of SO_2F_2☆

M. Rotger,[a,*] V. Boudon,[a] M. Loëte,[a,*] L. Margulès,[b] J. Demaison,[b] H. Mäder,[c] G. Winnewisser,[d] and H.S.P. Müller[d]

[a] *Laboratoire de Physique de l'Université de Bourgogne, CNRS UMR 5027, 9, Avenue Alain Savary, B.P. 47 870, F-21078 Dijon Cedex, France*
[b] *Laboratoire de Physique, Atomes et Molécules, CNRS UMR 8523, Université de Lille I, Bât. P5, 59655 Villeneuve d'Ascq Cedex, France*
[c] *Institut für Physikalische Chemie, Universität Kiel, Olshausenstr. 40, D-24098 Kiel, Germany*
[d] *I. Physikalisches Institut, Universität zu Köln, D-50937 Köln, Germany*

Received 1 April 2003; in revised form 11 June 2003

Abstract

The analysis of the ground state rotational spectrum of SO_2F_2 [K. Sarka, J. Demaison, L. Margulès, I. Merke, N. Heineking, H. Bürger, H. Ruland, J. Mol. Spectrosc. 200 (2000) 55] has been performed with the Watson's Hamiltonian up to sextic terms but shows some limits due to the *A* and *S* reductions. Since SO_2F_2 is a quasi-spherical top, it can also be regarded as derived from an hypothetical XY_4 molecule. Thus we have developed a new tensorial formalism in the $O(3) \supset T_d \supset C_{2v}$ group chain (M. Rotger, V. Boudon, M. Loëte, J. Mol. Spectrosc. 216 (2002) 297]. We test it on the ground state of this molecule using the same experimental data (10 GHz–1 THz region, *J* up to 99). Both fits are comparable even if the formalisms are slightly different. This paper intends to establish a link between the classical approach and the tensorial formalism. In particular, our tensorial parameters at a given order of the development are related to the usual ones. Programs for spectrum simulation and fit using these methods are named C_{2v}TDS. They are freely available at the URL: `http://www.u-bourgogne.fr/LPUB/c2vTDS.html`.

PACS: 33.15.Mt; 33.20.Sn; 33.20.Bx

Keywords: Microwave spectroscopy; Tensorial formalism; XY_2Z_2; Asymmetric tops

1. Introduction

The ground state rotational spectrum of sulfuryl fluoride, SO_2F_2, has been recently investigated [1]. In parallel to this work, the rovibrational spectra of some fundamental bands are being analyzed. The results for the isolated $\nu_8(b_2)$ band centered at 887.2 cm^{-1} have already been published [2] as well as those for the $\nu_3(a_1)/\nu_7(b_1)/\nu_9(b_2)$ triad around 550 cm^{-1} [3].

However the analyses are not satisfactory and in particular the *A* (asymmetric) and *S* (symmetric) reductions proposed by Watson [4] fail in the ground state analysis. The best results are obtained using the so-called 6 reduction. In fact, the *A*, *B*, and *C* rotational constants have very close values and in this case the *A* and *S* reductions lead to non-perturbative unitary transformations of the Hamiltonian [5].

In this paper, we will use another approach. According to the rotational constants values, in first approximation we can consider the SO_2F_2 molecule as a spherical top derived from an hypothetical SY_4 molecule.

For this we have developed an adapted tensorial formalism in the $O(3) \supset T_d \supset C_{2v}$ chain [6]. It is an extension of the usual formalism used in Dijon for XY_4 [7] spherical tops with tetrahedral symmetry.

This theory is presented here and is applied to the analysis of the ground state. Results are compared to the previous analysis. In addition the tensorial and Watson's models are compared and relations between the parameters of both models are established.

☆ Supplementary data associated with this article can be found at doi:10.1016/S0022-2852(03)00215-7

* Corresponding authors. Fax: +33-3-80-39-59-71.
E-mail address: Maud.Rotger@u-bourgogne.fr (M. Rotger).
URL: http://www.u-bourgogne.fr/LPUB/Equipe2A/Spectroscopy/spectro.html.

0022-2852/$ - see front matter © 2003 Elsevier Inc. All rights reserved.
doi:10.1016/S0022-2852(03)00215-7

2. Experimental details

The sample is the same as previously used [1]. In Kiel, the spectra were recorded in the frequency range from about 8–14 GHz, employing a Fourier transform microwave spectrometer for the X/Ku-band with automatic scan facility [8] and a waveguide-cell of quadratic cross-section and 12 m length [9]. Ambient temperature and sample pressures of about 0.3–0.6 Pa (2–4 mTorr) were used throughout. The transition frequencies were determined from a least-squares analysis of the transient emission signals, in most cases at an accuracy of better than 5 kHz.

The Cologne Terahertz spectrometer was used between 545 and 945 GHz. The radiation sources are Russian phase-locked backward-wave oscillators (BWOs). The detector is a magnetically tuned LHe cooled InSb hot electron bolometer. Further details of the spectrometer are given in [10]. The accuracy of the measurements is 30 up to 100 kHz for weak lines.

In Lille, a FIR laser sideband spectrometer [11] was used to cover selected regions between 600 and 1000 GHz. The output of a MW synthetizer (2–18 GHz) and that of an optically pumped FIR laser were mixed on a Schottky diode to generate terahertz sideband radiation which was detected by a heterodyne receiver. The laser was locked permitting an accuracy better than 300 kHz. In addition, the lines below 473 GHz were measured with a source-modulated spectrometer employing phase-locked French Thomson-CSF BWOs. The signal was detected with a LHe cooled InSb bolometer. In general, the accuracy of the measurements was better than 50 kHz.

3. Theory

3.1. The Hamiltonian operator

3.1.1. Watson's form

The usual sextic rotational Hamiltonian for an asymmetric rotor (which we call H_{Watson} or "Watsonian") can be written in terms of the operators J^2, J_Z, and $J_\pm = J_X \pm iJ_Y$ as follows [12]:

$$\begin{aligned} H_{\text{Watson}} = {} & B_{200}J^2 + B_{020}J_Z^2 + T_{400}(J^2)^2 + T_{220}J^2J_Z^2 \\ & + T_{040}J_Z^4 + \Phi_{600}(J^2)^3 + \Phi_{420}(J^2)^2J_Z^2 \\ & + \Phi_{240}J^2J_Z^4 + \Phi_{060}J_Z^6 + \frac{1}{2}[B_{002} + T_{202}J^2 \\ & + T_{022}J_Z^2 + \Phi_{402}(J^2)^2 + \Phi_{222}J^2J_Z^2 \\ & + \Phi_{024}J_Z^4, J_+^2 + J_-^2]_+ + \frac{1}{2}[T_{004} + \Phi_{204}J^2 \\ & + \Phi_{024}J_Z^2, J_+^4 + J_-^4]_+ + \Phi_{006}(J_+^6 + J_-^6) \end{aligned} \tag{1}$$

with

$$\begin{cases} B_{200} = \frac{B+C}{2}, \\ B_{020} = \frac{2A-B-C}{2}, \\ B_{002} = \frac{B-C}{4}, \end{cases} \tag{2}$$

in the I^r representation.

The use of capital letters (X, Y, Z) to label the angular momentum components in Eq. (1) is different from the standard notation and will be explained later.

In the S reduction [1], one quartic parameter, T, and three sextic parameters, Φ, are constrained to zero: $T_{022} = \Phi_{222} = \Phi_{042} = \Phi_{024} = 0$.

3.1.2. Distorted tetrahedron form

Let us now introduce our tensorial Hamiltonian for a distorted tetrahedral molecule.

The theoretical model described below to develop the Hamiltonian operator is based on the tensorial formalism and vibrational extrapolation methods used in Dijon. These methods have already been explained for example in [7,13–15]. We only recall here the basic principles and their applications to the case of XY_2Z_2 molecules [6] belonging to the C_{2v} group.

The background of the model is based on the idea of considering XY_2Z_2 molecules as distorted XY_4 molecules, by substitution of two ligands. Practically, this means that we start from the $O(3) \supset T_d$ formalism used for tetrahedral species [7] and make a symmetry reduction (or reorientation) into the C_{2v} subgroup. This procedure has been detailed in [6]. In the following, all the C_{2v} oriented tensor operators will be denoted in the form:

$$T^{(\ldots,\Gamma,\widetilde{\Gamma})},$$

with Γ ($= A_1, A_2, E, F_1, F_2$) and $\widetilde{\Gamma}$ ($= a_1, a_2, b_1, b_2$) denoting T_d and C_{2v} irreducible representations (irreps), respectively. This way of handling XY_2Z_2 molecules has some consequences on the labelling of Hamiltonian and transition moment parameters. The energy level labels are also different from the "usual" ones used in the standard treatment of asymmetric tops, as it will be detailed in Section 3.1.5.

If we consider an XY_2Z_2 molecule in its vibrational ground state, the Hamiltonian operator can be put in the following form (after performing some contact transformations):

$$H_{\text{Moret-Bailly}} = \sum_{\text{all indices}} t^{\Omega(K,n\Gamma,\widetilde{\Gamma})}\beta R^{\Omega(K,n\Gamma,\widetilde{\Gamma})}, \tag{3}$$

which we have called $H_{\text{Moret-Bailly}}$ since it is based on the rotational operators R defined by Moret-Bailly [16,17].

In Eq. (3), the $t^{\Omega(K,n\Gamma,\Gamma)}$ are the parameters to be determined and β is a numerical factor such that:

$$\beta = \begin{cases} \left(-\frac{\sqrt{3}}{4}\right)^{\Omega/2} & \text{if } (K,n\Gamma) = (0,0A_1), \\ 1 & \text{otherwise.} \end{cases} \tag{4}$$

$R^{\Omega(K,n\Gamma,\widetilde{\Gamma})}$ is the rotational operator of degree Ω. The order of each individual term is defined as $\Omega-2$.

Let us summarize here the construction of the $R^{\Omega(K,n\Gamma,\Gamma)}$ rotational operators. Further details can be found in [6,7]. A convenient classification of a complete set of rotational tensors requires two indices: the degree Ω in the angular momentum components and the tensorial rank K. This basic tensor as defined by Moret-Bailly [16,17] is denoted by

$$R^{1(1)} = 2J^{(1)},$$

where $J^{(1)}$ is the angular momentum vector. The general tensor $R^{\Omega(K)}$ is defined according to the following recursive expressions given by Zhilinskií [18]

$$R^{\Omega(K)} = R^{\Omega-K(0)} \times R^{K(K)}, \tag{5}$$

where

$$R^{\Omega-K(0)} = ((R^{1(1)} \times R^{1(1)})^{(0)})^{(\Omega-K)/2} = (R^{2(0)})^{(\Omega-K)/2} \tag{6}$$

and

$$R^{K(K)} = (R^{K-1(K-1)} \times R^{1(1)})^{(K)}. \tag{7}$$

In the T_d group, $R^{\Omega(K,n\Gamma)}_{\sigma}$ is the general form for a rotational tensor. Γ is an irrep of this group, σ a component of Γ and n is an index of multiplicity. They are linked to $O(3)$ tensors (5) thanks to the G coefficients [19,20]

$$R^{\Omega(K,n\Gamma)}_{\sigma} = \sum_{M}^{(K)} G^{M}_{n\Gamma\sigma} R^{\Omega(K)}_{M}. \tag{8}$$

Finally, the preceeding rotational tensor is re-oriented from T_d into our subgroup (C_{2v}) and is denoted $R^{\Omega(K,n\Gamma,\widetilde{\Gamma})}$, where $\widetilde{\Gamma}$ is a C_{2v} irrep. This re-orientation is done using the G' coefficients [6,21]:

$$R^{\Omega(K,n\Gamma,\widetilde{\Gamma})} = \sum_{\sigma}^{(\Gamma)} G'^{\sigma}_{\widetilde{\Gamma}} R^{\Omega(K,n\Gamma)}_{\sigma}. \tag{9}$$

3.1.3. Principal axes

Let us first consider only terms of order 0 (i.e., degree 2 in J_x, J_y, J_z) in (3)

$$H_{\text{Moret-Bailly}} = t_1 \beta R^{(2,0A_1,a_1)} + t_2 R^{(2,0E,a_1)} + t_3 R^{(2,0F_2,a_1)} + \cdots \tag{10}$$

In term of J_x, J_y, and J_z operators and according to (5)–(9), this leads to the following equation

$$\begin{aligned} H_{\text{Moret-Bailly}} = {} & \left(t_1 - 2\sqrt{\frac{2}{3}}t_2\right)J_x^2 + \left(t_1 - 2\sqrt{\frac{2}{3}}t_2\right)J_y^2 \\ & + \left(t_1 + 4\sqrt{\frac{2}{3}}t_2\right)J_z^2 + 2\sqrt{2}t_3(J_xJ_y \\ & + J_yJ_x) + \cdots, \end{aligned} \tag{11}$$

where x, y, and z denote the components in the axis system of the tetrahedral molecule (see Fig. 1).

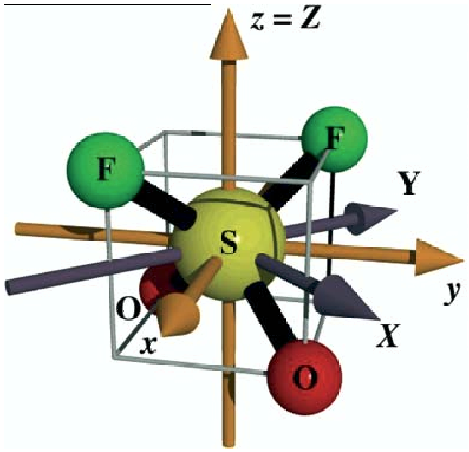

Fig. 1. The molecular axis frames in T_d and C_{2v}.

At the same order of development, the Watsonian can be written

$$\begin{aligned} H_{\text{Watson}} = {} & (B_{200} + 2B_{002})J_X^2 + (B_{200} - 2B_{002})J_Y^2 \\ & + (B_{020} + B_{200})J_Z^2 + \cdots \end{aligned} \tag{12}$$

We can see that our oriented Hamiltonian contains an additional term proportional to $J_xJ_y + J_yJ_x$. This can be easily understood because $H_{\text{Moret-Bailly}}$ has been derived from the reorientation of the tetrahedral Hamiltonian. For this one, the (x, y, z) axis frame that is used (see Fig. 1) is not the principal axis system of the "distorted" C_{2v} molecule. Thus, a coordinate change has to be made in order to eliminate the $J_xJ_y + J_yJ_x$ cross-term.

In term of angular momentum operators, this leads to the following relations for the components of the J angular momentum:

$$\begin{cases} J_X = -\frac{1}{\sqrt{2}}(J_x - J_y), \\ J_Y = \frac{1}{\sqrt{2}}(J_x + J_y), \\ J_Z = J_z \end{cases} \tag{13}$$

or

$$\begin{cases} J_x = -\frac{1}{\sqrt{2}}(J_X - J_Y), \\ J_y = \frac{1}{\sqrt{2}}(J_X + J_Y), \\ J_z = J_Z. \end{cases} \tag{14}$$

A correct phase choice for the J_X component has been made to be in agreement with the signs of the usual rotational constants. In other words, our C_{2v} molecular axis frame (or ($OXYZ$) frame) is deduced from the ($Oxyz$) molecular axis of the T_d group by a rotation of an angle equals to $\pi/4$ about the OZ axis as shown on Fig. 1.

3.1.4. Comparison of the two models

In the aim of comparing the two models, we give hereafter the expression of both Hamiltonians taken in the same ($Oxyz$) molecular frame, up to order 2 (i.e.,

degree 4 in J_x, J_y, J_z). By applying transformation (13) to Eq. (1), we get :

$$\begin{aligned}H_{\text{Watson}} &= B_{200}J^2 + B_{020}J_z^2 - 2B_{002}(J_xJ_y + J_yJ_x)\\ &+ T_{400}\left(J_x^2+J_y^2+J_z^2\right)\left(J_x^2+J_y^2+J_z^2\right)\\ &+ \frac{T_{220}}{2}\left[\left(J_x^2+J_y^2+J_z^2\right)J_z^2 + J_z^2\left(J_x^2+J_y^2+J_z^2\right)\right]\\ &+ T_{040}J_z^4 - T_{202}\left[\left(J_x^2+J_y^2+J_z^2\right)(J_xJ_y+J_yJ_x)\right.\\ &\left.+ (J_xJ_y+J_yJ_x)\left(J_x^2+J_y^2+J_z^2\right)\right]\\ &- T_{022}\left[J_z^2(J_xJ_y+J_yJ_x) + (J_xJ_y+J_yJ_x)J_z^2\right]\\ &- 2T_{004}\left[J_y^4 - J_y^2J_x^2 - J_x^2J_y^2 + J_x^4\right]\\ &+ 2T_{004}\left(J_xJ_yJ_xJ_y + J_yJ_xJ_yJ_x + J_xJ_y^2J_x + J_yJ_x^2J_y\right),\end{aligned} \tag{15}$$

to be compared with:

$$\begin{aligned}&H_{\text{Moret-Bailly}}\\ &= t_1\left(J_x^2+J_y^2+J_z^2\right) + \frac{4}{3}t_2\left(2J_z^2 - J_x^2 - J_y^2\right)\\ &+ 2\sqrt{2}t_3(J_xJ_y+J_yJ_x) + t_4\left(J_x^2+J_y^2+J_z^2\right)\left(J_x^2+J_y^2+J_z^2\right)\\ &- \frac{8\sqrt{2}}{6}t_5\left[\left(2J_z^2 - J_x^2 - J_y^2\right)\left(J_x^2+J_y^2+J_z^2\right)\right.\\ &\left.+ \left(J_x^2+J_y^2+J_z^2\right)\left(2J_z^2 - J_x^2 - J_y^2\right)\right]\\ &- \frac{8\sqrt{2}}{2\sqrt{3}}t_6\left[(J_xJ_y+J_yJ_x)\left(J_x^2+J_y^2+J_z^2\right)\right.\\ &\left.+ \left(J_x^2+J_y^2+J_z^2\right)(J_xJ_y+J_yJ_x)\right]\\ &+ \frac{8\sqrt{2}}{\sqrt{15}}t_7\left[5J_x^4 + 5J_y^4 + 5J_z^4 - 3\left(J_x^2+J_y^2+J_z^2\right)\right.\\ &\left.\times\left(J_x^2+J_y^2+J_z^2\right) + J_x^2+J_y^2+J_z^2\right]\\ &+ \frac{8\sqrt{2}}{\sqrt{21}}t_8\left[J_x^4 + J_y^4 - 2J_z^4 - 6\left(J_x^2J_y^2 + J_y^2J_x^2\right)\right]\\ &+ \frac{8\sqrt{2}}{\sqrt{21}}t_8\left[3\left(J_x^2J_z^2 + J_z^2J_x^2 + J_y^2J_z^2 + J_z^2J_y^2\right)\right.\\ &\left.+ 5J_x^2 + 5J_y^2 - 10J_z^2\right]\\ &+ \frac{8\sqrt{2}}{\sqrt{7}}t_9\left[3J_z^2(J_xJ_y+J_yJ_x) + 3(J_xJ_y+J_yJ_x)J_z^2\right]\\ &- \frac{8\sqrt{2}}{\sqrt{7}}t_9\left[\left(J_x^3J_y + J_yJ_x^3\right) - \left(J_yJ_x^3 + J_x^3J_y\right)\right.\\ &\left.- 4(J_xJ_y+J_yJ_x)\right].\end{aligned} \tag{16}$$

It is not possible to fit all quartic constants in both models using terms up to the order 2 only [1,6]. In order to identify these two expressions and also to be able to compare the results with experimental values, we use the so-called S reduction for H_{Watson} [1]. In this reduction, $T_{022} = 0$ which clearly corresponds to $t_9 = 0$ in $H_{\text{Moret-Bailly}}$. This ensures a full consistency between the two expressions. So, we get:

$$\begin{cases} t_1 = B_{200} + \frac{1}{3}B_{020} + \frac{2}{5}T_{004} - \frac{1}{15}T_{040} + \cdots\\ t_2 = \frac{\sqrt{6}}{84}(7B_{020} - 30T_{004} - 5T_{040}) + \cdots\\ t_3 = -\frac{1}{2}\sqrt{2}B_{002} + \cdots\\ t_4 = -\frac{8}{15}T_{004} + \frac{1}{5}T_{040} + \frac{1}{3}T_{220} + T_{400} + \cdots\\ t_5 = -\frac{\sqrt{2}}{112}(8T_{004} + 6T_{040} + 7T_{220}) + \cdots\\ t_6 = \frac{\sqrt{6}}{8}T_{202} + \cdots\\ t_7 = -\frac{\sqrt{30}}{240}(6T_{004} - T_{040}) + \cdots\\ t_8 = -\frac{\sqrt{42}}{336}(6T_{004} + T_{040}) + \cdots \end{cases} \tag{17}$$

In the reverse way, we obtain:

$$\begin{cases} B_{002} = -\sqrt{2}t_3 + \cdots\\ B_{020} = 2\sqrt{6}t_2 - \frac{40}{7}\sqrt{42}t_8 + \cdots\\ B_{200} = t_1 - \frac{2}{3}\sqrt{6}t_2 + \frac{8}{15}\sqrt{30}t_7 + \frac{40}{21}\sqrt{42}t_8 + \cdots\\ T_{400} = -D_J = t_4 + \frac{8}{3}\sqrt{2}t_5 - \frac{4}{15}\sqrt{30}t_7 - \frac{88}{21}\sqrt{42}t_8 + \cdots\\ T_{220} = -D_{JK} = -8\sqrt{2}t_5 - \frac{8}{3}\sqrt{30}t_7 + \frac{88}{21}\sqrt{42}t_8 + \cdots\\ T_{040} = -D_K = 4\sqrt{30}t_7 - 4\sqrt{42}t_8 + \ldots\\ T_{202} = d_1 = \frac{4}{3}\sqrt{6}t_6 + \cdots\\ T_{004} = d_2 = -\frac{2}{3}\sqrt{30}t_7 - \frac{2}{3}\sqrt{42}t_8 + \cdots \end{cases} \tag{18}$$

The dots indicate that these expressions are only approximate. The main reason is that Moret-Bailly's rotational operators are not homogeneous polynomials in J_x, J_y and J_z. $R^{\Omega(K)}$ terms contain monomials in J_x, J_y, J_z of maximum degree Ω. For instance, we can see that the term $R^{4(4,A_1,a_1)}$ with parameter t_7 in (16) contains also monomials of degree 2. Thus, the dots in the above expressions will contain additional contributions from $\Omega = 6, 8, \ldots$.

3.1.5. Matrix elements of the tensorial Hamiltonian

The matrix elements of a pure rotational operator are calculated in the following pure rotational basis

$$|\Psi^{(J,nC_r,\widetilde{C_r})}\rangle. \tag{19}$$

Expression of the matrix elements of the Hamiltonian from [6] is simplified in the following manner for purely rotational operators:

$$\begin{aligned}&\left\langle \Psi^{(J',n'C'_r,\widetilde{C'}_r)}\middle| R^{\Omega(K,n_r\Gamma_r,\widetilde{\Gamma})}\middle|\Psi^{(J,nC_r,\widetilde{C_r})}\right\rangle\\ &= K'\begin{pmatrix}\Gamma_r & C_r & C'_r\\ \widetilde{\Gamma} & \widetilde{C_r} & \widetilde{C'_r}\end{pmatrix}K\begin{pmatrix}K & J & J'\\ n_r\Gamma_r & nC_r & n'C'_r\end{pmatrix}\\ &\times\left\langle \Psi^{(J')}\middle\| R^{\Omega(K)}\middle\|\Psi^{(J)}\right\rangle.\end{aligned} \tag{20}$$

All the rovibrational levels are described by $(J, \tilde{\alpha}, \widetilde{C})$ labels where $\tilde{\alpha}$ is a numbering index for levels that have the same C_{2v} symmetry within a J block. This labelling is related to our group chain choice which considers XY_2Z_2 molecules like near-spherical tops.

In this way, the usual asymmetric-top K_a, K_c labels are hidden and related to the $\widetilde{C}$ symmetry. Thus, the (ΔK_a, ΔK_c) nomenclature does not occur in our transition labels.

3.1.6. Intensity calculations for the tensorial model

The strength of a transition between the molecular rovibrational states Φ_i (with energy E_i) and Φ_f (with energy E_f) is calculated using

Table 1
Rotational and centrifugal distortion constants in MHz of SO_2F_2 in S and 6 reductions

		S reduction			6 reduction
A		5134.877276(93)	A		5134.876906(51)
B		5073.078278(60)	B		5073.078441(36)
C		5057.056659(69)	C		5057.055567(36)
D_J	$\times 10^3$	1.478671(14)	D_J	$\times 10^3$	1.497054(26)
D_{JK}	$\times 10^3$	−1.529510(51)	D_{JK}	$\times 10^3$	−1.64148(15)
D_K	$\times 10^3$	1.850506(50)	D_K	$\times 10^3$	1.94409(13)
d_1	$\times 10^6$	−30.212(17)	d_1	$\times 10^6$	−30.1838(46)
d_2	$\times 10^3$	0.1372017(39)	R_5	$\times 10^3$	−0.16272(22)
			R_6	$\times 10^3$	0.146508(13)
H_J	$\times 10^9$	0.44338(95)	H_J	$\times 10^9$	0.71538(67)
H_{JK}	$\times 10^9$	0.565(11)	H_{JK}	$\times 10^9$	−1.5585(24)
H_{KJ}	$\times 10^9$	0.141(21)	H_{KJ}	$\times 10^9$	2.351(12)
H_K	$\times 10^9$	−0.730(18)	H_K	$\times 10^9$	−1.005(13)
h_1	$\times 10^9$	0.5891(34)	h_1	$\times 10^9$	−0.1012(10)
h_2	$\times 10^{12}$	95.05(90)	h_2	$\times 10^{12}$	−57.00(55)
h_3	$\times 10^9$	−0.67251(96)	h_3	$\times 10^{12}$	13.86(93)
L_{JJK}	$\times 10^{15}$	−59.23(97)			
L_{JK}	$\times 10^{12}$	−0.1431(24)			
L_{KKJ}	$\times 10^{15}$	−65.3(2.5)			
l_1	$\times 10^{15}$	−8.44(21)			
l_3	$\times 10^{15}$	7.73(12)			
σ^a	kHz	26			21
RMS	kHz	102.85			79.27

[a] Standard deviation of the fit calculated from the median of absolute residuals.

Table 2
Values of the ground state parameters with our tensorial formalism ($H_{\text{Moret-Bailly}}$)

t_i	$\Omega(K, n\Gamma, \widetilde{\Gamma})$	Value/MHz	
		Best fit	$t_9 = 0$ Reduction
t_1	$2(0, 0A_1, a_1)$	5088.337142(42)	5088.337190(42)
t_2	$2(2, 0E, a_1)$	14.250186(12)	14.250245(12)
t_3	$2(2, 0F_2, a_1)$	−2.832303(8)	−2.832273(8)
t_4	$4(0, 0A_1, a_1)$	−0.001338723(13)	−0.001338742(14)
t_5	$4(2, 0E, a_1)$	$2.835(3) \times 10^{-6}$	$5.0518(36) \times 10^{-6}$
t_6	$4(2, 0F_2, a_1)$	$-2.03114(28) \times 10^{-5}$	$-9.2687(26) \times 10^{-6}$
t_7	$4(4, 0A_1, a_1)$	$-7.68568(13) \times 10^{-5}$	$-7.35454(13) \times 10^{-5}$
t_8	$4(4, 0E, a_1)$	$-1.9084(12) \times 10^{-6}$	$-1.3551(12) \times 10^{-6}$
t_9	$4(4, 0F_2, a_1)$	1.689×10^{-5} (fixed)	0 (fixed)
t_{10}	$6(0, 0A_1, a_1)$	$5.235(17) \times 10^{-10}$	$5.256(17) \times 10^{-10}$
t_{11}	$6(2, 0E, a_1)$	$-1.5(3) \times 10^{-12}$	$-6.08(32) \times 10^{-12}$
t_{12}	$6(2, 0F_2, a_1)$	$-5.61(1.23) \times 10^{-12}$	$-1.751(10) \times 10^{-10}$
t_{13}	$6(4, 0A_1, a_1)$	$-1.87(63) \times 10^{-11}$	$-1.34(6) \times 10^{-11}$
t_{14}	$6(4, 0E, a_1)$	$-7.5(5.71) \times 10^{-13}$	$7.5(5.7) \times 10^{-13}$
t_{15}	$6(4, 0F_2, a_1)$	$-2.72(16) \times 10^{-11}$	$1.352(13) \times 10^{-10}$
t_{16}	$6(6, 0A_1, a_1)$	$1.02(8) \times 10^{-11}$	$1.1(9) \times 10^{-12}$
t_{17}	$6(6, 0E, a_1)$	$-1.08(3) \times 10^{-11}$	$-4.80(39) \times 10^{-12}$
t_{18}	$6(6, 0F_2, a_1)$	$-3.355(51) \times 10^{-11}$	$-2.69(42) \times 10^{-11}$
t_{19}	$6(6, 1F_2, a_1)$	$-1.986(16) \times 10^{-11}$	$-1.1762(14) \times 10^{-10}$
σ^a	kHz	23.29	23.47
RMS	kHz	69.87	72.85

[a] Standard deviation of the fit calculated from the median of absolute residuals.

$$S_{if} = K_{if} g_i e^{-(hcE_i)/kT} \sum_{M_i,M_f} |\langle \Phi_i | \tilde{\mu}_{\mathscr{Z}} | \Phi_f \rangle|^2, \quad (21)$$

where K_{if} is a numerical coefficient and g_i is the spin statistical weight of state Φ_i. The values of spin statistical weights in XY_2Z_2 (C_{2v}) molecules, with Y ligands having spin $\frac{1}{2}$ and Z ligands having a spin equal to 1 are listed in Table (6) of [6]. The sum is realized over the spherical components M_i and M_f of the two states in the Laboratory-Fixed Frame (LFF). $\mu_{\mathscr{Z}}$ is the $\mathscr{Z}$ component of the dipole moment in the ($\mathscr{O}\mathscr{X}\mathscr{Y}\mathscr{Z}$) LFF.

In order to calculate transition intensities, we have limited the development of the dipole moment operator through the zeroth order only using the methods explained in [6]. This reference also gives the expression of the matrix elements of the dipole moment operator.

4. Analysis and discussion

First, the assigned transitions (1071) were fitted to the Watsonian using I^r representation in the S and 6 reductions. The results are given in Table 1. Inspection of this table shows that all the determinable sextic centrifugal distortion constants are well determined and that the standard deviation of the fit in the 6 reduction is slightly smaller although the number of fitted parameters is smaller (16 instead of 20). It confirms the conclusion of [1] that, in the particular case of SO_2F_2, it is preferable to use a non-reduced Hamiltonian (at least up to quartic terms). It is also worth noting that the rotational constants have a smaller standard deviation in the 6 reduction and that the sextic constants are significantly different in the S and 6 reductions (another indication that the reduction parameter is too large).

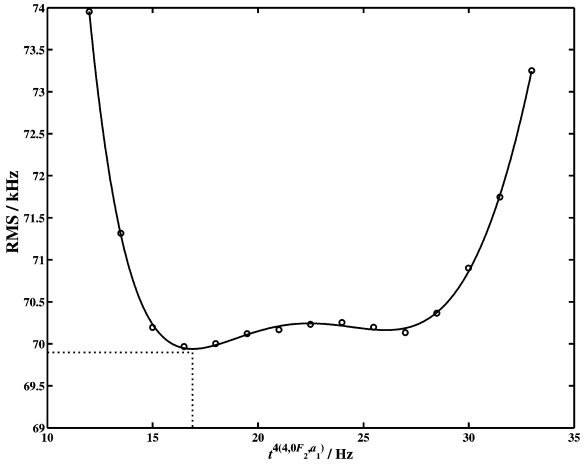

Fig. 2. The root mean square versus the values of the $t^{A(4,0F_2,a_1)}$ parameter.

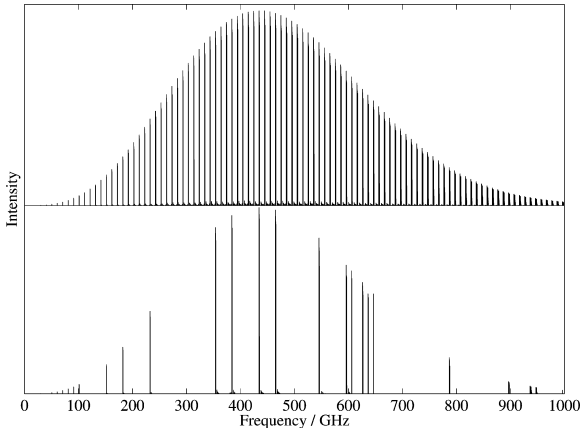

Fig. 3. Overview stick spectrum of the ground state of SO_2F_2: experiment and simulation.

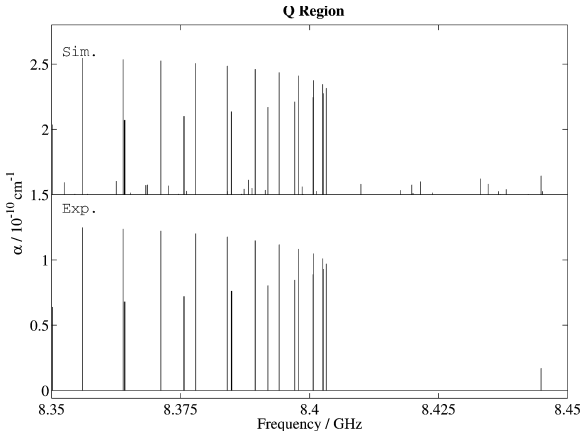

Fig. 4. Q region of the ground state of SO_2F_2: experiment and simulation.

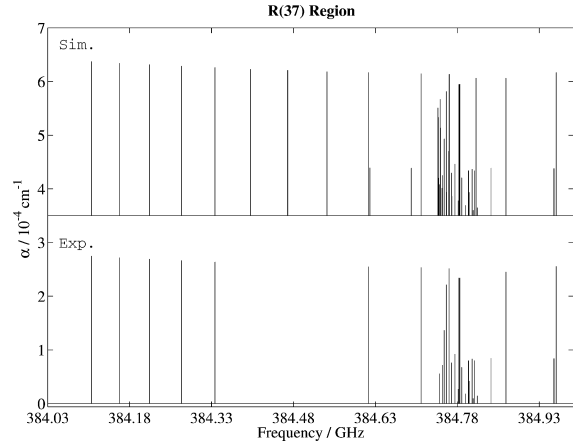

Fig. 5. $R(37)$ cluster of the ground state of SO_2F_2: experiment and simulation.

We have then performed an analysis of the ground state of SO_2F_2 using the tensorial model described above. For this, $\mathscr{H}_{\{\text{Moret-Bailly}\}}$ has been developed to the fourth order. Preliminary simulations of this region were obtained starting from the rotational parameters of Sarka et al. [1] and in taking the same value for A_0, B_0, and C_0 rotational constants. In the I^r representation, we obtain the following relations for our t_1, t_2 and t_3 tensorial parameters using (2) and (17)

$$t_1 \simeq \frac{A_0+B_0+C_0}{3}, \quad t_2 \simeq \frac{\sqrt{6}}{12}\left(A_0-\frac{B_0}{2}-\frac{C_0}{2}\right),$$
$$t_3 \simeq \frac{C_0-B_0}{4\sqrt{2}}. \tag{22}$$

A first simulation enabled us to begin the assignments and the fit procedure for low J values. More and more parameters have been successively released and the whole spectrum has been simulated. At the end, all the 1071 available transitions (see above) were used. So 18 parameters were adjusted together and the final standard deviation is equal to 23.29 kHz. The resulting parameters are listed in Table 2. Only one parameter, namely $t_9 = t^{A(4,0F_2,a_1)}$, is fixed because of an ambiguity problem. Its value is choosen as shown in Fig. 2 in the aim of decreasing the root mean square. Several root mean squares have been calculated for different values of the $t^{A(4,0F_2,a_1)}$ parameter. This curve has been fitted by a polynomial and the minimum has been found. The last column of this table also gives the values of our parameter in $t_9 = 0$ reduction.

Figs. 3–5 show synthetic spectra calculated with the parameters of the fit listed in Table 2. The detailed views show very good agreement between the simulation and the experiment.

In the experimental stick spectrum, only lines that have been actually observed are plotted. Fig. 7 displays the calculated and observed reduced energy levels for the ground state (observed levels are levels reached by observed transitions). They are obtained by subtracting the scalar terms, i.e.,

$$E_{\text{red}} = E(J,\tilde{\alpha},\tilde{C}) - t^{2(0,0A_1,a_1)}J(J+1) - t^{4(0,0A_1,a_1)}J^2(J+1)^2. \tag{23}$$

The Fig. 6 show the observed minus the calculated frequencies versus J. These residual values are quite similar in both models versus J.

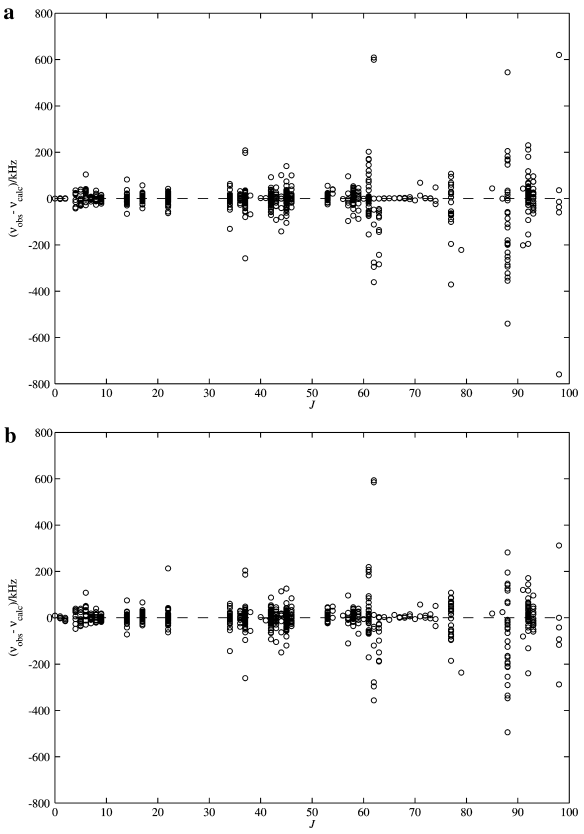

Fig. 6. Observed minus calculated wavenumbers versus J with the Watsonian (a) and Moret-Bailly's Hamiltonian (b).

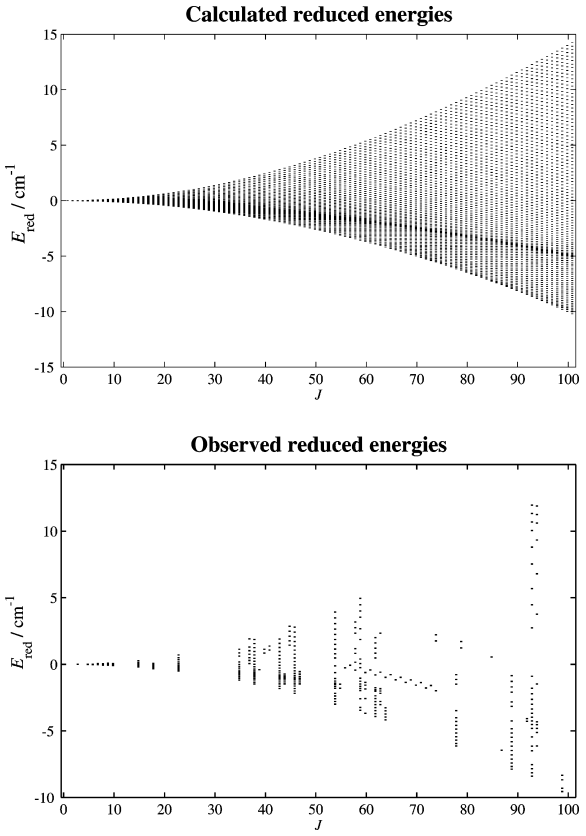

Fig. 7. Observed and calculated energies for the ground state of SO_2F_2 using the Moret-Bailly's model.

Table 3
Fitted values of the ground state parameters up to the quartic order with the tensorial model ($H_{\text{Moret-Bailly}}$)

t_i	$\Omega(K, n\Gamma, \widetilde{\Gamma})$	Value/MHz
t_1	$2(0, 0A_1, a_1)$	5088.3097(18)
t_2	$2(2, 0E, a_1)$	14.2468(5)
t_3	$2(2, 0F_2, a_1)$	−2.8291(3)
t_4	$4(0, 0A_1, a_1)$	$-0.133101(28) \times 10^{-2}$
t_5	$4(2, 0E, a_1)$	$4.530(75) \times 10^{-6}$
t_6	$4(2, 0F_2, a_1)$	$-7.657(39) \times 10^{-6}$
t_7	$4(4, 0A_1, a_1)$	$-7.2906(30) \times 10^{-5}$
t_8	$4(4, 0E, a_1)$	$-3.64(25) \times 10^{-7}$
t_9	$4(4, 0F_2, a_1)$	0 (fixed)

Table 4
Fitted values of the ground state parameters up to the quartic order with the Watson model compared to those obtained according to relation (18) and Table 3

Watson's Par.	Value/MHz	"Calc."/MHz
A	$5.1348351(28) \times 10^3$	$5.1348394(51) \times 10^3$
B	$5.0730374(21) \times 10^3$	$5.0730466(35) \times 10^3$
C	$5.0570357(24) \times 10^3$	$5.0570424(35) \times 10^3$
$D_J = -T_{400}$	$1.47055(19) \times 10^{-3}$	$1.2052(13) \times 10^{-3}$
$D_{JK} = -T_{220}$	$-1.53611(37) \times 10^{-3}$	$-1.0037(20) \times 10^{-3}$
$D_K = -T_{040}$	$1.85278(97) \times 10^{-3}$	$1.5879(13) \times 10^{-3}$
$d_1 = T_{202}$	$-24.374(94) \times 10^{-6}$	$-25.01(13) \times 10^{-6}$
$d_2 = T_{004}$	$13.3326(53) \times 10^{-5}$	$26.779(22) \times 10^{-5}$
$R_5 = \frac{1}{2}T_{022}$	0 (fixed)	0

In the aim of comparing the parameters obtained with the two models with the correspondence formula (17),(18), we decide to do in the both case a fit till order 2 only. So these fits are not the best ones but they are just performed to verify our relations of correspondence. In Tables 3 and 4, we give fitted values up to the quartic parameters in both models and according to relations (18), we recalculate the Watson's parameters. The values are in reasonably good agreement. We must keep in mind that our relations (18) are only approximate.

5. Conclusion

We have first presented the two theoretical models which have enabled us to analyze the ground state of the SO_2F_2 quasi-spherical top. Then, we give the two corresponding sets of parameters and relations between them. They clearly show an approximate numerical link between the two formalisms. We can conclude at this stage of comparison that both models give similar results in the analysis independently from the J values. A complete table of measured and assigned transitions in both models is available on the journal's home page. Our analysis has been performed thanks to the C_{2v} TDS software, which can be freely downloaded at the URL: `http://www.u-bourgogne.fr/LPUB/c2vTDS.html`.

Our next challenge is to apply the tensorial model to the $\nu_9(b_2)/\nu_7(b_1)/\nu_3(a_1)$ triad and particularly to the $\nu_4(a_1)/\nu_5(a_2)$ dyad where problems concerning the choice of axes are encountered with Watson's formalism.

Acknowledgments

The authors wish to thank Dr. Jean-Marie Flaud (LPPM, 91405 Orsay Cedex, France) for helpful discussions in Prague in September 2002. Support from the Région Bourgogne for the computer equipment of the Laboratoire de Physique de l'Université de Bourgogne is gratefully acknowledged. The work in Köln has been supported in part by the Deutsche Forschungsgemeinschaft (DFG) via grant SFB 494 and by special funding from the Land Nordrhein-Westfalen. L.M. acknowledges the Alexander von Humboldt-Stiftung for his stipend.

References

[1] K. Sarka, J. Demaison, L. Margulès, I. Merke, N. Heineking, H. Bürger, H. Ruland, J. Mol. Spectrosc. 200 (2000) 55–64.
[2] H. Bürger, H. Ruland, I. Merke, K. Sarka, L. Margulès, J. Demaison, J. Mol. Spectrosc. 203 (2000) 268–272.
[3] H. Bürger, J. Demaison, F. Hegelund, L. Margulès, I. Merke, J. Mol. Struct. 612 (2002) 133–141.
[4] J.K.G. Watson, in: J.R. Durig (Ed.), Vibrational Spectra and Structure, vol. 6, Elsevier, Amsterdam, 1977, pp. 1–89.
[5] A. Mekhtiev, J.T. Hougen, J. Mol. Spectrosc. 199 (2000) 284–301.
[6] M. Rotger, V. Boudon, M. Loëte, J. Mol. Spectrosc. 216 (2002) 297–307.
[7] J.-P. Champion, M. Loëte, G. Pierre, in: K.N. Rao, A. Weber (Eds.), Spectroscopy of the Earth's Atmosphere and Interstellar Medium, Academic Press Inc., San Diego, 1992, pp. 339–422.
[8] M. Krüger, H. Harder, C. Gerke, H. Dreizler, Z. Naturforsch. A 48 (1993) 737–738.
[9] C. Gerke, unpublished results (Kiel).
[10] G. Winnewisser, A.F. Krupnov, M. Yu Tretyakov, M. Liedtke, F. Lewen, A.A. Saleck, R. Schieder, A.P. Shkaev, S.V. Volokhov, J. Mol. Spectrosc. 165 (1994) 294–300.
[11] D. Boucher, R. Bocquet, J. Burie, W.D. Chen, J. Phys. III (France) 4 (1994) 1467–1480.
[12] D. Papoušek, M.R. Aliev, Molecular Vibrational–Rotational Spectra, Elsevier, Amsterdam/New York, 1982.
[13] N. Cheblal, M. Loëte, V. Boudon, J. Mol. Spectrosc. 197 (1999) 222–231.
[14] Ch. Wenger, V. Boudon, J.-P. Champion, G. Pierre, J. Quant. Spectrosc. Radiat. Transfer 66 (2000) 1–16.
[15] Ch. Wenger, J.-P. Champion, J. Quant. Spectrosc. Radiat. Transfer 59 (1998) 471–480.
[16] J. Moret-Bailly, Cah. Phys. 15 (1961) 237–316.
[17] J. Moret-Bailly, J. Mol. Spectrosc. 15 (1965) 344–354.
[18] B.I. Zhilinskiĭ, Opt. Spectrosc. (USSR) 51 (1981) 262–263.
[19] J.-P. Champion, G. Pierre, F. Michelot, J. Moret-Bailly, Can. J. Phys. 55 (1977) 512–520.
[20] M. Rey, V. Boudon, Ch. Wenger, G. Pierre, B. Sartakov, J. Mol. Spectrosc. 219 (2003) 313–325.
[21] M. Rotger, A. Decrette, V. Boudon, M. Loëte, S. Sander, H. Willner, J. Mol. Spectrosc. 208 (2001) 169–179.

Troisième partie

Chapitre

5

Banques de Données Spectroscopiques

Publications P16, P27, P33, P34
Article de revue B2

5.1 Introduction

Une préoccupation majeure liée aux travaux d'analyse spectroscopiques réalisés au LPUB concerne la diffusion de ces résultats et à leur mise à disposition de la communauté scientifique [P33]. Depuis de nombreuses années a été mise au point au LPUB la base de données STDS (*Spherical Top Data System*) qui permet aux utilisateurs de recalculer les spectres (absorption infrarouge et diffusion Raman) de diverses molécules tétraédriques sous différentes conditions de température et de pression. J'ai pu contribuer à l'amélioration de STDS, d'une part par l'inclusion de mes résultats d'ajustements récents (voir Chapitres III.2 et III.3), et d'autre part à l'aide d'un certain nombre d'améliorations techniques. Enfin, j'ai développé sur le même principe une base de données consacrée aux molécules octaédriques (HTDS, *Highly-spherical Top Data System*) et participé au développement d'autres bases similaires consacrées à des molécules de symétrie plus basse (C_{2v}, C_{4v}, ...).

5.2 Améliorations apportées à STDS

Les programmes inclus dans STDS sont basés sur l'implémentation du formalisme tensoriel. Une caractéristique essentielle est l'utilisation d'opérateurs tensoriels irréductibles et de bases orientés dans la chaîne de groupes $O(3) \supset T_d$. L'orientation se fait par l'intermédiaire d'une matrice notée G,

$$|j,nC\sigma\rangle = \sum_m {}^{(j)}G^m_{nC\sigma}\,|j,m\rangle\,. \tag{III.5.1}$$

Dans la référence [P34] qui est une partie du travail de thèse de Michaël Rey, nous avons exposé une méthode générale de calcul des éléments matriciels ${}^{(j)}G^m_{nC\sigma}$ pour j entier et demi-entier (nous reparlerons du cas demi-entier dans la Partie IV). Ceci nous a permis de repousser la limite initiale en J (nombre quantique rotationnel) de STDS de 96 à 199. Ceci est très important pour le calcul de spectres de molécules lourdes qui font intervenir des excitations rotationnelles élevées.

D'autre part, et d'un point de vue plus technique, les premières versions de STDS étaient basées sur le schéma des polyades vibrationnelles du méthane (la polyade P_n étant définie par les niveaux vibrationnels tels que $n = 2(v_1+v_3)+v_2+v_4$). Ceci n'est toutefois pas adapté à toutes les molécules. J'ai donc introduit une généralisation dans les programmes permettant de spécifier le schéma de polyade adapté à la molécule étudiée directement dans les paramètres d'entrée. Cette technique est décrite dans le référence [P16] reproduite ci-après.

5.3 Nouvelles bases de données

Plusieurs bases de données sont désormais en téléchargement libre sur le site Web du LPUB (ou le seront très prochainement),

`http://www.u-bourgogne.fr/LPUB/shTDS.html`

STDS (Spherical Top Data System) est consacrée aux molécules tétraédriques du type XY_4. STDS a servi de point de départ au développement des autres bases décrites ci-dessous [P33].

HTDS (Highly-spherical Top Data System) est consacrée aux molécules octaétriques de type XY_6 [P16,P33].

***C*$_{2v}$TDS** (C_{2v}-Top Data System) est consacrée aux molécules de type XY_2Z_2 de symétrie C_{2v} (voir Chapitre III.4).

***C*$_{4v}$TDS** (C_{4v}-Top Data System) est consacrée aux molécules de type XY_5Z de symétrie C_{4v} (voir Chapitre III.4) [P27].

***D*$_{2h}$TDS** (D_{2h}-Top Data System) est consacrée aux molécules de type X_2Y_4 de symétrie D_{2h} (voir Chapitre III.4).

GROUP permet de lister les coefficients ${}^{(j)}G^m_{nC\sigma}$ ainsi que divers autres coefficents de couplage et de recouplage pour les chaînes de groupes $O(3) \supset T_d$ et $O(3) \supset O_h$ [1] [P34].

L'ensemble des "packages" xTDS consiste d'une par en un jeu de programmes de simulation de spectres et d'ajustement de données spectroscopiques (fréquences et intensités) en FORTRAN 77 et, d'autre, part, en une base de données des fichiers de paramètres résultant des analyses de spectres effectuées au LPUB. Tous ces programmes sont conçus pour fonctionner sous UNIX (y compris Linux et Mac OS X). Un version Microsoft Windows de STDS est également disponible.

5.4 Article-clé

Est reproduit ici un article illustrant les principes utilisés pour l'ensemble des bases de données du type xTDS.

– [**P16 :** *J. Quant. Chem. Radiat. Transfer*, **66**, 1–16 (2000)] présente la base de données et le jeu de programmes HTDS, dédié aux molécules octaédriques de type XY_6. Notons que depuis la publication de cet article, les paramètres résultant des différentes analyses récentes de bandes de SF_6 (voir Chapitre III.1) ont été ajoutées à HTDS. De plus, conformément aux méthodes développées dans la Référence [P34], les programmes ont été modifiés afin de permettre la prise en compte de nombres quantiques rotationnels élevés (jusqu'à $J = 199$, actuellement).

1. GROUP permet également de lister ces mêmes coefficients pour des valeurs demi-enitères de j, ce dont nous reparlerons dans la Partie IV.

PERGAMON

Journal of Quantitative Spectroscopy & Radiative Transfer 66 (2000) 1–16

Journal of Quantitative Spectroscopy & Radiative Transfer

www.elsevier.com/locate/jqsrt

Highly-spherical Top Data System (HTDS) software for spectrum simulation of octahedral XY_6 molecules

Ch. Wenger, V. Boudon*, J-P. Champion, G. Pierre

Laboratoire de Physique de l'Université de Bourgogne-CNRS, B.P. 400, F-21011 Dijon, France

Abstract

The Spherical Top Data System (STDS) program suite developed in Dijon has been extended into two directions. First, the vibrational extrapolation is now possible for any kind of polyad scheme, this one being fully specified in the input parameters of the programs for hamiltonian and transition moment model calculations. This was not the case of the preceding version which was based on the polyad scheme of methane. Secondly, it is now possible to study any band and polyad of XY_6 molecule for which a complete treatment in the O_h group is made. Up to now, only some vibrational levels of these molecules (F_{1u} levels in particular) could be studied using equivalences with the T_d group. Some examples mainly concerning the SF_6 molecule are presented. As before, this suite is composed of a series of FORTRAN programs called by a UNIX script. The whole package is freely accessible through ftp (user anonymous) at jupiter.u-bourgogne.fr.

Keywords: Octahedral molecules; Tensorial formalism; Vibrational extrapolation

1. Introduction

In a previous paper [1], we have described STDS (Spherical Top Data System) for the simulation of spherical-top spectra. This package, however, is restricted to the study of XY_4 tetrahedral molecules (point group T_d). Moreover, STDS is based on the polyad definition scheme of methane.

In this article, we present an extension of STDS, named HTDS (Highly-spherical Top Data System) dedicated to the study of XY_6 octahedral molecules (point group O_h). This extension was first motivated by the possibility of studying vibrational bands of SF_6 other than simple ν_3 or

* Corresponding author. Tel.: -33-3-80-39-59-17; fax: -33-3-80-39-59-71.
E-mail address: boudon@jupiter.u-bourgogne.fr (V. Boudon)

0022-4073/00/$ - see front matter
PII: S0022-4073(99)00161-2

v_4F_{1u} fundamentals (these could be considered in STDS using some symmetry equivalences). In a forthcoming paper [2], we will describe our analysis of the $v_2 + v_6$ combination band of $^{32}SF_6$ using the HTDS programs. This case will therefore be largely used in the examples given in the present paper. The principal characteristics of HTDS are:

- A full treatment in the O_h group is made and parity is taken into account.
- The polyad scheme of the molecule under consideration is fully specified by the user in the form of command-line arguments.
- The package includes programs necessary to fit experimental data with Hamiltonian parameters.

HTDS thus constitutes a good complement to STDS for people who want to study XY_6 molecule spectra.

The HTDS package presented here is intended to provide direct access to the theoretical results achieved in high resolution research on XY_6 molecules as well as the tools for studying new spectra. It is freely accessible by anonymous ftp at the Internet address jupiter.u-bourgogne.fr. HTDS is designed for UNIX workstations or for PC computers running under LINUX. It consists of a complete set of FORTRAN routines managed by UNIX scripts. The aim of this paper is to provide the user, nonexpert in the theory of spherical tops, all information needed to exploit efficiently the software package.

2. General comments about octahedral molecules and their spectra

2.1. Remarkable spectroscopic features

XY_6 molecules possess six normal modes of vibration: three X–Y stretching modes named $v_1(A_{1g})$, $v_2(E_g)$ and $v_3(F_{1u})$, and three Y–X–Y bending modes that are $v_4(F_{1u})$, $v_5(F_{2g})$ and $v_6(F_{2u})$. We consider here only XY_6 molecules with an A_{1g} (totally symmetric) electronic ground state. Molecules like ReF_6, IrF_6, NpF_6,... (with a degenerate electronic ground state) would involve much more complex phenomena (rovibronic couplings) and are thus not studied here. In the present case, only the F_{1u} fundamentals are allowed in absorption spectra. A_{1g}, E_g and F_{2g} fundamentals are allowed in Raman scattering spectra. Thus, XY_6 molecules show a characteristic vibrational spectrum with two very strong infrared fundamentals (v_3 and v_4) and three intense Raman fundamentals (v_1,v_2 and v_5). The v_6 mode is inactive. The overtone and combination bands give much less intense and more complicated features [3,4]. Some vibrational levels may form polyads (groups of levels that are accidentally close to each other). But the polyad scheme is completely different from one molecule to the other, and no general rule can be derived.

Another important characteristic of these molecules is their relatively high molecular weight generally leading to highly congested spectra due to:

- Low B_0 rotational constant values (0.091 cm^{-1} for SF_6 [5], 0.057 cm^{-1} for PuF_6 [6], even lower for hexachlorides).
- Low energy bending fundamentals (especially v_6 that may be below 200 cm^{-1} for transition-metal hexahalides) leading to numerous hot bands.

This generally implies the use of high-resolution spectroscopic techniques [7–10] and of supersonic expansion jets [2,11–14] to resolve XY_6 spectra.

2.2. Theory

The theoretical model used in HTDS is based on the tensorial formalism and vibrational extrapolation methods developed in Dijon [15]. Let us consider an XY_6 molecule with vibrational levels grouped in a series of polyads designed by P_k ($k = 0, \ldots, n, \ldots$), P_0 being the ground state (GS). The Hamiltonian can be developed as a sum of operators specific to each polyad as

$$\mathscr{H} = \mathscr{H}_{\{P_0 \equiv \mathrm{GS}\}} + \mathscr{H}_{\{P_1\}} + \cdots + \mathscr{H}_{\{P_k\}} + \cdots + \mathscr{H}_{\{P_{n-1}\}} + \mathscr{H}_{\{P_n\}} + \cdots \tag{1}$$

The effective Hamiltonian for polyad P_n is obtained by projection in the corresponding subspace,

$$\begin{aligned} H^{\langle P_n\rangle} &= P^{\langle P_n\rangle}\mathscr{H}P^{\langle P_n\rangle} \\ &= H^{\langle P_n\rangle}_{\{\mathrm{GS}\}} + H^{\langle P_n\rangle}_{\{P_1\}} + \cdots + H^{\langle P_n\rangle}_{\{P_k\}} + \cdots + H^{\langle P_n\rangle}_{\{P_{n-1}\}} + H^{\langle P_n\rangle}_{\{P_n\}}. \end{aligned} \tag{2}$$

The different terms are written as

$$\mathscr{H}_{\{P_k\}} = \sum_{\text{all indexes}} t^{\Omega(K,n\Gamma)\Gamma_v\Gamma'_v}_{\{s\}\{s'\}} \left[{}^{\varepsilon}V^{\Omega_v(\Gamma_v\Gamma'_v)\Gamma}_{\{s\}\{s'\}} \otimes R^{\Omega(K,n\Gamma)}\right]^{(A_{1g})}. \tag{3}$$

The $t^{\Omega(K,n\Gamma)\Gamma_v\Gamma'_v}_{\{s\}\{s'\}}$ are the model parameters, ${}^{\varepsilon}V^{\Omega_v(\Gamma_v\Gamma'_v)\Gamma}_{\{s\}\{s'\}}$ and $R^{\Omega(K,n\Gamma)}$ are vibrational and rotational operators. Their construction is described in Ref. [15]. All parity indexes being g in this case, they are omitted in the following equations. Ω and Ω_v are the rotational and vibrational degree, respectively. The order of development is given by $\Omega + \Omega_v - 2$. Here are some examples of effective Hamiltonian matrices:

The ground state: $H^{\langle \mathrm{GS}\rangle} = H^{\langle \mathrm{GS}\rangle}_{\{\mathrm{GS}\}}$.

The ν_3 stretching band: $H^{\langle \nu_3\rangle} = H^{\langle \nu_3\rangle}_{\{\mathrm{GS}\}} + H^{\langle \nu_3\rangle}_{\{\nu_3\}}$.

The $\nu_2 + \nu_6$ combination band: $H^{\langle \nu_2+\nu_6\rangle} = H^{\langle \nu_2+\nu_6\rangle}_{\{\mathrm{GS}\}} + H^{\langle \nu_2+\nu_6\rangle}_{\{\nu_6\}} + H^{\langle \nu_2+\nu_6\rangle}_{\{\nu_2\}} + H^{\langle \nu_2+\nu_6\rangle}_{\{\nu_2+\nu_6\}}$.

The matrix elements are calculated in the coupled basis

$$\left|\left[{}^{v}\Psi^{(C_v)} \otimes {}^{r}\Psi^{(J,nC)}\right]^{(\Gamma)}_{\sigma}\right\rangle, \tag{4}$$

where ${}^{r}\Psi^{(J,nC)}_{\sigma_r}$ is a rotational wavefunction and ${}^{v}\Psi^{C_v}_{\sigma_v}$ a coupled vibrational wavefunction with

$$\begin{aligned} \left|{}^{v}\Psi^{(C)}_{\sigma_v}\right\rangle = \Big|\Big[\Big[\Big[\Big[{}^{\Psi}{}^{(A_{1g})}_{v_1} \otimes \Psi^{(l_2,n_2C_2)}_{v_2} \otimes \Psi^{(l_3,n_3C_3)}_{v_3}\Big]^{(C_{23})} \otimes \Psi^{(l_4,n_4C_4)}_{v_4}\Big]^{(C_{234})} \\ \otimes \Psi^{(l_5,n_5C_5)}_{v_5}\Big]^{(C_{2345})} \otimes \Psi^{(l_6,n_6C_6)}_{v_6}\Big]^{(C_v)}_{\sigma_v}\Big\rangle, \end{aligned} \tag{5}$$

the $\Psi^{(l_i,n_iC_i)}_{v_i}$ being symmetrized harmonic oscillator wave functions for the six normal vibrational modes of the XY_6 molecule that is considered.

The diagonalization of the effective Hamiltonian leads to eigenvalues (energies) and eigenstates that are simply denoted by

$$\left|\Psi^{(J,n,C)}_{\sigma}\right\rangle, \tag{6}$$

where n is an index to number the states ordered by increasing energy within a (J, C) block.

In order to perform intensity calculations, the dipole moment (for absorption spectra) and polarizability (for Raman spectra) operators are expanded in a similar way. This will be described in detail in a forthcoming paper [16] and is thus not explained here.

3. Description of the HTDS package

Once properly installed, the HTDS package has the directory structure described in Fig. 1 (assuming that the installation directory is named HTDS). The subdirectories contain the following files:

- bin: Executable files created by the compile script,
- ctrp: Examples of files containing constrains for parameter fits,
- exp: Some experimental files (line frequencies and assignments),
- gtd: Symmetrization coefficients ${}^{(J)}G^{m}_{nC\sigma}$ (see Ref. [15]),
- jobs: Examples of jobs for spectrum calculations and experimental data fits,
- para: Parameter files for all the molecules and band systems presently included in the package,
- prog: Scripts for compilation, program sources and some other files used by the scripts.

The calculation jobs (in jobs) are arranged by molecule. Their names are in the form

job_cal_NameOfTheBandSystem.

For example,.../jobs/32SF6/job_cal_nu2+nu6 calculates the $\nu_2 + \nu_6$ band of $^{32}SF_6$.

4. Calculating spectra with HTDS

The general structure of a job for spectrum calculation is given in Fig. 2. A commented example (for the $\nu_2 + \nu_6$ combination band of $^{32}SF_6$) is given in Table 1. First of all, the eigenvalues (energies) and eigenstates of the effective Hamiltonian are calculated for the upper and lower polyad (here a polyad can be a single vibrational state as well as a complex vibrational system). Then the transition moments for the transitions between these two polyads are evaluated and finally, the spectrum (line frequencies and intensities) is calculated for specific conditions (frequency range, temperature, ...). Let us first describe the Hamiltonian energy calculation.

The first program used is hmodel which determines the operators to be used in the Hamiltonian development for the vibrational levels and polyad scheme considered and up to the development order specified. The general command-line syntax for hmodel can be summarized as follows:

hmodel Pn N1 Dk_0 0 0 0 0 0 0 \
Nm_1 Dk_1 $v_{1_1}^1$ ... $v_{6_1}^1$ ... $v_{1_1}^{m_1}$ ... $v_{6_1}^{m_1}$ \
... ... \
Nm_i Dk_i $v_{1_i}^1$ ... $v_{6_i}^1$ ... $v_{1_i}^{m_i}$ ... $v_{6_i}^{m_i}$ \
... ... \
Nm_n Dk_n $v_{1_n}^1$ ... $v_{6_n}^1$ ... $v_{1_n}^{m_n}$ ... $v_{6_n}^{m_n}$

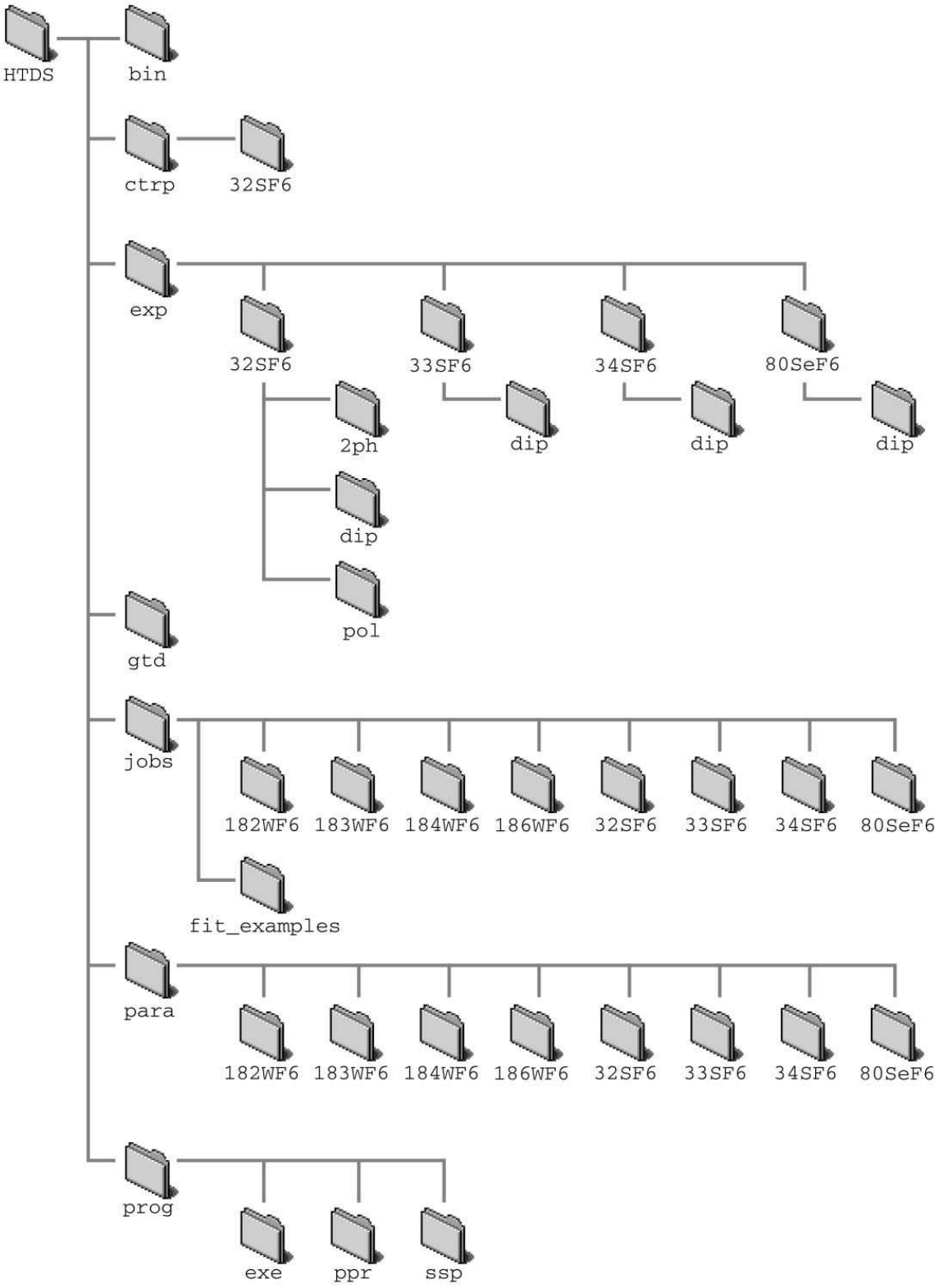

Fig. 1. The directory structure of HTDS.

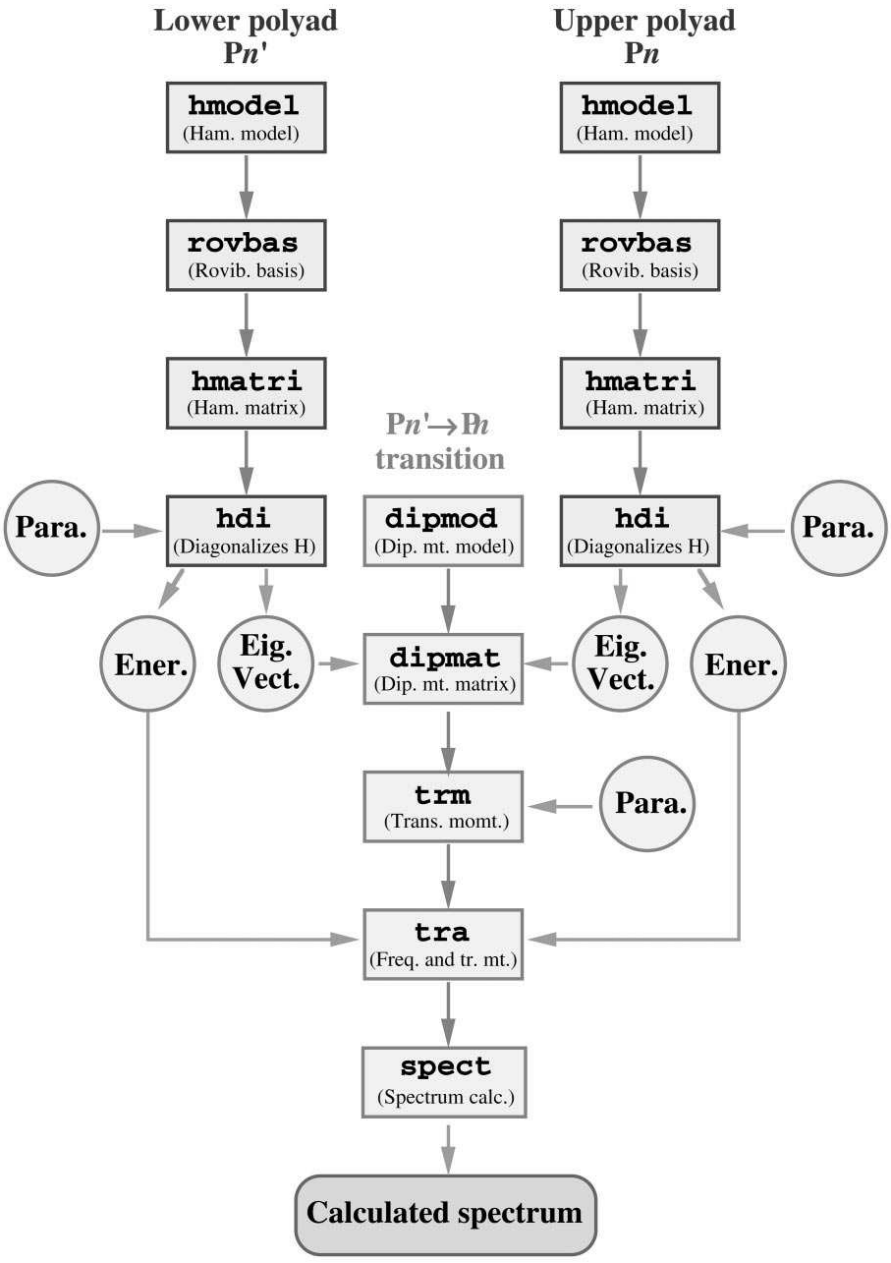

Fig. 2. Schematic description of the spectrum calculation. For Raman spectra, dipmod and dipmat are replaced by polmod and polmat, respectively.

The first argument must be the letter P immediately followed by an integer number n. This one indicates the running number of the polyad to consider. This argument is followed by $n + 1$ lines describing polyads $P_0, \ldots, P_i, \ldots, P_n$. Each line consists of:

- the number m_i of vibrational states for polyad P_i (following letter N),

Table 1
Example of a job for spectrum calculation: the $\nu_2 + \nu_6$ combination band of $^{32}SF_6$

```
# ! /bin/sh
  set -v
## Calculation of the absorption spectrum
## of nu2+nu6 of SF6.
##
BASD = .../.../HTDS                                   ⇒ HTDS installation directory.
#
  JOBD = $BASD/prog/exe
  PARD = $BASD/para
##
## Jmax values.
##
  JPinf_p = 36                                        ⇒ Maximum J value for lower level.
  JPsup_p = 35                                        ⇒ Maximum J value for upper level.
  JPsupminf_p = 35                                    ⇒ Maximum J value for the calculated spectrum
##
## Parameter file.
##                                                    ⇒ Parameters for H and μ (or α).
  PARA = $PARD/32SF6/Pa_010001m000000
##
##
####################################
##########
##
## Hamiltonien matrix elements.
##
## Lower Polyad.
##
  $JOBD/passx hmodel P0 N1 D2    0 0 0 0 0 0
##                                                    ⇒ Hamiltonian model for lower polyad.
  $JOBD/passx rovbas P0 N1 D2 $JPinf_p
##                                                    ⇒ Rovibrational basis for lower polyad.
  $JOBD/passx hmatri P0 N1 D2 $JPinf_p
##                                                    ⇒ H matrix elements for lower polyad.
  $JOBD/passx hdi      P0 N1 D2 $JPinf_p $PARA
##                                                    ⇒ Diagonalization of H for lower polyad.
## Upper Polyad.
##
  $JOBD/passx hmodel P3 N1 D2    0 0 0 0 0 0  \
                        N1 D2    0 0 0 0 0 1  \       ⇒ Hamiltonian model for upper polyad.
                        N1 D2    0 1 0 0 0 0  \
                        N1 D4    0 1 0 0 0 1
##
  $JOBD/passx rovbas P3 N1 D2224 $JPsup_p
##                                                    ⇒ Rovibrational basis for upper polyad.
  $JOBD/passx hmatri P3 N1 D2224 $JPsup_p
##                                                    ⇒ H matrix elements for upper polyad.
  $JOBD/passx hdi P3 N1 D2224 $JPsup_p $PARA          ⇒ Diagonalization of H for upper polyad.
##
## Dipole moment matrix elements.
##
## Upper – lower level transition.
```

Table 1. (*Continued*)

```
##
  $JOBD/passx dipmod P3 N1  0 0 0 0 0 0  \
                       N1  0 0 0 0 0 1  \          ⇒ Dipole moment model.
                       N1  0 1 0 0 0 0  \
                       N1  0 1 0 0 0 1  \
                    P0 N1  0 0 0 0 0 0  \
                    D1
##
  $JOBD/passx dipmat P3 N1 P0 N1 D1   \
                     $JPsupminf_p                 ⇒ Dipole moment matrix elements.
##
## Transition moment.
##
  $JOBD/passx trm   P3 N1 P0 N1 D1   \
                    $JPsupminf_p $PARA dip
##                                                ⇒ Transition moments.
  $JOBD/passx tra   P3   P0   D1   \
                    $JPsupminf_p
##                                                ⇒ Frequencies and transition moments.
## Spectrum calculation.
##
  $JOBD/passx spect 986.0 996.0 30.0 30.0 10.0
                                                   ⇒ Spectrum calculation.
```

Note: Some comments are given on the right.

- the order of development (following letter D) of $\mathscr{H}_{\{P_i\}}$,
- m_i sets of six vibrational quantum numbers $(v_1, v_2, v_3, v_4, v_5, v_6)$ defining the m_i vibrational states of polyad P_i.

The rovibrational basis (Eq. (4)) is then calculated by `rovbas` for $J = 0, \ldots, J_{\max}$. The matrix elements of the hamiltonian operators constructed by `hmodel` are calculated by `hmatri` in this basis. Finally, `hdi` uses the Hamiltonian parameter values to construct the hamiltonian matrix and then diagonalizes it.

The model and matrix elements of the dipole moment (resp. the polarizability) are calculated in a similar way by `dipmod` (resp. `polmod`) and `dipmat` (resp. `polmat`) for absorption (resp. Raman) spectra. The syntax for `dipmod` /`polmod` follows the same principles as for `hmodel`. This time, both the lower and upper polyads must be fully specified on the command-line (see example in Table 1). Programs `trm` and `tra` calculate the transition moments.

The final step is made by `spect` that calculates the line frequencies and intensities in the frequency range $[f_{\min}, f_{\max}]$ and for rotational and vibrational temperatures T_{rot} and T_{vib}, respectively. The command-line syntax for `spect` is

$$\texttt{spect}\ f_{\min} f_{\max} T_{\text{rot}} T_{\text{vib}} I_{\min}$$

$I_{\min}$ is the intensity threshold (all lines with intensity lower than $I_{\min}$ are not written in the output file). The main output file is `spectr.t`. An example is given in Table 2. The beginning of this file recalls the parameter values, the vibrational states involved and the calculation conditions. Then,

Table 2
Example of the spectr.t output file

```
Hamiltonian Parameters in Octahedral Formalism
518 Data ; Jmax 27 ; St Dev previous 3.592 , predicted 3.592
2. 10. 8. 6. 6.          0.5      Spin Statistics , Spin Y
nu1      nu2      nu3      nu4      nu5      nu6      (J = 0)      B0                  D0
773.5   641.7   939.0     614.0     525.0   347.0          0.090971          0.6058000D − 8
24      1.d − 21   8       Para Number   ;   Model Accuracy Parameters
SF6   000000 et 010001   Order 6
Sat May 23 15:24:02 WEIDST 1998            Hmn Frdm        Value/cm − 1        St.Dev./cm − 1
  1   2(0,0A1g) 000000A1g 000000A1g A1g 02      0   0.91078389192E − 01 0.0000000E+00
  2   4(0,0A1g) 000000A1g 000000A1g A1g 04   237  − 0.26999749845E − 06 0.2313801E − 07
… … … … … … … … … … … … … … … … … … … … … … … … … … … … … … … … … … … … … …
  23   2(2,0 Eg) 010001F2u 010001F2u   Eg 42   161  − 0.10457505336E − 03 0.1850921E − 04
  24   2(2,0F2g) 010001F2u 010001F2u F2g 42   218   0.34048941616E − 04 0.1557648E − 04
Transition Moment Parameters in Octahedral Formalism
*
*
*
  1 Arbitrary Units
  1 1.d-1
*
*
  1 0(0,0A1g) 000000A1g 010001F1u F1u 20        0    0.10000000000E+01     0.0000000E+00
  2 Upper Vibrational States
#          v1          v2          v3          v4          v5          v6       Cv
1 | [[[[ 0(0,0A1g)* 1(1,0 Eg)* 0(0,0A1g)]Eg* 0(0,0A1g)]Eg* 0(0,0A1g)]Eg* 1(1,0F2u)]F1u >
2 | [[[[ 0(0,0A1g)* 1(1,0 Eg)* 0(0,0A1g)]Eg* 0(0,0A1g)]Eg* 0(0,0A1g)]Eg* 1(1,0F2u)]F2u >
  1 Lower Vibrational States
#          v1          v2          v3          v4          v5          v6       Cv
1 | [[[[ 0(0,0A1g)* 0(0,0A1g)* 0(0,0A1g)]A1g* 0(0,0A1g)]A1g* 0(0,0A1g)]A1g* 0(0,0A1g)]A1g >
Spectroscopic Data Calculated through J = 35
Imposed Frequency Range:              986.000000 -              996.000000
Vibrational Temperature: 300.00 Kelvin
Rotational Temperature:   300.00 Kelvin
Intensity Lower Limit     0.10E+00     Arbitrary Units

  Calculated Transitions
   Frequency Intensity J C n #vib J C n #vib Lower Energy
990.478131      1.01E-01     P   6   A2   1    1    100%  5   A2  3   1    97%   3.824832
991.285997      1.16E-01     Q   6   A2   1    1    100%  6   A2  2   1    98%   3.824832
… … … … … … … … … … … … … … … … … … … … … … … … … … … … … … … … … … … … … …
987.415295      1.80E-01     P   36  F2   8    1    100%  35  F2  52  1    81%   120.861640
987.431784      1.86E-01     P   36  F2   9    1    100%  35  F2  53  1    82%   120.873879
Number of Calculated Transitions                    1248
First Transition →  987.226466 1.67E-01 P 36 F1
Strongest Transition →  991.383702 3.78E-01 Q 34 A2
Last Transition →  995.998186 2.12E-01 R 27   A2
Effective Jo range      →     6 – 36
Strongest Tr at Jmax    →      991.296938 3.02E-01 Q 35 A2
Intensity summations:
  0.20E+03   Arbitrary Units            with      threshold =      0.10E+00
  0.30E+03   Arbitrary Units             without   threshold
```

Note: See text for comments.

the list of calculated transitions is given. Each line is identified by the lower (J'', n'', C'') and upper (J, n, C) quantum numbers (same labels as in Eq. (6)). In each case, the (J, n, C) sets are followed by a vibrational identification consisting in the number of the vibrational state and in a percentage representing the projection of the "true" vibrational wave function on the specified normal mode basis.

5. Fitting parameters with HTDS

The HTDS package also provides the possibility to fit hamiltonian parameters using experimental data. The general procedure is described in Fig. 3. This necessitates an assignment file containing lines of the following form (the format must be respected):

```
19  995.718784+  0.008700    0.001620    26 E    2  27 E    16 SF010001mP0
20  995.707187+  0.013000    0.001490    25 A2   2  26 A2   8  SF010001mP0
20  995.707187+  0.013000    0.001490    19 F1   5  20 F1   22 SF010001mP0
```

Each line has the following structure:

Columns 1–6: running index on experimental lines.
Columns 9–18: experimental line wavenumber.
Column 20: the plus sign indicates that the line has been assigned and fitted. If any other character is placed here, this indicates that the line has been assigned but will not be fitted and will thus not be taken into account by the programs.
Columns 24–31: experimental line intensity.
Columns 36–43: experimental precision on line position.
Columns 53–70: assignment in the form $J''C''n''$ (lower level) $J'C'n'$ (upper level). Each experimental line can be assigned to several theoretical transitions if necessary.
Columns 72–83: character chain used to extract desired assignment lines.

Practically, two jobs must be used. A first job is used to calculate the Hamiltonian operators matrix elements (up to the desired order). This is done using `hmodel`, `rovbas` and `hmatri` for both lower and upper polyad, just as explained in the preceding section. In `jobs/fit_examples`, some examples of such jobs are given. Their names are in the form:

`job_hme_NameOfTheMolecule_NameOfTheBandSystem.`

In the same directory, one can find examples of the second type of job required, named in the form:

`job_fit_NameOfTheMolecule_NameOfTheBandSystem.`

This second job performs an iteration to determine a new parameter set. It is organized as follows. The first program used is `hdiag`. It diagonalizes the Hamiltonian matrix for the lower and upper polyad using the Hamiltonian initial parameter file. The difference between `hdi` (see preceding section) and `hdiag` is that the later also calculates energy derivatives with respect to the parameters.

The job `exasg` is used to extract the desired lines in the assignment file (see above) using a specified character chain. Then, `eq_tds` calculates the normal equations and `paradj` determines

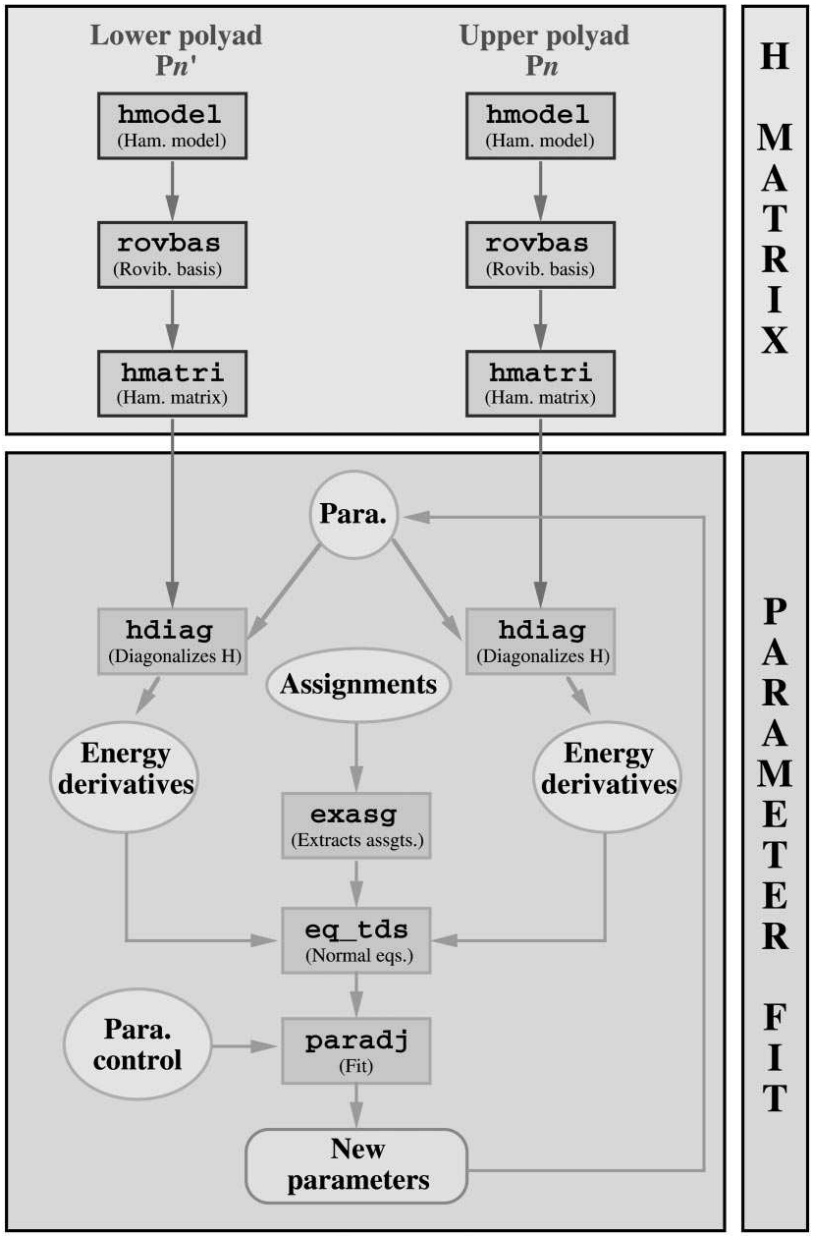

Fig. 3. Schematic description of the parameter fit.

the new parameter set. Further iterations can be done simply by renaming the output parameter file (its name is indicated at the end of the job) with a command line like

```
mv OutputParameterFile InputParameterFile
```

and by running the job again.

A commented example of a fit job is given in Table 3.

Table 3
Example of a job for parameter fit: the $\nu_2 + \nu_6$ combination band of $^{32}SF_6$.

```
#! /bin/sh
  set -v
## Example of parameter fitting :
## nu2+nu6 of 32SF6.
##
   BASD = /home/nep2/wenger/HTDS                    ⇒  HTDS installation directory.
#
   JOBD = $BASD/prog/exe
  PARD = $BASD/para
  EXPD = $BASD/exp
  CTRD = $BASD/ctrp
##
## Jmax values.
##
  JPlow = 28                                       ⇒  Maximum J value for lower level.
  JPupp = 27                                       ⇒  Maximum J value for upper level.
   JPupp_low = 27                                  ⇒  Maximum J value for the
##                                                     calculated spectrum.
## Parameter file.
##
  PARA = $PARD/32SF6/Pa_010001
##                                                 ⇒  Parameters for H.
## Assignment files.
##
   ASG = $EXPD/32SF6/dip/Herman.exp                ⇒  File containing experimental assigned lines.
##
## Parameter constrain file.
##
CLF = $CTRD/32SF6/010001
##                                                 ⇒  File defining the constrains on parameters.
##############################

##
## Hamiltonian diagonalization.
##
## 000000 level.
##
  $JOBD/passx hdiag P0 N1 D2 $JPlow $PARA          ⇒  Diagonalization of H for lower polyad.
##
## 010001 level.
##
  $JOBD/passx hdiag P3 N1 D2224 $JPupp $PARA
##
## nu2+nu6 fit.                                    ⇒  Diagonalization of H for upper polyad.
##
  $JOBD/exasg SF 010001mP0 $ASG
  mv ASG_EXP ASG_010001mP0
  cp ASG_010001mP0 assignments.t                   ⇒  Extraction of assigned lines.
##
  $JOBD/passx eq_tds P3 P0 p p ir $JPupp_low
  mv normal_eq.t        NQ_H_010001_010001mP0-mv   ⇒  Calculation of normal equations.
                        prediction_mix.t Pred_010001mP0
```

Table 3. (*Continued*)

```
##
## New hamiltonian parameter estimates.
##
  cp $CLF CL_H_010001
  $JOBD/passx paradj H CL_H_010001
          NQ_H_010001_010001mP0
##
###
### The new parameter file is:                    ⇒  New estimate of parameters.
###
###             NQ_H_010001_010001mP0_adj
###
```

Note: Some comments are given on the right.

6. Hardware and software requirements

The HTDS package includes source codes of all the executables. A FORTRAN compiler is necessary to generate these executable files using the installation script.

In principle, since almost only standard statements and UNIX commands are used, HTDS should be suitable for most UNIX workstations. It has been carefully tested on the following platforms: HP 9000/7xx operating under HP-UX 9.05 and 10.20, IBM RS/6000 operating under AIX 2.4 and SUN UltraSPARC operating under SUN-OS 5.5.1. A PC LINUX version of the package is also available. The user should refer to the `htds_README` file for more detailed instructions. DEC Alpha and SGI workstations can also run the HTDS package with a few modification. The authors can be contacted for such technical questions.

The minimum configuration for HTDS is 32 Mbytes RAM and 175 Mbytes of free disk space for the creation of temporary files of the most complex calculations.

7. Present status

Presently available molecules and band systems are given in Table 4. The calculation parameters, disk space and CPU time given in this table are only indicative. J_{max} corresponds to the maximum J value of spectral lines that could be assigned up to now in the spectra whose analysis lead to the parameter files included in the present package. $[f_{min}, f_{max}]$ is a rough wave number interval (in cm^{-1}) suitable for the band systems under consideration. The rotational and vibrational temperatures T_{rot} and T_{vib} correspond to the experimental conditions of the spectra used for the analyses. The CPU time was determined on a HP 9000/712-80 workstation.

Of course, the user can change the values of J_{max}, f_{min}, f_{max}, T_{rot} and T_{vib} in the jobs (see the jobs and command-line descriptions in the preceding sections). The only limitations are the disk space available to the user, and also that the programs cannot handle J values higher than 96. Extrapolation to higher J, T_{rot} or T_{vib} values than those indicated are possible, also the results should be considered very carefully.

Table 4
Molecules and band systems presently available from HTDS. See text for comments

Molecule/job_name	J_{max}	F_{min} (cm^{-1})	F_{max} (cm^{-1})	T_{vib} (K)	T_{rot} (K)	S_{min} (AU)[a]	DS[b] (Mo)	CPU time (hh:mm:ss)
$^{32}SF_6$/job_cal_nu2	90	620	665	293	293	0.2	51.6	00:46:28
$^{32}SF_6$/job_cal_nu3	95	900	996	300	300	0.004	134.7	02:29:24
$^{32}SF_6$/job_cal_2nu3 − nu3	60	900	996	300	300	0.00008	173.6	00:57:41
$^{32}SF_6$/job_cal_3nu3	32	2700	3000	300	300	0.01	59.2	00:05:21
$^{32}SF_6$/job_cal_nu2+nu6	35	986	996	30	30	1	10.4	00:01:38
$^{33}SF_6$/job_cal_nu3	35	935	941	30	30	0.01	4.8	00:01:22
$^{34}SF_6$/job_cal_nu3	35	928	933	30	30	0.01	4.8	00:01:21
$^{80}SeF_6$/job_cal_nu3	95	750	800	300	300	0.001	80.6	00:58:41
$^{182}WF_6$/job_cal_nu3	46	680	740	50	50	0.2	8.5	00:02:43
$^{183}WF_6$/job_cal_nu3	47	680	740	50	50	0.2	9.0	00:03:02
$^{184}WF_6$/job_cal_nu3	48	680	740	50	50	0.2	9.6	00:03:10
$^{186}WF_6$/job_cal_nu3	43	680	740	50	50	0.2	7.1	00:02:09

[a]AU = Arbitrary unit.
[b]DS = Disk space.

8. Getting, installing and running HTDS

The HTDS computer package can be accessed directly either by anonymous ftp at the Internet address

jupiter.u − bourgogne.fr

in the directory /dist/HTDS_UNIX or through the World Wide Web at the URL

http://www.u − bourgogne.fr/LPUB/shTDS.html.

As mentioned above, two versions are available: a general UNIX and a specific PC LINUX version. Both versions consist in a single compressed file in the standard tar format. Their size is 2.4 Mbytes for both of them. Instructions to get and install HTDS are given in Table 5.

Table 5
Instructions to get and install HTDS

1	Create a local directory to be used as the HTDS installation directory
2	Login by ftp, user anonymous, on jupiter.u-bourgogne.fr
3	Get (binary mode) the remote file dist/HTDS_UNIX/htds_96.tar.Z into the local directory
4	Quit ftp and start installation using uncompress < htds_96.tar.Z | tar xvf −
5	Continue installation following instructions in file "htds_README"

Note: To get the PC LINUX version, follow the same procedure using the file dist/HTDS_UNIX/htds_96_PC.tar.Z instead of dist/HTDS_UNIX/htds_96.tar.Z.

The execution of the instructions given in Table 5 creates automatically the appropriate directories and files according to the structure given in Fig. 1 and explained in Section 3. The final step of the installation is achieved using the included compiling script (refer to file `htds_README`).

During the execution of the jobs (spectrum calculation or parameter fit), the various steps are displayed on the session window. The sequences of routines previously described exchange data through temporary files created in the working directory. Since these files are automatically deleted after use, it is highly recommended to work in a dedicated directory (distinct from the HTDS installation directory), in order to avoid undesired removal of permanent files.

Although the use of HTDS does not require any particular knowledge in theory nor in programming, users are freely allowed to modify any of the files (source codes, parameter files or executable scripts). Of course, this is not recommended to users non-expert in the theory of spherical tops or in computer programming. The authors may be contacted for further information and developments on the present package.

9. Conclusion and perspectives

Compared to STDS [1], HTDS is certainly a little more difficult to use, because it is not launched by a single job using a simple command line. Here, the user who wants to use other conditions or molecules than those included in the examples provided has to modify the jobs. But on the other hand, this offers a greatest flexibility and an enormous amount of possibilities. The polyad scheme being entirely specified by the user, it is not linked to any particular molecule. Apart from this, the advantages of HTDS compared to other databases containing essentially experimental or precalculated data (fixed number of transitions) are the same as for STDS. Extrapolations to high J values, although they have obviously a limited reliability, are possible and can be very helpful at least for qualitative predictions. HTDS can also be used for theoretical studies of vibration-rotation features in XY_6 molecules simply by using appropriate parameter files to represent specific molecular quantum systems. STDS and HTDS constitute together a reference tool for the simulation of complex band systems of highly symmetrical molecules. Moreover, HTDS includes programs for Hamiltonian parameter fitting. This allows the use of HTDS with the user's own data.

The use of the command-line description of the polyad scheme will be soon adapted to STDS. The study of other vibrational bands of XY_6 molecules are planned and thus HTDS should be updated consequently in the future. The use of HTDS for the study of other octahedral molecules is also possible under some conditions. For example, we have used this package to study the ν_6 band of molybdenum hexacarbonyl, $Mo(CO)_6$ [17].

Acknowledgements

Support from the Région Bourgogne for the computer equipment of the Laboratoire de Physique de l'Université de Bourgogne and from the European Community (contract XCT94-0603) are gratefully acknowledged. HTDS benefited from many contributors (experimentalists and theoreticians) who are also thanked a lot.

References

[1] Wenger CH, Champion J-P. JQSRT 1998;59(3–5):471–80.
[2] Boudon V, Hepp M, Herman M, Pak I, Pierre G. J Mol Spectrosc 1998;192:359–67.
[3] McDowell RS, Krohn BJ, Flicker H, Vasquez MC. Spectrochim Acta 1986;42A(2/3):351–69.
[4] McDowell RS, Krohn BJ. Spectrochim Acta 1986;42A(2/3):371–85.
[5] Kim KC, Person WB, Seitz D, Krohn BJ. J Mol Spectrosc 1979;76:322–40.
[6] Kim KC, Krohn BJ, Briesmeister RA, David SJ. J Mol Spectrosc 1988;132:207–15.
[7] McDowell RS, Patterson CW, Harter WG, Los Alamos Science — Los Alamos National Laboratory. 1982, p. 38–65.
[8] Reiser C, Steinfeld JI, Galbraith HW. J Chem Phys 1981;74(4):2189–94.
[9] Dubs M, Harradine D, Schweitzer E, Steinfeld JI. J Chem Phys 1982;77(5):3824–39.
[10] Khelkhal M, Rusinek E, Legrand J, Herelemont F. J Chem Phys 1997;107(15):5694–701.
[11] Takami M. J Chem Phys 1986;84(1):73–7.
[12] Matsumoto Y, Takami M. J Chem Phys 1986;85(7):3785–90.
[13] Takami M, Matsumoto Y. Mol Phys 1988;64(4):645–58.
[14] Aldridge J-P, Brock EG, Filip H, Flicker H, Fox K, Galbraith HW, Holland RF, Kim KC, Krohn BJ, Magnuson DW, Maier II WB, Owell RS, Patterson CW, Person WB, Smith DF, Werner GK. J Chem Phys 1985;83(1):34–48.
[15] Champion J-P, Loëte M, Pierre G. Spherical top spectra. In: Narahari Rao K, Weber A. editors. Spectroscopy of the earth's atmosphere and interstellar medium. San Diego: Academic Press, 1992, p. 339–422.
[16] Cheblal N, Boudon V, Loëte M. J Mol Spectrosc 1999;197:222–31.
[17] Asselin P, Soulard P, Manceron L, Boudon V, Pierre G. J Mol Struct, 1999, in Press.

Quatrième partie

Spectroscopie Moléculaire dans un Etat Electronique dégénéré

QUATRIÈME PARTIE

Chapitre

1

Développement d'un Formalisme Rovibronique

Publications P1, P2, P3, P4, P6, P7, P11, P19, P23, P24, P29, P34, P35
Proceeding A2

1.1 Introduction

Les études décrites tout au long de la Partie III de ce rapport concernent exclusivement des problèmes de spectroscopie rovibrationnelle dans un état électronique non-dégénéré (singulet) isolé. Ces travaux se situent dans le cadre strict de l'approximation de Born-Oppenheimer et, par conséquent, les mouvements électroniques sont ignorés (on construit un hamiltonien effectif pour un état électronique singulet donné, l'effet des autres états électroniques étant inclus de manière perturbative).

Lorsque l'on considère des transitions vers des états électroniques excités, qui sont souvent dégénérés, l'approximation de Born-Oppenheimer n'est en général plus valable. Le problème devient alors très complexe, mais aussi très intéressant du point de vue théorique. Il est alors nécessaire de traiter ensemble les mouvements rotationnels, vibrationnels et électroniques. On parle alors de spectroscopie *rovibronique*.

Cependant, la communauté de spectroscopie rovibrationnelle (infrarouge et Raman) et celle de spectroscopie électronique (visible, ultraviolet) sont souvent disjointes et ont peu d'interactions entre elles. Il n'y a pourtant pas de raison pour que les méthodes et modèles qui ont fait le succès de la spectroscopie rovibrationnelle à haute résolution ne puissent pas s'adapter également à l'analyse de spectres rovibroniques. Un moyen de faire le pont entre ces deux domaines (et aussi de simplifier quelque peu le problème) est de considérer des transitions rovibroniques à l'intérieur d'un état électronique de base non-trivial. Les espèces possédant un état électronique fondamental dégénéré sont en fait très nombreuses, puisque ceci regroupe tous les radicaux et ions moléculaires (qui ont de nombreuses applications en chimie atmosphérique, en astrophysique, dans les combustions, les réactions chimiques, ...), mais aussi, comme nous allons le voir, des molécules stables (bien que très réactives) à sous-couche incomplète.

1.2 Présentation du problème

Une classe intéressante de molécules à sous-couche incomplète est celle des hexafluorures de métaux de transition (dits aussi hexafluorures colorés). Des espèces comme ReF_6 [P11,P29] ou IrF_6 [P3,P4,P6] possèdent ainsi un état électronique de base quatre fois dégénéré ; les deux états électroniques les plus bas de OsF_6 sont très proches l'un de l'autre, menant ainsi à un état de base quasi cinq fois dégénéré [P7]. Il intervient dans ce cas des phénomènes de couplages vibroniques (effet Jahn-Teller, ...) complexes. Ce type de molécule a été étudié dès les années 1950, mais l'élucidation de la structure rovibronique de ces molécules n'a pas été réalisée jusqu'à une période récente.

La spectroscopie des hexafluorures colorés a constitué mon sujet de thèse. Par la suite, le projet que j'ai présenté lors de ma candidature au CNRS était basé sur le même sujet. Une partie importante de mes recherches actuelles concernent la spectroscopie rovibronique.

L'étude de ce type de molécule présente principalement deux types de difficultés :

- Les couplages vibroniques du type Jahn-Teller sont de nature non-pertrubative et mènent, dans leur formulation usuelle, à des matrices infinies. Une nouvelle formulation doit être trouvée pour contourner cette difficulté.
- Le fait que certaines espèces comme ReF_6 possédent un nombre impair d'électrons implique dans ce cas l'existence de moments angulaires demi-entiers. Se pose alors le problème de la symétrisation des fonctions de moment angulaire demi-entier dans le groupe ponctuel de la molécule.

Les conséquences liées à ces deux points ainsi que des exemples sont détaillés dans la Référence [A2] reproduite ci-après.

1.3 Principes du formalisme

Au cours de ma thèse, j'ai tout d'abord appliqué au groupe O_h la méthode des représentations spinorielles [P1] qui permet la symétrisation des fonctions de moment angulaire demi-entier [1]. J'ai également, dans le même cadre, reformulé le modèle de couplage Jahn-Teller en termes d'opérateurs tensoriels irréductibles [P2,P3]. Cette nouvelle écriture ne permettait toutefois pas de s'affranchir du problème des matrices infinies. Celles-ci doivent par conséquent être tronquées à des valeurs relativement élevées des nombres quantiques vibrationnels. L'inclusion de la rotation moléculaire mène alors à des problèmes de taille irréaliste, même pour de puissants ordinateurs (typiquement, la diagonalisation de matrices 45000×45000, voire plus encore). Une nouvelle approche s'imposait donc.

En collaboration avec Maud Rotger, nous avons pu enregistrer à Dijon quelques spectres d'absorption à basse résolution de plusieurs hexafluorures colorés, dans les domaines proche infrarouge, visible et ultraviolet [2]. Ces spectres sont très complexes et seuls certains ont pu recevoir un début d'interprétation de leur structure rovibronique à l'aide du modèle vibronique tensoriel simplifié développé lors de ma thèse [P3,P6,P7,P11]. La Figure 1.1 montre l'exemple de transitions vibroniques de PtF_6.

Lors du stage de DEA et de la thèse de Michaël Rey, un nouveau formalisme a donc été élaboré [P19,P24,P34,A2], permettant la construction d'hamiltoniens rovibroniques effectifs pour des états électroniques deux, trois ou quatre fois dégénérés sous la forme générale

$$\mathcal{H} = \sum_i t_i \left(R_i \otimes V_i \otimes E_i\right)^{(A_{1g})}, \tag{IV.1.1}$$

où les t_i sont les paramètres du modèle et les R_i, V_i et E_i sont des opérateurs rotationnels, vibrationnels et électroniques, respectivement. Une méthode de construction des opérateurs électroniques E_i à partir des opérateurs du moment angulaire électronique a été développée [P19,P24]. Les moments de transition (moment dipolaire et polarisabilité) servant au calcul des intensités des transitions sont développés de manière similaire. Cette approche évite le problème des matrices infinies. Par contre, le problème du lien entre les paramètres obtenus par ce type de méthode avec les paramètres (ro)vibroniques "classiques" reste entier, la transformation permettant le passage entre les deux modèles étant de nature non perturbative. Cependant, ainsi que nous le verrons dans les chapitres suivants, notre modèle a pu d'ores et déjà être appliqué avec succès au cas des molécules $V(CO)_6$ [P23] et ReF_6 [P19,A2].

Dans la référence [P34] déjà mentionnée au Chapitre III.5, nous avons exposé de manière détaillée la méthode de calcul des coefficients de symétrisation des fonctions de moment angulaire demi-entier dans les groupes de l'octaèdre et du tétraèdre. Le programme GROUP décrit dans ce même Chapitre permet de lister les coefficients ${}^{(j)}G^m_{nC\sigma}$ ainsi que différents coefficients de couplage et de recouplage pour j demi-entier compris entre 1/2 et 399/2.

1. Cette méthode est une alternative élégante au concept de groupe double et permet d'éviter certains choix arbitraires inhérants à celui-ci.

2. Echantillons fournis par le Pr. Daniel Avignant de l'Université de Clermont-Ferrand et le Pr. Henry Selig de l'Université de Jérusalem, Israël.

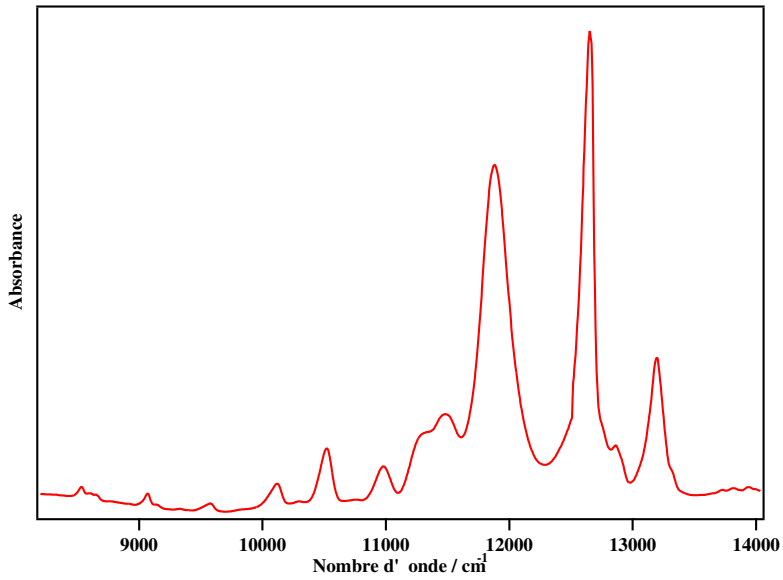

FIG. 1.1 – *Spectre d'absorption des transitions électroniques* $d \longleftarrow X$ *et* $e \longleftarrow X$ *de* PtF_6*. Un structure vibronique complexe est visible.*

Récemment, une approche algébrique utilisant le formalisme de $SU(4)$ pour les états électroniques quatre fois dégénérés a également été mise au point par Françoise Michelot [P35].

1.4 Articles-clés

Sont reproduits ici un acte de colloque et deux articles détaillant le formalisme tensoriel rovibronique développé dans le cadre de la thèse de Michaël Rey.

- [**A2 :** *Proceedings of SPIE*, **5311**, 1–13 (2003)] est extrait des actes du colloque "*XIVth Symposium on High Resolution Molecular Spectroscopy, HighRus 2003*" (06-11/07 2003, Krasnoïarsk – Yenisseisk – Kransoïarsk, Russie) pour lequel j'étais conférencier invité. Cet article est une introduction générale à la thématique des états électroniques dégénérés et au formalisme rovibronique que nous avons développé.
- [**P19 :** *J. Mol. Spectrosc.*, **204**, 106–119 (2000)] présente une première version du formalisme rovibronique, restreinte aux modes de vibration trois fois dégénérés et utilisant un schéma de couplage des opérateurs et des vecteurs de base dans $SU(2) \otimes C_I$.
- [**P24 :** *J. Mol. Struct.*, **599**, 125–137 (2001)] présente la version généralisée du formalisme rovibronique, utilisant un schéma de couplage des opérateurs et des vecteurs de base dans O_h^S.

Open-Shell Octahedral Molecules: A First Insight into the Full Rovibronic Problem

V. Boudon[a], M. Rey[a,b], M. Rotger[a] and M. Loëte[b]

[a] Laboratoire de Physique de l'Université de Bourgogne, CNRS UMR 5027, 9 Av. A. Savary, BP 47870, F-21078 Dijon Cedex, France

[b] Present address: Laboratorium für Physikalische Chemie, ETH-Hönggerberg, HCI, CH-8093, Zürich, Switzerland

ABSTRACT

Despite its great successes for the standard rovibrational problem, there is still a large domain in which high-resolution molecular spectroscopy lacks both extensive experimental data and a complete and convincing theory: the full rovibronic problem. This is the case of a molecule in a degenerate electronic state, *i.e.* when the Born-Oppenheimer approximation breaks down. It means that the electronic, vibrational and rotational degrees of freedom must be treated simultaneously. Complex (ro)vibronic couplings (Jahn-Teller "effect", *etc*) are then involved. Some octahedral transition metal hexafluorides and hexacarbonyls are known since many years to be stable open-shell systems with degenerate electronic ground states leading to very unusual absorption spectra. However, the extreme complexity of this kind of problem (from both experimental and theoretical sides) prevented to go any further in this direction until very recently. In this paper, we will give an overview of the tensorial rovibronic model that we have developed in the Dijon group for such systems. This model enables the systematic development of the rovibronic Hamiltonian and transition moments (dipole moment and polarizability) in a given degenerate electronic state. We will then review the current status of rovibronic spectroscopy of octahedral molecules. This includes the recent data obtained using supersonic expansion jet infrared spectroscopy of $V(CO)_6$ and ReF_6, for which we will present detailed analyses.

Keywords: Open-shell molecules, Jahn-Teller effect, degenerate electronic states, rovibronic couplings, hexafluorides, hexacarbonyls, ions, radicals, group theory, tensorial formalism, effective Hamiltonians and transition moments.

1. INTRODUCTION

During the last four decades, high-resolution rovibrational spectroscopic studies of small semi-rigid polyatomic molecules have reached a high degree of sophistication, from both experimental and theoretical (effective and *ab initio* models) point of views. Rovibrational fine structures can now be reproduced with a very high accuracy, even for complicated and excited vibrational groups of levels (or "polyads"). In our group, we have developed powerful tools and techniques (group theoretical methods, tensorial formalism, effective Hamiltonians and transitions moments) for the study of highly-symmetrical molecules, the so-called "spherical-tops".[1,2] Such tools have also been extended to lower symmetry species.[3–6]

However, until very recently all this well-established machinery still failed to allow the study of a large and extremely interesting class of molecules: open-shell systems like molecular ions and free radicals. These appear in many chemical processes like combustions and in chemically active media like planetary atmospheres, interstellar medium, *etc*. This failure of standard models is due to the fact that such species exhibit degenerate or quasi-degenerate electronic states for which the usual Born-Oppenheimer approximation fails. This implies to consider the electronic, vibrational and rotational degrees of freedom as a whole, that is the rovibronic problem. While the purely vibronic problem, and especially the Jahn-Teller effect, has been discussed in numerous papers (see

Further author information: Send correspondence to V. Boudon,
E-mail: Vincent.Boudon@u-bourgogne.fr, Telephone: +33 3 80 39 59 17, Fax: +33 3 80 39 59 71, Address: Laboratoire de Physique de l'Université de Bourgogne, CNRS UMR 5027, 9 Av. A. Savary, BP 47870, F-21078 Dijon Cedex, France

Refs.[7,8] for good reviews), accurate models for high-resolution (rovibronically resolved) spectra of molecules in a degenerate electronic states still represent an important challenge.

In this paper, we will review the most recent results obtained in our group concerning the rovibronic spectroscopy of hexafluorides and hexacarbonyls in a non-singlet electronic ground state. After reviewing the major differences observed in the spectra of such molecules, compared to usual closed-shell systems, we will present the effective rovibronic model that we have developed and its first applications to $V(CO)_6$ and ReF_6.

2. RECALLS ABOUT CLOSED-SHELL MOLECULES

Let us first review the very basic characteristics about the spectroscopy of closed-shell molecules, in the aim of stressing the differences that will appear when dealing with open-shell systems. Throughout this paper, we will only consider XY_n ($n = 4$ or 6) molecules, although many considerations can be extended to other species.

Closed-shell species always have a non-degenerate electronic ground state. The consequence is, as shown on the left part of Figure 1, that the structure of their vibronic levels is quite simple. Schematically, such molecules (like CH_4, SF_6, ...) are essentially transparent though the near infrared and visible regions. They absorb infrared light due to the vibrational levels of their singlet electronic ground state, and electronic transitions usually occur far in the UV region, due to charge transfers between the central atom and the ligands.[9]

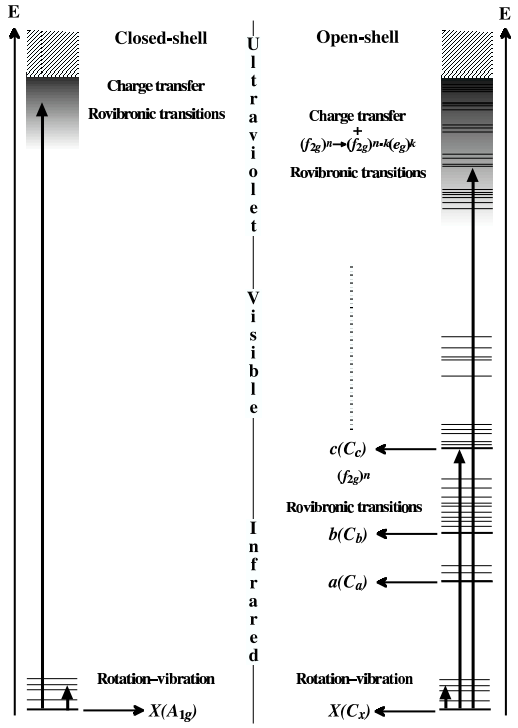

Figure 1. Schematic comparison of the electronic structures for closed- and open-shell XY_6 molecules.

2.1. The Born-Oppenheimer Approximation

Isolated singlet electronic states, like the ground states of closed-shell systems, are usually treated within the frame of the so-called Born-Oppenheimer approximation (BOA). This has been discussed in numerous papers (see for instance Ref.[8] and references therein). Let us just recall very briefly the general principle of this

approximation, since we will consider a modified version of the BOA when dealing with degenerate electronic states. Generally speaking, a full (non-relativistic) molecular Hamiltonian can be put in the form

$$H(r,Q) = \underbrace{T(Q)}_{\text{Nuclear kinetic energy}} + \underbrace{H_e(r)}_{\text{Electrons}} + \underbrace{V(r,Q)}_{\text{Electrons–nuclei and nuclei–nuclei}}, \tag{1}$$

where r and Q are the electronic and nuclear coordinates, respectively. $H_e(r)$ contains the electronic kinetic energy and the Coulomb electron-electron interactions. $V(r,Q)$ contains all other potential (Coulombic) terms. The Born-Oppenheimer (or "crude" Born-Oppenheimer) approximation is a variant of the adiabatic approximation,[8] for which we consider only small nuclear displacements in the vicinity of the reference configuration Q_0 (usually a stable minimum of the potential energy). Thus, if we consider the eigenfunctions $\psi_n(r)$ of the electronic Hamiltonian $H_e(r)+V(r,Q_0)$, then the total wavefunction of the molecule can be taken has

$$\psi(r,Q) = \sum_n \chi_n(Q)\psi_n(r). \tag{2}$$

By considering the matrix elements of the Hamiltonian (1) in the electronic basis $\psi_n(r)$, we can deduce that the nuclear wavefunctions $\chi_n(Q)$ are thus solutions of a system of coupled equations with the general form

$$\sum_m \left(\delta_{m,n}T(Q)+U_{nm}(Q)\right)\chi_m(Q) = E\chi_n(Q). \tag{3}$$

For an isolated electronic state $n=n_0$, we neglect all interaction terms with $m\neq n_0$ and we have thus simply

$$H_{n_0}(Q) = T(Q)+U_{n_0n_0}(Q) \quad \text{and} \quad \psi(r,Q) = \chi_{n_0}(Q)\psi_{n_0}(r). \tag{4}$$

2.2. Rovibrational Spectroscopy

In such an isolated electronic singlet state, the neat consequence of the BOA is that the electronic motion can be separated from the nuclear motion. The energy levels of molecule can thus be described by a rotation-vibration Hamiltonian. For a given polyad P_k, an effective tensorial Hamiltonian can be written as[1]

$$\mathcal{H}_{\{P_k\}} = \sum_i t_i \left(R_i^{(\Gamma)} \otimes V_i^{(\Gamma)}\right)^{(A_{1g})}, \tag{5}$$

where the t_i are parameters to determine thanks to experimental data. $R_i^{(\Gamma)}$ and $V_i^{(\Gamma)}$ are rotational and vibrational operators with symmetry Γ, respectively. Their construction through recursive couplings of elementary operators J_x, J_y, J_z on one hand and a_i^+ and a_i creation and annihilation operators on the other hand has been detailed elsewhere.[1] For tetrahedral and octahedral molecules, we symmetrize all the operators and wavefunctions in the $O(3)\supset T_d$ or O_h group chain thanks to a G orientation matrix whose determination has been detailed in References.[10,11] For instance, we orient $T_m^{(j)}$ tensors of $O(3)$ into T_d or O_h symmetrized tensors using:

$$T_\sigma^{(j,nC)} = \sum_m {}^{(j)}G_{nC\sigma}^m T_m^{(j)}. \tag{6}$$

In order to calculate intensities, transition moment operators (dipole moment and polarizability) can be expanded in the same way. The non-zero conditions on their matrix elements lead to the selection rules. For the absorption spectrum of an isolated fundamental band, the most basic selection rule concerns, of course, the rotational quantum number J:

$$\Delta J = -1,\ 0 \text{ or } 1, \tag{7}$$

leading to a characteristic band profile with three branches P, Q and R. Each J is further split by symmetry effects (the so-called fine and superfine structures). All this may seem obvious, but we will see now that the open-shell case generates much more complicated structures.

3. OPEN-SHELL MOLECULES

The existence of an incomplete electronic subshell leads to extremely rich and also much more complex spectroscopic features (see right part of Figure 1), since in this case it becomes impossible to separate the electronic and nuclear motions. Let us first review the molecular species of interest in this respect. While most open-shell systems are unstable short-life radicals or ions, there exist a few stable open-shell systems. Among diatomics, NO is a well-known example of a molecule with an odd number of electrons, for instance. But there exist also open-shell spherical-top molecules, as we will see in the next paragraphs.

3.1. Colored hexafluorides

A very interesting and quite large molecular family is that of hexafluorides (see Reference[12] and Table 1). Since the 1950's, various authors have noticed that several transition-metal hexafluorides are stable open-shell systems.[12–17] Although extremely reactive (especially with water)[18–20] they can be synthesized and kept forever in a dry environment (a sealed quartz cell or a passivated metallic bottle, for instance).[21]

Table 1. The hexafluoride molecules. The first column indicates the electronic structure of the central ion (for a ionic model), n being the number of non-bonding electrons. Quotation marks indicate more or less hypothetical molecules that have been mentioned by some authors but whose existence has never been clearly established. Boldface characters indicate open-shell systems (the so-called "colored hexafluorides").

n	0	1	2	3	4	5
$(2p)^n$						PF_6 ?
$(3s)^n$	SF_6					
$(3d)^n$	CrF_6 ?					
$(4s)^n$	SeF_6					
$(4d)^n$	MoF_6	**TcF_6**	**RuF_6**	**RhF_6**	**PdF_6 ?**	
$(5s)^n$	TeF_6	IF_6 ?	XeF_6			
$(5d)^n$	WF_6	**ReF_6**	**OsF_6**	**IrF_6**	**PtF_6**	**AuF_6 ?**
$(6s)^n$	PoF_6	AtF_6 ?	RnF_6 ?			
$(5f)^n$	UF_6	**NpF_6**	**PuF_6**	**AmF_6**	**CmF_6 ?**	

In a simple ionic picture,[9] second- and third-row transition-metal hexafluorides can be viewed as a central M^{6+} metallic ion (with a $(d)^n$ external subshell) surrounded by a regular octahedron formed by six F^- ions and having thus a $(f_{2g})^n$ electronic structure with n non-bonding electrons. Depending on n, this f_{2g} subshell leads to various electronic states in the visible or even near-infrared regions (see Figures 1 and 2). Moreover, spin-orbit coupling in this case is huge and causes further splitting of spin multiplets by several hundreds or thousands of cm^{-1}.[12,15] Molecules with $n > 0$ are thus usually heavily colored (IrF_6 is bright yellow and PtF_6 is deep red) and are therefore often called "colored hexafluorides". Most of these low-lying electronic states are degenerate, including the ground state in many cases. For example, and as we will discuss it in detail in Section 6.2, the ground-state of ReF_6 is a quadruplet with G'_g symmetry.[22]

In such degenerate electronic states, authors have noticed that even at low-resolution the spectra can be heavily perturbed, implying huge effects of electron-vibration (vibronic) couplings.[12,22,23] For example, the comparison between the Raman spectra of WF_6 and ReF_6 shown on figure 3 is particularly striking for the ν_2 fundamental: while WF_6 shows the usual $OP - Q - RS$ branch structure, ReF_6 exhibits a wide structureless band profile.

3.2. Other spherical open-shell systems

There are a few other similar interesting systems that we can consider. Among these, we can especially mention transition-metal hexacarbonyl molecules. While $Cr(CO)_6$, $Mo(CO)_6$ and $W(CO)_6$ are usual closed shell-systems,[24–26] $V(CO)_6$ is an open-shell molecule with a $^2F_{2g}$ electronic ground term[27,28] that we will consider in detail in the following. Finally, we can also mention VCl_4 which is one of the very few open-shell tetrahedral systems.[29,30]

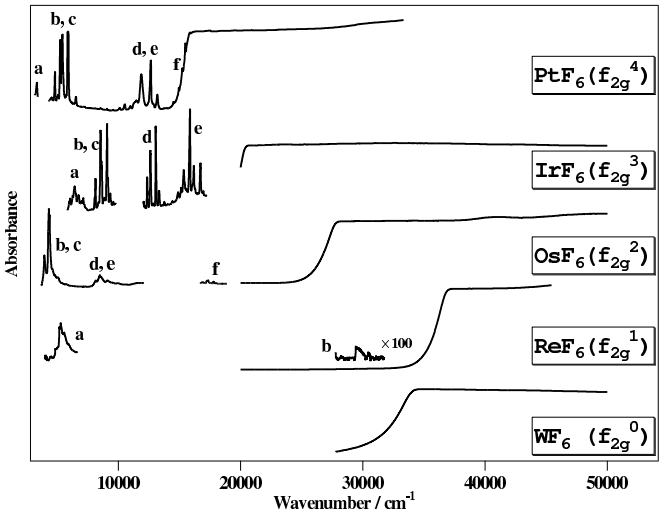

Figure 2. Overview of the electronic absorption spectra of the third row transition-metal hexafluorides. The resolution is about 2 cm^{-1}. Huge absorption features in the UV correspond to charge transfers between the central atom and the ligands (see also right part of Figure 1).

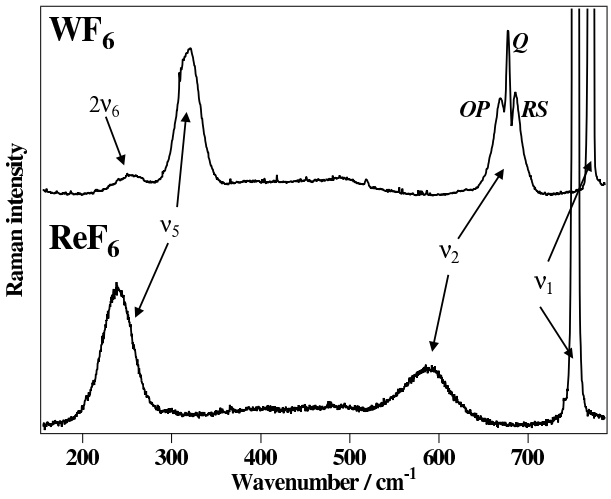

Figure 3. Spontaneous Raman spectra of WF_6 (B. Roussel, DILOR Company, Lille, France) and ReF_6 (A. Lorriaux, LASIR, Université de Lille I, France). The resolution is about 2 cm^{-1}.

4. VIBRONIC COUPLINGS

Before coming to our new model for rovibronic interactions, we will review here the problems associated to vibronic couplings in degenerate electronic states.

4.1. The Born-Oppenheimer approximation for degenerate electronic states

The first question we have to consider here is: what about the Born-Oppenheimer approximation in the case of an electronic degeneracy ? As we only consider here isolated electronic states with a "true" degeneracy (*i.e.*

strictly due to symmetry reasons), the answer is that we can use a modified version of the BOA. In an electronic state with symmetry Γ, we can thus re-write Eq. (3) as[8]

$$\sum_{m=1}^{[\Gamma]} \left(\delta_{m,n} T(Q) + U_{nm}(Q)\right) \chi_m(Q) = E\chi_n(Q), \quad (n = 1, \ \ldots \ [\Gamma]), \tag{8}$$

where the sum has been restricted to the $[\Gamma]$ degenerate states ($[\Gamma]$ being the dimension of the irreducible representation Γ), that is to treat the $[\Gamma]$ electronic surfaces as a whole. In other words, in this new approximation, all the non-adiabatic interactions with other distinct electronic states are neglected, but all such interactions between the set of $[\Gamma]$ degenerate electronic states are taken into account.

4.2. Half-integer angular momenta

Another important problem is that some open-shell systems possess an odd number of electrons. Due to the electronic spin, this leads to the existence of half-integer angular momenta. The question that thus arise is: how to symmetrize half-integer momentum wavefunctions into the symmetry point group of the molecule ? This can be done thanks to two methods. The first one uses the *double group* concept originally introduced by Bethe.[31] However, as pointed out in References,[32–34] this technique leads to some difficulties (quite large groups with doubled number of elements) and ambiguous definitions (the quite non-physical "2π-rotation" R and the non-unique multiplication rules). This is why we prefer a second method based on the more mathematically strict concept of *spinorial representations* (SR) developed in a series of papers by Altmann and coworkers.[32,35,36] In Reference,[34] we have applied this method to the case of the O_h group. In short, it is possible to define a special kind of irreducible representations that can be used to reduce half-integer angular momentum states. As shown in Table 2, the O and T_d groups have three such SR, namely E_1', E_2' and G' of respective dimension 2, 2 and 4. We add the S superscript to the group names (like T_d^S or O_h^S) to indicate that we consider the group with its SR.

Table 2. Character table for the O^S and T_d^S groups. E_1', E_2' and G' are spinorial representations.

T_d^S	E	$8C_3$	$3S_4^2$	$6S_4$	$6\sigma_d$
O^S	E	$8C_3$	$3C_4^2$	$6C_4$	$6C_2$
A_1	1	1	1	1	1
A_2	1	1	1	−1	−1
E	2	−1	2	0	0
F_1	3	0	−1	1	−1
F_2	3	0	−1	−1	1
E_1'	2	1	0	$\sqrt{2}$	0
E_2'	2	1	0	$-\sqrt{2}$	0
G'	4	−1	0	0	0

For example, we have the reduction rules:

$$\mathcal{D}^{(1/2)} \downarrow O = E_1', \quad \mathcal{D}^{(3/2)} \downarrow O = G', \quad \mathcal{D}^{(5/2)} \downarrow O = E_2' \oplus G', \quad \ldots \tag{9}$$

The G orientation matrix of Equation (6) can be extended to half-integer j values (C being a SR in this case) in order to symmetrize spin states, for instance.[11,34]

4.3. The Jahn-Teller effect

The most famous vibronic interaction to occur in a degenerate electronic state is known as the so-called Jahn-Teller effect (JTE). This "effect" (or, more strictly speaking, this coupling) was first demonstrated in 1937 by H. A. Jahn and E. Teller[37] and extended in 1938 by H. A. Jahn[38] to systems with an odd number of electrons. The Jahn-Teller theorem states that a non-linear molecule in a degenerate electronic state (excluding Kramers' spin doublets) is always unstable with respect to at least one vibrational mode. This instability can either

result in a static distortion (which removes the degeneracy), or in a dynamic coupling between electronic and vibrational motions. In this case, which is the most common for gas-phase molecules, the molecule experiences an instantaneous distortion, but its mean configuration is the most symmetrical one (although it never stays in this configuration).

Let us reformulate the Jahn-Teller coupling in a "modern" way.[8,39] First, we consider a set of symmetrized coordinates $\left\{Q_{\sigma_i}^{(C_i)}\right\}$ in which we expand the potential part of the Hamiltonian:

$$H(r,Q) = H_e(r,Q_0) + T(Q) + \sum_{C,\sigma}\left(\frac{\partial V(r,Q)}{\partial Q_\sigma^{(C)}}\right)_{Q_0} Q_\sigma^{(C)} + \frac{1}{2}\sum_{C_1,\sigma_1}\sum_{C_2,\sigma_2}\left(\frac{\partial^2 V(r,Q)}{\partial Q_{\sigma_1}^{(C_1)}\partial Q_{\sigma_2}^{(C_2)}}\right)_{Q_0} Q_{\sigma_1}^{(C_1)}Q_{\sigma_2}^{(C_2)} + \dots \qquad (10)$$

If we now take the matrix elements of this Hamiltonian in the electronic basis

$$\left\{\left|\psi_\gamma^{(\Gamma)}\right\rangle,\ \gamma = 1,\ \dots\ ,[\Gamma]\right\}$$

of a degenerate electronic state with symmetry Γ, we get the matrix form

$$\widehat{H} = \left(\ \left\langle\psi_{\gamma'}^{(\Gamma)}\right| H \left|\psi_\gamma^{(\Gamma)}\right\rangle\ \right) = \widehat{H}_e + T\widehat{I} + \widehat{V}, \qquad (11)$$

(where the $\widehat{\ }$ denotes matrices). The Jahn-Teller theorem can thus be expressed as follows: there are always vibrational coordinates such that $\widehat{V}$ has off-diagonal elements. As far as linear terms in the development (10) are concerned (linear JTE), only coordinates with symmetry E_g or F_{2g} of octahedral molecules are implied. Of course, other coordinates can be involved when considering higher order terms, as we will discuss it later.

But first, and in order to illustrate the problems encountered with this standard approach of the JTE, we now focus on a very simple and illustrative case. We consider an octahedral molecule in a fourfold degenerate electronic state with symmetry G_g' (say, the electronic ground state of ReF_6). The $\nu_5(F_{2g})$ mode (coordinates $Q_\sigma^{(F_{2g})} = q_{5x}$, q_{5y} and q_{5z}) leads to a JTE and up to the linear term only, we get the following vibronic Hamiltonian (in both tensor and usual form)[21]:

$$\frac{H}{\hbar\omega_5} = \left(N_5 + \frac{3}{2}\right) - 2\sqrt{6D_5}\ \left(q_5^{(1)} \otimes \Sigma^{(1)}\right)_0^{(0)} = \frac{1}{2}\left(\mathbf{p}_5^2 + \mathbf{q}_5^2\right) + 2\sqrt{2D_5}\ \mathbf{q}_5 \cdot \mathbf{\Sigma}. \qquad (12)$$

The first term in the above Hamiltonian is the harmonic oscillator (N_5 being the number operator) while the second one is the linear coupling term with parameter D_5. In this case, the three matrices of first derivatives (with respect to q_{5x}, q_{5y} and q_{5z}) of Eq. (10) in the electronic basis can be written in the form of a pseudo 1/2-spin Σ_x, Σ_y and Σ_z. Thus, in a vibronic basis $|v_5, l_5, \Sigma = 1/2, j_5, m_5\rangle$ (l_5 being the vibrational angular momentum quantum number for the triply degenerate vibration ν_5), j_5 is a good quantum number ($\mathbf{j}_5 = \mathbf{l}_5 + \mathbf{\Sigma}$) and the matrix of (12) can be expressed as a series of infinite tridiagonal blocs, one for each j_5 value:

$$\frac{\widehat{H}_{j_5}}{\hbar\omega_5} = \begin{pmatrix} j_5+1 & \sqrt{2D_5(j_5+1)} & & & & \\ \sqrt{2D_5(j_5+1)} & j_5+2 & \sqrt{2D_5} & & & \\ & \sqrt{2D_5} & j_5+3 & \sqrt{2D_5(j_5+2)} & & \\ & & \sqrt{2D_5(j_5+2)} & j_5+4 & \sqrt{4D_5} & \\ & & & \sqrt{4D_5} & \ddots & \ddots \\ & & & & \ddots & \ddots \end{pmatrix}. \qquad (13)$$

This illustrates very well one major difficulty which arises when handling the JTE in this way: since JTE terms couple together successive vibrational quantum number values, one gets infinite matrices. One solution consists in truncating the vibronic basis at some sufficiently high v_5 value. Figure 4 shows the eigenvalues for

the above example for $0 \leq D_5 \leq 1$ and a truncation at $v_5 = 12$. The many avoided crossings observed in this typical D_5 range clearly show that the JTE is a non-perturbative effect and thus usual perturbation techniques (contact transformations, ...) are useless in this case. It is then easy to imagine that for a "real" rovibronic case, with inclusion of higher order coupling terms and of the rotation, the dimensions of the matrices involved become enormous, making the problem numerically intractable. For instance, the size of matrix blocks for a triply degenerate mode in a fourfold degenerate electronic state of an octahedral molecule at $J = 28.5$ (quite a low rotational excitation for the heavy transition-metal hexafluoride molecules) and $v_{\max} = 11$ is $\sim 45,000 \times 45,000$! This clearly illustrates the need for a new model that overcomes this kind of problem.

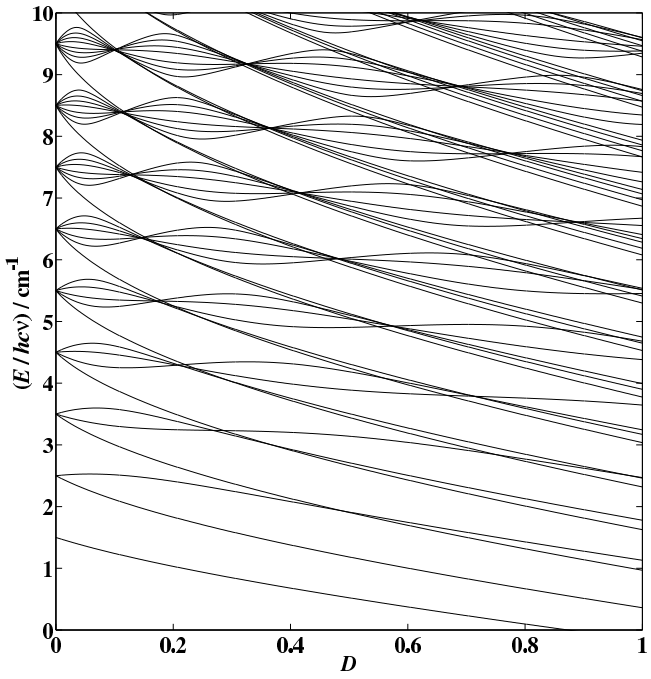

Figure 4. Vibronic energy levels for the linear $G'_g \otimes F_{2g}$ system as a function of $D(= D_5)$.

5. A NEW ROVIBRONIC MODEL

In order to re-write such rovibronic problems in a tractable way, we have elaborated a new model for effective Hamiltonians and transition moment suitable for any vibronic polyad of spherical tops in an isolated degenerate electronic state. Since this model has already been explained in detail elsewhere,[40,41] we only outline here its main features.

5.1. Electronic operators

The basic idea first consists in building suitable electronic operators for the electronic state under consideration. To do this, we associate an effective electronic angular momentum $\mathbf{J}_e$ to the electronic state. For instance, if the electronic symmetry is G'_g, we have the electronic quantum number $J_e = 3/2$*. We can then construct general electronic operators by recursive couplings of the elementary operators $2J_e^{(1)}$ in the same way as Moret-Bailly did for rotational operators.[1,44–46] The main difference here is that, since the quantum number J_e has a fixed

*We can notice that such a procedure is more difficult to apply to integer states with E symmetry, since there is no simple branching rule from $O(3)$ to the E representation of T_d and O_h. Anyway, this problem can be overcome using a non-standard $SU(2)$ orientation.[42,43]

value, the number of independent operators is limited: the electronic degree Ω_e must be equal to the electronic rank K_e and moreover $K_e \leq 2J_e$. The construction is thus symbolically[40,41]:

$$E^{(K_e,n_e\Gamma_e)} = 2^{K_e} \underbrace{\left(J_e^{(1)} \otimes J_e^{(1)} \otimes \ldots \otimes J_e^{(1)}\right)^{(K_e,n_e\Gamma_e)}}_{K_e \text{ terms}}. \tag{14}$$

5.2. Rovibronic effective Hamiltonian and transition moments

We can now construct effective rovibronic Hamiltonians as a sum of rovibronic operators,[40,41]

$$\mathcal{H}_{\{P_k\}} = \sum_i t_i \left(R_i^{(\Gamma)} \otimes \left(V_i^{(\Gamma_v)} \otimes E_i^{(\Gamma_e)}\right)^{(\Gamma)}\right)^{(A_{1g})}, \tag{15}$$

which is a generalization of Equation (5). Just as for the rovibrational problem, the operators are, by construction, restricted to a given vibronic polyad and thus the matrix blocks to diagonalize are no longer infinite. All matrix elements can be calculated in a rovibronic basis coupled in the same manner:

$$\left|\left(\psi_r^{(C_r)} \otimes \left(\psi_v^{(C_v)} \otimes \psi_e^{(C_e)}\right)^{(C_{ev})}\right)^{(C)}\right\rangle. \tag{16}$$

In order to calculate transition intensities, we construct transition moment operators (dipole moment and polarizability) using the same methods.

6. APPLICATION TO $V(CO)_6$ AND ReF_6

We now present two detailed examples for which recent experimental data exist and have been analyzed using the new formalism described above.

6.1. Vanadium hexacarbonyl

The $V(CO)_6$ molecule has 107 electrons and its ground electronic term is $^2F_{2g}$. According to the literature, its spin-orbit coupling constant should be very small.[27,28] We thus consider here that the electronic ground-state symmetry is F_{2g}, neglecting spin effects.

As for all hexacarbonyl molecules, the triply degenerate C–O stretch vibration ν_6 is interesting to study because i) its fundamental ($v_6 = 1$) level is well isolated and ii) it has a very big overall intensity due to a huge dipole moment. Due to the high mass of this molecule and to the existence of floppy V–C–O bending modes, only a tiny portion of the molecules lie in the ground-state at room temperature and thus spectra recorded under these conditions essentially consist in hot bands. The only way to study correctly the rovibronic spectroscopy in such a case is to use cold molecules, for instance in a supersonic expansion jet.

In Reference,[47] we have presented the first analysis of the jet-cooled FTIR spectrum of ν_6. We briefly recall here the main results of this work. Due to large rovibronic coupling, the individual transitions are spread out over a wide wavenumber range. This implies that, even if the total band intensity is big (see above), the intensity for each wavenumber value is low. Thus, the sensitivity of the FTIR experiment was not sufficient to allow a resolution better than 0.1 cm^{-1}. However, as shown on Figure 5, it was possible to satisfactorily reproduce the band profile using the model described above.

It appears that the three prominent features that we observe correspond to a quadratic Jahn-Teller splitting of the four vibronic sublevels (since $F_{2g} \otimes F_{1u} = A_{2u} \oplus E \oplus F_{1u} \oplus F_{2u}$). The total splitting is quite large, almost 40 cm^{-1}. The observed discrepancies (especially in the two lateral features) may be due to the zero spin-orbit coupling approximation. However, it seems clear that the spin-orbit constant should be very small (compared to transition-metal hexafluorides like ReF_6, see below), maybe only a very few cm^{-1}. This study tends to definitely prove the existence of a dynamic Jahn-Teller effect in this molecule, eliminating the possibility of a static distortion (at least in the gas phase).

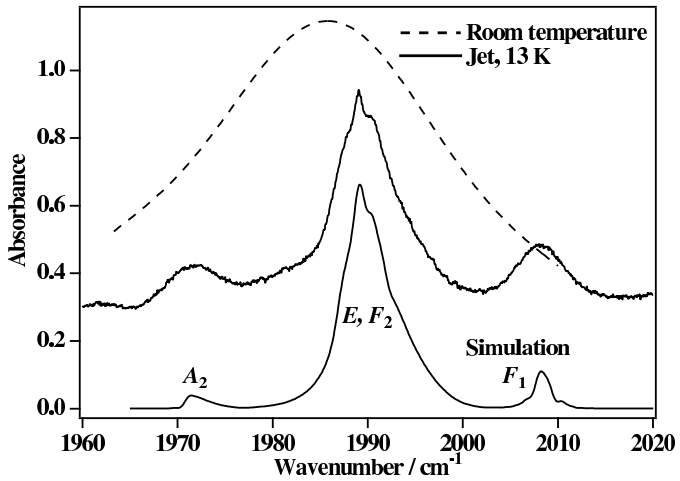

Figure 5. Supersonic expansion jet FTIR spectrum of the ν_6 band of $V(CO)_6$ (resolution is 0.1 cm^{-1}, rotational temperature is *ca.* 13 K) compared to the simulation. Symmetries of the $v_6 = 1$ sublevels are indicated. The dashed line shows the band profile at room temperature. Data taken from Ref..[47]

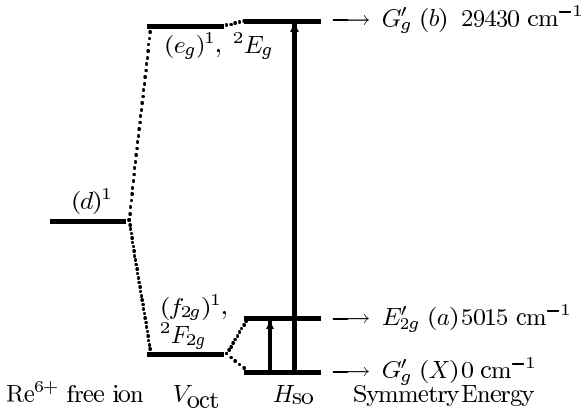

Figure 6. The lowest electronic energy levels of ReF_6 in a ligand-field scheme (see text). Arrows indicate the $a \longleftarrow X$ and $b \longleftarrow X$ electronic absorption transitions (see Figure 2 and Ref.[49]).

6.2. Rhenium hexafluoride

ReF_6 with its 189 electrons is, as already mentioned above, a $(d)^1$ system with a large spin-orbit coupling constant leading to a fourfold degenerate electronic ground state with G'_g spinorial symmetry (see Figure 6).[48,49]

Just as in the preceeding case, it was possible to record low-resolution (0.5 cm^{-1}) jet-FTIR spectra of this heavy molecule[50] and to simulate the band profile using our effective model, as shown on Figure 7.

Again, we have four vibronic sublevels ($G'_g \otimes F_{1u} = E'_{1u} \oplus E'_{2u} \oplus 2G'_g$) with a large splitting (~ 17 cm^{-1}) mainly due to a quadratic dynamic Jahn-Teller effect. To better take into account the absorption intensity above 735 cm^{-1}, we also added the $\nu_2 + \nu_6$ combination band (but with lowest order terms only in the Hamiltonian and dipole moment developments).

As explained in Reference,[50] it was also possible for this molecule to record high-resolution (0.0007 cm^{-1}) diode laser spectra in a supersonic expansion jet. As diode laser only provide a few small spectral windows[†] (< 1

[†]But on the other hand, this technique has the advantage of being very sensitive.

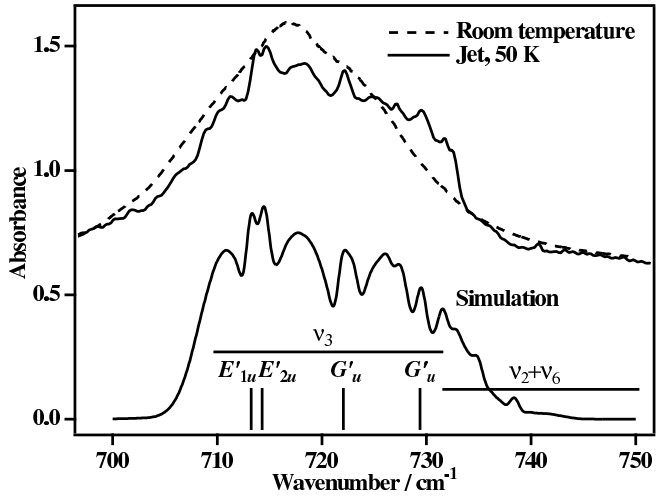

Figure 7. Supersonic expansion jet FTIR spectrum of the ν_3 band region of ReF_6 (resolution is 0.5 cm^{-1}, rotational temperature is *ca.* 50 K) compared to the simulation (which includes ν_3 and $\nu_2 + \nu_6$). Positions of the $v_3 = 1$ sublevels are indicated. The dashed line shows the band profile at room temperature. Experimental data taken from Ref..[50]

cm^{-1}) wide, the detailed analysis of this ν_3 region using only these data will probably be extremely difficult. But it already appeared that high-resolution simulations using the parameters coming from the band profile analysis show characteristic structures that are very similar to those observed in the corresponding regions recorded with the diode laser. This is very encouraging and convincing in respect to the validity of the present approach. These preliminary results concerning high-resolution spectra will be detailed in a forthcoming paper.[51]

7. CONCLUSION AND PERSPECTIVES

We have presented a new approach for the rovibronic spectroscopy of octahedral molecules in a degenerate electronic state. The model presented here has two major advantages: firstly, it avoids the problem of infinite matrices usually encountered with the "standard" approach of vibronic couplings and, secondly, it allows a systematic treatment of all possible rovibronic interactions up to a given order of the development. One drawback is that it is almost impossible to obtain a formal link between the untransformed and effective Hamiltonians since the transformation between these two is non-perturbative (because Jahn-Teller terms are themselves non-perturbative). Further developments could be the extension of the present methods to other symmetry groups in order to treat some free radicals like CH_3O or CH_3S, for instance. It could also be very interesting to complete this work by an *ab initio* approach.

ACKNOWLEDGMENTS

Région Bourgogne is gratefully acknowledged for supporting the Laboratoire de Physique de l'Université de Bourgogne. We also thank Pr. M. Quack, Dr. H. Hollenstein (ETH Zürich, Switzerland), Dr. P. Asselin, Dr. P. Soulard, Dr. L. Manceron (LADIR, Université Pierre et Marie Curie, Paris, France), Dr. A. Lorriaux (LASIR, Université de Lille I, France) and Mr. B. Roussel (DILOR Company, Lille, France) for the recording of experimental spectra and for useful comments and discussions. Finally, we acknowledge Mr. A. Jourdan (COMURHEX Company, Pierrelatte, France), Pr. D. Avignant (Université de Clermont-Ferrand, France) and Pr. H. Selig (University of Jerusalem, Israel) for providing us with hexafluoride samples and Pr. F. Michelot (LPUB, Dijon) for very helpful discussions and advices.

REFERENCES

1. J.-P. Champion, M. Loëte, and G. Pierre, "Spherical top spectra," in *Spectroscopy of the Earth's atmosphere and interstellar medium*, K. N. Rao and A. Weber, eds., pp. 339–422, Academic Press, San Diego, 1992.
2. N. Cheblal, M. Loëte, and V. Boudon, *J. Mol. Spectrosc.* **197**, pp. 222–231, 1999.
3. M. Rotger, V. Boudon, and M. Loëte, *J. Mol. Spectrosc.* **200**, pp. 123–130, 2000.
4. M. Rotger, V. Boudon, and M. Loëte, *J. Mol. Spectrosc.* **200**, pp. 131–137, 2000.
5. M. Rotger, V. Boudon, and M. Loëte, *J. Mol. Spectrosc.* **216**, pp. 297–307, 2002.
6. A. Nikitin, L. R. Brown, L. Féjard, J.-P. Champion, and V. G. Tyuterev, *J. Mol. Spectrosc.* **216**, pp. 225–251, 2002.
7. R. Englman, *The Jahn-Teller effect in molecules and crystals*, Wiley & Sons, New-York, 1972.
8. I. Bersuker and V. Polinger, *Vibronic interactions in molecules and crystals*, Springer-Verlag, Berlin, 1989.
9. B. Figgis, *Introduction to ligand fields*, Interscience, New-York, 1966.
10. J.-P. Champion, G. Pierre, F. Michelot, and J. Moret-Bailly, *Can. J. Phys.* **55**, pp. 512–520, 1977.
11. M. Rey, V. Boudon, C. Wenger, G. Pierre, and B. Sartakov, *J. Mol. Spectrosc.* **219**, pp. 313–325, 2003.
12. B. Weinstock and G. Goodman, *Adv. Chem. Phys.* **9**, pp. 169–319, 1965.
13. H. Mattraw, N. Hawkins, D. Carpenter, and W. Sabol, *J. Chem. Phys.* **23**, pp. 985–986, 1955.
14. W. Moffit and W. Thorson, *Phys. Rev.* **108**(5), pp. 1251–1255, 1957.
15. W. Moffit, G. Goodman, M. Fred, and B. Weinstock, *Mol. Phys.* **2**, pp. 109–122, 1959.
16. B. Weinstock, *Rec. Chem. Prog.* **23**(1), pp. 23–50, 1962.
17. B. Weinstock, *Chem. Eng. News* **42**(38), pp. 86–100, 1964.
18. N. Bartlett, *Angew. Chem. Int. Ed. Engl.* **7**(6), pp. 433–439, 1968.
19. R. Burns and T. O'Donnell, *J. Inorg. Nucl. Chem.* **42**, pp. 1285–1291, 1980.
20. R. Burns and T. O'Donnell, *J. Inorg. Nucl. Chem.* **42**, pp. 1613–1619, 1980.
21. V. Boudon, M. Rotger, and D. Avignant, *J. Mol. Spectrosc.* **175**, pp. 327–339, 1996.
22. R. McDowell and L. Asprey, *J. Mol. Spectrosc.* **45**, pp. 491–493, 1973.
23. H. Claassen and H. Selig, *Israel J. Chem.* **7**, pp. 499–504, 1969.
24. G. Hansford and P. Davies, *J. Mol. Spectrosc.* **168**, pp. 540–555, 1994.
25. G. Hansford, M. Loroño, and P. Davies, *J. Chem. Phys.* **112**(8), pp. 3620–3625, 2000.
26. P. Asselin, P. Soulard, L. Manceron, V. Boudon, and G. Pierre, *J. Mol. Struct.* **517**(1), pp. 145–155, 2000.
27. H. Haas and R. Sheline, *J. Am. Chem. Soc.* **88**(14), pp. 3219–3220, 1966.
28. S. Bratt, A. Kassyk, R. Perutz, and M. Symons, *J. Am. Chem. Soc.* **104**, pp. 490–494, 1982.
29. T. Parameswaran, J. Koningstein, and L. Haley, *J. Mol. Spectrosc.* **66**, pp. 350–356, 1977.
30. K. Stavrev and M. Zerner, *Chem. Phys. Lett.* **263**, pp. 667–670, 1996.
31. H. A. Bethe, *Ann. Phys.* **3**, pp. 133–206, 1929.
32. S. Altmann, *Mol. Phys.* **38**(2), pp. 489–511, 1979.
33. S. Altmann, *Rotations, quaternions, and double groups*, Clarendon Press, Oxford, 1986.
34. V. Boudon and F. Michelot, *J. Mol. Spectrosc.* **165**, pp. 554–579, 1994.
35. S. Altmann and F. Palacio, *Mol. Phys.* **38**(2), pp. 513–526, 1979.
36. S. Altmann and P. Herzig, *Mol. Phys.* **45**(3), pp. 585–604, 1982.
37. H. A. Jahn and E. Teller, *Proc. Roy. Soc. A (London)* **A161**, pp. 220–235, 1937.
38. H. A. Jahn, *Proc. Roy. Soc. A (London)* **164**, pp. 117–131, 1938.
39. V. Boudon, F. Michelot, and J. Moret-Bailly, *J. Mol. Spectrosc.* **166**, pp. 449–470, 1994.
40. M. Rey, V. Boudon, M. Loëte, and F. Michelot, *J. Mol. Spectrosc.* **204**, pp. 106–119, 2000.
41. M. Rey, V. Boudon, and M. Loëte, *J. Mol. Struct.* **599**, pp. 125–137, 2001.
42. V. Boujut and F. Michelot, *J. Mol. Spectrosc.* **173**, pp. 237–261, 1995.
43. F. Michelot, M. Rey, and V. Boudon, *J. Mol. Spectrosc.* **220** , pp. 19–44, 2003.
44. J. Moret-Bailly, *Cah. Phys.* **15**, pp. 237–316, 1961.
45. J. Moret-Bailly, *J. Mol. Spectrosc.* **15**(3), pp. 344–354, 1965.
46. B. I. Zhilinskií, *Opt. Spectrosc. (USSR)* **51**, pp. 262–263, 1981.

47. M. Rey, V. Boudon, M. Loëte, P. Asselin, P. Soulard, and L. Manceron, *J. Chem. Phys.* **114**(24), pp. 10773–10779, 2001.
48. J. Brand, G. Goodman, and B. Weinstock, *J. Mol. Spectrosc.* **38**, pp. 449–463, 1971.
49. M. Rotger, V. Boudon, and H. Selig, *Spectrochim. Acta A* **55**, pp. 1575–1584, 1999.
50. V. Boudon, M. Rotger, Y. He, H. Hollenstein, M. Quack, and U. Schmitt, *J. Chem. Phys.* **117**(7), pp. 3196–3207, 2002.
51. M. Rey, V. Boudon, M. Rotger, M. Loëte, H. Hollenstein, and M. Quack. work in progress, 2003.

Journal of Molecular Spectroscopy **204,** 106–119 (2000)
doi:10.1006/jmsp.2000.8193, available online at http://www.idealibrary.com on IDEAL®

A Tensorial Formalism Adapted to the Rovibronic Couplings in the Colored Hexafluorides: Application to the $\nu_5(F_{2g})$ and $\nu_3(F_{1u})$ Modes

M. Rey, V. Boudon, M. Loëte, and F. Michelot

Laboratoire de Physique de l'Université de Bourgogne, CNRS, B.P. 47870, F-21078 Dijon Cedex, France

E-mail: Boudon@jupiter.u-bourgogne.fr

Received May 15, 2000; in revised form June 20, 2000

A tensorial formalism adapted to the case of transition-metal hexafluorides in a degenerate electronic state has been developed on the basis of preceding works about spherical-top molecules in a nondegenerate electronic state. We have introduced electronic operators constructed using group theory features and some physical considerations. Vibronic couplings (Jahn–Teller effect, *etc.*) have been reviewed for the triply degenerate vibrational modes $\nu_5(F_{2g})$ and $\nu_3(F_{1u})$ leading to the identification of the main vibronic parameters. For the first time, an effective rovibronic Hamiltonian as well as the effective transition moment operators (dipole moment and polarizability) for rovibronic transitions have been studied qualitatively thanks to the tensorial algebra properties. © 2000 Academic Press

Key Words: tensorial formalism; colored hexafluorides; Jahn–Teller effect; rovibronic couplings.

1. INTRODUCTION

Some transition-metal fluorides (often called colored hexafluorides) such as ReF_6, IrF_6, OsF_6, PtF_6, PuF_6, etc., have the particularity of possessing an incomplete electronic shell leading to the existence of low-lying electronic states (including the ground state) that can be degenerate. This implies that low-energy electronic transitions occur in the visible or near-infrared regions (*1*). Furthermore, the study of such molecules having an odd number of electrons represents an interesting case due to the presence of half-integer angular momenta (*2*). With such an electronic structure, many complex couplings, called rovibronic couplings, appear. All this results in very particular spectra (without the usual *PQR* pattern for isolated fundamental bands, for instance, see Refs. (*3–6*) compared to those which are usually observed for molecules in a nondegenerate electronic state (SF_6, etc. (*7, 8*). This necessitates the consideration of the vibrational, rotational, and electronic motions altogether. In particular, many previous works dealt with the Jahn–Teller effect (*1, 9, 10*), which is the simplest vibronic (vibration–electronic) coupling and that leads to some "abnormalities" in the molecular electronic and vibrational spectra. In the past few years, several authors have treated this subject; Boudon *et al.* (*11, 12*) took advantage of group theory methods and tensorial formalism. They suggested an extension of the usual $O(3) \supset O_h$ chain used for the "classical" spherical-top molecules, considering the presence of half-integer states and thus introducing the $SU(2) \otimes C_I \supset O_h^S$ chain, where O_h^S is the octahedral group with its spinorial representations. This leads to a first tensorial writing of the vibronic Hamiltonian with a systematic construction of all operators. However, the vibronic problem, as it was treated in these papers, has the disadvantage of leading to infinite matrices.

The present paper deals with the rovibronic interactions written in purely tensorial form in quite the same way, as for rovibrational problems already treated in Dijon (*13–16*). An XY_6 molecule possesses six normal modes of vibration, namely (O_h symmetry is indicated in parentheses):

$$\underbrace{\nu_1(A_{1g}),\ \nu_2(E_g),\ \nu_3(F_{1u})}_{\text{(Stretching)}},\quad \underbrace{\nu_4(F_{1u}),\ \nu_5(F_{2g}),\ \nu_6(F_{2u})}_{\text{(Bending)}}.$$

The $\nu_5(F_{2g})$ and $\nu_3(F_{1u})$ triply degenerate vibrational modes are examined here in detail. This choice is due to the fact that ν_5 is the simplest case which presents a linear Jahn–Teller effect and that there exits some experimental data about ν_3 (*17*) for the ReF_6 molecule.

We wish here to stress the facts that (*i*) this paper introduces a new model of vibronic couplings in order to get rid of the problem of infinite matrices and (*ii*) this work is a first attempt of a tensorial writing adapted to a rovibronic Hamiltonian. The particular symmetry for the ν_5 and ν_3 modes leads us to couple all operators and wavefunctions in the $SU(2) \otimes C_I$ group.

Some recollections about the Jahn–Teller effect will be first carried out, in particular for the case of an octahedral XY_6 molecule in a fourfold degenerate electronic state of G'_g symmetry in O_h^S (*11*).

We present here three models adapted to three particular cases.

First, we present a vibronic Hamiltonian in the $SU(2) \otimes C_I$ group in order to try to reproduce the linear Jahn–Teller levels

0022-2852/00 $35.00

for the $\nu_5(F_{2g})$ Raman-active bending mode with finite matrices. The theory of transition-moment operators being essential for the study and prediction of transition intensities, we will expand the polarizability operator within the same scheme.

Second, we present a complete rovibronic model (Hamiltonian and polarizability) in the full chain $SU(2) \otimes C_I \supset O_h^S$ for $\nu_5(F_{2g})$.

Third, we present a vibronic and a complete rovibronic model (Hamiltonian and dipole moment) in the full chain for the $\nu_3(F_{1u})$ infrared active stretching mode with a different construction of electronic operators. The ν_3 mode does not present a *linear* Jahn–Teller effect but is subject to quadratic and higher order couplings.

2. THE JAHN–TELLER EFFECT

We first recall the basic principles of the Jahn–Teller theory as given in Refs. (*18–20*). Most of the electronic states of colored hexafluorides are degenerate and this implies couplings between the different molecular motions. The main vibronic coupling is called the Jahn–Teller (JT) effect. It is considered as a limiting case when the correction to the Born–Oppenheimer approximation becomes comparable to the vibrational energy. These terms in the Hamiltonian are nonperturbative and then must be treated exactly.

The vibronic Hamiltonian in a degenerate electronic state (of degeneracy d) can be written in the form

$$\mathcal{H} = \mathcal{H}_0 + \tilde{\mathcal{H}}^{(e)}, \qquad [1]$$

where

$$\mathcal{H}_0 = \frac{1}{2} \sum_{\alpha,i} \omega_\alpha (\mathcal{P}_{\alpha i}^2 + \mathcal{Q}_{\alpha i}^2) \qquad [2]$$

is the sum of harmonic oscillator Hamiltonians. The $\mathcal{Q}_{\alpha i}$ and $\mathcal{P}_{\alpha i}$ are dimensionless normal coordinates and conjugate momenta for the α mode; the subscript i distinguishes between the different components of degenerate vibrations.

$\tilde{\mathcal{H}}^{(e)}$ is the vibronic (JT) part and is expanded as a power series in normal coordinates. It contains anharmonic terms, in particular, linear terms which are typical of the Jahn–Teller effect. In Ref. (*21*), Moffit and Thorson have shown that these terms could be written

$$\tilde{\mathcal{H}}^{(e)} = \tilde{\mathcal{H}}_1^{(e)} + \cdots = \sum_{\alpha,i} k_\alpha \mathcal{Q}_{\alpha i} \mathcal{T}_{\alpha i} + \cdots, \qquad [3]$$

$\mathcal{T}_{\alpha i}$ is an electronic operator; k_α is a parameter.

If the electronic level is d-fold degenerate, then $\mathcal{T}_{\alpha i}$ is a $d \times d$ Hermitian matrix (expressed in an orthonormal basis $\{\psi_K^{(e)}\}_{K=1,\ldots,d}$). If we consider linear terms only, then all vibrational modes whose coordinates do not appear in $\tilde{\mathcal{H}}_1^{(e)}$ do not present a Jahn–Teller effect. In fact, if we take two electronic functions Φ_ρ and Φ_σ and two vibrational functions Ψ_β and Ψ_χ, then there is always at least one nontotally symmetric coordinate $\mathcal{Q}_{\alpha i}$ so that the matrix element between two vibronic states $\Phi_\rho\Psi_\beta$ and $\Phi_\sigma\Psi_\chi$

$$\langle \tilde{\mathcal{H}}_1^{(e)} \rangle = \sum_{\alpha,i} k_\alpha \langle \mathcal{Q}_{\alpha i} \rangle_{\beta\chi} \int \Phi_\rho \mathcal{T}_{\alpha i} \Phi_\sigma d\gamma \qquad [4]$$

are nonvanishing. This is the expression of the Jahn–Teller theorem (*22, 23, 9*). The vibrational modes implied in Eq. [4] lift electronic degeneracy.

For an octahedral XY_6 molecule (point group O_h^S) in a fourfold degenerate electronic state, only the $\nu_1(A_{1g})$, $\nu_2(E_g)$, and $\nu_5(F_{2g})$ modes are affected by the linear coupling. The other modes ($\nu_3(F_{1u})$, $\nu_4(F_{1u})$, $\nu_6(F_{1u})$) are only affected by higher order couplings (quadratic, etc.).

3. LINEAR VIBRONIC MODEL IN $SU(2) \otimes C_I$ FOR THE $\nu_5(F_{2g})$ BENDING MODE

3.1. Previous Works

The threefold degenerate bending mode $\nu_5(F_{2g})$ presents a linear Jahn–Teller effect in a fourfold electronic degenerate state of symmetry $\Gamma = G'_g$. Then, the vibronic Hamiltonian can be written for such an $(F_{2g} \times G'_g)$ problem as

$$H(\nu_5) = H_0 + H_{\text{JTL}} + H_{\text{JTQ}}^{(E_g)} + H_{\text{JTQ}}^{(F_{2g})} + \cdots, \qquad [5]$$

where

$$H_0 = \hbar\omega_5 (N_5 + 3/2) = \hbar\omega_5 (a^{+(F_{2g})} a^{(F_{2g})} + 3/2) \qquad [6]$$

is the threefold degenerate harmonic oscillator. The second term is the linear JT term written as (*12*):

$$H_{\text{JTL}} = 6\sqrt{2D_5}\, \hbar\omega_5 (Q_5^{(F_{2g})} \otimes T^{(F_{2g})})^{(A_{1g})}. \qquad [7]$$

D_5 ($k_5 = \sqrt{2D_5}$) is the linear parameter. There are two possible quadratic terms (*12*):

$$H_{\text{JTQ}}^{(E_g)} = 2\sqrt{6}\, \hbar\omega_5 \times Q_{E_g}((Q_5^{(F_{2g})} \otimes Q_5^{(F_{2g})})^{(E_g)} \otimes T^{(E_g)})^{(A_{1g})}, \qquad [8]$$

$$H_{\text{JTQ}}^{(F_{2g})} = 2\sqrt{6}\, \hbar\omega_5 \times Q_{F_{2g}}((Q_5^{(F_{2g})} \otimes Q_5^{(F_{2g})})^{(F_{2g})} \otimes T^{(F_{2g})})^{(A_{1g})}. \qquad [9]$$

(Q_{E_g}, $Q_{F_{2g}}$) are the quadratic parameters.

Moreover, in the pure vibronic case, the particular symmetry of ν_5 allows us to take advantage of the spherical formalism in $SU(2) \otimes C_I$. In fact, as shown in (*24*), any triply degenerate mode for an XY_6 molecule can be identified with a F_{1u} oscillator recalling the natural subduction $\mathcal{D}^{(1u)} \downarrow O_h = F_{1u}$.

As a matter of fact, we can write here

$$Q_{5\sigma}^{(1u,F_{1u})} = I^{(A_{2u})} Q_{5\sigma}^{(F_{2g})}, \qquad [10]$$

where $I^{(A_{2u})}$ is a trivial operator with the main property $[I^{(A_{2u})}]^2 = I$ (identity). Thus, the Hamiltonian can be rewritten

$$H(\nu_5) = H_0 + H_{\text{JTL}} + H_{\text{JTQ}}^{(0_g,A_{1g})} + H_{\text{JTQ}}^{(4_g,A_{1g})} + \cdots, \qquad [11]$$

with

$$\begin{cases} H_0 = \hbar\omega_5(N_5 + 3/2), \\ H_{\text{JTL}} = 6\sqrt{2D_5}\,\hbar\omega_5 I^{(A_{2u})}(Q_5^{(1u)} \otimes T^{(2g)})^{(3u,A_{2u})}, \\ H_{\text{JTQ}}^{(0_g,A_{1g})} = 2\sqrt{6}\,\hbar\omega_5 Q_0 (Q_5^{2(2g)} \otimes T^{(2g)})^{(0_g,A_{1g})}, \\ H_{\text{JTQ}}^{(4_g,A_{1g})} = 2\sqrt{6}\,\hbar\omega_5 Q_4 (Q_5^{2(2g)} \otimes T^{(2g)})^{(4_g,A_{1g})}. \end{cases} \qquad [12]$$

$Q_5^{2(2g)}$ is defined as $(Q_5^{(1u)} \otimes Q_5^{(1u)})^{(2g)}$. Q_0 and Q_4 are the quadratic Jahn–Teller parameters. Quadratic terms in the vibronic interaction are essential for the complete understanding of intrastate vibronic coupling (*25*). However, let us first concentrate on the linear term itself since it will help us to illustrate the basic principles of our method to construct (ro)vibronic operators.

Boudon *et al.* have suggested (*5*) a new writing in $SO(3)$ for the linear term itself which only requires the use of group theory and tensorial algebra propertes in $SU(2)$:

$$H(\nu_5) = \hbar\omega_5\left(N_5 + \frac{3}{2}\right) - 2\hbar\omega_5\sqrt{6D_5}(Q_5^{(1)} \otimes \Sigma^{(1)})_0^{(0)}. \qquad [13]$$

$\boldsymbol{\Sigma}$ is called the pseudo-spin because of the commutation rules of its components:

$$[\Sigma_\alpha, \Sigma_\beta] = i\epsilon_{\alpha\beta\gamma}\Sigma_\gamma \quad (\alpha, \beta, \gamma = x, y, \text{or } z). \qquad [14]$$

The quantum number Σ is $\frac{1}{2}$. The Hamiltonian [13] is an invariant of $SU(2)$ and commutes with the total angular momentum

$$\mathbf{j}_5 = \mathbf{l}_5 + \boldsymbol{\Sigma}, \qquad [15]$$

where l_5 is the vibrational angular momentum. Therefore, j_5 is a good quantum number ($\mathbf{j}_5^2$ being an invariant of the $SU(2)$ group) and each eigenvalue characterized by j_5 is $(2j_5 + 1)$-fold degenerate. Figure 1 shows the vibronic energy levels

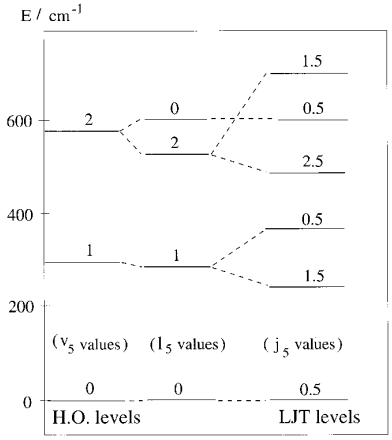

FIG. 1. Linear Jahn–Teller (LJT) energy levels for $\nu_5 = 286$ cm^{-1} and $D_5 = 0.103$. (H.O. = harmonic oscillator.)

in the case $D_5 = 0.103$ (electronic ground state of ReF_6 (*6*), see next paragraph).

With the introduction of quadratic (or other) terms, j_5 is no longer a good quantum number for the problem (although it can be considered as an approximate quantum number if these terms are weak).

This simple model has the disadvantage of leading the treatment of infinite matrices (*5*) because H_{JTL} couples v_5 with $v_5 \pm 1$. The previous works have brought out mainly two methods to solve this problem: either (*i*) a perturbative method which is only valid for the low D_5 values or (*ii*) a method based on truncated matrices at high v_5 values (say, 15 or more) which leads in practice to a difficult problem when adding rotational terms: the matrices obtained in this case would be difficult to handle because of their very large size. That is why, in the next paragraph, we will try to skirt this problem by writing a new effective model in $SU(2) \otimes C_I$.

3.2. *Effective Vibronic Hamiltonian in SU(2) ⊗ C_I*

The previous paragraph intended only to express vibronic coupling under a systematical tensorial writing. Here we construct electronic operators based on symmetry properties.

In the case of a fourfold (G_g') degenerate electronic state, we have chosen to construct electronic operators in the same way as rotational tensor operators introduced by Moret-Bailly in Ref. (*13*), noticing that the elementary components Σ_x, Σ_y, and Σ_z introduced previously form an irreductible spherical tensor of rank 1 (similar to the rotational operators J_x, J_y, and J_z).

Let us write an electronic tensor as $E^{\Omega_e(K_{eg})}$ in the group $O(3)$ where Ω_e is the degree (in the $\boldsymbol{\Sigma}$ components) and K_{eg} is the rank of the tensor. For more coherence with the rotational operator construction, the elementary tensor is

$$E_\alpha^{1(1_g)} = 2\Sigma_\alpha. \qquad [16]$$

The other operators are constructed as

$$E^{\Omega_e(K_{eg})} = \left(\left(E^{1(1_g)} \otimes E^{1(1_g)}\right)^{(0_g)}\right)^{(\Omega_e - K_e)/2} \times \left(E^{K_e - 1((K_e-1)_g)} \otimes E^{1(1_g)}\right)^{(K_{eg})}. \quad [17]$$

The nonvanishing operators involve K_e values such that

$$K_e = \Omega_e, \Omega_e - 2, \Omega_e - 4, \ldots, 1 \text{ or } 0. \quad [18]$$

In our case, $\Sigma = \frac{1}{2}$ and

$$E^{2(0_g, A_{1g})} = -\frac{4}{\sqrt{3}} \mathbf{\Sigma}^2 = \text{constant}. \quad [19]$$

This term appears in the first part of Eq. [17] and leads to some restrictions about tensor powers. In fact, one can show that

$$E^{\Omega_e(K_{eg})}_{K_e} \sim \left(E^{1(1_g)}_1\right)^{K_{eg}}, \quad [20]$$

where $E^{1(1_g)}_1$ is proportional to $\Sigma_+ = \Sigma_x + i\Sigma_y$. Moreover, if we consider $\epsilon_{ps} = \{|\frac{1}{2}, -\frac{1}{2}\rangle, |\frac{1}{2}, \frac{1}{2}\rangle\}$, the space which is generated by the pseudo-spin, we have $(\Sigma_+)^2 = 0$. Thus, the nonvanishing electronic operators are obtained only for Ω_e, $K_e \leq 1$; this is the main difference with the rotational operators (since the rotational quantum number $J = 0, 1, \ldots, \infty$). Therefore, we can conclude that only the

$$E^{0(0_g)} = I \quad \text{and} \quad E^{1(1_g)} = 2\Sigma^{(1_g)} \quad [21]$$

operators will be present in the developments. The other electronic operators are proportional to these.

The vibrational operators constructed in $O(3)$ can be expanded as those of Champion (*14*) in T_d thanks to Eq. [10] as

$$^{\epsilon}V^{K_{1\mu}K_{2\mu}(K_{vg})}_{\{5\}\{5\}} = \frac{e^{i\phi}}{[K_v]^{1/2}} \left(\left(A_5^{+(K_{1\mu})} \otimes A_5^{(K_{2\mu})}\right)^{(K_{vg})} + \epsilon(-1)^{K_v}\left(A_5^{+(K_{2\mu})} \otimes A_5^{(K_{1\mu})}\right)^{(K_{vg})}\right), \quad [22]$$

with

$$\begin{cases} A_5^{(K_{i\mu})} = \left(I^{(A_{2u})}\right)^{\Omega_v/2}\left(\cdots\left(a_5^{(1_u)} \otimes a_5^{(1_u)}\right) \otimes a_5^{(1_u)}\cdots\right)^{(K_{i\mu})}, \\ A_5^{+(K_{i\mu})} = \left(I^{(A_{2u})}\right)^{\Omega_v/2}\left(\cdots\left(a_5^{+(1_u)} \otimes a_5^{+(1_u)}\right) \otimes a_5^{+(1_u)}\cdots\right)^{(K_{i\mu})} \end{cases} \quad [23]$$

where $\epsilon = \pm 1$ is the parity under time-reversal and $e^{i\phi} = 1$ (respectively $-i$) for $\epsilon = +$ (respectively $-$). We have denoted the dimension of the $\mathcal{D}^{(K_v)}$ representation of $O(3)$ by $[K_v] = (2K_v + 1)$. Here, μ is either g ($\Omega_v/2$ even) or u ($\Omega_v/2$ odd).

As in vibration–rotation studies, one uses an effective Hamiltonian which has the advantage of having a completely diagonal or block-diagonal form with respect to a vibronic subspace corresponding to a group (or polyad) of vibronic levels (*15*). Thus, one defines the effective vibronic Hamiltonian

$$\tilde{H}_{ev} = \mathcal{P}^{\langle \text{polyad} \rangle} T H_{ev} T^{-1} \mathcal{P}^{\langle \text{polyad} \rangle} \quad [24]$$

obtained by applying a unitary transformation using a unitary operator $T = e^{iS}$ (S is Hermitian). $\mathcal{P}^{\langle \text{polyad} \rangle}$ is the projector on the Hilbert subspace spanned by the vibronic states of the polyad. Then, the vibronic contribution to the effective molecular Hamiltonian for the linear effect is written as:

$$\tilde{H}_{ev} = \sum_{\text{all indexes}} \tilde{t}^{\Omega_e K_{1\mu} K_{2\mu}(K_{eg})}_{\{5\}\{5\}} \zeta \left(E^{\Omega_e(K_{eg})} \otimes {}^{\epsilon}V^{K_{1\mu}K_{2\mu}(K_{eg})}_{\{5\}\{5\}}\right)^{(0_g)}, \quad [25]$$

where the $\tilde{t}$ are the vibronic parameters are ζ is a numerical factor equal to $[K_1]^{1/2}$ if $(\Omega_e, K_{eg}) = (0, 0_g)$ and to 1 otherwise. The vibronic Hamiltonian H_{ev} must be invariant under time-reversal. That is why we must have $\epsilon = +$ (respectively $-$) for Ω_e even (respectively odd). We have chosen to define the order of the Hamiltonian development (Ω) in the same way as for the rovibrational Hamiltonian (*15*) as:

$$\Omega = \Omega_v + \Omega_e - 2. \quad [26]$$

Let us note that this choice is in fact somewhat arbitrary. However, the order of the development intends to characterize the contribution of the operators and not the order of magnitude of the parameters.

The calculation of matrix elements of irreducible tensor operators requires the use of the Wigner–Eckart theorem in $SU(2) \otimes C_I$ which is given in Appendix B. In the present case, the adapted vibronic basis is of the form

$$\left|\left(\Phi^{(1/2_g)} \otimes \Psi^{(l_{5\tau})}_{v_5}\right)^{(j_{5\tau})}_{m_5}\right\rangle, \quad [27]$$

$\Psi^{(l_{5\tau})}$ being the vibrational function ($\tau = g$ or u). The effective Hamiltonian is diagonal in v_5. So, we can write the matrix elements in $SU(2) \otimes C_I$ as

$$\begin{aligned} &\left\langle\left(\Phi^{(1/2_g)} \otimes \Psi^{(l_{5\tau})}_{v_5}\right)^{(j_{5\tau})}_{m_5}\right| \left(E^{\Omega_e(K_{eg})} \otimes {}^{\epsilon}V^{K_{1\mu}K_{2\mu}(K_{eg})}_{\{5\}\{5\}}\right)^{(0_g)}\Big| \\ &\quad \times \left(\Phi^{(1/2_g)} \otimes \Psi^{(l_{5\tau})}_{v_5}\right)^{(j_{5\tau})}_{m_5}\Big\rangle \\ &= (-1)^{K_e + l_g + j_5 + 1/2}[K_e]^{-1/2} \begin{Bmatrix} 1/2_g & j_{5\tau} & l_{5\tau} \\ l'_{5\tau} & K_{eg} & 1/2_g \end{Bmatrix} \\ &\quad \times \left\langle \Psi^{(l_{5\tau})}_{v_5}\right\| {}^{\epsilon}V^{K_{1\mu}K_{2\mu}(K_{eg})}_{\{5\}\{5\}} \left\|\Psi^{(l_{5\tau})}_{v_5}\right\rangle \left\langle \Phi^{(1/2_g)}\right\| E^{\Omega_e(K_{eg})} \left\|\Phi^{(1/2_g)}\right\rangle. \end{aligned} \quad [28]$$

The reduced matrix elements (RME) are given in Appendix C.

TABLE 1
Effective Vibronic Parameters for the ν_5 Mode of ReF_6

Level	$\Omega_e(K_e)$	$K_1K_2(K_e)$	Order	Para.	Value/cm^{-1} (see text)
$v_5 = 1$	0(0)	11(0)	0	$\tilde{t}_1$	287.5333
	1(1)	11(1)	1	$\tilde{t}_2$	95.6117

It is interesting to relate the Jahn–Teller model (with truncated matrices) and this effective model which has the advantage of possessing finite matrices. As a very simple illustration, let us list the Hamiltonian parameters up to order 1 (Table 1). Thanks to Eq. [28], we have calculated the nonvanishing matrix elements in the $\{|v_5, l_5, \frac{1}{2}; j_5, m_5\rangle\}$ ($v_5 = 0, 1$) basis. Then, we can relate the two models [13] and [25] and plot the new parameters according to D_5 values.

The first step to obtain this result is to calculate the eigenvalues of the model given by Boudon [13] in the same basis. This calculation is obtained by truncating the infinite matrices at a high v_5 value ($v_5 = 15$ here). Then one just has to equal the eigenvalues of the two models to find the values of our parameters. The results are shown in Fig. 2. For a given D_5 value, the $\tilde{t}_1$ and $\tilde{t}_2$ parameters are totally determined.

Knowing the D_5 value for ReF_6 ($D_5 = 0.103$ (*6*)) in its ground electronic state $X(G'_g)$, we deduce the corresponding parameters (Table 1). The $\tilde{t}_2$ parameter can be thought of as a kind of vibronic "Coriolis-coupling" constant which is responsible for the splitting between the different j_5 components of a ν_5 level.

3.3. Raman Transitions

The theory of transition moments operators (dipole moment and polarizability) is essential for the study and prediction of transition intensities. We present here a simple model of a polarizability operator in $SU(2)$ for the ν_5 band which is Raman active. Thanks to [10], we can write for the vibronic transitions of the ν_5 mode,

$$\tilde{\alpha} = \tilde{\alpha}_0 I^{(A_{2u})}(E^{0(0_g)} \otimes a^{+(1_u)})^{(1_u,F_{1u})} \rightarrow \text{vibrational},$$
$$\left.\begin{aligned} &+\tilde{\alpha}_1 I^{(A_{2u})}(E^{1(1_g)} \otimes a^{+(1_u)})^{(1_u,F_{1u})} \\ &+\tilde{\alpha}_2 I^{(A_{2u})}(E^{1(1_g)} \otimes a^{+(1_u)})^{(2_u,E_u)} \end{aligned}\right\} \rightarrow \text{vibronic}, \quad [29]$$

$E^{0(0_g)}$ and $E^{1(1_g)}$ being the elementary electronic operators introduced previously and $\tilde{\alpha}_0$, $\tilde{\alpha}_1$, $\tilde{\alpha}_2$ are the parameters. The selection rules between the $v_5 = 0$ ($j_5 = \frac{1}{2}$) level and the $v_5 = 1$ ($j'_5 = \frac{1}{2}, \frac{3}{2}$) level and the expression of intensities are given in Table 2.

TABLE 2
Selection Rules and Intensity for the $\nu_5 = 1$ Transition

	Vibrational part	Vibronic part
$\Delta j_5 = j'_5 - 1/2$	0, 1	0, 1
Intensity	$I \sim \lvert\langle j'_5 \rvert \tilde{\alpha} \rvert \frac{1}{2}\rangle\rvert^2$	
$j'_5 = 1/2$	$I \sim \frac{2}{3}(\sqrt{2}\tilde{\alpha}_1 - \tilde{\alpha}_0)^2$	
$j'_5 = 3/2$	$I \sim \frac{2}{3}(\sqrt{2}\tilde{\alpha}_0 + \tilde{\alpha}_1 + \sqrt{5}\tilde{\alpha}_2)^2$	

3.4. Example: The Case of ReF_6

To better illustrate the origin of the abnormalities in the spectra of hexafluoride molecules, we have plotted the peak positions observed (*2*) for ν_5 (Fig. 3) for the hexafluorides of the second and third transition-metal series. We note that the variation trend of the fundamental vibrational frequency as a function of the nonbonding electrons shows very marked deviations for ReF_6, TcF_6, OsF_6, and RuF_6.

For these molecules, the value of the ν_5 peak position is seen to be, respectively, 39, 42, 24, and 21 cm^{-1} lower than the value ν_5^0 expected. These observations are the result of a linear Jahn–Teller effect. Let us now consider the case of ReF_6 and see how it is possible to understand its Raman spectrum which has been differently interpreted by several authors.

According to Weinstock and Goodman (*1*), certain abnormalities observed in the spectrum of rhenium hexafluoride have been referred to as dynamic Jahn–Teller coupling. However, they assigned several peaks for vibronic transition that could not be observed by other authors. In particular, Claassen and Selig (*4*) asserted that the spectrum of ReF_6 looks like other typical hexafluoride spectra, so they forsaw no Jahn–Teller effect for ν_5. If we look at Figs. 1 and 3, we realize that the observation of a unique peak at about 250 cm^{-1} for ν_5 in the ground electronic state G'_g, that is somewhat lower than the

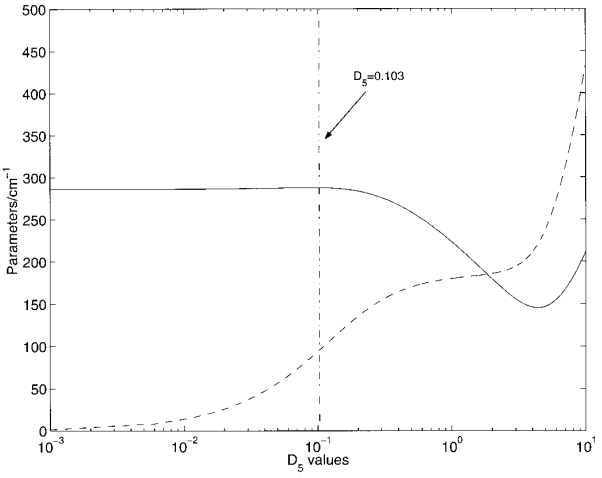

FIG. 2. Vibronic parameters of Table 1 as a function of D_5 values for $\nu_5 = 286$ cm^{-1} (ReF_6 (*6*)). In this figure, $\tilde{t}_1$ (solid line) and $\tilde{t}_2$ (dashed line) are represented.

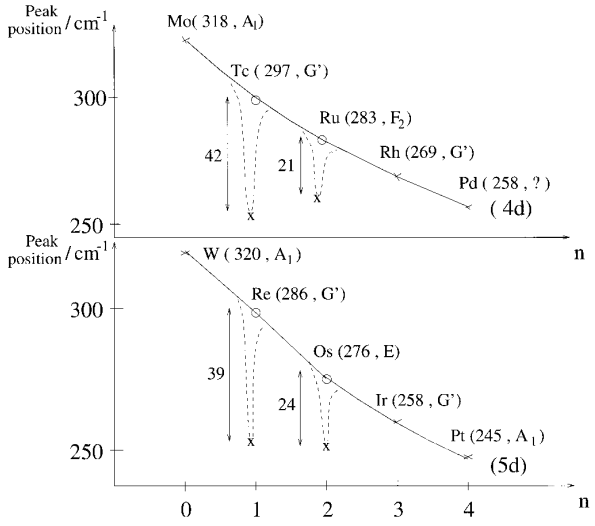

FIG. 3. Frequency variations of the Raman-active fundamental $\nu_5(F_{2g})$ as a function of the number of nonbonding valence electrons for the transition–metal hexafluoride molecules. The frequency shift for ReF_6, TcF_6, OsF_6, and RuF_6 arises from linear vibronic coupling. Inside the parentheses, the frequency (in cm^{-1}) and the symmetry of the ground electronic state are given.

expected harmonic oscillator transition, would be possible if only the

$$(v_5 = 0, j_5 = 1/2) \mapsto (v_5 = 1, j_5 = 3/2)$$

transition was allowed. This implies $\tilde{\alpha}_0 \simeq \sqrt{2}\,\tilde{\alpha}_1$. The existence of a large Jahn–Teller splitting ($\simeq$110 cm^{-1} for $D_5 = 0.103$ (see Fig. 1)) is thus not incompatible with the observation of a unique peak. The transition to the other level of component $j_5 = 1/2$ is present in the spectrum but it should correspond to a weak transition.

4. EFFECTIVE ROVIBRONIC MODEL IN $SU(2) \otimes C_I \supset O_h^S$ FOR THE $\nu_5(F_{2g})$ MODE

In this section, we construct a formal rovibronic Hamiltonian as well as the polarizability operator for rovibronic transitions by adding rotational operators.

We now take into account nonlinear Jahn–Teller terms which appear in the rovibronic Hamiltonian expansion. That is why we must introduce different electronic operators (see next paragraph) in order to consider all possible terms of the Hamiltonian.

Most studies of vibration–rotation spectra of molecules with a high symmetry in a nondegenerate electronic state use the tensorial formalism originally developed in Dijon by Moret-Bailly and Champion (*13, 14*).

Champion (*14*) has considered a Hamiltonian developed to any order and taking into account all possible interactions. His work is based on the construction of vibration–rotation operators symmetrized in the $O(3) \supset T_d$ chain. The case of octahedral molecules (XY_6, $X(YZ)_6$) has also been considered (*16*) in the $O(3) \supset O_h$ chain. We can extend this formalism to the $SU(2) \otimes C_I \supset O_h^S$ chain in the same way as Champion, considering the particular symmetry of a triply degenerate mode.

4.1. Electronic Tensor Operators

Using the same approach as for the linear Jahn–Teller model, our electronic tensor operators are constructed thanks to elementary operators but these ones are defined differently. Instead of using the pseudo-spin properties, we define more general electronic operators through the symmetry of the electronic state only.[1]

In our case, we have the electronic symmetry G'_g in O_h^S. Considering the natural subduction $\mathcal{D}^{(3/2_g)} \downarrow O_h^S = G'_g$, we define an effective electronic momentum $\mathbf{J}'$ with the property $J' = \frac{3}{2}$. Therefore, the basic tensor will be denoted

$$E_\alpha^{1(1_g)} = 2J'_\alpha, \qquad [30]$$

the other operators being constructed as in Ref. (*17*).

Thus, the electronic tensor operators coupled in the $SU(2) \otimes C_I$ group are written $E^{\Omega_e(K_{eg})}$, where the allowed values of K_e are $K_e = 0$, 1, 2, and 3. Only operators with the $\Omega_e = K_e$ condition are independent. The other operators (as well as for $\Omega_e \geq 4$) are deduced from these.

It is useful to consider the effective vibronic angular momentum (*12*)

$$\mathbf{J}_5 = \mathbf{l}_5 + \mathbf{J}'. \qquad [31]$$

4.2. Rovibronic Hamiltonian

Operators and wavefunctions are still coupled in $SU(2) \otimes C_I$ but oriented with respect to O_h^S (J_5 is not a good quantum number) through the unitary transformation

$$\Lambda_\sigma^{(j_\tau, nC_\tau)} = \sum_m {}^{(j_\tau)}G^m_{nC_\tau\sigma}\Lambda_m^{(j_\tau)}, \qquad [32]$$

where the G orientation matrices as well as variance choices are defined in Ref. (*11*).

We do not recall the construction of rotational operators $R^{\Omega_r(K_{rg})}$ since this has been well described elsewhere (*15*).

Thus, all possible effective rovibronic operators are constructed by coupling in $O(3)$ as

[1] We note here that relating this second model with that using the pseudo-spin (especially concerning symmetry properties) is not a simple task, although it is feasible. This problem will be treated in a forthcoming paper where we will discuss the pseudo-spin approach in more detail.

$$T^{(\{t\},K_g,n_0A_{1g})}_{\{5\}\{5\}} = T^{\Omega_r\Omega_e,K_{rg}K_{eg}K_{1\mu}K_{2\mu}K_{vg},K_{evg}(K_g,n_0A_{1g})}_{\{5\}\{5\}}$$
$$= (R^{\Omega_r(K_{rg})} \otimes (E^{\Omega_e(K_{eg})} \otimes {}^{\epsilon}V^{K_{1\mu}K_{2\mu}(K_{vg})}_{\{5\}\{5\}})^{(K_{evg})})^{(K_g,n_0A_{1g})}, \quad [33]$$

with $(\Omega_e, K_e) \leq 3$ (see Section (4.1)).

The effective Hamiltonian ($\tilde{H} = THT^{-1}$) is expressed as a linear combination of rovibronic operators

$$\tilde{H} = \sum_{\text{all indexes}} \tilde{t}^{(\{t\},K_g,n_0A_{1g})}_{\{5\}\{5\}}\eta \times T^{(\{t\},K_g,n_0A_{1g})}_{\{5\}\{5\}}, \quad [34]$$

where $\tilde{t}$ are the parameters and η is a numerical factor which allows coincidence between the standard and tensorial notations for scalar terms,

$$\eta = [K_{1\mu}]^{1/2}(-\sqrt{3}/4)^{(\Omega_r)/2}, \quad [35]$$

if $(K_{rg}, K_{eg}) = (0_g, 0_g)$ and 1 otherwise.

The complete Hamiltonian is a Hermitian operator which must be totally symmetric in O_h (but not in $O(3)$) and invariant under time-reversal. Thus, operators [33] selected for $\tilde{H}$ are those for which the V, E, and R operators have the same parity in elementary momentum oeprators. As a consequence, one has $\epsilon = +$ (respectively $-$) for $(\Omega_r + \Omega_e)$ even (respectively odd).

The matrix elements of operators [33] calculated in the appropriate basis function

$$|\Psi^{(\mathcal{J}_\tau,n\tilde{C}_\tau)}_\sigma\rangle = |(\Psi^{(J_g)}_r \otimes (\Phi^{(3/2_g)} \otimes \Psi^{(l_{5\tau})}_{v_5})^{(J_{5\tau})})^{(\mathcal{J}_\tau,n\tilde{C}_\tau)}_\sigma\rangle \quad [36]$$

are

$$\langle\Psi^{(\mathcal{J}'_{\tau'},n'\tilde{C}_{\tau'})}_\sigma|T^{(\{t\},K_g,n_0A_{1g})}_{\{5\}\{5\}}|\Psi^{(\mathcal{J}_\tau,n\tilde{C}_\tau)}_\sigma\rangle$$
$$= (-1)^{2C+2\mathcal{J}'}[\tilde{C}]^{-1/2}\sqrt{[K][K_{ev}][J_5][J'_5][\mathcal{J}][\mathcal{J}']}$$
$$\times \begin{Bmatrix} J_g & J_{5\tau} & \mathcal{J}_\tau \\ K_{rg} & K_{evg} & K_g \\ J_g & J'_{5\tau'} & \mathcal{J}'_{\tau'} \end{Bmatrix} \begin{Bmatrix} 3/2_g & l_{5\tau} & J_{5\tau} \\ K_{eg} & K_{vg} & K_{evg} \\ 3/2_g & l'_{5\tau'} & J'_{5\tau'} \end{Bmatrix} \quad [37]$$
$$\times K \begin{pmatrix} (K_g & \mathcal{J}_\tau & \mathcal{J}'_{\tau'}) \\ (n_0A_{1g} & n\tilde{C}_\tau & n'\tilde{C}_{\tau'}) \end{pmatrix}$$
$$\times \langle\Psi^{(g_{\tau'})}_{v_5}\|{}^{\epsilon}V^{K_{1\mu}K_{2\mu}(K_{vg})}_{\{5\}\{5\}}\|\Psi^{(l_{5\tau})}_{v_5}\rangle\langle\Phi^{(3/2_g)}\|E^{\Omega_e(K_{eg})}\|\Phi^{(3/2_g)}\rangle$$
$$\times \langle\Psi^{(J_g)}_r\|R^{\Omega_r(K_{rg})}\|\Psi^{(J_g)}_r\rangle,$$

(the operators being diagonal in v_5 and J). The "true" symmetry of the state is $C_\chi = (A_{2u})^{v_5} \otimes \tilde{C}_\tau$.

4.3. Effective Polarizability Operator for Rovibronic Raman Transitions

In this part, we are going to try to construct a formal model for the calculation of rovibronic Raman transition intensities.

4.3.1. Definition. To build rovibronic polarizability operators, let us first recall some basic principles.

The application of an electric field **E** to the molecules induces a dipole moment μ related to the α polarizability (*16*) by

$$\mu_{\Theta_1} = \sum_{\Theta_2} \alpha_{\Theta_1\Theta_2}E_{\Theta_2}. \quad [38]$$

The $\alpha_{\Theta_1\Theta_2}$ laboratory-fixed frame (LFF) components (Θ_1, $\Theta_2 = X, Y, Z$) can be related to the $\alpha_{\theta_1\theta_2}$ molecule-fixed frame (MFF) components (θ_1, $\theta_2 = x, y, z$) with the aid of direction cosines

$$\alpha_{\Theta_1\Theta_2} = \sum_{\theta_1\theta_2} \lambda_{\Theta_1\theta_2}\lambda_{\Theta_1\theta_2}\alpha_{\theta_1\theta_2}. \quad [39]$$

$\alpha_{\theta_1\theta_2}$ can be expanded in power series of normal coordinates

$$\alpha_{\theta_1\theta_2} = \alpha^e_{\theta_1\theta_2} + \sum_{s,\sigma}\left(\frac{\partial\alpha_{\theta_1\theta_2}}{\partial q_{s\sigma}}\right)q_{s\sigma}$$
$$+ \frac{1}{2}\sum_{s,s',\sigma\sigma'}\left(\frac{\partial^2\alpha_{\theta_1\theta_2}}{\partial q_{s\sigma}q_{s'\sigma'}}\right)q_{s\sigma}q_{s'\sigma'} + \cdots, \quad [40]$$

where $\alpha^e_{\theta_1\theta_2}$ is the permanent polarizability (if it exists).

4.3.2. Tensorial formalism in O^S_h. An extension to a tensorial formalism is undertaken here for a degenerate electronic state in order to perform the calculation of (ro)vibronic transitions. We will still work in the full chain $SU(2) \otimes C_I \supset O^S_h$.

According to Stone (*26*) and Eq. [32], we can define a transformation which links spherical components to Cartesian components by

$$\alpha_{\theta_1\theta_2} = \sum_{K_{ev},k} \langle K_{ev}; k|\theta_1\theta_2\rangle\alpha^{(K_{ev})}_k, \quad [41]$$

$$\alpha_{\Theta_1\Theta_2} = \sum_{K_{ev},m} \langle K_{ev}; m|\Theta_1\Theta_2\rangle\alpha^{(K_{ev})}_m, \quad [42]$$

where $\langle K_{ev}; k|\theta_1\theta_2\rangle$ and $\langle K_{ev}; m|\Theta_1\Theta_2\rangle$ are Stone coefficients (*26*) calculated by Pascaud and Poussigue (*27*) for spherical top molecules.

In the (MFF), one writes

$$\begin{aligned}\alpha_{\sigma}^{(\Gamma_g)} &= \sum_{\text{all indexes}} \alpha_{\{5\}\{5\}}^{(\{i\},K_{ev\nu},n_0\tilde{\Gamma}_\nu,\Gamma_g)} P_{\sigma}^{(\{i\},K_{ev\nu},n_0\tilde{\Gamma}_\nu,\Gamma_g)} \\ &= \sum_{\text{all indexes}} \alpha_{\{5\}\{5\}}^{(\{i\},K_{ev\nu},n_0\tilde{\Gamma}_\nu,\Gamma_g)} (I^{(A_{2u})^{\Omega_v}} \otimes \mathbb{O}_{ev}^{(K_{ev\nu},n_0\tilde{\Gamma}_\nu)})^{(\Gamma_g)},\end{aligned} \quad [43]$$

where $\alpha_{\{5\}\{5\}}^{(\{i\},K_{ev\nu},n_0\tilde{\Gamma}_\nu,\Gamma_g)}$ are the parameters. Here, α is built thanks to the *vibronic* operators. We have $\Gamma_g = A_{1g}$, E_g, or F_{2g}, where the A_{1g} symmetry represents the isotropic part and the E_g, F_{2g} symmetries correspond to the anisotropic part. Γ_g is obtained from the branching rules

$$\mathcal{D}^{(K_{ev\nu})} \supset n_0\tilde{\Gamma}_\nu \quad \text{and} \quad \Gamma_g = \tilde{\Gamma}_\nu \otimes (A_{2u})^{\Omega_v}, \quad [44]$$

where $\nu = u$ if Ω_v is odd and $\nu = g$ otherwise.

It is necessary to consider an effective polarizability operator obtained by applying the same transformation T as to the effective Hamiltonian [34] that is

$$\tilde{\alpha}_{\theta_1\theta_2} = T\alpha_{\theta_1\theta_2}T^{-1}. \quad [45]$$

Such a transformation contains rotational operators (*16*). Therefore, the effective polarizability is written with the aid of rovibronic operators [33]

$$\tilde{\alpha}_{\sigma}^{(\Gamma_g)} = \sum_{\text{all indexes}} \tilde{\alpha}_{\{5\}\{5\}}^{(\{i\},L'_\nu,n_0\tilde{\Gamma}_\nu,\Gamma_g)} P_{\sigma}^{(\{i\},L'_\nu,n_0\tilde{\Gamma}_\nu,\Gamma_g)}. \quad [46]$$

If we want to work in the LFF, then we need to take into account the direction cosines tensor. From [39], [42], and Appendix A, we obtain the tensorial expression of the components of the polarizability

$$\begin{aligned}\tilde{\alpha}_{\Theta_1\Theta_2} = \sum_{K',\Gamma,L',m,\rho,\{i\}} &(-1)^{K'}([\Gamma][K'])^{1/2}\langle L';\, m|\Theta_1\Theta_2\rangle \\ &\times K \begin{pmatrix} L_g & L'_\nu & K'_\nu \\ 0\Gamma_g & n_0\tilde{\Gamma}_\nu & \bar{n}\tilde{\bar{\Gamma}}_\nu \end{pmatrix} \times {}^{(L'\nu)}G_m^{n_0\tilde{\Gamma}_\nu\rho}\tilde{\alpha}_{\{5\}\{5\}}^{(\{i\},L'_\nu,n_0\tilde{\Gamma}_\nu,\Gamma_g)} \\ &\times (I^{(A_{2u})^{\Omega_v}} \otimes [C^{(L_g)} \otimes P^{(\{i\},L'_\nu)}]^{(K'_\nu,\bar{n}\tilde{\bar{\Gamma}}_\nu)})^{(A_{1g})},\end{aligned} \quad [47]$$

with

$$\mathcal{D}^{(K'_\nu)} \supset \bar{n}\tilde{\bar{\Gamma}}_\nu \quad \text{and} \quad \tilde{\bar{\Gamma}}_\nu \otimes (A_{2u})^{\Omega_v} = A_{1g}. \quad [48]$$

The brackets indicate the use of a symmetrized tensor product (because C and R do not commute) defined as

$$\begin{aligned}[A^{(j_1)} \otimes B^{(j_2)}]^{(j)} = \tfrac{1}{2}\,&((A^{(j_1)} \otimes B^{(j_2)})^{(j)} \\ &+ (-1)^{j+j_1+j_2}(B^{(j_2)} \otimes A^{(j_1)})^{(j)}).\end{aligned} \quad [49]$$

Let us note that the parameters $\tilde{\alpha}_{\{5\}\{5\}}^{(\{i\},L'_\nu,n_0\tilde{\Gamma}_\nu,\Gamma_g)}$ depend on the Hamiltonian parameters through transformation [45].

4.3.3. Intensity: Selection rules. The Raman intensities between two transformed rovibronic states are given by

$$I_{if} = R_{ij}g_i e^{-(hcE_i/kT)} \sum_{M_i,M_f} \sum_{\Theta,\Theta'} |\langle\tilde{\Phi}_i|\tilde{\alpha}_{\Theta\Theta'}|\tilde{\Phi}_f\rangle|^2, \quad [50]$$

where R_{ij} is a numerical factor which depends on the frequency and the temperature and g_i is the spin–statistical weight of the $\tilde{\Phi}_i$ state.

The calculation of matrix elements between two rovibronic basis function given in [36] requires once again the use of Wigner–Eckart theorem. One obtains

$$\begin{aligned}&\langle(\Psi^{(A_{2u})^{\nu'_5}} \otimes \Psi^{(\mathcal{J}'_\tau,n'\tilde{C}'_\tau)})_{\sigma}^{(C_\chi)}|(I^{(A_{2u})^{\Omega_v}} \otimes [C^{(L_g)} \otimes P^{(\{i\},L'_\nu)}]^{(K'_\nu,\bar{n}\tilde{\bar{\Gamma}}_\nu)})^{(A_{1g})}|(\Psi^{(A_{2u})^{\nu_5}} \otimes \Psi^{(\mathcal{J}_\tau,n\tilde{C}_\tau)})_{\sigma}^{(C_\chi)}\rangle \\ &= \frac{1}{2}\sum_{L''}(-1)^{2\mathcal{J}'+2\tilde{C}'+K'+K_r+K_{ev}+L+L''+J+J'}[L'']\sqrt{[C][\mathcal{J}][\mathcal{J}'][K'][J_5][J'_5][K_{ev}][L']}\begin{Bmatrix} K_{ev\nu} & K_{rg} & L'_\nu \\ L_g & K'_\nu & L''_g \end{Bmatrix} \times \begin{Bmatrix} 3/2_g & l_{5\tau} & J_{5\tau} \\ K_{eg} & K_{\nu\nu} & K_{ev\nu} \\ 3/2_g & l'_{5\tau'} & J'_{5\tau'} \end{Bmatrix} \\ &\times \begin{Bmatrix} J_g & J_{5\tau} & \mathcal{J}_\tau \\ L_g & K_{ev\nu} & K'_\nu \\ J'_g & J'_{5\tau'} & \mathcal{J}'_{\tau'} \end{Bmatrix}\begin{Bmatrix} (A_{2u})^{\Omega_v} & (A_{2u})^{\nu_5} & (A_{2u})^{\nu'_5} \\ \tilde{\bar{\Gamma}}_\nu & \tilde{C}_\tau & \tilde{C}'_{\tau'} \\ A_{1g} & C_\chi & C_\chi \end{Bmatrix}\langle\Psi^{(A_{2u})^{\nu'_5}}\|I^{(A_{2u})^{\Omega_v}}\|\Psi^{(A_{2u})^{\nu_5}}\rangle \times \langle\Psi_{\nu'_5}^{(I'_{5\tau})}\|\epsilon V_{\{5\}\{5\}}^{K_1\mu K_2\chi(K_{\nu\nu})}\|\Psi_{\nu_5}^{(I_{5\tau})}\rangle \\ &\times \langle\Phi^{(3/2_g)}\|E^{\Omega_e(K_{eg})}\|\Phi^{(3/2_g)}\rangle\langle\Psi_r^{(J'_g)}\|C^{(L_g)}\|\Psi_r^{(J_g)}\rangle K \begin{pmatrix} K'_\nu & \mathcal{J}_\tau & \mathcal{J}'_{\tau'} \\ \bar{n}\tilde{\bar{\Gamma}}_\nu & n\tilde{C}_\tau & n'\tilde{C}'_{\tau'} \end{pmatrix} \\ &\times \left[\begin{Bmatrix} L_g & K_{rg} & L''_g \\ J_g & J'_g & J_g \end{Bmatrix}\langle\Psi^{(J_g)}\|R^{\Omega_r(K_{rg})}\|\Psi^{(J_g)}\rangle + (-1)^{L+K_r+L''}\begin{Bmatrix} K_{rg} & L_g & L''_g \\ J_g & J'_g & J'_g \end{Bmatrix}\langle\Psi_r^{(J'_g)}\|R^{\Omega_r(K_{rg})}\|\Psi_r^{(J'_g)}\rangle\right].\end{aligned} \quad [51]$$

TABLE 3
Rovibronic Selection Rules in *SU*(2)

	$\tilde{H}$	$\tilde{\alpha}^{(A_1)}$	$\tilde{\alpha}^{(E,F_2)}$
$\triangle J$	0	0	$0, \pm 1, \pm 2$
$\triangle M$	0	0	$0, \pm 1, \pm 2$
$\triangle l_5$	$0, \pm 1, ..., \pm K_v$	$0, \pm 1, ..., \pm K_v$	$0, \pm 1, ..., \pm K_v$
$\triangle J_5$	$0, \pm 1, ..., \pm K_{ev}$	$0, \pm 1, ..., \pm K_{ev}$	$0, \pm 1, ..., \pm K_{ev}$
$\triangle \mathcal{J}$	$0, \pm 1, ..., \pm K$	$0, \pm 1, ..., \pm K'$	$0, \pm 1, ..., \pm K'$
$\tau \otimes \tau'$	g	ν	ν

We set here

$$\langle \Psi^{(A_{2u})v_5'} \| I^{(A_{2u})\Omega_v} \| \Psi^{(A_{2u})v_5} \rangle = (-i)^{\Omega_v} \delta_{v_5', v_5 \pm \Omega_v} \qquad [52]$$

in order to make matrices real since K factors with $\tilde{\tilde{\Gamma}} = A_2$ are imaginary.

The selection rules (Table 3) come from the nonzero condition of the matrix elements of Hamiltonian and polarizability operators in the rovibronic basis. We define the order of the development by

$$\Omega_t = \Omega_v + \Omega_r + \Omega_e - k, \qquad [53]$$

with $k_2 = 2$ for the Hamiltonian and $k = 1$ for the polarizability.[2] We have listed rovibronic operators up to order 2 for the Hamiltonian and polarizability in Table 4.

5. EFFECTIVE ROVIBRONIC MODEL IN $SU(2) \otimes C_I \supset O_h^S$ FOR THE $\nu_3(F_{1u})$ STRETCHING MODE

As we pointed out in paragraph 2, the Hamiltonian for the ν_3 mode does not possess linear vibronic coupling terms in a G' electronic state. However, other couplings (quadratic, etc.) are allowed, as shown for instance, in Ref. (*12*). Many years ago, McDowell and Asprey (*28*) noted a strange structure in the infrared spectrum of ReF_6 for the ν_3 fundamental. They attributed this feature to a quadratic vibronic coupling that splits the $v_3 = 1$ level into four sublevels according to:

$$F_{1u} \otimes G_g' = E_{1u}' \oplus E_{2u}' \oplus 2G_u'. \qquad [54]$$

For such a fundamental, one can expect to have a more complex rotational contour than that of a "normal" molecule (such as SF_6 for instance). This has been confirmed recently at high resolution by Boudon *et al.* (*17*).

[2] To restore the correct symmetry, the tensorial extension relation [10] is taken into account for the polarizability.

As previously, Boudon *et al.* have proposed writing $H(\nu_3)$ still considering the natural subduction $\mathcal{D}^{(1u)} \downarrow O_h = F_{1u}$. So we have

$$H(\nu_3) = H_0 + H_{\mathrm{JTQ}}^{(0_g, A_{1g})} + H_{\mathrm{JTQ}}^{(4_g, A_{1g})}, \qquad [55]$$

with

$$\begin{cases} H_0 = \hbar\omega_3(N_3 + 3/2), \\ H_{\mathrm{JTQ}}^{(0_g, A_{1g})} = 2\sqrt{6}\,\hbar\omega_3 Q_0 (Q_3^{2(2g)} \otimes T^{(2g)})^{(0_g, A_{1g})}, \\ H_{\mathrm{JTQ}}^{(4_g, A_{1g})} = 2\sqrt{6}\,\hbar\omega_3 Q_4 (Q_3^{2(2g)} \otimes T^{(2g)})^{(4_g, A_{1g})}. \end{cases} \qquad [56]$$

We have set $Q_3^{2(2g)} = (Q_3^{(1u)} \otimes Q_3^{(1u)})^{(2g)}$. Q_0 and Q_4 are the quadratic Jahn–Teller parameters. Again, this writing leads to infinite matrices. In the next paragraph, we will use the same method as before to write an effective Hamiltonian with finite matrices.

5.1. *Effective Vibronic Hamiltonian in $SU(2) \otimes C_I \supset O_h^S$*

In this paragraph, we want just to try to relate the two vibronic models.

Let us consider the effective vibronic angular momentum (*12*)

$$\mathbf{J}_3 = \mathbf{l}_3 + \mathbf{J}', \qquad [57]$$

which allows us to label the vibronic levels ($\mathbf{l}_3$ being the vibrational angular momentum).

As previously for ν_5, we are going to relate the effective vibronic parameters of our model in $SU(2) \otimes C_I \supset O_h^S$ and the quadratic parameters (Q_0, Q_4) defined in the same way as in Eq. [12] (see Ref. (*12*)). Operators and wavefunctions are still coupled in $SU(2) \otimes C_I$ and oriented with respect to O_h^S through the unitary transformation [32].

So, the effective Hamiltonian is written as

$$\tilde{H} = \sum_{\text{all indexes}} \tilde{t}_{\{3\}\{3\}}^{\Omega_e K_{1\mu} K_{2\mu}, K_{vg}(K_{evg}, n_0 A_{1g})} \times \zeta (E^{\Omega_e(K_{eg})} \otimes {}^{\epsilon} V_{\{3\}\{3\}}^{K_{1\mu} K_{2\mu}(K_{vg})})^{(K_{evg}, n_0 A_{1g})}, \qquad [58]$$

with the $\mathcal{D}^{(K_{evg})} \downarrow O^S \supset n_0 A_{1g}$ condition. ζ is a numerical factor defined previously for ν_5. Therefore, $\tilde{H}$ is no more invariant under $O(3)$ but only under O_h.

The matrix elements are calculated in the coupled basis

$$|(\Phi^{(3/2_g)} \otimes \Psi_{v_3}^{(l_{3\tau})})_{\sigma}^{(J_{3\tau}, nC_\tau)}\rangle, \qquad [59]$$

where $\Phi^{(3/2_g)}$ is the electronic wavefunction associated with a fourfold degenerate state and n_0 is the multiplicity index. Thus, the matrix elements are

TABLE 4
Effective Parameters for the ν_5 Mode

Hamiltonian						Polarizability				
Parameter $\tilde{t}^{(\{i\},K_g,n_0A_{1g})}_{\{5\}\{5\}}$						Parameter $\tilde{\alpha}^{(\{i\},L'_\nu,n_0\tilde{\Gamma}_\nu\Gamma_g)}_{\{5\}\{5\}}$				
Level	Order	$\Omega_r(K_r)$	$\Omega_e(K_e)$	K_v	K	Transition	Order	$\Omega_r(K_r)$	$\Omega_e(K_e)$	$K_v, K_{ev}(L')$
Ground state	0	2(0)	0(0)	0	0	ν_5	0	0(0)	0(0)	1, 1(1)
$(K_1 = K_2 = 0)$	0	1(1)	1(1)	0	0	$(K_1 = 1, K_2 = 0)$	1	1(1)	0(0)	1, 1(1)
	2	4(0)	0(0)	0	0		1	1(1)	0(0)	1, 1(2)
	2	4(4)	0(0)	0	4		1	0(0)	1(1)	1, 1(1)
	2	3(1)	1(1)	0	0		1	0(0)	1(1)	1, 1(2)
	2	3(3)	1(1)	0	4		2	2(0)	0(0)	1, 1(1)
	2	2(2)	2(2)	0	0		2	2(2)	0(0)	1, 1(1)
	2	2(2)	2(2)	0	4		2	2(2)	0(0)	1, 1(2)
	2	1(1)	3(3)	0	4		2	2(2)	0(0)	1, 1(3)
$v_5 = 1$	0	0(0)	0(0)	0	0		2	1(1)	1(1)	1,0(1)
$(K_1 = K_2 = 1)$	1	1(1)	0(0)	1	0		2	1(1)	1(1)	1,1(1)
	1	0(0)	1(1)	1	0		2	1(1)	1(1)	1,1(2)
	2	2(0)	0(0)	0	0		2	1(1)	1(1)	1,2(1)
	2	2(2)	0(0)	2	0		2	1(1)	1(1)	1,2(2)
	2	2(2)	0(0)	2	4		2	1(1)	1(1)	1,2(3)
	2	1(1)	1(1)	0	0		2	0(0)	2(2)	1,1(1)
	2	1(1)	1(1)	2	0		2	0(0)	2(2)	1,2(2)
	2	1(1)	1(1)	2	4		2	0(0)	2(2)	1,3(3)
	2	0(0)	2(2)	2	0					
	2	0(0)	2(2)	2	4					

$$\langle(\Phi^{(3/2_g)}\otimes\Psi_{v_3}^{(l'_{3\tau})})_{\sigma}^{(J'_{3\tau},n'C_\tau)}|(E^{\Omega_e(K_{eg})}\otimes\epsilon V_{\{3\}\{3\}}^{K_{1\mu}K_{2\mu}(K_{vg})})^{(K_{evg},n_0A_{1g})}|(\Phi^{(3/2)}\otimes\Psi_{v_3}^{(l_{3\tau})})_{\sigma}^{(J_{3\tau},nC_\tau)}\rangle$$
$$= (-1)^{2C+2J'_3}\left(\frac{[K_{ev}][J_3][J'_3]}{[C]}\right)^{1/2} K\begin{pmatrix}(K_{evg} & J_{3\tau} & J'_{3\tau})\\ (n_0A_{1g} & nC_\tau & n'C_\tau)\end{pmatrix}\begin{Bmatrix} l_{3\tau} & 3/2_g & J_{3\tau}\\ K_{eg} & K_{vg} & K_{evg}\\ l'_{3\tau} & 3/2_g & J'_{3\tau}\end{Bmatrix} \quad [60]$$
$$\times\langle\Psi_{v_3}^{(l'_{3\tau})}\|\epsilon V_{\{3\}\{3\}}^{K_{1\mu}K_{2\mu}(K_{vg})}\|\Psi_{v_3}^{(l_{3\tau})}\rangle\langle\Phi^{(3/2_g)}\|E^{\Omega_e(K_{eg})}\|\Phi^{(3/2_g)}\rangle.$$

Table 5 is the list of the independent vibronic parameters for $v_3 = 1$ ($K_1 = K_2 = 1$) and up to order 3. To relate this model to that described by Eq. [56], we should first note that we have here five parameters for only four levels (Eq. [54]). So, one parameter, say $\tilde{t}_5$, has to be fixed to a chosen value. Figure 4 shows parameters $\tilde{t}_1$ to $\tilde{t}_4$ as a function of $\tilde{t}_5$ (in the domain where all parameters are real) obtained by equaling the eigenvalues of both models and with $\nu_3 = 719.3\ \text{cm}^{-1}$, $Q_0 = 0.006$, $Q_4 = -0.008$. These values were estimated in Ref. (*17*) from the general aspect of the ν_3 band of ReF_6 at 300 K. Values for $\tilde{t}_1$ to $\tilde{t}_4$ in this case are given in Table 5 for $\tilde{t}_5$ fixed to -1. These parameters might be used in a next step to assign the ν_3 band of ReF_6 rovibronic spectra. The $(\mathbf{J}'\,\mathbf{l}_3)$ term corresponding to the $\tilde{t}_2$ parameter is actually responsible for the splitting of $v_3 = 1$ into vibronic sublevels. This leads to a partial degeneracy lifting of the 12-fold degenerate $v_3 = 1$ level. Thus, one can describe this term as "pseudo-Coriolis" coupling.

TABLE 5
Effective Vibronic Parameters for the Hamiltonian

Level	$\Omega_e(K_e)$	$\Omega_v(K_v)$	K_{ev}	Order		Value/cm^{-1} (see text)
$v_3 = 1$	0(0)	2(0)	0	0	$\tilde{t}_1$	719.2778
	1(1)	2(1)	0	1	$\tilde{t}_2$	-0.3902
	2(2)	2(2)	0	2	$\tilde{t}_3$	-2.5735
	2(2)	2(2)	4	2	$\tilde{t}_4$	1.0326
	3(3)	2(1)	4	3	$\tilde{t}_5$	-1

5.2. Rovibronic Hamiltonian in SU(2) ⊗ C_I ⊃ O_h^S

As previously, a rovibronic effective Hamiltonian $\tilde{H} = THT^{-1}$ (T being a unitary transformation) is developed as a series of rovibronic operators

$$\tilde{H} = \sum_{\text{all indexes}} \tilde{t}^{(\{i\},K_g,n_0A_{1g})}_{\{3\}\{3\}}\eta\times T^{(\{i\},K_g,n_0A_{1g})}_{\{3\}\{3\}}, \quad [61]$$

where η is a numerical factor defined in [35].

The required coupled rovibronic basis is constructed in the same way as those used for the ν_5 study; thus using the Wigner–Eckart theorem, the matrix elements are given by:

$$\langle(\Psi_r^{(J_g)}\otimes(\Phi^{(3/2_g)}\otimes\Psi_{v_3}^{(l'_{3\tau'})})^{(J'_{3\tau'})})_\sigma^{(\mathcal{J}_\tau,n'C_{\tau'})}|T^{([i],K_g,n_0A_{1g})}_{\{3\}\{3\}}|(\Psi_r^{(J_g)}\otimes(\Phi^{(3/2_g)}\otimes\Psi_{v_3}^{(l_{3\tau})})^{(J_{3\tau})})_\sigma^{(\mathcal{J}_\tau,nC_\tau)}\rangle$$

$$= (-1)^{2C+2\mathcal{J}'}[C]^{-1/2}\sqrt{[K][K_{ev}][J_3][J'_3][\mathcal{J}][\mathcal{J}']}\times\begin{Bmatrix}J_g & J_{3\tau} & \mathcal{J}_\tau\\ K_{rg} & K_{evg} & K_g\\ J'_g & J'_{3\tau'} & \mathcal{J}'_{\tau'}\end{Bmatrix}\begin{Bmatrix}3/2_g & l_{3\tau} & J_{3\tau}\\ K_{eg} & K_{vg} & K_{evg}\\ 3/2_g & l'_{3\tau'} & J'_{3\tau'}\end{Bmatrix} \quad [62]$$

$$\times K\begin{pmatrix}K_g & \mathcal{J}_\tau & \mathcal{J}'_{\tau'}\\ n_0A_{1g} & nC_\tau & n'C_{\tau'}\end{pmatrix}\langle\Psi_{v_3}^{(l'_{3\tau'})}\|\epsilon V^{K_1\mu K_2\mu(K_{vg})}_{\{3\}\{3\}}\|\Psi_{v_3}^{(l_{3\tau})}\rangle\langle\Phi^{(3/2_g)}\|E^{\Omega_e(K_{eg})}\|\Phi^{(3/2_g)}\rangle\langle\Psi_r^{(J_g)}\|R^{\Omega_r(K_{rg})}\|\Psi_r^{(J_g)}\rangle.$$

We note here that this model is formally identical to that for ν_3 (Eq. [37]). The "initial" (untransformed) Hamiltonian being different (there is no linear Jahn–Teller effect for ν_3), the difference resides in the unitary transformation T relating the initial and effective Hamiltonian. However, this transformation being not a usual contact (perturbative) transformation, it is not possible to express it explicitly.

5.3. *Effective Dipole Moment Operators for Rovibronic Transitions*

The ν_3 band is only active in absorption, so in this part, we present a systematic approach to construct the dipole moment operators and to calculate the intensities for a given rovibronic polyad.

5.3.1. Definition. One can relate the dipole moment components μ_θ in the MFF to those (μ_Θ) in the LFF through

$$\mu_\Theta = \sum_\theta \lambda_{\Theta\theta}\mu_\theta, \quad [63]$$

and each component μ_θ can be developed as power series in the dimensionless normal coordinates

$$\mu_\theta = \mu_\theta^e + \sum_{s,\sigma}\left(\frac{\partial\mu_\theta}{\partial q_{s\sigma}}\right)q_{s\sigma} + \frac{1}{2}\sum_{s,s',\sigma\sigma'}\left(\frac{\partial^2\mu_\theta}{\partial q_{s\sigma}q_{s'\sigma'}}\right)q_{s\sigma}q_{s'\sigma'} + \cdots, \quad [64]$$

where μ_θ^e is the permanent dipole moment (if it exists). The other terms are induced by molecular vibration.

5.3.2. Tensorial extension. Through the relation [32], we can link Cartesian tensor to spherical tensor by

$$\mu_\theta = \sum_{k,K_{ev}}\langle K_{ev};\, k|\theta\rangle\mu_k^{(K_{ev})}, \quad [65]$$

$$\mu_\Theta = \sum_{m,K_{ev}}\langle K_{ev};\, m|\Theta\rangle\mu_m^{(K_{ev})}, \quad [66]$$

where $\langle K_{ev};\, k|\theta\rangle$ and $\langle K_{ev};\, m|\Theta\rangle$ are Stone coefficients calculated in Ref. (*27*).

Each component of a transition moment operator in the MFF is written as a sum of vibronic operators. Therefore, the tensor components oriented in O_h have the form

$$\mu_\sigma^{(F_{1u})} = \sum_{\text{all indexes}}\mu^{([i],K_{evu},n_0F_{1u})}_{\{3\}\{3\}}M_\sigma^{([i],K_{evu},n_0F_{1u})} = \sum_{\text{all indexes}}\mu^{([i],K_{evu},n_0F_{1u})}_{\{3\}\{3\}} \times (E^{\Omega_e(K_{eg})}\otimes\epsilon V^{K_1\chi K_2\tilde{\pi},(K_{vu})}_{\{3\}\{3\}})^{(K_{evu},n_0F_{1u})}. \quad [67]$$

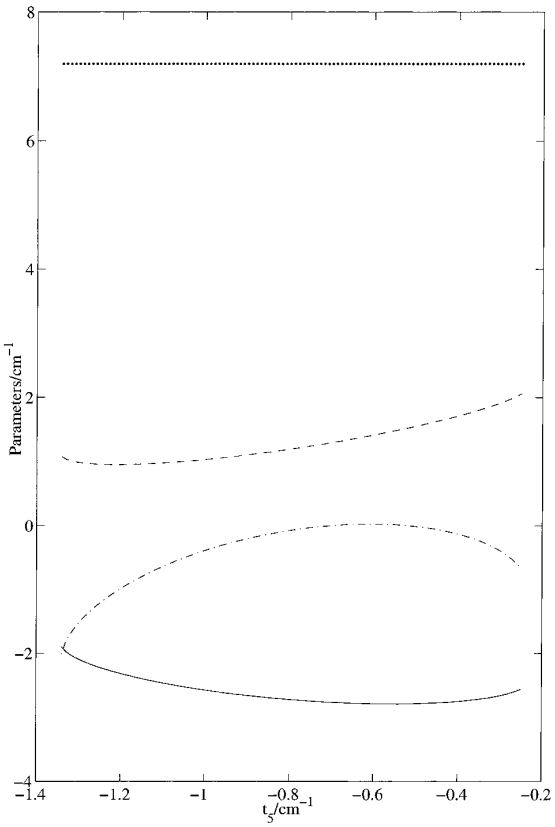

FIG. 4. Vibronic parameter $\tilde{t}_1/100$ (dotted line), $\tilde{t}_2$ (dash-dotted line), $\tilde{t}_3$ (solid line), and $\tilde{t}_4$ (dashed line) as a function of $\tilde{t}_5$ for $Q_0 = 0.008$ and $Q_4 = -0.006$.

TABLE 6
Selection Rules in $SU(2) \otimes C_I$

	$\tilde{H}$	$\tilde{\mu}$
$\triangle J$	0	$0, \pm 1$
$\triangle M$	0	$0, \pm 1$
$\triangle l_3$	$0, \pm 1, ..., \pm K_v$	$0, \pm 1, ..., \pm K_v$
$\triangle J_3$	$0, \pm 1, ..., \pm K_{ev}$	$0, \pm 1, ..., \pm K_{ev}$
$\triangle \mathcal{J}$	$0, \pm 1, ..., \pm K$	$0, \pm 1, ..., \pm K'$
$\tau' \otimes \tau$	g	u

The eigenfunctions of the transformed effective Hamiltonian are related to the initial eigenfunctions by a unitary transformation T. Thus, the effective dipole moment has to be transformed as

$$\tilde{\mu}_\theta = T\mu_\theta T^{-1}. \qquad [68]$$

Just as for the polarizability, the transformed dipole moment

$$\tilde{\mu}_\sigma^{(F_{1u})} = \sum_{\text{all indexes}} \tilde{\mu}_{\{3\}\{3\}}^{(\{i\},L'_u,n_0F_{1u})} M_\sigma^{(\{i\},L'_u,n_0F_{1u})} \qquad [69]$$

is expanded as a series of rovibronic operators.

The development of the transformed components in the LFF is deduced from [63] and [66], giving

$$\tilde{\mu}_\Theta = \sqrt{3} \sum_{L',K',\rho,m,\{i\}} [K']^{1/2}(-1)^{K'} \langle L', m|\Theta\rangle \times {}^{(L'_u)}G_m^{n_0F_{1u}\rho} \tilde{\mu}_{\{3\}\{3\}}^{(\{i\},L'_u,n_0F_{1u})} K \begin{pmatrix} 1_g & L'_u & K'_u \\ (0F_{1g} & n_0F_{1u} & n'_0A_{1u}) \end{pmatrix} \times [C^{(1_g)} \otimes M^{(\{i\},L'_u)}]^{(K'_u,n'_0A_{1u})}, \qquad [70]$$

where $C^{(1_g)}$ are the tensor director cosines. Contrary to polarizability tensor, $\tilde{\mu}_\Theta$ is not invariant under the inversion operation.

5.3.3. Intensity: Selection rules. The strength of a vibration–rotation–electronic transition between two transformed rovibronic states is given by

$$S_{if} = K_{if} g_i e^{-(hcE_i/kT)} \sum_{M_i,M_f} |\langle \tilde{\Phi}_i|\tilde{\mu}_Z|\tilde{\Phi}_f\rangle|^2, \qquad [71]$$

where K_{if} is a numerical factor which depends on the frequency and the temperature and g_i is the spin statistic weight of the $\tilde{\Phi}_i$ state:

$$\langle [\Psi_r^{(J'_g)} \otimes [\Phi^{(3/2_g)} \otimes \Psi_{v'_3}^{(l'_{3\tau'})}]^{(J'_{3\tau'})}]_\sigma^{(\mathcal{J}_{\tau'},n'C_{\tau'})} | [C^{(1_g)} \otimes M^{(\{i\},L'_u,n_0F_{1u})}]^{(K'_u,n'_0A_{1u})} | [\Psi_r^{(J_g)} \otimes [\Phi^{(3/2_g)} \otimes \Psi_{v_3}^{(l_{3\tau})}]^{(J_{3\tau})}]_\sigma^{(\mathcal{J}_\tau,n'C_\tau)} \rangle$$
$$= \frac{1}{2} \sum_{L''} (-1)^{2\mathcal{J}'+2C+K'+K_r+L'+1+L''+J+J'} [C]^{-1/2} [L''] \sqrt{[\mathcal{J}][\mathcal{J}'][K'][J_3][J'_3][K_{ev}][L']} \begin{Bmatrix} 1_g & K_{rg} & L''_g \\ K_{evu} & K'_u & L'_u \end{Bmatrix}$$
$$\times \begin{Bmatrix} 3/2_g & l_{3\tau} & J_{3\tau} \\ K_{eg} & K_{vu} & L'_u \\ 3/2_g & l'_{3\tau'} & J'_{3\tau'} \end{Bmatrix} \begin{Bmatrix} J_g & J_{3\tau} & \mathcal{J}_\tau \\ L''_g & L'_u & K'_u \\ J'_g & J'_{3\tau'} & \mathcal{J}'_{\tau'} \end{Bmatrix} K \begin{pmatrix} K'_u & \mathcal{J}_\tau & \mathcal{J}'_{\tau'} \\ (n'_0A_{1u} & nC_\tau & n'C_{\tau'}) \end{pmatrix} \times \langle \Psi_{v'_3}^{(l'_{3\tau'})} \| \epsilon V_{\{3\}\{3\}}^{K_1\chi K_2\tilde{\chi}(K_{vu})} \| \Psi_{v_3}^{(l_{3\tau})} \rangle \langle \Phi^{(3/2_g)} \| E^{\Omega_e(K_{eg})} \| \Phi^{(3/2_g)} \rangle$$
$$\times \langle \Psi_r^{(J'_g)} \| C^{(1_g)} \| \Psi_r^{(J_g)} \rangle \times \left[\begin{Bmatrix} 1_g & K_{rg} & L''_g \\ J_g & J'_g & J_g \end{Bmatrix} \langle \Psi^{(J_g)} \| R^{\Omega_r(K_{rg})} \| \Psi^{(J_g)} \rangle + (-1)^{1+K_r+L''} \begin{Bmatrix} K_{rg} & 1_g & L''_g \\ J_g & J'_g & J'_g \end{Bmatrix} \langle \Psi_r^{(J'_g)} \| R^{\Omega_r(K_{rg})} \| \Psi_r^{(J'_g)} \rangle \right]. \qquad [72]$$

The selection rules (Table 6) come from the nonzero condition of the matrix elements of Hamiltonian and dipole moment operators in the rovibronic basis.

In Table 7, we have listed the rovibronic operators up to order for the Hamiltonian and dipole moment. We find four purely vibronic parameters for $v_3 = 1$ for the Hamiltonian (see Table 5).

6. CONCLUSION

We have developed a tensorial formalism (operators and matrix elements) by extending preceding works about molecules in a non-degenerate electronic state to XY_6 molecules (especially colored hexafluorides) in a degenerate electronic state. Our purely tensorial study has been carried out considering an extension of $O(3)$ ($\supset O_h$) to $SU(2) \otimes C_I$ ($\supset O_h^S$) in order to take into account half-integer angular momenta. We have introduced new electronic tensor operators in order to avoid the problem of infinite matrices. These operators have allowed us to construct for the first time a rovibronic Hamiltonian as well as transition moment operators for rovibronic transitions. This has been expanded for the triply degenerate vibrational states $\nu_3(F_{1u})$ and $\nu_5(F_{2g})$ in the case of a fourfold degenerate electronic state. We have determined values of the new vibronic parameters from previous works.

TABLE 7
Effective Parameters for the ν_3 Mode

Hamiltonian						Dipole moment				
Parameter $\tilde{t}^{(\{i\},K_g,n_0A_{1g})}_{\{3\}\{3\}}$						Parameter $\tilde{\mu}^{(\{i\},L'_u,n_0F_{1u})}_{\{3\}\{3\}}$				
Level	Order	$\Omega_r(K_r)$	$\Omega_e(K_e)$	K_v	K	Transition	Order	$\Omega_r(K_r)$	$\Omega_e(K_e)$	$K_v, K_{ev}(L')$
Ground state	0	2(0)	0(0)	0	0	ν_3	0	0(0)	0(0)	1, 1(1)
$(K_1 = K_2 = 0)$	0	1(1)	1(1)	0	0	$(K_1 = 1, K_2 = 0)$	1	1(1)	0(0)	1, 1(1)
	2	4(0)	0(0)	0	0		1	0(0)	1(1)	1, 1(1)
	2	4(4)	0(0)	0	4		2	2(0)	0(0)	1, 1(1)
	2	3(1)	1(1)	0	0		2	2(2)	0(0)	1, 1(1)
	2	3(3)	1(1)	0	4		2	2(2)	0(0)	1, 1(3)
	2	2(2)	2(2)	0	0		2	1(1)	1(1)	1, 0(1)
	2	2(2)	2(2)	0	4		2	1(1)	1(1)	1, 1(1)
	2	1(1)	3(3)	0	4		2	1(1)	1(1)	1, 1(3)
$v_3 = 1$	0	0(0)	0(0)	0	0		2	1(1)	1(1)	1, 2(1)
$(K_1 = K_2 = 1)$	1	1(1)	0(0)	1	0		2	1(1)	1(1)	1, 2(3)
	1	0(0)	1(1)	1	0		2	0(0)	2(2)	1, 1(1)
	2	2(0)	0(0)	0	0		2	0(0)	2(2)	1, 1(3)
	2	2(2)	0(0)	2	0					
	2	2(2)	0(0)	2	4					
	2	1(1)	1(1)	0	0					
	2	1(1)	1(1)	2	0					
	2	1(1)	1(1)	2	4					
	2	0(0)	2(2)	2	0					
	2	0(0)	2(2)	2	4					

Now that this qualitative study is done, we intend

- to apply this formalism to the ν_3 high-resolution rovibronic absorption spectrum of ReF_6 (*17*),
- to extend this formalism to other groups (spherical-top molecules (T_d^S), symmetric-top molecules (C_{3v}^S), etc.) by constructing operators and matrix elements,
- to generalize this study to the case of transitions between two different electronic states.

APPENDIX A

Subduction $SU(2) \otimes C_I \supset O_h^S$

j integer	$\mathcal{D}^{(j)} \downarrow O_h$	j half integer	$\mathcal{D}^{(j)} \downarrow O_h^S$
0	A_1	1/2	E'_1
1	F_1	3/2	G'
2	$E + F_2$	5/2	$E'_2 + G'$
3	$A_2 + F_1 + F_2$	7/2	$E'_1 + E'_2 + G'$
4	$A_1 + E + F_1 + F_2$	9/2	$E'_1 + 2G'$
5	$E + 2F_1 + F_2$	11/2	$E'_1 + E'_2 + 2G'$
6	$A_1 + A_2 + E + F_1 + 2F_2$	$6+j'$	$E'_1 + E'_2 + 2G' + (j',\ E'_1 \leftrightarrow E'_2)$
7	$A_2 + E + 2F_1 + 2F_2$	$12k + j'$	$2k(E'_1 + E'_2 + 2G') + (j')$
8	$A_1 + 2E + 2F_1 + 2F_2$		
9	$A_1 + A_2 + E + 3F_1 + 2F_2$		
10	$A_1 + A_2 + 2E + 2F_1 + 3F_2$		
11	$A_2 + 2E + 3F_1 + 3F_2$		
$12p + q$	$p(A_1 + A_2 + 2E + 3F_1 + 3F_2) + (q)$		

$SU(2) \otimes C_I$–O_h^S Connection

$$(A^{(j_{1\tau})} \otimes B^{(j_{2v})})^{(j_\chi)}_{nC_\chi\sigma} = (-1)^{\varphi(j)+2C}\left(\frac{[j]}{[C]}\right)^{1/2} \sum_{n_1C_1,n_2C_2,\beta_0} \beta_0 K \begin{pmatrix} n_1C_{1\tau} & n_2C_{2v} & nC_\chi \\ j_{1\tau} & j_{2v} & j_\chi \end{pmatrix} \times (A^{(j_{1\tau},n_1C_{1\tau})} \otimes B^{(j_{2v},n_2C_{2v})})^{(\beta_0C_\chi)}_\sigma. \quad [A.1]$$

APPENDIX B

Wigner–Eckart Theorem in $SU(2)$

$$\langle \gamma' j' m' | T^{(k_0)}_{m_0} | \gamma j m \rangle = [j']^{-1/2} F \begin{pmatrix} k_0 & j & m' \\ m_0 & m & (j') \end{pmatrix} \langle \gamma' j' \| T^{(k_0)} \| \gamma j \rangle. \quad [B.1]$$

APPENDIX C

Reduced Matrix Elements in $SU(2) \otimes C_I$

Electronic Operators

$$\langle j_g \| E^{\Omega_e(K_{eg})} \| j_g \rangle = \left[-\frac{4j(j+1)}{\sqrt{3}} \right]^{(\Omega_e - K_e)/2} \times \left[\frac{K_e!(2j+K_e+1)!}{(2K_e-1)!!(2j-K_e)!} \right]^{1/2}. \quad [C.1]$$

Direction Cosine Tensors

$$\langle J'_g \| C^{(L_g)} \| J_g \rangle = (-1)^{L+J-M} ([J][J'])^{1/2} \begin{pmatrix} J_g & L_g & J'_g \\ -M & M_L & M' \end{pmatrix}, \quad [C.2]$$

where $(\cdots)$ is a $3-J$ symbol.

The $Q_s^{(1_u)}$ Tensor

We recall that

$$Q_s^{(1_u)} = \frac{1}{\sqrt{2}} (A_s^{(1_u)} + A_s^{+(1_u)}), \quad [C.3]$$

with $s = 3$ or 5. Thus,

$$\langle v_s + 1, (l_s + 1)_{\tau'} \| A_s^{+(1_u)} \| v_s, l_{s\tau} \rangle = -[(l_s+1)(v_s+l_s+3)]^{1/2}, \quad [C.4]$$

$$\langle v_s + 1, (l_s - 1)_{\tau'} \| A_s^{+(1_u)} \| v_s, l_{s\tau} \rangle = [l_s(v_s - l_s + 2)]^{1/2}, \quad [C.5]$$

$$\langle v_s - 1, (l_s + 1)_{\tau'} \| A_s^{(1_u)} \| v_s, l_{s\tau} \rangle = -[(l_s+1)(v_s - l_s)]^{1/2}, \quad [C.6]$$

$$\langle v_s - 1, (l_s - 1)_{\tau'} \| A_s^{(1_u)} \| v_s, l_{s\tau} \rangle = -[l_s(v_s + l_s + 1)]^{1/2}. \quad [C.7]$$

These formulas are used for the calculation of matrix elements of the vibrational operators V.

ACKNOWLEDGMENTS

Région Bourgogne is gratefully acknowledged for supporting the Laboratoire de Physique de l'Université de Bourgogne.

REFERENCES

1. B. Weinstock, *Adv. Chem. Phys.* **9,** 169–319 (1965).
2. V. Boudon, PhD thesis, Dijon, France, 1995.
3. J. C. D. Brand, G. L. Goodman, and B. Weinstock, *J. Mol. Spectrosc.* **37,** 436–437 (1960).
4. H. H. Claassen and H. Selig, *Israel J. Chem.* **7,** 499–504 (1969).
5. V. Boudon, M. Rotger, and D. Avignant, *J. Mol. Spectrosc.* **175,** 327–339 (1996).
6. M. Rotger, V. Boudon, and H. Selig, *Spectrosc. Acta, Part A* **55,** 1575–1584 (1999).
7. O. Acef, Ch. J. Bordé, A. Clairon, G. Pierre, and B. Sartakov, *J. Mol. Spectrosc.* **199,** 188–204 (2000).
8. V. Boudon, M. Hepp, M. Herman, and I. Pak, *J. Mol. Spectrosc.* **192,** 359–367 (1998).
9. R. Englman, "The Jahn–Teller Effect in the Molecules and Crystals," Wiley, New York, 1972.
10. M. S. Child and H. C. Longuet-Higgins, *Philos. Trans. Roy. Soc. London Ser. A* **254,** 259–294 (1961).
11. V. Boudon and F. Michelot, *J. Mol. Spectrosc.* **165,** 554–579 (1994).
12. V. Boudon, F. Michelot, and J. Moret-Bailly, *J. Mol. Spectrosc.* **166,** 449–470 (1994).
13. J. Moret-Bailly, *Cah. Phys.* **15,** 237–314 (1961).
14. J. P. Champion, *Can. J. Phys.* **15,** 1802–1828 (1977).
15. J. P. Champion, M. Loëte, and G. Pierre, "Spectroscopy of the Earth's Atmosphere and Interstellar Medium," pp. 339–422, Academic Press, San Diego, 1992.
16. N. Cheblal, V. Boudon, and M. Loëte, *J. Mol. Spectrosc.* **197,** 222–231 (1999).
17. V. Boudon, M. Rotger, Y. He, U. Schmitt, H. Hollenstein, and M. Quack, unpublished manuscript.
18. M. S. Child, *J. Mol. Spectrosc.* **10,** 357–365 (1963).
19. W. Moffit and W. Thorson, *Phys. Rev.* **168,** 362–369 (1968).
20. B. R. Judd, *J. Chem. Phys.* **67,** 1174–1179 (1977).
21. W. Moffit and W. Thorson, *Phys. Rev.* **108,** 1251–1255 (1957).
22. H. A. Jahn and E. Teller, *Proc. Roy. Soc. London Ser. A* **161,** 220–225 (1937).
23. J. K. G. Watson, *J. Mol. Spectrosc.* **50,** 281–285 (1974).
24. F. Michelot and T. Schwartzmann, *Mol. Phys.* **80,** 1269–1296 (1993).
25. E. R. Bernstein and J. D. Webb, *Mol. Phys.* **36,** 1113–1118 (1978).
26. J. Stone, *Mol. Phys.* **29,** 1461–1471 (1975).
27. E. Pascaud and G. Poussigue, *Can. J. Phys.* **56,** 1577–1593 (1978).
28. R. S. McDowell and L. B. Asprey, *J. Mol. Spectrosc.* **45,** 491–493 (1973).

ELSEVIER

Journal of Molecular Structure 599 (2001) 125–137

Journal of
MOLECULAR
STRUCTURE

www.elsevier.com/locate/molstruc

Tensorial development of the rovibronic Hamiltonian and transition moment operators for octahedral molecules ☆

Michaël Rey*, Vincent Boudon, Michel Loëte

Laboratoire de Physique de l'Université de Bourgogne — CNRS UMR 5027, B.P. 47870, F-21078 Dijon cedex, France

Received 6 July 2000; accepted 27 September 2000

Abstract

We present a development of the Hamiltonian, dipole moment and polarizability operators of octahedral XY_6 molecules in a degenerate electronic state. These rovibronic operators are written with the aid of a tensorial formalism derived from the one already used in Dijon in the case of molecules in a non-degenerate electronic state. Electronic operators are defined from the group theory properties. Transition moment operators are introduced in order to consider rovibronic transitions. Spectrum simulations are made thanks to a new version of the HTDS sofware [J. Quant. Spectrosc. Radiat. Transfer 66 (2000) 16] used for the calculation of rovibrational spectra. © 2001 Elsevier Science B.V. All rights reserved.

Keywords: Tensorial formalism; Rovibronic operators; HTDS sofware

1. Introduction

The theory of rovibrational spectra for XY_4 molecules [1–3] and more recently for XY_6 molecules [4] in a non-degenerate electronic state (CH_4, SiH_4, SF_6, WF_6, ...) is well-established. However, some molecules such as transition–metal fluorides (ReF_6, IrF_6, OsF_6, ...) possess an incomplete electronic subshell so that their electronic states can be degenerate. This particular electronic structure can be compared to that of molecular ions or free radicals, i.e. of unstable species which are difficult to handle but also of significant interest in many domains such as chemical reactions, atmospheric and interstellar studies, etc. Moreover, these kind of hexafluoride molecules are good candidates for studying many complex interactions such as vibronic (Jahn–Teller effect [5–8], etc.) or rovibronic couplings. Their spectra show low energy electronic transitions occuring in the visible or near infrared region [9]. Jahn and Teller [5] remarked that electronic and nuclear motions can be coupled together and Weinstock and Goodman [9] have noted that each time there is an electronic degeneracy, then some qualitative evidence for a Jahn–Teller effect appear. In particular, certain abnormalities observed in the spectrum of rhenium hexafluoride have been assigned to this effect. All this leads in very particular spectra [10–13] compared to those of 'classical' hexafluorides [14,15].

Our motivation comes mainly from the fact that there still exists a very few theorical studies of these molecules. Until now, there existed only some low resolution spectra, but recently the first high resolution rovibronic absorption spectra for these kind of

☆ This paper is dedicated to Professor Alfred Bauder in appreciation of his significant contributions to the field of microwave spectroscopy.

* Corresponding author.
E-mail address: michael.rey@u-bourgogne.fr (M. Rey).

PII: S0022-2860(01)00841-9

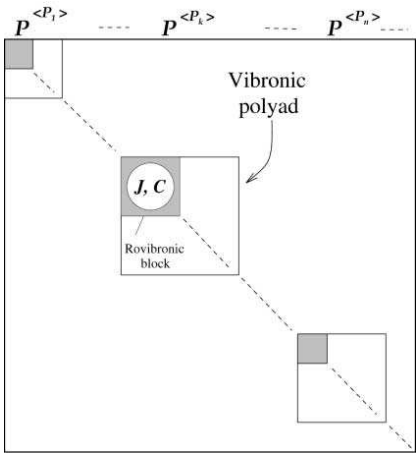

Fig. 1. Matricial representation of the effective rovibronic Hamiltonian.

molecules appeared for ReF_6 [16]. So, a complete model (operators and matrix elements) for the study and prediction of rovibronic transitions is necessary to analyse these rovibronic spectra. In a previous issue [17], we have derived a theoretical model suitable for the triply degenerate vibrational modes $\nu_3(F_{1u})$ and $\nu_5(F_{2g})$ in a degenerate electronic state G'_g. The particular symmetry of these modes has allowed to couple all operators and wavefunctions in the $SU(2) \otimes C_I$ chain. However, this model cannot be generalized easily to other vibrational modes.

The aim of the present paper is to provide a tensorial development that is valid for all vibrational modes in a given degenerate electronic state except those of symmetry E. This development will follow the same general principles as works about XY_6 molecules and more recently about XY_5Z molecules [18,19] in a non-degenerate electronic state. The usual $O(3) \supset O_h$ chain used for the 'classical' XY_6 molecules has been extended to the full chain $SU(2) \otimes C_I \supset O_h^S$ so that integer or half-integer electronic states can be considered [20]. Section 2 recalls briefly basic principles about the theory (Hamiltonian and transition moment operators). In Section 3, we construct an electronic operator set associated with a degenerate electronic state. The rovibronic Hamiltonian as well as the transition moment operators for (ro)vibronic transitions are thus defined. Finally, we present a program suite based on the HTDS software [21] in order to calculate rovibronic spectra. A full treatment in the O_h^S group is made.

2. Basic principles

The aim of this section is to recall briefly the theory of the Hamiltonian and the transition moments (dipole moment and polarizability) for octahedral molecules.

2.1. Contact transformations

In all quantum mechanical problems, it is more easy to work with operators having a completely diagonal or block diagonal form in an appropriate basis function set. This one is found by applying successive contact transformations to these operators. If $\mathscr{A}$ represents the Hamiltonian or a transition moment operator, then the transformed operators $\tilde{A}$ express themselves as

$$\tilde{A} = e^{iS} A e^{iS}, \tag{1}$$

where S is a sum of Hermitian operators invariant under the point group operations and called the generator of the contact transformation. Let us note that S contains some rotational operators of odd degrees in J_α (rotational angular momentum components) and also that this unitary transformation is not necessarily perturbative, thus the transformed operator $\tilde{A}$ cannot always be expanded as a converging series [17].

We can now define an effective rovibronic Hamiltonian for a given vibronic polyad (or group of vibronic levels) by

$$\tilde{\mathscr{H}}^{\langle polyad\rangle} = \mathscr{P}^{\langle polyad\rangle} \underbrace{e^{iS} H e^{-iS}}_{\tilde{H}} \mathscr{P}^{\langle polyad\rangle}, \tag{2}$$

$\mathscr{P}^{\langle polyad\rangle}$ being the projector operator on the considered vibronic Hilbert subspace.

The effective Hamiltonian for a given polyad P_n can be written as a sum of Hamiltonian contributions

$$\tilde{H}^{\langle P_n\rangle} = \tilde{H}^{\langle P_n\rangle}_{\langle GS\rangle} + \tilde{H}^{\langle P_n\rangle}_{\langle P_1\rangle} + \cdots + \tilde{H}^{\langle P_n\rangle}_{\langle P_{n-1}\rangle} + \tilde{H}^{\langle P_n\rangle}_{\langle P_n\rangle}. \tag{3}$$

As shown in Fig. 1, the contribution of the P_n polyad necessarily contains those of lower polyads.

2.2. Dipole moment

The molecular vibration changes the electronic density and induces an electric dipole moment. One can relate the dipole moment components μ_θ ($\theta = x,y,z$) in the molecule-fixed frame (MFF) to those (μ_Θ, $\Theta = X,Y,Z$) in the laboratory-fixed frame (LFF) through the relation

$$\mu_\Theta = \sum_\theta \lambda_{\Theta\theta}\mu_\theta, \tag{4}$$

where $\lambda_{\Theta\theta}$ are the direction cosines. Each component μ_θ can be developed as power series in the dimensionless normal coordinates

$$\mu_\theta = \mu_\theta^e + \sum_{s,\sigma}\left(\frac{\partial\mu_\theta}{\partial q_{s\sigma}}\right)q_{s\sigma} + \frac{1}{2}\sum_{s,s',\sigma\sigma'}\left(\frac{\partial^2\mu_\theta}{\partial q_{s\sigma}q_{s'\sigma'}}\right)q_{s\sigma}q_{s'\sigma'} + \cdots, \tag{5}$$

where μ_θ^e is the permanent dipole moment (if it exists). The other terms are induced by molecular vibration.

From Eq. (1) and to satisfy the Hermiticity condition, the LFF components of the transformed dipole moment are written in the form [22]

$$\tilde{\mu}_\Theta = \frac{1}{2}\sum_\theta(\lambda_{\Theta\theta}\tilde{\mu}_\theta + \tilde{\mu}_\theta\lambda_{\Theta\theta}), \tag{6}$$

where μ_Θ and $\tilde{\mu}_\Theta$ are linked together through the same contact transformation as in Eq. (2).

2.3. Polarizability operator

With the application of an electric field **E**, each molecule develops an induced dipole moment **μ** whose components are written as

$$\mu_{\Theta_1} = \sum_{\Theta_2}\boldsymbol{\alpha}_{\Theta_1\Theta_2}E_{\Theta_2}. \tag{7}$$

The $\boldsymbol{\alpha}_{\Theta_1\Theta_2}$ tensor (called polarizability tensor) is responsible for Rayleigh and Raman scattering.

The $\boldsymbol{\alpha}_{\Theta_1\Theta_2}$ LFF components ($\Theta_1, \Theta_2 = X,Y,Z$) are related to the $\boldsymbol{\alpha}_{\theta_1\theta_2}$ MFF ones ($\theta_1, \theta_2 = x,y,z$) through

$$\boldsymbol{\alpha}_{\Theta_1\Theta_2} = \sum_{\theta_1\theta_2}\lambda_{\Theta_1\theta_2}\lambda_{\Theta_1\theta_2}\alpha_{\theta_1\theta_2}. \tag{8}$$

$\alpha_{\theta_1\theta_2}$ can be expanded as a power series of normal coordinates

$$\alpha_{\theta_1\theta_2} = \alpha^e_{\theta_1\theta_2} + \sum_{s,\sigma}\left(\frac{\partial\alpha_{\theta_1\theta_2}}{\partial q_{s\sigma}}\right)q_{s\sigma} + \frac{1}{2}\sum_{s,s',\sigma\sigma'}\left(\frac{\partial^2\alpha_{\theta_1\theta_2}}{\partial q_{s\sigma}q_{s'\sigma'}}\right)q_{s\sigma}q_{s'\sigma'} + \cdots, \tag{9}$$

$\alpha^e_{\theta_1\theta_2}$ being the permanent polarizability (if it exists).

Just as for the dipole moment, the LFF components of the transformed polarizability are given by [4]

$$\tilde{\alpha}_{\Theta_1\Theta_2} = \frac{1}{2}\sum_{\theta_1\theta_2}(\lambda_{\Theta_1\theta_2}\lambda_{\Theta_1\theta_2}\tilde{\alpha}_{\theta_1\theta_2} + \tilde{\alpha}_{\theta_1\theta_2}\lambda_{\Theta_1\theta_2}\lambda_{\Theta_1\theta_2}). \tag{10}$$

3. Tensorial formalism for octahedral molecules

In this section, we present a systematic approach to construct a rovibronic Hamiltonian as well as the transition moments for a given degenerate electronic state. First, we will give a few details about symmetry conditions for single and double-valued states and about the construction of electronic operators.

3.1. Symmetry conditions

It is useful to do some recalls about the symmetry condition for a rovibronic level of species C in the O^S group [20]. O^S represents the octahedral group O with its spinorial representations, i.e. if the rovibronic basis (oriented with respect to the $SU(2) \supset O^S$ chain) is labeled $|J,nC\sigma\rangle$ (n being a multiplicity index) thus

representations C with **J** integer are single-valued (vectorial),
representations C with **J** half-integer are double-valued (spinorial).

A particular application concerns the symmetry conditions for a degenerate electronic state. Let us design first by Γ_e the symmetry of a electronic operator $^{\epsilon_e}\mathcal{O}^{(\Gamma_e)}$, $\epsilon_e = +$ or $-$ is the symmetry under the time-reversal operation. So, the electronic matrix elements (for a given electronic state with symmetry C_e)

$$\langle J_c, n_c C_c \sigma_c | {}^{\epsilon_e}\mathcal{O}^{(\Gamma_e)} | J'_e, n'_e C_e \sigma'_e \rangle$$

Table 1
Expression of the electronic coefficients (the δ are Kronecker's symbols)

	$[^{(K_{eg})}E^{(\Gamma_{eg})}]^{\alpha_1\ldots\alpha_{K_e}}_{\sigma_e}$
$[^{(0_g)}E^{(A_{1g})}]$	1
$[^{(1_g)}E^{(F_{1g})}]^{\alpha}_{\sigma_1}$	$2\delta_{\alpha,\sigma_1}$
$[^{(2_g)}E^{(E_g)}]^{\alpha_1\alpha_2}_{\sigma_2}$	$4F^{F_{1g}\alpha_1F_{1g}\alpha_2(2_g)}_{(1_g1_g)E_g\sigma_2}\delta_{\alpha_1,\alpha_2}$
$[^{(2_g)}E^{(F_{2g})}]^{\alpha_1\alpha_2}_{\sigma_3}$	$4F^{F_{1g}\alpha_1F_{1g}\alpha_2(2_g)}_{(1_g1_g)F_{2g}\sigma_2}$
$[^{(3_g)}E^{(\Gamma_e)}]^{\alpha_1\alpha_2\alpha_3}_{\sigma_e}$	$8F^{F_{1g}\alpha_1F_{1g}\alpha_2(2_g)}_{(1_g1_g)\gamma_2}F^{\gamma_2F_{1g}\alpha_3(3_g)}_{(2_g1_g)\Gamma_e\sigma_e}$

vanish if the following rules are not respected [23]:

- If C_e is single-valued and $\epsilon_e = +$ (resp. $-$), then Γ_e must belong to the representation $[C_e \times C_e]$ (resp. $\{C_e \times C_e\}$).
- If C_e is double-valued and $\epsilon_e = +$ (resp. $-$), then Γ_e must belong to the representation $\{C_e \times C_e\}$ (resp. $[C_e \times C_e]$).

Here, [ ] (resp. { }) is the symmetric (resp. antisymmetric) part of the product $C_e \times C_e$.

This is the expression of the Jahn–Teller theorem [5,23]. In our case, the O^S group possesses five single-valued (vectorial) representations named A_1, A_2, E, F_1 and F_2 and three double-valued (spinorial) representations named E'_1, E'_2 and G' (of dimension two, two and four, respectively). The different possible cases are given below

$$\begin{cases} A_1 \times A_1 = A_2 \times A_2 = [A_1], \\ E \times E = [A_1 + E] + \{A_2\}, \\ F_1 \times F_1 = F_2 \times F_2 = [A_1 + E + F_2] + \{F_1\}, \\ E'_1 \times E'_1 = E'_2 \times E'_2 = [F_1] + \{A_1\}, \\ G' \times G' = [A_2 + 2F_1 + F_2] + \{A_1 + E + F_2\}. \end{cases} \tag{11}$$

3.2. Electronic tensor operators: generalities

As shown in Ref. [17], we define electronic operators in the same way as rotational operators introduced previously by Moret-Bailly [1]. All possible operators $E^{\Omega_e(K_{eg})}$ in $O(3)$ are constructed by successive couplings of the basic tensor

$$\mathbf{E}^{1(1_g)}_{\alpha} = 2J_{e\alpha} \qquad (\alpha = x, y, z). \tag{12}$$

The electronic angular momentum J_e is obtained by symmetry considerations (see next paragraph). Initially, such electronic operators have been introduced to construct an effective theoretical model in order to get rid of infinite matrices which could appear in the initial vibronic problem (i.e. the untransformed vibronic Hamiltonian) [12]. As we have mentioned in Ref. [17], only operators with

$$\Omega_e = K_e \leq 2J_e \tag{13}$$

are independent. This result comes from the fact that we stay in a given electronic state (i.e. with a fixed J_e value).

A complete set of independent electronic tensors is thus given by

$$\mathbf{E}^{K_e(K_{eg})} = (\mathbf{E}^{K_e-1((K_e-1)_g)} \otimes \mathbf{E}^{1(1_g)})^{(K_{eg})}. \tag{14}$$

Symmetry adapted tensors are deduced from the G orientation matrices [20] through

$$\mathbf{E}^{K_e(K_{eg}n_e\Gamma_{eg})}_{\sigma_e} = \sum_{m_e} {}^{(K_{eg})}G^{m_e}_{n_e\Gamma_{eg}\sigma_e}\mathbf{E}^{K_e(K_{eg})}_{m_e}, \tag{15}$$

where n_e is a multiplicity index distinguishing redundant symmetries.

However, it is also useful to express these operators in terms of the different components of the electronic angular momentum $J_{e\alpha}$ $(\alpha = x, y, z)$. This can be achieved through the stretched tensor product

$$\mathbf{E}^{K_e(K_{eg})}_{p_e} = ((\mathbf{E}^{1(1_g)}_{p_1} \times \mathbf{E}^{1(1_g)}_{p_2})^{(2_g)}_{p_{12}} \times \cdots \times \mathbf{E}^{1(1_g)}_{p_m})^{(K_{eg})}_{p_e}, \tag{16}$$

where the p_i correspond to the triplet $(n_i\Gamma_i\sigma_i)$.

In the case of spherical top molecules, the subduction $\mathbf{E}^{1(1_g)}_{p_e} = \mathbf{E}^{1(1_g)}_{F_1\alpha} = 2J_{e\alpha}$ allows us to write Eq. (16) as

$$E^{K_e(K_{eg})}_{p_e} = F^{p_1p_2(2_g)}_{(1_g1_g)p_{12}}F^{p_{12}p_3(3_g)}_{(2_g,1_g)p_{123}}\ldots F^{p_{1\ldots n-1}p_n(K_{eg})}_{((K_e-1)_g1_g)p_e} \times (2)^{K_e}J_{e\alpha_1}J_{e\alpha_2}\ldots J_{e\alpha_{K_e}}, \tag{17}$$

with $p_j = F_1\alpha_j$ $(j = 1,\ldots n)$. The F symbols are the Clebsch–Gordan coefficients oriented in $O(3) \supset O_h$ [24].

Finally, expression (17) can be written in the

notation of Ref. [25] as

$$\mathbf{E}_{\sigma_e}^{K_e(K_{eg},n_e\Gamma_{eg})} = [^{(K_{eg})}\mathbf{E}^{(n_e\Gamma_{eg})}]_{\sigma_e}^{\alpha_1\ldots\alpha_{K_e}} J_{e\alpha_1}J_{e\alpha_2}\ldots J_{e\alpha_{K_e}}, \quad (18)$$

where the $[^{(K_{eg})}\mathbf{E}^{(n_e\Gamma_{eg})}]_{\sigma_e}^{\alpha_1\ldots\alpha_{K_e}}$ coefficients will be calculated in the following (see Table 1).

We have also (see Section 3.1)

$$\epsilon_e = (-1)^{\Omega_e} = (-1)^{K_e}. \quad (19)$$

3.3. Application to a degenerate electronic state

In this part, we define general electronic operators thanks to the symmetry of the electronic state $C_{e\chi}$ ($\chi = g$ or u). However, let us note that the E_χ integer twofold degenerate states will not be dealt with here. This is due to the fact that no angular momentum can be associated to this symmetry in a simple way. This special case will be treated in a forthcoming paper.

3.3.1. Non-degenerate state

No problem appears here since

$$A_{1\chi} = A_{1g} \times A_{1\chi}, \qquad A_{2\chi} = A_{1g} \times A_{2\chi}, \quad (20)$$

and we have the natural subduction $\mathscr{D}^{(0_g)} \downarrow O_h^S = A_{1g}$. Consequently, only the operator

$$E^{0(0_g,A_{1g})} = I \quad (21)$$

is present. No rovibronic coupling appears in this case and we have a usual rovibrational problem.

3.3.2. Triply degenerate state

As mentioned previously [25], any triply degenerate state $\Phi^{(C_{e\chi})}$ for an XY_6 molecule can be treated as an F_{1u} state through the relations

$$F_{1\chi} = F_{1u} \times A_{\overline{\chi}} \qquad (\chi = g,u;\ \overline{\chi} = u \times \chi = u,g),$$

$$F_{2\chi} = F_{1u} \times A_{2\overline{\chi}}. \quad (22)$$

Under this consideration, it is straightfoward to associate with each state an effective angular momentum $\mathbf{J}_e$ with $J_e = 1$.

We recall that the redution $SO(3) \supset O$ is

$$\mathscr{D}^{(0)} \supset A_1, \qquad \mathscr{D}^{(1)} \supset F_1, \qquad \mathscr{D}^{(2)} \supset E + F_2, \quad (23)$$

Thus, noticing that $J_e \times J_e = [0+2] + \{1\}$, the allowed values for K_e are $K_e = 0,1,2$ and the electronic operators are

$$\mathbf{E}^{0(0_g,A_{1g})} = 1, \qquad \mathbf{E}_{\sigma_1}^{1(1_g,F_{1g})} = [^{(1_g)}\mathbf{E}^{(F_{1g})}]_{\sigma 1}^{\alpha} J_{e\alpha_1},$$

$$\mathbf{E}_{\sigma_2}^{2(2_g,E_g)} = [^{(2_g)}E^{(E_g)}]_{\sigma_2}^{\alpha_1\alpha_2} J_{e\alpha_1}J_{e\alpha_2}, \quad (24)$$

$$\mathbf{E}_{\sigma_3}^{2(2_g,F_{2g})} = [^{(2_g)}\mathbf{E}^{(F_{2g})}]_{\sigma_3}^{\alpha_1\alpha_2} J_{e\alpha_1}J_{e\alpha_2},$$

with $\sigma_1, \sigma_3, \alpha, \alpha_1, \alpha_2 = x, y$ or z and $\sigma_2 = 1$ or 2.

3.3.3. Half-integer doubly degenerate state

Half-integer (spinorial) irreps $E'_{1\chi}$ and $E'_{2\chi}$ are twofold degenerate in the O_h^S group. Just as for the triply degenerate state, we can merge the study of E'_1 and E'_2 into only one according to

$$E'_{1\chi} = E'_{1g} \times A_{1\chi}, \qquad E'_{2\chi} = E'_{1g} \times A_{2\chi}. \quad (25)$$

As pointed out in Ref. [20], $\mathscr{D}^{(1/2)}$ is irreductible in O^S and its characters are those of E'_1, so we can associate the E'_1 state with an angular momentum $\mathbf{J}_e$ with $J_e = 1/2$. From the fact that $(1/2) \times (1/2) = [1] + \{0\}$, the only possible electronic operators are

$$\mathbf{E}^{0(0g,A_{1g})} = I \quad \text{and} \quad \mathbf{E}_{\sigma_1}^{1(1_g,F_{1g})}. \quad (26)$$

In that case, the only vibronic contribution to the untransformed Hamiltonian is proportional to $J_{e\alpha}^{(F_{1g})} q_{s\alpha}^{(F_{1g})}$ which is not allowed for octahedral XY_6 molecules (there are no vibrational modes with the symmetry F_{1g}) and thus there is no Jahn-Teller effect. This result is coherent with the fact that E'_1 and E'_2 states are *Kramers doublet* [26] whose degeneracy is a spin degeneracy that cannot be removed by electrostatic forces such as Jahn–Teller ones.

3.3.4. Fourfold degenerate state

In that case, a fourfold degenerate state is denoted by the symmetry G'_χ in O_h^S with

$$G'_\chi = G'_g \times A_{1\chi}. \quad (27)$$

As for E'_1 and considering the natural subduction $\mathscr{D}^{(3/2)} \downarrow O^S = G'$, we can define an effective electronic momentum $\mathbf{J}_e$ with $J_e = 3/2$. If we make the product $3/2 \times 3/2 = [1+3] + \{0+2\}$, it appears that only electronic operators with $K_e = 0,1,2,3$ are allowed,

i.e.

$$\mathbf{E}^{0(0_g,A_{1g})},\ \mathbf{E}_{\sigma_1}^{1(1_g,F_{1g})},\ \mathbf{E}_{\sigma_2}^{2(2_g,E_g)},\ \mathbf{E}_{\sigma_3}^{2(2_g,F_{2g})},\ \text{and}\ \mathbf{E}_{\sigma_e}^{3(3_g,\Gamma_e)} = [^{(3_g)}\mathbf{E}^{(\Gamma_e)}]_{\sigma_e}^{\alpha_1\alpha_2\alpha_3} J_{e\alpha_1} J_{e\alpha_2} J_{e\alpha_3}, \tag{28}$$

with

$$\mathscr{D}^{(3)} \supset \Gamma_e = A_2 + F_1 + F_2. \tag{29}$$

In the following, we will omit the n_e index since it is always equal to 0 (no multiplicity). The electronic coefficients $[^{(K_{eg})}\mathbf{E}^{(\Gamma_{eg})}]_{\sigma_e}^{\alpha_1\ldots\alpha_{K_e}}$ defined in Eq. (18) are given in Table 1.

Let us well note that the product $G'_\chi \times G'_\chi$ has multiplicities for the F_{1g} and F_{2g} symmetries which will be denoted by the β index. Ref. [20] labels these ones by

$$\begin{cases} \beta = 1 \text{ and } 3 \text{ if } F_1 \subset [G' \times G'], \\ \beta = s \text{ (resp. } a) \text{ if } F_2 \subset [G' \times G'] \text{ (resp.}\{G' \times G'\}). \end{cases} \tag{30}$$

This is the main difference with the O_h group. Because of these multiplicity labels, recoupling coefficients $(6C, 9C, \ldots)$ of O_h^S are more difficult to handle than those of O_h.

3.4. Expression of the effective rovibronic Hamiltonian

At this stage, we can construct a formal rovibronic Hamiltonian by extending works about XY_6 molecules in a non-degenerate electronic state (rovibrational studies [13] to the case of molecules in a degenerate electronic state. Vibrational (V), rotational (R) and electronic (E) operators and wavefunctions are thus coupled in $O(3) \supset O_h$ or $SU(2) \otimes C_I \supset O_h^S$ so that half-integer states are taken into account when necessary (see Section 3.3).

Starting from the untransformed Hamiltonian H, we define a transformed rovibronic Hamiltonian $\tilde{H}$ which is a function of rotational, electronic and vibrational variables by applying the unitary transformation (1)

$$\begin{aligned} H &= H(J_\alpha, J_{e\beta}, q_{s\sigma}, p_{s\sigma}) \\ &\quad \downarrow e^{iS} \\ \tilde{H} &= \tilde{H}(J_\alpha, J_{e\beta}, q_{s\sigma}, p_{s\sigma}) \end{aligned} \tag{31}$$

The untransformed and effective Hamiltonians are linked here together through a unitary transformation which is a priori a non-perturbative transformation, impossible to express explicitely.

The expansion of vibrational operators is given by [3]

$$\epsilon V_{\{n_s\}\{m_s\}}^{\Gamma_{1\mu}\Gamma_{2\mu}(\Gamma_{vg})} = \frac{1}{N} e^{i\phi}\left(\left(A_{\{n_s\}}^{+(\Gamma_{1\mu})} \otimes A_{\{m_s\}}^{(\Gamma_{2\mu})}\right)^{(\Gamma_{vg})} + \epsilon(-1)^{\Gamma_1+\Gamma_2+\Gamma_v}\left(A_{\{m_s\}}^{+(\Gamma_{2\mu})} \otimes A_{\{n_s\}}^{(\Gamma_{1\mu})}\right)^{(\Gamma_{vg})}\right) \tag{32}$$

where the tensors $\mathbf{A}^+$ and $\mathbf{A}$ are built from elementary operators of creation $a_{s\sigma}^+$ and annihilation $a_{s\sigma}$ (the σ's are the components of the degenerate vibration s). The complete Hamiltonian is a Hermitian operator which must be totally symmetric in O_h, so we obtain all possible rovibronic operators by coupling systematically E, V, R operators in the O_h group in the following way:

$$T_{\{n_s\}\{m_s\}}^{\Omega_r(K_{rg},n_{0r},\Gamma_{evg})(K_{eg},\Gamma_{eg})\Gamma_{1\mu}\Gamma_{2\mu}(\Gamma_{vg})} = (R^{\Omega_r(K_{rg},n_{0r},\Gamma_{evg})} \otimes (\mathbf{E}^{K_e(K_{eg},\Gamma_{eg})} \otimes \epsilon V_{\{n_s\}\{m_s\}}^{\Gamma_{1\mu}\Gamma_{2\mu}(\Gamma_{vg})})^{(\Gamma_{evg})})^{(A_{1g})}. \tag{33}$$

The transformed effective rovibronic Hamiltonian is expressed as a linear combination of rovibronic operators (33)

$$\tilde{H} = \sum_{\text{all indexes}} \tilde{t}_{\{n_s\}\{m_s\}}^{(\{i\})} \eta T_{\{n_s\}\{m_s\}}^{(\{i\})}, \tag{34}$$

where $\{i\}$ summarizes all indexes. $\tilde{t}_{\{n_s\}\{m_s\}}^{(\{i\})}$ are the parameters. η is a numerical factor which allows coincidence between the standard and tensorial notations for scalar terms

$$\eta = [\Gamma_1]^{1/2}(-\sqrt{3}/4)^{(\Omega_r)/2}, \tag{35}$$

if $(K_{rg}, K_{eg}) = (0_g, 0_g)$ and $\eta = 1$ otherwise.

The Hamiltonian is invariant under time-reversal, thus the V, E and R operators must have the same parity in elementary momentum operators (J, p). This results in

$$\epsilon = (-1)^{\Omega_r + K_e}. \tag{36}$$

We have chosen to define the order of the rovibronic Hamiltonian development in the same way as for the rovibrational Hamiltonian [3] as we did in Ref.

Table 2
Expressions of the different phase factors

$\varphi(J_e)$	$\begin{cases} J_e \text{ if } J_e \text{ integer}, \\ 2J_e \text{ if } J_e \text{ half integer} \end{cases}$
$e^{i\Phi(\Gamma_e)}$	$\begin{cases} -i \text{ if } \Gamma_e = A_2 \text{ or } F_1, \\ 1 \text{ otherwise} \end{cases}$
$e^{i\Phi(\Gamma_e,C_e,\beta,\beta')}$	$\delta_{\beta,1}\delta_{\beta',1}$

[17]

$$\Omega = \Omega_v + \Omega_r + K_e - 2. \tag{37}$$

The calculation of matrix elements of irreducible tensor operators requires the use of the Wigner–Eckart theorem (WET) and of recoupling formulas in O_h^S which are given in Appendix B. In order to apply the WET, the basis must be constructed with the same coupling scheme as the operators (33). So we have

$$\left\| \left[\Psi_r^{(J_g,nC_{rg})} \otimes \left[\Phi_e^{(J_{eg},C_{e\chi})} \otimes \Psi_{v,I_\tau}^{(C_{v\tau})} \right]^{(C_{ev\tau})} \right]_\sigma^{(C_\tau)} \right\rangle, \tag{38}$$

where

$$\left| \Phi_e^{(J_{eg},C_{e\chi})} \right\rangle = \left| \Phi_e^{(J_{eg},\tilde{C}_{eg})} \right\rangle |I^{(A)}\rangle. \tag{39}$$

In Eqs. (38) and (39) J_e and J are both integer (resp. half integer) angular momentum quantum numbers, if the number of electrons is even (resp. odd).

We have also

$$\mathcal{D}^{(J_{eg})} \downarrow O_h^S = \tilde{C}_{eg} \qquad \text{and} \qquad \tilde{C}_{eg} = A \times C_{e\chi} \tag{40}$$

with

$$A = \begin{cases} A_{1\chi} \text{ if } C_{e\chi} = A_{1\chi}, F_{1\chi}, E'_{1\chi} \text{ or } G'_\chi, \\ A_{2\chi} \text{ if } C_{e\chi} = A_{2\chi}, F_{2\chi} \text{ or } E'_{2\chi}. \end{cases} \tag{41}$$

Each electronic operator is implicitly multiplied by the identity operator $I_e^{(A_{1g})}$ associated with the wavefunction $|I^{(A)}\rangle$.

So, the matrix elements of the Hamiltonian are

$$\left\langle \beta 2\beta 4 \left[\Psi_r^{(J_g,n'C'_{rg})} \otimes \left[\left[\Phi_e^{(J_{eg},C_{e\chi})} \otimes \Psi_{v',I'_{\tau'}}^{(C'_{v\tau'})} \right]^{(C'_{ev\tau'})} \right]_\sigma^{(C_{\tau'})} \right| \right.$$

$$\times T^{(\{i\},A_{1g})}_{\{n_s\}\{m_s\}} \times \left| \beta_1\beta_3 \left[\Psi_r^{(J_g,nC_{rg})} \right. \right.$$

$$\left. \left. \otimes \left[\Phi_e^{(J_{eg},C_{e\chi})} \otimes \Psi_{v,I_\tau}^{(C_{v\tau})} \right]^{(C_{ev\tau})} \right]_\sigma^{(C_\tau)} \right\rangle$$

$$= (-1)^{\varphi(J)+\varphi(J_e)}(-1)^{C_{ev}+C'_r+2C_e-C-\Gamma_{ev}}([C'_{ev}]$$

$$\times [C_{ev}])^{1/2} \sum_{\beta_r} \beta_r K \begin{pmatrix} K_{rg} & J_g & J_g \\ n_{0r}\Gamma_{evg} & nC_{rg} & n'C'_{rs} \end{pmatrix}$$

$$\times \sum_{\beta,\beta'\beta} {}^{\beta'}K \begin{pmatrix} K_{eg} & J_{eg} & J_{eg} \\ \Gamma_{eg} & \tilde{C}_{eg} & \tilde{C}_{eg} \end{pmatrix} \begin{Bmatrix} C_{rg} & C_{\bar{\tau}} & C_{ev\bar{\tau}} \\ C'_{ev\tau'} & \Gamma_{evg} & C'_{rg} \end{Bmatrix}_{\beta_r\beta_2\bar{\beta}\beta_1}$$

$$\times \begin{Bmatrix} \Gamma_{eg} & C_{e\chi} & C_{e\chi} \\ \Gamma_{vg} & C_{v\tau} & C'_{v\tau'} \\ \Gamma_{evg} & C_{ev\bar{\tau}} & C'_{ev\tau'} \end{Bmatrix}_{\beta 1\bar{\beta}1\beta_3\beta_4}$$

$$\times e^{\Psi(\Gamma_e,C_e,\beta,\beta')} \left\langle \Psi_{v',I'_{\tau'}}^{(C'_{v\tau'})} \right\| \epsilon V^{\Gamma_{1\mu}\Gamma_{2\mu}(\Gamma_{vg})}_{\{n_s\}\{m_s\}} \left|$$

$$\times \left| \Psi_{v,I_\tau}^{(C_{v\tau})} \right\rangle \langle J_{eg} \| E^{K_e(K_{eg})} \| J_{eg} \rangle \langle J_g \| R^{\Omega_r(K_{rg})} \| J_g \rangle. \tag{42}$$

The $(-1)^C$ phases as well as recoupling symbols ($6C$ and $9C$) are defined in Ref. [20].

We have set

$$e^{i\Psi(\Gamma_e,C_e,\beta,\beta')} = [C_e][\Gamma_e]^{1/2} \begin{Bmatrix} A_{1g} & A & A \\ \Gamma_{eg} & \tilde{C}_{eg} & \tilde{C}_{eg} \\ \Gamma_{eg} & C_{e\chi} & C'_{e\chi} \end{Bmatrix}_{1\beta'\beta 111}, \tag{43}$$

which is calculated in Table 2.

The reduced matrix element (RME) for the identity operator $I_e^{(A_{1g})}$ is

$$\left\langle I^{(A)} \right\| I_e^{(A_{1g})} \left\| I^{(A)} \right\rangle = F^{(A_{1g}A)}_{(A)} = 1, \tag{44}$$

and the electronic RME is given by

$$\langle J_{eg}|E^{K_e(K_{eg})}||J_{eg}\rangle = e^{i\Phi(\Gamma_e)}\left[\frac{K_e!(2j+K_e+1)!}{(2K_e-1)!!(2j-K_e)!}\right]^{1/2}, \quad (45)$$

where $e^{i\Phi(\Gamma_e)}$ is a phase factor given in Table 2.

3.5. Expression of the dipole moment

A development of a tensorial formalism in $SU(2) \otimes C_I \supset O_h^S$ is undertaken here for a degenerate electronic state in order to perform the calculation of (ro)vibronic transitions for absorption spectra.

According to Stone [27], we can link cartesian tensors to spherical tensors by

$$\mu_\theta = \sum_k \langle 1;k|\theta\rangle \mu_k^{(1)}, \quad (46)$$

$$\mu_\Theta = \sum_m \langle 1;m|\Theta\rangle \mu_m^{(1)}, \quad (47)$$

where $\langle 1;k|\theta\rangle$ and $\langle 1;m|\Theta\rangle$ are Stone coefficients.

Contrary to the case of non-degenerate electronic states, each component of the untransformed dipole moment in the (MFF) is written as a sum of *vibronic* operators

$$\mu_\theta^{(F_{1u})} = \sum_{\{i\}} \mu_{\{n_s\}\{m_s\}}^{(\{i\},F_{1u})} (E^{K_e(K_{eg},\Gamma_{eg})} \otimes \epsilon V_{\{n_s\}\{m_s\}}^{\Gamma_{1\mu}\Gamma_{2\bar{\mu}}(\Gamma_{vu})})^{(F_{1u})}, \quad (48)$$

where $\{i\}$ summarizes all indexes.

The eigenfunctions of the transformed effective Hamiltonian are related to the initial eigenfunctions by the unitary transformation e^{iS}. Thus, the effective dipole moment has to be transformed as

$$\tilde{\mu} = e^{iS}\mu\, e^{-iS}. \quad (49)$$

So, the transformed dipole moment

$$\tilde{\mu}_\theta^{(F_{1u})} = \sum_{\{i\}} \tilde{\mu}_{\{n_s\}\{m_s\}}^{(\{i\},F_{1u})} M_\theta^{(\{i\},F_{1u})} \quad (50)$$

is formed by a series of rovibronic operators

$$M^{(\{i\},F_{1u})} = M_{\{n_s\}\{m_s\}}^{\Omega_r(K_{rg},n_{0r}\Gamma_{rg})(K_{eg},\Gamma_{eg})\Gamma_{1\mu}\Gamma_{2\bar{\mu}}(\Gamma_{vg})(\Gamma_{evg})(F_{1u})}$$
$$= (R^{\Omega_r(K_{rg},n_{0r}\Gamma_{rg})} \otimes \left(E^{K_e(K_{eg},\Gamma_{eg})} \otimes \epsilon V_{\{n_s\}\{m_s\}}^{\Gamma_{1\mu}\Gamma_{2\bar{\mu}}(\Gamma_{vg})}\right)^{(\Gamma_{evg})})^{(F_{1u})}. \quad (51)$$

Using Eqs. (6) and (46), the transformed components in the (LFF) are expressed as

$$\tilde{\mu}_\Theta^{(A_{1u})} = \sqrt{3}\sum_m \langle 1,m|\Theta\rangle \sum_{\{i\}} \tilde{\mu}^{(\{i\},F_{1u})} [\mathbf{C}^{(F_{1g})} \otimes M^{(\{i\},F_{1u})}]^{(A_{1u})}, \quad (52)$$

where the $\mathbf{C}^{(F_{1g})}$ is the direction cosine tensor.

The square brackets indicate the use of a symmetrized tensor product (because C and R do not commute) defined as

$$[A^{(\Gamma_1)} \otimes B^{(\Gamma_2)}]^\Gamma = \tfrac{1}{2}((A^{(\Gamma_1)} \otimes B^{(\Gamma_2)})^{(\Gamma)} + (-1)^{\Gamma+\Gamma_1+\Gamma_2}(B^{(\Gamma_2)} \otimes A^{(\Gamma_1)})^{(\Gamma)}). \quad (53)$$

The strength of a vibration–rotation–electronic transition between two transformed rovibronic states is given by

$$S_{if} = K_{if} g_i e^{-(hcE_i/kT)} \sum_{M_i,M_f} |\langle \tilde{\Phi}_i|\tilde{\mu}_Z|\tilde{\Phi}_f\rangle|^2 \quad (54)$$

where K_{if} is a numerical factor which depends on the frequency and the temperature and g_i is the spin statistic weight of the $\tilde{\Phi}_i$ state (with energy E_i).

The expression of the matrix elements of the transformed dipole moment is given Appendix A.

3.6. Expression of the polarizability

A complete model (operators and matrix elements) is necessary for the prediction and the calculation of rovibronic Raman transition intensities.

The spherical and cartesian components are linked through

$$\alpha_{\theta_1\theta_2} = \sum_{L,k} \langle L;k|\theta_1\theta_2\rangle \alpha_k^{(L)}, \quad (55)$$

Table 3
Rovibronic selection rules for the Hamiltonian, dipole moment and polarizability operators

	$\tilde{H}$	$\tilde{\mu}$	$\tilde{\alpha}^{(0)}$	$\tilde{\alpha}^{(2)}$
ΔJ	0	0, ±1	0	0, ±1, ±2
ΔM	0	0, ±1	0	0, ±1, ±2
Symmetry	$C' = C$	$C' = C$	$C' = C$	$C' = C$
$\tau' \otimes \tau$	g	u	g	g
Components	$\sigma' = \sigma$	$\sigma' = \sigma$	$\sigma' = \sigma$	

$$\boldsymbol{\alpha}_{\Theta_1\Theta_2} = \sum_{L,m} \langle L; m|\Theta_1\,\Theta_2\rangle \alpha_m^{(L)}, \tag{56}$$

where $\langle L; k|\theta_1\,\theta_2\rangle$ and $\langle L; m|\Theta_1\,\Theta_2\rangle$ are Stone coefficients [27].

In the MFF, one writes

$$\alpha_\theta^{(L_g,\Gamma_g)} = \sum_{\{i\}} \alpha_{\{n_s\}\{m_s\}}^{(\{i\},\Gamma_g)} (E^{K_e(K_{eg},\Gamma_{eg})} \otimes {}^{\epsilon}V_{\{n_s\}\{m_s\}}^{\Gamma_{1\mu}\Gamma_{2\mu}(\Gamma_{vg})})^{(\Gamma_g)}, \tag{57}$$

where L_g is the rank in $O(3)$ and $\alpha_{\{n_s\}\{m_s\}}^{(\{i\},\Gamma_g)}$ are the parameters

$$\Gamma_g = A_{1g} \otimes E_g \otimes F_{2g} \Leftrightarrow L_g = 0_g, 2_g. \tag{58}$$

The $\tilde{\alpha}^{(0_g A_{1g})}$ tensor is the isotropic part and the $\tilde{\alpha}^{(2_g E_g \text{ or } F_{2g})}$ tensor corresponds to the anisotropic part.

It is necessary to consider an effective polarizability

$$\tilde{\alpha} = e^{iS} \alpha\, e^{-iS} \tag{59}$$

obtained by applying the same transformation e^{iS} as to the effective Hamiltonian. Thus the tensorial expression for the transformed polarizability is given by

$$\tilde{\alpha}_\theta^{(L_g,\Gamma_g)} = \sum_{\{i\}} \tilde{\alpha}_{\{n_s\}\{m_s\}}^{(\{i\},\Gamma_g)} P_\theta^{(\{i\},\Gamma_g)}, \tag{60}$$

Table 4
List of some hexafluorides with their electronic ground state symmetry

TcF_6	RuF_6	RhF_6	ReF_6	OsF_6	IrF_6	NpF_6	AmF_6
G_g'	F_{2g}	G_g'	G_g'	E_g	G_g'	E_{2u}'	G_u'

where $P_\theta^{(\{i\},\Gamma_g)}$ are rovibronic operators expressed as

$$P^{(\{i\},\Gamma_g)} = P_{\{n_s\}\{m_s\}}^{\Omega_r(K_{rg},n_{0r}\Gamma_{rg})(K_{eg},\Gamma_{eg})\Gamma_{1\mu}\Gamma_{2\mu}(\Gamma_{vg})(\Gamma_{evg})(\Gamma_g)}$$
$$= (R^{\Omega_r(K_{rg},n_{0r}\Gamma_{rg})} \otimes \left(E^{K_e(K_{eg},\Gamma_{eg})} \otimes {}^{\epsilon}V_{\{n_s\}\{m_s\}}^{\Gamma_{1\mu}\Gamma_{2\mu}(\Gamma_{vg})}\right)^{(\Gamma_{evg})})^{(\Gamma_g)}. \tag{61}$$

In the (LFF), we need to take into account the direction cosines tensor so we obtain the expression of the components of the polarizability

$$\tilde{\alpha}_{\Theta_1\Theta_2}^{(A_{1g})} = \sum_{L,\Gamma,m} [\Gamma]^{1/2} \langle L, m|\Theta_1, \Theta_2\rangle \sum_{\{i\}} \tilde{\alpha}_{\{n_s\}\{m_s\}}^{(\{i\},\Gamma_g)} [C^{(L_g,\Gamma_g)} \otimes P^{(\{i\},\Gamma_g)}]^{(A_{1g})}. \tag{62}$$

The Raman intensities between two rovibronic states are given by

$$I_{if} = R_{if} g_i\, e^{-(hcE_i/kT)} \sum_{M_i,M_f,\theta} \left|\left\langle \tilde{\Phi}_i \middle| \tilde{\alpha}_\theta^{(L_g,\Gamma_g)} \middle| \tilde{\Phi}_f \right\rangle\right|^2, \tag{63}$$

where R_{if} is a numerical factor which depends on the frequency and the temperature.

3.7. Selection rules

The order of the development for transition moments is defined as [17]

$$\Omega = \Omega_v + \Omega_r + K_e - 1. \tag{64}$$

The calculation of matrix elements (given in Appendix A) between two rovibronic basis function requires the use of the WET and leads to the selection rules given in Table 3.

4. Calculating rovibronic spectra

In this section, we present briefly programs necessary for calculating rovibronic spectra.

4.1. Presentation

Potential candidates for study such spectra are given in Table 4. Other potential molecules are given in Ref. [28].

The highly-spherical top data system (HTDS) software [21] for the calculation of rovibrational spectra of octahedral XY_6 molecules has been modified since

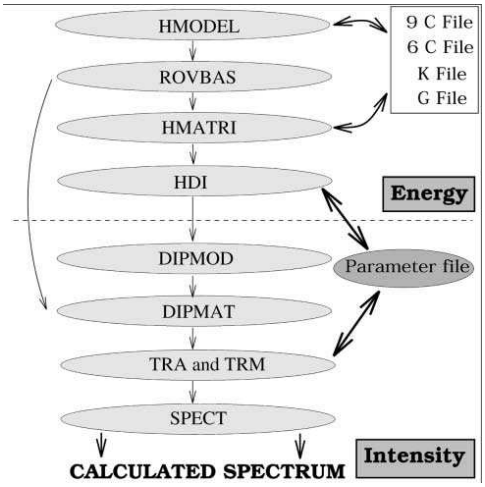

Fig. 2. Schematic description of the program chain leading to the calculated absorption spectrum. The Raman spectra are obtained by the substitution of DIPMOD (DIPMAT) to POLMOD (POLMAT).

it is only devoted to molecules in a non-degenerate electronic state. We have introduced the electronic operators (14) into this program chain.

Programs calculating rovibronic Raman spectra (ν_1, ν_2 and ν_5 bands) and rovibronic absorption spectra (ν_3 and ν_4 bands) for any kind of polyads are included. However, let us notice that molecules in a degenerate electronic state of symmetry E are not handled by these programs.

4.2. Description

The general structure of HTDS has not been modified. Modifications appear only inside programs with the adding of:

- electronic operators (14) with its associated eigenfunctions (39),
- half-integer represention E'_1, E'_2 and G' (multiplication table, etc.),
- recoupling coefficient files (6*C*, 9*C*) and *K*-factor files [20] (computation of rovibronic matrix elements),
- multiplicity indexes for eigenfunctions (see Section 3.3).

A schematic description of necessary programs for the calculation of spectra is given Fig. 2. This set of programs is available upon request to the authors.

For the energy part, the first program used is HMODEL. It lists rovibronic operators for a given polyad and development order. The vibronic reduced matrix elements are calculated too. Secondly, ROVBAS constructs the rovibronic basis until $J_{max} \leq 100$ and HMATRI calculates the matrix elements of rovibronic operators. Finally, HDI diagonalises the Hamiltonian matrix by using Hamiltonian parameters.

- For the intensity part, we have DIPMOD (resp. POLMOD) which gives a list of the operators of the dipole moment (resp. polarizability). Matrix elements of these operators are calculated by DIPMAT (resp. POLMAT). Programs TRA and TRM calculate the transition moments. Finally, SPECT calculates the line frequencies and intensities.

5. Conclusion

A tensorial formalism (operators and matrix elements) has been written by extending preceding works about XY_6 molecules in a non-degenerate electronic state to open-shell systems (especially colored hexafluorides) where the electronic states can be degenerate. We have considered an extension of $O(3) \supset O_h$ to $SU(2) \otimes C_I \supset O_h^S$ in order to take into account half-integer rovibronic angular momenta as well as half-integer representations. A preliminary new version of the HTDS sofware has been described briefly. The computation of matrix elements of the rovibronic operators (Hamiltonian, dipole moment and polarizability) allows the simulation of rovibronic infrared or Raman spectra for all vibrational modes. Now, it remains to study quantitatively such spectra with this formalism. A interesting extension would be also to consider a electronic state of E symmetry by an algebraic approach. We also intend to extend this formalism to the case of transitions between two different electronic states.

Acknowledgements

Région Bourgogne is gratefully acknowledged for supporting the Laboratoire de Physique de l'Université de Bourgogne.

Appendix A

A.1. Matrix elements for the dipole moment and polarizability operators

Dipole moment

$$\left\langle {}_{\beta 2\beta 4}[\Psi_{\mathrm{r}}^{(J_g,n'C'_{\mathrm{rg}})} \otimes \left[\Phi_{\mathrm{e}}^{(J_{\mathrm{eg}},C_{\mathrm{e}\chi})} \otimes \Psi_{\mathrm{v}',l'_{\tau'}}^{(C'_{\mathrm{v}\tau'})}\right]^{(C'_{\mathrm{ev}\tau'})}\right]_{\sigma}^{(C_{\tau'})} \left\| \left[C^{(F_{1g})} \otimes T^{(\{i\},F_{1u})}\right]^{(A_{1u})} \right| {}_{\beta 1\beta_3}[\Psi_{\mathrm{r}}^{(J_g,nC_{\mathrm{rg}})}$$

$$\otimes \left[\Phi_{\mathrm{e}}^{(J_{\mathrm{eg}},C_{\mathrm{e}\chi})} \otimes \Psi_{\mathrm{v},l_\tau}^{(C_{\mathrm{v}\tau})}\right]^{(C_{\mathrm{ev}\bar{\tau}})}\right]_{\sigma}^{(C_{\bar{\tau}})} \Big\rangle = \frac{1}{2}(-1)^{\varphi(J_{\mathrm{e}})}(-1)^{\Gamma_{\mathrm{r}}+2C_{\mathrm{e}}+F_1+C_{\mathrm{r}}-C'_{\mathrm{r}}}([C][C_{\mathrm{ev}}][C'_{\mathrm{ev}}])^{1/2}$$

$$\times [\Gamma_{\mathrm{ev}}] \sum_{\beta,\beta',\bar{\beta},\beta_{\mathrm{r}}} {}^{\beta'}K \begin{matrix}(K_{\mathrm{eg}} & J_{\mathrm{eg}} & J_{\mathrm{eg}})\\ (\Gamma_{\mathrm{eg}} & \tilde{C}_{\mathrm{eg}} & \tilde{C}_{\mathrm{eg}})\end{matrix}^{\beta} \begin{Bmatrix} \Gamma_{\mathrm{evg}} & C_{\mathrm{rg}} & C'_{\mathrm{rg}} \\ \Gamma_{\mathrm{ev}u} & C_{\mathrm{ev}\bar{\tau}} & C'_{\mathrm{ev}\bar{\tau}'} \\ A_{1u} & C_{\bar{\tau}} & C'_{\bar{\tau}'} \end{Bmatrix}_{\beta_{\mathrm{r}}\beta 11\beta_1\beta_2} \begin{Bmatrix} \Gamma_{\mathrm{eg}} & C_{\mathrm{e}\chi} & C_{\mathrm{e}\chi} \\ \Gamma_{\mathrm{v}g} & C_{\mathrm{v}\tau} & C'_{\mathrm{v}\tau'} \\ \Gamma_{\mathrm{evg}} & C_{\mathrm{ev}\bar{\tau}} & C'_{\mathrm{ev}\bar{\tau}'} \end{Bmatrix}_{\beta 1\bar{\beta}1\beta_3\beta_4}$$

$$\times \left\langle \Psi_{\mathrm{v}',l'_{\tau'}}^{(C'_{\mathrm{v}\tau'})} \| \epsilon V_{\{n_{\mathrm{s}}\}\{m_{\mathrm{s}}\}}^{\Gamma_{1\mu}\Gamma_{2\hat{\mu}}(\Gamma_{\mathrm{v}u})} \| \Psi_{\mathrm{v},l_\tau}^{(C_{\mathrm{v}\tau})} \right\rangle \langle J_{\mathrm{eg}} \| E^{K_{\mathrm{e}}(K_{\mathrm{eg}})} \| J_{\mathrm{eg}} \rangle \langle J'_g \| C^{(1_g)} \| J_g \rangle \, \mathrm{e}^{\mathrm{i}\Psi(\Gamma_{\mathrm{e}},C_{\mathrm{e}},\beta,\beta')} \Big\{ \langle J'_g \| R^{\Omega_{\mathrm{r}}(K_{\mathrm{rg}})} \| J'_g \rangle, \tag{A1}$$

$$\times \sum_{\beta_{1\mathrm{r}},\beta_{2\mathrm{r}}} \left[\sum_{C''_{\mathrm{r}}} \begin{Bmatrix} \Gamma_{\mathrm{rg}} & F_{1g} & \Gamma_{\mathrm{evg}} \\ C_{\mathrm{rg}} & C'_{\mathrm{rg}} & C''_{\mathrm{rg}} \end{Bmatrix}_{\beta_{1\mathrm{r}}\beta_{2\mathrm{r}}\beta_{\mathrm{r}}1} \sum_{n''} {}^{\beta 2\mathrm{r}}K \begin{matrix}(1_g & J_g & J'_g)\\ (0F_{1g} & nC_{\mathrm{rg}} & n''C''_{\mathrm{rg}})\end{matrix}^{\beta 1\mathrm{r}} K \begin{matrix}(K_{\mathrm{rg}} & J'_g & J'_g)\\ (n_{0\mathrm{r}}\Gamma_{\mathrm{rg}} & n''C''_{\mathrm{rg}} & n'C'_{\mathrm{rg}})\end{matrix} \right]$$

$$+ (-1)^{\varphi(J)+\varphi(J')}(-1)^{F_1+\Gamma_{\mathrm{r}}+\Gamma_{\mathrm{ev}}} \langle J_g \| R^{\Omega_{\mathrm{r}}(K_{\mathrm{rg}})} \| J_g \rangle \sum_{\beta'_{1\mathrm{r}},\beta'_{2\mathrm{r}}} \left[\sum_{C''_{\mathrm{r}}} \begin{Bmatrix} F_{1g} & \Gamma_{\mathrm{rg}} & \Gamma_{\mathrm{evg}} \\ C_{\mathrm{rg}} & C'_{\mathrm{rg}} & C''_{\mathrm{rg}} \end{Bmatrix}_{\beta'_{2\mathrm{r}}\beta'_{1\mathrm{r}}\beta_{\mathrm{r}}1} \right.$$

$$\left. \times \sum_{n''} {}^{\beta'_{2\mathrm{r}}}K \begin{matrix}(1_g & J_g & J'_g)\\ (0F_{1g} & n''C''_{\mathrm{rg}} & n'C'_{\mathrm{rg}})\end{matrix}^{\beta'_{1\mathrm{r}}} K \begin{matrix}(K_{\mathrm{rg}} & J_g & J_g)\\ (n_{0\mathrm{r}}\Gamma_{\mathrm{rg}} & nC_{\mathrm{rg}} & n''C''_{\mathrm{rg}})\end{matrix} \right] \Big\}$$

Polarizability

$$
\begin{aligned}
&\left\langle {}_{\beta_2\beta_4}\left[\Psi_{\mathrm{r}}^{(J_g,n'C'_{\mathrm{rg}})} \otimes \left[\Phi_{\mathrm{e}}^{(J_{\mathrm{eg}},C_{\mathrm{eg}})} \otimes \Psi_{\mathrm{v}',l'_{\tau'}}^{(C'_{\mathrm{v}\tau'})} \right]^{(C'_{\mathrm{ev}\tau'})} \right]_{\sigma}^{(C_{\tau'})} | [C^{(F_{1g})} \right. \\
&\left. \otimes T^{(\{i\},F_{1u})}]^{(A_{1u})}|_{\beta_1\beta_3} \left[\Psi_{\mathrm{r}}^{(J_g,nC_{\mathrm{rg}})} \otimes \left[\Phi_{\mathrm{e}}^{(J_{\mathrm{eg}},C_{\mathrm{e}\chi})} \otimes \Psi_{\mathrm{v},l_\tau}^{(C_{\mathrm{v}\tau})} \right]^{(C_{\mathrm{ev}\bar{\tau}})} \right]_{\sigma}^{(C_{\bar{\tau}})} \right\rangle \\
&= \frac{1}{2}(-1)^{\varphi(J_{\mathrm{e}})}(-1)^{\Gamma_{\mathrm{r}}+2C_{\mathrm{e}}+\Gamma_1+C_{\mathrm{r}}+C_{\mathrm{ev}}-C-\Gamma_{\mathrm{ev}}}([\Gamma_{\mathrm{ev}}][C_{\mathrm{ev}}][C'_{\mathrm{ev}}])^{1/2} \\
&\quad \times \sum_{\beta,\beta',\bar{\beta},\beta_{\mathrm{r}}} {}^{\beta'}K \begin{pmatrix} K_{\mathrm{eg}} & J_{\mathrm{eg}} & J_{\mathrm{eg}} \\ \Gamma_{\mathrm{eg}} & \tilde{C}_{\mathrm{eg}} & \tilde{C}_{\mathrm{eg}} \end{pmatrix} \begin{Bmatrix} C_{\mathrm{rg}} & C_{\bar{\tau}} & C'_{\mathrm{ev}\tau} \\ C'_{\mathrm{ev}\bar{\tau}'} & \Gamma_{\mathrm{evg}} & C'_{\mathrm{rg}} \end{Bmatrix}_{\beta_{\mathrm{r}}\beta_2\bar{\beta}\beta_1} \begin{Bmatrix} \Gamma_{\mathrm{eg}} & C_{\mathrm{e}\chi} & C_{\mathrm{e}\chi} \\ \Gamma_{\mathrm{vg}} & C_{\mathrm{v}\tau} & C'_{\mathrm{v}\tau'} \\ \Gamma_{\mathrm{evg}} & C_{\mathrm{ev}\bar{\tau}} & C'_{\mathrm{ev}\bar{\tau}'} \end{Bmatrix}_{\beta_1\bar{\beta}_1\beta_3\beta_4} \\
&\quad \times \left\langle \Psi_{\mathrm{v}',l'_{\tau'}}^{(C'_{\mathrm{v}\tau'})} \middle\| \epsilon V_{\{n_{\mathrm{s}}\}\{m_{\mathrm{s}}\}}^{\Gamma_{1\mu}\Gamma_{2\mu}(\Gamma_{\mathrm{vg}})} \middle\| \Psi_{\mathrm{v},l_\tau}^{(C_{\mathrm{v}\tau})} \right\rangle \langle J_{\mathrm{eg}} \| E^{K_{\mathrm{e}}(K_{\mathrm{eg}})} \| J_{\mathrm{eg}} \rangle \langle J'_g \| C^{(L_g)} \| J_g \rangle \, \mathrm{e}^{\mathrm{i}\Psi(\Gamma_{\mathrm{e}},C_{\mathrm{e}},\beta,\beta')} \Big\{ \langle J'_g \| R^{\Omega_{\mathrm{r}}(K_{\mathrm{rg}})} \| J'_g \rangle, \\
&\quad \times \sum_{\beta_{1\mathrm{r}},\beta_{2\mathrm{r}}} \left[\sum_{C''_{\mathrm{r}}} \begin{Bmatrix} \Gamma_{\mathrm{rg}} & \Gamma_g & \Gamma_{\mathrm{evg}} \\ C_{\mathrm{rg}} & C'_{\mathrm{rg}} & C''_{\mathrm{rg}} \end{Bmatrix}_{\beta_{1\mathrm{r}}\beta_{2\mathrm{r}}\beta_{\mathrm{r}}1} \sum_{n''} {}^{\beta_{2\mathrm{r}}}K \begin{pmatrix} L_g & J_g & J'_g \\ 0\Gamma_g & nC_{\mathrm{rg}} & n''C''_{\mathrm{rg}} \end{pmatrix} {}^{\beta_{1\mathrm{r}}}K \begin{pmatrix} K_{\mathrm{rg}} & J'_g & J'_g \\ n_{0\mathrm{r}}\Gamma_{\mathrm{rg}} & n''C''_{\mathrm{rg}} & n'C'_{\mathrm{rg}} \end{pmatrix} \right] \\
&\quad + (-1)^{\varphi(J)+\varphi(J')}(-1)^{\Gamma+\Gamma_{\mathrm{r}}+\Gamma_{\mathrm{ev}}} \langle J_g \| R^{\Omega_{\mathrm{r}}(K_{\mathrm{rg}})} \| J_g \rangle \sum_{\beta'_{1\mathrm{r}},\beta'_{2\mathrm{r}}} \left[\sum_{C''_{\mathrm{r}}} \begin{Bmatrix} \Gamma_g & \Gamma_{\mathrm{rg}} & \Gamma_{\mathrm{evg}} \\ C_{\mathrm{rg}} & C'_{\mathrm{rg}} & C''_{\mathrm{rg}} \end{Bmatrix}_{\beta'_{2\mathrm{r}}\beta'_{1\mathrm{r}}\beta_{\mathrm{r}}1} \right. \\
&\quad \left. \times \sum_{n''} {}^{\beta'_{2\mathrm{r}}}K \begin{pmatrix} L_g & J_g & J'_g \\ 0\Gamma_g & n''C''_{\mathrm{rg}} & n'C'_{\mathrm{rg}} \end{pmatrix} {}^{K}_{\beta'_{1\mathrm{r}}} \begin{pmatrix} K_{\mathrm{rg}} & J_g & J_g \\ n_{0\mathrm{r}}\Gamma_{\mathrm{rg}} & nC_{\mathrm{rg}} & n''C''_{\mathrm{rg}} \end{pmatrix} \right]
\end{aligned}
\tag{A2}
$$

Appendix B

B.1. Wigner–Eckart theorem and recoupling formulas in O^S

Winger–Eckart theorem in O^{S}

$$
\left\langle \Psi_{\sigma'}^{(C')} \middle| T_{\sigma_0}^{(C_0)} \middle| \Psi_{\sigma}^{(C)} \right\rangle = [C']^{-1/2} \sum_{\beta} F \begin{pmatrix} C_0 & C & \sigma' \\ \sigma_0 & \sigma & (C') \end{pmatrix} \langle \beta C' \| T^{(C_0)} \| C \rangle, \tag{B1}
$$

with $C_0 \times C \supset \beta C'$.

Recoupling formula for two operators acting on the same space

$$
\begin{aligned}
&\langle \beta C' \| [T^{(C_1)} \otimes T^{(C_2)}]^{(\beta_0 C_0)} \| C \rangle = \sum_{C'',\beta''_1,\beta''_2} (-1)^{C_1+C_2+C+C'} [C_0]^{1/2} \begin{Bmatrix} C_1 & C_2 & C_0 \\ C & C' & C'' \end{Bmatrix}_{\beta''_1\beta''_2\beta\beta_0} \\
&\langle \beta''_1 C' \| T^{(C_1)} | C'' \rangle \langle \beta''_2 C'' \| T^{(C_2)} \| C \rangle.
\end{aligned}
\tag{B2}
$$

Recoupling formula for two operators acting on two different spaces

$$\langle C_1' C_2', \beta\beta_{12}' C' \| [T^{(\Gamma_1)} \otimes U^{(\Gamma_2)}]^{(\beta_0 \Gamma_0)} \| C_1 C_2, \beta_{12} C \rangle$$

$$= ([C][C'][\Gamma_0])^{1/2} \sum_{\beta_1 \beta_2} \begin{Bmatrix} \Gamma_1 & C_1 & C_1' \\ \Gamma_2 & C_2 & C_2' \\ \Gamma_0 & C & C' \end{Bmatrix}_{\beta_1 \beta_1 \beta \beta_0 \beta_{12} \beta_{12}'}$$

$$\times \langle \beta_1 C_1' \| T^{(\Gamma_1)} \| C_1 \rangle \langle \beta_2 C_2' \| U^{(\Gamma_2)} \| C_2 \rangle. \quad \text{(B3)}$$

References

[1] J. Moret-Bailly, Cah. Phys. 15 (1961) 237.
[2] J.P. Champion, Can. J. Phys. 55 (1977) 1802.
[3] J.P. Champion, M. Loëte, G. Pierre, Spectroscopy of the Earth's Atmosphere and Interstellar Medium, Academic Press, San Diego, 1992 p. 339.
[4] N. Cheblal, V. Boudon, M. Loëte, J. Mol. Spectrosc. 222 (1999) 197.
[5] H.A. Jahn, E. Teller, Proc. Roy. Soc. (London) Ser. A 161 (1937) 220.
[6] M.S. Child, J. Mol. Spectrosc. 10 (1963) 357.
[7] W. Moffit, W. Thorson, Phys. Rev. 168 (1968) 362.
[8] V. Boudon, F. Michelot, J. Moret-Bailly, J. Mol. Spectrosc. 166 (1994) 449.
[9] B. Weinstock, G.L. Goodman, Adv. Chem. Phys. 9 (1965) 169.
[10] J.C.D. Brand, G.L. Goodman, B. Weinstock, J. Mol. Spectrosc. 37 (1960) 436.
[11] H.H. Claassen, H. Selig, Isr. J. Chem. 7 (1969) 499.
[12] V. Boudon, M. Rotger, D. Avignant, J. Mol. Spectrosc. 175 (1996) 327.
[13] M. Rotger, V. Boudon, H. Selig, Spectrosc. Acta A 55 (1999) 1575.
[14] O. Acef, Ch.J. Bordé, A. Clairon, G. Pierre, B. Sartakov, J. Mol. Spectrosc. 199 (2000) 188.
[15] V. Boudon, M. Hepp, M. Herman, I. Pak, J. Mol. Spectrosc. 192 (1998) 359.
[16] V. Boudon, M. Rotger, Y. He, U. Schmitt, H. Hollenstein, M. Quack, submitted for publication.
[17] M. Rey, V. Boudon, M. Loëte, F. Michelot, 204 (2000) 106–119.
[18] M. Rotger, V. Boudon, M. Loëte, J. Mol. Spectrosc. 200 (2000) 123.
[19] M. Rotger, V. Boudon, M. Loëte, J. Mol. Spectrosc. 200 (2000) 131.
[20] V. Boudon, F. Michelot, J. Mol. Spectrosc. 165 (1994) 554.
[21] Ch. Wenger, V. Boudon, J.P. Champion, G. Pierre, J. Quant. Spectrosc. Radiat. Transfer 66 (2000) 1.
[22] M. Loëte, Can. J. Phys. 61 (1983) 1242.
[23] J.K.G. Watson, J. Mol. Spectrosc. 50 (1974) 281.
[24] J.P. Champion, G. Pierre, F. Michelot, J. Moret-Bailly, Can. J. Phys. 55 (1977) 512.
[25] F. Michelot, T. Schwartzmann, Mol. Phys. 80 (1993) 1269.
[26] H.A. Kramers, Proc. Acad. Sci. Amsterdam 33 (1930) 959.
[27] J. Stone, Mol. Phys. 29 (1975) 1461.
[28] V. Boudon, PhD Thesis, Dijon France, 1995.

Quatrième partie

Chapitre 2

Application à la Spectroscopie de l'Hexacarbonyle de Vanadium

Publication P23
Proceeding A2

2.1 Introduction

Si la plus grande famille de molécules de type toupies sphériques possédant une sous-couche électronique incomplète est celle de hexafluorures de métaux de transition (voir Chapitre IV.1) et si les tous premiers spectres rovibroniquement résolus l'ont été sur ReF_6 (voir Chapitre IV.3), la première analyse rovibronique dans un état électronique dégénéré que nous ayons pu mener à bien concerne un hexacarbonyle, $V(CO)_6$. C'est pourquoi je lui consacre ici un chapitre complet.

Un spectre en jet supersonique du profil de la bande d'élongation C–O ν_6 de cette molécule a en effet pu être enregistré par Pierre Asselin et ses collègues (Université Pierre et Marie Curie, Paris), dans la suite du travail réalisé sur l'hexacarbonyle "classique" $Mo(CO)_6$ [P15,P17].

2.2 La molécule $V(CO)_6$

$V(CO)_6$ est un hexacarbonyle octaédrique comme illustré sur la Figure 2.1. Elle possède 107 électrons et son terme électronique de base est $^2F_{2g}$.

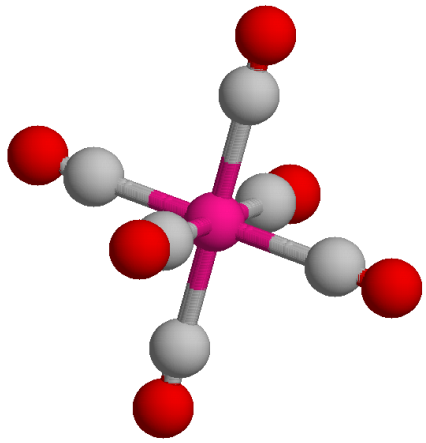

Fig. 2.1 – *La molécule $V(CO)_6$.*

Cette molécule possède 13 modes normaux de vibration, dont certains sont des modes de pliage V–C–O très "mous" à bas nombre d'onde, d'où un nombre extrêmement grand de bande chaudes à température ambiante, rendant indispensable l'utilisation d'un jet supersonique pour pouvoir observer

les bandes froides. Par contre, comme tous les hexacarbonyles, $V(CO)_6$ possède un mode d'élongation C–O, ν_6 à la fois très intense et bien isolée des autres vibrations.

2.3 Article-clé

Est reproduit ici l'article illustrant l'utilisation du modèle d'hamiltonien tensoriel rovibronique effectif pour l'analyse du profil de la bande ν_6 d'élongation C–O de $V(CO)_6$.

– [**P23 :** *J. Chem. Phys.*, **114**, 10773–10779 (2001)] présente ces résultats obtenus en collaboration avec Pierre Asselin et ses collègues.

JOURNAL OF CHEMICAL PHYSICS VOLUME 114, NUMBER 24 22 JUNE 2001

The spectrum of an octahedral molecule in a degenerate electronic state: The ν_6 fundamental band of jet-cooled $V(CO)_6$

M. Rey, V. Boudon,[a] and M. Loëte
Laboratoire de Physique de l'Université de Bourgogne (UMR CNRS 5027), 9 av. A. Savary, B.P. 47 870-21078 Dijon Cedex, France

P. Asselin, P. Soulard, and L. Manceron
LADIR/Laboratoire de Spectrochimie Moléculaire (UMR CNRS 7075), Université Pierre et Marie Curie, Case Courrier 49, Bâtiment F74, 4 Place Jussieu, 75252 Paris Cedex 05, France

(Received 12 February 2001; accepted 6 April 2001)

The jet-cooled FTIR spectrum of the ν_6 fundamental band (C–O stretch) of vanadium hexacarbonyl, $V(CO)_6$, is studied for the first time. The spectrum shows a very unusual structure consisting of three well-defined broad subbands, without the usual PQR structure. $V(CO)_6$ being an open-shell system this is attributed to a dynamical $F_{2g}\otimes F_{1u}$ Jahn–Teller coupling which considerably complicates the analysis. A new theoretical model based on group theory and tensorial algebraic techniques is developed in this paper for the very first attempt to analyze such a rovibronic spectrum. The assumption of a negligible spin–orbit coupling is validated by the overall agreement between predicted and observed band profiles. The rovibronic Hamiltonian and dipole moment operators have been expanded in order to enable a simultaneous treatment of the four vibronic sublevels. We were able to satisfactorily reproduce the band profile and thus to give the first estimation of some rovibronic parameters for this molecule. © *2001 American Institute of Physics.* [DOI: 10.1063/1.1374957]

I. INTRODUCTION

Since the original discovery of vanadium hexacarbonyl in 1959,[1] considerable effort has been devoted to the elucidation of structural and electronic properties of the molecule. Once the monomeric nature of this unique compound was established,[2] and the molecular entity recognized as $V(CO)_6$, a stable 17-electron monomeric complex, a number of techniques has been applied to the determination of the molecular shape and the electronic ground state. In an early infrared study, Haas and Sheline[3] concluded from the extreme broadening of the room-temperature gas phase IR absorption spectrum that the molecule *probably* experienced no static distorsion from an average octahedral configuration, but a dynamic Jahn–Teller effect. Magnetic susceptibility measurements show that the complex has one unpaired electron as expected for the d^5 (t_{2g}^5) configuration,[4] but below 66 K weak antiferromagnetic coupling has been observed in the solid state.[5] Gas phase diffraction data[6] and x-ray diffraction structure (at 245 K) (Ref. 7) indicate *approximate* octahedral symmetry near room temperature, but with rather large error bars. EPR spectroscopy has of course been applied in several studies, but is restricted to the condensed phase.[8–10] At low temperature, a small static distorsion is concluded, leading to a $^2B_{2g}$ term, but no clear consensus has been reached concerning the exact nature of the distorsion. The electronic spectrum giving its color to the dark crystal has also motivated solid state UV-visible absorption[11] and MCD (Ref. 12) studies in the neat solid and matrix isolated phases, interpreting the UV spectrum of the isolated molecule in term of a rather large static distorsion. Vibrational studies on the same phase were of little help, however, as the splitting observed on the triply degenerate, F_{1u} symmetry, ν_6 mode which were interpreted as indicating a D_{4h} ground state geometry also exist for the related, *bona fide*, octahedral molecules $Cr(CO)_6$ and $Mo(CO)_6$ (Refs. 13–15) due to matrix perturbations.

One factor limiting the range of the seminal vibrational study of Haas and Sheline was the fact that, as for the better known $Cr(CO)_6$ and $Mo(CO)_6$ hexacarbonyl complexes, the IR room temperature absorption spectrum is also broadened by overlapping of the many hot band transitions, arising from the existence of the numerous low-lying vibrations. This broadening leads to a complete loss of the rotational structure, even for perfectly octahedral molecules with closed-shell configuration. The low vapor pressure of these compounds does not permit quenching of the excited vibrational levels in equilibrium conditions. Jet-cooling techniques combined with high resolution IR absorption spectroscopy has proved to be a powerful technique to elucidate the rotational structure of these fluxional molecules by the cooling effect of the adiabatic expansion.

Davies and co-workers studied $Ni(CO)_4$, $Cr(CO)_6$, and other hexacarbonyl complexes using IR-diode laser scanning and double modulation techniques[16–19] which present unsurpassed sensitivity when narrow (around the Doppler limit) absorption lines are observable. FTIR techniques are so far less sensitive but have some advantages regarding frequency calibration, broad spectral coverage[20] and most important, studies involving molecules for which extensive anharmonic couplings[21] or dynamical processes broaden the spectral fea-

[a]Author to whom correspondence should be addressed. Electronic mail: boudon@jupiter.u-bourgogne.fr

tures beyond the point where wavelength-modulation techniques are no longer usable.

In this study we report Fourier transform infrared spectra and analysis of the ν_6 band of $V(CO)_6$. After a brief description of the experimental part, an original rovibronic treatment will be developed.

II. EXPERIMENT

The supersonic jet-FTIR spectrometer device for observing the gas phase IR spectrum of the jet-cooled molecule is similar to that used for the study on $Mo(CO)_6$.[22] Briefly, $V(CO)_6$ is seeded in argon at about 2% by sweeping the rare gas over the metal carbonyl kept constant at 25 °C, which corresponds to a vapor pressure of about 2.0 mbar (measured with a baratron gauge) vs 0.4 mbar for $Mo(CO)_6$. Consequently it is not necessary to overheat the injection nozzle for this compound. The gas mixture is expanded through a circular nozzle of 1 mm diam D and 1 mm length and then evacuated by a $18\,m^3\,s^{-1}$ Varian four stage diffusion pump. As evidenced for the $Mo(CO)_6$ study,[22] the argon flow rate is maintained at about $1\,mol\,h^{-1}$ for $D=1$ mm, which corresponds to the optimal conditions for sweeping $V(CO)_6$ vapor efficiently. In these conditions the stagnation pressure is about 70 Torr for a background pressure equal to 10^{-3} Torr. The supersonic beam is finally probed by the 16-pass arrangement of the IR beam issued from a Bruker IFS 120 HR interferometer and then focused on an InSb detector fitted directly in the expansion chamber.

Sodium hexacarbonyl vanadate as the diglyme-stabilized salt was purchased from Strem Chemicals. About 3 g of neutral $V(CO)_6$ was synthesized by oxydation of the anion with orthophosphoric acid[23] in an evacuated cell and distilled around 60 °C into a glass trap cooled around −60 °C. The black solid was kept in the dark and under its own vapor pressure without noticeable decomposition when not heated. The purity of the product was checked by argon matrix isolation IR spectroscopy. The product was first handled exclusively with glassware, but showed no sign of decomposition when streamed down stainless steel tubing.

Figure 1 displays two experimental spectra of the CO stretching ν_6 band of $V(CO)_6$, the room temperature cell spectrum (a) recorded at $0.3\,cm^{-1}$ resolution by Haas and Sheline[3] and the jet spectrum (b) recorded at $0.1\,cm^{-1}$ with our experimental device, as well as the jet spectrum of the CO stretching ν_6 band of $Mo(CO)_6$ (c) recorded at $0.004\,cm^{-1}$ from our latter work[22] and shifted down by $16.6\,cm^{-1}$ to make the comparison easier. Another jet spectrum of $V(CO)_6$ recorded in the same experimental conditions but at higher resolution ($0.01\,cm^{-1}$) does not reduce the width of the bands observed.

Some notable differences exist between the band contours of these three spectra. The cell spectrum (a) shows only one broad band ($20\,cm^{-1}$ FWHM) around $1980\,cm^{-1}$. Due to the rovibrational cooling of the supersonic expansion, the jet spectrum (b) is structured into three narrower bands ($6\,cm^{-1}$ FWHM) located, respectively, at 1972, 1989, and $2008\,cm^{-1}$. The conditions of dilution for $V(CO)_6$ in argon being very similar to those used for the $Mo(CO)_6$ study, the rotational temperature derived from the simulation of the resolved rovibrational band (13 K) is hereafter assumed to be about the same for both hexacarbonyls. However, the absence of a resolved PQR pattern in the jet spectrum (b) of $V(CO)_6$ compared to (c) of $Mo(CO)_6$ clearly proves the existence of a dynamic Jahn–Teller effect as suggested previously.[3] The following paragraph describes the theoretical formalism necessary to build the spectrum of an octahedral molecule in a degenerate electronic state.

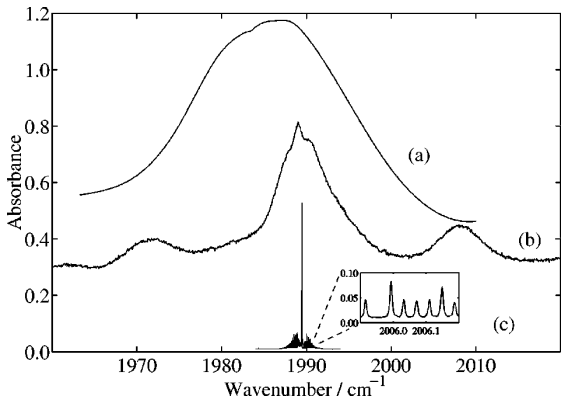

FIG. 1. Experimental spectra of the ν_6 band, (a) of $V(CO)_6$ in cell, (b) of $V(CO)_6$ in jet (magnified by a factor of 30), and (c) of $Mo(CO)_6$ in jet (shifted by $-16.6\,cm^{-1}$ for the sake of presentation). Note the expanded view of a part of the R branch ($J=10$–17) displaying the resolved rovibrational lines.

III. THEORY

The $V(CO)_6$ molecule has 107 electrons which implies the existence of an incomplete electronic subshell. There are only a very few informations about the true symmetry of its electronic ground state in the literature. According to Haas and Sheline,[3] $V(CO)_6$ is an octahedral molecule pertaining to the O_h point group and the electronic ground state term is $^2F_{2g}$. However, Ref. 3 does not give any value for the spin–orbit coupling, but it is suggested that this should be very weak. Barton *et al.*[12] predicted a spin–orbit coupling for $V(CO)_6$ of $\approx 100\,cm^{-1}$. This case is somewhat different from that of open-shell transition-metal hexafluorides[24] which exhibit very large spin–orbit coupling. For these molecular species (ReF_6, IrF_6, …) the states are classified according to the value of their total electronic angular momentum (spin plus orbital). In the present work, following Ref. 3, we have neglected the spin–orbit coupling and thus assumed that $V(CO)_6$ has an electronic ground state of symmetry F_{2g} in O_h. In spite of this approximation, the electronic degeneracy implies of course the existence of complex rovibronic couplings and complex spectra.

The model used here is based on previous works about the spectroscopy of octahedral molecules in a fourfold degenerate electronic state.[25–29] In Refs. 28 and 29 we have developed a new model for the expansion of the Hamiltonian and transition moment operators (dipole moment and polarizability) for an electronic state of G_g' symmetry in the O_h^S group.[25] The main advantage of this model is to avoid infinite matrices that usually arise in vibronic couplings[26,27] such

TABLE I. Hamiltonian and dipole moment effective parameters for the ν_6 band of $V(CO)_6$.

Hamiltonian parameters

Parameter $\tilde{t}^{\Omega_r(K_{rg},n\Gamma_{evg})\,(K_{eg},\Gamma_{eg})\Gamma_{1\mu}\Gamma_{2\mu}\,(\Gamma_{vg})}_{\{n_s\}\{m_s\}}$

Level	Ω[a]		$\Omega_r(K_{rg},n\Gamma_{evg})$	$K_e(K_{eg},\Gamma_{eg})$	$\Gamma_{1\mu}$	$\Gamma_{2\mu}$	Γ_{vg}	Value/cm^{-1}	Comment
GS	0		$1(1,0F_{1g})$	$1(1,F_{1g})$	A_{1g}	A_{1g}	A_{1g}	8.0×10^{-5}	
	0		$2(0,0A_{1g})$	$0(0,A_{1g})$	A_{1g}	A_{1g}	A_{1g}	$1.954\,11\times10^{-2}$	B_0
$v_6=1$	0		$0(0,0A_{1g})$	$0(0,A_{1g})$	F_{1u}	F_{1u}	A_{1g}	1994.48	ν_6
	1	$\tilde{t}_1$	$0(0,0A_{1g})$	$1(1,F_{1g})$	F_{1u}	F_{1u}	F_{1g}	−16.61	
	1	$\tilde{t}_2$	$0(0,0A_{1g})$	$2(2,E_g)$	F_{1u}	F_{1u}	F_{2g}	−7.51	
	1	$\tilde{t}_3$	$0(0,0A_{1g})$	$2(2,F_{2g})$	F_{1u}	F_{1u}	E_g	1.79	
	1		$1(1,0F_{1g})$	$0(0,A_{1g})$	F_{1u}	F_{1u}	F_{1g}	-3.6418×10^{-4}	$3\sqrt{2}(B\xi)_6$
	2		$1(1,0F_{1g})$	$1(1,F_{1g})$	F_{1u}	F_{1u}	A_{1g}	-3.0×10^{-2}	
	2		$1(1,0F_{1g})$	$1(1,F_{1g})$	F_{1u}	F_{1u}	E_g	8.0×10^{-2}	
	2		$1(1,0F_{1g})$	$1(1,F_{1g})$	F_{1u}	F_{1u}	F_{2g}	-7.0×10^{-2}	
	2		$2(0,0A_{1g})$	$0(0,A_{1g})$	F_{1u}	F_{1u}	A_{1g}	$-1.285\,274\times10^{-5}$	B_6-B_0
	2		$2(2,0E_g)$	$0(0,A_{1g})$	F_{1u}	F_{1u}	E_g	-1.0×10^{-5}	
	2		$2(2,0F_{2g})$	$0(0,A_{1g})$	F_{1u}	F_{1u}	F_{2g}	1.332×10^{-6}	
	3		$1(1,0F_{1g})$	$2(2,E_g)$	F_{1u}	F_{1u}	F_{1g}	-1.0×10^{-2}	
	3		$1(1,0F_{1g})$	$2(2,F_{2g})$	F_{1u}	F_{1u}	F_{1g}	1.5×10^{-2}	
	3		$2(0,0A_{1g})$	$1(1,F_{1g})$	F_{1u}	F_{1u}	F_{1g}	-7.0×10^{-4}	
	3		$2(2,0E_g)$	$1(1,F_{1g})$	F_{1u}	F_{1u}	F_{1g}	-8.0×10^{-4}	
	3		$2(2,0F_{2g})$	$1(1,F_{1g})$	F_{1u}	F_{1u}	F_{1g}	8.0×10^{-4}	
	3		$3(1,0F_{1g})$	$0(0,A_{1g})$	F_{1u}	F_{1u}	F_{1g}	-1.53×10^{-8}	
	3		$3(3,0F_{1g})$	$0(0,A_{1g})$	F_{1u}	F_{1u}	F_{1g}	1.39×10^{-8}	

Dipole moment parameters

Parameter $\tilde{\mu}^{\Omega_r(K_{rg},n\Gamma_{evg})\,(K_{eg},\Gamma_{eg})\Gamma_{1\mu}\Gamma_{2\bar{\mu}}(\Gamma_{vu})(\Gamma_{evu})}_{\{n_s\}\{m_s\}}$

Trans.	Ω[a]	$\Omega_r(K_{rg},n\Gamma_{rg})$	$K_e(K_{eg},\Gamma_{eg})$	$\Gamma_{1\mu}$	$\Gamma_{2\bar{\mu}}$	$\Gamma_{vu}(\Gamma_{evu})$	Value/arb. unit
ν_6	0	$0(0,0A_{1g})$	$0(0,A_{1g})$	A_{1g}	F_{1u}	$F_{1u}(F_{1u})$	1.0
	1	$0(0,0A_{1g})$	$1(1,F_{1g})$	A_{1g}	F_{1u}	$F_{1u}(F_{1u})$	1.8×10^{-2}
	1	$1(1,0F_{1g})$	$0(0,A_{1g})$	A_{1g}	F_{1u}	$F_{1u}(F_{1u})$	2.5×10^{-3}
	1	$0(0,0A_{1g})$	$2(2,E_g)$	A_{1g}	F_{1u}	$F_{1u}(F_{1u})$	7.5×10^{-2}
	1	$0(0,0A_{1g})$	$2(2,F_{2g})$	A_{1g}	F_{1u}	$F_{1u}(F_{1u})$	-2.0×10^{-1}
	2	$1(1,0F_{1g})$	$1(1,F_{1g})$	A_{1g}	F_{1u}	$F_{1u}(A_{1u})$	1.0×10^{-3}
	2	$1(1,0F_{1g})$	$1(1,F_{1g})$	A_{1g}	F_{1u}	$F_{1u}(E_u)$	0.0
	2	$1(1,0F_{1g})$	$1(1,F_{1g})$	A_{1g}	F_{1u}	$F_{1u}(F_{1u})$	0.0
	2	$1(1,0F_{1g})$	$1(1,F_{1g})$	A_{1g}	F_{1u}	$F_{1u}(F_{2u})$	5.0×10^{-4}
	2	$2(0,0A_{1g})$	$0(0,A_{1g})$	A_{1g}	F_{1u}	$F_{1u}(F_{1u})$	0.0
	2	$2(2,0E_g)$	$0(0,A_{1g})$	A_{1g}	F_{1u}	$F_{1u}(F_{1u})$	0.0
	2	$2(2,0F_{2g})$	$0(0,A_{1g})$	A_{1g}	F_{1u}	$F_{1u}(F_{1u})$	0.0

[a]Order in the development.

as the Jahn–Teller effect.[30,31] Using exactly the same principles as in Ref. 28, we have extended this model to the case of a threefold F_{2g} electronic symmetry.[29] Here we will simply recall the basic principles of the method, focusing on the differences with the G'_g symmetry case only.

Following the same scheme as Champion and co-workers,[32,33] the effective Hamiltonian for a given polyad P_n can be written as a sum of Hamiltonian contributions,

$$\tilde{H}^{\langle P_n\rangle}=\tilde{H}^{\langle P_n\rangle}_{\langle GS\rangle}+\tilde{H}^{\langle P_n\rangle}_{\langle P_1\rangle}+\cdots+\tilde{H}^{\langle P_n\rangle}_{\langle P_{n-1}\rangle}+\tilde{H}^{\langle P_n\rangle}_{\langle P_n\rangle}. \tag{1}$$

Each term is developed as a sum of rovibronic operators,[29]

$$\tilde{H}=\sum_{\text{all indexes}}\eta\tilde{t}^{\Omega_r(K_{rg},n\Gamma_{evg})\,(K_{eg},\Gamma_{eg})\Gamma_{1\mu}\Gamma_{2\mu}\,(\Gamma_{vg})}_{\{n_s\}\{m_s\}}\times(R^{\Omega_r(K_{rg},n\Gamma_{evg})}\otimes(E^{K_e(K_{eg},\Gamma_{eg})}\otimes{}^{\varepsilon}V^{\Gamma_{1\mu}\Gamma_{2\mu}\,(\Gamma_{vg})}_{\{n_s\}\{m_s\}})^{(\Gamma_{evg})})^{(A_{1g})}. \tag{2}$$

The Hamiltonian parameters are denoted by $\tilde{t}$; η is a numerical factor which allows coincidence between standard and tensorial notations for scalar terms.[29] $R^{\Omega_r(K_{rg},n\Gamma_{evg})}$ and ${}^{\varepsilon}V^{\Gamma_{1\mu}\Gamma_{2\mu}\,(\Gamma_{vg})}_{\{n_s\}\{m_s\}}$ are rotational and vibrational operators, respectively,[33] and $E^{K_e(K_{eg},\Gamma_{eg})}$ are the electronic operators defined in Ref. 28. The latter operators are constructed by successive couplings of the basic tensor,

$$E^{1(1)}=2J_e, \tag{3}$$

and then symmetrized in the O_h point group. The main difference with the G'_g case lies in the value of the electronic angular momentum J_e. For an electronic symmetry G'_g, we defined an effective electronic momentum $\mathbf{J}_e$ with $J_e=3/2$,[28] whereas the value for a triply degenerate electronic state F_{2g} is $J_e=1$.[29] The order of each term in the development is defined as $\Omega=\Omega_v+\Omega_r+\Omega_e-2$, where Ω_v, Ω_r, and Ω_e $=K_e$ are the vibrational, rotational, and electronic degrees, respectively.

In the present work we consider the isolated ν_6 fundamental band. So expression (1) reduces to

$$\tilde{H}^{\langle \nu_6 \rangle} = \tilde{H}^{\langle \nu_6 \rangle}_{\langle GS \rangle} + \tilde{H}^{\langle \nu_6 \rangle}_{\langle \nu_6 \rangle}. \tag{4}$$

For the line strength calculations, the effective dipole moment first introduced by Loete for XY_4 molecules[34] and generalized afterwards for XY_6 molecules[35] is constructed following the same coupling scheme as for the Hamiltonian. It is expressed in the laboratory fixed frame as[29]

$$\tilde{\mu}^{(A_{1u})}_{\Theta} \propto \sum_{\text{all indexes}} \tilde{\mu}^{\Omega_r(K_{rg},n\Gamma_{rg})(K_{eg},\Gamma_{eg})\Gamma_{1\mu}\Gamma_{2\bar{\mu}}(\Gamma_{vu})(\Gamma_{evu})}_{\{n_s\}\{m_s\}} \times [C^{(F_{1g})} \otimes M^{(F_{1u})}]^{(A_{1u})}, \tag{5}$$

where $\Theta = X$, Y or Z; $C^{(F_{1g})}$ is the direction cosine tensor and $M^{(F_{1u})}$ is a rovibronic operator written as

$$M^{(F_{1u})} = (R^{\Omega_r(K_{rg},n\Gamma_{rg})} \otimes (E^{K_e(K_{eg},\Gamma_{eg})} \otimes^{\varepsilon} V^{\Gamma_{1\mu}\Gamma_{2\bar{\mu}}(\Gamma_{vu})}_{\{n_s\}\{m_s\}})^{(\Gamma_{evu})})^{(F_{1u})}. \tag{6}$$

The $\tilde{\mu}$ are the parameters and the order of each term of the dipole moment is defined as $\Omega = \Omega_v + \Omega_r + \Omega_e - 1$.

The basis functions necessary for the calculation of the matrix elements in an electronic state F_{2g} are written[29]

$$|[\Psi^{(J_g,nC_{rg})}_r \otimes [[\Phi^{(1_g,F_{2g})}_e \otimes \Psi^{(F_{1u})}_v]^{(C_{evu})}]^{(C_u)}_{\sigma}\rangle. \tag{7}$$

In order to make the connection between the F_{2g} electronic state symmetry and the effective electronic angular momentum,[29] we have set

$$|\Phi^{(1_g,F_{2g})}_e\rangle = |\Phi^{(1_g,F_{1g})}_e\rangle |I^{(A_{2g})}\rangle. \tag{8}$$

As it is usual for spherical top molecules, the only "good" quantum numbers are J and C. The Hamiltonian eigenstates (and thus the energy levels) are labeled as

$$|\Psi^{(J_g,\alpha,C_\tau)}_{\sigma}\rangle, \tag{9}$$

with $\tau = g$ for the ground state and u for the $v_6 = 1$ state. α is a multiplicity index distinguishing states with the same symmetry, i.e., states within a (J, C) bloc. The selection rules are deduced from the nonzero conditions of the dipole moment matrix elements. In the case of the ν_6 band and for a transition between two states $(J''_{\tau''}, \alpha'', C''_{\tau''})$ and $(J'_{\tau'}, \alpha', C'_{\tau'})$ we simply have

$$\begin{aligned} &\Delta J = J' - J'' = 0, \pm 1, \\ &C' = C'', \\ &\tau' = \tau'' \otimes u. \end{aligned} \tag{10}$$

Let us now discuss briefly the main purely vibronic contributions in the Hamiltonian expansion. Some terms have a stronger influence on the spectrum structure than others. The vibronic term

$$\tilde{t}^{0(0_g,A_{1g})(1_g,F_{1g})F_{1u}F_{1u}(F_{1g})}_{\{6\}\{6\}} \mathbf{J}_e \cdot \mathbf{l}_6 = \tilde{t}_1 \mathbf{J}_e \cdot \mathbf{l}_6$$

($\mathbf{l}_6$ being the vibrational angular momentum with $l_6 = 1$) can be regarded as a "vibronic-Coriolis" term that splits the $v_6 = 1$ level into three sublevels since the vibronic angular momentum,

$$\mathbf{j} = \mathbf{J}_e + \mathbf{l}_6, \tag{11}$$

takes the values 0, 1, and 2.

Two other vibronic parameters, namely,

$$\tilde{t}_2 = \tilde{t}^{0(0_g,A_{1g})(2_g,E_g)F_{1u}F_{1u}(E_g)}_{\{6\}\{6\}}$$

and

$$\tilde{t}_3 = \tilde{t}^{0(0_g,A_{1g})(2_g,F_{2g})F_{1u}F_{1u}(F_{2g})}_{\{6\}\{6\}},$$

also act on the vibronic pattern. In particular, they further split the $j = 2$ level into two sublevels giving finally four sublevels [taking into account the true symmetry by multiplying by A_2 as in Eq. (8)],

$$(\mathcal{D}^{(0)} + \mathcal{D}^{(1)} + \mathcal{D}^{(2)}) \times A_2 = A_2 + F_2 + (E + F_1) = F_2 \times F_1. \tag{12}$$

IV. ANALYSIS

In this study, $\tilde{H}^{\langle \nu_6 \rangle}_{\langle GS \rangle}$ has been developed to the zeroth-order only and $\tilde{H}^{\langle \nu_6 \rangle}_{\langle \nu_6 \rangle}$ has been developed to the third order giving 20 Hamiltonian parameters. The dipole moment is written up to the second order (12 parameters).

All the simulations have been carried out using a modified version of the *Highly-spherical Top Data System* (HTDS) software[36] in which the electronic contribution has been added. Basically these programs were written for octahedral XY_6 molecules. However, the $\nu_6(F_{1u})$ band of $V(CO)_6$ can be treated as a $\nu_3(F_{1u})$ or a $\nu_4(F_{1u})$ band of an XY_6 molecule.

It seemed reasonable to start our study by using the rovibrational parameters determined in Ref. 22 for $Mo(CO)_6$, this molecule being the "closest" hexacarbonyl compared to $V(CO)_6$ and also the only one [with $W(CO)_6$ (Ref. 19)] for which such parameters are available. Only the harmonic frequency ν_6 has been shifted to 1994.48 cm^{-1} for $V(CO)_6$. In Table I, a few of these "classical" rovibrational parameters are indicated by more usual labels. For instance, B_0 is the ground state rotational constant and $(B\xi)_6$ is the Coriolis interaction in the $v_6 = 1$ state. However, as explained in Ref. 29, the molecular parameters (i.e., the parameters of the untransformed Hamiltonian) and these of the present effective

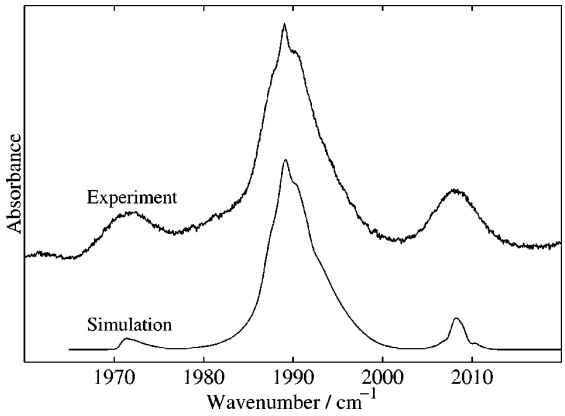

FIG. 2. Low resolution calculated band profile compared to the experiment.

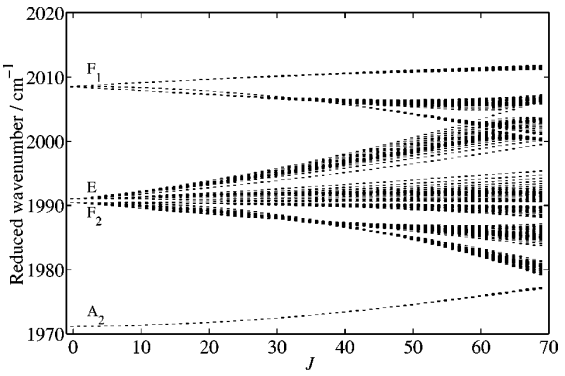

FIG. 3. Calculated reduced energy levels for the ν_6 vibronic polyad of $V(CO)_6$. The vibronic symmetries of the $F_1 \times F_2$ system are pointed out on the left.

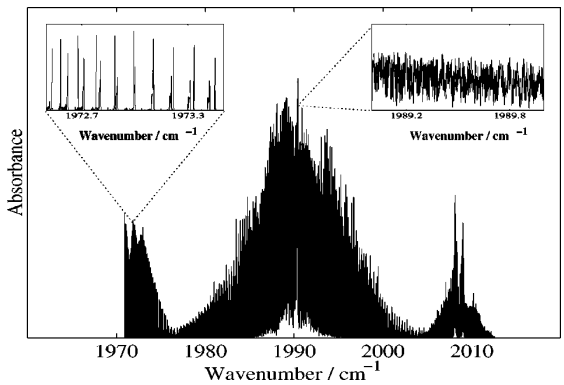

FIG. 4. Global view of the calculated ν_6 band of $V(CO)_6$ at high resolution. Two detailed portions of the spectrum around 1973.0 cm^{-1} and 1989.5 cm^{-1} are shown in the top left and top right corners of the figure, respectively.

Hamiltonian are linked through a nonperturbative transformation which would be extremely difficult to perform in practice. This makes difficult to go much further into the "physical" explanation of the rovibronic parameters. The next step was to find correct values for the rovibronic parameters by adjusting them by hand.

We have made several trial simulations up to $J=70$ at different rotational temperatures T_R. It appeared that the parameter set given in Table I for a rotational temperature of about 15 K is suitable if we compare the experimental spectrum with the simulated spectrum as shown in Fig. 2.

Figure 3 displays the reduced energies,

$$E_{\text{red}} = E - B_0 J(J+1) \tag{13}$$

for $\upsilon_6 = 1$ and with $B_0 = \tilde{t}^{2(0_g^+,A_{1g})(0_g^+,A_{1g})A_{1g}A_{1g}(A_{1g})}_{\{0\}\{0\}}$. We can observe the four vibronic sublevels as well as the octahedral splitting due to the coupling between the degenerate electronic system and the rotational and vibrational motions. Of course, the level positions in this figure are only indicative. Other sets of rovibronic parameters could certainly give a similar band profile. A detailed analysis would require rovibronically resolved spectra.

Concerning line intensities, the values of the rovibronic parameters for the dipole moment used in the simulation are also given in Table I. All of them take part in the intensity of each peak with a strong sensibility. Figure 2 shows quite good agreement between experimental and simulated rovibronic spectra. The PQR pattern usually met in rovibrational problems is absent in $V(CO)_6$. That strongly consolidates the existence of a dynamic Jahn–Teller effect. Figure 4 displays a calculated spectrum showing what this band could look like if recorded at high resolution (7×10^{-4} cm^{-1}, a typical diode laser resolution). One must carefully keep in mind, however, that the structures observed in this figure only constitute an indication of what such a spectrum *could* look like at high resolution. Again, it is necessary to say that the knowledge of precise structures would require a much more detailed analysis. Another point to notice is that the inclusion of interactions that were neglected in the present study (such as the spin-orbit interaction) would certainly further complicate the spectrum and will very likely mask the few regular structures visible in Fig. 4.

V. DISCUSSION

In order to better illustrate the influence of the vibronic terms, let us move some vibronic parameters of the Hamiltonian and see the consequences of this change. For that, we have recalculated the eigenvalues of the Hamiltonian by substituting one parameter $\tilde{t}$ by the value $\tilde{t}+\Delta\tilde{t}$. The $\Delta\tilde{t}$ term corresponds to a variation of the parameter around its optimum value (see Table I). Figure 5 gives the result of some variations for the $\tilde{t}_1$, $\tilde{t}_2$, and $\tilde{t}_3$ parameters (see above), respectively. In each case, only one parameter has been

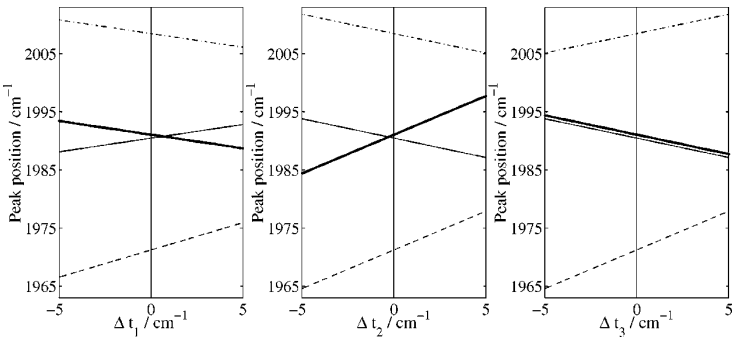

FIG. 5. Vibronic level positions as a function of the variation of one vibronic parameter. Curves for the vibronic sublevels: A_2 (dashed line), E (bold line), F_1 (dashed–dotted line), and F_2 (solid line) appear on these figures.

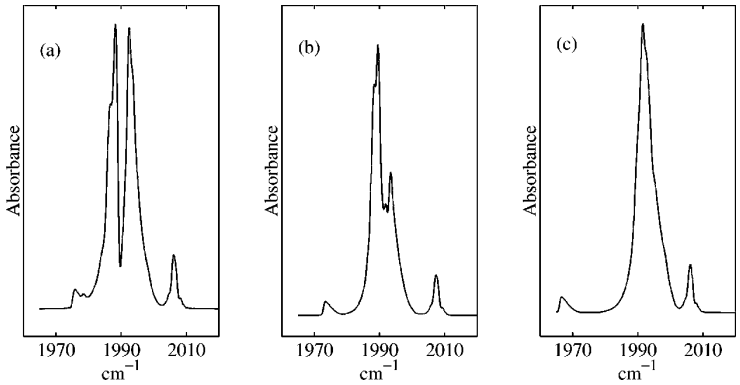

FIG. 6. Influence of the main vibronic parameters on the spectrum for (a) $\Delta\tilde{t}_1 = 4.6\ \mathrm{cm}^{-1}$, (b) $\Delta\tilde{t}_2 = 1.5\ \mathrm{cm}^{-1}$, and (c) $\Delta\tilde{t}_3 = -3.6\ \mathrm{cm}^{-1}$.

changed, the other ones take the values of Table I. The figure displays the vibronic level positions as a function of $\Delta\tilde{t}$.

Let us take some examples to illustrate these alterations.

Case (a): As we mentionned previously, the $\tilde{t}_1$ parameter is identified as the "vibronic Coriolis" term. It splits the vibronic sublevels and then, acts on the position of the peaks. This is clearly shown in Fig. 6(a).

Case (b): The $\tilde{t}_2$ parameter acts mainly on the structure of the (E, F_2) sublevels (the large central peak), the outer peaks remain essentially unchanged [Fig. 6(b)].

Case (c): The $\tilde{t}_3$ parameter acts on the position of the (A_2, F_1) sublevels and has no big influence on the two central peaks [Fig. 6(c)].

We can also notice that many parameters for the dipole moment are still constrained to zero so it is also important to add that this work is a first attempt to better understand the vast complexity of such a rovibronic spectrum. A high resolution spectrum in Fig. 4 has been simulated for a resolution of $7\times10^{-4}\ \mathrm{cm}^{-1}$ with the parameter set given in Table I. This figure throws light on the difficulty that one should expect for the analysis the detailed structure of the spectrum.

VI. CONCLUSION

We have seen in this paper that the Jahn–Teller effect considerably complicates the ν_6 band of $V(CO)_6$, even at low temperature, compared to the spectrum of a molecule in a nondegenerate electronic state [$Mo(CO)_6$, for example, Ref. 22]. The electron spin was not taken into account here, assuming that the spin–orbit interaction was small.[12] The effect of this spin–orbit coupling on the $^2F_{2g}$ state would be to split it into two states of species E'_{2g} and G'_g (twofold and fourfold degeneracy, respectively). Thus, a detailed analysis of the rovibronic structure would imply to build a new model to perform a simultaneous analysis of two interacting electronic states. An *ab initio* calculation to estimate, if possible, the value of the spin-orbit coupling constant would be of great help.

However, the good agreement between the observed and calculated band profile (Fig. 2) strongly suggests that the spin–orbit constant should not exceed a few cm^{-1}, which is even lower than the estimation of Barton *et al.*[12] We also see that our study almost certainly eliminates the possibility of a static Jahn–Teller distorsion. The next challenge for the future of this study would be to achieve the recording of rovibronically resolved spectra.

ACKNOWLEDGMENT

Support for the Région Bourgogne for the computer equipment of the Laboratoire de Physique de l'Université de Bourgogne is gratefully acknowledged.

[1] G. Natta, R. Ercoli, F. Calderazzo, A. Alberola, P. Corradini, and P. Allegra, J. Am. Chem. Soc. **82**, 2966 (1960).
[2] F. Calderazzo, R. Cini, P. Corradini, R. Ercoli, and G. Natta, Chem. Ind. **1960**, 500.
[3] H. Haas and R. K. Sheline, J. Am. Chem. Soc. **88**, 3219 (1966).
[4] F. Calderazzo, R. Cini, and R. Ercoli, Chem. Ind. **1960**, 934.
[5] J. C. Bernier and O. Kahn, Chem. Phys. Lett. **19**, 414 (1960).
[6] D. Schmiddling, J. Mol. Struct. **24**, 1 (1960).
[7] S. Bellard, K. Rubinson, and G. Scheldrick, Acta Crystallogr., Sect. B: Struct. Crystallogr. Cryst. Chem. **35**, 271 (1979).
[8] K. A. Rubinson, J. Am. Chem. Soc. **98**, 5188 (1976).
[9] S. W. Bratt, A. Kassyk, R. N. Perutz, and M. C. Symons, J. Am. Chem. Soc. **104**, 490 (1982).
[10] M. P. Boyer, Y. Lepage, J. R. Morton, and K. F. Preston, Can. J. Spectrosc. **26**, 181 (1981).
[11] G. F. Holland, M. C. Manning, D. E. Ellis, and W. C. Trogler, J. Am. Chem. Soc. **105**, 2308 (1983).
[12] T. J. Barton, R. Grinter, and A. J. Thomson, J. Chem. Soc. Dalton Trans. **1978**, 608.
[13] T. A. Ford, H. Huber, W. Klotzbücher, M. Moskovits, and G. A. Ozin, Inorg. Chem. **15**, 1666 (1976).
[14] N. A. Graham, M. Poliakoff, and J. J. Turner, J. Chem. Soc. A **1971**, 2939.
[15] D. Tevault and K. Nakamoto, Inorg. Chem. **14**, 237 (1975).
[16] J. R. Burie, P. B. Davies, G. M. Hansford, N. A. Martin, J. Gang, and D. K. Russell, Mol. Phys. **74**, 919 (1991).
[17] G. M. Hansford and P. B. Davies, J. Mol. Spectrosc. **168**, 540 (1994).
[18] G. M. Hansford and P. B. Davies, J. Chem. Phys. **104**, 8292 (1996).
[19] G. M. Hansford, M. Loroño, and P. B. Davies, J. Chem. Phys. **112**, 3620 (2000).
[20] P. Asselin, P. Soulard, G. Tarrago, N. Lacome, and L. Manceron, J. Chem. Phys. **104**, 4427 (1996).
[21] P. Asselin, P. Soulard, M. E. Alikhani, and J. P. Perchard, Chem. Phys. **256**, 195 (2000).
[22] P. Asselin, P. Soulard, L. Manceron, V. Boudon, and G. Pierre, J. Mol. Struct. **517**, 145 (2000).
[23] L. V. Interrante and G. V. Nelson, J. Organomet. Chem. **25**, 153 (1970).
[24] B. Weinstock and G. L. Goodman, Adv. Chem. Phys. **9**, 169 (1965).
[25] V. Boudon and F. Michelot, J. Mol. Spectrosc. **165**, 554 (1994).
[26] V. Boudon, F. Michelot, and J. Moret-Bailly, J. Mol. Spectrosc. **166**, 449 (1994).
[27] V. Boudon, M. Rotger, and D. Avignant, J. Mol. Spectrosc. **175**, 327 (1996).

[28] M. Rey, V. Boudon, M. Loëte, and F. Michelot, J. Mol. Spectrosc. **204**, 106 (2000).
[29] M. Rey, V. Boudon, and M. Loëte, J. Mol. Struct. (in press).
[30] H. A. Jahn and E. Teller, Proc. R. Soc. London, Ser. A **161**, 220 (1937).
[31] R. Englman, *The Jahn–Teller Effect in the Molecules and Crystals* (Wiley, New York, 1972).
[32] J. P. Champion, Can. J. Phys. **55**, 1802 (1977).
[33] J. P. Champion, M.Loëte, and G. Pierre, in *Spectroscopy of the Earth's Atmosphere and Interstellar Medium*, edited by K. N. Rao and A. Weber (Academic, San Diego, 1992), pp. 339–422.
[34] M. Loëte, Can. J. Phys. **61**, 1242 (1983).
[35] N. Cheblal, V. Boudon, and M. Loëte, J. Mol. Spectrosc. **197**, 222 (1999).
[36] Ch. Wenger, V. Boudon, J. P. Champion, and G. Pierre, J. Quant. Spectrosc. Radiat. Transf. **66**, 1 (2000).

QUATRIÈME PARTIE

Chapitre

3

Application à la Spectroscopie de l'Hexafluorure de Rhénium

Publications P11, P29
Proceeding A2

3.1 Introduction

La seconde molécule dont nous avons pu étudier en détail la spectroscopie rovibronique est l'hexafluorure de rhénium, ReF_6. Lors de mon stage postdoctoral à l'ETH Zürich (Suisse), j'ai pu participer activement à l'enregistrement des tous premiers spectres (en jet supersonique et diode laser) rovibroniquement résolus de cette molécule, autrement dit des tous premiers spectres rovibroniquement résolus d'une molécule toupie sphérique dans un état électronique dégénéré. Mais ce n'est que plus récemment, au cours du travail de thèse de Michaël Rey, qu'une interprétation détaillée de ces spectres a pu être entreprise.

3.2 La molécule ReF_6

ReF_6 possède 189 électrons et présente un très fort couplage spin-orbite (contrairement à $V(CO)_6$, voir Chapitre IV.2) [P11]. Son état électronique de base est quatre fois dégénéré.

Comme tous les hexafluorures, ReF_6 est une molécule lourde dont le spectre à température ambiante présente un très grand nombre de bandes chaudes (voir Chapitre III.1). Il est donc nécessaire d'utiliser la technique du jet moléculaire supersonique afin de simplifier les spectres et de pouvoir observer les bandes froides. Notons que dans le cas d'une espèce aussi agressive et réactive qu'un hexafluorure de métal de transition, ceci est expérimentalement difficile. A l'ETH Zürich, nous avons employé des pompes contenant une huile spéciale, capable de résister aux produits fluorés [P29].

Les deux références reproduites à la fin de ce chapitre présentent les différents spectres expérimentaux à l'enregistrement desquels j'ai pu participer. Nous nous sommes plus particulièrement focalisés sur la bande d'élongation ν_3 dans l'état électronique de base. Dans le paragraphe suivant, je résume succinctement les résultats obtenus récemment pour cette région lors de la thèse puis du stage postdoctoral de Michaël Rey et qui sont en cours de publication. Le lecteur pourra également se référer au Chapitre IV.1 et à l'extrait d'acte de colloque [A2] qui y est reproduit.

3.3 Avancées récentes

Ainsi qu'on peut le voir dans l'article [P29] reproduit ci-après, les spectres de la bande ν_3 de ReF_6 s'avèrent extrêmement complexes et, bien entendu, très différents des spectres rovibrationnels d'une bande fondamentale d'une molécule "ordinaire" (dans un état électronique singulet). L'interprétation que nous pouvons donner de ces spectres n'en est encore qu'à un stade préliminaire, mais donne toutefois dès à présent des résultats très intéressants et, je pense, très convaincants dans le sens où ils permettent de valider pleinement notre approche.

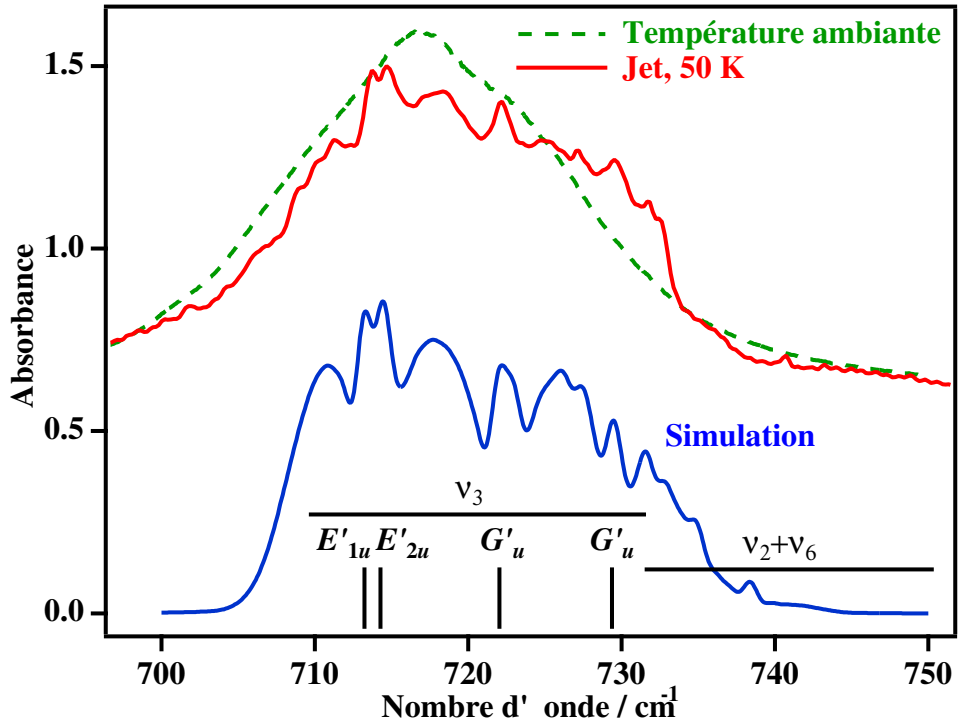

FIG. 3.1 – *Spectre d'absorption par transformée de Fourier en jet supersonique de la région de la bande ν_3 de ReF_6 (résolution de 0.5 cm^{-1}, température rotationnelle d'environ 50 K) comparée à la simulation (incluant ν_3 et $\nu_2 + \nu_6$). Les positions des sous-niveaux de $v_3 = 1$ sont indiquées. Les pointillés montrent le profil de la même région à température ambiante (l'échelle d'intensité n'est pas la même pour cette dernière courbe).*

Le niveau vibrationnel $v_3 = 1$ est trois fois dégénéré, de symétrie F_{1u}. L'état électronique de base de ReF_6 est quatre fois dégénéré, de symétrie G'_g (dans la notation des représentations spinorielles du groupe de l'octaèdre, voir Chapitre IV.1). Le couplage vibronique (essentiellement l'effet Jahn-Teller quadratique) donne donc quatre sous-niveaux vibroniques, puisque

$$F_{1u} \otimes G'_g = E'_{1u} \oplus E'_{2u} \oplus 2G'_u. \tag{IV.3.1}$$

Une remarque importante (également valable pour le cas de la bande ν_6 de $V(CO)_6$, voir chapitre IV.2) est que même si la bande étudiée est globalement très intense (intensité totale grande), l'éclatement vibronique provoque un étalement des raies sur une zone spectrale relativement large. Il y a de plus un très grand nombre de raies rovibroniques, chacune étant en réalité peu intense, individuellement. Ceci fait que l'intensité en chaque point du spectre rovibronique est faible. En spectroscopie par transformée de Fourier dans un jet moléculaire supersonique, la sensibilité de l'expérience s'est donc avérée insuffisante pour effectuer des enregistrements à un résolution meilleure que 0.5 cm^{-1}. Par contre, comme nous le verrons plus bas, la spectroscopie par diode laser, beaucoup plus sensible, nous a permis d'enregistrer quelques portions de spectre à haute résolution.

Tout comme pour $V(CO)_6$, nous avons donc commencé par considérer le profil à basse résolution de la bande considérée. Pour la région ν_3 de ReF_6, celui-ci est également assez caractéristique, bien que plus complexe. Une difficulté supplémentaire concernant cette molécule vient de la présence, en abondance naturelle, de deux isotopomères, $^{185}ReF_6$ (37.40 %) et $^{187}ReF_6$ (62.60 %). Pour chacun de ces isotopomères, l'hamiltonien effectif pour le niveau $v_3 = 1$ a été développé à l'ordre 3 en utilisant le formalisme du Chapitre IV.1 (21 paramètres, dont 4 purement vibroniques). L'hamiltonien effectif pour l'état de base a été développé à l'ordre 0 seulement (2 paramètres) et le moment dipolaire à l'ordre 2 (4 paramètres). Les paramètres purement rovibrationnels ont été fixés aux valeurs obtenues pour la molécule WF_6, très voisine [P29]. La valeur optimale des paramètres vibroniques a alors été

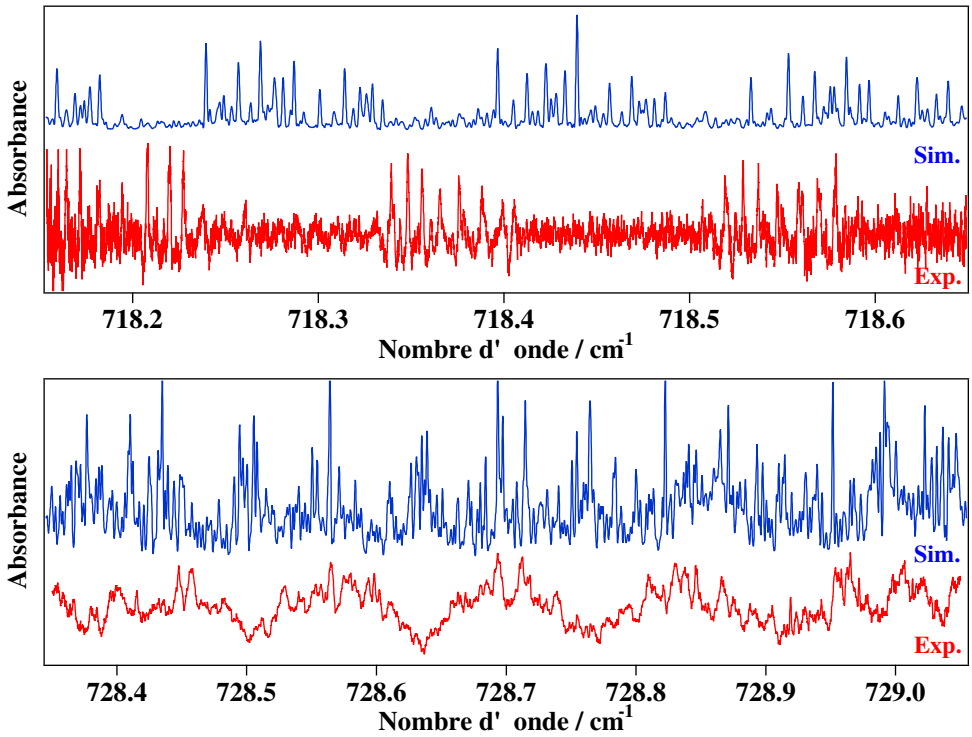

FIG. 3.2 – *Deux spectres d'absorption par diode laser en jet supersonique dans la région de la bande ν_3 de ReF_6 (résolution de 0.0007 cm^{-1}, température rotationnelle d'environ 50 K) comparés à la simulation préliminaire. On peut constater des similarités importantes dans les structures (voir texte).*

recherchée à la main, afin d'obtenir la meilleure reproduction possible du profil de bande. Celui-ci a encore été amélioré en "ajustant" de la même manière quelques paramètres rovibroniques.

Le résultat est présenté sur la Figure 3.1. Pour tenir compte de l'absorption au-delà de 730 cm^{-1}, la bande $\nu_2 + \nu_6$ a été ajoutée, selon le même principe. Ceci est justifié par le fait que cette bande de combinaison est la bande proche de ν_3 la plus intense pour tous les hexafluorures (voir le cas de SF_6 au Chapitre III.1). Pour les quatre sous-niveaux vibroniques, nous trouvons les positions suivantes, en très bon accord avec l'étude préliminaire de la Référence [P11].

$$\begin{array}{lcl} E'_{1u} & : & 713.68\ cm^{-1} \\ E'_{2u} & : & 714.97\ cm^{-1} \\ G'_{u} & : & 722.29\ cm^{-1} \\ G'_{u} & : & 726.71\ cm^{-1} \end{array} \qquad \text{(IV.3.2)}$$

Comme déjà mentionné ci-dessus, il a été possible, toujours lors de mon stage post-doctoral à l'ETH Zürich, d'enregistrer des spectres d'absorption en jet supersonique de la même région ν_3, mais cette fois-ci à l'aide de diodes laser. Grâce à la grande sensibilité de celles-ci (sachant également que nous disposions d'un jet fente de 30 mm et d'un dispositif optique à quatre passages), des spectres à la résolution 0.0007 cm^{-1} ont été obtenus, mais seulement pour quelques portions de moins d'un cm^{-1} chacune.

Très récemment, lors de son stage post-doctoral au sein du même groupe de l'ETH Zürich, Michaël Rey a pu effectuer des simulations à haute résolution des régions étudiées par diode laser, en utilisant les paramètres obtenus via l'analyse du profil à basse résolution. Une partie de ces résultats préliminaires sont montrés sur les Figures 3.2 et 3.3. Bien évidemment, ces simulations ne reproduisent pas précisément les spectres expérimentaux, mais il est très encourageant d'observer de grandes similitudes entre les structures observées et calculées.

Il est clair qu'un gros travail reste à accomplir pour une analyse détaillée de la région de la bande ν_3 à haute résolution. Ceci nécessitera sans doute l'obtention de nouvelles données expérimentales.

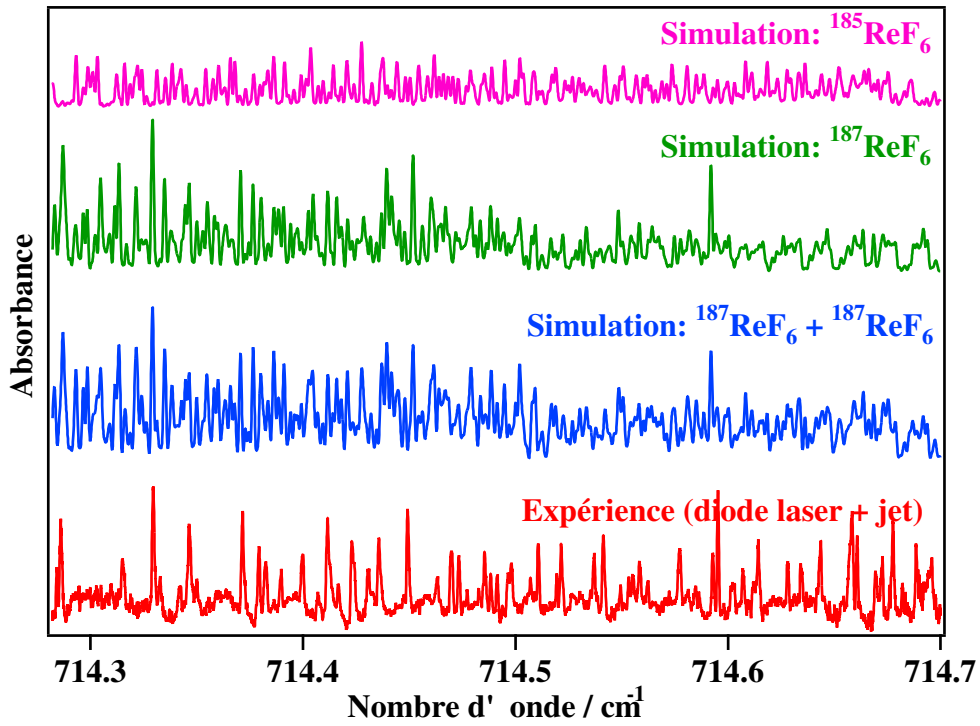

FIG. 3.3 – *Idem Figure 3.2 pour une autre région de la bande ν_3. La superposition des spectres des deux isotopomères est ici explicitée.*

Néanmoins, il est clair que les résultats obtenus sont très encourageants et montrent que le modèle élaboré permet une bonne compréhension de ce problème.

3.4 Articles-clés

Sont reproduits deux articles à caractère principalement expérimental concernant la spectroscopie de ReF_6.

- [**P11 :** *Spectrochim. Acta A*, **55**, 1575–1584 (1999)] présente le spectre rovibronique de ReF_6, du proche nfrarouge à l'ultraviolet.
- [**P29 :** *J. Chem. Phys.*, **117**, 3196–3207 (2002)] présente les spectres en jet supersonique (transformée de Fourier et diode laser) de WF_6 er ReF_6 enregistés à l'ETH Zürich (Suisse) lors de mon stage post-doctoral. Un petit modèle préliminaire très simplifié est présenté pour ReF_6. Celui-ci est antérieur au modèle complet développé lors de la thèse de Michaël Rey. Cependant, les résultats des deux approches sont très similaires en ce qui concerne la position des sous-niveaux (voir ci-dessus).

Voir aussi, sur le même sujet, la Référence [A2] reproduite au Chapitre IV.1.

ELSEVIER

Spectrochimica Acta Part A 55 (1999) 1575–1584

SPECTROCHIMICA ACTA PART A

Absorption spectrum of the $a(E'_{2g}) \leftarrow X(G'_g)$ and $b(G'_g) \leftarrow X(G'_g)$ electronic transitions of ReF_6

M. Rotger [a,*], V. Boudon [a], H. Selig [b]

[a] *Laboratoire de Physique de l'Université de Bourgogne, (Unité associée au C.N.R.S.), B.P. 400–21011 Dijon Cedex, France*
[b] *Department of Inorganic and Analytical Chemistry, The Hebrew University of Jerusalem, Jerusalem 91904, Israel*

Received 24 October 1998; received in revised form 24 November 1998; accepted 24 November 1998

Abstract

The absorption spectra of the near-infrared and ultraviolet bands of ReF_6 have been recorded with a commercial spectrophotometer. The vibronic assignments previously published by different authors are critically revised. A non-perturbative method has been used to calculate the linear Jahn–Teller levels for the ν_5 mode in the ground electronic state. Some new vibronic parameter values are derived. The ν_5 linear Jahn–Teller parameter in the $X(G'_g)$ electronic state is found to be $D_5 = 0{,}103(9)$. The ultraviolet absorption spectrum has enabled us to determine relatively accurate values of the crystal-field ($10Dq$) and spin-orbit (ζ_d) parameters.

Keywords: Rhenium hexafluoride; Absorption spectroscopy; Vibronic transitions

1. Introduction

In two previous papers [1,2], we have analysed in detail the vibronic bands of IrF_6 and also the visible band of OsF_6 [3]. We present here a preliminary study of another third-row transition-metal hexafluoride, namely ReF_6. This molecule is used in chemical vapour deposition for anti-corrosion layers and in microelectronics (deposition of rhenium–tungsten alloys) [4–8]. There exist only a very few studies on the near-infrared and ultraviolet absorption spectroscopy of this molecule. Some low resolution absorption spectra have been recorded and partially assigned by Moffit et al. [9], Brand et al. [10], McDiarmid [11], and Holloway et al. (ReF_6 in a matrix) [12]. These different studies were sometimes contradictory, so it appeared to us necessary to re-examine the vibronic spectrum of this molecule in view of our preceding work on iridium and osmium hexafluorides. In this paper, we present a detailed analysis and parameter values arising from the analysis of the vibronic transitions between the ground and the first excited electronic state of ReF_6, this one being well isolated from the others. This enabled us to obtain an indirect determination of the ground state linear Jahn–Teller parameter for the ν_5 mode. We also show the

* Corresponding author. Tel.: +33-3-80-39-59-67; fax: +33-3-80-39-59-71.
E-mail address: rotger@jupiter.u-bourgogne.fr (M. Rotger)

1386-1425/99/$ - see front matter
PII: S1386-1425(98)00338-2

ultraviolet region. Although this latter spectrum is still to be interpreted, it allowed us to determine the electronic parameters $10Dq$ and ζ_d.

2. Experiment

Rhenium hexafluoride is a colourless gas, with a vapour pressure of 590 Torr at 300 K [13]. We filled a 35 mm length quartz cell with this substance, using a method similar to that described in Ref. [1], and explained in detail hereafter. Pure ReF_6 was obtained by heating the volatile fluorination products of rhenium metal to 400°C in the presence of excess Re metal. Any ReF_7 present originally is reduced to ReF_6 in this process [14]. The absence of ReF_7 and of $ReOF_5$ in our sample was verified by the fact that no trace could be seen of the strong ReF_7 bands at 300 and 355 cm^{-1} and of the $ReOF_5$ band at 990 cm^{-1} in the infrared spectrum [15]. Additional purification from HF and other impurities was carried by repeated trap-to-trap sublimation under high vacuum in as described elsewhere [16].

A sample cell of fused silica about 25 mm in diameter and 35 mm long was attached to the vacuum line via a graded seal and a Kovar-to-glass connection. It was baked out at 400°C under high vacuum. After cooling to room temperature the cell was pre-treated with ClF_3 which was then pumped off. The cell was again baked out at 400°C under vacuum, following which the appropriate amount of ReF_6 was distilled in and the cell was sealed off, while the ReF_6 was maintained at liquid nitrogen temperature. Final ReF_6 pressure in the ampoule was estimated at 200 Torr at room temperature.

Fig. 1 shows the near-infrared absorption spectrum of the $a(E'_{2g}) \leftarrow X(G'_g)$ transition, recorded using a Cary 5E (Varian) commercial spectrophotometer. The apparatus resolution was a few wavenumbers in this region. Some HF lines are visible.

3. Analysis of the $a(E'_{2g}) \leftarrow X(G'_g)$ transition

Using the simple crystal-field model described in Ref. [17], we can see that ReF_6 is a $(d)^1$ system (a single d electron in an octahedral field). This leads to three degenerate electronic states, the ground state $X(G'_g)$ and the $a(E'_{2g})$ and $b(G'_g)$ ones. We first focus on the case of the $a(E'_{2g})$ state. This one is quite well isolated and since it is a Kramers doublet, no vibronic couplings can occur in this case [17]. However, such vibronic (Jahn–Teller) couplings do appear in the ground electronic state [18], especially linear coupling terms for the ν_2 and ν_5 modes. Since for such a heavy molecule at room temperature many such levels are thermally populated, the Jahn–Teller effect in the $X(G'_g)$ state has to be taken into account for the analysis of the hot vibronic bands of the $a \leftarrow X$ transition. Since ν_5 has a much lower frequency than ν_2, we expect to see many more hot transitions originating from the ν_5 levels.

We started from the assignments of Brand et al. [10], and McDiarmid [11]. The overall spectrum appears to be very dense. The pure electronic transition being forbidden ($g \leftrightarrow g$ transitions are not electric dipole allowed in XY_6 molecules), it is not itself visible and the global absorption is small. The intensity (and the main peaks observed) comes from transitions implying modes of u parity (ν_4, ν_6) in either the X or a state. Surprisingly, but just as in the case of the $a(G'_g)$ electronic state of IrF_6 [1], there seems to appear no transition implying the ν_3 stretching mode. But this one is known to be strongly perturbed in the $X(G'_g)$ state [19]. In Table 1, we give the observed frequencies and the results of the fit that we have realised using a least-squares fit method. The theoretical model taking into account the linear Jahn–Teller in the ground electronic state effect is explained in Ref. [1]. A non-perturbative treatment has been used which give better results that the perturbation theory developed by Brand et al. [20], or McDiarmid [11]. We work in a $|v_5(l_5\Sigma)j_5m_5\rangle$ basis set, $\mathbf{l_5}$ being the vibrational angular momentum for the ν_5 mode ($l_5 = v_5, v_5 - 2, \ldots, 0$ or 1), $\mathbf{\Sigma}$ the $X(G'_g)$ pseudo-spin ($\Sigma = 1/2$) [1], and $\mathbf{j_5} = \mathbf{l_5} + \mathbf{\Sigma}$. The Jahn–Teller matrix is of infinite dimension, since the linear Jahn–Teller Hamiltonian couples v states with $v+1$ ones (see Ref. [1]). For a given j_5 value, we have for the Hamiltonian matrix:

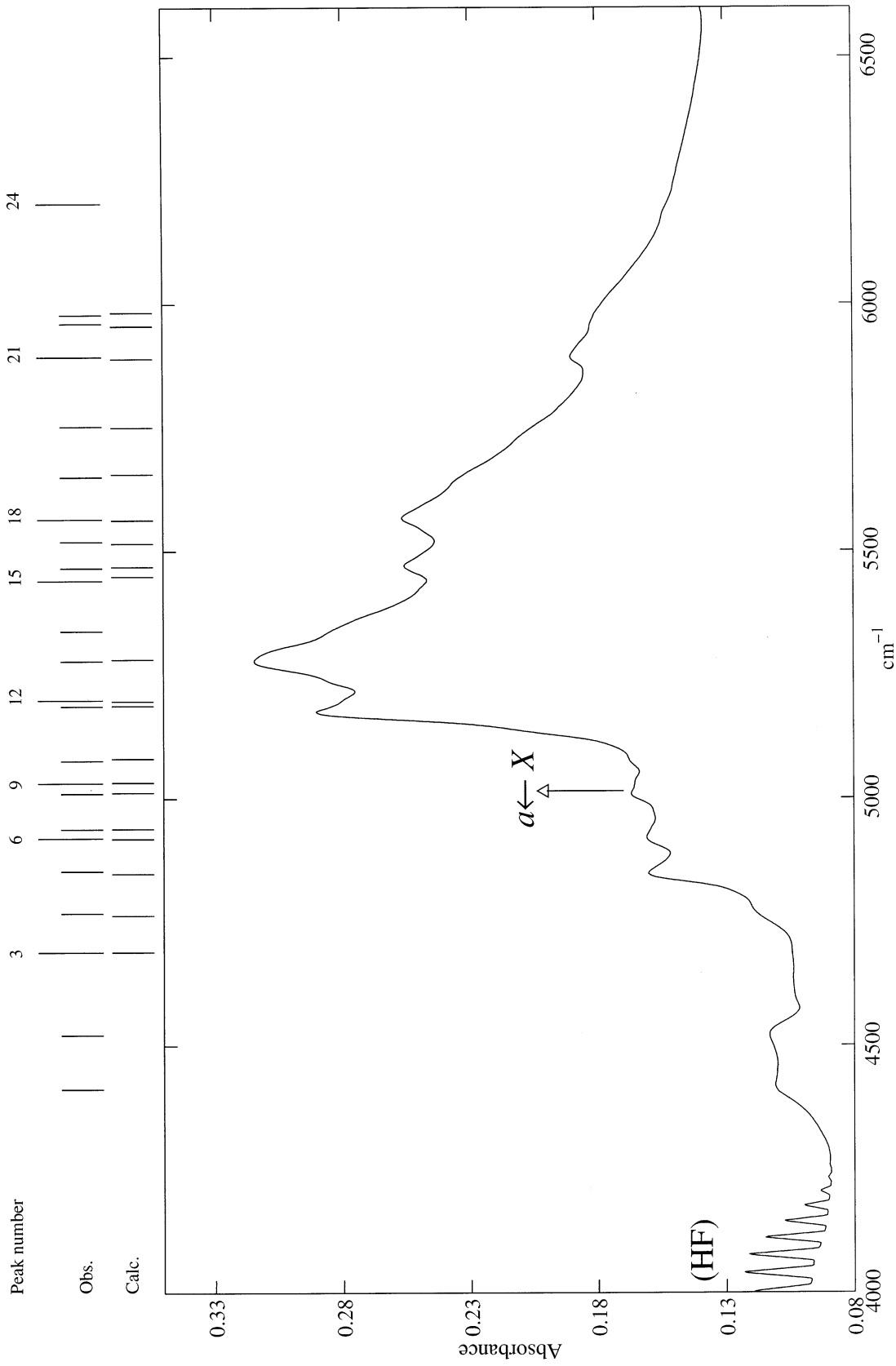

Fig. 1. Absorption spectrum of the $a(E'_{2g}) \leftarrow X(G'_g)$ transition (wavenumber in cm^{-1}), with observed and calculated peak positions.

$$\hat{H}(v_5, j_5) = \hbar\omega_5 \times$$

$$\begin{bmatrix} j_5+1 & \sqrt{2D_5(j_5+1)} & & & & \\ \sqrt{2D_5(j_5+1)} & j_5+2 & \sqrt{2D_5} & & & \\ & \sqrt{2D_5} & j_5+3 & \sqrt{2D_5(j_5+2)} & & \\ & & \sqrt{2D_5(j_5+2)} & J_5+4 & \sqrt{4D_5} & \\ & & & \sqrt{4D_5} & \ddots & \ddots \\ & & & & \ddots & \ddots \end{bmatrix} \quad (1)$$

Table 1
Assignments and fit for the $a(E'_{2g}) \leftarrow X(G'_g)$ transition (wavenumber in cm^{-1})[a]

Peak number	R. McDiarmid		Brand et al.		This work			
$a \leftarrow X$	ν_{obs}	Assignment	ν_{obs}	Assignment	ν_{obs}	Assignment	ν_{calc}	$\nu_{obs}-\nu_{calc}$
1	–	–	–	–	412.61_p	?	–	–
2	–	–	–	–	4522.26_p	?	–	–
3	–	–	–	–	4689.60_{sh}	$\boldsymbol{\nu'_4-2\nu''_5(\frac{1}{2})}$	4689.79	−0.19
4	4760	$-\nu''_6+\nu'_5-\nu''_5(\frac{1}{2})$	–	–	4768.69_{sh}	$-\nu''_6+\nu'_5-\nu''_5(\frac{1}{2})$	4763.90	4.78
5	4850	$-\nu''_6+2\nu'_4-2\nu''_4$	4834	$-\nu''_6$	4853.50_p	$-\nu''_6$	4848.54	4.96
6	–	–	–	–	4920.50_p	$\boldsymbol{\nu'_6-\nu''_4}$	4918.81	1.69
7	4910	$\nu'_6-\nu''_5(\frac{3}{2})$	4920	$\nu'_6-\nu''_5(\frac{1}{2})$	4939.13_{sh}	$\nu'_6-\nu''_5(\frac{3}{2})$	4939.33	−0.20
8	–	–	–	–	5011.00_p	$\boldsymbol{\nu'_4-\nu''_4}$	5012.69	−1.69
9	5009	$\nu'_4-\nu''_5(\frac{3}{2})$	–	–	5032.17_{sh}	$\nu'_4-\nu''_5(\frac{3}{2})$	5033.21	−1.03
10	5065	–	–	–	5077.00_{sh}	$\boldsymbol{\nu'_2-\nu''_2}$	5081.09	−4.09
11	5158	ν'_6	5167	ν'_6	5187.00_p	ν'_6	5188.15	−1.14
12	5193	$\nu'_4+\nu'_5-\nu''_5(\frac{1}{2})$	–	–	5199.78_{sh}	$\nu'_4+\nu'_5-\nu''_5(\frac{1}{2})$	5197.40	2.38
13	5261	ν'_4	5271	ν'_4	5279.00_p	ν'_4	5282.03	−3.03
14	–	–	–	–	5339.50_{sh}	?	–	–
15	5415	$\nu'_6+4\nu'_5-3\nu''_5(\frac{3}{2})$	–	–	5441.30_{sh}	$\nu'_6+4\nu'_5-3\nu''_5(\frac{3}{2})$	5449.57	−8.27
16	–	–	5470	$\nu'_5+\nu'_6$	5467.00_p	$\nu'_5+\nu'_6$	5469.50	−2.50
17	5484	$\nu'_6+4\nu'_5-3\nu''_5(\frac{3}{2})$ $+\nu'_2-\nu''_2$	–	–	5520.21_{sh}	$\nu'_6+4\nu'_5-3\nu''_5(\frac{3}{2})$ $+\nu'_2-\nu''_2$	5516.11	4.09
18	–	–	5568	$\nu'_1+\nu'_5$	5565.50_p	$\nu'_4+\nu'_5$	5563.39	2.11
19	5630	ν'_2	–	–	5650.40_{sh}	ν'_2	5656.05	−5.65
20	–		–	–	5753.00_{sh}	$\boldsymbol{2\nu'_5-\nu'_6}$	5750.86	2.14
21	5882	$\nu'_1+\nu'_6$	5888	$\nu'_1+\nu'_6$	5894.00_p	$\nu'_1-\nu'_6$	5889.81	4.19
22	–	–	–	–	5961.74_{sh}	$\boldsymbol{\nu'_5-\nu'_6(\frac{3}{2})+\nu'_4-\nu'_2}$	5956.08	5.65
23	–	–	5981	$\nu'_1+\nu'_4$	5979.50_{sh}	$\nu'_1+\nu'_4$	5983.69	−4.19
24	–	–	–	–	6204.35_{sh}	?	–	–

[a] ν'_i and ν''_i are the vibrational frequencies of mode i in the $a(E'_{2g})$, and $X(G'_g)$ electronic states, respectively. The peak numbers are the same as in Fig. 1. For levels implying ν''_5, the j_5 value is indicated in parentheses. New assignments appear in boldface.

Table 2
Vibronic parameters for ReF_6 (in cm^{-1})[a]

Electronic state	Vibrational wavenumber (cm^{-1})							JT Parameter
	v_0	$v_1(A_{1g})$	$v_2(E_g)$	$v_3(F_{1u})$	$v_4(F_{1u})$	$v_5(F_{2g})$	$v_6(F_{2u})$	D_5
$X(G'_g)$	–	–	575.0(5.9)	–	269.3(4.5)	286.3(2.3)	166.0 (fixed)	0.103(9)
$a(E'_{2g})$	5014.5(3.4)	701.7(4.5)	641.5(5.0)	–	267.5(4.3)	281.3(1.9)	173.6(5.0)	–

[a] The column v_0 gives the energy of the $a(E'_{2g})$ electronic state. The standard deviation is given in parentheses in the unit of the last two figures.

Rows and columns are indexed by the v_5 values:

$$v_5 = j_5 - \tfrac{1}{2}, j_5 + \tfrac{1}{2}, j_5 + \tfrac{3}{2}, j_5 + \tfrac{5}{2}, \ldots \quad (2)$$

So, it was necessary to truncate this matrix at some high v_5 values and we chose $(v_5)_{max} = 15$. The other modes were treated as being harmonic oscillators.

The corresponding peak positions (observed and calculated) are displayed at the top of Fig. 1. As we mentioned before, the origin of the electronic transition is extremely weak ($a(E'_{2g}) \leftarrow X(G'_g)$) being even invisible). Most of the assignments are in good agreement with those found by Brand et al. and R. McDiarmid. Some new ones have been added and are indicated in the table in boldface. We can notice some small discrepancies between observed and calculated line positions as indicated in the last column of this Table. However, the global root-mean squares of the fit is quite good, about 1.14 cm^{-1}. We have assigned 20 peaks or shoulders and this leads to the determination of the vibronic parameter values listed in Table 2. The only Jahn–Teller parameter that could be derived was that for the v_5 band in the electronic ground state. The v_2 band also presents some linear Jahn–Teller effect and this should explain the rather low vibronic value found for this band in the $X(G'_g)$ electronic ground state. The v''_2 value that we determined probably corresponds to the $v''_2(1/2)$ component (the lowest $v_2 = 1$ component with $j_2 = 1/2$). As v''_2 appears only one time in our assignments, it was not possible to fit the D_2 linear Jahn–Teller parameter. As one of our criteria was to obtain ground state parameters close to those reported in the literature [10,11], we found it necessary to fix v''_6 at 166.0 cm^{-1}. A few observed bands remain unassigned (especially the two features around 4500 cm^{-1}).

Table 3 lists the theoretical and experimental values for the linear Jahn–Teller levels corresponding to the v_5 band. These experimental values have been derived from the few assignments of Table 1 involving some Jahn–Teller components. They are in good agreement with the computed ones obtained using a non-perturbative model [1]. These levels are also displayed on Fig. 2.

4. The UV spectrum of ReF_6

Fig. 3 is an overview absorption spectrum of the ultraviolet region. Such a study has already been investigated by R. McDiarmid [11], and Holloway et al. [12]. We present here the first detailed spectrum of this ultraviolet region of ReF_6. The huge absorption above 35 000 cm^{-1} corresponds to $\pi(F) \rightarrow d(Re)$ charge-transfer bands [2,9,12]. Around 30 000 cm^{-1}, a very faint structure appears. This corresponds to the $b(G'_g) \leftarrow X(G'_g)$ transition (see below). This is in

Table 3
Observed and calculated linear Jahn–Teller levels for the v_5 mode in the $X(G'_g)$ electronic ground state

v_5	j_5	v_5 X state	
		Calc. (cm^{-1})	Obs. (cm^{-1})
0	1/2	0	0
1	3/2	249.4	247.3
1	1/2	361.0	362.3
2	1/2	587.2	592.4
3	3/2	856.6	865.8

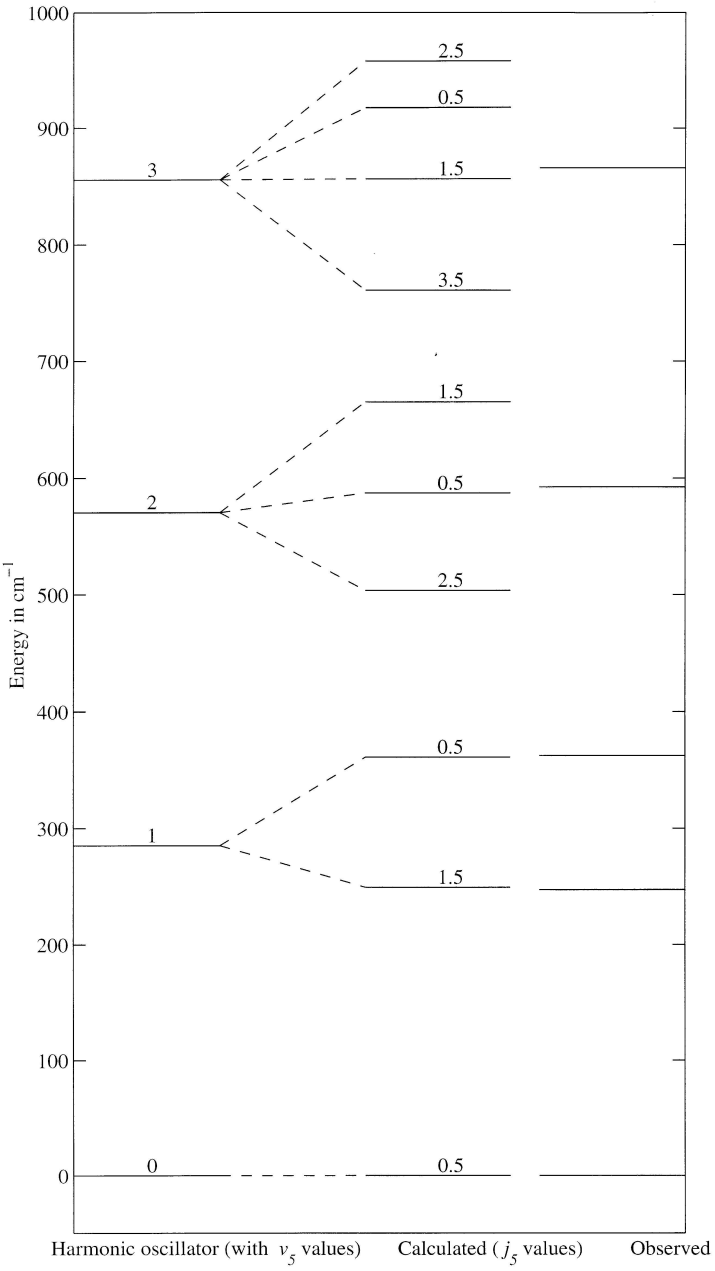

Fig. 2. Observed and calculated linear Jahn–Teller levels for ReF_6.

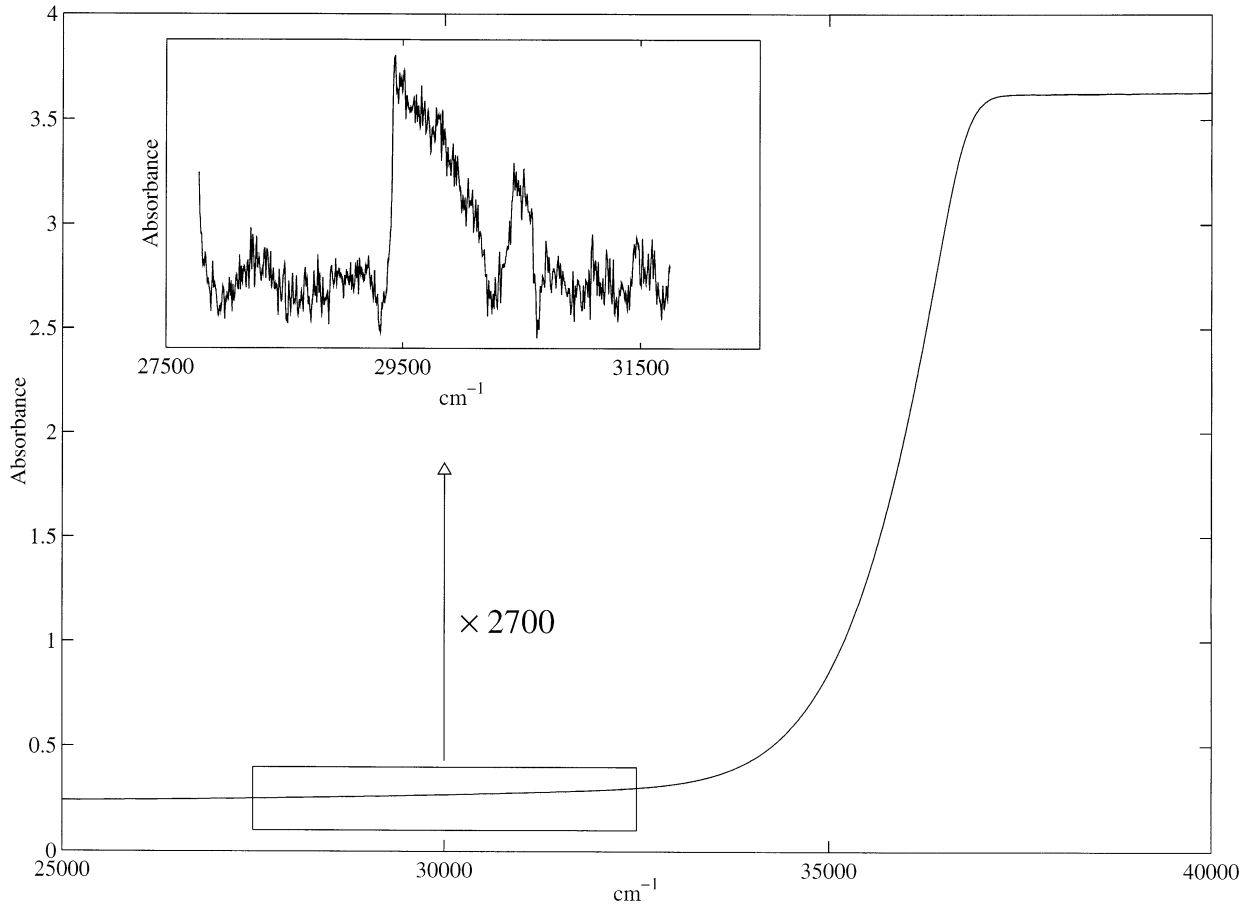

Fig. 3. UV spectrum of ReF_6 (wavenumber in cm^{-1}). The detail shows the absorption spectrum of the $b(E'_g) \leftarrow X(G'_g)$ transition.

fact an $(e_g)^1 \leftarrow (f_{2g})^1$ interconfigurational transition [2]. The details of this transition on Fig. 3 have been obtained by subtracting the continuous absorption in this region after having fitted the latter with a polynomial of degree 9.

Since both the b and X states are strongly perturbed by Jahn–Teller couplings and since this extremely weak absorption led us to a quite poor quality spectrum, it was not possible to analyse the $b \leftarrow X$ transition in detail. However, its precise location allows us to obtain a good determination of the electronic parameters.

5. Electronic parameters

From a simple theoretical point of view, the central Re^{6+} ion has only one d-type electron placed in the octahedral potential created by the six F^- ions. As a consequence, the electronic part of the Hamiltonian can be written:

$$\tilde{H}_{el} = \underbrace{H_0}_{\substack{\text{Kinetic energy + spherical} \\ \text{part of the potentials}}} + \underbrace{H_C}_{\substack{\text{Coulombian} \\ \text{interaction}}} + \underbrace{H_{SO}}_{\substack{\text{Spin-orbit} \\ \text{interaction}}} + \underbrace{V_{OCT}}_{\substack{\text{Octahedral} \\ \text{potential}}} \quad (3)$$

It is possible to express the octahedral potential in the following manner:

$$V_{oct} = 10Dq \times \frac{2\sqrt{21\pi}}{5} Y^{(4,A_1)}, \quad (4)$$

$10Dq$ being the crystal-field parameter and $Y^{(4,A1)}$ a totally symmetric combination of $Y_m^{(4)}$ spherical harmonics, say:

$$Y^{(4,A_1)} = \sqrt{\frac{5}{24}}(Y_4^{(4)} + Y_{-4}^{(4)}) + \sqrt{\frac{7}{12}} Y_0^{(4)}. \quad (5)$$

Table 4
Comparisons between $10Dq$ and ζ_d (values in cm^{-1})

	McDiarmid	Moffit et al.	Holloway et al.	This work
a origin location	4993	5200	?	5014.5(3.4)[b]
b origin location	?	32 500	30 190	29 430
$10\ D_q$	?	30 766[a]	28 000	27 759[a]
ζ_q	?	3467[a]	3300	3343[a]

[a] Calculated with Eqs. (10) and (11).
[b] Standard deviation in the unit of the last two figures given in parentheses.

If we consider just one d-type electron, there is no Coulombian interaction and H_0 is a constant term, we can write H_{so} as:

$$H_{so} = \zeta_d \mathbf{l}\cdot\mathbf{s} = \frac{\zeta_d}{2}(\mathbf{j}^2 - \mathbf{l}^2 - \mathbf{s}^2), \tag{6}$$

$\mathbf{l}$ and $\mathbf{s}$ being the orbital, and spin electronic angular momenta, respectively, and $\mathbf{j} = \mathbf{l} + \mathbf{s}$. In our case, $V_{oct} \gg H_{so}$ (this is the so-called strong-field case [9]) and if we use the following basis set:

$$|l\Gamma_b, s\Gamma_s, \Gamma\sigma\rangle = |2\Gamma_b, \tfrac{1}{2}E'_1, \Gamma\gamma\rangle,\ \Gamma_l = E\ or\ F_2, \tag{7}$$

the Γ's being O_h^S irreducible representations [21], the electronic Hamiltonian matrix can be written as:

$$\tilde{H}_{el}^{(n=1)} =$$

$$\begin{bmatrix} E'_2 & G' & G' \\ \zeta_d - 4Dq & 0 & 0 \\ 0 & \frac{1}{2}\zeta_d - 4Dq & -\sqrt{\frac{3}{2}\zeta_d} \\ 0 & -\sqrt{\frac{3}{2}\zeta_d} & 6Dq \end{bmatrix} \begin{matrix} |l\Gamma_b, s\Gamma_s, \Gamma\rangle \\ |2F_2, \tfrac{1}{2}E'_1, E'_2\rangle \\ |2F_2, \tfrac{1}{2}E'_1, G'\rangle \\ |2E, \tfrac{1}{2}E'_1, G'\rangle \end{matrix} \tag{8}$$

The corresponding eigenvalues give the energies of the three electronic states:

$$E(a) = E(E'_2) = \zeta_d - 4Dq,$$
$$E(b) = E_+(G') \simeq 6Dq,$$
$$E(X) = E_-(G') \simeq -\frac{\zeta_d}{2} - 4Dq, \tag{9}$$

(with the approximation that $10D_q \gg \zeta_d$). If we evaluate thanks to our experimental spectra the a and b state origins, it enables us to calculate the $10Dq$ and ζ_d values listed in the last column of Table 4, thanks to:

$$E(a \leftarrow X) = E(a) - E(X) = \tfrac{3}{2}\zeta_d, \tag{10}$$

$$E(b \leftarrow X) = E(b) - E(X) = 10Dq + \tfrac{1}{2}\zeta_d. \tag{11}$$

Our results are in good agreement with those of Holloway et al. [12]. Fig. 4 illustrates our results for the electronic structure of ReF_6.

6. Conclusion

This study is based theoretically on a linear Jahn–Teller model described in Ref. [1]. After describing the methods for synthesis and purification of ReF_6, we have recorded the near-infrared and ultraviolet low resolution absorption spectra. Some of our assignments complete those of Brand et al. [10] and those of McDiarmid [11]. New values for the vibronic parameters have been derived. We also present a first detailed ultraviolet absorption spectrum. This study has enabled us to give reasonable values for the electronic parameters $10Dq$ and ζ_d. As a perspective to the present work, we intend to investigate the near-infrared bands of OsF_6 and the very rich near-infrared and visible band system of PtF_6, which are very perturbed by Jahn–Teller and pseudo Jahn–Teller (in case of quasi-degenerate electronic states) effects.

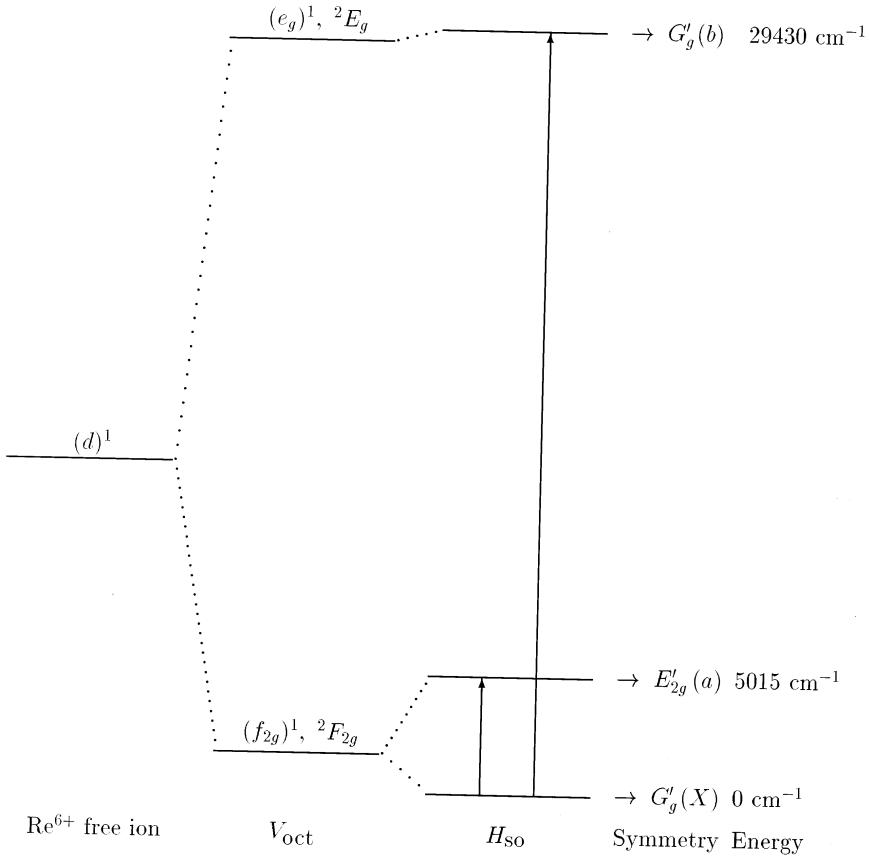

Fig. 4. Some of the lower electronic levels of ReF_6. The two arrows correspond to the observed $a(E'_{2g}) \leftarrow X(G'_g)$ and $b(G'_g) \leftarrow X(G'_g)$ transitions.

Acknowledgements

The authors thank Dr Alain Tabard (LIMSAG, Dijon, FRANCE) for having given us the opportunity of using the Varian spectrophotometer.

References

[1] V. Boudon, M. Rotger, D. Avignant, J. Mol. Spectrosc. 175 (1996) 327.
[2] V. Boudon, M. Rotger, D. Avignant, Spectrochim. Acta Part A 52 (1996) 1175.
[3] M. Rotger, V. Boudon, H. Selig, Spectrochim. Acta Part A 53 (1997) 991.
[4] C. Bernard, R. Madar, Y. Pauleau, Solid State Technol. 2 (1989) 79.
[5] F.W. Hoertel, J.G. Donaldson, Electrodepos. Surf. Treat. 2 (1973) 343.
[6] L.W. Roberts, The properties of CVD deposits of W and W–Re alloys in High Temperature Materials, 6th Plansee Seminar, June 1968, Reutte (Austria), (1969) 880.
[7] Yu.V. Laklatkin, A.I. Krosovskiy, Russ. Metall. Metally 1 (1983) 21.
[8] M. Pons, A. Benezech, P. Huguet, R. Gaufrès, P. Diez, J. Lafforet, J.C.V.D. 2 (1993) 135.
[9] W. Moffit, G.L. Goodman, M. Fred, B. Weinstock, Mol. Phys. 2 (1959) 109.
[10] J.C.D. Brand, G.L. Goodman, B. Weinstock, J. Mol. Spectrosc. 38 (1971) 449.
[11] R. McDiarmid, J. Mol. Spectrosc. 38 (1971) 495.
[12] J.H. Holloway, G. Stanger, E.G. Hope, W. Levason, J.S. Ogden, J. Chem. Soc. Dalton Trans., (1988) 1341.
[13] J.S. Malm, H. Selig, J. Inorg. Nucl. Chem. 20 (1961) 184.
[14] J.G. Malm, H. Selig, S. Fried, J. Am. Chem. Soc. 82 (1960) 1510.
[15] J.H. Holloway, H. Selig, H.H. Claassen, J. Chem. Phys. 54 (1971) 4305.

[16] B. Weinstock, J.G. Malm, J. Inorg. Nucl. Chem. 2 (1956) 380.
[17] V. Boudon, F. Michelot, J. Moret-Bailly, J. Mol. Spectrosc. 166 (1994) 449.
[18] B. Weinstock, G.L. Goodman, Adv. Chem. Phys. 9 (1965) 169.
[19] R.S. McDowell, L.B. Asprey, J. Mol. Spectrosc. 45 (1973) 491.
[20] J.C.D. Brand, G.L. Goodman, B. Weintstock, J. Mol. Spectrosc. 37 (1971) 464.
[21] V. Boudon, F. Michelot, J. Mol. Spectrosc. 165 (1994) 554.

JOURNAL OF CHEMICAL PHYSICS VOLUME 117, NUMBER 7 15 AUGUST 2002

High-resolution spectroscopy of the ν_3 band of WF_6 and ReF_6 in a supersonic jet

V. Boudon and M. Rotger
Laboratoire de Physique de l'Université de Bourgogne (UMR CNRS 5027), 9 av. A. Savary, B.P. 47870, F-21078 Dijon, France

Y. He, H. Hollenstein, M. Quack,[a] and U. Schmitt[b]
Physical Chemistry, ETH Zürich, CH-8093 Zürich, Switzerland

(Received 17 October 2000; accepted 13 March 2002)

We have recorded the Fourier-transform infrared (FTIR) spectrum of the ν_3 fundamental band of WF_6 in a continuous supersonic jet expansion with an instrumental bandwidth of 0.0024 cm^{-1} (FWHM, full width at half maximum, unapodized), using a Bomem DA.002 spectrometer. Some parts of this band have also been recorded with 0.0007 cm^{-1} bandwidth using a diode laser spectrometer combined with a pulsed slit jet expansion. A multiple-pass arrangement has been used for the slit jet to observe low-intensity lines. In each case, we have used a WF_6:He mixture with a seeding ratio 1:3 leading to a rotational temperature of ca. 50 K. This work extends the previous investigation of Takami and Kuze [J. Chem. Phys. **80**, 5994 (1984)] to much higher J transitions. In both P and R branches, rotational lines have been recorded for J up to 46–48. We have used a tensorial Hamiltonian adapted to the group chain $O(3)\supset O_h$ and developed to the third order for the analysis of the spectra. A least-squares fit for each of the four main isotopic species: $^{182}WF_6$, $^{183}WF_6$, $^{184}WF_6$, and $^{186}WF_6$ results in band centers (in this order) 714.538 19, 714.214 06, 713.895 44, and 713.266 21 cm^{-1}. We report furthermore first results on the high-resolution spectra of ν_3 of ReF_6, which exhibits a fourfold degenerate electronic ground state of G_g' species in the O_h^S group. Supersonic jet-FTIR spectra show a moderately structured relatively broad band, whereas the diode laser spectroscopy of the seeded jet in the range 708–733 cm^{-1} results in line resolved spectra of high complexity. A preliminary analysis is discussed, while a complete analysis still represents an appreciable challenge. © *2002 American Institute of Physics.* [DOI: 10.1063/1.1475754]

I. INTRODUCTION

The present paper aims at contributing to a systematic understanding of the ν_3 fundamental rovibronic structure of transition metal hexafluorides in general and WF_6 and ReF_6 in particular. These constitute the interesting first two members of this group of molecules arising from the third row elements and provide a striking contrast to each other. While WF_6 shows a relatively simple band structure of the degenerate $\nu_3(F_{1u})$ fundamental in the infrared spectrum, which has been the subject of several previous investigations also at high-resolution,[1–4] ReF_6 is an open-shell molecule, which exhibits a fourfold degenerate electronic ground state resulting in the prediction that ν_3 should consist of four transitions to four vibronic sublevels.[5] The observed spectra previously revealed only broad structures.[5–8]

In the present work we first provide an extended high-resolution analysis for ν_3 of WF_6 and then proceed to a first attempt at the high-resolution rovibronic spectroscopy of ReF_6. Tungsten hexafluoride is the first member of the third-row transition-metal hexafluoride series. It has a high vapor pressure (more than one atmosphere at room temperature[9]) and this leads to interesting opportunities for applications. First of all, this material is currently used to deposit tungsten thin films in microelectronics by chemical vapor deposition techniques.[10,11] WF_6 could also be a good candidate for laser isotope separation of tungsten. But this requires an accurate knowledge of the spectroscopic constants.[12] Furthermore, tungsten isotopes are of interest in isotope geology and dating.[13–15] The spectroscopy of W compounds as part of the group 6 elements has also gained further recent interest because of the proof that the transuranium element 106 Seaborgium (Sg) falls in this group,[16,17] and a corresponding conclusion holds presumably true for element 107 (Nielsbohrium, Ns or Bohrium, Bh) in relation to Re. The low resolution infrared[1,5] and Raman[18,19] spectra of this molecule have been known for a long time. But no rotational structure has been resolved in these early papers. Indeed, for such heavy transition-metal hexafluorides, high-resolution spectroscopy is not a simple task, since room temperature spectra are completely congested by hot bands due to the presence of low energy vibrational modes.[20,21] For WF_6, the ν_6 mode lies at 127 cm^{-1} (Ref. 20) and the ground vibrational state has a population of only 1.3% at 300 K. The thermal congestion is illustrated in the survey spectrum of Fig. 1, showing the FTIR spectrum of the ν_3 stretching fundamental region (around 14 μm). At room temperature, the structure is dominated by hot bands, even if some faint structures can be

[a]Author to whom correspondence should be addressed. Electronic mail: martin@quack.ch
[b]Present address: Institut für Physikalische Chemie der Universität Göttingen, Tammannstrasse 6, D-37077 Göttingen, Germany.

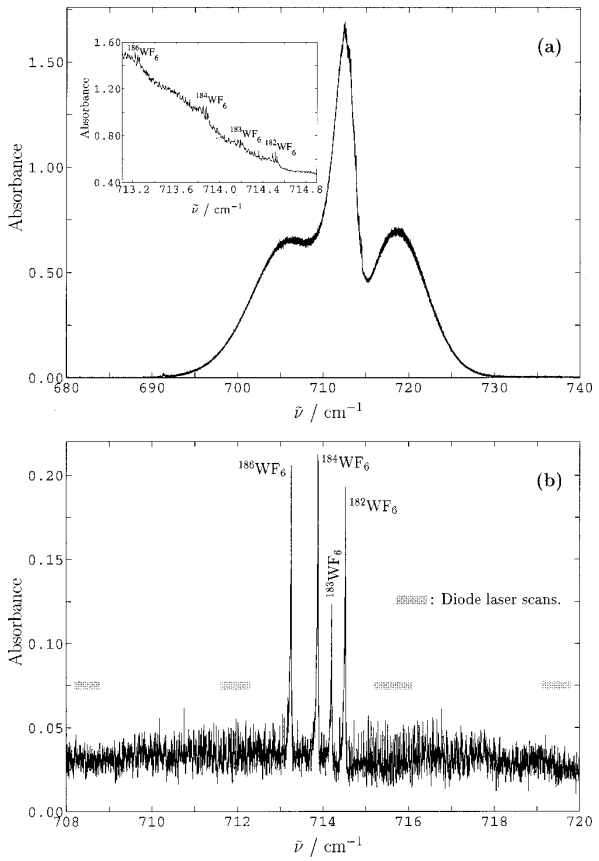

FIG. 1. (a) Overview FTIR spectrum of the ν_3 band of WF_6 at room temperature (0.3 mbar WF_6 in a 18 cm length glass cell with KBr windows), with an instrumental bandwidth of 0.0024 cm^{-1} (FWHM, unapodized). A detail is shown near the band center region, with the ν_3 Q branches of the four isotopomers. (b) Overview FTIR spectrum of the same region using a WF_6:He supersonic jet with a seeding ratio 1:3. The rotational temperature is estimated to 50 K. The gray sticks show the regions covered by the jet +diode laser experiment.

resolved, such as the ν_3 Q branches of the four isotopomers of natural abundance WF_6, and some very high J structures on top of the P and R wings. At low temperature in the supersonic jet expansion, the Q-branch structures of the four isotopomers emerge prominently.

Several authors have used a supersonic free jet of WF_6 in the past in order to achieve low temperature (vibrational and rotational) spectra and thus to resolve the rotational structure.[2–4] The most complete previous work was that of Takami and Kuze[4] who determined rotational constants for the four main isotopic species. They obtained a rotational temperature of 30 K. Under these conditions, rotational lines could be seen only up to $J=29$. In this paper we report a reinvestigation of the supersonic jet expansion spectroscopy of WF_6 with a higher rotational temperature (50 K) in which we were able to observe and identify rotational lines up to $J=48$. This enables us to give some refined values for the parameters.

Rhenium hexafluoride is the second member of the third-row transition series. Its vapor pressure is lower than that of WF_6 but still relatively high (590 torr at 300 K[9]). This molecule is used for the chemical vapor deposition of rhenium anticorrosion layers and in microelectronics in association with WF_6 (deposition of tungsten–rhenium alloys[10,22–24]). However, a particular interest of this molecule is its electronic structure having an unpaired d electron.[25–29] As explained, for example, in Ref. 29, this leads to a fourfold degenerate electronic ground state of G_g' species in the group O_h^S (symmetry group of the octahedron with its spinorial representations, see Ref. 30) as well as to the presence of half-integer angular momenta. ReF_6 pertains to a family of molecules often called "colored hexafluorides" since these open-shell systems (ReF_6,OsF_6,IrF_6,PtF_6,...) possess some low-lying electronic states leading to the absorption of visible or near infrared light. For instance, the first excited electronic state of ReF_6 lies at 5000 cm^{-1}.[29] The degeneracy of the electronic ground state implies complex rovibronic couplings. The unusual band profile observed at low resolution for the ν_3 fundamental[5,7,8] led McDowell and Asprey[5] to suspect that a quadratic vibronic coupling could be responsible for a splitting of the $v_3=1$ vibrational level (F_{1u} symmetry) into four vibronic sublevels (since $G_g'\otimes F_{1u}=E_{1u}'\oplus E_{2u}'\oplus 2G_u'$ in O_h^S), but this theoretical suggestion has never been supported by experiment through a high-resolution study which necessitates the use of a supersonic jet expansion, for the same reasons as explained above for WF_6. Moreover, the extremely aggressive nature of ReF_6 makes such a study difficult.

We report here the first supersonic jet expansion spectroscopy of rhenium hexafluoride. We present FTIR-jet and diode laser spectra of a seeded jet in the range 708–733 cm^{-1} which are to our knowledge the first resolved rovibronic spectra of an open-shell transition-metal hexafluoride ever recorded. The spectra show very complex and extensive line structures. An approximate model enables us to obtain a first estimate of the order of magnitude of the vibronic coupling parameters. A preliminary account of the present work has been presented in Ref. 31.

II. EXPERIMENT

Natural abundance tungsten hexafluoride (<0.2% $^{180}WF_6$, 26.4% $^{182}WF_6$, 14.4% $^{183}WF_6$, 30.6% $^{184}WF_6$, and 28.4% $^{186}WF_6$) and rhenium hexafluoride (37.40% $^{185}ReF_6$, 62.60% $^{187}ReF_6$) were furnished by the COMURHEX company in Pierrelatte (France). The BF_3 calibration gas was purchased from Elf Atochem (France). All substances were used without any further purification. The identity of the compounds was obvious from the spectra and the precise purity is not relevant for the present investigation, not attempting the measurement of quantitative band strengths.

A. WF_6 spectra

We have recorded the spectra in two different ways: (i) A Fourier-transform infrared spectrum is obtained for WF_6 in a continuous supersonic jet expansion setup described in Refs. 32 and 33 with an instrumental bandwidth of 0.0024 cm^{-1} (FWHM, unapodized), using a Bomem DA.002 spectrom-

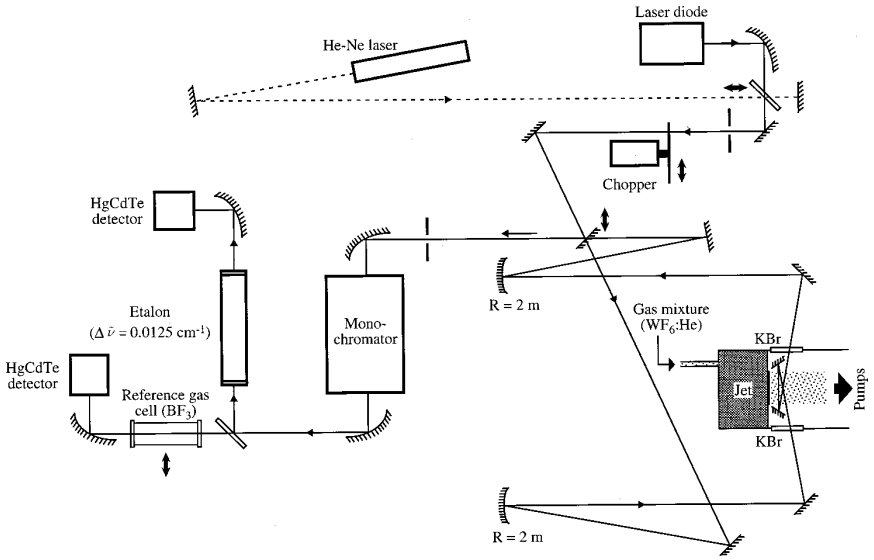

FIG. 2. Schematic drawing of the jet +diode laser experimental setup. $\Delta\tilde{\nu}$ is the free spectral range of the étalon.

eter. (ii) Diode laser spectra are taken with an instrumental bandwidth of 0.0007 cm^{-1} using a pulsed slit jet apparatus described in Ref. 34. The Doppler widths for WF_6 and ReF_6 fall in the range 0.0002 to 0.0005 cm^{-1} between 50 and 300 K (a range also expected to be relevant for the jet expansion) and thus the effective resolution in our experiments is largely determined by the instrumental bandwidths. For the present investigation, various parts of the jet system have been improved and exchanged to guarantee resistance to chemically very aggressive substances. The pumping system consisted of a 2000 m^3/h roots pump (WKP 2000, Balzers/Pfeiffer), which was backed by a 63 m^3/h rotary pump (Alcatel 2063CP). The pump oil was FOMBLIN® for both.

We have used a mixture of tungsten hexafluoride with helium, to achieve a better vibrational cooling. The WF_6:He seeding ratio was 1:3. Under these conditions, the rotational temperature was approximately T_{rot}=50 K. No hot band lines were observed. The vibrational ground state population should be about 95% at 50 K vibrational temperature.[21]

Figure 2 describes schematically the "jet+diode laser" experiment. The slit was 0.5×35 mm in dimension and operated below 0.5 Hz with an opening time of 2.5 ms. The diode laser frequency was scanned by modulating its current with a triangle signal.[34] The backing pressure was 350 mbar. A monochromator was used to select only one emission mode of the multimode diode laser output at a time. Using two small mirrors placed on both sides of the slit, we were able to perform up to nine passes in the jet. This was necessary for observing the high-J transitions (below 709 cm^{-1} and above 719 cm^{-1}) where the absorption was very weak. Figure 1(b) shows the wavenumber ranges where diode laser scans were carried out for WF_6.

The frequency calibration of the diode laser absorption spectra was realized as follows (see Fig. 3). First, the absorption spectrum was recorded simultaneously with the transmission fringes of a 40 cm long Fabry–Perot étalon. Then the spectrum of a reference gas (BF_3) in the cell was recorded, again together with étalon fringes. Etalon fringes were used to linearize the frequency scale, while the BF_3 lines from a FTIR spectrum gave the absolute calibration. We have chosen BF_3 as a reference gas, since it has a dense spectrum in the whole 660–740 cm^{-1} region.[35] For this purpose, we have recorded a FTIR spectrum of natural BF_3 (20% $^{10}BF_3$, 80% $^{11}BF_3$) at room temperature at the highest resolution (see above). This spectrum is displayed in Fig. 4. The BF_3 FTIR spectrum was itself calibrated against CO_2 and H_2O lines with an accuracy of about 0.0005 cm^{-1} in the 720 cm^{-1} region.[36]

B. ReF_6 spectra

For ReF_6, we have used the same experimental setup as described above. Diode laser spectra were calibrated in the same way, using BF_3 lines. We have used various seeding ratios with helium and argon to optimize the conditions. Figure 5 shows the survey FTIR spectra and the regions where diode laser scans were carried out. ReF_6 experiments are

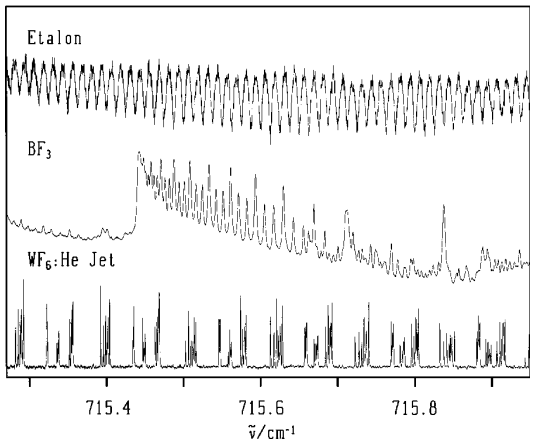

FIG. 3. Typical raw experimental data, showing transmission fringes of the étalon, reference gas peaks (10 mbar of BF_3 in a 18 cm long glass cell with KBr windows) and jet spectrum of the WF_6:He mixture.

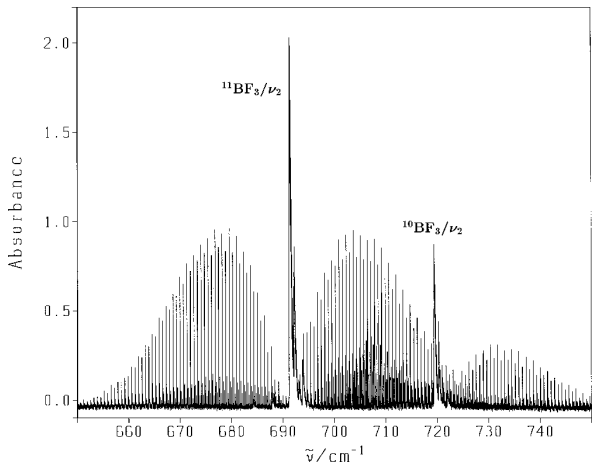

FIG. 4. FTIR spectrum of the ν_2 band of BF_3 at room temperature (0.5 mbar of BF_3 in a 18 cm long glass cell with KBr windows).

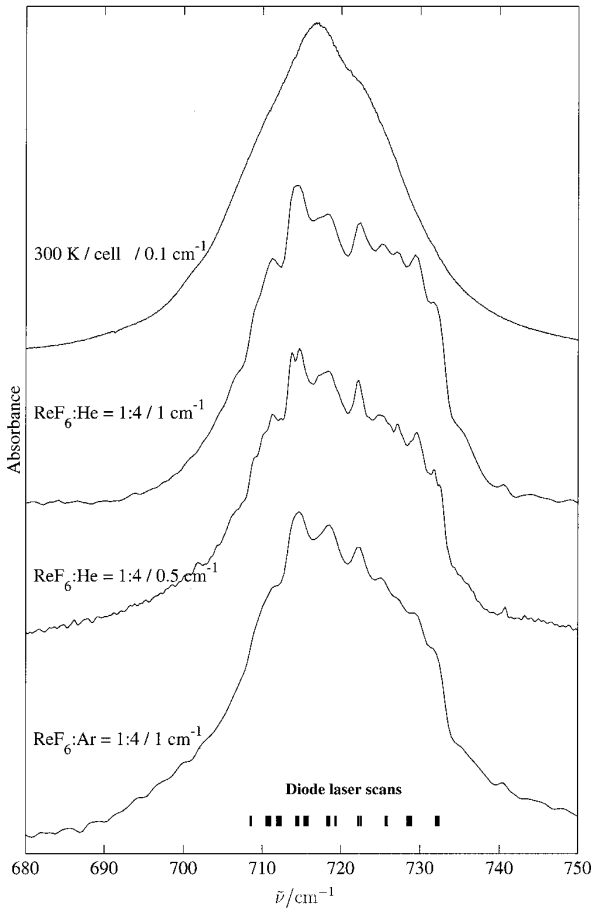

FIG. 5. Overview low-resolution FTIR spectra of the ν_3 band of ReF_6 at room temperature (0.3 mbar ReF_6 in a 18 cm length glass cell with KBr windows) and in a supersonic jet at different mixtures and instrumental bandwidths conditions.

more difficult to realize due to the chemical reactivity which is much greater for this species than for WF_6. As can be seen from Fig. 5, jet-cooled spectra of the ν_3 band show a band which is about as broad as that at room temperature. This is due to the rovibronic interactions which spread the quantum levels over a large energy range and thus the cooling effect does not result in the same band narrowing as for WF_6 (see Fig. 1). A consequence of this is that the effective absorption of ν_3 of ReF_6 is rather low since the absorption strength is distributed over a very large number of lines in a rather large wave number range. This low intensity prevented us to record high-resolution jet-FTIR spectra. However, it was possible to record diode laser spectra of the ReF_6:He supersonic expansion jet as will be described in Sec. IV B, using up to nine passes in the jet, corresponding to an effective optical pathlength up to 315 mm.

III. THEORY

A. The WF_6 closed-shell molecule and general aspects

The theory used here is based on the model developed by Champion, Loëte, and Pierre[37] for the analysis of spherical-top spectra. Since we consider here the ν_3 band as isolated, we can use the completely transformed Hamiltonian,

$$\tilde{H}=\tilde{H}_{\{0\}}+\tilde{H}_{\{\nu_3\}}+\cdots. \tag{1}$$

Here, $\tilde{H}_{\{0\}}$ is the purely rotational contribution which can be written as

$$\tilde{H}_{\{0\}}=\sum_{\Omega_r,K_r} t_0^{\Omega_r(K_r)}\beta^0_{\Omega_r,K_r}R^{\Omega_r(K_r,A_1)}, \tag{2}$$

the $R^{\Omega_r(K_r,A_1)}$ operators being defined as usual.[37,38] Here, $t_0^{\Omega_r(K_r)}$ is a parameter and $\beta^0_{\Omega_r,K_r}$ is a coefficient used to match the traditional spectroscopic notations[39] for the scalar terms [see below, Eq. (4)]. The ν_3 contribution is then

$$\tilde{H}_{\{\nu_3\}}=\sum_{K_v,\Omega_r,K_r,K} t_{3,3}^{2\Omega_r((K_vK_r)K)} \times\beta^2_{\Omega_r,K_r}[{}^{\varepsilon}V_{3,3}^{2(K_v)}\otimes R^{\Omega_r(K_r)}]^{(K,A_1)}, \tag{3}$$

where we realize the coupling of the vibrational $({}^{\varepsilon}V_{3,3}^{2(K_v)})$ and rotational operators in the $O(3)$ group. This is not the usual method,[40] but we choose it for consistency with the coupling scheme we use for molecules with a degenerate electronic ground state, like ReF_6 (see next paragraph). The $t_{3,3}^{2\Omega_r((K_vK_r)K)}$ are again parameters, and the $\beta^{\Omega_v}_{\Omega_r,K_r}$ factors are defined as

$$\beta^{\Omega_v}_{\Omega_r,K_r}=\begin{cases}\left(-\dfrac{\sqrt{3}}{4}\right)^{\Omega_r/2}(\sqrt{3})^{\Omega_v/2} & \text{if } K_r=0,\\ 1 & \text{if } K_r\neq 0.\end{cases} \tag{4}$$

Four vibrational operators are involved in Eq. (3), which are

$${}^{+}V_{3,3}^{0(0)}=\mathbb{I}\ \text{(identity operator)}, \tag{5}$$

$$ {}^{+}V^{2(0)}_{3,3} = -[a_3^{+(1)} \otimes a_3^{(1)}]^{(0)} = \frac{1}{\sqrt{3}} N_3^{(0)}, \tag{6} $$

$$ {}^{-}V^{2(1)}_{3,3} = -\frac{1}{\sqrt{3}} [a_3^{+(1)} \otimes a_3^{(1)}]^{(1)} = -\frac{1}{\sqrt{6}} l_3^{(1)}, \tag{7} $$

$$ {}^{+}V^{2(2)}_{3,3} = -\frac{1}{\sqrt{5}} [a_3^{+(1)} \otimes a_3^{(1)}]^{(2)}. \tag{8} $$

$N_3^{(0)}$ is the usual "number" operator and $l_3^{(1)}$ is the vibrational angular momentum. The upper left index $\epsilon = \pm$ gives the parity (even/odd) in the conjugate momenta $p_\sigma^{(F_{1u})}$ ($\sigma = x$, y, or z). Note that the parity index g or u has been omitted here for simplicity, since it is u for $a_3^{(1)}$ and $a_3^{+(1)}$ and g everywhere else. Overall parity could be defined as well by using the nonrigid molecule group S_6^*,[41,42] but this is not needed for the present analysis, which assumes a semirigid molecular framework, although it might be of interest at high energy or for reactive processes.[42]

Effective Hamiltonians for the ground and $v_3 = 1$ vibrational states are obtained simply by projecting the completely reduced Hamiltonian [Eq. (1)] on the subspaces spanned by the vibrational functions of these states, that is

$$ \mathbf{H}^{\langle 0 \rangle} = P^{\langle 0 \rangle} \tilde{H} P^{\langle 0 \rangle} = \mathbf{H}^{\langle 0 \rangle}_{\{0\}}, \tag{9} $$

$$ \mathbf{H}^{\langle \nu_3 \rangle} = P^{\langle \nu_3 \rangle} \tilde{H} P^{\langle \nu_3 \rangle} = \mathbf{H}^{\langle \nu_3 \rangle}_{\{0\}} + \mathbf{H}^{\langle \nu_3 \rangle}_{\{\nu_3\}}. \tag{10} $$

Practically, we use a coupled rovibrational basis of the type

$$ |\Psi_{\mathrm{IV}}\rangle = |v_3, (J, l_3) R, n C \sigma\rangle, \tag{11} $$

by setting $\mathbf{R} = \mathbf{J} - l_3$, $\mathbf{J}$ being the total and $\mathbf{R}$ the rotational angular momentum, where

$$ |R - l_3| \leqslant J \leqslant R + l_3 \tag{12} $$

and l_3 and thus R and C have u parity. It should be noted here, that g and u "parity" do not refer to the total parity. For a more detailed discussion of this point and the role of total (positive or negative) parity, we refer to Ref. 43, in conjunction with a more detailed analysis of the ReF_6 spectrum. C is the rovibrational symmetry in the O_h point group and σ its component. The matrix elements for $\mathbf{H}_{\{0\}}$ and $\mathbf{H}_{\{\nu_3\}}$ are then given by

$$ \langle v_3 = 0, (J, l_3 = 0) J n'' C \sigma | \mathbf{H}_{\{0\}} | v_3 = 0, (J, l_3 = 0) J n' C \sigma \rangle = \sum_{\Omega_r, K_r} (-1)^J \beta^0_{\Omega_r, K_r} F^{(K_r \; J \; J)}_{A_1 \; n'C\sigma \; n''C\sigma} \langle J \| R^{\Omega_r(K_r)} \| J \rangle t_0^{\Omega_r(K_r)}, \tag{13} $$

and

$$ \begin{aligned} &\langle \nu_3 = 1, (J, l_3 = 1) R'' n'' C \sigma | \mathbf{H}_{\{\nu_3\}} | v_3 = 1, (J, l_3 = 1) R' n' C \sigma \rangle \\ &= \sum_{\Omega_v, K_v, \Omega_r, K_r, K} (-1)^{R''} \beta^{\Omega_v}_{\Omega_r, K_r} F^{(K \; R' \; R'')}_{A_1 \; n'C\sigma \; n''C\sigma} \sqrt{[R'][R''][K]} \begin{Bmatrix} K_r & J & J \\ K_v & 1 & 1 \\ K & R' & R'' \end{Bmatrix} \langle J \| R^{\Omega_r(K_r)} \| J \rangle \\ &\quad \times \langle 1,1 \| V^{\Omega_v(K_v)}_{3,3} \| 1,1 \rangle t^{\Omega_v \Omega_r((K_v K_r) K)}_{3,3}. \end{aligned} \tag{14} $$

The F are oriented coupling coefficients in the group chain $O(3) \supset O_h$.[44] The necessary reduced matrix elements can be expressed as follows:

$$ \langle J \| R^{\Omega_r(K_r)} \| J \rangle = \left(-\frac{4J(J+1)}{\sqrt{3}} \right)^{(\Omega_r - K_r)/2} \times \left(\frac{2^{K_r} (K_r!)^2 (2J + K_r + 1)!}{(2K_r)! (2J - K_r)!} \right)^{1/2}, \tag{15} $$

$$ \langle 1,1 \| V^{\Omega_v(K_v)}_{3,3} \| 1,1 \rangle = 1, \quad \Omega_v \neq 0, \tag{16} $$

$$ \langle 1,1 \| V^{0(0)}_{3,3} \| 1,1 \rangle = \sqrt{3}. \tag{17} $$

As we only study here an isolated fundamental band, the dipole moment operator necessary for transition moment calculations was simply developed to order zero and the corresponding parameter was set to 1 (as we do not consider absolute intensities). Relative line intensities were computed using the Boltzmann rotational partition function and the nuclear spin statistical weights for XY_6 molecules having Y ligands with a 1/2 spin.[45,46]

To conclude this paragraph, let us mention that in their work, Takami and Kuze[4] used Hamiltonians for the ground and $v_3 = 1$ states using the Amat–Nielsen ordering scheme[39] and expressed as

$$ H_{\{0\}} = B_0 J(J+1) - D_0 J^2 (J+1)^2 - D_{044} T_{044}, \tag{18} $$

$$ \begin{aligned} H_{\{\nu_3\}} = {} & \nu_3 + B_3 J(J+1) - D_3 J^2 (J+1)^2 \\ & + [-2B\zeta_3 + F_{110} J(J+1)] T_{110} \\ & + \alpha_{220} T_{220} - D_{044} T_{044} + \alpha_{224} T_{224} + F_{134} T_{134}. \end{aligned} \tag{19} $$

This formulation is not so different from ours since the T_{ijk}'s and F_{ijk}'s are also spherical tensor operators and the matrix elements of these two Hamiltonians can be calculated through formulas very similar to (13) and (14). However, our formulation has some important advantages: First, it is more

TABLE I. Effective parameters for the ν_3 band of WF_6 (in cm^{-1}). J_{max} is the maximum J value observed in the P or R branch, and σ is the root mean square of the residuals.

Level	Order	Parameter	$^{182}WF_6$ (26.4%)	$^{183}WF_6$ (14.4%)	$^{184}WF_6$ (30.6%)	$^{186}WF_6$ (28.4%)	Notation of Ref. 39
$\upsilon_3=0$	0	$t_0^{2(0)}$ [a]	0.066 1000	0.066 1000	0.066 1000	0.066 1000	B_0
$\upsilon_3=1$	0	$t_{3,3}^{20(00)0)}$	714.557 65(22)	714.233 387(21)	713.914 60(21)	713.285 14(19)	ν_3
	1	$t_{3,3}^{21((11)0)}$	−0.041 253(27)	−0.040 994(27)	−0.040 634(17)	−0.040 149(27)	$-3\sqrt{2}B\zeta_3$
	2	$t_{3,3}^{22((00)0)}$	$-4.558(41)\times10^{-5}$	$-4.574(37)\times10^{-5}$	$-4.989(52)\times10^{-5}$	$-4.809(40)\times10^{-5}$	$\Delta B=B_3-B_0$
		$t_{3,3}^{22((22)0)}$	$-2.496(65)\times10^{-5}$	$-1.156(96)\times10^{-5}$	$-0.831(91)\times10^{-5}$	$-0.622(73)\times10^{-5}$	$-\frac{5}{4}\alpha_{220}$
		$t_{3,3}^{22((22)4)}$	$-9.169(54)\times10^{-5}$	$-9.141(64)\times10^{-5}$	$-9.301(60)\times10^{-5}$	$-9.259(56)\times10^{-5}$	$-\frac{30}{\sqrt{6}}\alpha_{224}$
	3	$t_{3,3}^{23((11)0)}$	$-0.64(14)\times10^{-7}$	$-1.36(13)\times10^{-7}$	$0.28(14)\times10^{-7}$	$-0.31(15)\times10^{-7}$	$-\frac{3\sqrt{6}}{8}F_{110}$
		$t_{3,3}^{23((13)4)}$ [b]	0.0	0.0	0.0	0.0	$\frac{3\sqrt{5}}{2}F_{134}$
	$\tilde{\nu}_0$ [c]		714.538 19	714.214 06	713.895 44	713.266 21	
	$J_{max}(P/R)$		46	47	48	43	
	Assigned transitions		260	201	232	253	
	$\sigma/10^{-3}$ cm^{-1}		1.2	1.3	1.3	1.2	

[a]Fixed to the value of electron diffraction measurement of Ref. 48.
[b]Fixed to zero (see text).
[c]Band center (see text, the uncertainty is of the same order as in line 2 of the table). The full list of wave numbers of measured and calculated line positions is available through EPAPS (Ref. 70).

general as it enables the systematic expansion of the rovibrational Hamiltonian with a straightforward extension to any vibrational level or polyad. Second, it uses the so-called "vibrational extrapolation" [37] in which the Hamiltonian for a given polyad (here ν_3) contains the parameters of all the lower polyads (here the ground state). The correspondence between our parameters and those of Ref. 4 is easy to establish and is given in the last column of Table I.

B. The ReF_6 open-shell molecule

It has been shown in Ref. 47 that the vibronic Hamiltonian for the $\nu_3(F_{1u})$ mode in a G_g' electronic state can be written as

$$H=\hbar\omega_3(N_3^{(0)}+\tfrac{3}{2})+H_{JTQ}^{(0,A_1)}+H_{JTQ}^{(4,A_1)}, \quad (20)$$

where $\omega_3/2\pi$ is the harmonic oscillator frequency, $N_3^{(0)}=a_3^{+(1)}\cdot a_3^{(1)}$ is the number operator and the two quadratic vibronic terms are

$$H_{JTQ}^{(0,A_1)}=2\sqrt{6}\hbar\omega_3 Q_0[[q_3^{(1)}\otimes q_3^{(1)}]^{(2)}\otimes T^{(2)}]^{(0,A_1)}, \quad (21)$$

$$H_{JTQ}^{(4,A_1)}=2\sqrt{6}\hbar\omega_3 Q_4[[q_3^{(1)}\otimes q_3^{(1)}]^{(2)}\otimes T^{(2)}]^{(4,A_1)}, \quad (22)$$

where $q_3^{(1)}=(a_3^{(1)}+a_3^{+(1)})/\sqrt{2}$, $T^{(2)}$ is an electronic operator,[47] $\omega_3/2\pi$ is the harmonic oscillator frequency and Q_0, Q_4 are the quadratic vibronic parameters. Formulæ for the calculation of the matrix elements of this Hamiltonian in a coupled vibronic basis

$$|\Psi_{ev}\rangle=|[\Psi_{\upsilon 3}^{(l_3)}\otimes\Phi^{(3/2)}]_{\sigma_0}^{(J_3,n_0C_0)}\rangle \quad (23)$$

are given in Ref. 47. Here,

$$|l_3-\tfrac{3}{2}|\leq J_3\leq l_3+\tfrac{3}{2}, \quad (24)$$

$\mathbf{J}_3$ being the vibronic angular momentum. As this Hamiltonian matrix is of infinite dimension, we can calculate the energy levels in practice by truncating υ_3 at some high value (say, $\upsilon_3=20$). Figure 6 shows the four resulting eigenvalues for $\upsilon_3=1$ (as a function of Q_0 and Q_4) that correspond to the four vibronic sublevels expected for the ν_3 band.

As the complete treatment of the rovibronic interactions

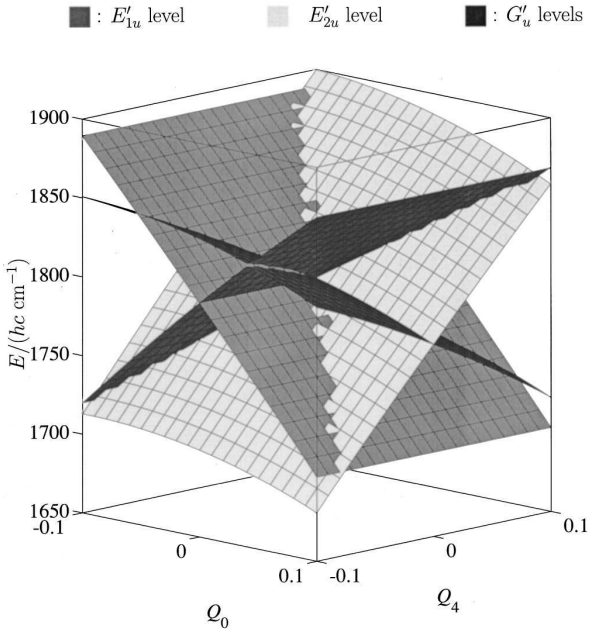

FIG. 6. Eigenvalues of the vibronic Hamiltonian for $\upsilon_3=1$ plotted as a function of Q_0 and Q_4 for $\tilde{\nu}_3=719.5$ cm^{-1} of ReF_6 (including the zero point energy for ν_3 only). The four sublevels E_{1u}', E_{2u}' and $2G_u'$ are shown with avoided crossings for the latter.

TABLE II. Effective parameters for the ν_3 band of WF_6 (in cm^{-1}) from Ref. 4.

Level	Order	Parameter	$^{182}WF_6$	$^{183}WF_6$	$^{184}WF_6$	$^{186}WF_6$
$\nu_3=1$	0	$t_{3,3}^{20((00)0)}$	714.557 67(12)	714.234 30(14)	713.915 20(13)	713.286 31(13)
	1	$t_{3,3}^{21((11)0)}$	−0.041 027(20)	−0.040 763(27)	−0.040 528(20)	−0.039 983(14)
	2	$t_{3,3}^{22((00)0)}$ [a]	-4.312×10^{-5}	-4.393×10^{-5}	-4.616×10^{-5}	-5.010×10^{-5}
		$t_{3,3}^{22((22)0)}$	-1.68×10^{-5} [b]	-1.68×10^{-5} [b]	-1.68×10^{-5} [b]	$-1.68(8)\times10^{-5}$
		$t_{3,3}^{22((22)4)}$	$-9.23(8)\times10^{-5}$	$-9.06(16)\times10^{-5}$	$-9.06(12)\times10^{-5}$	$-9.044(65)\times10^{-5}$
	3	$t_{3,3}^{20((11)0)}$	$-1.3(3)\times10^{-7}$	$-1.1(3)\times10^{-7}$	$-1.5(2)\times10^{-7}$	$-2.1(2)\times10^{-7}$
		$\tilde{\nu}_0$ [c]	714.538 32	714.215 08	713.896 09	713.267 46

[a]Calculated from the B_3 value through $t_{3,3}^{22((00)0)}=\Delta B=B_3-B_0$.
[b]Fixed to the value determined for $^{186}WF_6$ (see Ref. 4).
[c]Band center (see text).

(i.e., including rotation) remains a very difficult problem, we will only use a very crude model in this paper in order to get a preliminary qualitative interpretation of the spectra. We can apply the following simple effective Hamiltonian:

$$\tilde{H}=H_{\mathrm{JTQ}}^{(^0{}_g,{}^1A_{1g})}+H_{\mathrm{JTQ}}^{(^4{}_g,{}^1A_{1g})}+\tilde{H}_{\{0\}}+\tilde{H}_{\{\nu_3\}}+\cdots \tag{25}$$

with

$$\tilde{H}_{\{0\}}=B_0\mathbf{J}^2-2B_0\zeta_0\mathbf{J}\cdot\mathbf{J}_3+\cdots, \tag{26}$$

$$\tilde{H}_{\{\nu_3\}}=\Delta B\mathbf{J}^2-2\Delta(B\zeta)\mathbf{J}\cdot\mathbf{J}_3+\cdots, \tag{27}$$

where B_0 is the ground state rotational constant and the ζ are "Coriolis-type" coupling constants. ΔB and $\Delta(B\zeta)$ are the differences between the $\upsilon_3=1$ and ground state values, i.e., $\Delta B=B_3-B_0$ and $\Delta(B\zeta)=B_3\zeta_3-B_0\zeta_0$. If we set

$$\Delta E_{\mathrm{JT}}^{J_3}(\nu_3,Q_0,Q_4)=E_{\mathrm{JT}}^{1,J_3}(\nu_3,Q_0,Q_4)-E_{JT}^{0,3/2}(\nu_3,Q_0,Q_4), \tag{28}$$

where $E_{\mathrm{JT}}^{0,3/2}$ and E_{JT}^{1,J_3} are the eigenvalues of the vibronic Hamiltonian (20) for $\upsilon_3=0$ and $\upsilon_3=1$, respectively, the transition energies are (with $\mathbf{R}=\mathbf{J}-\mathbf{J}_3$):

$$\Delta E=\Delta E_{\mathrm{JT}}^{J_3}(\nu_3,Q_0,Q_4)+B_3(1-\zeta_3)J'(J'+1)-B_0(1-\zeta_0)J''(J''+1)+\Delta(B\zeta)R(R+1)+\cdots. \tag{29}$$

It seems reasonable to assume that the main term responsible of the octahedral splitting of the R levels is the same as that for "normal" molecules (A_{1g} electronic state), i.e., we can add the term

$$H_{\mathrm{oct}}=-\frac{\sqrt{2}}{5\sqrt{35}}g[[a^{+(1)}\otimes a^{(1)}]^{(2)}\otimes R^{2(2)}] \tag{30}$$

(this is the lowest order anisotropic vibration–rotation interaction term), where g is the octahedral-splitting parameter. The matrix elements of this operator can be calculated in the same way as in Eq. (14).

IV. ANALYSIS OF THE SPECTRA

A. WF_6

We have developed the effective Hamiltonian $\mathbf{H}_{\{\nu_3\}}^{\langle\nu_3\rangle}$ defined in the preceding section up to the third order ($\Omega_v+\Omega_r-2\leqslant3$). $\mathbf{H}_{\{0\}}^{\langle0\rangle}$ ($\equiv\mathbf{H}_{\{0\}}^{\langle\nu_3\rangle}$) has been developed to the zeroth order only, as in Refs. 4 and 40. The value of $t_0^{0(0)}=B_0$ has been fixed to 0.0661 cm^{-1} obtained from the electron diffraction.[48] A least-squares-fit program has then been used to determine the effective parameters for each of the four isotopic species. Preliminary assignments have been realized using the parameters of Takami and Kuze.[4] These have been refined in the high-J regions after several fits. We have used both sets of data (Fourier transform and diode laser spectra) described in Sec. II. All the observed lines in the diode laser spectra could be assigned. The parameter $t_{3,3}^{23((13)4)}$ has been fixed to zero, since all attempts to determine it led to a value lower than the uncertainty in terms of one standard deviation. Attempts to determine fourth order parameters were also unsuccessful. Thus, six parameters could be determined for each isotopomer.

The results are summarized in Table I. When we use the parameters from Ref. 4 (Table II) the simulation shows severe discrepancies when compared to our measurements (more than 0.02 cm^{-1}) in the high-J regions ($J\geqslant30$) which were not observed previously.[4] With our new sets of parameters, the agreement of experiment and simulation is good over the whole range observed.

Figures 7–9 show examples of comparisons between experimental and calculated spectra. The simulations were computed for a rotational temperature $T_{\mathrm{rot}}=50$ K and a Gaussian linewidth (FWHM) of 0.0007 cm^{-1} (diode laser spectra) or 0.004 cm^{-1} (FTIR spectra, apodized).

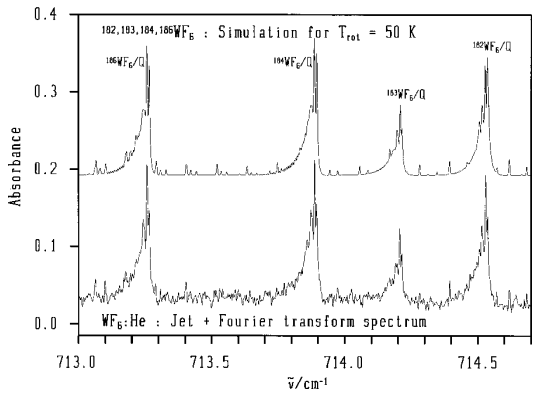

FIG. 7. WF_6 jet-FTIR spectrum and simulation of the ν_3 Q branch region.

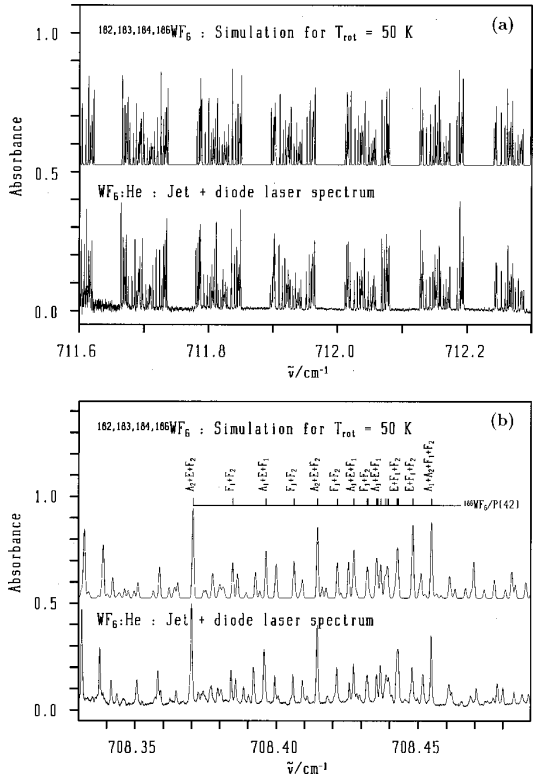

FIG. 8. (a) WF_6 jet+diode laser spectrum and simulation: part of the ν_3 P branch region. (b) WF_6 jet+diode laser spectrum and simulation in the region of the $^{186}WF_6$ $P(42)$ lines of the ν_3 band. Symmetry species (group O) are given for some of these lines.

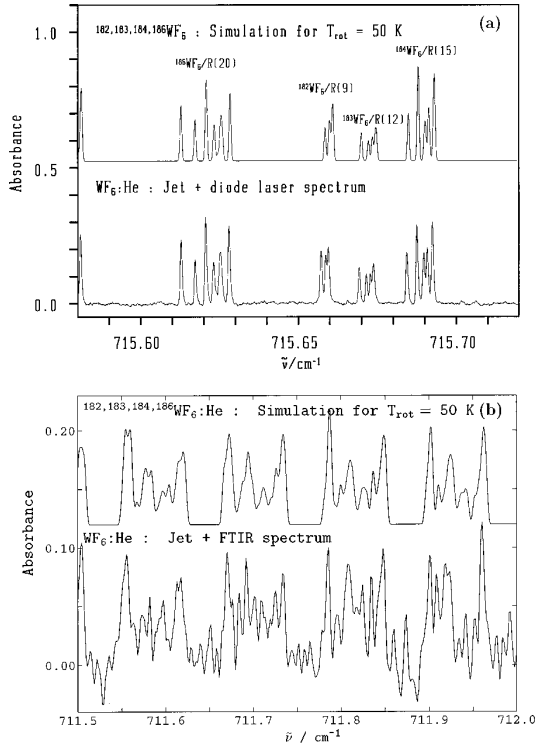

FIG. 9. (a) WF_6 jet+diode laser spectrum and simulation: detail in the ν_3 R branch region. (b) WF_6 jet-FTIR spectrum and simulation: detail in the ν_3 P branch region.

The cluster structure[49] is very well developed for high-J values as it can be seen in the case of the $P(42)$ lines of $^{186}WF_6$ [Fig. 8(b)]. As Harter and Patterson have shown,[49–51] for high-J values, the levels tend to group into sixfold and eightfold degenerate clusters. In a semiclassical interpretation, these clusters correspond to an angular momentum $\mathbf{J}$ precessing around a C_4 or a C_3 symmetry axis, respectively. In Fig. 8(b), the C_4 clusters of the $P(42)$ lines are seen on the left ($A_2+E+F_2, F_1+F_2, A_1+E+F_1, \ldots$) and the C_3 clusters appear on the right ($A_1+A_2+F_1+F_2, E+F_1+F_2, \ldots$). In other words, this means that the corresponding rotational energy surface $E(J_x, J_y, J_z)$ obtained by calculating the energy for continuous "classical" values of the angular momentum vector components J_x, J_y, J_z, has minima on C_4 axes and maxima on C_3 axes. We do not detail this point any further here, since the structure of rovibrational clusters of a degenerate vibrational level from the semiclassical point of view has already been discussed by Harter and co-workers in the case of tetrahedral molecules[52–54] (including the treatment of the Coriolis interaction[53]). More recently, the case of the ν_6 band of $Mo(CO)_6$ (Ref. 55) and of various bands of P_4 (Ref. 56) have been investigated, from both semiclassical and fully classical point of views. The cluster ordering observed here is consistent with the positive value of α_{224} (see Table I) just as in the case of GeF_4,[57] for instance.

Figure 10 displays the reduced energies for the $v_3=1$ vibrational level of $^{182}WF_6$. In the upper part of this figure, the distribution among the different J values of the rotational levels that we observed is shown.

The band center ν_0 can be calculated through[58]

$$\nu_0=\nu_3-2B\zeta_3-\frac{\alpha_{220}}{2}+\cdots$$

$$=t_{3,3}^{20((00)0)}+\frac{\sqrt{2}}{3}t_{3,3}^{21((11)0)}+\frac{2}{5}t_{3,3}^{22((22)0)}+\cdots. \quad (31)$$

This gives the following values:

$$\tilde{\nu}_0(^{182}WF_6)=714.538\,19\ \mathrm{cm}^{-1}, \quad (32)$$

$$\tilde{\nu}_0(^{183}WF_6)=714.214\,06\ \mathrm{cm}^{-1}, \quad (33)$$

$$\tilde{\nu}_0(^{184}WF_6)=713.895\,44\ \mathrm{cm}^{-1}, \quad (34)$$

$$\tilde{\nu}_0(^{186}WF_6)=713.266\,21\ \mathrm{cm}^{-1}. \quad (35)$$

Thus, the isotopic shift for WF_6 can be estimated to be

$$\Delta\tilde{\nu}_0/\Delta m=-0.3176\ \mathrm{cm}^{-1}u^{-1}. \quad (36)$$

This can also be read approximately directly from the Q branches from Fig. 1(b) and is consistent with Ref. 4. The band center of the remaining isotopomer $^{180}WF_6$ would be roughly

$$\tilde{\nu}_0(^{180}WF_6)\simeq 715.170\ \mathrm{cm}^{-1}, \quad (37)$$

but its very low natural abundance (0.135%) prevents it from being identified under our experimental conditions. The apparent higher precision of $t_{3,3}^{20((00)0)}$ for $v_3=1$ in line 2 of Table I for the isotope $^{183}WF_6$ results from a combination of correlation effects and accidental statistics of the lines. Thus, while numerically significant, it has no physical meaning.

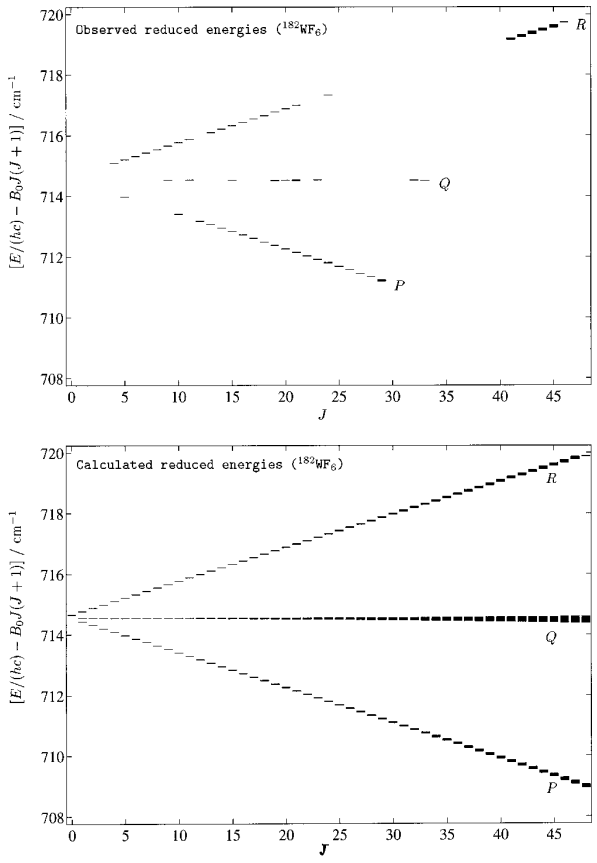

FIG. 10. Observed (upper) and calculated (lower part) reduced energy levels for the $v_3=1$ vibrational level of $^{182}WF_6$.

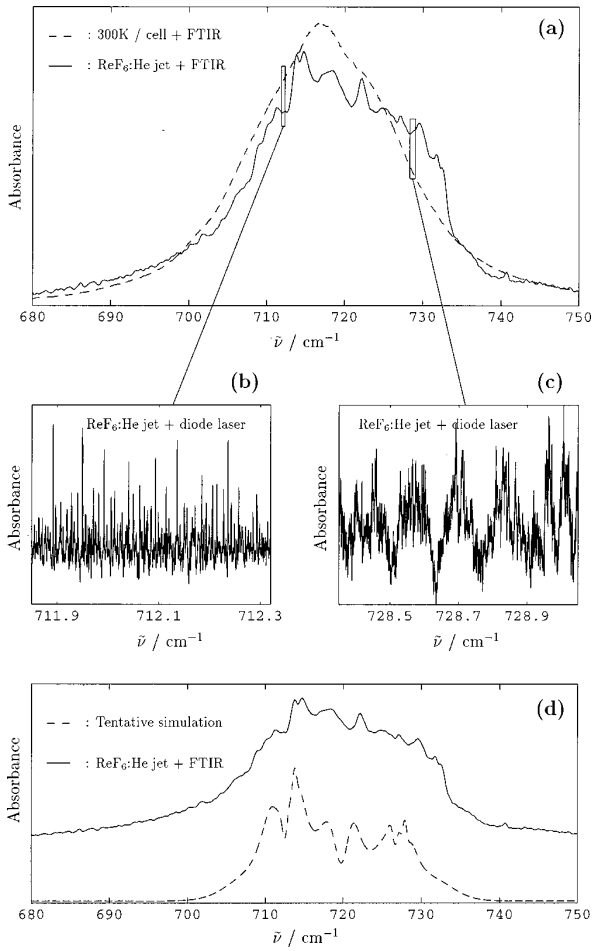

FIG. 11. (a) Overview low-resolution FTIR spectra of the ν_3 band of ReF_6 at room temperature and in a ReF_6:He jet (the instrumental bandwidth is 0.1 and 0.5 cm^{-1}, respectively). (b), (c) Jet+diode laser spectra of a ReF_6:He jet in the ν_3 band region. (d) Low-resolution (instrumental bandwidth of 0.5 cm^{-1}) jet-FTIR spectrum of the ν_3 band of ReF_6 compared to our tentative simulation (see text).

B. ReF_6

Figures 5, 11, and 12 show surveys and examples of low and high-resolution spectra for ν_3 of ReF_6. The differences to the surveys of ν_3 in WF_6 shown in Fig. 1 are most striking. Even in the FTIR supersonic jet spectra of ReF_6 shown in Figs. 11(a) and 11(d) the fine structure is just about becoming visible in form of some humps superimposed on a broad background. However, this "broad background" at high resolution can be resolved into a rich substructure of numerous lines that are well separated, with spacings that are of the order of frequently 0.01 cm^{-1} or less. This can be seen particularly in the diode laser spectra shown in Fig. 12, where the reproducibility of the traces demonstrates that all the stronger lines are clearly real line structure, well above the noise level. The total number of unambiguously assigned lines just in the regions covered by our diode laser scans indicated in Fig. 5 exceeds 700. The linewidths are frequently 0.001 cm^{-1} and less, although some lines are broader, which may indicate blending of several lines. At present, a full analysis of this extremely rich and dense fine structure is not possible. However, the line density is of the expected order of magnitude in agreement with our simulations and agrees with theoretical expectations of the complexity of these spectra.

The coarse superstructure appearing in the FTIR-jet spectra is amenable to at least a very preliminary analysis. In order to compute a "tentative simulation" using the simple rovibronic model described in Sec. III B, we have used the following parameters for both isotopomers of ReF_6: (i) $\tilde{\nu}_3 = 720.13$ cm^{-1} for $^{185}ReF_6$ and $\tilde{\nu}_3 = 719.50$ cm^{-1} for $^{187}ReF_6$, (ii) $B_0 = 0.066\,23$ cm^{-1}, value from electron diffraction measurements,[48] (iii) $\Delta B = B_3 - B_0 = -5 \times 10^{-5}$ cm^{-1}, $g = -0.97 \times 10^{-5}$ cm^{-1} and $\zeta_3 = 0.14$ (WF_6 values), (iv) $\zeta_0 = -0.80$ a tentative value, (v) $Q_0 = 0.008$ and $Q_4 = -0.006$ a "reasonable" order of magnitude, considering the general aspect of the band at 300 K. Much smaller or much larger values would lead to a band profile incompatible with what is observed. The resulting simulation [Fig. 11(d)] at a resolution of 0.5 cm^{-1} seems quite reasonable compared to the jet-FTIR spectrum and taking into account the crudeness of the model employed. This seems to confirm at least the order of magnitude of the quadratic vibronic coupling parameters given above. Table III summarizes the vibrational fundamentals for ReF_6 as far as known today, including the

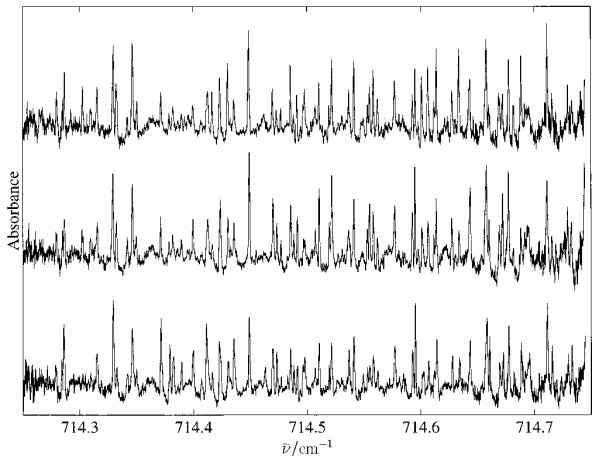

FIG. 12. Three jet+diode laser scans of a ReF_6:He=1:4 mixture (backing pressure of about 750 mbar) in the 714.5 cm^{-1} region.

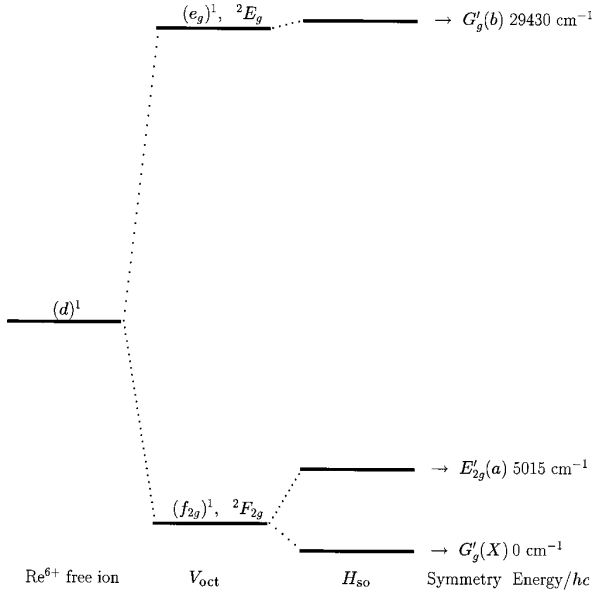

FIG. 13. The electronic levels of ReF_6. V_{oct} is the ligand field potential and H_{SO} is the spin–orbit coupling operator.

preliminary band center estimates of ν_3 from the present work. It is clear that much remains to be done on the vibronic level structure in this molecule.

V. CONCLUSIONS AND OUTLOOK

The high resolution FTIR and diode laser spectra obtained and analyzed in the present work confirm the theoretical expectation of completely different spectral structure for these two prototypes for a closed shell hexafluoride molecule with a nondegenerate ground state on the one hand and for an open shell molecule with a degenerate electronic ground state on the other. The rovibrational spectra of the ν_3 stretching fundamental of WF_6 show a simple structure under conditions of supersonic jet cooling, allowing for a straightforward analysis. Our results extend significantly the previous work[4] but agree with it, where there is overlap. There are no obvious interactions of ν_3 with other vibrational levels even at high J, the closest vibrational level expected in this region being far away [$\nu_2+\nu_5$ at 810 cm^{-1} (Ref. 5)]. Our analysis could be extended to other levels such as the ν_4 fundamental at 258 cm^{-1} (Ref. 5) or combination and overtones with some technical difficulties but no fundamental obstacles to be expected. Besides an improved understanding of the rovibrational level structure our results on WF_6 are potentially useful for two frequency laser isotope separation of W isotopes with selective preexcitation around 700 cm^{-1}, using, for instance, coincidences with the lines of the Raman shifted CO_2 laser or other high power lasers.[12,59,60]

The ν_3 fundamental of ReF_6 stands in stark contrast to the relatively simple structures observed for WF_6. Even under conditions of supersonic jet cooling the overall structure in the FTIR spectrum remains unresolved, with some broad features but no prominent Q-branch structures being visible. At the highest resolutions achieved in the diode laser spectra, this structure is, however, largely resolved into an extremely large number of closely spaced lines. While the broader features of the overall structure was amenable to a preliminary analysis with a simple model Hamiltonian, providing a first estimate of some of the ν_3 band parameters, the understanding of the detailed fine structure is at present not available, and remains a task to be handled in the future once the theory is further developed.[43,61] The complexity of this spectrum is indeed expected because of the complex electronic structure with a $G'_g(X)$ electronic ground state leading to complex rovibronic effects. The overall electronic structure of ReF_6 is summarized in Fig. 13. It indicates that beyond the complexities arising in the range of fundamental vibrations, the near infrared overtone spectrum might be of considerable interest because of potential vibronic interactions with the E'_{2g} electronic state near 5000 cm^{-1}. Such high vibrational levels might become accessible via recent high

TABLE III. The vibrational fundamentals of ReF_6 in its ground electronic state (in cm^{-1}).

Vibration	Symmetry	Activity	$^{185}ReF_6$	$^{187}ReF_6$	Reference
$\tilde{\nu}_1$	A_{1g}	Raman	753.7		66
$\tilde{\nu}_2$	E_g	Raman	575.0 (593[a])		29, 66
$\tilde{\nu}_3$	F_{1u}	Infrared	720.13 (715[a])	719.50 (715[a])	This work (7)
$\tilde{\nu}_4$	F_{1u}	Infrared	269.3 (257[a])		29, 7
$\tilde{\nu}_5$	F_{2g}	Raman	286.3 (246[a])		29, 66
$\tilde{\nu}_6$	F_{2u}	Inactive	166.0 (193[a])		29, 7

[a]First value reported in the literature [7, 66].

sensitivity techniques such as cw diode laser supersonic jet cavity ring down spectroscopy.[62,63] Of course also the higher electronic states have some interest in their own right.[27,64,65]

While the high resolution infrared spectroscopy of ReF_6 is still in its infancy, it offers some interesting opportunities for the future. Besides laser isotope separation, which might be more difficult because of the complex spectra, the very dense ultrahigh resolution spectra of open shell compounds of this type might reveal effects from parity mixing under the weak nuclear force which will be less efficient than in chiral molecules, but potentially much more efficient than in light atom closed shell molecules,[67,68] both in the absence or the presence of level crossings in magnetic fields.[69] Full understanding of the high resolution spectra which are the first ever recorded for such a case might open the route towards such investigations.

ACKNOWLEDGMENTS

We are very grateful to Alex Jourdan from COMURHEX company (Pierrelatte, France) for giving us substantial samples of WF_6 and ReF_6. Our work is supported financially by the Schweizerischer National Fonds (including a postdoctoral fellowship extended to V.B. during his stay at ETH Zürich) and by ETH Zürich (including the AGS, C^4 and CSCS projects). This work has also profited from stimulus and discussions with Jacques Moret-Bailly and Françoise Michelot.

[1] J. Gaunt, Trans. Faraday Soc. **49**, 1122 (1953).
[2] D. Travis, J. McGurk, D. McKeown, and R. Denning, Chem. Phys. Lett. **45**, 287 (1977).
[3] G. Baronov, A. Britov, S. Karavaev, A. Karachevskii, S. Kulikov, A. Merzlyakov, S. Sivachenko, and Y. I. Shcherbina, Sov. J. Quantum Electron. **11**, 947 (1981).
[4] M. Takami and H. Kuze, J. Chem. Phys. **80**, 5994 (1984); see also Y. Mitzugai, H. Kuze, H. Jones, and M. Takami, Appl. Phys. B: Photophys. Laser Chem. **32**, 43 (1983).
[5] R. McDowell and L. Asprey, J. Mol. Spectrosc. **45**, 491 (1973).
[6] J. Gaunt, Trans. Faraday Soc. **50**, 209 (1954).
[7] H. Claassen, J. Malm, and H. Selig, J. Chem. Phys. **36**, 2890 (1962).
[8] I. Levin, S. Abramowitz, and A. Müller, J. Mol. Spectrosc. **41**, 415 (1972).
[9] G. Cady and B. Hargreaves, J. Chem. Soc. **1961**, 1563.
[10] C. Bernard, R. Madar, and Y. Pauleau, Solid State Technol. **2**, 79 (1989).
[11] N. Desatnik and B. Thompson, J. Electrochem. Soc. **141**, 3532 (1994).
[12] M. Quack, Infrared Phys. **29**, 441 (1989); J. Chem. Phys. **69**, 1282 (1978).
[13] A. N. Halliday, Contemp. Phys. **38**, 103 (1997).
[14] D. C. Lee and A. N. Halliday, Nature (London) **378**, 771 (1995).
[15] D. C. Lee and A. N. Halliday, Science **274**, 1876 (1996).
[16] M. Schädel, W. Brüchle, R. Dressler *et al.*, Nature (London) **388**, 55 (1997).
[17] C. Nash and B. Bursten, J. Am. Chem. Soc. **121**, 10830 (1999).
[18] K. Tanner and A. Duncan, J. Am. Chem. Soc. **73**, 1164 (1951).
[19] H. Claassen and H. Selig, Isr. J. Chem. **7**, 499 (1969).
[20] H. Claassen, G. Goodman, J. Holloway, and H. Selig, J. Chem. Phys. **53**, 341 (1970).
[21] D. Jackson, Informal report LA-6025-MS, Los Alamos National Laboratory.
[22] L. Roberts, The properties of C.V.D. deposits of W and W–Re alloys, High temperature materials, 6th Plansee seminar, June 1968, Reutte, Austria, 1969.
[23] Y. Lakhotkin and A. Krasovskiy, Russ. Metall. **1**, 21 (1983).
[24] M. Pons, A. Benezech, P. Huguet, R. Gaufres, P. Diez, and J. Lafforet, J. Chem. Vap. Deposition **2**, 135 (1993).
[25] W. Moffit, G. Goodman, M. Fred, and B. Weinstock, Mol. Phys. **2**, 109 (1959).
[26] J. Brand, G. Goodman, and B. Weinstock, J. Mol. Spectrosc. **37**, 161 (1971).
[27] R. McDiarmid, J. Mol. Spectrosc. **38**, 495 (1971).
[28] J. Holloway, G. Stanger, E. Hope, W. Levason, and J. Ogden, J. Chem. Educ. **1988**, 1341.
[29] M. Rotger, V. Boudon, and H. Selig, Spectrochim. Acta, Part A **55**, 1575, 734 (1999).
[30] V. Boudon and F. Michelot, J. Mol. Spectrosc. **165**, 554 (1994).
[31] V. Boudon, Y. He, U. Schmitt, M. Quack, and M. Rotger, in *15th Colloquium on High Resolution Molecular Spectroscopy* (Glasgow, United Kingdom, 1997); V. Boudon, M. Rotger, Y. He, U. Schmitt, and M. Quack, in *16th Colloquium on High Resolution Molecular Spectroscopy* (Dijon, France, 1999).
[32] A. Amrein, M. Quack, and U. Schmitt, J. Phys. Chem. **92**, 5455 (1988).
[33] M. Quack, Annu. Rev. Phys. Chem. **41**, 839 (1990).
[34] H. Hollenstein, M. Quack, and E. Richard, Chem. Phys. Lett. **222**, 176 (1994).
[35] S. Yamamoto, R. Kuwabara, M. Takami, and K. Kuchitsu, J. Mol. Spectrosc. **115**, 333 (1986).
[36] G. Guelachvili and K. N. Rao, *Handbook of Infrared Standards* (Academic, Orlando, FL, 1986).
[37] J.-P. Champion, M. Loëte, and G. Pierre, in *Spectroscopy of the Earth's Atmosphere and Interstellar Medium*, edited by K. N. Rao and A. Weber (Academic, San Diego, CA, 1992), pp. 339–422.
[38] J. Moret-Bailly, Can. J. Phys. **15**, 237 (1961).
[39] A. Robiette, D. Gray, and F. Briss, Mol. Phys. **32**, 1591 (1976).
[40] M. Terki-Hassaine, G. Pierre, H. Bürger, and H. Willner, J. Mol. Spectrosc. **185**, 93 (1997).
[41] H. C. Longuet-Higgins, Mol. Phys. **6**, 445 (1963).
[42] M. Quack, Mol. Phys. **34**, 477 (1977).
[43] V. Boudon, M. Rey, M. Rotger, M. Loëte, H. Hollenstein, and M. Quack (unpublished).
[44] J. Champion, G. Pierre, F. Michelot, and J. Moret-Bailly, Can. J. Phys. **55**, 512 (1977).
[45] C. Cantrell and H. Galbraith, J. Mol. Spectrosc. **58**, 158 (1975).
[46] H. Berger, J. Phys. (France) **38**, 1371 (1977).
[47] V. Boudon, F. Michelot, and J. Moret-Bailly, J. Mol. Spectrosc. **166**, 449 (1994).
[48] M. Kimura, V. Schomaker, D. Smith, and B. Weinstock, J. Chem. Phys. **48**, 4001 (1968).
[49] W. Harter and C. Patterson, J. Chem. Phys. **66**, 4872 (1977).
[50] W. Harter and C. Patterson, J. Chem. Phys. **66**, 4886 (1977).
[51] W. Harter, Comput. Phys. Rep. **8**, 319 (1988).
[52] W. G. Harter, H. W. Galbraith, and C. W. Patterson, J. Chem. Phys. **69**, 4888 (1978).
[53] W. G. Harter, C. W. Patterson, and H. W. Galbraith, J. Chem. Phys. **69**, 4896 (1978).
[54] C. W. Patterson, H. W. Galbraith, B. J. Krohn, and W. G. Harter, J. Mol. Spectrosc. **77**, 457 (1979).
[55] G. Dhont, D. Sadovskiĭ, B. Zhilinskiĭ, and V. Boudon, J. Mol. Spectrosc. **201**, 95 (2001).
[56] Ch. Van-Hecke, D. Sadovskiĭ, B. Zhilinskiĭ, and V. Boudon, Eur. Phys. J. D **17**, 13 (2001).
[57] V. Boudon, H. Bürger, and E. B. Mkadmi, J. Mol. Spectrosc. **206**, 172 (2001).
[58] B. Bobin and K. Fox, J. Phys. (Paris) **34**, 571 (1973).
[59] D. Lupo and M. Quack, Chem. Rev. **1987**, 87.
[60] M. Quack, Infrared Phys. Technol. **36**, 365 (1995).
[61] M. Rey, V. Boudon, M. Loëte, and F. Michelot, J. Mol. Spectrosc. **204**, 106 (2000).
[62] M. Hippler and M. Quack. J. Chem. Phys. **116**, 6045 (2002).
[63] M. Hippler and M. Quack, Chem. Phys. Lett. **314**, 273 (1999).
[64] J. C. D. Brand, G. L. Goodman, and B. Weinstock, J. Mol. Spectrosc. **38**, 445 (1971).
[65] G. R. Meredith, J. D. Webb, and E. R. Bernstein, Mol. Phys. **34**, 995 (1977).
[66] H. H. Claassen and H. Selig, Isr. J. Chem. **7**, 499 (1969); H. H. Claassen, G. L. Goodman, J. H. Holloway, and H. Selig, J. Chem. Phys. **53**, 341 (1970).

[67] A. Bakasov, T.-K. Ha, and M. Quack, J. Chem. Phys. **109**, 7263 (1998).
[68] R. Berger and M. Quack, J. Chem. Phys. **112**, 3148 (2000).
[69] M. J. M. Pepper, I. Shavitt, P. Von Ragué Schleyer, M. N. Glukhovtsev, R. Janoschek, and M. Quack, J. Comput. Chem. **16**, 207 (1995).
[70] See EPAPS Document No. E-JCPSA6-116-005222 for four tables containing the observed and calculated transition wave numbers for WF_6 (Table I: $^{182}WF_6$, Table II: $^{183}WF_6$, Table III: $^{184}WF_6$, Table IV: $^{186}WF_6$). This document may be retrieved via the EPAPS homepage (http://www.aip.org/pubservs/epaps.html) or from ftp.aip.org in the directory /epaps/. See the EPAPS homepage for more information.

QUATRIÈME PARTIE

Chapitre

4

Perspectives : Spectroscopie des Ions et Radicaux

4.1 Introduction

Ainsi que je l'ai déjà mentionné dans les Chapitres précédents, le modèle rovibronique que nous avons développé ces dernières années peut être étendu à d'autres espèces moléculaires à sous couches incomplètes. Hormis d'autres types de molécules toupies sphériques "open-shell" telles que VCl_4, par exemple, auxquelles la théorie pourrait être appliquée directement, nous pouvons en particulier penser aux ions et radicaux de symétrie moindre que l'on rencontre dans de nombreux domaines : atmosphères planétaires, milieu interstellaires, milieux en combustion, intermédiaires de réactions chimiques diverses, *etc*.

Ainsi, l'extension du formalisme tensoriel à des molécules de type toupies symétriques ou asymétriques que j'ai présentée au Chapitre III.4 pourrait être associée à une construction d'opérateurs rovibroniques du type de celle décrite au Chapitre IV.1 pour obtenir un modèle rovibronique pour des ions ou radicaux de symétries diverses. Je décris ici très succinctement un travail qui est en train de se mettre en place sur ce type de sujet, ainsi que les perspectives à plus long terme en matière de spectroscopie rovibronique.

4.2 Les radicaux méthoxy et thiométhyle

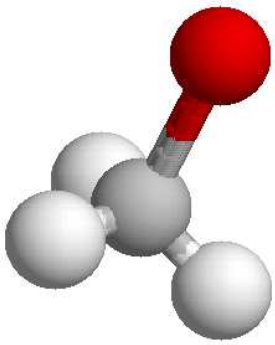

FIG. 4.1 – *Le radical CH_3O.*

Un stage de DEA débute cette année sous ma responsabilité concernant la spectroscopie des

radicaux méthoxy (CH_3O, Figure 4.1) et thiométhyle (CH_3S). Ces deux radicaux interviennent de manière importante dans diverses réactions chimiques troposphériques, dont la chimie de l'ozone (O_3).

Le terme électronique de base de ces radicaux est ^2E, ce qui implique des couplages rovibroniques, en particulier pour les modes de vibration deux fois dégénérés. Divers travaux récents à haute résolution ont produit des spectres dans l'état électronique de base [1] ou dans des états électroniques excités [2]. Toutefois, les modèles Jahn-Teller employés dans ces travaux semblent incomplets, le couplage étant traité soit de manière perturbative (ce qui, strictement, n'est pas valide ainsi que nous l'avons vu précédemment), soit de manière empirique (en prenant l'énergie de chaque sous-niveau vibronique comme un paramètre).

Le stage de DEA d'Abdollatyf El Hilali consiste à suivre un programme similaire à ce qui a été fait pour les molécules octaédriques, à savoir : étudier les représentations spinorielles du groupe C_{3v}, élaborer un formalisme tensoriel pour la chaîne $O(3) \supset C_{3v}^S$, et construire un Hamiltonien et des moments de transition rovibroniques pour des molécules du type XY_3Z dans un état électronique dégénéré. Par la suite, nous pourrons, à l'aide de ce nouvel outil, entreprendre l'interprétation des spectres existants.

4.3 Futurs développements

A plus long terme, l'idée générale de cette thématique est d'aboutir à des outils permettant l'analyse globale de spectres rovibroniques, avec un niveau de précision et de détail similaire à ce qui existe en spectroscopie rovibrationnelle. Les futurs développements devront donc permettre :

- L'analyse de transitions rovibroniques à l'intérieur d'un état électronique de symétrie quelconque pour différents types de molécules.
- L'analyse de spectres rovibroniques correspondant à des transitions entre états électroniques différents.

Il s'agit bien entendu d'un travail considérable qui ne peut s'envisager que sur de nombreuses années et dans le cadre de collaborations avec d'autres équipes, tant au niveau théorique, qu'expérimental. Encore une fois, il existe un recouvrement important entre les différentes thématiques présentées dans le présent rapport. Ainsi, les nouvelles techniques que nous envisageons d'appliquer au cas des spectres très complexes de polyades élevées du méthane, seront sans aucun doute utiles pour l'étude des spectres rovibroniques, dont le niveau de complexité, même dans les états les plus bas, peut être lui aussi considérable.

1. J.-X. Han, Yu. G. Utkin, H.-B. Chen, L. A. Burns and R. F. Curl, *J. Chem. Phys.*, **117**(14), 6538–6545 (2002)
2. D. E. Powers, M. B. Pushkarsky and T. Miller, *J. Chem. Phys.*, **106**(17), 6863–6877 (1997)

Cinquième partie

Conclusion

J'ai essayé de décrire dans ce mémoire mes activités de chercheur aussi bien à l'Ecole Polytechnique Fédérale de Zürich qu'au Laboratoire de Physique de l'Université de Bourgogne.

Après un bref récapitulatif de mon parcours scientifique et des différentes responsabilités (administratives et collectives, d'encadrement et d'animation scientifique) que j'assume, j'ai abordé la présentation des résultats de recherche. J'ai distingué deux grandes parties, selon le type d'état électronique moléculaire considéré. Premièrement, j'ai présenté mes travaux en spectroscopie rovibrationnelle dans un état électronique singulet. Deuxièmement, j'ai exposé mes recherches sur la spectroscopie rovibronique dans un état électronique dégénéré.

Comme on a pu le voir dans ce document, une grande partie de mon activité a consisté, tout en s'appuyant sur l'acquis des méthodes tensorielles utilisées au Laboratoire, à rechercher et à développer de nouvelles ouvertures et applications pour ce type d'approches. Dans ce cadre, le formalisme a été adapté et étendu à de nouveaux types de problèmes (toupies sphériques "déformées", molécules piégées, spectroscopie rovibronique). Une partie de mon propos a consisté à montrer que l'approche "dijonnaise" ne se limite pas à la seule spectroscopie rovibrationnelle des molécules toupies sphériques, mais constitue un ensemble d'outils puissants permettant d'aborder de nombreux problème de physico-chimie moléculaire.

J'ai par ailleurs mis l'accent sur la diffusion des résultats auprès de la communauté scientifique à travers les bases de données et sur les applications en chimie atmosphérique et en astrophysique.

La partie concernant la spectroscopie rovibronique doit beaucoup à l'excellent travail de DEA puis de thèse réalisé par Michaël Rey de 1998 à 2002.

Dans l'avenir, je compte bien entendu poursuivre parallèlement les deux grandes thématiques développées ici. L'étude des polyade élevées du méthane et des bandes chaudes de SF_6 demandera encore beaucoup de travail et la complexité de ces problèmes amènera inévitablement au développement de nouvelles méthodes d'analyse.

La spectroscopie de molécules piégées dans des solides (zéolithes, matrices, ...) me semble un thème très porteur pour l'avenir, avec de nombreuses applications potentielles (dépollution, *etc*).

Enfin, malgré les progrès importants réalisés récemment, les études concernant la spectroscopie rovibronique dans un état électronique dégénéré n'en sont encore qu'à leur début. Une stage de DEA est actuellement en cours pour l'application dess méthodes que nous avons mises en place à certains radicaux importants en chimie atmosphérique. Ceci est une porte ouverte vers une meilleure compréhension de la spectroscopie des ions moléculaires et des radicaux libres qui interviennent dans de nombreux domaines (atmosphères, combustions, réactions chimiques, ...). A plus long terme, le but de cette thématique est de construire les outils permettant une analyse globale de spectres rovibroniques pour des transitions entre deux états électroniques quelconques.

Sixième partie

Annexe : Liste des Travaux

Thèse de doctorat

"Spectroscopie des Hexafluorures à Nombre Impair d'Electrons",
V. Boudon,
Thèse, Dijon, (1995).

Articles dans des revues à comité de lecture

[P1] "Spectroscopy of Hexafluorides with an Odd Number of Electrons. A Tensorial Formalism Adapted to the Chain $SU(2) \otimes C_I \supset O_h^S$",
V. Boudon and F. Michelot,
Journal of Molecular Spectroscopy, **165**, 554–579, (1994).

[P2] "Spectroscopy of Hexafluorides with an Odd Number of Electrons. Operators of Interest for Electronic Spectroscopy and for the Jahn-Teller Effect",
V. Boudon, F. Michelot and J. Moret-Bailly,
Journal of Molecular Spectroscopy, **166**, 449–470, (1994).

[P3] "Spectroscopy of Hexafluorides with an Odd Number of Electrons. The Vibronic Bands of IrF_6",
V. Boudon, M. Rotger and D. Avignant,
Journal of Molecular Spectroscopy, **175**, 327–339, (1996).

[P4] "Spontaneous Raman Scattering Spectrum of Gaseous IrF_6 in the Ground Electronic State",
M. Rotger, V. Boudon, A.T. Nguyen and D. Avignant,
Journal of Raman Spectroscopy, **27**, 145–148, (1996).

[P5] "Theoretical Comparison of the Three Most Widely Used Resonators for High Power Nd-YAG Lasers",
M. Rotger and V. Boudon,
Journal d'Optique, **27**(3), 121–128, (1996).

[P6] "Ultraviolet Absorption Spectrum of Gaseous IrF_6 in the 200–500 nm Region",
V. Boudon, M. Rotger and D. Avignant,
Spectrochimica Acta A, **52**, 1175–1182, (1996).

[P7] "Absorption Spectrum of the $f(A_{1g}) \leftarrow X(E_g)$, $a(F_{2g})$ Electronic Transition of OsF_6",
M. Rotger, V. Boudon and H. Selig,
Spectrochimica Acta A, **53**, 991–994 (1997).

[P8] "*Ab Initio* Calculations and High Resolution Spectroscopy of the Bending Pentad of SiH_2D_2 in the 10-16 μm Region"
M. Rotger, V. Boudon, B. Lavorel, S. Sommer, H. Bürger, J. Breidung, W. Thiel, M. Bétrencourt and J.-C. Deroche,
Journal of Molecular Spectroscopy, **192**, 294–308 (1998).

[P9] "High-Resolution Jet-Cooled Spectroscopy of SF_6: The $\nu_2+\nu_6$ Combination Band of $^{32}SF_6$ and the ν_3 Band of the Rare Isotopomers",
V. Boudon, M. Hepp, M. Herman, I. Pak and G. Pierre,
Journal of Molecular Spectroscopy, **192**, 359–367 (1998).

[P10] "High-Resolution Fourier Transform Infrared Spectroscopy and Analysis of the ν_3 Fundamental Band of P_4 ",
V. Boudon, E. B. MKadmi, H. Bürger and G. Pierre,
Chemical Physics Letters, **305**, 21–27 (1999).

[P11] "Absorption Spectrum of the $a(E'_{2g}) \leftarrow X(G'_g)$ and $b(G'_g) \leftarrow X(G'_g)$ Electronic Transitions

of ReF_6",
M. Rotger, V. Boudon and H. Selig,
Spectrochimica Acta A, **55**, 1575–1584 (1999).

[**P12**] "Development of the Dipole Moment and Polarizability Operators of Octahedral Molecules ",
N. Cheblal, M. Loëte and V. Boudon,
Journal of Molecular Spectroscopy, **197**, 222–231 (1999).

[**P13**] "Spectroscopy of XY_5Z (C_{4v}) Molecules. A Tensorial Formalism Adapted to the $O(3) \supset O_h \supset C_{4v}$ Chain ",
M. Rotger, V. Boudon and M. Loëte,
Journal of Molecular Spectroscopy, **200**, 123–130 (2000).

[**P14**] "Spectroscopy of XY_5Z (C_{4v}) Molecules. Development of the Hamiltonian and of the Transition Moment Operators Using a Tensorial Formalism ",
M. Rotger, V. Boudon and M. Loëte,
Journal of Molecular Spectroscopy, **200**, 131–137 (2000).

[**P15**] "High-Resolution Fourier Transform Infrared Spectroscopy and Analysis of the ν_6 Band of Jet-Cooled $Mo(CO)_6$",
P. Asselin, P. Soulard, L. Manceron, V. Boudon and G. Pierre,
Journal of Molecular Structure (numéro spécial en l'honneur de G. Graner), **517**(1), 145–155 (2000).

[**P16**] "Highly-Spherical Top Data System (HTDS) Software for the Spectrum Simulation of Octahedral XY_6 Molecules",
Ch. Wenger, V. Boudon, J.-P. Champion and G. Pierre,
Journal of Quantitative Spectroscopy and Radiative Transfer, **66**(1), 1–16 (2000).

[**P17**] "Analysis of the "Unusual" Vibrational Components of Triply Degenerate Vibrational Mode ν_6 of $Mo(CO)_6$ Based on the Classical Interpretation of the Effective Rotation-Vibration Hamiltonian",
G. Dhont, D. Sadovskii, B. Zhilinskii and V. Boudon,
Journal of Molecular Spectroscopy, **201**, 95–108 (2000).

[**P18**] "Simultaneous Analysis of the ν_2 Raman and $\nu_2+\nu_6$ Infrared Spectra of the SF_6 Molecule",
D. Bermejo, R. Z. Martinez, E. Loubignac, V. Boudon and G. Pierre,
Journal of Molecular Spectroscopy, **201**, 164–171 (2000).

[**P19**] "A Tensorial Formalism Adapted to the Rovibronic Couplings in the Colored Hexafluorides. Application to the $\nu_5(F_{2g})$ and $\nu_3(F_{1u})$ modes",
M. Rey, V. Boudon, M. Loëte and F. Michelot,
Journal of Molecular Spectroscopy, **204**, 106–119 (2000).

[**P20**] "High Resolution Spectroscopy and Analysis of the ν_4 Bending Region of SF_6 Near 615 cm^{-1}",
V. Boudon, G. Pierre and H. Bürger,
Journal of Molecular Spectroscopy, **205**, 304–311 (2001).

[**P21**] "High Resolution Spectroscopy and Analysis of the ν_3 and ν_4 Fundamentals of Monoisotopic $^{70}GeF_4$",
V. Boudon, H. Bürger and E. B. MKadmi,
Journal of Molecular Spectroscopy, **206**, 172–180 (2001).

[**P22**] "High Resolution Spectroscopy and Analysis of the ν_4 Band of $^{80}SeF_6$",
M. Rotger, V. Boudon, H. Bürger and H. Willner,
Chemical Physics Letters, **339**, 83–88 (2001).

[**P23**] "The Spectrum of an Octahedral Molecule in a Degenerate Electronic State: The ν_6 Fundamental Band of Jet-Cooled $V(CO)_6$",
M. Rey, V. Boudon, M. Loëte, P. Asselin, P. Soulard and L. Manceron,
Journal of Chemical Physics, **114**(24), 10773–10779 (2001).

[**P24**] "Tensorial Development of the Rovibronic Hamiltonian and Transition Moment Operators for Octahedral Molecules",
M. Rey, V. Boudon and M. Loëte,
Journal of Molecular Structure (numéro spécial en l'honneur de A. Bauder), **599**, 125–137 (2001).

[**P25**] "High Resolution Spectroscopy and Analysis of the ν_1/ν_8 Dyad of $SF_5{}^{35}Cl$",
M. Rotger, A. Decrette, V. Boudon, M. Loëte, S. Sander and H. Willner,
Journal of Molecular Spectroscopy, **208**, 169–179 (2001).

[**P26**] "Rotational-Vibrational Relative Equilibria and the Structure of Quantum Energy Spectrum of the Tetrahedral Molecule P_4",
Ch. Van-Hecke, D. A. Sadovskii, B. I. Zhilinskii and V. Boudon,
European Physical Journal D, **17**, 13–35 (2001).

[**P27**] "C_{4v} Top Data System (C_{4v}TDS) Software for Infrared Spectrum Simulation of XY_5Z Symmetric Molecules",
Ch. Wenger, M. Rotger and V. Boudon,
Journal of Quantitative Spectroscopy and Radiative Transfer, **74**, 621–636 (2002).

[**P28**] "First High-Resolution Raman Spectrum and Analysis of the ν_5 Bending Fundamental of SF_6",
V. Boudon and D. Bermejo,
Journal of Molecular Spectroscopy, **213**, 139–144 (2002).

[**P29**] "High Resolution Spectroscopy of the ν_3 Band of WF_6 and ReF_6 in a Supersonic Jet",
V. Boudon, M. Rotger, Y. He, H. Hollenstein, M. Quack and U. Schmitt,
Journal of Chemical Physics, **117**, 3196–3207 (2002).
Supplément: Document EPAPS No. E-JCPSA6-116-005222, "Four Tables Containing the Observed and Calculated Transition Wavenumbers for WF_6".
Cf. `http://www.aip.org/pubservs/epaps.html`.

[**P30**] "Spectroscopy of XY_2Z_2 (C_{2v}) Molecules: A Tensorial Formalism Adapted to the $O(3) \supset T_d \supset C_{2v}$ Chain. Application to the Ground State of SO_2F_2",
M. Rotger, V. Boudon and M. Loëte,
Journal of Molecular Spectroscopy, **216**, 297–307 (numéro spécial en l'honneur de H. Bürger, 2002).

[**P31**] "Study of the Fundamental Bands of $^{70}GeD_4$ by High-Resolution Raman and Infrared Spectroscopy. First Experimental Determination of the Equilibrium Structure of Germane",
G. Pierre, V. Boudon, E.B. MKadmi, H. Bürger, D. Bermejo and R. Martinez,
Journal of Molecular Spectroscopy, **216**, 408–418 (numéro spécial en l'honneur de H. Bürger, 2002).
Supplément: "ASCII Files of Measured Transitions".
Cf. `http://www.elsevier.com/homepage/sap/suppmat/S0022285202986625/`.

[**P32**] "Spectroscopy of X_2Y_4 (D_{2h}) Molecules: Tensorial Formalism Adapted to the $O(3) \supset D_{2h}$ Chain, Hamiltonian and Transition Moment Operators",
W. Raballand, M. Rotger, V. Boudon and M. Loëte,
Journal of Molecular Spectroscopy, **217**, 239–248 (2003).

[**P33**] "Spectroscopic Tools for Remote Sensing of Greenhouse Gases CH_4, CF_4 and SF_6",

V. Boudon, J.-P. Champion, T. Gabard, G. Pierre, M. Loëte and Ch. Wenger, *Environmental Chemistry Letters*, **1**, 86–91 (2003).

[**P34**] "Orientation of $O(3)$ and $SU(2) \otimes C_I$ Representations in Cubic Point Groups (O_h, T_d) for Application to Molecular Spectroscopy",
M. Rey, V. Boudon, Ch. Wenger, G. Pierre and B. Sartakov,
Journal of Molecular Spectroscopy, **219**, 313–325 (2003).

[**P35**] "$SU(4)$ Approach to Fourfold Degenerate Electronic States of Some Hexafluoride Molecules",
F. Michelot, M. Rey and V. Boudon,
Journal of Molecular Spectroscopy, **220**, 19–44 (2003).

[**P36**] "The Ground State Rotational Spectrum of SO_2F_2",
M. Rotger, V. Boudon, M. Loëte, L. Margulès, J. Demaison, H. Mäder, G. Winnewisser and H. S. P. Müller,
Journal of Molecular Spectroscopy, **222**, 172–179 (2003).
Supplément: "Complete Table of Measured and Assigned Transitions".
Cf. `http://www.sciencedirect.com/science/journal/00222852`.

[**P37**] "High-Resolution FTIR Spectrum and Analysis of the $\nu_2 + \nu_4$ Combination Band of SF_6",
V. Boudon and N. Lacome,
Journal of Molecular Spectroscopy, **222**, 291–295 (2003).

[**P38**] "Diode Laser Spectroscopy of the ν_8 Band of the SF_5Cl Molecule",
W. Raballand, N. Benoit, M. Rotger and V. Boudon,
Spectrochimica Acta A, **accepté**, (numéro spécial à l'occasion de *TDLS 2003: 4th International Conference on Tunable Diode Laser Spectroscopy*, 14-18/07 2003, Zermatt, Suisse).

[**P39**] "Symmetry-Adapted Tensorial Formalism to Model Rovibrational and Rovibronic Spectra of Molecules Pertaining to Various Point Groups",
V. Boudon, J.-P. Champion, T. Gabard, M. Loëte, F. Michelot, G. Pierre, M. Rotger, Ch. Wenger and M. Rey,
Journal of Molecular Spectroscopy, **accepté** (2004).

Publications soumises

[**P40**] "High-Resolution Raman Spectroscopy of the ν_1 Region and Raman-Raman Double Resonance Spectroscopy of the $2\nu_1 - \nu_1$ Band of $^{32}SF_6$ and $^{34}SF_6$. Determination of the Equilibrium Bond Length of Sulfur Hexafluoride",
V. Boudon, J. L. Doménech, D. Bermejo and H. Willner,
Journal of Molecular Spectroscopy, **soumis**, (2004).

[**P41**] "C_{2v} Top Data System (C_{2v}TDS) Software for Infrared Spectrum Simulation of XY_2Z_2 Asymmetric Molecules. Some Improvements to the TDS Packages",
Ch. Wenger, M. Rotger and V. Boudon,
Journal of Quantitative and Radiative Transfer, **soumis**, (2004).

Contributions à des ouvrages collectifs

[**B1**] "Rovibrational Spectroscopy of Sulphur Hexafluoride: A Review",
V. Boudon and G. Pierre,
In *Recent Research Developments in Molecular Spectroscopy*, vol. 1, pp 25-55, Transworld Research Network (Trivandrum, Inde), (2002).

[**B2**] "Spectroscopic Tools for Remote Sensing of Greenhouse Gases CH_4, CF_4 and SF_6",

V. Boudon, J.-P. Champion, T. Gabard, G. Pierre, M. Loëte and Ch. Wenger, **Accepté pour publication** dans *Environmental Chemistry*, Springer (2003).

Actes de colloques

[**A1**] "Molecular Absorbers in the Atmospheres of Methane Dwarfs",
D. Homeier, F. Allard, P. H. Hauschildt and V. Boudon,
IAU Symposium No. 210, *Modelling of Stellar Atmospheres* (17-20/06 2002, Uppsala, Suède),
N. E. Piskunov, W. W. Weiss and D. F. Gray, Eds., Astr. Soc. Pacific (2003).

[**A2**] "Open-Shell Octahedral Molecules: A First Insight into the Full Rovibronic Problem",
V. Boudon, M. Rey, M. Rotger and M. Loëte,
Proceedings of SPIE, *XIVth Symposium on High Resolution Molecular Spectroscopy, HighRus 2003*, (06-11/07 2003, Krasnoïarsk – Yenisseisk – Krasnoïarsk, Russie), **5311**, 1–13 (2003).

Conférences invitées

[**I1**] " *Workshop of the HCM Network : Laser Controlled Dynamics of Molecular Processes and Applications*", 23-25/09 1998, Kaiserslautern (Allemagne):
"A New Set of Analysis Programs for XY_6 Molecules : Application to $\nu_2+\nu_6$ of SF_6",
V. Boudon.

[**I2**] "*Saint Flour PICS 599 Workshop on Local Modes*", 11-12/09 1999, Saint-Flour (France):
"Spectroscopy of Spherical Tops: Methods and Perspectives",
V. Boudon.

[**I3**] "*Oberwolfach PICS 599 Workshop on Reductions of the Rovibrational Hamiltonian*", 28/09-01/10 2000, Oberwolfach (Allemagne) :
"Reductions and (Ro)vibronic Spectroscopy of Octahedral Molecules: The Case of Non-Perturbative Contact Transformations",
V. Boudon.

[**I4**] "*17th Colloquium on High Resolution Molecular Spectroscopy*", 09/09-13/09 2001, Nimègue (Pays-Bas) :
"Rovibronic Spectroscopy of Octahedral Molecules in a Degenerate Electronic State"
V. Boudon.

[**I5**] "*XIVth Symposium on High Resolution Molecular Spectroscopy – HighRus 2003*", 06/07-11/07 2003, Krasnoïarsk – Yenisseisk – Krasnoïarsk (Russie) :
"Open-Shell Octahedral Molecules: A First Insight into the Full Rovibronic Problem"
V. Boudon.

Posters présentés lors de colloques

[**C1**] "*13th Colloquium on High Resolution Molecular Spectroscopy*", Sept. 1993, Riccione (Italie), **un poster** présenté :

- "Spectroscopy of hexafluorides with an odd number of electrons",
  V. Boudon and J. Moret-Bailly.

[**C2**] "*14th Colloquium on High Resolution Molecular Spectroscopy*", 11-15/09 1995, Dijon (France), **deux posters** présentés :

- "A Tensorial Formalism Adapted to Octahedral Molecules or Ions Having an Odd Number of Electrons",
  V. Boudon and F. Michelot.

– "Spectroscopy of the Ground and Excited Electronic States of IrF_6",
V. Boudon and M. Rotger.

[C3] "*15th Colloquium on High Resolution Molecular Spectroscopy*", 31/08-05/09 1997, Glasgow (Royaume-Uni), **un poster** présenté :

– "High Resolution Spectroscopy of the ν_3 Band of WF_6 in a Supersonic Jet",
V. Boudon, M. Rotger, Y. He, U. Schmitt and M. Quack.

[C4] "*3ième Colloque Journées de Spectroscopie Moléculaire*", 07-08/07 1998 à Reims (France), **deux posters** présentés :

– "Calculs des Spectres Rovibrationnels des Divers Types de Polyades des Molécules Toupies Sphériques XY_4 et XY_6 : Une extension de STDS",
Ch. Wenger, V. Boudon, G. Pierre et J.-P. Champion.

– "Calculs *Ab Initio* et Spectroscopie Haute Résolution de la Pentade de Pliage de SiH_2D_2 dans la Région 10-16 μm",
M. Rotger, V. Boudon, B. Lavorel, S. Sommer, H. Bürger, J. Breidung, W. Thiel, M. Bétrencourt et J.-C. Deroche.

[C5] "*Praha 98 : 15th Conference on High Resolution Molecular Spectroscopy*", 30/08-03/09 1998, Prague (Rép. Tchèque), **deux posters** présentés :

– "*Ab Initio* Calculations and High Resolution Spectroscopy of the Bending Pentad of SiH_2D_2 in the 10-16 μm Region",
M. Rotger, V. Boudon, B. Lavorel, S. Sommer, H. Bürger, J. Breidung, W. Thiel, M. Bétrencourt and J.-C. Deroche.

– "High Resolution Jet-Cooled Spectroscopy and Analysis of the $\nu_2+\nu_6$ combination band of SF_6",
V. Boudon, M. Hepp, M. Herman, I. Pak and G. Pierre.

[C6] "*Fourteenth Winter Fluorine Conference*", 17-22/01 1999, St. Petersburg Beach (Floride, USA), **un poster** présenté :

– "Absorption Spectrum of the $a(E'_{2g}) \leftarrow X(G'_g)$ and $b(G'_g) \leftarrow X(G'_g)$ Electronic Transitions of ReF_6",
M. Rotger, V. Boudon and H. Selig.

[C7] "*Thirteenth International Symposium and School on High Resolution Molecular Spectroscopy – HighRus-99*", 04-10/07 1999, Tomsk (Russie), **un poster** présenté :

– "Study of ν_2 Raman spectra of SF_6 molecule",
D. Bermejo, R. Martinez, E. Loubignac, V. Boudon and G. Pierre.

[C8] "*Atmospheric Spectroscopy Applications – ASA Reims 99*", 01-03/09 1999, Reims (France), **un poster** présenté :

– "Absorption of SF_6 in the ν_3 Band",
N. Lacome, R. R. Gamache, E. Loubignac, V. Boudon and G. Pierre.

[C9] "*16th Colloquium on High Resolution Molecular Spectroscopy*", 06-10/09 1999, Dijon (France), **huit posters** présentés :

– "High Resolution Infrared Spectroscopic Study of the ν_3 Band of ReF_6 in a Supersonic Jet Expansion",
V. Boudon, M. Rotger, Y. He, H. Hollenstein, M. Quack and U. Schmitt.

– "High Resolution Fourier Transform Infrared Spectroscopy an Analysis of the ν_3 Fundamental Band of P_4",
V. Boudon, G. Pierre, E. B. MKadmi and H. Bürger.

– "Classical Interpretation of The Rotational Structure of the v_6=1 Vibrational Level of $Mo(CO)_6$",

G. Dhont, B. Zhilinskii, D. Sadovskii and V. Boudon.

- "Spectroscopy of XY_5Z (C_{4v}) Symmetric Top Molecules : A Tensorial Formalism Adapted to the Chain $O(3) \supset O_h \supset C_{4v}$ Chain",
  M. Rotger, V. Boudon and M. Loëte.
- "Transition Moments for the XY_5Z (C_{4v}) Symmetric Top Using the Tensorial Formalism",
  M. Rotger, V. Boudon and M. Loëte.
- "Spontaneous Raman Spectroscopy of Closed and Open-Shell Transition-Metal Fluorides",
  M. Rotger, M. Rey, V. Boudon, M. Loëte, A. Lorriaux and H. Selig.
- "Study of the Infrared Absorption Spectrum of SF_6 Near 950 cm^{-1}",
  E. Loubignac, V. Boudon, G. Pierre, N. Lacome, R. R. Gamache, F. Herlemont, M.Khelkhal and J. Legrand.
- "Study of the Fundamental Bands of $^{70}GeD_4$ by Raman and Infrared Spectroscopy",
  G. Pierre, V. Boudon, E. B. MKadmi, H. Bürger, D. Bermejo and R. Martinez.

[C10] "*Colloque Bilan et Prospective du PNCA* ", 01-03/12 1999, Clermont-Ferrand (France), **deux posters** présentés :

- "Détermination des Paramètres de ν_6 de SF_6 à Partir de l'Analyse Simultanée de ν_2 et $\nu_2+\nu_6$ en Vue de l'Etude de la Bande Chaude $\nu_3+\nu_6-\nu_6$",
  D. Bermejo, R. Martinez, E. Loubignac, V. Boudon et G. Pierre.
- "Etude de l'Absorption de SF_6 dans la Région de la Bande ν_3",
  N. Lacome, R. Gamache, E. Loubignac, V. Boudon et G. Pierre.

[C11] "*Praha 2000 : 16th Conference on High Resolution Molecular Spectroscopy*", 03-07/09 2000, Prague (Rép. Tchèque), **trois posters** présentés :

- "High Resolution Spectroscopy and Analysis of the ν_4 Bending Region of SF_6 Near 615 cm^{-1}",
  V. Boudon, G. Pierre and H. Bürger.
- "High Resolution Spectroscopy and Analysis of the ν_3 Stretching Fundamental of $^{70}GeF_4$",
  V. Boudon, H. Bürger and E. B. MKadmi.
- "C_{4v}TDS Software and its application to the ν_1/ν_8 Dyad of $SF_5{}^{35}Cl$",
  M. Rotger, A. Decrette, V. Boudon, M. Loëte, H. Bürger, S. Sander and H. Willner.

[C12] "*17th Colloquium on High Resolution Molecular Spectroscopy*", 09-13/09 2001, Nimègue (Pays-Bas), **six posters** présentés :

- "The Spectrum of an Octahedral Molecule in a Degenerate Electronic State : The ν_6 Fundamental Band of Jet-Cooled $V(CO)_6$",
  M. Rey, V. Boudon, M. Loëte, P. Asselin, P. Soulard and L. Manceron.
- "Rotational-Vibrational Relative Equilibria and the Structure of Quantum Energy Spectrum of the Tetrahedral Molecule P_4",
  Ch. Van-Hecke, D. A. Sadovskii, B. I. Zhilinskii and V. Boudon.
- "High-Resolution Spectroscopy and Analysis of the ν_4 Band of $^{80}SeF_6$",
  M. Rotger, V. Boudon, H. Bürger and H. Willner.
- "Spectroscopy of XY_2Z_2 (C_{2v}) Asymmetric Top Molecules: A Tensorial Formalism Adapted to the $O(3) \supset T_d \supset C_{2v}$ Chain",
  M. Rotger, V. Boudon and M. Loëte.
- "Transition Moments for XY_2Z_2 (C_{2v}) Asymmetric Top Using The Tensorial Formalism – C_{2v} Top Data System Software",
  M. Rotger, V. Boudon and M. Loëte.
- "High Resolution Spectroscopy on the Chiral Molecule CDBrClF : A Rovibrational Analysis of the ν_5 State",
  S. Albert, V. Boudon and M. Quack.

[C13] "*2nd European Meeting on Environmental Chemistry*", 12-15/12 2001, Dijon (France), **un poster** présenté :

- "Spectroscopic Tools for the Remote Sensing of Some Greenhouse Gases : CH_4, CF_4, SF_6, ...",
  V. Boudon, J.-P. Champion, T. Gabard, G. Pierre, M. Loëte and Ch. Wenger.

[C14] "*Praha 2002 : 17th Conference on High Resolution Molecular Spectroscopy*", 01-05/09 2002, Prague (Rép. Tchèque), **cinq posters** présentés :

- "Rovibronic Couplings in a Fourfold Degenerate Electronic State of an Octahedral Molecule: The ν_3 band of ReF_6",
  M. Rey, V. Boudon, M. Loëte and F. Michelot. **Note :** Pour cette contribution, M. Rey a reçu le *Prix Pliva 2002* du meilleur poster.
- "Orientation of $O(3)$ and $SU(2) \otimes C_I$ Representations in Cubic Point Groups (O_h, T_d) for Application to Molecular Spectroscopy",
  M. Rey, V. Boudon, Ch. Wenger, G. Pierre and B. Sartakov.
- "First High-Resolution Raman Spectrum and Analysis of the ν_5 Bending Fundamental fo SF_6",
  V. Boudon and D. Bermejo.
- "Study of Quasi-Spherical XY_2Z_2 Molecules Using Symmetry-Adapted Tensorial Formalism: Application to SO_2F_2",
  M. Rotger, V. Boudon and M. Loëte.
- "Spectroscopy of the Ethylene Molecule: A Tensorial Formalism Adapted to the $O(3) \supset D_{2h}$ Chain",
  W. Raballand, M. Rotger, V. Boudon and M. Loëte.

[C15] "TDLS 2003: 4th International Conference on Tunable Diode Laser Spectroscopy", 14-18/07 2003, Zermatt (Suisse), **un poster** présenté :

- "Diode Laser Spectroscopy of the ν_5 band of the SF_5Cl Molecule",
  W. Raballand, N. Benoit, M. Rotger and V. Boudon.

[C16] "*18th Colloquium on High Resolution Molecular Spectroscopy*", 08-12/09 2003, Dijon (France), **neuf posters** présentés :

- "Stark Spectroscopy of the Ethylene Molecule: Tensorial Formalism for Spectrum Simulations",
  W. Raballand, M. Rotger, V. Boudon and M. Loëte.
- "D_{2h} Top Data System (D_{2h}TDS) Software for Spectrum Simulation of X_2Y_2 Asymmetric Molecules",
  W. Raballand, Ch. Wenger, M. Rotger, V. Boudon and M. Loëte.
- "Detailed Investigation of the Icosad (1.3 – 1.5 μm) of $^{12}CH_4$ at High-Resolution: Preliminary Analysis of the ν_2+$2\nu_3$ Region",
  V. Boudon, M. Loëte, M. Hippler, M. Quack and M. Rey.
- "Summary of Recent Analyses of the First Four Polyads of Methane",
  M. Loëte, J.-P. Champion, O. Robert, J.-C. Hilico, V. Boudon, S. Toumi and L. R. Brown.
- "Spectroscopy of Octahedral Molecules in a Degenerate Electronic State: Detailed Investigation of the 720 cm^{-1} Region of Jet-Cooled ReF_6",
  M. Rey, V. Boudon, M. Rotger, M. Loëte, H. Hollenstein and M. Quack.
- "$SU(4)$ in Electronic Spectroscopy of Molecules with an Odd Number of Electrons",
  F. Michelot, M. Rey and V. Boudon.
- "*Ab Initio* Calculations on the SF_5Cl Molecule",
  N. Zvereva, M. Rotger, V. Boudon and M. Loëte.

- "High-Resolution Infrared Absorption Spectrum and Analysis of the $\nu_2+\nu_4$ Combination Band of SF_6",
  V. Boudon and N. Lacome.
- "The Ground State Rotational Spectrum of SO_2F_2",
  M. Rotger, V. Boudon, M. Loëte, L. Margulès, J. Demaison, H. Mäder, G. Winnewisser and H. S. P. Müller.

[C17] "*Colloque Bilan et Prospective du PNCA*", 22-25/09 2003, Saint-Jean-de-Luz (France), **deux posters** présentés :

- "Etat des Lieux de la Spectroscopie du Méthane",
  V. Boudon, M. Loëte, J.-P; Champion, M. Hippler, M. Quack et L. R. Brown.
- "Modélisation de l'Absorption de SF_6 dans la Région de 10 μm",
  V. Boudon et N. Lacome.

[C18] "*39 th Symposium on Theoretical Chemistry - Molecular Spectroscopy and Dynamics*", 28/09-02/10 2003, Gwatt (Suisse), **un poster présenté** :

- "Detailed Investigation of the Icosad (1.3 – 1.5 μm) of $^{12}CH_4$ at High-Resolution: Preliminary Analysis of the $\nu_2 + 2\nu_3$ Region",
  V. Boudon, M. Loëte, M. Hippler, M. Quack and M. Rey.

Communications orales présentées lors de colloques

[O1] "*55th Ohio State University International Symposium on Molecular Spectroscopy*", 12-16/06 2000, Columbus, Ohio (USA) : **une communication** présentée :

- "Tensorial Development for the Rovibronic Hamiltonian and Transition Moments of Octahedral XY_6 Molecules in a Fourfold Degenerate Electronic State",
  V. Boudon, M. Rey, M. Loëte and F. Michelot. *Présenté par V.* Boudon,
  Mini-symposium "*Vibronic Interactions*".

[O2] "*56th Ohio State University International Symposium on Molecular Spectroscopy*", 11-15/06 2001, Columbus, Ohio (USA) : **deux communications** présentées :

- "STDS and HTDS Software for the Calculation and Analysis of Spherical-Top Spectra",
  V. Boudon, Ch. Wenger, J.-P. Champion and G. Pierre. *Présenté par V.* Boudon,
  Mini-symposium "*Spectroscopic Freeware*".
- "Extension of the STDS/HTDS Software to Rovibronic Spectroscopy and to Lower Symmetry Problems",
  V. Boudon, M. Rey, M. Rotger and M. Loëte. *Présenté par V.* Boudon,
  Mini-symposium "*Spectroscopic Freeware*".

[O3] "*57th Ohio State University International Symposium on Molecular Spectroscopy*", 17-21/06 2002, Columbus, Ohio (USA) : **trois communications** présentées :

- "Rovibrational Spectroscopy of Sulphur Hexafluoride: A Review",
  V. Boudon and G. Pierre. *Présenté par V.* Boudon.
- "Rovibronic Couplings in a Fourfold Degenerate Electronic State of an Octahedral Molecule: The ν_3 band of ReF_6",
  M. Rey, V. Boudon and M. Loëte. *Présenté par M.* Rey.
- "Study of Distorted Spherical Tops Using Symmetry-Adapted Tensorial Formalism: Application to SF_5Cl and SO_2F_2",
  M. Rotger, V. Boudon and M. Loëte. *Présenté par M.* Rotger.

[O4] "*Atmospheric Spectroscopy Applications – ASA Moscow 02*", 25-28/08 2002, Moscou (Russie) : **une communication** présentée :

- "The $^{12}CH_4$ Spectrum in the 1.6 – 2 μm Region: The $4\nu_4$ Band",

O. Robert, M. Rey, J.-C. Hilico, M. Loëte, V. Boudon and J.-P. Champion. *Présenté par M. Loëte.*

[O5] "*Séminaire National de Spectroscopie – SNS'02*", 15-17/12 2002, Saïda (Algérie) : **deux communications** présentées :

- "Spectroscopie Moléculaire à l'Aide d'Opérateurs Tensoriels Irréductibles: Théorie et Applications",
  G. Pierre, J.-P. Champion and V. Boudon. *Présenté par G. Pierre.*
- "STDS, HTDS, C_{2v}TDS, C_{4v}TDS, MIRS, GROUP : Un Ensemble de Logiciels Développés pour la Spectroscopie Moléculaire",
  Ch. Wenger, V. Boudon, M. Rotger, M. Rey, J.-P. Champion, A. Nikitin and G. Pierre. *Présenté par Ch. Wenger.*

[O6] "*58th Ohio State University International Symposium on Molecular Spectroscopy*", 16-20/06 2003, Columbus, Ohio (USA) : **quatre communications** présentées :

- "Databases and Programs for the Spectroscopy of some Greenhouse Gases: CH_4, SF_6 and CF_4",
  V. Boudon, J.-P. Champion, T. Gabard, G. Pierre, M. Loëte and Ch. Wenger. *Présenté par V.* Boudon,
  Mini-symposium "*Atmospheric Chemistry / Spectroscopy*".
- "The Symmetrization of Angular Momentum Wavefunctions and its Applications to Molecular Spectroscopy",
  V. Boudon, M. Rey, Ch. Wenger, G. Pierre and B. Sartakov. *Présenté par V.* Boudon.
- "The Ground State Rotational Spectrum of SO_2F_2",
  M. Rotger, V. Boudon, M. Loëte, L. Margulès, J; Demaison, H. Mäder, G. Winnewisser and H. S. P. Müller. *Présenté par M.* Rotger.
- "Spectroscopy of X_2Y_4 (D_{2h}) Molecules: Tensorial Formalism Adapted to the $O(3) \supset D_{2h}$ Chain, Hamiltonian and Transition Moment Operators. Application to the ν_{12} and ν_2 Bands of C_2H_4",
  M. Rotger, W. Raballand, V. Boudon and M. Loëte. *Présenté par M.* Rotger.

Séminaires et communications orales diverses

[S1] **Séminaire** présenté au *Laboratorium für Physikalische Chemie* de *l'Ecole Polytechnique Fédérale de Zürich* (Suisse) le 10/07/1996 à l'invitation du Pr. M. Quack.
"Spectroscopy of Transition-Metal Hexafluorides",
M. Rotger and V. Boudon. *Présenté par V.* Boudon et M. Rotger.

[S2] **Séminaire** présenté à l'*Institut für Anorganische und Analytische Chemie, Farbereich Chemie, Freie Universität Berlin* (Allemagne) le 24/04/1997 à l'invitation du Pr. K. Seppelt.
"Spectroscopy of Transition-Metal Hexafluorides",
V. Boudon. *Présenté par V.* Boudon.

[S3] **Séminaire** présenté au *Laboratorium für Physikalische Chemie* de *l'Ecole Polytechnique Fédérale de Zürich* (Suisse) le 23/08/2000 à l'invitation du Pr. M. Quack.
"Reductions and (Ro)vibronic Spectroscopy of Octahedral Molecules : The Case of Non-Perturbative ContactTransformations",
V. Boudon. *Présenté par V.* Boudon.

[S4] **Séminaires** présentés au *Laboratorium für Physikalische Chemie* de *l'Ecole Polytechnique Fédérale de Zürich* (Suisse) le 02/05/2002 à l'invitation du Pr. M. Quack.

- "Rovibrational Spectroscopy of Sulphur Hexafluoride: A Review",
  V. Boudon and G. Pierre. *Présenté par V.* Boudon.

– "Rovibronic Couplings in a Fourfold Degenerate Electronic State of an Octahedral Molecule: The ν_3 band of ReF_6",
M. Rey, V. Boudon and M. Loëte. *Présenté par M.* Rey.

[S5] Séminaire présenté à la *Société COMURHEX* (Pierrelatte) le 06/11/2002 à l'invitation de Mme C. Belhomme et de Mr. B. Morel.
"Eléments de Spectroscopie Moléculaire",
M. Rotger et V. Boudon. *Présenté par M.* Rotger *et V.* Boudon.